



**An integrated seismic-scale analysis  
of reservoir compartmentalisation  
on continental margins: the Espírito  
Santo Basin, SE Brazil**

**Davide Alexandre da Costa Gamboa**

**Submitted in partial fulfilment of the requirements for the  
degree of Ph.D.**

**Cardiff University**

**December 2011**





## **Author note and status of publications**

The results chapters presented in this thesis have been prepared as scientific papers for publication in international journals. The present status of publication is as follows:

Chapter 4 has been published as Gamboa, D., Alves, T., Cartwright, J., and Terrinha, P., 2010, MTD distribution on a 'passive' continental margin: The Espírito Santo Basin (SE Brazil) during the Palaeogene: *Marine and Petroleum Geology*, v. 27, p. 1311-1324.

Chapter 5 has been published as Gamboa, D., Alves, T., and Cartwright, J., 2011, Distribution and characterization of failed (mega) blocks along salt ridges, southeast Brazil: Implications for vertical fluid flow on continental margins: *Journal of Geophysical Research*, v. 116, p. B08103.

At the time of thesis submission, Chapter 6 has been re-submitted after revision and acceptance to publication in *Marine and Petroleum Geology* as: Gamboa, D., Alves, T., and Cartwright, J., A submarine channel confluence classification for topographically confined slopes.

Additional work published during this project: Gamboa, D., Alves, T.M. and Cartwright, J., 2011. Seismic-Scale Rafted and Remnant Blocks over Salt Ridges in the Espírito Santo Basin, Brazil. In: Y. Yamada et al. (Eds.), *Submarine Mass Movements and Their Consequences*. Springer, pp. 629-638.

Although the articles are jointly co-authored with the project supervisors, the work presented in the publications is that of the lead author, Davide Gamboa. Editorial work was provided by the project supervisors in accordance with a normal thesis chapter.

## Acknowledgements

This project benefited from the support of a great number of people who, directly or indirectly, helped me during this project. I would like to thank my main supervisor, Tiago Alves, for his guidance and support. His knowledge and good ideas helped to make this experience more productive and stimulating. I also thank him for the support on all other non-PhD matters and for a couple of relaxing drinks every once in a while. I am grateful to my co-supervisors Joe Cartwright for his constructive comments on my work. I must thank Fundação para a Ciência e Tecnologia (Portugal) for funding of the SFRH/BD/38819/2007 scholarship that allowed me to undertake this project. A sincere thank you goes to my pastoral supervisor, Richard Lisle, for all the help and support he provided and also for all that I have learned from him during the various fieldtrips in Wales and Spain. Gwen Pettigrew is thanked for the indispensable IT support for the 3D Lab. I would like to thank L. Moscardelli, W. Mohriak, A. Tripsanas, R. Urgeles, M. Huuse, J. Frey-Martínez for the reviews of my published papers. A word of appreciation goes to Kiichiro Kawamura for his invaluable help that greatly made my trip to Japan much less stressful.

My thanks to all the Cardiff people with whom I got along in the last few years. Thank you Ana, Ricardo, Cristina, Duarte, Dan, Alessia, Mostyn, Aggie, Jennie, Suze, Ian, Bledd, Paola, Andy, Kate, Laura, Martino and all other past and present Cardiff University students I met for the knowledge and good moments shared. Ruben and the Portuguese “bio-people” are thanked for all the good times shared outside the university life.

I am grateful for the unconditional support provided by my parents, Rosa and José, throughout my life that allowed me to follow my choices and ambitions. Without them, none of this would have been possible. Last but not least, my deepest gratitude goes to my girlfriend Ana Maia. I thank her for all the support given in the last four years and for being by my side during all the ups and downs of real life. Her patience and belief were invaluable to overcome the grey days, and her smile made the good moments last longer. Thank you for making me a better person.

## **Abstract**

Deepwater continental margins constitute one of the ultimate exploration frontiers where giant oilfields have been discovered. These comprise reservoir units affected by multi-scale compartmentalisation resultant from stratigraphic, structural and/or diagenetic processes that compromise the lateral and/or vertical connectivity of permeable strata.

A 3D seismic dataset from the deepwater Espírito Santo Basin (SE Brazil) was analysed to assess and quantify the architectural elements that influence the compartmentalisation of reservoir units. Mass-Transport Deposits (MTDs) have growing importance on reservoir studies as they highly impact the compartmentalisation of contemporaneous reservoir-prone turbidite strata. More significant compartmentalisation occurs in areas with higher MTD proportion, which are associated to wider dimensional ranges of laterally limited turbidites. However, salt diapirs constitute important barriers for MTD erosion, thus aiding the preservation of reservoir-prone turbidites. The internal compositional heterogeneities and cohesed strata on remnant and rafted blocks identified within the studied MTDs constitute important fluid flow or accumulation compartments, particularly when linked to underlying permeable faults.

Submarine channels in Palaeocene and Neogene Units comprise important reservoir-prone strata, thus it is crucial to understand their spatial distribution. Large channels are focused along the axis of salt-withdrawal basins, whereas in sub-units with numerous smaller channels these are laterally scattered across the basin. A new quantitative method used in this study shows that channel confluences and topographic confinement control significantly the density and spatial distribution patterns of submarine channels. A novel classification for submarine channel confluences is proposed, based on channel morphology and distribution of sediment facies within the tributaries.

The key aim of this thesis was to undertake a seismic-scale qualitative and quantitative analysis of the compartmentalisation of reservoir units on the Brazilian margin using methodologies that can be applied to other continental margins worldwide. As such, the results of this study can provide significant contributions for hydrocarbon exploration.

## **Table of Contents**

### **Chapter 1: Introduction**

1.1. Rationale .....	2
1.2. Depositional systems on continental slopes .....	4
1.2.1 – Mass Transport Deposits .....	7
1.2.2. Submarine Canyons and Channels.....	14
1.2.2.1. Evolution of submarine channel systems .....	20
1.3. Halokinesis on passive continental margins .....	24
1.4. Reservoirs and reservoir compartmentalisation .....	26
1.4.1. Hydrocarbon Reservoirs .....	26
1.4.2 – Reservoir Compartmentalization .....	30
1.4.2.1. Stratigraphic compartmentalization .....	33
1.4.2.2. Structural compartmentalization .....	38
1.4.2.3. Diagenetic compartmentalisation .....	40
1.4.2.4. Mixed Compartmentalisation .....	42
1.5. Aims of this research.....	42
1.6. Thesis layout .....	44

### **Chapter 2: Geological Setting – Espírito Santo Basin, SE Brazil**

2.1 Tectono-Stratigraphic Evolution .....	47
2.2. Late Cretaceous-Cenozoic Halokinesis .....	55
2.3. Local setting .....	56
2.4. Seismic Stratigraphy.....	57

2.4.1. Unit 1.....	57
2.4.1. Unit 2.....	58
2.4.3. Unit 3.....	58

## **Chapter 3: Methods**

3.1. 3D Seismic .....	62
3.1.1. Seismic resolution .....	67
3.1.2. 3D seismic volume visualisation and interpretation .....	71
3.1.2.1. Interpretation of seismic facies.....	74
3.1.3. Seismic Attributes .....	76
3.1.4 3D seismic survey parameters and time-depth conversions.....	80
3.2. Quantitative seismic analysis.....	81
3.2.1. Spatial Statistics .....	82

## **Chapter 4: MTD on the Espírito Santo Basin during the Palaeogene**

4.1. Abstract.....	87
4.2. Introduction .....	88
4.3. Results and observations .....	91
4.3.1- Description of MTD intervals.....	91
4.3.1.1- Interval M1 .....	93
4.3.1.2- Interval M2 .....	96
4.3.2- Absence of headwall scarps.....	101
4.3.3 – Distribution of stratified lithologies .....	101
4.4. Statistical analysis of unit variability.....	108

4.4.1- Thickness variations in the Abrolhos Unit .....	108
4.4.2- Thickness variations of MTDs in the Abrolhos Unit.....	108
4.5. Slope Profiles .....	110
4.6. Discussion.....	114
4.6.1. Significance of variability in MTD-Turbidite couplets .....	114
4.6.2. Influence of MTD deposition in slope profiles and margin evolution .....	116
4.7. Conclusions .....	118

## **Chapter 5: Distribution and characterization of failed (mega) blocks along salt ridges, SE Brazil: Implications for vertical fluid flow on continental margins**

5.1. Abstract.....	120
5.2. Introduction .....	121
5.3. Studied stratigraphic interval .....	126
5.4. Character of the basal MTD-A1 .....	126
5.4.1. Internal character of the MTD .....	127
5.4.1.1. Remnant and rafted blocks .....	132
5.4.1.2. Internal imbrication.....	135
5.4.1.3. Fault distribution and relation to failed blocks .....	137
5.4.2. Peridiapiric block distribution .....	138
5.4.2.1. Block surface area .....	140
5.4.2.2. Block Orientation.....	140
5.4.2.3. Block Density .....	141
5.4.2.4. Block Height.....	142
5.4.2.5. Width/Length Ratio .....	143
5.4.3. Block deformation.....	145
5.4.3.1. Deformation styles .....	145

5.4.3.2. Quantification and distribution of deformation types.....	145
5.5. Discussion.....	150
5.5.1. Halokinetic structures as triggers of slope instability.....	150
5.5.2. Can blocks constitute preferential fluid-flow paths? .....	156
5.6. Conclusions .....	160

## **Chapter 6: Submarine confluence classification for topographically confined slopes**

6.1. Abstract.....	164
6.2. Introduction .....	165
6.3. Chapter-specific Methods.....	171
6.3.1. Seismic data analysis.....	171
6.3.2. Channel Spatial analysis.....	172
6.4. Results.....	175
6.4.1 Morphology of submarine channel confluences .....	175
6.4.1.1. Channel C1 (sub-unit 3a) .....	175
6.4.1.2. Channel C4 (Modern Channel) .....	177
6.4.2. Geomorphic channel parameters in relation to confluence .....	181
6.4.3. Channel density and distribution.....	185
6.4.4. Spatial analysis of channel distribution: a new quantitative method .....	188
6.5. Discussion.....	193
6.5.1. Controls on channel clustering on submarine environments .....	193
6.5.2. Comparison between fluvial and submarine confluences .....	198
6.5.2. Classification of submarine confluences .....	204
6.6 Conclusions .....	207

## **Chapter 7: Summary and discussion**

7.1 Introduction and summary of major findings.....	210
7.1.1. Chapter 4.....	210
7.1.2. Chapter 5.....	211
7.1.3. Chapter 6.....	212
7.2. Styles and scales of compartmentalization on the Espírito Santo Basin.....	215
7.2.1- Scale of MTD and Turbidite compartmentalization .....	219
7.2.1.1. Scale relationships between MTDs of distinct units .....	219
7.2.1.2. Scale relationships between MTDs and turbidites in Unit 2 .....	221
7.2.1.3. Scale of MTD blocks and relationship to turbidites .....	223
7.2.1.4. Scale relationships between MTD blocks and submarine channels .....	225
7.2.2. Channel styles and compartmentalisation .....	228
7.2.3- Scale of fault-bounded compartments.....	231
7.3. Can MTDs be reservoirs? .....	237
7.4. Does channel compartmentalization change alongslope? .....	238
7.4.1. Channel distribution .....	238
7.4.2. Changes in channel accommodation space.....	241
7.4.3. Morphological depressions as isolated compartments.....	244
7.5. Primary and secondary controls of halokinesis on reservoir compartmentalisation ....	247
7.6. Limitations of this research.....	251
7.7. Further Work.....	253

## **Chapter 8: Conclusions**

8.1. Main conclusions .....	257
8.2. Conclusions from Chapter 4.....	258
8.3. Conclusions from Chapter 5.....	259



8.4. Conclusions from Chapter 6.....	260
<b>References .....</b>	<b>263</b>
<b>Annexes .....</b>	<b>297</b>
A1. Seismic acquisition and processing parameters of BES-2 survey.....	298
A2. Supplementary data for Chapter 4.....	299
A3. Supplementary data for Chapter 5.....	306
A4. Supplementary data for Chapter 6.....	317
A5. Supplementary data for Chapter 7 .....	449

## List of Figures

<b>Figure 1.1.</b> Controls on the development of deep-marine clastic systems .....	5
<b>Figure 1.2.</b> (a) Schematic representation of the distinct MTD domains and compositional features (modified from Bull et al., 2009). (b) Representation of MTD sub-classes according to their degree of internal cohesion. Deformation and disaggregation tends to increase downslope as travel distance increases (modified from Shanmugam, 2006). .....	11
<b>Figure 1.3.</b> Diagram representing submarine slope canyon and channel systems, with frontal lobes present on the distal basin regions. Canyons have high thalwegs that fully confine the turbiditic flows. Leveed channels are characterised by lower thalwegs, which allows flow stripping and overspill of finer sediment on the overbanks. Crevasse splays can be created at channel bends when turbidite flows breach through the levee. Frontal lobes are characterised by decreases of flow energy and confinement, favouring sediment deposition.....	16
<b>Figure 1.4.</b> (a) Hierarchical arrangement of channel complexes, from the single elements to complex systems (modified from Slatt, 2006). (b) Channel arrangement resultant from the interplay of lateral and vertical amalgamation (from Clark and Pickering, 2006). (c) Comparison of channel architecture resultant from gradual lateral migration (accretion) and rapid shifts in channel course (avulsion) (from Abreu et al., 2003). .....	23
<b>Figure 1.5.</b> (a) Vertical sections showing the patterns of faulting and folding associated with growing salt structures. (b) Plan view of radial and concentric faults developing around salt diapirs. (c) Gravity spreading of fragmented overburden sections (rafts) on top of salt units (modified from Stewart, 2006). .....	27
<b>Figure 1.6.</b> Section representative of the main halokinetic structures along passive margins. The proximal margin is characterised by thick overburdens and a salt extensional domain, favouring the development of salt rollers attached to large listric faults. This is followed by a transitional domain at mid-slope regions characterised by the development of vertical diapirs. Compressional domains on the distal slope are characterised by salt-generated fold-and-thrust belts that actively deform the sea-floor, creating significant topographic relief which exert important controls on sediment distribution at such regions. ....	28
<b>Figure 1.7.</b> (a) Orders of compartment scales. (b) Representation of closed and open compartments, and the connectivity concept of dynamic and closed compartments. (c) Representation of elements influencing lateral and vertical compartmentalisation. Faults are important controls of lateral connectivity. (d) Sand-body amalgamation and connectivity as a function of accommodation/sedimentation ratios. (e) Amalgamation on accretion packages and impact on lateral connectivity. Non-amalgamated LAPs are fully compartmentalised. ....	37

<b>Figure 2.1.</b> Map representing the location and geographic limits of the Espírito Santo Basin, Southeast Brazilian Margin. The area in black shows the location of the BES-2 3D seismic volume/block .....	48
<b>Figure 2.2.</b> Simplified regional section across the Espírito Santo Basin depicting the three salt domains (extensive, transitional and compressive) and associated deformation structures. The major depositional mega-sequences and their interaction with salt structures are also represented (Modified from Fiduk et al., 2004). .....	49
<b>Figure 2.3.</b> Paleogeography outline of the Brazilian margin showing main tectonic phases. <b>(a)</b> Syn-rift phase, with predominance of continental environments. <b>(b)</b> Transitional phase, marked by deposition of evaporites in a restricted basin. <b>(c)</b> Early drift phase, with formation of shallow-water carbonate platforms. <b>(d)</b> Late drift phase characterised by open marine sedimentation. The relative location of the Espírito Santo Basin is highlighted by the red box (Modified from Ojeda, 1982). .....	50
<b>Figure 2.4.</b> Stratigraphic chart of the Espírito Santo Basin showing regional stratigraphic units, main tectonic phases and magmatic events (modified from França et al., 2007). .....	54
<b>Figure 2.5.</b> Seafloor dip-map of the studied area, Espírito Santo Basin. The figure highlights the presence of several salt diapirs (D1 to D7) that control the distribution of the modern sedimentary systems. The diapir alignments form two northwest-oriented ridges that bound main salt-withdrawal basins. ....	59
<b>Figure 2.6.</b> Seismic section showing the principal seismo-stratigraphic units in the northern region of the Espírito Santo Basin. Three main units are identified based on their seismic character, and stratigraphic and structural features .....	60
<b>Figure 3.1.</b> Schematic representation of 3D marine seismic surveys. A towed acoustic source near the surface emits a sound wave that travels through the water. When the acoustic properties of the rock change, the P-waves reflected to the surface are detected by hydrophones mounted in a long cable towed behind the boat. The hydrophone spacing partly controls the horizontal resolution of the seismic data (modified from Bacon et al. 2003). ....	65
<b>Figure 3.2. (a)</b> Schematic representation of the seismic waves in SEG normal polarity zero phased data. In variable area wiggle display, peaks are displayed in black and troughs in white. In variable density display, individual traces are represented as colour-coded voxels indicative of their amplitude (modified from Hart, 1999). <b>(b)</b> Schlumberger Geoframe interpretation environment with examples of a seismic section both in variable area wiggle and variable density displays, with the latter type providing a clearer visualisation of data. ....	66

<b>Figure 3.3.</b> Effect of vertical resolution and tuning thickness. The resolution of the reflections from the top and bottom of a bed is dependant of the interaction between closely spaced wavelets (adapted from Brown, 2004).....	69
<b>Figure 3.4. (a)</b> Pre- and post-migration area of the Fresnel zone. In 3D seismic, the initial large circle is reduced to a smaller one with a radius of $\frac{1}{4}$ of the wavelength, represented by the black dot in the centre (modified from Brown, 2004). <b>(b)</b> Representation of data summation paths in 3D seismic processing (from Bacon et al., 2003).....	70
<b>Figure 3.5. (a)</b> Diagram illustrative of a data volume. Vertical seismic sections can be taken through the volume in any desired direction, and (horizontal) time slices can be taken at any desired time depth (modified from Kearey et al., 2002). <b>(b)</b> Example of seismic volume showing sections along inlines, crossline, and partially along a time slice (top limit). The volume in the figure was set to only represent data below an interpreted horizon. ....	72
<b>Figure 3.6.</b> Diagram presenting the different seismic facies associated with Mass-Transport Deposits (MTDs). Comparative outcrop-scale examples of the correspondent seismic facies are also shown. ....	77
<b>Figure 3.7.</b> Diagram representing non-MTD seismic facies associated with turbidite deposits (submarine channels and turbidite fans) and fine grained sediments (hemipelagites and contourites).....	78
<b>Figure 3.8.</b> Representation of spatial distribution patterns. <b>(a)</b> Uniform distribution. <b>(b)</b> Random distribution. <b>(c)</b> Clustered distribution.....	85
<b>Figure 4.1.</b> Sea-bed dip map of the 3-D seismic survey. Defined sub-areas are outlined and labelled A1 to A4. D1 to D7: Salt diapirs. ....	90
<b>Figure 4.2. a)</b> Seismic section across slope representing the character of stratigraphic units. Note the faults in Unit 1 limited at the base of the Abrolhos Unit. Horizon1 to Horizon 7 represent interpreted horizons bounding defined intervals. <b>b)</b> Detail of seismic section to highlight the chaotic character of interval M1 and the continuous reflections of interval M2.....	92
<b>Figure 4.3.</b> Attribute maps for interval M1. <b>a)</b> Isochron map of interval M1, predominantly consisting in MTDs. Note the high thickness over 100 ms TWTT in the western diapir area, represented by dark colours. Thickness of the interval gradually decreases towards the MTD limit close to the eastern salt diapirs to values bellow 50 ms TWTT. Contour spacing is 25 ms twtt. <b>b)</b> RMS amplitude map for interval M1. Moderate amplitudes characterize the MTDs. High amplitudes are seen in the central area of the basin, gradually decreasing to the east. Note the amplitude contrast on both flanks of diapir D3. <b>c)</b> Coherence slice across interval M1. The dark irregular patterns represent chaotic MTDs. Light colours represent lower deformation. Note the varied	

coherence patterns for the MTD. MTD lateral limit is marked by intersection of the coherence slice with an underlying less deformed interval. ....	94
<b>Figure 4.4.</b> Seismic section representative of the eastward thickness decrease of the MTD defined by interval M1. The overall decrease of amplitude and chaotic character of the seismic reflections follows the MTD thinning towards the salt diapirs on the Eastern section.....	95
<b>Figure 4.5.</b> Vertical seismic section representative of interval M2. <b>a)</b> North-South oriented profile showing high amplitude continuous reflections of this interval. Reflector continuity is compromised close to diapir deformed areas. <b>b)</b> Detail showing the termination of continuous strata by overlying MTD flow. <b>c)</b> Detail of a section with disturbed reflectors. ....	98
<b>Figure 4.6. a)</b> Section representing the transition from MTD to continuous strata within interval M2. Note the predominant presence of MTDs in the west section of the stratigraphic succession. <b>b)</b> Detail of the disrupted reflections within M2. <b>c)</b> Detail of the continuous, less deformed strata of M2, also coincident with the thickening of the interval. Notice the segmentation of the strata on this transition area. ....	99
<b>Figure 4.7.</b> Attribute maps computed for interval M2. <b>a)</b> Isochron map for interval M2. Thicker stratigraphic accumulations over 100 ms TWTT are seen close to the diapirs and along parts of the central salt withdrawal basin. <b>b)</b> RMS amplitude map for interval M2. Very high amplitudes predominate in the centre of the basin when compared to peripheral areas. Notice the marked amplitude contrasts on the flanks of diapir D3, and the gradual amplitude decrease towards the East. <b>c)</b> Coherence slice for interval M2. Light coloured coherent patterns predominate, reflecting the continuous undeformed nature of most of its composing strata. The dark, low coherence areas correspond to areas of higher MTD deformation. Note the slump between diapirs D2 and D6, with the lateral limits and internal compression structures well evidenced by this attribute.....	100
<b>Figure 4.8.</b> Uninterpreted ( <b>a</b> ) and interpreted ( <b>b</b> ) seismic section highlighting continuous strata. Solid lines highlight horizons represented in Figure 4.9. Note the higher proportion of continuous, less deformed strata above interval S2, when compared to the lower half of the Abrolhos Unit. The extent of interval S1 is limited by the MTD of interval M1, suggesting erosion by the mass-flow. Interval S2, included in interval M2, contains continuous reflections, with localized thicker packages close to the diapirs. Interval S3 is bounded by relatively thin (~40 ms TWTT) MTDs (or partially deformed strata). ....	102
<b>Figure 4.9.</b> Isochron maps of selected interval bounding continuous reflections, also representing their lateral extent. <b>a)</b> Interval S1, located bellow interval M1, and restricted to the NW salt structures. <b>b)</b> Interval S2, within interval M2, covering large areas in the salt withdrawal basin.	

Note thickening along the basin axis. <b>c)</b> Interval S3, continuous within the diapiric area. Contour spacing is 10 ms twtt in <b>a</b> and <b>c</b> , and 20ms twtt in <b>b</b> . .....	104
<b>Figure 4.10.</b> Amplitude map of the continuous reflections depicted in Figure 4.9. Lateral variations of the amplitude values are common, representative of lateral heterogeneities in the stratigraphic accumulations. The majority of the high-amplitude patches is elongated and are preferentially trending northwest to southeast. Low-amplitude features commonly separate the high-amplitude regions, either representing stratigraphic or structural (faults) discontinuities. ....	107
<b>Figure 4.11.</b> Graphic representation of statistical data representing variations of Abrolhos Unit and MTD thickness, and MTD proportion in the Abrolhos Unit. Plots represent variations along and across slope according to a North-South and East-West direction, respectively. ....	111
<b>Figure 4.12.</b> <b>a)</b> Seismic section across slope representing Horizon 2, Horizon 4 and Horizon 6. Inset shows location of seismic line. <b>b to d)</b> Plots representing the profiles of Horizon 2, Horizon 4 and Horizon 6, respectively, along with dip measurements along slope. The dip change area divides the profile in upper and lower segment, based on the dip values. “m” represents the slope value calculated for a best-fit line applied to each segment of the profile.....	113
<b>Figure 5.1.</b> Seismic section representing the character of the identified seismo-stratigraphic units in northern Espírito Santo Basin. Unit 1 (Late Cretaceous-Palaeogene) is characterized by low amplitude reflections. Crestal faults are present above buried salt ridges. Unit 2 is characterized by high-amplitudes and chaotic character of the seismic reflections, contrasting with the remaining units 1 and 3. MTD-A1 is the lowermost deposit identified in Unit 2, bounded by Horizon 1 and Horizon 2. This section also evidences thinning of the MTD towards the rims of the diapir ridge. ....	124
<b>Figure 5.2.</b> Coherence slice taken 20 ms TWTT above Horizon 1, intersecting the studied MTD. The studied MTD overlies a northwest-trending diapir ridge where five diapirs are present. This area was divided in three zones representative of upper, middle and lower slope, respectively. Numerous high coherence remnant/rafted blocks (light colours) are observed within the limit of Diapir Ridge 1. Blocks clusters are observed in Zone 3 and rims of Zone 2. No blocks are observed either in the salt-withdrawal basins, or the region of Diapir Ridge 2. ....	128
<b>Figure 5.3.</b> Seismic sections depicting the relation between faults and blocks. <b>a)</b> Map showing the location of seismic sections in this figure. <b>b)</b> Stepped profile of Horizon 1, evidencing the influence of pre-existing faults on the mass-failure. The small steps in the horizon irregular profile are due to fault activity, whereas high steps are due to remobilization of failed strata. The latter is confirmed by the height of the deformed block, similar to the height of the erosional step. <b>c)</b> section of MTD-A1 depicting the relation between faulting and remnant	

strata/blocks. The remnant features show evident vertical continuity with the underlying unit, limited by the erosional surface. Notice the thicker accumulations on the eastern sector underlain by faults. **d)** and **e)** illustrate in more details the link between blocks and pre-failure faults. The blocks commonly show their limits aligned with the faults, especially less deformed ones. Fractures are commonly identified within the bigger blocks. Rafted blocks show tilted or folded internal reflections, implying lateral movement. Fault-block alignments are less evident in this type..... 129

**Figure 5.4.** **a)** Time map of Horizon 1, representing the base of MTD-A1. The grey shapes represent the blocks identified in MTD-A1, occurring along the northwest-trending depressions flanking the ridge. Notice the higher abundance of blocks below 3000 ms TWTT. **b)** Isochron map of MTD-A1. The thickest MTD accumulations are present along the depressions of Horizon 1 pointed in a), reaching close to 200 ms TWTT, also coincident with the presence of the blocks. Other higher thickness deposits of the MTD are observed upslope of diapir D2, where no blocks occur. **c)** Thickness map between Horizon 1 and Horizon 0, evidencing the Late Cretaceous deformation in the study area. Lower thickness (<750ms TWTT) highlight the presence of buried salt ridges (BR1 and BR2) related with the smaller diapirs D5 and D2. **d)** Slope profiles of Horizon 1 along the West and East flanks of the diapir ridge. The slope dip decrease coincides with slope regions where blocks occur..... 130

**Figure 5.5.** Seismic profiles illustrating the thinning of MTD-A1 towards the western and eastern limits. **a)** and **b)** evidence the morphological step of Horizon 1 which limits the regions of higher thickness of the MTD. **b), c)** and **d)** show blocks in the morphological depressions where thicker accumulations occur. The thickness of MTD-A1 is commonly defined by the block height, and these are absent in the thinner regions..... 131

**Figure 5.6.** **a)** RMS (Root-Mean-Square) amplitude map of a time window within MTD-A1 between 20 and 40 ms TWTT above Horizon 1. Higher amplitudes are observed closer to the rims of the MTD, whereas the axial area of the ridge shows lower amplitudes. The blocks are evidenced by higher rms amplitude values. **b)** Detail of blocks with dipping internal strata evidenced by the alternations of pattern in rms amplitude. **c)** Detail of blocks with variable internal dip. The rms amplitude maps provides an indicator of block deformation as tilted blocks show the banded internal aspect, whereas non-tilted ones have relatively uniform amplitude patterns..... 134

**Figure 5.7.** Seismic sections depicting internal imbrications in the MTD, used as kinematic indicators of the MTD transport direction. **a)** Seismic section north of diapir D2, showing imbrications dipping towards the diapir, indicating eastwards flow towards the salt-withdrawal basin. The evident imbrications on the top and flanks of the diapir suggest a flow collision with the chaotic

masses in the salt-withdrawal basin. **b)** Section on the northern flank of diapir D3. Imbricated strata indicate southward movement of this MTD component, buttressing against the diapir. **c)** Section on the rim of MTD-A1, where imbricated blocks evidence eastwards flow of a peripheral component towards the diapir ridge (d) Example of imbricated strata on the eastern regions of the salt ridge. This section evidences differential MTD internal flow. Rotated blocks have their movement hindered by larger, less remobilized blocks. .... 136

**Figure 5.8.** Relation between faults and blocks. **a)** Coherence map of a slice taken 100 ms TWTT bellow Horizon 1, showing the faults in Unit 1. **b)** Coherence map of a slice taken 20 ms TWTT bellow Horizon 1. These maps show important faulting of Unit 1 along the southern and eastern regions of the diapiric ridge. **c)** Map evidencing the buried salt ridges and the modern diapirs with the overlay of the faults in Unit 1 and the blocks in MTD-A1. The ridges, faults and blocks show a close relation in Zone 3 and the eastern region of Zone 2. Note how the more fractured areas correspond to the ones where block frequency is higher. (d) Rose diagrams with the fault and block orientation along the diapir ridge. Both features show preferential northwest trending directions. .... 139

**Figure 5.9.** Graphic representation of the statistical data obtained from the interpreted blocks in MTD-A1, evidencing their properties in the three different zones and distance to the diapir ridge axis. Bars on right-hand side represent the minimum, maximum and average values of each parameter at a given Zone. **a)** Block area distribution in the salt ridge. **b)** Block density and their distance to the salt ridge axis. **c)** Block height. **d)** Width and length of blocks. **e)** Width-Length ratio of blocks in relation to their distance to the salt ridge axis. Blocks are distributed asymmetrically in relation to the ridge axis. The results show a general similarity of blocks alongslope, indicating similar genesis and remobilization in the three studied regions. Plotted best-fit lines represent the entire block data series, regardless of the zone. .... 144

**Figure 5.10.** Different styles of block deformation. **a)** Minor deformation represented by sub-horizontal internal strata. **b)** Moderate deformation with folding and low tilt of blocks. **c)** Major deformation, represented by steeply dipping strata ( $>15^\circ$ ) due to block rotation. **d)** Distribution of block deformation styles along the salt ridge. **e)** Graph of the frequency of deformation styles in relation to the distance from the ridge axis. The plot in **e)** is a projection of the blocks distribution shown in **d)**, and no zone distinction is represented. Note the relatively uniform distribution of deformation styles, with the exception of the western rim of the MTD where major deformation is prevalent. .... 147

**Figure 5.11.** Schematic diagram with the evolution of the diapir ridge. Salt ridges developed deformed the overburden, forming a northwest-oriented relief (**a** and **e**). Early deformation and



faulting of the overburden along the buried salt ridges also led to partial subsidence on the crest of the salt ridges and diapirs (**b** and **f**). Failure and deposition of MTD-A1 with numerous blocks located along the main diapir ridge. Remnant blocks/strata are limited by faults, whereas the presence of rafted blocks is not strictly dependant of underlying crestal faults (**c** and **g**). **d**) Diagram illustrating the relative movement of the MTD components. Higher remobilization is interpreted to occur in the area north of diapir D3, with convergence of flow directions. Short remobilization is interpreted to have occurred along the axis of the diapir ridge, with MTD components spreading perpendicularly to the latter. Moderate remobilization occurred predominantly along the western rim of the MTD with these components flowing eastwards, colliding with the ones in the central regions. .... 152

**Figure 5.12.** Acoustic anomalies in the seismic data evidence the presence of fluids in the studied strata. (**a** to **e**). Faults in Unit 1 are associated with fluid migration, sourced from Late Cretaceous strata. Brightening in or above fault-bounded blocks, or the block-matrix contact suggest permeability enhancement features within the MTD. When blocks are absent, fluids are trapped underneath the impermeable debrites. **f**) Diagram representing the fluid flow potential within MTD-A1. Areas with higher block frequency and faults have higher potential, whereas areas where no blocks or faults are observed have the lowest. Moderate potential is expected in faulted regions with fewer blocks, or where blocks show no evident relation to underlying faults. **g**) Schematic drawing representing fluid bypass through MTD units suggested by the close relation of faults and remnant/rafted blocks. Faults act as vertical fluid conduits in pre-failure strata. Migration through the MTD is made along permeable strata and fractures in the blocks..... 161

**Figure 6.1.** Sea-floor dip map of the studied slope, depicting the geometry of the modern Rio Doce Turbidite System within a salt-withdrawal basin confined by salt diapirs. The greater confined is observed in area A2, where diapir spacing is smaller. .... 169

**Figure 6.2.** Seismic profiles representative of **a**) Area 1, **b**) Area 2 and **c**) Area 3. Three sub-units are identified, 3a, 3b, 3c and the modern channel. Sub-unit 3a and the modern channel consist in 'Y' shaped canyons located on the axis of the basin. Sub-units 3b and 3c are composed by multiple channels dispersed along width of the basin. Salt diapirs in Area 2 imposed significant topographic confinement at the mid-slope section..... 170

**Figure 6.3.** Schematic representation of the channel analysis method. Channel thalweg height and width were measured from a reference Channel Point (CP) at its base. This was applied to all channel features identified on evenly spaced seismic profiles..... 173

<b>Figure 6.4.</b> Representation of the channel analysis method workflow. Step 1 corresponds to the channel analysis and data acquisition. Step 2 is related to the statistical analysis and tests applied.....	174
<b>Figure 6.5.</b> Profiles of maximum thalweg depth, in time, of Channel C1 (sub-unit 3a) and Channel C4 (modern). Colours represent different tributaries and the post-confluence channel. Profiles indicate that tributaries join at equal levels in canyon C1, whereas in canyon C4 tributary depths are offset. Nevertheless, the eastern tributary in C4 is at a concordant level with the post-confluence channel. $s$ = channel sinuosity. ....	176
<b>Figure 6.6.</b> Maps and graphical data for Channel C1. <b>a)</b> Time map of the base of channel C1. Incision depth of tributaries is identical at the junction. A central depression at the confluence point is interpreted as a plunge pool, analogous to those observed in fluvial systems. Contour spacing is 25 ms TWTT. <b>b)</b> Maximum amplitude map within channel C1. The high amplitude values along the eastern tributary and post-confluence branch suggest that these form the main channel. <b>c)</b> 3D view of the confluence geometry in channel C1. <b>d)</b> Plots of thalweg height and width variations along slope. ....	179
<b>Figure 6.7.</b> Maps and graphical data of channel C4. <b>a)</b> Time map of modern channel, which evidences unequal junctions. High sinuosity is observed at the post-confluence reaches. Contour spacing is 25 ms TWTT <b>b)</b> Rms amplitude from a 40 ms time window below the seafloor. Here, the confluence point shows a low amplitude patch, interpreted to represent sediment erosion by increase flow velocity at the junction. <b>c)</b> 3D view of the confluence geometry in channel C4. A limited plunge pool is present close to the tributary at the highest topographic level. <b>d)</b> Plots of thalweg height and width variation along slope.....	180
<b>Figure 6.8.</b> Scatter plots representing CP width and height in the studied stratigraphic sub-units. Data for sub-unit 3ca and Modern Channel highlight width and height variations related with the confluence region. In sub-units 3b and 3c there is no clear distinction between the different slope regions. ....	183
<b>Figure 6.9.</b> <b>a)</b> Plot illustrating the frequency of CP per sub-unit, in each area. <b>b)</b> Map representing the spatial distribution of CP in the studied area, for each sub-unit. CP distribution provides a close proxy to assess the path and orientation of the various slope channels. <b>c)</b> Map representing the density of CP per cell in the study area. High densities in the pre-confluence area are coincident with location of main tributaries. In post-confluence areas, higher densities are observed on the flanks of salt diapirs. White arrows indicate regions with higher channel densities. Dashed white lines mark the limits of zones A1, A2 and A3. Red line delimits the area of data analysed by the statistical models.....	187

<b>Figure 6.10.</b> Plots illustrating the observed CP frequencies, and ones expected from distribution models. <b>a)</b> Negative Binomial distributions provide a good fit to explain the CP distribution in the slope (see also Table 6.2). <b>b), c)</b> and <b>d)</b> represent the observed and Poisson (normal) expected frequencies. The significant data scattering between the observed frequencies and the expected frequencies calculated by the Poisson distribution show that this model does not provide a good fit to describe the distribution of channels on the slope. Nevertheless, areas of higher CP density (Area A1) show an approach to normal distributions.....	194
<b>Figure 6.11.</b> Plot representing the confluence-tributary width ratio observed in different margins of the world. This value is obtained by dividing the confluence width by the sum of tributary widths. Dotted line represents a width ratio equal to 1, which is expected when the confluence width is equal to the sum of tributary widths. (data from Barnes, 1992; Bellaiche, 1993; Canals et al., 2000; Cronin et al., 2005; Dalla Valle and Gamberi, <i>in press</i> ; Ercilla et al., 2000; Greene et al., 2002; L'Heureux et al., 2009; McGregor, 1985; McHugh and Ryan, 2000; Mitchell, 2004; Pirmez et al., 2000; Pratson and Coakley, 1996; Scholl et al., 1970; Schwab et al., 2007; Shepard and Dill, 1966). .....	203
<b>Figure 6.12.</b> Diagram illustrative of the submarine confluence classification. Symmetric confluences are Y-shaped and nomenclature is based on the position of the main active tributary, i.e. left or right symmetric. Asymmetric confluences are pure asymmetric if principal channel activity is along the alignment made by the main tributary and post-confluence channel. Secondary asymmetric describes cases where channel activity is not along the main alignment. ....	206
<b>Figure 7.1.</b> Schematic representation of the study area with a synthesis of the principal observations and results.....	214
<b>Figure 7.2.</b> Plot representing the width and height of the different geological features identified in the slope. Two major dimensional groups are present. The largest values correspond to MTDs and associated turbidite intervals. The smaller dimensions correspond to channel systems and intra-MTD blocks. ....	218
<b>Figure 7.3.</b> Plot representing the average width and height of MTDs in Units 2 and 3, and of turbidites in Unit 2. ....	226
<b>Figure 7.4.</b> Plot representing the width and length of blocks in MTD-A1 and of turbidites in Unit 2. ....	227
<b>Figure 7.5.</b> Plots of channel data. <b>(a)</b> and <b>(b)</b> show the width and height of the numerous channel sections measured in sub-units 3b and 3c. <b>(c)</b> Width and height of measured sections of the Palaeocene Channel, Channel C1 and the modern channel. Blocks in MTD-A1 are also represented for comparison with the dimensions of channel sections. Regression lines of each	

data series are colour-coded for clearer distinction. (d) Average width and height of the distinct channels systems. The buried systems show identical scale relationships where, on average, channel width is about 12 times the height.....	232
<b>Figure 7.6.</b> (a) Plot with throw and spacing of the crestal and synclinal faults. Both families have identical scale relationships of these parameters. (b) Plot representing length and spacing of the two fault families. Synclinal faults are prone to delimit larger compartments when compared to crestal ones. ....	236
<b>Figure 7.7.</b> (a) Time and maximum amplitude maps of Channel C1. The time map shows that several morphological constrictions along the channel path, being better evidenced at downslope locations. The amplitude map shows that these constrictions bound channel sections, or compartments, with higher amplitude values, interpreted to represent higher amounts of coarse-grained sediment. (b) Schematic representation of the effect of morphologic constrictions within channels on the formation of higher volume compartments, and on sediment distribution. Constrictions are associated with sharp knickpoints are prone to compromise connectivity between compartments.....	243
<b>Figure 7.8.</b> Circular to elongated depressions in sub-unit 3b. (a) Coherence slice with several depressions evidenced by red dashed lines. Depressions upslope are smaller and aligned with channels. Depressions at mid-slope position are larger and have higher spacing. (b) amplitude map highlighting ring-shaped amplitude patterns associated with the depression. (c) Seismic profile representing the Neogene units in the study area. Depressions cannot be easily distinguished from channels on vertical sections. (d) Plots representing dimensional data from the morphological depressions.....	246
<b>Figure A.1.</b> Plot representing the area of individual turbidites in Unit 2. ....	305
<b>Figure A.2.</b> Plot representing the percentage of high-amplitude areas in relation to the total area of individual turbidites in Unit 2.....	305
<b>Figure A.3.</b> Plot representing width and length of deformed blocks. D1=low deformation, D2=moderate deformation, D3= Major deformation.....	315
<b>Figure A.4.</b> Plot with height and W/L ratio of deformed blocks. D1=low deformation, D2=moderate deformation, D3= Major deformation. ....	315
<b>Figure A.5.</b> Plot representing the frequency of variably deformed blocks and the distance from the diapir ridge axis. D1=low deformation, D2=moderate deformation, D3= Major deformation. .	316
<b>Figure A.6.</b> Plot contrasting the Poisson expected frequency and observed frequencies in the total area.....	447

<b>Figure A.7.</b> Plot contrasting the Negative Binomial expected frequency and observed frequencies in the total area.....	447
<b>Figure A.8.</b> Plots representing the Negative Binomial expected frequencies and the observed frequencies in the three studied areas. ....	448
<b>Figure A.9.</b> Linear regression residual plots of the width-height, or fault spacing-throw, relations obtained for the different data series analysed in this thesis. ....	452
<b>Figure A.10.</b> Log-Log plot comparing the width and length of MTD Blocks and morphological depressions, and spacing and length of crestal faults and synclinal faults. The size of blocks overlaps the sizes of crestal faults, thus confirming their genetic relation. ....	453

## List of tables

<b>Table 5.1.</b> Average values of blocks properties according to style of deformation and slope zone. .	149
<b>Table 6.1.</b> Synthesis of $c$ and $a$ values obtained from power trend lines in the each Area/Sub-unit couplet. ....	184
<b>Table 6.2.</b> Summary table of the goodness-of-fit test results to the distribution models. In <b>a)</b> and <b>b)</b> , corresponding to uniform and random distribution tests, the test values exceed the critical values, hence $H_0$ is rejected. c) test results are lower than the critical values, hence it is valid to consider a negative binomial distribution for the analysed channel in all areas of the slope. ..	191
<b>Table 6.3.</b> Summary table of observed frequencies, estimated mean, variance and distribution patterns in the total and individualised areas. ....	195
<b>Table 6.4.</b> (Previous page) Comparative table of channel width and height at submarine confluences from several continental margins. Left and right tributary assignment is based on the upstream tributary position in relation to the confluence.....	202
<b>Table 7.1.</b> Synthesis table of the $\alpha$ and $\beta$ values obtained for the different depositional features. .	220
<b>Table 7.2.</b> Table representing the average length, throw and spacing, and the constants $\gamma$ and $\eta$ that represent the scale relationships of the families of crestal and synclinal faults .....	235
<b>Table A.1.</b> Table with thickness of MTDs identified at each measuring point. ....	299
<b>Table A.2.</b> Unit 2 thickness at each measuring point. ....	303
<b>Table A.3.</b> Percentage of MTDs in Unit 2 at each measuring point.....	304
<b>Table A.4.</b> Table with block measurement data and deformation style. ....	306
<b>Table A.5.</b> Table with location, size, perpendicular distance to salt ridge axis and deformation style of the studied blocks. Negative distances are indicative of westward position in relation to the ridge axis, positive distance values are eastward positions.....	311
<b>Table A.6.</b> Table with location, area and unit ID, and morphometric parameters of each CP identified in the Neogene stratigraphic units.....	317
<b>Table A.7.</b> Table with calculated Poisson probability, Poisson expected CP frequency and observed CP frequencies in the total area of the slope analysed in Chapter 6.....	431
<b>Table A.8.</b> Table with calculated Poisson probability, Poisson expected CP frequency and observed CP frequencies in Area A1. ....	433
<b>Table A.9.</b> Table with calculated Poisson probability, Poisson expected CP frequency and observed CP frequencies in Area A2. ....	435
<b>Table A.10.</b> Table with calculated Poisson probability, Poisson expected CP frequency and observed CP frequencies in Area A3. ....	437

<b>Table A.11.</b> Table with calculated Negative Binomial probability and expected CP frequency, and observed CP frequencies in the total area. ....	439
<b>Table A.12.</b> Table with calculated Negative Binomial probability and expected CP frequency, and observed CP frequencies in Area A1. ....	441
<b>Table A.13.</b> Table with calculated Negative Binomial probability and expected CP frequency, and observed CP frequencies in area A2. ....	443
<b>Table A.14.</b> Table with calculated Negative Binomial probability and expected CP frequency, and observed CP frequencies in area A3. ....	445
<b>Table A.15.</b> Average dimensions of MTDs in Units 2 and 3.....	449
<b>Table A.16.</b> Average dimensions of turbidites in Unit 2. ....	449
<b>Table A.17.</b> Length, Throw and Spacing data of the Crestal and Synclinal fault families.....	450
<b>Table A.18.</b> Table with dimensional data of the morphometric depressions in sub-unit 3b. ....	451

# **Chapter 1**

## **Introduction**



## **1. Introduction**

### **1.1. Rationale**

Deepwater continental slopes are prolific hydrocarbon exploration provinces that have been gaining great relevance in the last decade. Recent discoveries of giant oil fields on South Atlantic salt margins have confirmed their enormous potential, thus setting the drive for increased exploration of these offshore environments. The latest advances in 3D Seismic technology have been significant for the comprehension of deep offshore dynamics and morphology (Posamentier, 2004). The higher definition of new datasets has revealed that these environments are far more complex than previous knowledge allowed, leading to new qualitative and quantitative approaches to characterise submarine depositional systems (Deptuck et al., 2007b; Mayall and Stewart, 2000, McHargue et al., 2001).

Large canyon and channel systems are a dominant feature in continental slopes. These systems constitute conduits that stretch for thousands of kilometres, establishing main routes for sediment transport from the upper slope towards distal submarine lobes and fans (Posamentier and Walker, 2006; Shepard and Emery, 1973). The high proportions of sand in these stratigraphic features constitute important reservoirs of great interest for hydrocarbon exploration (Clark et al., 1996; Mayall et al., 2006). Slope failures are also a dominant process in deepwater settings. The resultant Mass-Transport Deposits (MTDs) are capable of remobilising very large volumes of sediment downslope and can significantly alter the stratigraphic architecture of the slope either by reworking of previous deposits, or by conditioning the distribution of posterior sedimentary accumulations (Armitage et al., 2009; Hampton et al., 1996; Piper et al., 1997). The importance of MTDs on exploration has

been increasing in recent years not only due to the important impact that they can have on the erosion of good-quality reservoirs, but also due to a growing potential of these units as reservoirs (Meckel III, 2011; Weimer and Shipp, 2004). Furthermore, South Atlantic margins are influenced by the diachronic growth of salt or mud diapirs that variably deform the overlying stratigraphic units and have a direct influence on the architecture and distribution of the submarine depositional systems (Fiduk et al., 2004; Mayall et al., 2010).

By knowing what processes act in these margins, it is aimed to predict what can be the resulting architectural arrangement of deep-water reservoirs. This gains particular relevance as reservoirs tend to be compartmentalised (Slatt, 2006). Each compartment is partially or totally delimited by low permeability barriers or baffles resultant from multi-scale stratigraphic, structural or diagenetic processes (Ortoleva, 1994). Despite its relevance, the full extent of compartmentalisation is only assessed during production and development of the oil fields (Jolley et al., 2010). As the exploration of deepwater reservoirs implies increasing challenges and costs, early assessments of compartmentalisation are required. As such, high-quality 3D seismic data is a powerful tool to characterise the architecture, morphology and deformation processes imposed on reservoir-prone strata and estimate the degree of compartmentalisation of reservoir units prior to drilling operations.

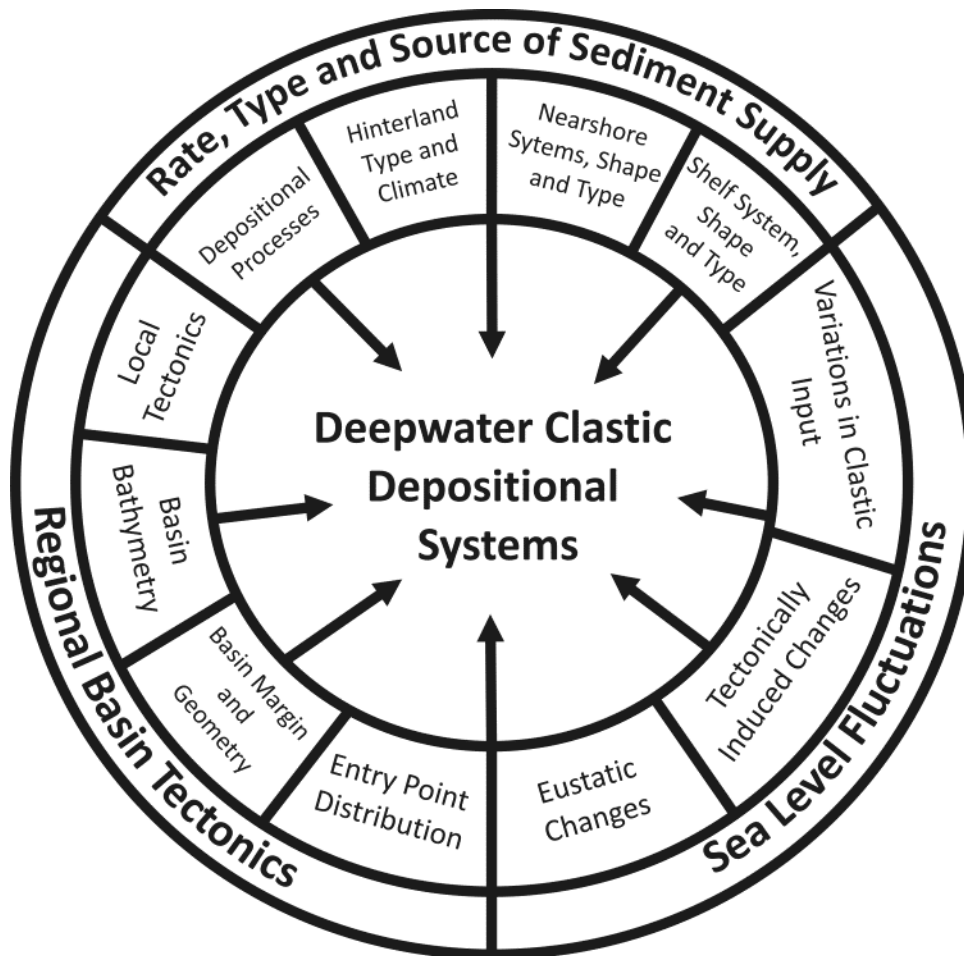
The key aim of this thesis is to undertake a seismic-scale a quantitative analysis of the compartmentalisation imposed by the stratigraphic architecture of potential reservoir units on continental slopes, and how these are influenced by the growth of salt structures.

## 1.2. Depositional systems on continental slopes

The continental slope can be considered as the frontier between the deep-marine and shallow shelf environment (Leeder, 1999). The continental slope extends from the shelf-break, where water depths do not exceed a few hundred metres, to water depths of 1.5–3.5 km, although depths are even greater for slopes that descend into oceanic trenches (Pratson et al., 2007). Seafloor gradients on the slope are similarly variable, ranging from  $< 1^\circ$  to  $> 25^\circ$ , with the overall average being  $\sim 4^\circ$  (Kennett, 1982; Stow et al., 1996).

These deep-marine systems are complex settings where a wide range of sedimentary and dynamic processes take place (Shanmugam, 2006). Several studies have attempted to provide general comprehensive models for continental slope settings (Bouma et al., 1962; Mutti and Normark, 1991; Normark, 1978; Posamentier and Allen, 1993, amongst others). With the proliferation of 3D seismic these models turned out to be over-simplified as improvements in the amount and quality of acquired data revealed that the morphological elements from deep water settings (canyons, channels, levees, lobes and bottom currents) have a complex and variable interaction among themselves (Baas et al., 2005; Eschard, 2001; Flint and Hodgson, 2005; Gee et al., 2007; Posamentier and Kolla, 2003).

Clastic sedimentation on continental slopes is controlled by an interaction of different factors that include climate, sea-level fluctuations, basin tectonics, type and nature of sediment and rate of supply, which are frequently interdependent (Baas et al., 2005; Posamentier and Walker, 2006; Reading and Richards, 1994; Richards et al., 1998) (Fig. 1.1). Sea-level variations in sequence stratigraphy models are cyclic events that can be described



**Figure 1.1.** Controls on the development of deep-marine clastic systems (from Richards et al., 1998)

by two end members: (1) relative sea level lowstands characterized by incision and deposition of coarse material in deeper setting, while during (2) relative sea level high stands there is a predominance of fine-grained (hemipelagic) sediments reaching the slope. A typified cycle has periods of high sediment supply represented by mass transport deposits overlaying fine sediments, followed by a decrease in sediment supply rate and deposition of turbidite successions, culminating with draping by hemipelagic sediment (Covault and Graham, 2010; Eschard, 2001; Posamentier and Kolla, 2003). This should not be taken as rule as it has been shown that sandy turbidites still occur during relative sea level high stands with significant sand supply to distal slope areas, as seen for example in the Mississippi Fan or offshore Angola (Abreu et al., 2003; Reading and Richards, 1994).

The type of sediment supply and physiographic characteristics of the shelf/slope play an important role in slope evolution and classification (Adams et al., 2002; Adams and Schlager, 2000; Baas and Best, 2002; Carvajal et al., 2009; Hurst et al., 1999; Richards et al., 1998). The relation between these two controlling factors is thoroughly described in works of Reading and Richards (1994) and Richards et al (1998), establishing a classification system based on the grain size of sediment and number of entry points to slope system. This classification relates prevailing architectural elements with the dominant type of sediment,. Sand rich systems (high sand:mud ratio) settle proximal to the base of slope having low degrees of reservoir heterogeneity. Mud rich systems (low sand:mud ratios) have high reservoir heterogeneity and locate at a significant distance from slope (Richards et al., 1998).

The architectural elements on slope depositional systems are influenced by the

process by which sediment is delivered to the deep sea (Bouma, 2004; Piper and Normark, 2009; Posamentier and Walker, 2006; Pratson et al., 2007; Stow et al., 1996; Stow and Johansson, 2000; Weaver et al., 2000). Stow et al. (1996) distinguishes three main groups of processes to supply sediment to deep sea systems: episodic resedimentation processes (channels and mass transport), semi-permanent bottom currents (contourites) and pelagic settling. A description of the main architectural elements relevant for the study of reservoirs, channels and mass-transport deposits, is presented in the following sub-sections.

### **1.2.1 – Mass Transport Deposits**

Mass Transport Deposits (MTDs) are considered to include all types of submarine mass movement deposits. These are common depositional elements in deep sea environments that originate from slope failure and move downslope by the action of gravity (Hampton et al., 1996; Masson et al., 2006; Mulder and Cochonat, 1996; Posamentier and Walker, 2006; Varnes, 1978). Mass transport complexes can occur at various scales: large basin-wide MTDs in the order of tenths or hundreds of kilometres, better visualised on seismic scale, can form by shelf break or mid-slope failure, while comparable smaller ones can form by collapse of canyon walls or flanks of salt domes (Cronin et al., 2005; Hampton et al., 1996; Masson et al., 2006; Mayall et al., 2006; Posamentier and Martinsen, 2011; Posamentier and Walker, 2006; Tripsanas et al., 2004). MTDs can constitute significant proportions of the submarine stratigraphic successions in excess of 50 or 75% (Moscardelli et al., 2006; Nelson et al., 2011; Posamentier and Martinsen, 2011; Weimer and Shipp, 2004). Their occurrence has been predominantly associated with margin erosion through retrogressive failures (Hampton et al., 1996; Masson et al., 2010; Masson et al., 2006; Mulder and Cochonat, 1996; Pratson and Coakley, 1996; Solheim et al., 2005). Nevertheless,

recent studies have shown that MTDs promote the transport of large volumes of sediment to slope and distal slope settings, thus playing important roles in the construction and progradation of continental margins (Boyd et al., 2010; Gamboa et al., 2010; Haughton et al., 2003; Huppertz et al., 2010).

Slope failure occurs when the shear strength of a geological surface or layer fails to resist the downslope shear stress imposed by gravity forces, being also related with the type of environment of the slope (Garziglia et al., 2008; Hampton et al., 1996; Stow et al., 1996; Varnes, 1978). Several failure mechanisms have been established as triggers of submarine MTDs, from which the more common are oversteepening, presence of weak geological layers, overpressure due to rapid sediment accumulation, earthquakes, dissociation of gas hydrates, high pore pressure and groundwater seepage, glacial loading, volcanic activity and salt growth (Bünz et al., 2005; Canals et al., 2004; Frey-Martínez et al., 2011; Hampton et al., 1996; Hudec and Jackson, 2006; Lastras et al., 2002; Masson et al., 2010; Masson et al., 2006; Tripsanas et al., 2004). MTDs are considered to result from a combined effect of several of these factors over time, although the main trigger for failure could be preferentially linked to a specific one.

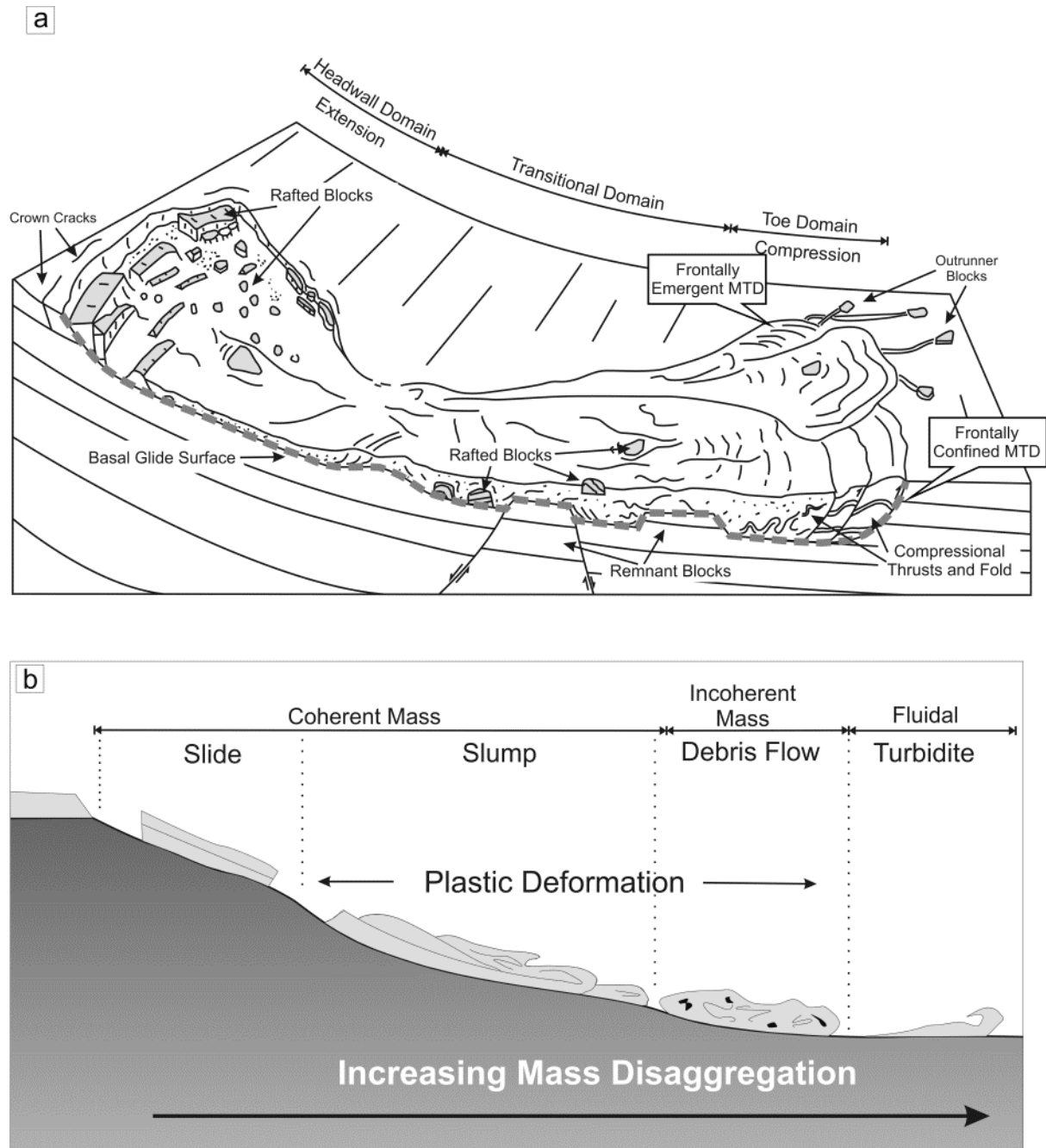
Two essential features of MTDs are the glide surfaces and the displaced masses of sediment that travel downslope (Hampton et al., 1996) (Fig. 1.2a). Glide of MTDs along basal rupture surfaces is often considered to occur along individualised weak surfaces (Frey-Martínez et al., 2011; Hampton et al., 1996; Masson et al., 2010). Nevertheless, variable thicknesses and degrees of deformation of the MTD basal features indicates that it can be a more complex basal shear zone than a single surface or layer (Alves and Lourenço, 2010). In addition, multiple glide surfaces can be present in MTDs, particularly at the proximal or

distal areas (Bull et al., 2009; Hampton et al., 1996; Masson et al., 2010). The failed masses commonly rest on the shear surfaces but can also flow beyond them (Bull et al., 2009; Frey-Martínez et al., 2006; Hampton et al., 1996). Idealised MTD models define a source, transition and depositional domains (Bull et al., 2009; Lastras et al., 2002; Posamentier and Martinsen, 2011; Posamentier and Walker, 2006) (Fig. 1.2). The source domain is limited upslope by the headwall scarp and corresponds to the region where failure has originated. Headwall scarps are sinuous or arcuate steep rupture planes that result from upward ramping of the basal surface (Bull et al., 2009; Hampton et al., 1996; McAdoo et al., 2000) (Fig. 1.2a). Extension predominantly takes place in the source area, with normal faults being common within localised failed masses. Crown cracks are also common in non-failed slope strata resultant from extensional stresses in the vicinities of the main headwall scarp, and the presence of such features is prone to cause posterior retrogressive slope failures (Bull et al., 2009; Pratson and Coakley, 1996). Although a common feature in most MTDs, the presence of headwall scarps is not always evident, being this particularly noted when slope failures are related to active deformation of mobile strata (Gamboa et al., 2010; Richardson et al., 2011).

The transitional domain is the main depositional region for the body of the MTD (Bull et al., 2009; Posamentier and Martinsen, 2011) (Fig. 1.2a). This includes variably deformed internal features resultant from either the extensional or compressional stresses suffered by the failed masses during transport (Frey-Martínez et al., 2005; Hampton et al., 1996; Martinsen and Bakken, 1990; Naruse and Otsubo, 2011; Posamentier, 2004; Posamentier and Walker, 2006). Relevant MTD features within this domain are the lateral margins, the morphology of the basal surface and internal deformation represented by folds and blocks



(Bull et al., 2009; Dunlap et al., 2010; Frey-Martinez et al., 2005; Frey-Martínez et al., 2006; Gafeira et al., 2007; Gamboa et al., 2011b; Gee et al., 2005; Gee et al., 2006; Moscardelli et al., 2006; Posamentier, 2004). When present, lateral margins constitute confining limits to the MTD that tend to be parallel to the flow direction (Bull et al., 2009). The general slip movement taking place at these locations can favour lateral collapse of strata and the additional inclusion of material within the MTD (Frey-Martinez et al., 2005; Martinsen, 1994). The basal surface is a key feature of MTDs (Fig. 1.2a). It can have a relatively flat and continuous morphology, especially on seismic-based studies, if MTDs have low erosive potential and predominantly hydroplaning flow (Ilstad et al., 2004a; Ilstad et al., 2004b). Irregular basal surfaces are associated with erosive MTDs. These often show numerous linear basal grooves that run parallel to the main flow direction (Bull et al., 2009; Gee et al., 2005; Moscardelli et al., 2006). More pronounced irregularities of the MTD basal surface (in the order of various tenths or hundred of metres) also occur. These can be represented by erosive “slots” if a depression was created below the average level of the MTD base (Bull et al., 2009), or by variably sized portions of remnant strata that was not remobilised by the MTD (Fig. 1.2a). These remnants can be of limited height, thus being covered by the remobilised material, or consist in completely intact portions of strata surrounded by the MTD (Alves, 2010; Alves and Cartwright, 2009; Deptuck et al., 2007a; Frey-Martinez et al., 2005). Irregular basal surfaces are prone to occur in MTDs affecting faulted regions. This can lead to marked lateral changes when relatively continuous basal surfaces present in non-faulted sections acquire irregular and stepped morphologies within the faulted regions (Gamboa et al., 2011b).



**Figure 1.2.** (a) Schematic representation of the distinct MTD domains and compositional features (modified from Bull et al., 2009). (b) Representation of MTD sub-classes according to their degree of internal cohesion. Deformation and disaggregation tends to increase downslope as travel distance increases (modified from Shanmugam, 2006).

At the termination of depositional domain is the MTD toe area (Fig. 1.2a). This is characterised by the presence of compressional structures resultant from arrest of the translating mass (Bull et al., 2009; Flint et al., 2011; Frey-Martínez et al., 2006; Hampton et al., 1996; Posamentier, 2004). Thus, internal deformation of the MTDs at this region is dominated by thrust and fold systems (Fig. 1.2a). These features induce the formation of arcuate pressure ridges on the top surface of the MTD that develop perpendicularly to the direction of flow. The frontal termination of the remobilised masses can be classified as 'frontally confined' or 'frontally emergent' (Frey-Martínez et al., 2006) (Fig. 1.2a). Frontally confined MTDs have their remobilised masses underlain by the basal glide surface, and their toe is characterised by buttressing of the remobilised strata against an abrupt frontal ramp (Frey-Martínez et al., 2006). In contrast, frontally emergent MTDs flow beyond the limits of their original glide surface by overriding their frontal limit, flowing freely over the substrate and possibly with increasing disaggregation (Frey-Martínez et al., 2006).

The internal geometry of MTDs is not uniform and it reflects the main process, or processes, that occurred during the deposition of the mass failure. Thus, subdivisions of MTD classification into slides, slumps and debris flows are common based on their increasing degree of internal deformation, which is also associated with the remobilisation distance (Coleman and Prior, 1988; Masson et al., 2006; Mulder and Cochonat, 1996; Posamentier and Martinsen, 2011; Slatt, 2006) (Fig. 1.2b). Slides consist in remobilised strata with low or no internal deformation that flow by translational movement of coherent masses. The original bedding can be slightly deformed or faulted at the headwall area, but it is predominantly intact on the middle regions which can make the recognition of such deposits problematic. The toe region is characterised by the typical compressional

structures. Slumps imply higher degrees of deformation and larger travel distances than slides, but this is still not significant enough to obliterate evidences of internal stratification. In general, slump deformation is marked by upslope extension, evidencing extension or listric faults, and by contraction at the toe area with formation of the characteristic folds and thrusts (Bull et al., 2009; Masson et al., 2006; Posamentier and Walker, 2006). Debris flows consist on cohesive to non-cohesive laminar flows that transport clasts and rock fragments within a fine-grained matrix (Coleman and Prior, 1988; Hampton et al., 1996; Posamentier and Walker, 2006). Internal cohesion and stratification is majorly absent within debris flows and these can flow for long distances, even in low angle slopes. These different classifications imply increasing movement of grains composing the MTDs, and consequently the internal deformation. This also implies that the different internal geometries are part of a continuous process where early stages are characterized by sliding tabular blocks that follow into slumps and debris flows as the mass movement accelerates, ultimately evolving into classical turbidity currents (Gee et al., 2005; Posamentier and Martinsen, 2011; Shanmugam, 2006) (Fig. 1.2b).

MTDs can include massive undeformed blocks that preserve the original structure and with sizes ranging from cobbles to outcrop scale features ((Alves and Cartwright, 2009; Alves and Lourenço, 2010; Callot et al., 2008; Dunlap et al., 2010; Minisini et al., 2007; Moscardelli et al., 2006; Posamentier and Walker, 2006; Spence and Tucker, 1997) (Fig. 1.2a). Such blocks are essential constituents of slides, although they are also common in slumps and debris flows. Blocks can be divided into two main groups, remnant and rafted. Remnant blocks are in situ and haven't been remobilised by the mass flow (Fig. 1.2a). They show vertical stratigraphic continuity with strata underlying the MTD and often show sharp

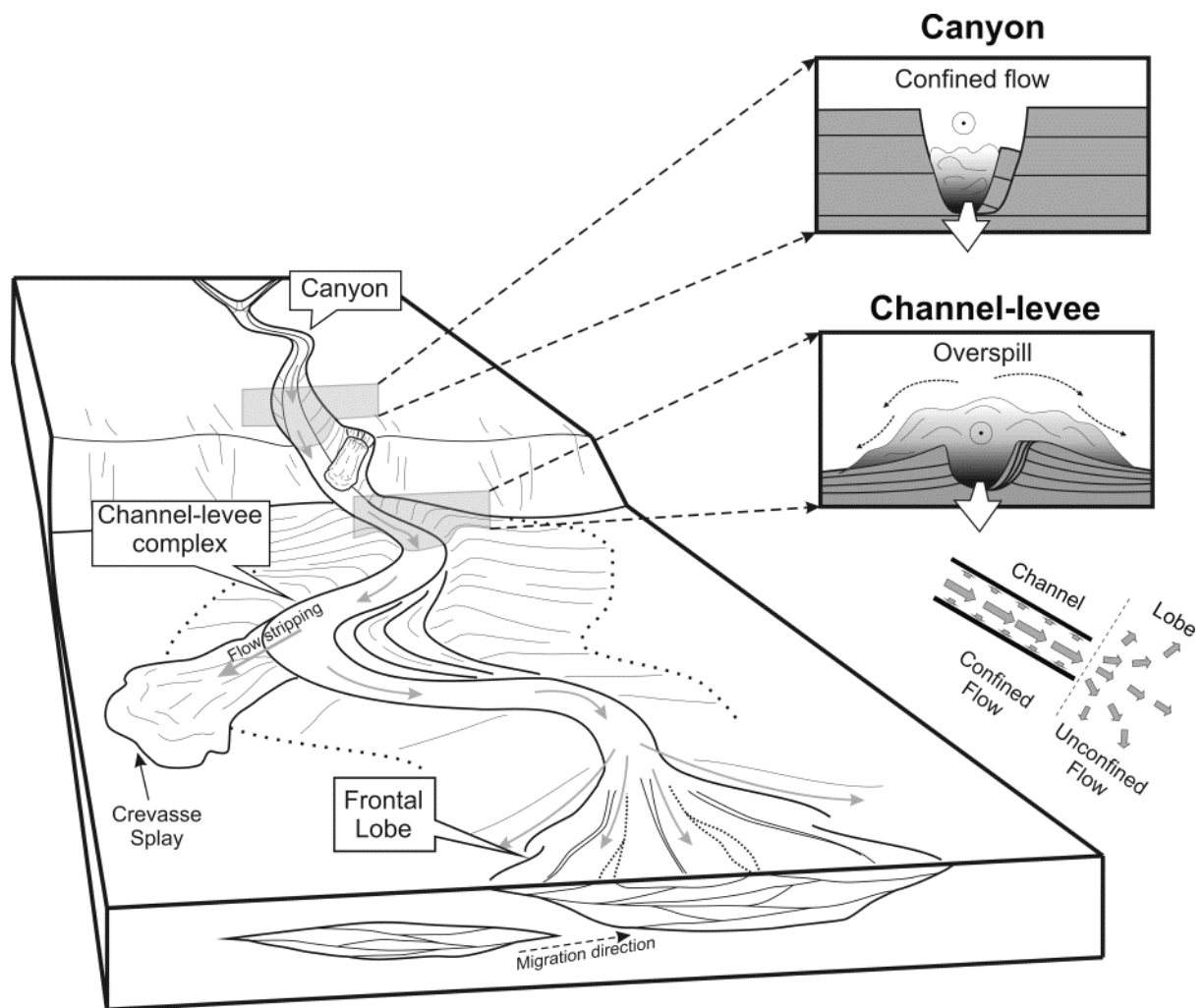
edges, although erosional smoothing of these features can occur. Contrastingly, rafted blocks have been remobilised from their original location by the mass flows (Alves and Cartwright, 2009; Gamboa et al., 2011a; Moscardelli and Wood, 2008). They can be dragged within the lower levels of the MTD, particularly larger ones, or floating and pushed towards the top of the flow (Fig. 1.2a). Although the presence of blocks is majorly restricted to the main body of the MTD, out-runner blocks that glide beyond their toe can occur (Bull et al., 2009; Nissen et al., 1999). As a general rule, block size tends to decrease downslope. Thus, larger blocks with low remobilisation are expected near the headwall areas. As the remobilisation distance increases, blocks are expected to get gradually smaller and more disaggregated (Homza, 2004; Laberg and Vorren, 2000). The regions with higher block density are also variable. Headwall areas could be expected to have higher block density, especially if remnant strata are present. Nevertheless the highest occurrence of blocks can take place in the proximal transitional zone (Lastras et al., 2002), or even towards the toe region where blocks would be expected to be smaller and/or less represented (Naruse and Otsubo, 2011).

### **1.2.2. Submarine Canyons and Channels**

Submarine canyons and channels are important components of deepwater continental margins. They form the main conduits for sediment transport from proximal areas into distal regions of continental slopes and ocean basins by means of turbidite flows (Deptuck et al., 2007b; Flint and Hodgson, 2005; Mutti and Normark, 1991; Normark et al., 1993; Piper, 1970; Piper and Normark, 2009; Shepard, 1981). These consist of episodic downslope density currents characterized by turbulent sediment suspension within the flow (Bouma, 2004; Normark et al., 1993; Piper and Normark, 2009; Posamentier and Walker,

2006; Stow et al., 1996). Their characteristics are controlled by slope steepness, type and concentration of sediment supplied, basin physiography and flow confinement (Bouma, 2004; Posamentier and Walker, 2006; Smith, 2004b). Slope steepness influences the velocity of turbidity currents flowing inside the canyons or channels. Thus, steeper slopes are prone to generate higher velocity flows which tend to wane as the gradient decreases. Theoretically, turbidity flows tend to erode or bypass the steeper proximal sections until a point along the channel is reached where lower gradients allow sediment deposition and aggradation (Kneller, 2003; Pirmez et al., 2000; Pirmez and Imran, 2003). In practice this has limited validity as distinct flows have distinct properties, namely velocity and density. Thus, sediment erosion and deposition can occur on identical channel locations at different times. This is further influenced by factors as large or small scale channel rugosity, height of available relief or slope breaks. Complex physiography also implies more obstacles that can force flow diversions or velocity changes, as well as providing places that promote sediment deposition (Kolla, 2007; Reading and Richards, 1994; Richards et al., 1998; Smith, 2004a).

These submarine systems typically extend for hundreds of kilometres and are characterised by predictable architecture changes along slope. These are, ordered from proximal to distal locations, **canyons**, **leveed channels complexes** and **frontal lobe complexes** (Deptuck et al., 2003; Normark, 1978; Normark and Piper, 1969; Posamentier and Walker, 2006; Posamentier and Kolla, 2003) (Fig. 1.3). **Canyons** are considered to be major erosive features of marine slopes and can be very complex systems, reaching over 10 km wide and 1 km deep (Cronin et al., 2005; Normark et al., 1993; Posamentier and Walker, 2006; Shepard, 1965). The origin of submarine canyons is often linked to the occurrence of large slumps or landslides. These create depressions on the slope that trap recurrent



**Figure 1.3.** Diagram representing submarine slope canyon and channel systems, with frontal lobes present on the distal basin regions. Canyons have high thalwegs that fully confine the turbiditic flows. Leveed channels are characterised by lower thalwegs, which allows flow stripping and overspill of finer sediment on the overbanks. Crevasse splays can be created at channel bends when turbidite flows breach through the levee. Frontal lobes are characterised by decreases of flow energy and confinement, favouring sediment deposition.

erosive currents, leading to the development of deep incisions (Cronin et al., 2005; Gee et al., 2007; Shepard and Dill, 1966; Slatt, 2006) (Fig. 1.3). Their development is also linked to eustatic cycles, with pronounced erosion and sediment bypass during sea-level lowstands followed by progressive canyon fill and decrease of activity during transgressions (Campbell and Mosher, 2010; Cronin et al., 2005; Slatt, 2006). The canyon morphology is generally straight, with steep V-shaped upper sections that tend to acquire a U-shape downslope as they widen (Cronin et al., 2005). The margins of the upper and medial canyon sections are often characterised by multiple scarps due to rotational slumping of the sidewall, creating variable-sized terraces along its path (Babonneau et al., 2004; Babonneau et al., 2002; Sawyer et al., 2007) (Fig. 1.3). Sediment supply to canyons can be made by direct connection to large fluvial systems or supplied by alongshore shelf drift processes (Posamentier and Walker, 2006; Stow et al., 1996). Downslope remobilization of sediment accumulated at the canyon head region downslope can be triggered by intermittent events (as earthquakes or storms), slope instability (rapid sedimentation, oversteepening or changes in pore pressure) or be more continuous in time as in canyon systems fed by large rivers (Arzola et al., 2008; Normark et al., 1993; Slatt, 2006). The high relief of the canyon walls tends to fully confine turbidity flows (Fig. 1.3). These seldom overtop the higher canyon margins, but the confinement effectiveness tends to decrease downslope towards the transition to channel-levee systems (Babonneau et al., 2004; Cronin et al., 2005; Posamentier, 2003; Skene et al., 2002).

**Leveed channels** are genetically linked with canyon channels (Deptuck et al., 2003; Posamentier and Walker, 2006) (Fig. 1.3). They can be constructional if aggradation occurs, erosional if formed by channel erosion, or mixed (Stow and Mayall, 2000). Channels can



develop in a fixed position over a period of time, or can grow by lateral and down-slope migration (Deptuck et al., 2007b; Kolla, 2007; Mayall et al., 2006; Posamentier and Kolla, 2003; Sylvester et al., 2011). The associated levees are generally asymmetric concave-up, gull shaped deposits that flank the channels and have an important role on the confinement of the turbidity flow (Deptuck et al., 2007a; Kane et al., 2007; Mayall et al., 2006; Posamentier, 2003) (Fig. 1.3). Sediments on the axis of the channels are predominantly coarse grained, whereas the levees are characterized by deposition of mud, silt and fine sands (Beaubouef, 2004; Kane et al., 2007; Mayall et al., 2006; Slatt, 2006; Weimer et al., 2000). The further the levees get from the channel axis they decrease in thickness and only the finer sediments are deposited until they fade into the sea-floor (Beaubouef, 2004; Deptuck et al., 2003; Normark et al., 1993). Levee areas close to the channel axis are thicker and with the coarser fraction of the fine sediments. In wider channels (and canyons) the development of inner levees can form terraces between the outer levee and channel axis where sediment can settle (Babonneau et al., 2004; Deptuck et al., 2003; Posamentier and Kolla, 2003). Leveed channels range from straight to moderately or highly sinuous paths, in many aspects similar to the ones seen in alluvial channels (Kolla, 2007). The sinuosity of the channel reflect the slope steepness: steeper areas will have straighter or low sinuosity channels whereas low gradients will develop high sinuosity channels. Sinuous channels are generally associated with lateral (sweep) and downslope (swipe) migration, which can result in complex channel evolution patterns (Deptuck et al., 2003; Kolla, 2007; Mayall et al., 2006). The highest sinuosity channels are commonly associated with major river sources (Abreu et al., 2003; Kolla et al., 2001; Normark et al., 1993; Posamentier and Kolla, 2003). The channel shape is also strongly conditioned by the basin physiography as channels will tend to adapt to the existing relief. Tectonically induced relief as, for example, mud/salt

diapirs, salt walls or fault scarps can force channels to acquire a straighter flow path, or divert them through complex routes downslope (Clark and Cartwright, 2011; Gee and Gawthorpe, 2006; Mayall et al., 2010; Prather, 2003; Smith, 2004a). Sediment deposition and growth of the levees is favoured by flow stripping and overspill resultant from the decrease in channel thalweg and flow confinement (Fig. 1.3). The sudden decrease in energy promotes the deposition of thin, fine grained turbidites over the levee flank (Bouma, 2004; Mayall et al., 2006; Peakall et al., 2007; Slatt, 2006). Due to the sinuous paths that channels acquire, outer bends tend to have thicker crests relatively to inner bends. The formation of sediment waves on levee flanks is related to flow stripping of turbidity currents, and its interaction with bottom currents (Posamentier and Walker, 2006). Crevasse splays also constitute an important type of overbank deposit (Fig. 1.3). These result from levee breaching by the denser fractions of the turbidity currents, preferentially occurring at channel bends. This leads to the deposition of coarse grained sediment within the silt- and mud-dominated middle and distal levee (Posamentier and Walker, 2006; Slatt, 2006).

**Frontal lobe complexes** can form either at the terminus of leveed channels complexes when the turbidity flow is partially or totally unconfined (Fig. 1.3), or at locations with significant breaks in slope (Normark, 1970; Posamentier, 2003; Wynn et al., 2002). Lobes have a tabular shape and are predominantly formed by sandstone, thus being also referred to as sandstone sheets (Lee and Watkins, 1996; Normark, 1970; Slatt and Weimer, 2001). They are characterized by distributary channels although braided patterns may also occur (Fig. 1.3). Channels are usually shallow with low relief sandy levees (Normark et al. 1993; Posamentier and Kolla 2003). The transition point from a leveed channel to a frontal lobe is controlled by the turbidity flow characteristics (sand:mud ratio, volume, height and

velocity)(Posamentier and Walker, 2006). Lobes are formed when decreasing confinement induced by the reduction in channel width, depth, sinuosity and levee height allows a lateral dispersal of flow vectors (Fig. 1.3), with consequent velocity decrease and sediment deposition in distributary channels (Posamentier and Kolla 2003; Posamentier and Walker 2006). Lobes can also exist in intra-slope mini-basins associated with salt-withdrawal or other type of sea floor depression-forming phenomenon (Beaubouef and Friedmann, 2000; Posamentier, 2003; Smith, 2004a).

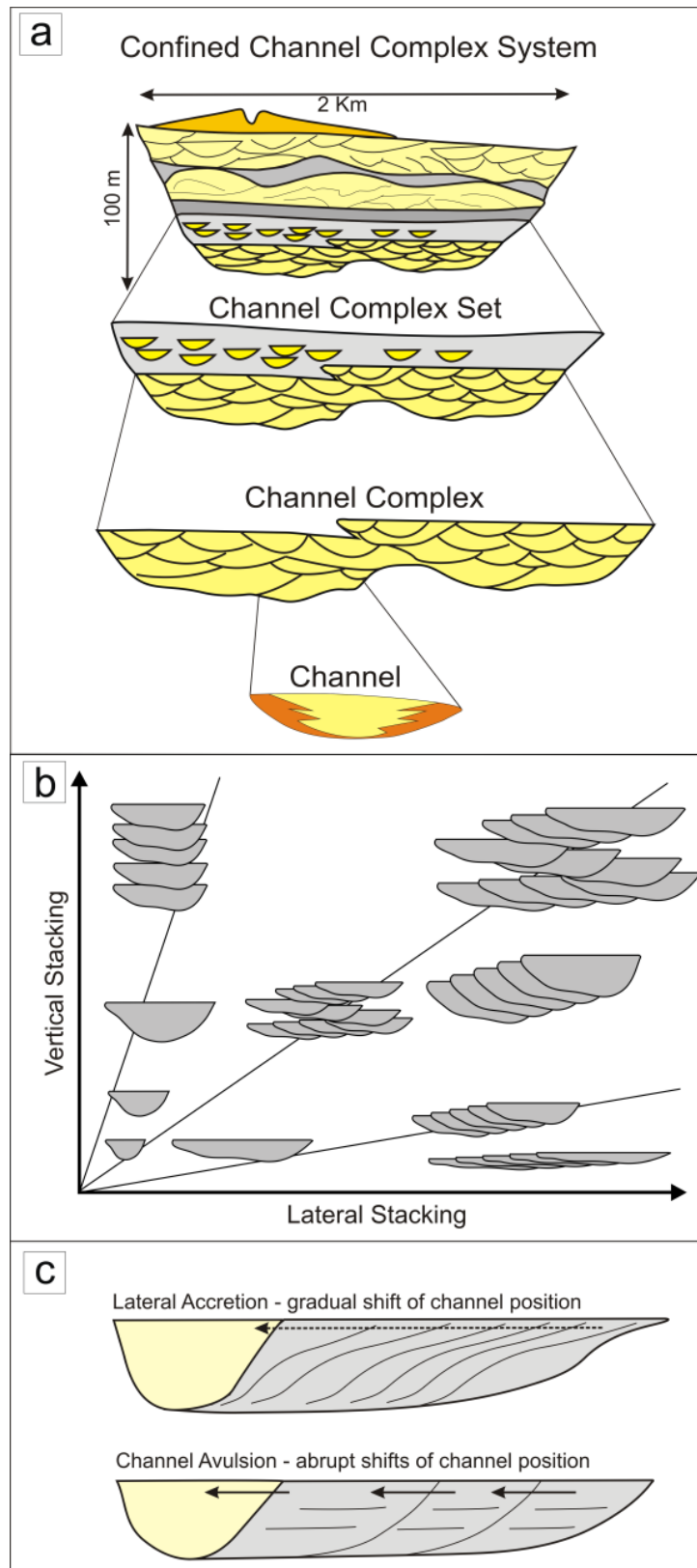
#### **1.2.2.1. Evolution of submarine channel systems**

The evolution of a submarine slope channel can be assessed by its fill history resultant from the recurrent erosion and/or deposition induced by turbidity flows. Thus, channel fill can be defined as “the product of a cycle of channel cutting, filling, and avulsion or abandonment” (Abreu et al., 2003). The type of sedimentary facies deposited in the channel (or canyon) is highly variable, reflecting the periods in which the deepwater turbidite system is active or inactive (Mayall et al., 2006; Normark et al., 1993; Pirmez et al., 2000; Slatt, 2006). Thus, active systems are characterised by deposition of coarse-grained sediment, in contrast with low activity channels where mud and silt should prevail. In general, channel-fill deposits follow an upward fining sequence composed by four main sedimentary facies, namely basal lags, slumps and debris flows, stacked sand-rich channels and channel levees (Beaubouef, 2004; Deptuck et al., 2003; Flint et al., 2011; Mayall et al., 2006; McHargue et al., 2011). Coarse-grained basal lags are commonly composed by conglomerates and sand, although mudclast conglomerates or shale drapes can also be present at the base of the channels. These deposits represent remnants of the channel erosive phase and bypass of turbidity currents (Mayall et al., 2006). The stacked channels

facies comprises the stacking and amalgamation of sedimentary beds. These are dominated by massive sands on the axial regions, with finer granulometries deposited towards the channel margins (Beaubouef, 2004; Mayall et al., 2006; McHargue et al., 2011). Collapse structures like slumps or slides are also common in channel-fill sequences, being more common in the erosional stages (Godo, 2006; Mayall et al., 2006; Meckel III et al., 2011; Posamentier and Kolla, 2003; Sawyer et al., 2007). These can be composed by different lithologies, ranging from mud, or muddy sand to clean sands. The slumps and debris flows fill deposits can represent sections of channel wall collapse or derive from long distance transport from further upslope (Mayall et al., 2006). Nevertheless, intra-channel failures can also occur, leading to deposition of sand-rich slumps and debris-flows resultant from reworking of previous turbidite deposits (Meckel III et al., 2011). On the later stages of channel fill, fine-grained sediments associated to lower density turbidity currents are predominant. This can lead to the development of highly sinuous leveed channel with complex internal architecture, which often spread beyond the original confinement of the erosional channels (Deptuck et al., 2007b; Mayall et al., 2006)(Mayall et al. 2006). As the channel is progressively abandoned, there is an upward increase of mudstone inter-beds (McHargue et al., 2011).

Submarine channels systems are characterized by repeated cycles of waxing and waning flows, being more frequent in long-lived channels. In essence, waxing flows are associated with erosive cycles whereas waning flows correspond to period of aggradation and channel fill, with the separation between both cycles being typically marked by channel avulsion (McHargue et al., 2011; Sprague et al., 2005). Submarine channel systems are organised by hierarchies where large complexes are filled by various smaller order channels

(Mayall et al., 2006; Slatt, 2006; Sprague et al., 2005) (Fig. 1.4a). The smallest level is represented by single channel elements, which organise into channel complexes made by several elements. In turn, channel complexes can create larger channel complex sets (Fig.1.4a). The organisation of these hierarchic orders is based on the relations of geometry of channel fill strata, the vertical and lateral stacking of channels, and the distribution of their bounding surfaces (Abreu et al., 2003; Mayall et al., 2006; Sprague et al., 2005; Sylvester et al., 2011). Vertical stacking is frequent in confined channels, with these focusing the cut and fill phases on a relatively fixed position (Clark and Pickering, 1996) (Fig. 1.4b). Lateral stacking is more common in sinuous, less confined channels (Abreu et al., 2003; Dykstra and Kneller, 2009). This channel arrangement can derive from gradual or abrupt channel shifts (Fig. 1.4c). Gradual shifts, also related to lateral accretion of channels, commonly take place on sinuous channels during meander migration (Fig. 1.4c). The syn-migration deposits tend to form sub-parallel arrangements better known as Lateral Accretion Packages (LAPs) (Abreu et al., 2003). In contrast, abrupt shifts created by channel avulsion tend to show abrupt contacts between adjacent channel elements marked by an erosive surface (Fig. 1.4c). Vertical or lateral stacking may predominate on a system, although both patterns commonly occur together and are expected to change along the channel (Deptuck et al., 2007b; Mayall and Stewart, 2000; Sylvester et al., 2011) (Fig. 1.4b).



**Figure 1.4.** (a) Hierarchical arrangement of channel complexes, from the single elements to complex systems (modified from Slatt, 2006). (b) Channel arrangement resultant from the interplay of lateral and vertical amalgamation (from Clark and Pickering, 2006). (c) Comparison of channel architecture resultant from gradual lateral migration (accretion) and rapid shifts in channel course (avulsion) (from Abreu et al., 2003).

### 1.3. Halokinesis on passive continental margins

Passive continental margins are generally characterized by low tectonic activity, which can be predominantly represented by gravity-driven thin-skinned tectonics. These processes lead to a wide range of deformation structures overlying a deep décollement interval composed by ductile lithologies like evaporites and mudstones (Brun and Fort, 2011). The most dramatic structural deformation is associated with evaporite deformation processes which are commonly termed salt tectonics. The principle of salt tectonics lies on the flow and rise of an originally flat evaporitic unit that deforms into variably complex structures (Demercian et al., 1993; Hudec and Jackson, 2007; Jackson et al., 1994). The main driver of salt movement is differential loading derived from gravitational, displacement or thermal effects, which have distinct preponderance depending of the depth of burial and geometry of the salt body, geological setting or thermal conditions (Hudec and Jackson, 2007). In general, salt moves laterally from higher loading salt withdrawal areas to areas of lower loading, with the major restriction being derived from frictional forces at the base of the salt bodies and the strength of the overburden (Hudec and Jackson, 2007; Seni and Jackson, 1983a). The initiation of salt movement is favoured during regional extensional events, in which decoupling and weakening or complete removal of the overburden occurs (Hudec and Jackson, 2006; Jackson and Vendeville, 1994; Vendeville, 2005; Vendeville and Jackson, 1992b).

The overburden deformation resultant from halokinesis creates folds and faults with distinct geometries (Demercian et al., 1993; Fort et al., 2004; Rowan et al., 2003; Seni and Jackson, 1983a; Seni and Jackson, 1983b; Stewart, 2006; Trudgill, 2011; Trudgill et al., 1999;

Vendeville, 2005; Vendeville and Jackson, 1992a; Vendeville and Jackson, 1992b) (Fig. 1.5a). Folding of the overburden is expressed by rim synclines on the salt-withdrawal areas and doming on the crest of the structures (Rowan et al., 2003; Stewart, 2006) (Fig. 1.5a). Drag folds are also common on the flanks of salt structures and can variably affect the thickness of flanking strata, with its most significant expression being given by significant bed thinning and overturning (Alsop et al., 2000; Giles and Lawton, 2002; Rowan et al., 2003; Schultz-Ela, 2003). Faults developed on the vicinities of salt have various geometries (Alsop, 1996; Rowan et al., 1999; Stewart, 2006). Radial faults develop perpendicularly to diapirs (Fig. 1.5b). Faults parallel to the structure are commonly formed during the extensional phase (Hudec and Jackson, 2007; Vendeville, 2005; Vendeville and Jackson, 1992b). In the case of diapirs, parallel faults can have concentric patterns surrounding the structure (Fig 1.5a and 1.5b). Crestal faults often have complex arrangements and can exhibit normal or inverse behaviour (Dooley et al., 2009). Fractured overburdens develop crestal grabens that gradually increase in size during salt flow (Demercian et al., 1993; Gaullier and Vendeville, 2005). Consequently, segmented overburden sections often develop into rafts that glide on top of the salt units as separated compartments spreading further apart (Fig. 1.5c)

On passive continental margins, different salt architectures are observed along the slope (Fig. 1.6). At the upper slope regions extensional processes prevail, leading to the development of salt rollers attached to large listric faults (Fig. 1.6). At mid-slope domains a transitional area is present, characterised by growth of salt diapirs and salt walls. Towards the distal domains of the slope, a compressive domain is present, forcing the growth of salt structures (Fig. 1.6). Structures like salt-cored anticlines, salt ridges, thrusts and canopies resultant from salt deformation are common at the distal slope locations, and their



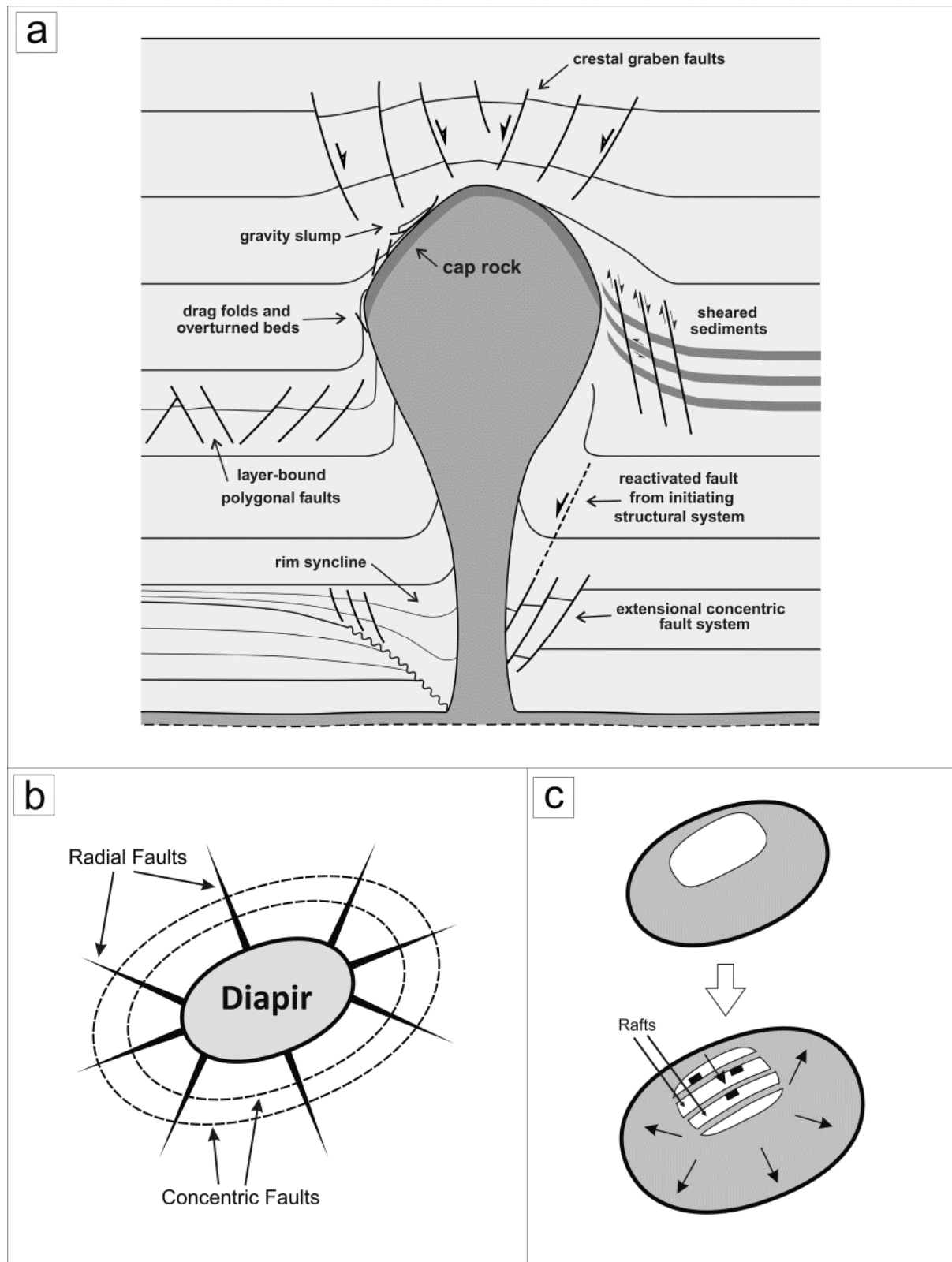
development is often associated with intense deformation of the sea-floor (Brun and Fort, 2004; Duval et al., 1992; Fiduk et al., 2004; Fort et al., 2004; Jackson et al., 1994; Leyden et al., 1976; McBride et al., 1998; Mohriak, 1995).

Halokinesis has an important influence on the stratigraphic architecture of the basin resultant from continuous salt-sediment interactions (Beaubouef and Friedmann, 2000; Clark and Cartwright, 2011; McBride et al., 1998; Prather, 2003; Prather et al., 1998; Rowan and Weimer, 1998; Smith, 2004a). Salt withdrawal and rise of structures control the accommodation space on the slope, and consequently the location of sedimentary depocentres. These have various shapes, depending of the complexity of deformation, ranging from enclosed mini-basins to elongated basins interconnected by tortuous pathways (Gee and Gawthorpe, 2006; Prather, 2003; Smith, 2004a). Salt-generated topography creates conduits that confine turbiditic flows and consequently influence the distribution and amalgamation of clastic sediment in deepwater settings. In addition, diachronic salt growth and changes of accommodation in the basin forces the sedimentary systems to adapt to the new topographic conditions. This is often expressed by deviation of channel paths, shift of depocentres and/or slope failure (Clark and Cartwright, 2011; Hudec and Jackson, 2006; Mayall et al., 2010; Tripsanas et al., 2004).

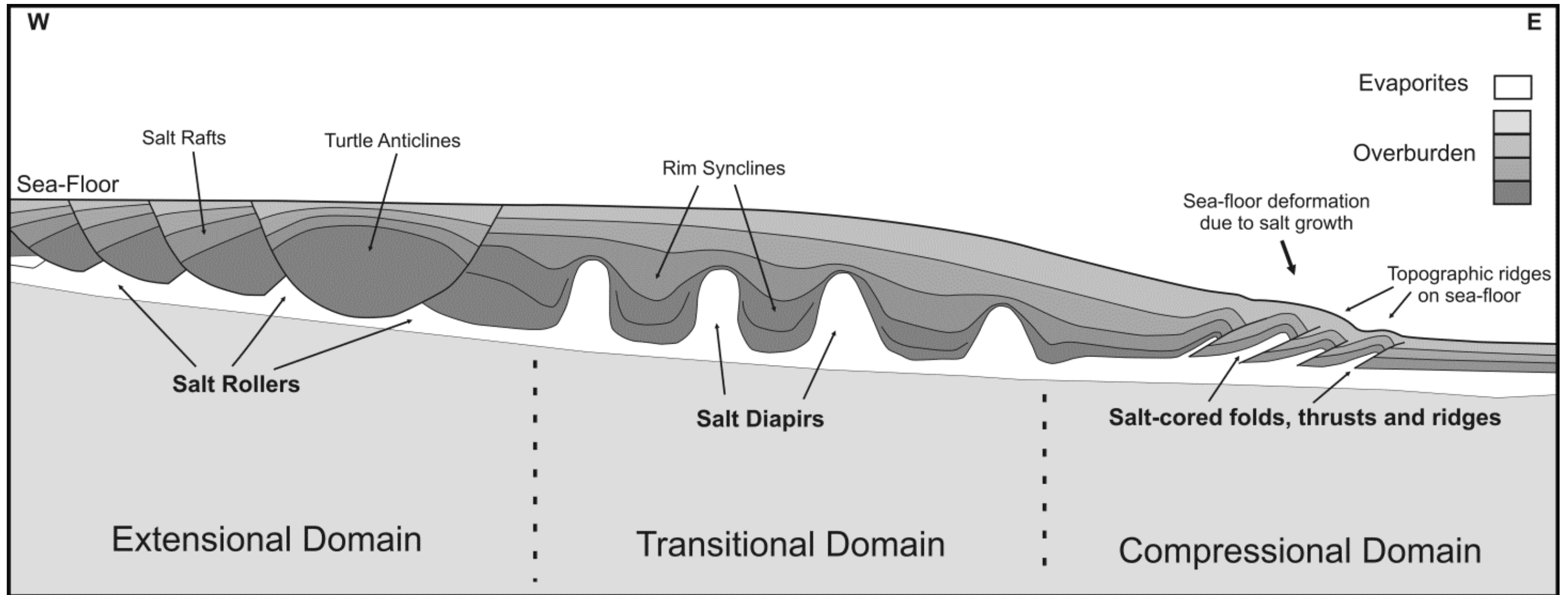
## **1.4. Reservoirs and reservoir compartmentalisation**

### **1.4.1. Hydrocarbon Reservoirs**

Hydrocarbon reservoirs are rocks with good capacity for oil and gas to accumulate, thus constituting the principal targets in exploration (Biddle and Wielchowsky, 1994). The



**Figure 1.5.** (a) Vertical sections showing the patterns of faulting and folding associated with growing salt structures. (b) Plan view of radial and concentric faults developing around salt diapirs. (c) Gravity spreading of fragmented overburden sections (rafts) on top of salt units (modified from Stewart, 2006).



**Figure 1.6.** Section representative of the main halokinetic structures along passive margins. The proximal margin is characterised by thick overburdens and a salt extensional domain, favouring the development of salt rollers attached to large listric faults. This is followed by a transitional domain at mid-slope regions characterised by the development of vertical diapirs. Compressional domains on the distal slope are characterised by salt-generated fold-and-thrust belts that actively deform the sea-floor, creating significant topographic relief which exert important controls on sediment distribution at such regions.

properties of a reservoir are broadly defined by its depositional environment, structure and diagenesis (Ainsworth, 2010; Jahn et al., 2003). The depositional environment is a primary control on reservoir lithology, being defined as an area with specific properties that define a specific type of rock. The characteristics of the latter depend of the intensity and duration of the depositional processes. Consequently, different processes within the depositional environment imply differences in reservoir units (Ainsworth, 2005; Jahn et al., 2003; Mayall et al., 2006; Slatt and Weimer, 2001). The depositional processes influence rock porosity and permeability, and these are the main factors to consider when evaluating the reservoir potential of a stratigraphic interval (Ainsworth, 2005; Allen and Allen, 2005; Clark et al., 1996; Jahn et al., 2003). Porosity controls the fluid storage capacity and permeability controls the flow properties of the rock (Slatt, 2006). The primary porosity and permeability of siliciclastic rocks are also dependent of the composition and textural properties (grain size, sorting, roundness and sphericity) (Allen and Allen, 2005; Selley, 1998; Slatt, 2006). The non-uniform deposition and later alterations of reservoir forming rocks, associated with internal structural deformation, lead to variable degrees of reservoir heterogeneity (Ainsworth, 2010; Slatt, 2006). The classification of heterogeneity is based on the scale, origin and influence on the flow. First order or megascopic heterogeneities are fieldwide and considered on a kilometric scale. Second order or macroscopic heterogeneities occur in an inter-well scale on a field. Third order or mesoscopic heterogeneities are observed on well-scale and recognized by the analyzing cores and logs. Analysis at this scale aims to distinguish rock types and stratification styles. Fourth order or microscopic heterogeneities focus on the type of grains and their contact and inter grain properties like the porosity, pore size and shape, and fabric ((Allen and Allen, 2005; Slatt, 2006). For the purpose of this

thesis, the analysis of reservoir-prone strata is mainly based on first and second order, metric to kilometric scales.

Buried reservoir-prone lithologies tend to suffer compaction and diagenetic alterations that will change the original depositional textures, thus affecting the porosity and permeability of the lithified rock (Chilingar et al., 2005; Jahn et al., 2003; Slatt, 2006). The diagenetic alterations may improve or decrease the rocks quality as a reservoir, depending on the alteration of the original components as well as on the later cements or clays that may precipitate in the pore space (Allen and Allen, 2005; Jahn et al., 2003; Slatt, 2006).

#### **1.4.2 – Reservoir Compartmentalization**

Reservoir compartmentalization has revealed to be the rule instead of the exception in basins all over the world (Rahimpour-Bonab, 2007; Slatt, 2006). The sedimentary basins are typically divided into a network of **compartments** isolated by sealing rocks (Bradley and Powley, 1994; Jolley et al., 2010; Larue and Hovadik, 2006; Snedden et al., 2007). The recognition of compartmentalisation in sedimentary basins has been largely based on the detection of isolated pressure compartments identified on well data that where either on over- or under-pressured states in relation to their surrounding lithologies (Bradley and Powley, 1994; Lee and Deming, 2002; Ortoleva, 1994). The geochemical characterization of reservoir fluids (oil, gas or water) also proves useful on the recognition (or absence) of reservoir complexity, as different compartments can be characterized by different geochemical signatures (Bhullar et al., 1998; Chuparova et al., 2010; Permanyer et al., 2007; Rahimpour-Bonab, 2007). In more recent years, the widespread use of 3D and 4D

seismic have provided further insights on the nature and dynamics of compartmentalisation, in particular of the larger scale extent of basin compartments (Chapin et al., 2002; Hardage et al., 1998a; Hardage et al., 1998b; Milkov et al., 2007; Scott et al., 2010; Slatt et al., 2009; Slatt and Weimer, 2001; Wonham et al., 2010).

The principle of compartmentalisation is similar to the one of trap and implies the presence of subsurface uncertainties that result of structural and/or stratigraphic complexity and diagenesis (Ainsworth, 2010; Snedden et al., 2007). These relate to the presence of barriers or baffles for fluid flow between different compartments that compromise the connectivity within the reservoir units (Larue and Hovadik, 2006; Ortoleva, 1994; Rahimpour-Bonab, 2007; Slatt and Weimer, 2001; Sweet and Sumpter, 2007). Compartments occur in a very large range of scales, from less than 2 Km<sup>2</sup> to tens of hundreds of squared kilometres (Al-Shaieb et al., 1994a; Bradley and Powley, 1994; Ortoleva, 1994). Each large compartment is composed by a variable number of progressively smaller architectural elements (Fig. 1.7a) that individually control the volume of hydrocarbons and production of the reservoir units (Ortoleva, 1994; Slatt, 2006). Three hierarchic orders of compartmentalisation have been defined for marginal marine reservoirs (Ainsworth, 2010), which are also valid for deepwater slope environments (Fig. 1.7a). The first order relates to large megascale (>100 Km) inter-parasequence connectivity, where the major flow units are separated by maximum flooding surfaces. The second order refers to macroscale (1-10 Km) inter-sand body connectivity, which is a product of the dominant processes at the time of sediment deposition. The third order relates to intra-sand body heterogeneities where existing shale and coal beds or shale plugs in channels constitute the major connectivity barriers (Fig. 1.7a). Higher orders can be established for heterogeneities

that compromise connectivity at microscales related to rock type and texture. Macroscale distribution of channels or lobes can influence the continuity or connectivity of good reservoir facies, while microscale properties and diagenetic changes cause the fill of intra-pore space and consequent loss of permeability (Chapin et al., 2002; Richards and Bowman, 1998; Richards et al., 1998; Slatt and Weimer, 1999; Slatt and Weimer, 2001).

Compartments have been classified as either static or dynamic (Jolley et al., 2010; Lee and Deming, 2002; Sweet and Sumpter, 2007) (Fig. 1.7b). **Static** compartments are completely sealed and do not allow fluid movement with adjacent strata over substantial periods of time in the order of thousands of years (Lee and Deming, 2002). **Dynamic** compartments are considered to have low permeability baffles that allow slow fluid mobility between adjacent compartments on a geological time scale, but have a significant impact on flow impedance on a production time scale. The dynamic of compartments is influenced by the geometry of their bounding surfaces. **Closed** compartments present permeability barriers or baffles on all four directions, but **open** compartments can occur if impermeable features only bound three directions (Snedden et al., 2007) (Fig. 1.7b). The spatial arrangement of isolated or poorly connected compartments in the reservoir units leads to **vertical** and **lateral** compartmentalisation (Fig. 1.7c and 1.7d). **Vertical** compartmentalisation occurs when a laterally continuous impermeable barrier is present between permeable units (Ainsworth, 2005; Ainsworth, 2010; Bradley and Powley, 1994; Clark et al., 1996; Larue and Hovadik, 2006; McKie et al., 2010; Slatt, 2006). **Lateral** compartmentalisation related to the areal separation of compartments and can result from various situations, from which channel position or the presence of faults are probably the most representative (Ainsworth, 2005; Ainsworth, 2006; Ainsworth, 2010; Clark et al., 1996;

Jolley et al., 2007b; Jolley et al., 2010; Knipe et al., 1998; Labourdette et al., 2006; Larue and Hovadik, 2006) (Fig. 1.7c). These two types of compartmentalisation seldom occur alone. One may be prevalent over the other during a certain period of time, although significant vertical and lateral compartmentalisation can also be contemporaneous in very dynamic systems. Consequently, the presence and degree of vertical and/or lateral compartmentalisation on a basin is likely to change between stratigraphic units of different age (Ainsworth, 2010; Clark et al., 1996).

There are 3 types of reservoir compartmentalization, namely **stratigraphic**, **structural** and **diagenetic**. It is common for one compartmentalisation type to predominate over the others, but even so the secondary ones can also have important impacts on the connectivity of the reservoir units (Slatt, 2006).

#### 1.4.2.1. Stratigraphic compartmentalization

The outline of deepwater reservoirs, and consequently their lateral and vertical heterogeneities, is conditioned by the processes and stratigraphic architecture of the depositional systems (Ainsworth, 2005; Labourdette, 2011; Lee and Watkins, 1996; Slatt and Weimer, 2001). These also constitute the basic building block with certain stratigraphic, lithologic or hydrodynamic properties upon which the remaining styles act upon (Ainsworth, 2010; Allan et al., 2006; Puckette and Al-Shaieb, 2003). Stratigraphic compartmentalisation is strongly controlled by the amalgamation of the permeable strata (Fig. 1.7d and 1.7e). This is primarily influenced by accommodation space in the basin and related external controls on sedimentation (Fig. 1.7d), from which sea-level changes are particularly important (Ainsworth, 2010; Chapin et al., 2002; Clark et al., 1996). High accommodation-



sedimentation ratios during sea-level rise are prone to decrease amalgamations and compartmentalise the reservoir by increasing the vertical separation of sand bodies (Ainsworth, 2010) (Fig. 1.7d). Contrastingly, lowering of the relative sea-level and lower accommodation-sedimentation ratios favour vertical stacking of sand bodies (Fig. 1.7d), but this also favours lateral compartmentalisation due to the presence of prograding or accreted shingled strata (Ainsworth, 2010; Larue and Hovadik, 2006) (Fig. 1.7e).

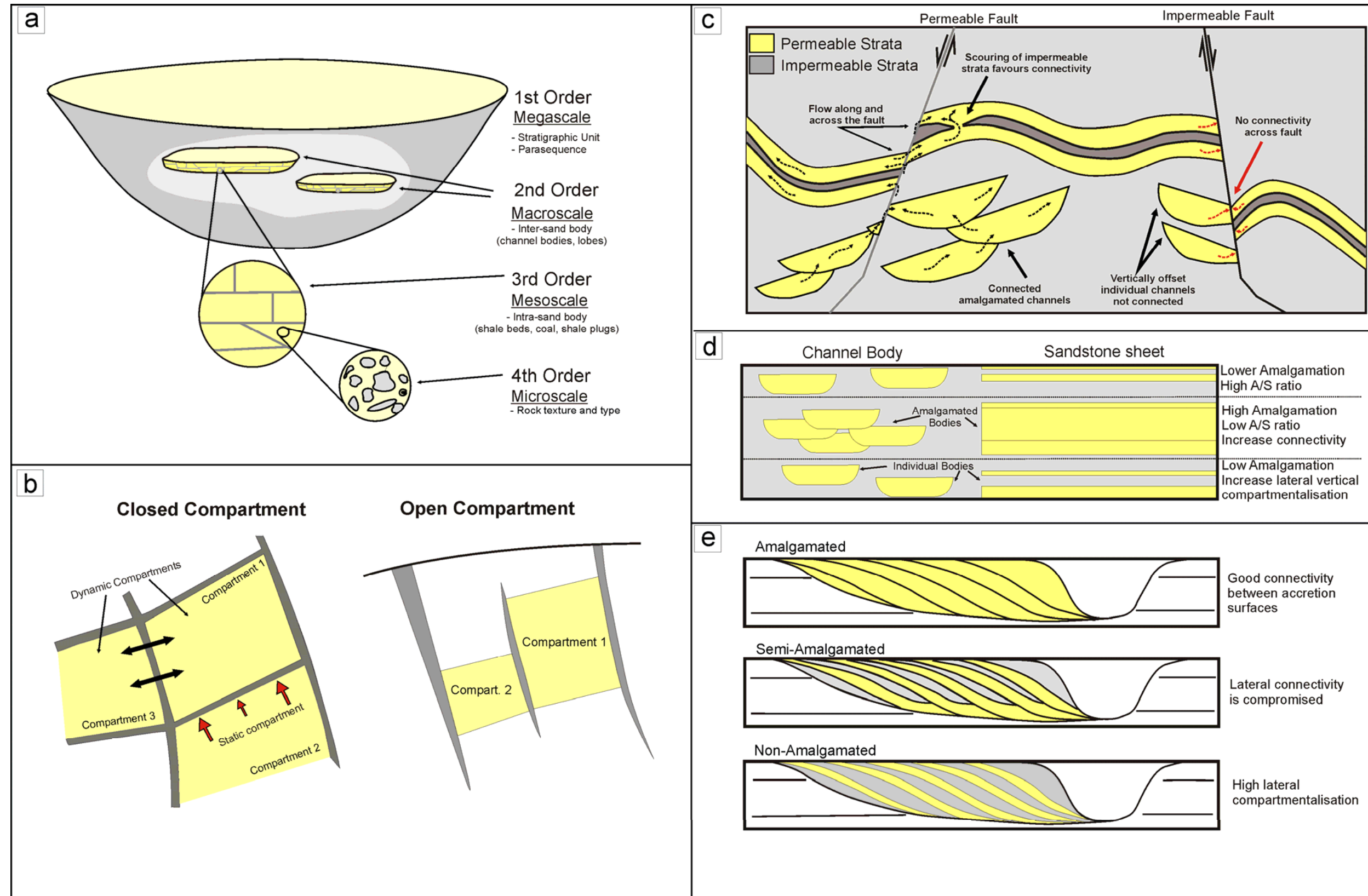
Laterally continuous sand sheets are prone to constitute good reservoirs, particularly if reworked during transgressions (Puckette and Al-Shaieb, 2003). These can be vertically compartmentalised due to the presence of impermeable shale drapes, particularly when accommodation space increases and the sedimentation rate is comparatively low (Ainsworth, 2010; Allen and Allen, 2005; Clark et al., 1996; Ramon and Fajardo, 2006; Slatt and Weimer, 2001) (Fig. 1.7d). In comparison, canyons and channels constitute smaller scale compartments with higher internal complexity (Slatt and Weimer, 2001). The evolution of the channel system dictates the degree of internal lateral and vertical compartmentalisation, which is closely related to the patterns of channel migration (Fig. 1.4b). Heterogeneities and zonation of sediment facies of channel-fill deposits is a primary control of compartmentalisation (Beaubouef, 2004; Labourdette, 2011; Larue and Hovadik, 2006; Mayall et al., 2006). In particular, the frequent occurrence of shale drapes or fine grained turbidites compromises the vertical connectivity between sand bodies, especially if the lateral extent of impermeable strata is equal or superior to the reservoir strata (Adeogba et al., 2005; Slatt, 2006). Nevertheless, the recurrence of erosive flows can scour the shale beds and enhance vertical connectivity between permeable strata (Labourdette et al., 2006). Sandstone bodies within channels often show limited extent or tortuous paths,

thus increasing internal lateral heterogeneity (Beaubouef, 2004; Puckette and Al-Shaieb, 2003; Slatt and Weimer, 2001). Furthermore, the occurrence of muddy slumps is also prone to increase both lateral and vertical heterogeneity within the channel fill deposits (Godo, 2006; Sawyer et al., 2007). At the scale of the channel complex, the vertical and lateral connectivity is a function of the repeated between cut-and-fill and amalgamation patterns of individual bodies (Clark et al., 1996; Mayall et al., 2006; McHargue et al., 2011; Slatt, 2006). Lateral compartmentalisation in channel complexes can result from fast (avulsion) or slower (lateral aggradation, or accretion) migration. The lateral migration of the channel can be reflected in alternations of permeable and impermeable lithologies in the LAPs. Depending of the extent of the impermeable lithologies, different degrees of lateral compartmentalisation can be present (Abreu et al., 2003) (Fig. 1.7e).

Unconfined depositional architectures like leveed channels can have reservoir-prone lithologies not only in their axis but also covering extensive areas on the overbank regions. The low channel height allows for fine sand and silt to be deposited over the levees, and coarse sand in crevasse splays can also be present in these regions (Beaubouef, 2004; Beaubouef and Friedmann, 2000; Posamentier et al., 2007). These coarser deposits are prone to form relative isolated compartments surrounded by low permeability muddy sediments. Consequently, vertical compartmentalisation is a major issue in these sequences, but uncertainty is very high as the overbank beds may have low lateral continuity or homogeneity (Beaubouef, 2004; Kane and Hodgson, 2011). Permeable overbank strata may be linked to the sandy constituents of channel-fill, but this commonly implies a complex connectivity issues at the channel margin due to slumping, scouring or faulting (Beaubouef and Friedmann, 2000; Kendrick, 1998; Slatt and Weimer, 2001). Channel overbank strata

can also have the better quality reservoir lithologies if mud-filled channels are present, particularly in the distal sections of the channel-levee systems and transition to the sediment. Besides the vertical compartmentalisation imposed by the presence of laterally continuous shale drapes in the distal slope, mud-plugged channels dissecting the lobe regions constitute important lateral barriers for flow that isolate the overbank compartments lobes (Adeogba et al., 2005; Chapin et al., 2002; Shanmugam, 2006).

MTDs play important and distinct roles on stratigraphic compartmentalisation. The occurrence of MTDs often implies the deposition of mud-rich lithologies that commonly constitute vertical permeability barriers between permeable flow units (Godo, 2006; Labourdette et al., 2006; Posamentier and Martinsen, 2011). The presence of low permeability MTDs also induces the total or partial lateral compartmentalisation of the permeable units, depending on the degree of vertical incision imposed by the erosive flow. Incision is variable, ranging from the smaller and numerous erosive scours to large slots of remobilised strata (Bull et al., 2009; Gee et al., 2005; Moscardelli et al., 2006). Nevertheless, the erosive power of MTDs can also be a key element on the decrease of margin compartmentalisation. The scouring resultant from their flow can erode any low permeability lithologies and expose buried permeable strata (Larue and Hovadik, 2006). This gains particular relevance if the scours are filled by posterior coarse-grained flows, thus allowing fluid communication between otherwise isolated permeable intervals. The irregular MTD topography is also an inducer of lateral compartmentalisation of immediately posterior turbiditic flows, resulting on an irregular distribution of disconnected sand bodies (Algar et al., 2011; Armitage et al., 2009; Cossey and Jacobs, 1992). In recent years MTDs have also started to be considered as potential reservoirs as many present fine to coarse grained



**Figure 1.7.** (a) Orders of compartment scales. (b) Representation of closed and open compartments, and the connectivity concept of dynamic and closed compartments. (c) Representation of elements influencing lateral and vertical compartmentalisation. Faults are important controls of lateral connectivity. (d) Sand-body amalgamation and connectivity as a function of accommodation/sedimentation ratios. (e) Amalgamation on accretion packages and impact on lateral connectivity. Non-amalgamated LAPs are fully compartmentalised.

components of clastic or carbonated nature with potential to accumulate fluids (Dykstra et al., 2011; Meckel III, 2011; Meckel III et al., 2011; Weimer and Shipp, 2004; Welbon et al., 2007). Nevertheless, their internal connectivity is uncertain and the risk of compartmentalisation in such deposits is very high.

#### **1.4.2.2. Structural compartmentalization**

Deformation of the stratigraphic successions that contain the reservoir by action of fold and faults will create different structures that will affect fluid flow and accumulation within them (Ainsworth, 2006). Fold-generated compartments are generally related to antiform structures created by tectonic effects, but these can also derive from depositional effects like slumping or compaction (Bacciotti et al., 2011; Biddle and Wielchowsky, 1994; Clark et al., 1996). Fluid accumulation in folded compartments is often associated with the compositional and dynamic conditions of the deformed reservoir strata. The presence of impermeable beds can lead to the formation of various fluid contacts at the fold crest region (Clark et al., 1996).

More relevant is the multi-scale impact of faulting on the compartmentalisation of reservoir units (Jolley et al., 2007a; Jolley et al., 2010; Knipe et al., 1998). Thus, it is important to know the structural complexity and fault geometry that affect a reservoir in order to determine the hydrocarbon accumulation areas as well as the presence of static or dynamic flow connectivity between each compartment (Knipe et al., 1998). Faults form either by compressive or extensional stresses and they can act as pathways or seals to fluid flow within a rock (Allen and Allen, 2005; Caine et al., 1996). If faults are not sealed, they may constitute conduits for fluid flow and increase connectivity within compartments in reservoir units (Fig. 1.7c). On the opposite situation, sealing faults act as barriers or baffles that compromise fluid flow between adjacent compartments (Fig.

1.7c). Fault displacement is important to consider on connectivity analysis, as displaced sandstones can either juxtapose other permeable intervals, favouring connectivity, or come in contact with impermeable shales and form efficient lateral flow barriers (Allen and Allen, 2005; Jolley et al., 2007a; Knipe, 1997). Fault permeability is dependant of the deformation along its core, where higher displacement takes places, and on its surrounding damage zone (Knipe et al., 1998; Zhang et al., 2010). Increasing displacement at the fault core is prone to create proportionally finer smears within the fault gouge, thus impacting on fault permeability (Allen and Allen, 2005; James, 1997; Ligtenberg, 2005). Shale smears constitute major permeability barriers, whereas sand smears can induce increased permeability across faults (Hooper, 1991). Nevertheless, the fault gouge composition can be significantly heterogeneous and result on a tortuous fluid path composed by complex arrangements of shingled shale and sand smears (James, 1997).

The fault density and presence of two or more fault families dictates the overall degree of structural compartmentalisation of the reservoir units, and also the size and shape of the compartments. This can lead to the formation of closed compartments, which tend to be more frequent in heavily faulted strata. Open compartments also occur and may have larger sizes if related to lower fault densities. The behaviour of faults as barriers or conduits for fluid flow can change with time as a result of various episodic processes, and consequently the dynamic or static connectivity between compartments.

Halokinesis has a profound impact in reservoir compartmentalisation. Salt displacement produces structures like pillows, salt rollers, salt walls or salt diapirs that cause a wide deformation of the surrounding lithologies expressed by concentric and radial faults, rim synclines, overturned beds and doming at the diapir crest (Rowan et al., 1999; Rowan et al., 2003; Stewart, 2006). Reservoir units overlying salt structures are likely to be cut by dense families of crestal faults and form numerous closed compartments. Radial faults flanking salt diapirs and ridges are likely to have a lower impact on the field

compartmentalisation when compared to crestal ones (Fig. 1.5b). The radial faults tend to form open compartments that may allow continuous replenishment of hydrocarbons towards the updip trap formed by either strata pinch-out or impermeable salt. The open direction of radial faults may even allow the contact between adjacent compartments in case their extent is lower than the area covered by the hydrocarbon column. Nevertheless, this situation is compromised when concentric faults are also present (Stewart, 2006), with consequent decrease in compartment connectivity and size (Fig. 1.5b). The growth of salt ridges and salt canopies is another compartmentalising process by which vertical and horizontal impermeable salt barriers are created within the stratigraphic units.

#### **1.4.2.3. Diagenetic compartmentalisation**

Diagenetic processes can change the porosity and permeability of the reservoir rock and therefore create either vertical or lateral barriers to fluid flow (Ortoleva, 1994; Slatt, 2006; Taghavi et al., 2006). Compaction, cementation or dolomitization are some of the processes that affect the inter-grain properties of rocks and their quality as reservoirs (Slatt, 2006). Compaction occurs due to the overburden load of the sedimentary succession. This causes a rearrangement of grain contact and consequent reduction of pore space, with the end result being influenced by the composition of the rock grains (de Souza et al., 1995; Taghavi et al., 2006). Ductile grains (e.g. mudstones, micaceous metamorphics, altered volcanic products, or glauconite) suffer higher compaction, with consequent porosity destruction, whereas silica rich clasts are more resistant (de Souza et al., 1995). Breakdown of rock minerals due to compaction can also constitute a trigger for chemical diagenesis (Slatt 2006). Cementation is another common diagenetic process resulting from mineral precipitation in inter-grain space, reducing or completely eliminating rock porosity and its

fluid flow or storage capacity (Cunha et al., 2001; Slatt, 2006). The secondary minerals forming the cement can derive from dissolution of previously existing components of the rock, or can be supplied from elsewhere diluted in percolating fluids (Slatt 2006). Minerals like carbonates, silica, clays or iron are the most common cements (Slatt 2006). Dolomitisation diverges from the processes described above, as it promotes an increase in porosity of the rocks (de Souza et al. 1995). Phase changes of rock constituting from gas to liquid or solid can also create fluid barriers. Examples include Permafrost in high latitudes, or frozen gas hydrates in marine sediments (Allen and Allen 1990; Allen et al. 2006).

The small-scale diagenetic reactions within sedimentary bodies can have variable lateral extents. Localised reactions within permeable beds can variable affect the flow properties of the rocks, with homogeneous reduction of porosity and permeability being the most significant. Isolated compartments can also be created if the diagenetic processes induce the formation of an impermeable shell surrounding a specific stratum (Ortoleva, 1994). Diagenetic reactions can take place bellow trapped hydrocarbon accumulations, forming a trapped pocket isolated from other reservoir compartments (Allen and Allen, 2005). Rock transformations through diagenesis also occur on basin-wide scales. Differential compaction can lead to important changes on the architecture of stratigraphic units, thus influencing fluid flow paths and accumulation areas (Clark et al., 1996). Basin-wide reaction fronts that cut across stratigraphic limits, like the ones resultant from carbonate diagenesis or opal A-Ct transformations, are also important features influencing the compartmentalisation of stratigraphic units (Al-Shaieb et al., 1994b, Davie and Cartwright, 2007; Neagu et al., 2010).



#### **1.4.2.4. Mixed Compartmentalisation**

Modern reservoirs may show a predominance of a determined type of compartments, but the overall fluid communication network is more likely to be the mixed result of stratigraphic, structural and diagenetic compartmentalisation processes acting together (Ainsworth, 2010; Richards et al., 2010; Van Hulten, 2010). Stratigraphic architecture will be the first control on compartmentalisation, and it is upon this that deformation resultant from folds and faults will act to impose the genesis of structural compartments. In addition, syn-tectonic deposition associated with growth faults or growing salt structures can induce the migration of channels or occurrence of MTDs, thus re-arranging the depositional architecture of the deepwater environments. On quiescent periods the sedimentary systems re-arrange and adapt to the new topographic conditions, only to be subjected to deformation resultant from younger growth phases. Contemporaneous diagenetic processes are likely to occur at any stage as well, although being more relevant in deeper buried intervals. In essence, the compartmentalisation of reservoir strata is based on the alternation or synchronicity of stratigraphic, structural and diagenetic processes.

#### **1.5. Aims of this research**

The research presented in this thesis aims to broaden our knowledge on the stratigraphic and structural processes operating on deepwater continental margins that influence the large scale compartmentalisation of target reservoir units. The study is based on a 3D seismic dataset from the northern Espírito Santo Basin, located on the Southeast Brazilian margin. Despite being a region with on-going exploration and high potential for the

future, this basin is still poorly understood. Thus, the analyses undertaken in this study are valid for the exploration objectives ongoing on this basin, but there is also an underlying aim of general applicability of the used methodologies for the characterisation of other continental margins. The specific project aims are as follows:

- 1) To document the stratigraphic architectures in distinct units on the Espírito Santo Basin.
- 2) To understand the impact and potential of MTDs on hydrocarbon exploration.
  - a) Analyse and quantify the distribution of MTDs in confined salt-withdrawal basins.
  - b) Investigate the influence of MTDs on the compartmentalisation of reservoir-prone strata, alongside the influence of growing salt diapirs.
  - c) Assess the role of MTDs on margin construction during periods of frequent mass-wasting.
  - d) Apply a qualitative and quantitative analysis of internal heterogeneities of submarine MTDs, and the implications of their internal compartmentalisation for the accumulation or flow of fluids in sedimentary basins.
  - e) Investigate genetic relations between mass-wasting and halokinesis on deepwater continental margins, alongside the application of MTDs as markers for periods of salt growth.
- 3) To improve the understanding of submarine channel confluences on confined basins.
  - a) Investigate the relation between submarine channel confluences and variable structural confinement.

- b) Apply a new methodology to analyse the spatial distribution patterns of submarine channels in confined salt-withdrawal basins.
  - c) Investigate channel density as a response to topographic confinement and salt tectonics, and its relation to slope compartmentalisation.
  - d) Characterise, quantify and classify the morphologies of confluence points on submarine channels
- 4) To do a quantitative analysis and establish scale relationships of the distinct geological features influencing the compartmentalisation of reservoir units on continental margins.

### **1.6. Thesis layout**

This thesis is divided into eight chapters. Chapter 1 consists of the presented Introduction where the principal concepts of reservoir compartmentalisation are covered, alongside an overview of submarine depositional systems and the principles of salt tectonics on continental margins. This is followed by the Geological Setting section and a synthesis of the Meso-Cenozoic evolution of the Southeast Brazilian continental margins section in Chapter 2. Chapter 3 presents the Methods used on this thesis, with a description of 3D seismic acquisition and visualisation, interpretation procedure and the use of seismic attributes. The quantitative methods and statistical analysis used in this thesis are also presented. Chapters 4, 5 and 6 present the main results of this thesis. Chapter 4 investigates the relative distribution of MTDs and turbidites of Eocene-Oligocene age present on the studied basin, and what is their relation with growing salt diapirs. Chapter 5 analyses the morphology and characteristics of a heterogeneous mid-Eocene MTD, within which several

remnant and rafted blocks were identified. Chapter 6 studies the confluence Neogene submarine channels in diapir-confined basins, and how this affects the channel spatial distribution. Chapter 7 presents a summary of the major findings and a Discussion of the scales involved in each of the compartmentalising features studied in the thesis. The main conclusions of this thesis are presented in Chapter 8

# **Chapter 2**

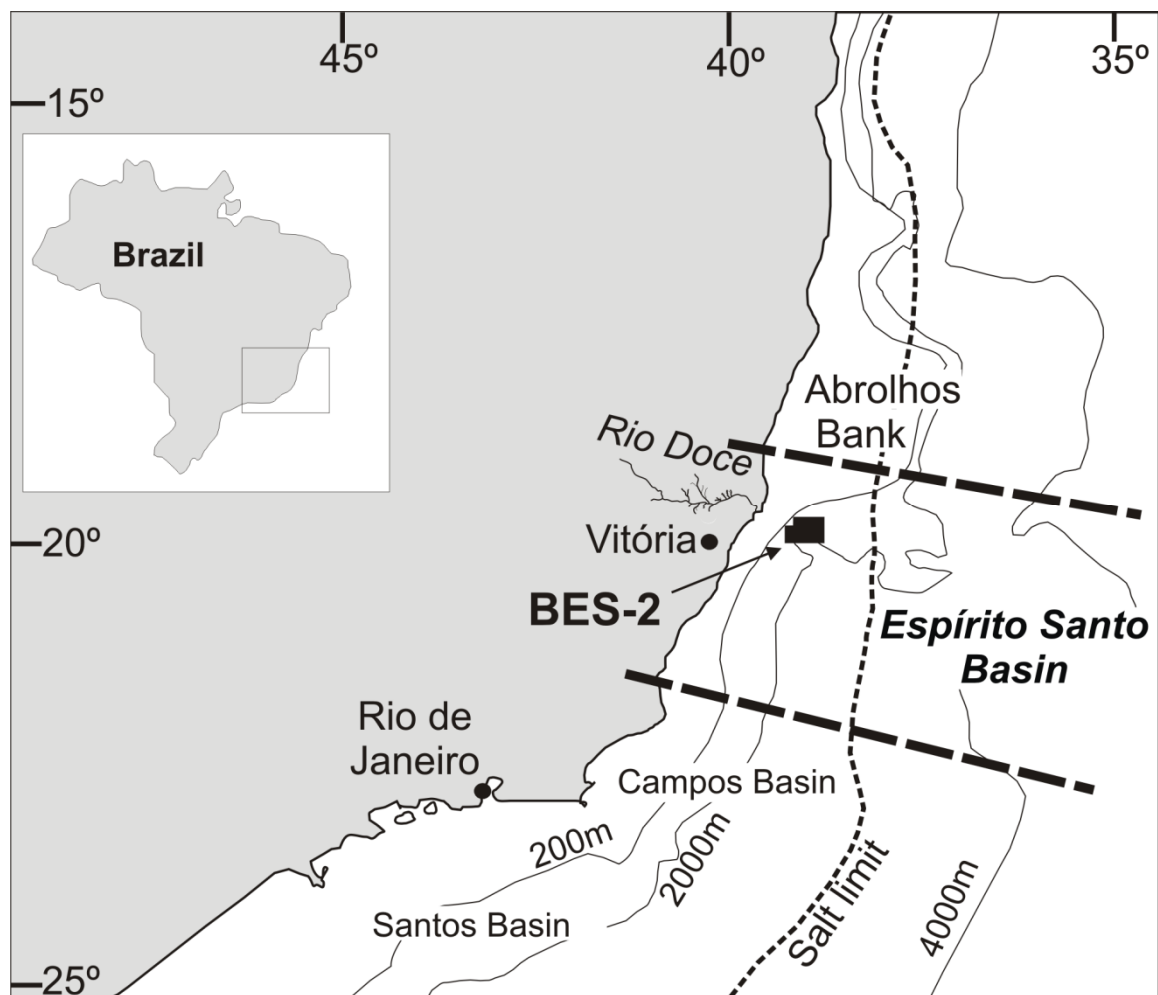
**Geological Setting:**

**Espírito Santo Basin, SE Brazil**

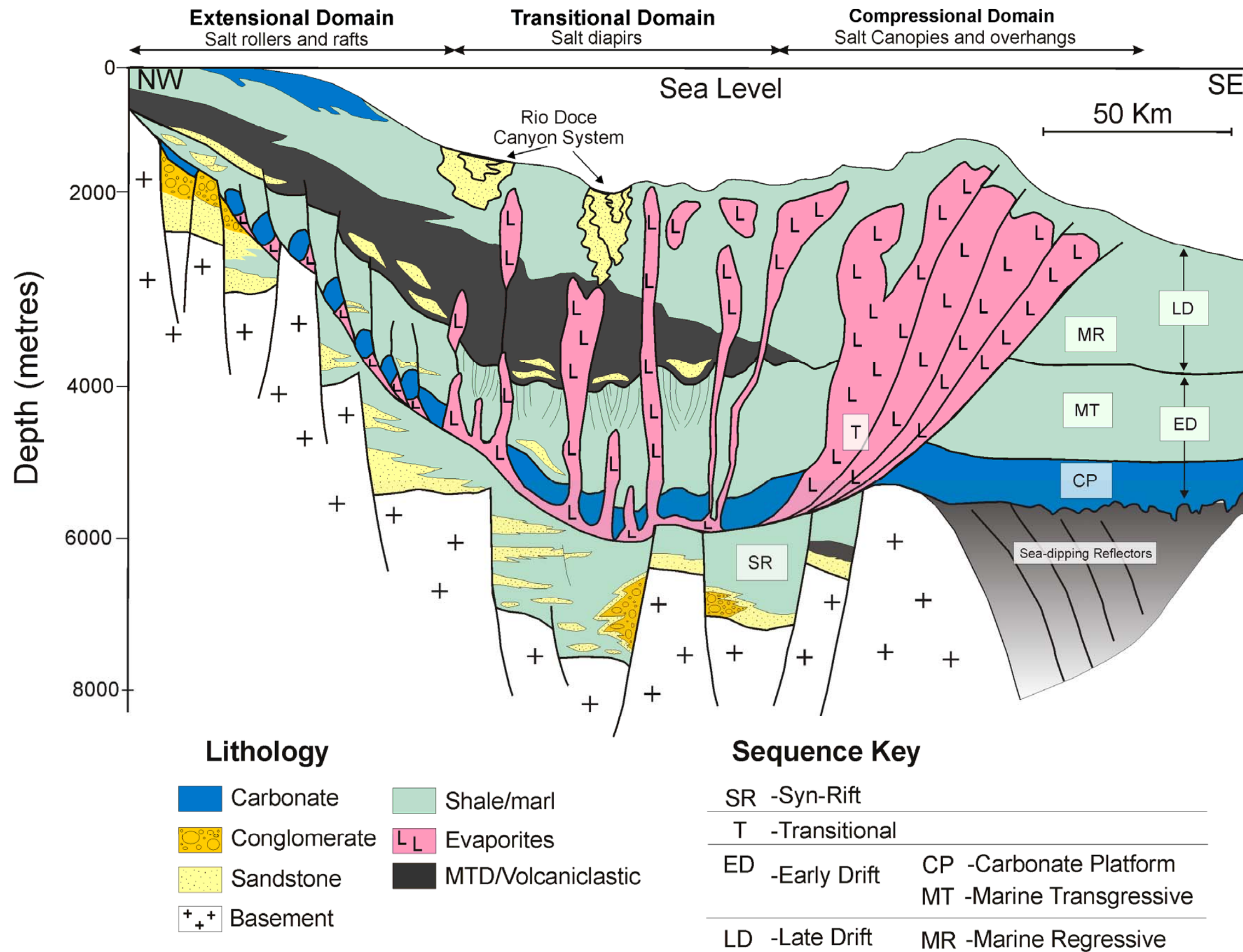
## 2. Geological Setting - Espírito Santo Basin, SE Brazil

### 2.1 Tectono-Stratigraphic Evolution

The Espírito Santo Basin is located on the southeast continental margin of Brazil, covering an approximate area of 18 000 km<sup>2</sup> onshore and c. 200 000 km<sup>2</sup> on its submarine domain (Mohriak, 2003). It is bounded in the north by the volcanic Abrolhos Plateau and in the south it is separated from the Campos Basin by the Victoria Arch (Fig. 2.1). The tectono-stratigraphic evolution of the Espírito Santo Basin is typical of a rifted passive margin and shares identical deformation histories with other basins in the southeastern Brazilian margin, in particular with the Santos and Campos basins located further south (Fig. 2.1). Four evolutionary stages have been identified, pre-rift, transitional and drift stage (Ojeda, 1982), which correlate to five depositional mega-sequences (Fiduk et al., 2004) (Fig. 2.2). The pre-rift phase marks the onset of crustal uplift that preceded the break-up of Western Gondwana in the Late Jurassic/Early Cretaceous, forming wide depressions filled by shallow water sediments. (Chang et al., 1992; Mohriak, 2003; Mohriak et al., 2008; Ojeda, 1982). The syn-rift phase (Fig. 2.2a) is estimated to have lasted from the late Berriasian/Valanginian to early Aptian, being marked by intense tectonic activity and formation of rift basins associated with the divergent movement of the South American and African plates (Demercian et al., 1993; França et al., 2007; Mohriak, 2008; Ojeda, 1982). During the syn-rift phase there was a predominance of lacustrine sedimentation within fault-controlled basins showing marked fluvial input at their flanks, and carbonate deposition on structural highs. In the Espírito Santo Basin, the syn-rift mega-sequence is characterised by the deposition of

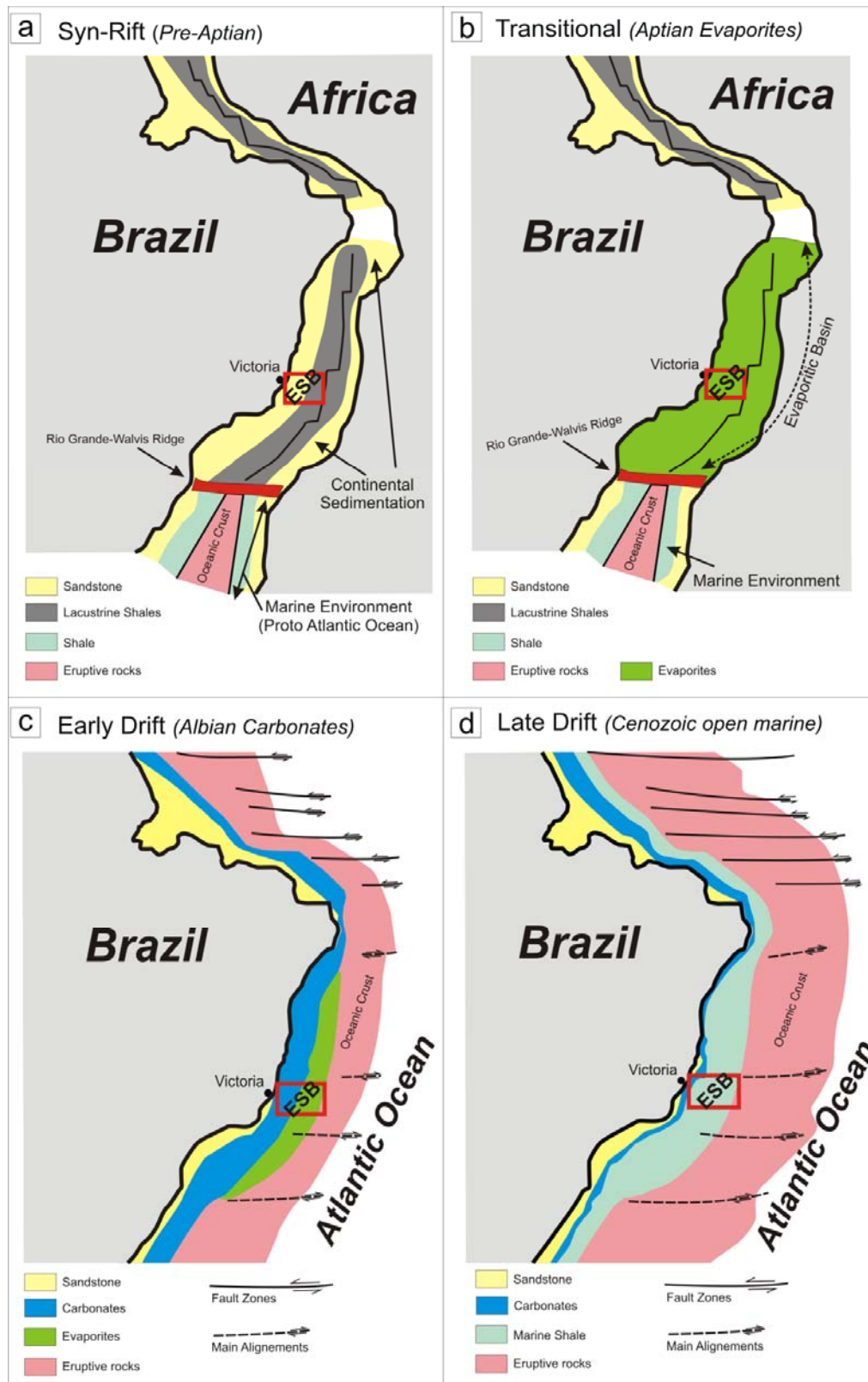


**Figure 2.1.** Map representing the location and geographic limits of the Espírito Santo Basin, Southeast Brazilian Margin. The area in black shows the location of the BES-2 3D seismic volume/block



**Figure 2.2.** Simplified regional section across the Espírito Santo Basin depicting the three salt domains (extensive, transitional and compressive) and associated deformation structures. The major depositional mega-sequences and their interaction with salt structures are also represented (Modified from Fiduk et al., 2004).





**Figure 2.3.** Paleogeography outline of the Brazilian margin showing main tectonic phases. (a) Syn-rift phase, with predominance of continental environments. (b) Transitional phase, marked by deposition of evaporites in a restricted basin. (c) Early drift phase, with formation of shallow-water carbonate platforms. (d) Late drift phase characterised by open marine sedimentation. The relative location of the Espírito Santo Basin is highlighted by the red box (Modified from Ojeda, 1982).

the Cricaré and Mariricu formations (Fig. 2.4), which comprise fluvial sandstones and syn-tectonic conglomerates in the proximal domains of individual rift basins, intercalated with volcanic rocks (França et al., 2007). Fine-grained sediment deposited in the lacustrine depocentres are characterised by fine sand, silts and dark shales (Chang et al., 1992; Fiduk et al., 2004; Milani et al., 2001; Mohriak, 2003; Ojeda, 1982). The extreme anoxic conditions in these lacustrine settings allowed the preservation of organic matter in extensive shale units, which constitute major source intervals for hydrocarbons on the SE Brazilian margins (Mello et al., 1994; Mohriak, 2003; Mohriak, 2004).

The transitional phase (Aptian to Early Albian) is bounded at its base by the break-up unconformity, being coincident with the beginning of a period of tectonic quiescence and cessation of basement fault activity during the Aptian. This sets the transition from the continental syn-rift to the marine drift phase characterised by the first marine incursions into the central graben of the southeast Brazilian rift basins (Dias, 2005; Ojeda, 1982). Within this phase are recorded crestal erosion of rotated rift blocks and generalised topographic smoothing of the margin (França et al., 2007; Mohriak, 2003; Mohriak, 2004). This same event is marked by the bypass of the topographic barrier created by the volcanic Rio Grande-Walvis ridge, creating an extensive gulf along the margin that supplied marine water to the evaporitic basins located over the rift valleys (Fig. 2.3b). Thus, the Aptian is marked by the deposition of thick evaporitic sequences, predominantly composed by halite and anhydrite, resulting from extreme brine evaporation in an arid climate (França et al., 2007; Mohriak, 2003; Mohriak et al., 2008). The late Aptian to lower Albian marks the initiation of salt movement, creating complex halokinetic deformation structures which also

controlled sedimentation in regions of salt withdrawal (Fiduk et al., 2004; Mohriak, 2003; Mohriak, 2004).

During the Late Cretaceous to Holocene drift phase there was a continued spreading of the South American and African plates with generalised eastward tilting and increasing subsidence of the deeper sections of the basin deriving from thermal subsidence and sediment loading (Bruhn and Walker, 1997; Mohriak, 2003). This phase is dominated by an open marine environment and by the complete bypass of the topographic barriers that constrained the proto-ocean. The drift phase is divided in an early drift transgressive mega-sequence and a late drift regressive mega-sequence (Fiduk et al., 2004; Ojeda, 1982). The early drift is marked by two marine transgressive sequences. The lower sequence consists of a shallow water Albian succession, with intercalated (proximal) coarse sandstones (São Mateus Formation). At this same time the Regência Formation carbonate platform was formed on the distal slope (Figs. 2.3c and 2.4) (Demercian et al., 1993; França et al., 2007; Milani et al., 2001). A late Albian unconformity limits the top of this first sequence, which is also associated with the erosion of the Regência and Fazenda Cedro paleo-canyons onshore and on the continental shelf. The late Albian to Palaeocene sequence reflects a deepening of the basin and drowning of the Albian carbonate platform. Basal deposits in this sequence consist of dark mudstones, turbiditic sandstones and local carbonated breccias resulting from the erosion of Albian carbonates. These are overlain by thick sequences of mudstones (Urucutuca Formation), with turbiditic sandstones linked to the Fazenda Cedro, Regência (França et al., 2007) and other submarine canyons (Alves et al., 2009; Fiduk et al., 2004).

The Late Drift marine-regressive mega-sequence, of Eocene to Holocene age, reflects important tectonic activity marked by the reactivation of ancient rift structures and uplift of

hinterland mountain chains. It resulted in a generalised sea-level drop and creation of a regional unconformity (Cobbold et al., 2001; Demercian et al., 1993; França et al., 2007). This eustatic event is also associated with important volcanic activity during the early/mid Eocene to Oligocene times, culminating on the development of the Abrolhos Bank, a plateau of volcanic origin covering c. 30000 Km<sup>2</sup> (Fainstein and Summerhayes, 1982; Sobreira and França, 2005). The plateau is shallow, but its margins show an abrupt shelf break and a relatively narrow slope area (Mohriak, 2003). Reactivation of older fault zones is suggested to explain the mid-plate volcanism, which was also associated with the presence of a hotspot in the Victoria-Trindade region (Fainstein and Summerhayes, 1982). A shallow-water carbonate platform (Caravelas Formation) developed on the Abrolhos Bank, creating a confined sub-basin delimited by the coast on the west and the volcanic build-ups and carbonates on the east. Erosion of the hinterland mountain ranges and ongoing volcanic activity led to a high input of mixed siliciclastic and volcanoclastic sediment to the continental slope. Prograding siliciclastic units of this age consist of fine to coarse lobate massive sandstones, conglomerates and local siltstones, whereas the volcanoclastic lithologies are represented by tuffs, volcanic breccias and hyaloclastites (Mohriak, 2004). Carbonates are also present in these prograding sequences, derived from erosion in the Abrolhos Bank region. Sediment was mainly transported by turbiditic flows deposited along submarine channel systems or as submarine fans (Bruhn and Walker, 1997; França et al., 2007; Mohriak, 2003), although submarine mass-wasting also played an important role in sediment supply to the basin in the northern limits of the Espírito Santo Basin (Fig. 2.2) (Gamboa et al., 2010). Neogene sedimentation is marked by the predominance of mudstones and turbidites in the deepwater domains (Urucutuca Formation), but there is an

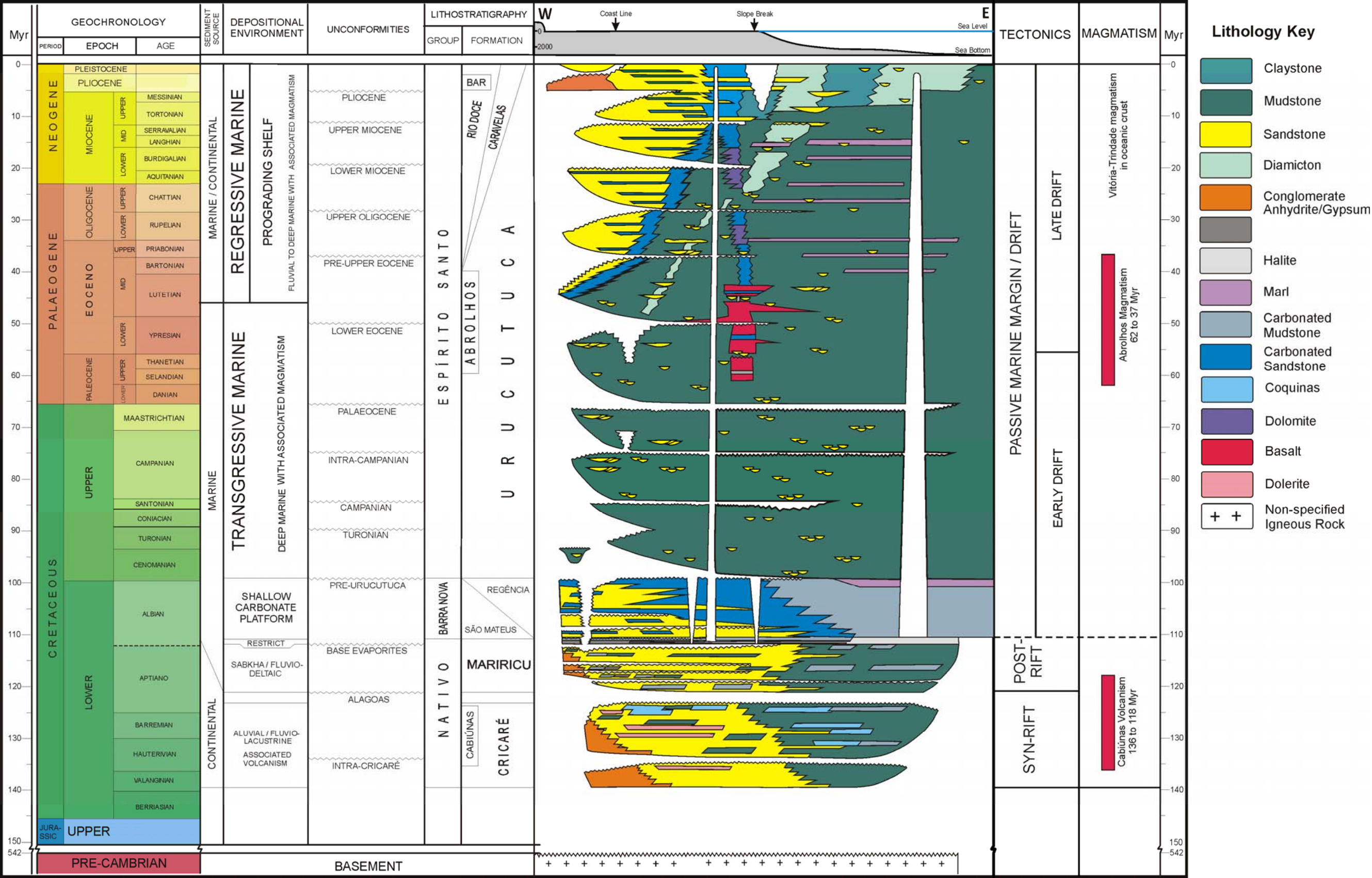


Figure 2.4. Stratigraphic chart of the Espírito Santo Basin showing regional stratigraphic units, main tectonic phases and magmatic events (modified from França et al., 2007)

increasing predominance of sandstones (Rio Doce Formation) and bioclastic calcarenites from the Caravelas formation further into the basin (França et al., 2007).

## **2.2. Late Cretaceous-Cenozoic Halokinesis**

The Late Cretaceous and Cenozoic evolution of the Espírito Santo Basin is predominantly controlled by thin-skinned gravitational gliding above Aptian evaporites (Demercian et al., 1983; Fiduk et al., 2004). The type of salt structures and associated sediment deformation in the basin are divided into three main tectonic domains (Fig. 2.2). The extensional domain, located on the inclined margin of the basin in proximal areas, is characterised by salt rollers, salt walls along conjugate normal faults, turtle anticlines and rafts (Mohriak 2008). This is followed by a transitional mid-slope domain where salt diapirs predominate, and by a compressional domain on the distal slope where allochthonous salt canopies and overhangs are observed (Davison, 2007; Demercian et al., 1993; Fiduk et al., 2004). The growth of salt structures in the Espírito Santo Basin is often limited to the Cretaceous. Nevertheless, several diapirs and canopies developed significantly through the whole Cenozoic as a result of increase in sediment input onto the continental slope, with this growth being evidenced by marked deformation of the modern seafloor (Lima, 2003; Fiduk et al., 2004). Regional tectonic uplift resulting from the emplacement of the Abrolhos Plateau is also considered to have controlled salt deformation. This led to a marked tilting of the margin and subsequent acceleration of gravitational gliding, with consequent deformation of several salt structures during the early Cenozoic (Fiduk et al., 2004). Distinct faulting stages have been identified in the Espírito Santo Basin in association with the sudden growth of salt structures (Alves et al., 2009; Baudon and Cartwright, 2008). A first

episode of faulting resulted in the formation of closely spaced synclinal and crestal faults that propagate through the Late Cretaceous and Palaeocene strata. These faults are mostly truncated by the Early/Mid-Eocene unconformity. Faulting of Late Eocene to Holocene strata is less significant, occurring predominantly by reactivation of older faults over collapsed salt anticlines, but with poor or no expression on the modern sea-floor (Alves et al., 2009; Baudon and Cartwright, 2008). Salt growth played an important role on the sedimentary evolution of the Espírito Santo Basin. Since its early deformation phases, salt structures and associated faults delimited confining sediment fairways that trapped the turbidite deposits, and conditioned the development of Cenozoic submarine canyons (Mohriak, 2004). The sediment fairways tend to follow a generalised NW-SE orientation, running parallel to the main halokinetic structures deforming the seafloor (Fiduk *et al.*, 2004).

### **2.3. Local setting**

The 3D seismic survey analysed in this thesis covers a section located on the northern limit of the Espírito Santo Basin (Figs. 2.1 and 2.5), totalling 1670 Km<sup>2</sup>. The northern limit of the study area coincides with the southern flank of the Abrolhos Plateau, where water depths reach c. 100 metres. The studied slope gradually deepens following a southeast direction to water depths up to 1800 m (Fig. 2.1). Main structural features evidenced on the modern sea-floor consist of a series of aligned diapirs that form two main northwest-oriented salt ridges (Fig. 2.5). These ridges delimit confined salt-withdrawal basins with identical orientation, which constitute the major fairways for sediment transported to the lower slope. Modern sedimentary architectures consist of a series of

south-southeast submarine channels flowing from the Rio Doce Canyon System that coexist alongside less confined turbidites and MTDs (Fig. 2.5).

## **2.4. Seismic Stratigraphy**

The stratigraphic successions in the study area are divided into three seismic-stratigraphic units (Fig. 2.6).

### **2.4.1. Unit 1**

The lowermost Unit 1 is Upper Cretaceous to Paleocene in age (Baudon and Cartwright, 2008), with its top marked by the Mid-Eocene unconformity (*Fiduk et al.*, 2004; *Gamboa et al.*, 2010). This unit is characterized by moderate-amplitude, sub-parallel, continuous reflections. The bottom reflections show local thickening of strata and onlap towards buried salt structures, changing into continuous, moderate amplitude reflections towards its top. At the top of Unit 1, reflections tend to be sub-parallel, with minor thickness changes. High-amplitude reflection packages are related to the Palaeocene submarine channel systems developed within axial salt-withdrawal basins (Alves et al., 2009). Other continuous high-amplitude deposits are likely to represent unconfined clastic deposition. Unit 1 is densely faulted, with normal faults occurring predominantly on the crest of buried salt diapirs and ridges. Their upper tips are commonly truncated by a Mid-Eocene unconformity (Fig. 2.6).

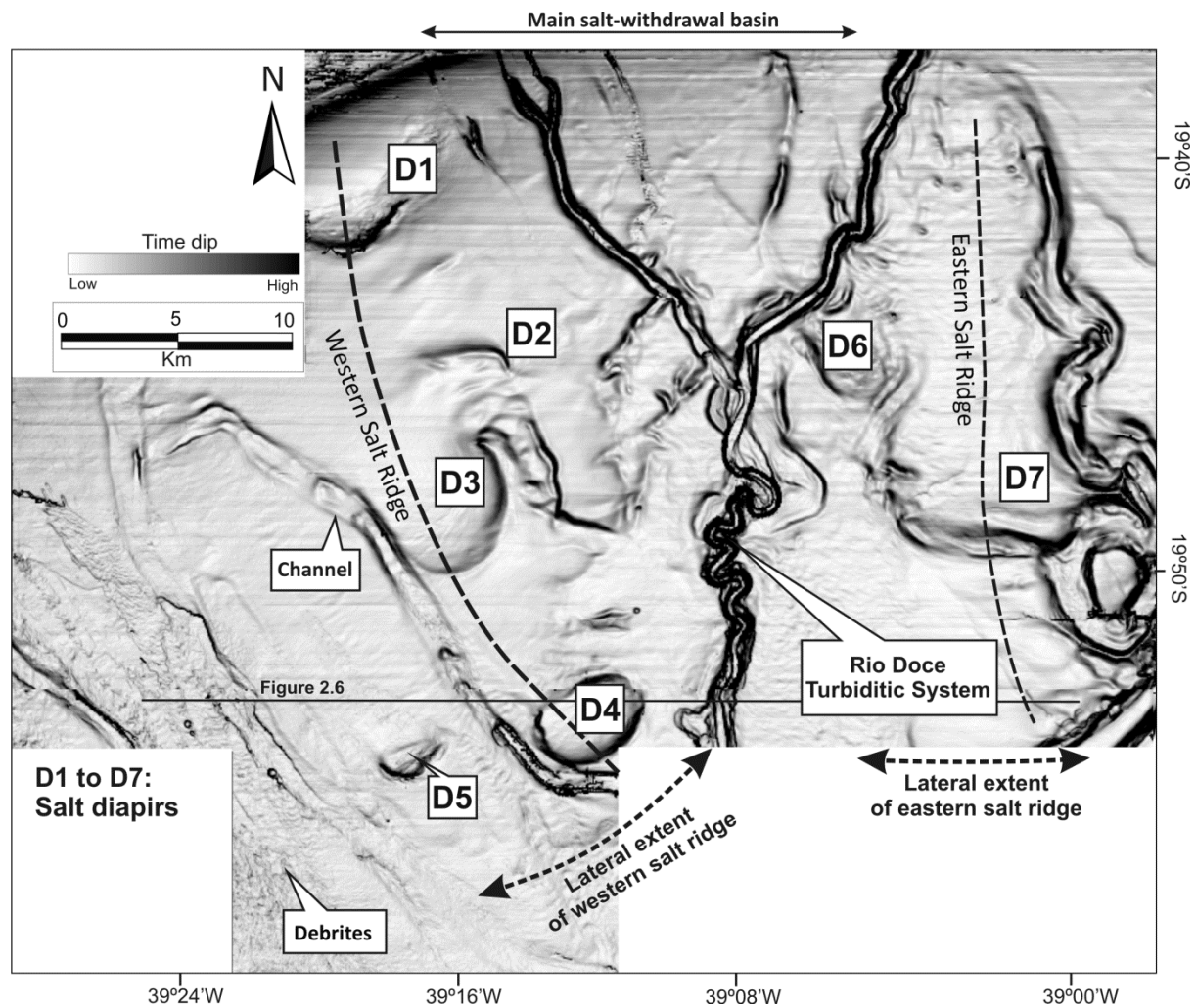


**2.4.2. Unit 2**

Unit 2 corresponds to the Abrolhos Unit, as its estimated age coincides with the period of volcanic activity that developed the Abrolhos Plateau. Its base is marked by the Mid-Eocene unconformity (Gamboa et al., 2010) while the top is inferred to be of early Miocene age. Unit 2 is characterised by moderate to very high amplitude, sub-parallel to chaotic seismic reflections. Chaotic to transparent reflections comprise mass-transport deposits, which are intercalated with laterally continuous turbidites. The high seismic amplitudes observed in this unit are, according to Fiduk et al. (2004), due to the high supply of siliciclastic sediment from the margin and to the predominance of reflective volcanoclastic material derived from the Abrolhos Plateau (Fig. 2.6).

**2.4.3. Unit 3**

The base of unit 3 is inferred to be early Miocene and its top coincides with the modern sea floor. Unit 3 can be divided in three sub-units (Fig. 2.6). Sub-unit 3a shows a single channel system incising at the base of the unit, and it is characterised by high-amplitude sub-parallel reflections. Sub-unit 3b shows low to moderate amplitude sub-parallel reflections, representative of continuous hemipelagic/contouritic deposits. This seismic character also reflects the presence of channel fill deposits, although these also show less-frequent high amplitude reflections. Sub-unit 3c corresponds to the upper stratigraphic package, interpreted to represent strata of Pliocene to Holocene age. Seismic reflections in the sub-unit are of high amplitude, and are often laterally continuous and sub parallel, associated with submarine channels and fans. Chaotic packages with moderate to high amplitudes are representative of MTDs in this interval.



**Figure 2.5.** Seafloor dip-map of the studied area, Espírito Santo Basin. The figure highlights the presence of several salt diapirs (D1 to D7) that control the distribution of the modern sedimentary systems. The diapir alignments form two northwest-oriented ridges that bound main salt-withdrawal basins.



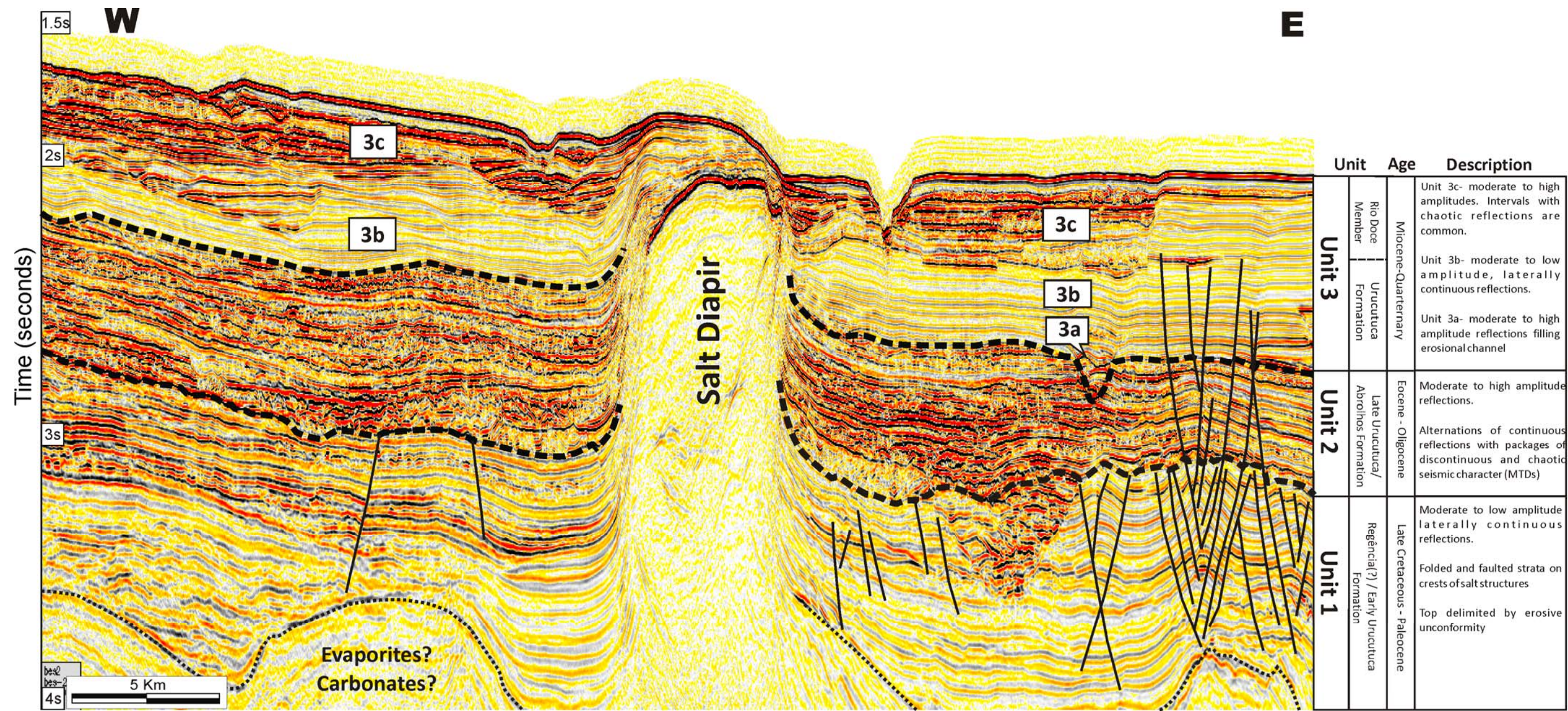


Figure 2.6. Seismic section showing the principal seismo-stratigraphic units in the northern region of the Espírito Santo Basin. Three main units are identified based on their seismic character, and stratigraphic and structural features



# **Chapter 3**

## **Methods**

### 3. Methods

The results presented in this work are based on the interpretation of 3D seismic data, followed by the quantitative analysis of geological features of interest. This chapter aims to provide a brief overview of the marine 3D seismic method, namely acquisition and interpretation, and to describe the dataset and statistical methods used in this thesis.

#### 3.1. 3D Seismic

The principle of 3D seismic is the acquisition of very closely-spaced seismic-reflection data, providing detailed information of the subsurface both in horizontal and vertical directions (Bacon et al., 2003). This allows improved spatial interpretations of the subsurface geological features when compared to 2D data, particularly in areas of complex 3D structural and/or stratigraphic geological features (Hart, 1999; Kearey et al., 2002; Posamentier et al., 2007, Yilmaz, 2001). The design of 3D seismic marine surveys consists on a series of marine seismic sources, usually an array of airguns, and a series of hydrophones towed behind the acquisition vessel (Fig. 3.1). The shooting direction is called the inline direction, being coincident with the boat track and orientation of the hydrophone arrays, and perpendicular to this is the crossline direction. Typically, trace spacing in 3D surveys are 12.5 to 25m for inlines and 25 to 50 m for crosslines, thus an accurate knowledge of the shot and receiver locations is required to provide the best quality data (Yilmaz, 2001). To produce the final 3D cube, the data has to be processed. The basic principles consist on the stacking and posterior migration of the data. Stacking combines individual traces into a common-cell gather (or bin), commonly coincident with a common-midpoint (CMP) gather, which tend to have cell sizes of 12.5 X 25 m (Yilmaz, 2001). Next, the data has to be

migrated in order to provide the correct location and geometry of the seismic reflectors. In essence, the migrations process collapses the diffraction patterns produced by sub-surface features, greatly improving the quality of the seismic image provided (Yilmaz, 2001).

The acquisition of commercial seismic reflection data is primarily focused on the detection of compressional P-waves reflected at subsurface geological interfaces (Kearey et al., 2002; Sheriff and Geldart, 1995). In marine environments, 3D seismic surveys comprise the acquisition of data generated by the energy sources below the sea surface, which are designed to concentrate downward energy pulses. The sum of the signals fired simultaneously from each airgun provides a far-field wavelet which has a range of frequency components. This wavelet propagates through the water column to reflect off the seafloor and through subsequent geological layers to provide reflection signals. The energy reflected is then detected by hydrophones towed behind the vessel, which record the in milliseconds two-way time (TWTT) that the P-wave reflections take to travel from the source until the return to the surface (Fig. 3.1).

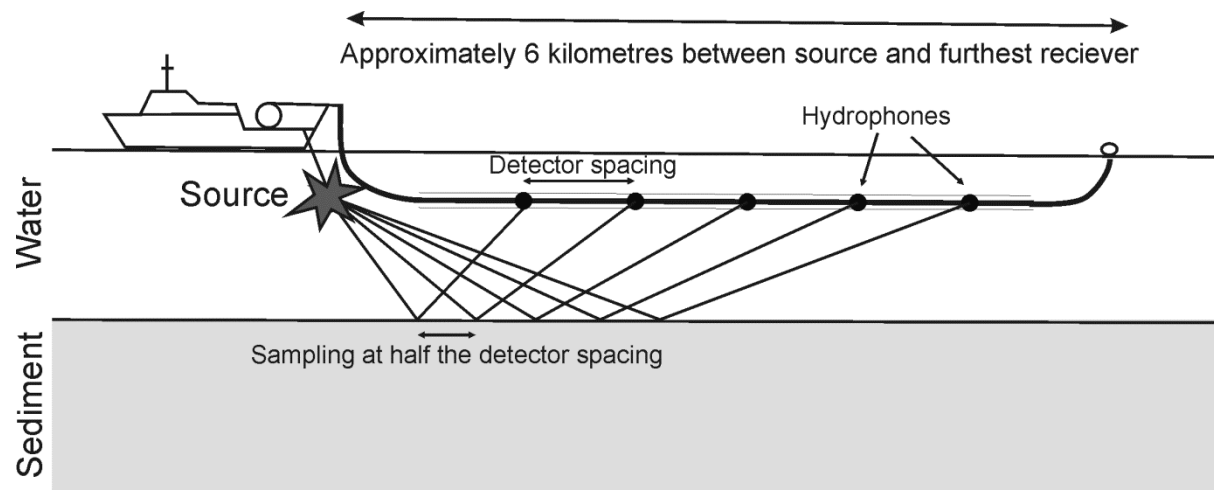
Two important parameters of the seismic P-waves are their velocity and frequency. The P-wave velocity is variable through the stratigraphic successions, being directly controlled by of the lithological composition, porosity, density, texture, pore-water, compaction, elastic modulus and also fluid content. In general, velocity tends to increase with depth as rocks become more compacted (Brown, 2004; Kearey et al., 2002). In contrast, acoustic frequency consists in the number of wave cycles passing by one point per second, and this tends to decrease with depth as the higher frequencies preferentially attenuate while travelling through the rock. This has a direct influence on the spatial

resolution of the seismic data, which also decreases as deeper stratigraphic levels are reached (Brown, 2004).

The strength of the reflections on seismic data reflects the contrast in physical properties across geological interfaces. Thus, reflector strength depends on the acoustic impedance (Z) which is defined as a function between the rock density ( $\rho$ ) and seismic velocity (v) (Brown, 2004; Kearey et al., 2002; Veeken, 2007), such that:

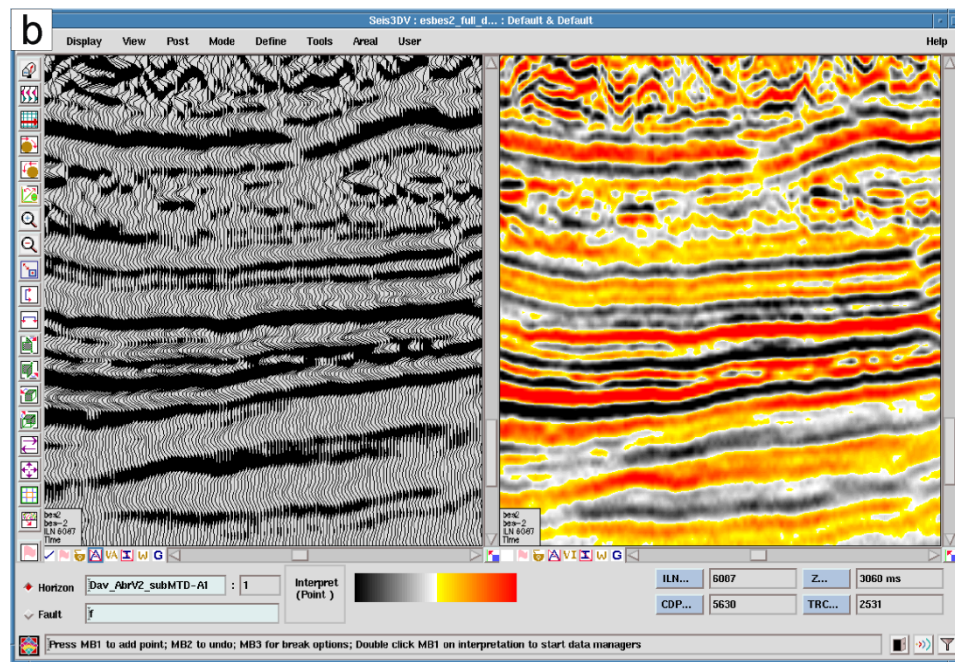
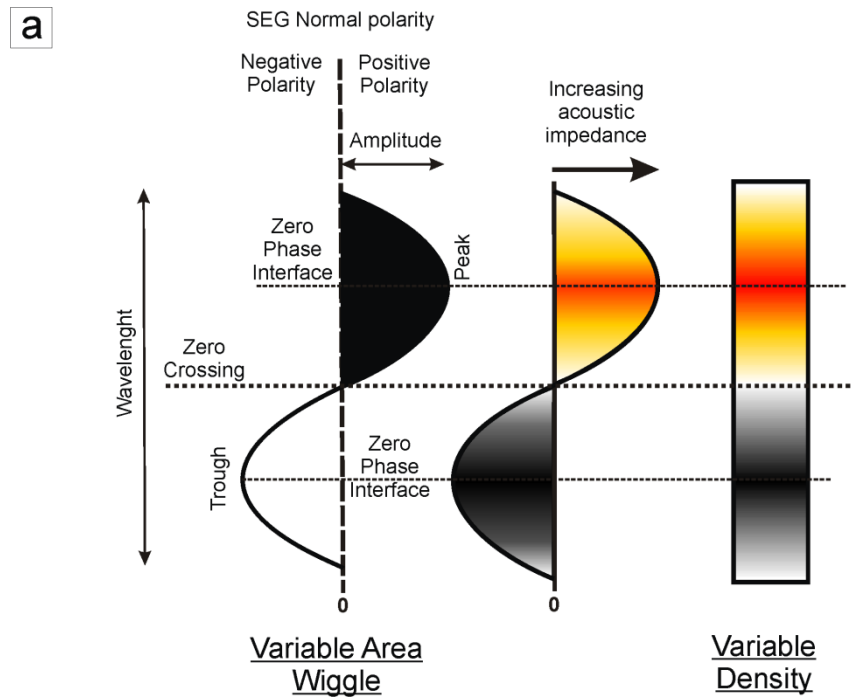
$$Z = \rho \cdot v \quad (\text{eq. 3.1})$$

Increasing acoustic impedances, which for example may be created by a sand interval underlying a shale, are commonly displayed as 'peaks' on the seismic wavelet and considered as positive amplitudes, while decreasing amplitudes are considered as negative amplitudes or 'troughs' (Kearey et al., 2002; Sheriff and Geldart, 1995). Wave displays are traditionally represented in distinct colours in what is termed the 'SEG (Society of Exploration Geophysicists) normal polarity' classification (Brown, 2004), being this the convention used in this thesis (Fig. 3.2). The data classification also considers phase. The surveys can be maximum, minimum and zero phase, but nowadays the latter type has gained the preference of seismic interpreters (Brown, 2004). The zero-phase data means that the wavelet is symmetrical and the majority of energy is coincident with its peak, which has a great advantage on seismic stratigraphic interpretations as the centre of the wavelet is coincident with the geological interface causing the reflections (Fig. 3.2).



**Figure 3.1.** Schematic representation of 3D marine seismic surveys. A towed acoustic source near the surface emits a sound wave that travels through the water. When the acoustic properties of the rock change, the P-waves reflected to the surface are detected by hydrophones mounted in a long cable towed behind the boat. The hydrophone spacing partly controls the horizontal resolution of the seismic data (modified from Bacon et al. 2003).





**Figure 3.2. (a)** Schematic representation of the seismic waves in SEG normal polarity zero phased data. In variable area wiggle display, peaks are displayed in black and troughs in white. In variable density display, individual traces are represented as colour-coded voxels indicative of their amplitude (modified from Hart, 1999). **(b)** Schlumberger Geoframe interpretation environment with examples of a seismic section both in variable area wiggle and variable density displays, with the latter type providing a clearer visualisation of data.

### 3.1.1. Seismic resolution

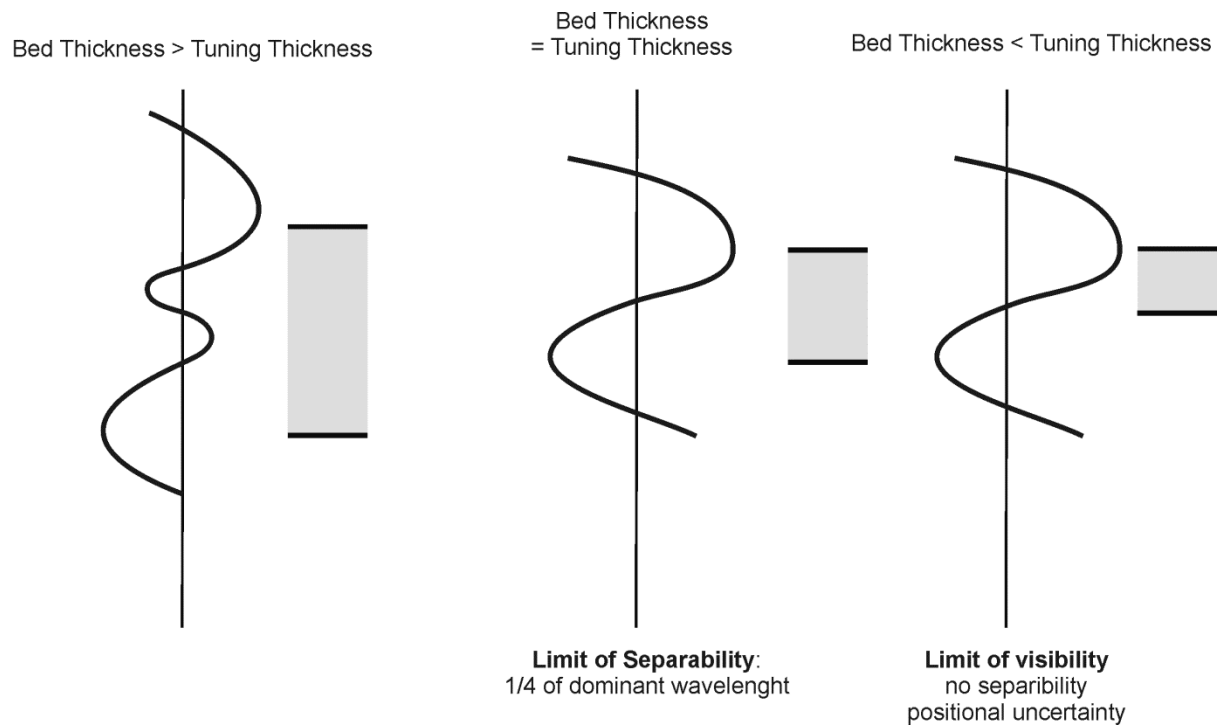
The key objective of any 3D seismic acquisition campaign is to provide high-resolution data of the subsurface, but this tends to decrease with depth as the rocks get increasingly more compacted (Brown, 2004). The resolution is related to the minimum proximity of two points that can still be identified as individual elements in the seismic data, with both vertical and lateral resolution being taken into account (Yilmaz, 2001).

Vertical resolution is mainly restricted by the dominant wavelength ( $\lambda$ ), which is defined by the wave velocity ( $v$ ) divided by the dominant frequency ( $f$ ), such that:

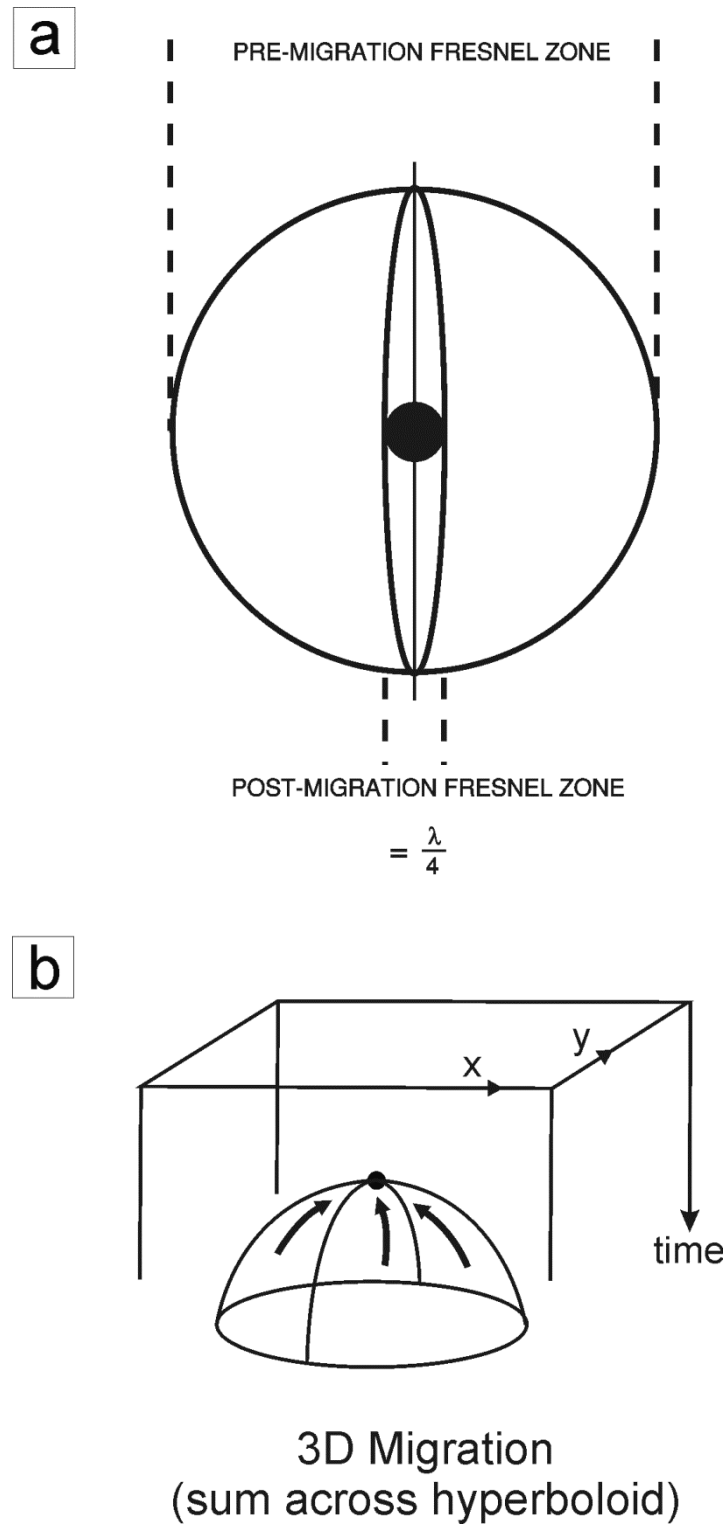
$$\lambda = v/f \quad (\text{eq. 3.2})$$

Seismic wavelength vary between 40 to 250 metres and tend to increase with depth, thus the deeper features must be thicker in order to be identifiable in the seismic data (Yilmaz, 2001). The vertically resolution is marked by the limit of visibility, which is typically  $\frac{1}{4}$  of the dominant seismic wavelength and it defines the potential to distinguish individual layers in the seismic data (Fig. 3.3). If the layers are too closely spaced, i.e. less than the limit of visibility, the reflected seismic energy creates variable interference patterns (Veeken, 2007). Constructive interference, or tuning, occurs when positive reflections overlap and the signal amplitude is boosted as the bed thins (Sheriff and Geldart, 1995; Veeken, 2007). As beds become thinner, they get attenuated until invisible. Nevertheless, in some cases it is possible to detect beds within resolutions of  $\lambda/30$ , although their true thickness is not possible to determine (Sheriff and Geldart, 1995) (Fig. 3.3).

The horizontal resolution refers to the minimal lateral proximity between two points that can still be recognized as individual points rather than one (Yilmaz, 2001). Determining the horizontal resolution is complex due to the areal component involved in 3D seismic and has two main controls, namely the detector spacing and intrinsic physical processes of the reflection (Kearey et al., 2002). The trace spacing normally ranges between 50 and 12.5 metres, thus influencing the spacing of the individual depth estimates from which the reflector geometry is reconstructed. In general, the horizontal sampling distance at a flat reflector is equivalent to half the hydrophone spacing (Kearey et al., 2002; Veeken, 2007). The other limiting control of the horizontal resolution is the size of the Fresnel Zone (Fig. 3.4), which depends on the depth of the reflector, the velocity above the reflector and the dominant frequency (Yilmaz, 2001). This is a circular area defined by the energy returned to the hydrophone, within half a wavelength of the one initially reflected, that arrives in phase and interferes constructively to build up the signal at the reflection point (Bacon et al., 2003; Kearey et al., 2002). To improve the horizontal resolution of a seismic volume, data has to be migrated in order to correct the spatial location of the reflectors and focus the energy spread over the Fresnel Zone (Bacon et al., 2003; Brown, 2004), with smaller areas meaning increased spatial resolution (Yilmaz, 2001). In perfect 3D migration, the Fresnel zone is reduced to a small circle with a radius of a quarter of the wavelength, but in practice it is only reduced to half of it (Brown, 2004).



**Figure 3.3.** Effect of vertical resolution and tuning thickness. The resolution of the reflections from the top and bottom of a bed is dependant of the interaction between closely spaced wavelets (adapted from Brown, 2004).

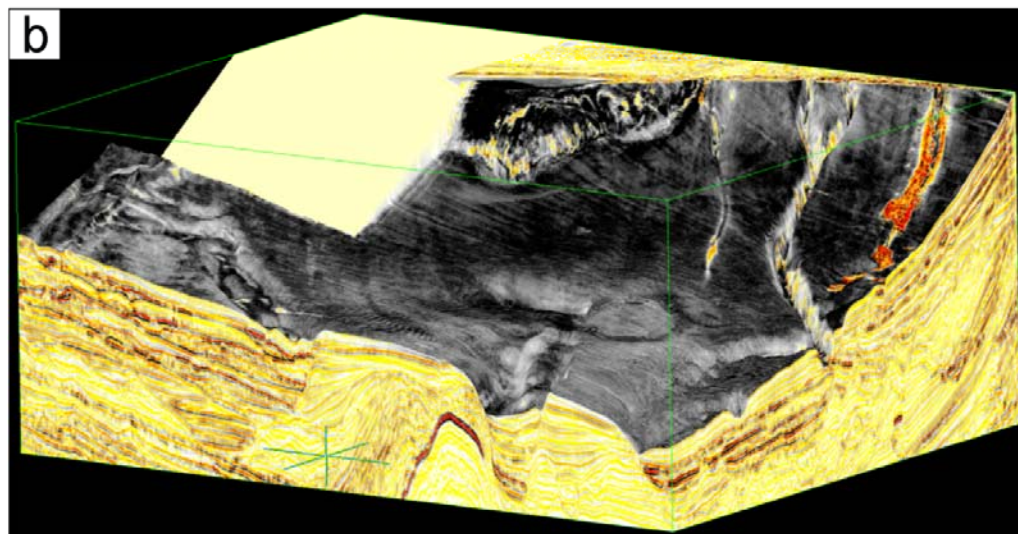
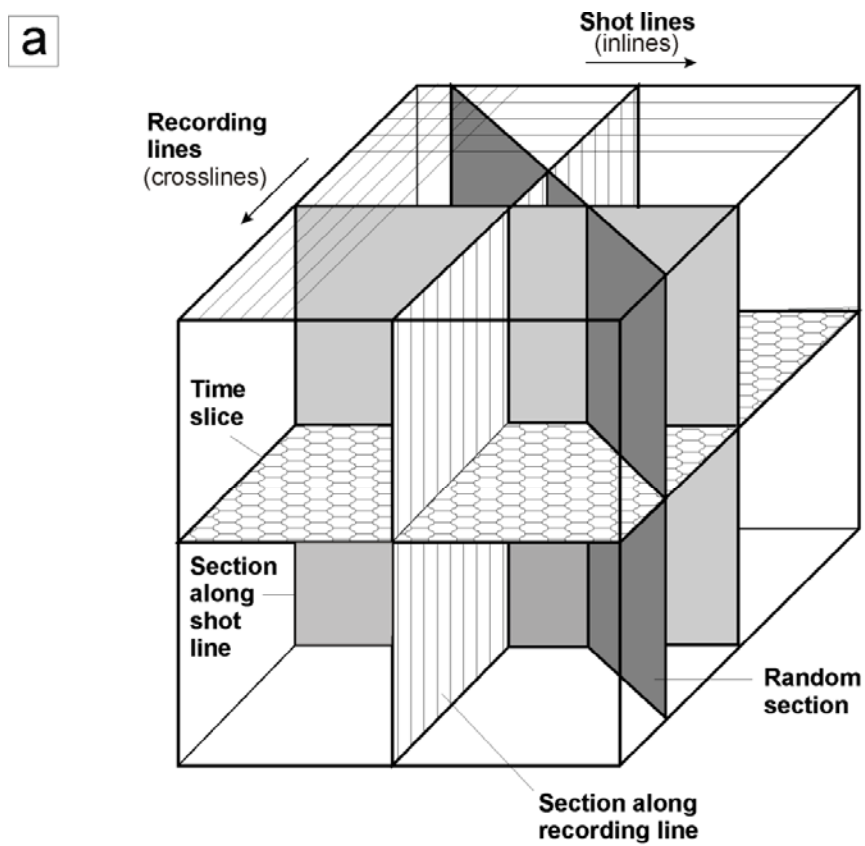


**Figure 3.4.** (a) Pre- and post-migration area of the Fresnel zone. In 3D seismic, the initial large circle is reduced to a smaller one with a radius of  $\frac{1}{4}$  of the wavelength, represented by the black dot in the centre (modified from Brown, 2004). (b) Representation of data summation paths in 3D seismic processing (from Bacon et al., 2003).

### 3.1.2. 3D seismic volume visualisation and interpretation

The 3D seismic survey is a volume of data that represents the reflection coverage of each subsurface reflector within the surveyed area (Kearey et al., 2002). Each volume can be considered to be made by a series of voxels, which consist in smaller 3D cubic units with specific dimensions (x,y,and z) and attribute values (Hart, 1999; Veeken, 2007). The 3D volumes can be manipulated in various ways by using interpretation workstations with high graphical processing capacity. The data can be visualised as a series of seismic wavelets that present seismic traces as continuous curves defining the amplitude peaks and troughs, although this has limitations in terms of its general overview. To overcome this limitation the data can be displayed in variably intensity mode, where each trace is displayed as a column of colour-coded voxels to display particular amplitude samples (Fig. 3.1) (Bacon et al., 2003). Independently of the display mode, the data can be visualised as 2D vertical sections defined along the inline or crossline direction, or along any arbitrary path through the volume (Fig. 3.5). Horizontal time-slices can also be obtained to display the patterns of reflections intersected by any time plane of constant two-way travel time, allowing the lateral trace of structures along the data volume (Hart, 1999; Kearey et al., 2002).

The manual pick and autotracking of relevant reflections is the base procedure in stratigraphic interpretation of 3D seismic data. In its early stages, seismic interpretation should be based on the definition of the structural and stratigraphic framework of the region by mapping major structures, unconformities and unit boundaries of the depositional sequences (Hart, 1999; Mitchum et al., 1977). The following step includes a detailed seismic



**Figure 3.5. (a)** Diagram illustrative of a data volume. Vertical seismic sections can be taken through the volume in any desired direction, and (horizontal) time slices can be taken at any desired time depth (modified from Kearey et al., 2002). **(b)** Example of seismic volume showing sections along inlines, crossline, and partially along a time slice (top limit). The volume in the figure was set to only represent data below an interpreted horizon.

facies analysis of relevant intervals based on the configuration, continuity and amplitude of the reflection patterns (Mitchum et al., 1977).

The computer-based interpretation of the 3D seismic volume in this thesis was made using Schlumberger's Geoframe Interpretation and Visualisation software. This process was based on reflection picking in order to obtain a horizon representative of both structural and stratigraphic features. The initial mapping procedure consisted on the manual picking of the reflections of interest along a series of parallel lines, often coincident with both the original inline and crossline directions in order to obtain a grid that covers its full area extent. The line spacing is defined by the interpreter and should be adapted to the complexity of the target reflection. The work developed in this thesis followed an initial interpretation with 20 line spacing, although a larger spacing up to 50 lines could be used to map laterally consistent reflections. Smaller intervals were used to mapping irregular surfaces in detail, as the ones created by erosional processes resultant from channel incision or MTDs. In such cases, a spacing of 2 to 5 lines was used. The manually mapped grid was then used as the seed point for automated horizon tracking. This consists in a series of algorithm operations that automatically attempt to identify the seismic events with phase and amplitude identical to the manually interpreted network of seed points. The final auto-tracked horizon was checked and edited to correct any erroneous data (see Hart, 1999). Alternatively, interpretation interpolation can be used in complex surfaces where autotracking is not suitable. This operation is simpler and is based on a direct connection between the seed points, disregarding any phase or amplitude properties. Consequently, manual horizon picks must be closely spaced (2 to 5 lines) in order to obtain an adequate representation of the subsurface reflector.



### 3.1.2.1. Interpretation of seismic facies

The interpretation of the stratigraphic features on the 3D seismic data is based on the grouping of reflections with similar character. By analysing the reflection termination patterns and their continuity it is possible to delimit the discontinuities bounding individual seismic sequences and facies, which provide good indicators of the depositional processes that occurred in the studied basins (Mitchum et al., 1977). Thus, each of the stratigraphic features studied in this thesis can be recognized on 3D seismic data characteristic reflection geometries associated to each seismic facies (Figs. 3.6 and 3.7).

Mass-Transport Deposits (MTDs) can present various types of reflection configurations on 3D seismic data, bounded by top and base surfaces. Regardless of their internal character, MTDs are underlain by a variable basal surface that can be planar, have irregular relief and/or present a stepped morphology. On map sections, these basal surfaces can show elongated scours of variable sizes (Gee et al., 2005; Weimer and Slatt, 2004). The MTD upper surface is generally irregular, but this aspect can be altered by the later erosion and reworking of sediment by channels or contour currents (Weimer and Slatt, 2004).

The seismic character MTDs is highly variable, depending of their internal stratigraphy. Mass-failures which show preservation of the internal stratigraphy are commonly described as slides (Masson et al. 2006, Weimer and Slatt, 2004). The preserved sections of strata are generally represented as remnant and rafted blocks, which on seismic data are distinguishable as laterally limited features with continuous parallel reflections (Fig. 3.6). The disaggregated material surrounding the blocks is generally represented by chaotic, discontinuous reflections of low seismic amplitude. The resolution of the seismic data is a

key factor determining the resolution of cohesive strata on slides. Outcrop-scale examples show that distinct bedding structures can still be observed within the matrix (Posamentier and Martinsen, 2001; Spence and Tucker, 1997), but these would not be possible to identify on a seismic-scale analysis. Slumps are identified by seismic facies that exhibit a relative preservation of the seismic reflections with associated faulting and folding, especially at the toe areas of MTDs (Bull et al., 2009; Frey-Martínez et al., 2006) (Fig. 3.6). Slump facies commonly exhibits moderate to high-amplitude reflections, which facilitates their recognition on the seismic data. Outcrop-scale examples of slumps commonly mimic the features observed on the seismic data. Debris-flows represent the mass-failures with the highest internal disaggregation, with little or no preservation of internal structures. On seismic data, these are identified as seismic packages of low to moderate amplitude with a generally uniform character, with no resolvable internal stratification (Masson et al., 2006; Posamentier and Walker, 2006). Outcrop examples of debris-flows are also characterised by the lack of internal stratification (Posamentier and Walker, 2006) (Fig. 3.6).

Submarine canyons and channels are identified on seismic data by identifying V or U shaped erosional features (Mayall et al., 2006; Mitchum et al., 1977). The seismic facies of channel-fill deposits can be varied, but these are commonly characterised as moderate to high-amplitude reflections that onlap onto the channel margins (Abreu et al., 2003; Clark and Cartwright, 2001; Mayall et al., 2006; Weimer and Slatt, 2004). (Fig. 3.7) Channel overbank deposits typically exhibit lower amplitudes, associated with the deposition of finer sediments (Deptuck et al., 2003; Mayall et al., 2006). Turbidites deposited in submarine lobes and fans are, on seismic data, recognised by packages of laterally continuous, generally high amplitude reflections (Fig. 3.7). The termination of seismic packages

representative of such deposits can be marked either by lateral thinning and pinch-out, or have abrupt terminations resultant from interactions with structures or erosive flows (MTDs) (Weimer and Slatt, 2004).

Fine grained sediments deposited on continental slopes, commonly correspondent to hemipelagites and contourites, are characterised by seismic facies with laterally continuous, parallel to sub-parallel reflections with low to moderate amplitudes (Fig. 3.8). Hemipelagites tend to form deposits of relatively uniform thickness and high lateral extents that drape pre-existing morphologies (Stow, 2006; Stow et al., 1984). Contourite deposits present identical amplitude features, but have characteristic mounded geometries (Hernández-Molina et al., 2008). Steeper angles and/or truncation of the reflectors and thicker accumulations are commonly observed closer to the focus of the current (Fig. 3.7.)

### 3.1.3. Seismic Attributes

The use of seismic attributes is of great value when interpreting 3D seismic data as they provide increased detail of the stratigraphic and structural. Several types of attributes are available in interpretation software packages. Attributes used in this thesis include time-dip, amplitude and coherence. The **time-dip** magnitude is a time-derived attribute that measures the horizon gradient changes by comparing the time value between adjacent points. The resultant dip maps are good indicators of the seismic horizon morphology, often highlighting subtle features at the limit of seismic resolution. The detailed morphology provided by time-dip maps also aids on the data acquisition from the horizons of interest.



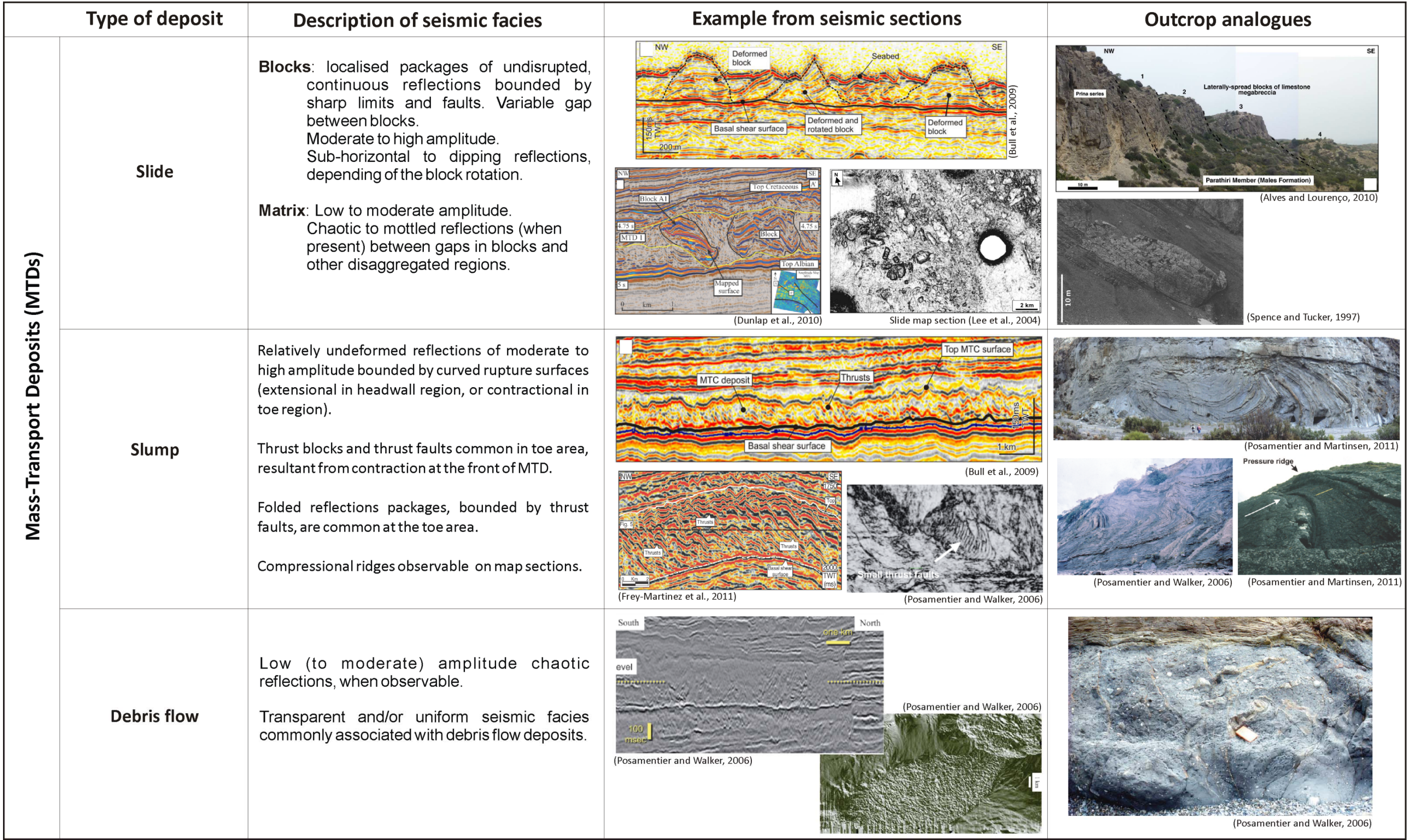


Figure 3.6. Diagram presenting the different seismic facies associated with Mass-Transport Deposits (MTDs). Comparative outcrop-scale examples of the correspondent seismic facies are also shown.



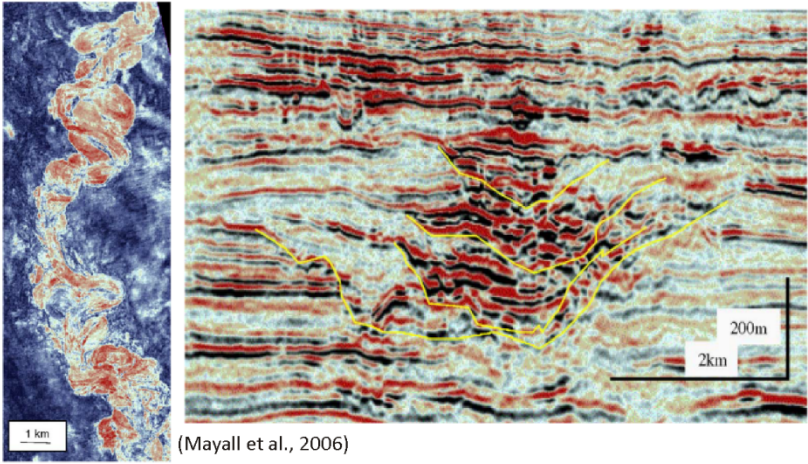
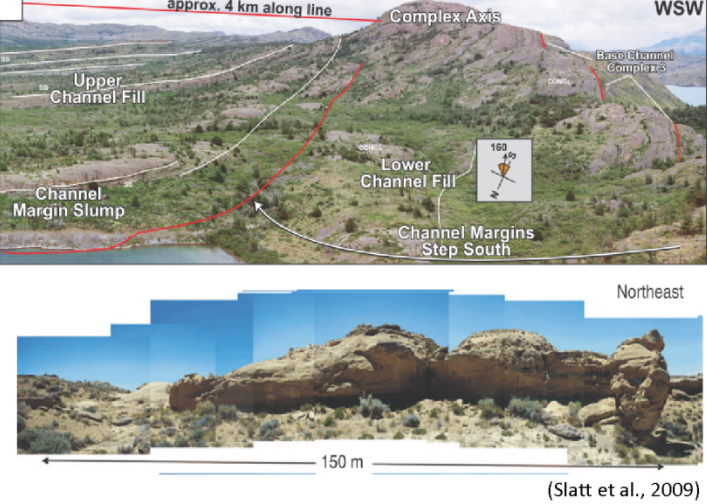
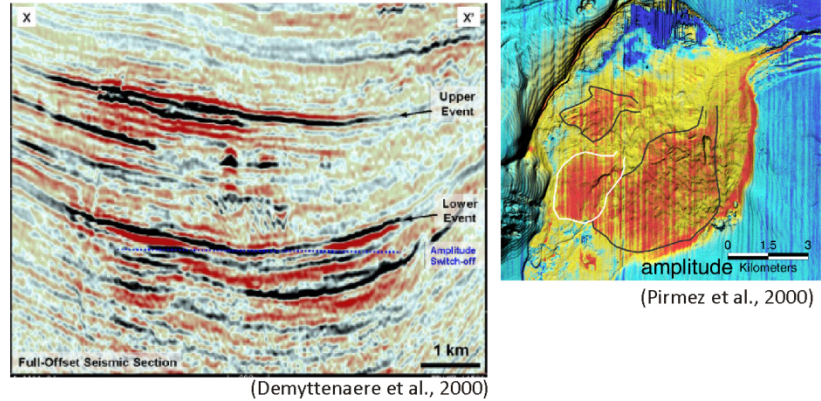
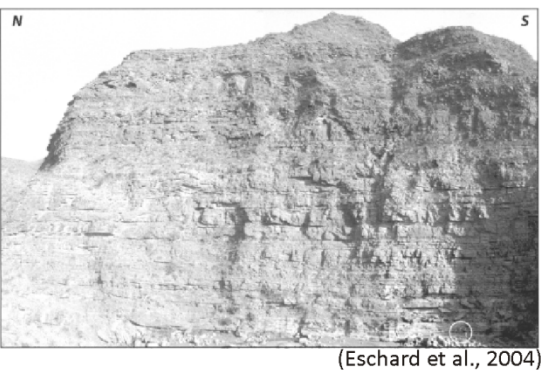
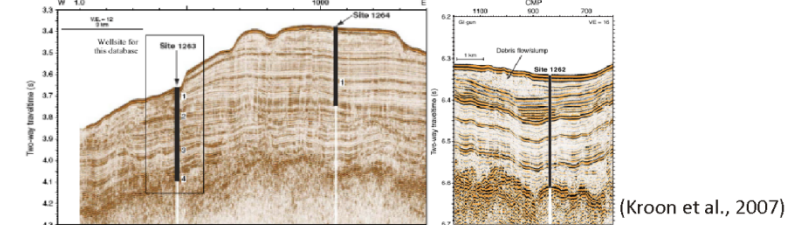

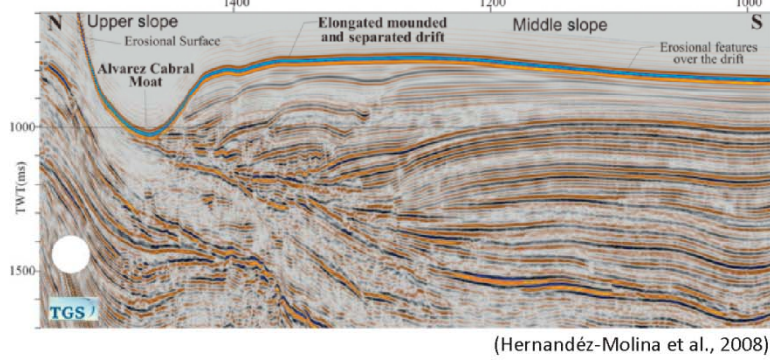
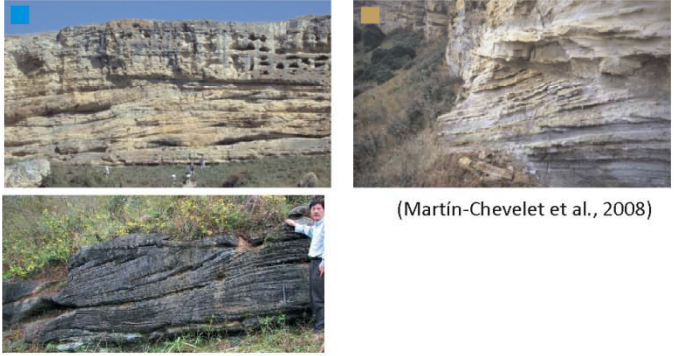
Type of deposit		Description of seismic facies	Example from seismic data	Outcrop analogues
Channels and Turbidites	Canyons and Channels	<p>Negative relief features when observed in vertical seismic profiles.</p> <p>Channel-fill deposits commonly represented by moderate to very high amplitude reflections, which contrast with lower reflection strength of overbank deposits</p> <p>A variety of geometries: lateral accretion packages, offset patterns, aggradational fill. Hierarchical organisation of single channels in higher complexity complexes.</p> <p>Variable geometry on attribute maps, from straight to high sinuous.</p>	 <p>(Mayall et al., 2006)</p>	 <p>(Beaubouef, 2004)</p> <p>(Slatt et al., 2009)</p>
	Turbidite Fans	<p>One to multiple reflections with good lateral continuity.</p> <p>Moderate to high amplitude reflections.</p> <p>Terminate laterally against the edge of the basin, or local topographic features. Lateral limits may also correspond to bed thinning beneath the resolution of the seismic data.</p>	 <p>(Demyttenaere et al., 2000)</p> <p>(Pirmez et al., 2000)</p>	 <p>(Eschard et al., 2004)</p>
Fine-grained sediments	Hemipelagites	<p>Sub-parallel laterally continuous reflections with general low amplitude.</p> <p>Seismic-stratigraphic intervals with relatively uniform thickness resultant from draping of paleo-seafloor.</p>	 <p>(Kroon et al., 2007)</p>	 <p>(Stow et al., 1984)</p>
	Contourites	<p>Low to moderate amplitude relatively continuous reflections, but chaotic and discontinuous ones may also occur. Wavy reflectors and migrating sediment waves common.</p> <p>Sheeted or mounded, lens-shaped and concave upward geometries. Thicker accumulations and steeper reflection dip are common adjacent to a erosive moat.</p>	 <p>(Hernández-Molina et al., 2008)</p>	 <p>(Martin-Chevelet et al., 2008)</p>

Figure 3.7. Diagram representing non-MTD seismic facies associated with turbidite deposits (submarine channels and turbidite fans) and fine grained sediments (hemipelagites and contourites)

Seismic **amplitude** is a fundamental attribute used in this research, and it represents the positive or negative value measured at the crest of the reflection wavelet. On map view, the horizon amplitude patterns are prone to change due to lateral variations in acoustic impedance, which are ultimately related to changes in the lithological properties or fluid content along the horizon (Brown, 2004). Amplitude maps are extremely useful not only to identify the extent of stratigraphic facies variations caused by the presence of channels or mass-wasting deposits, but also to detect the distribution of faults (Brown, 2004). **Root Mean Square (RMS) amplitude** is a key attribute that shows the average squared amplitude values from individual amplitude samples within a defined time interval, which can be variably defined (Brown, 2004). A common method is to extract arbitrary time windows, often between 20 to 50 ms TWTT, above or below a reference horizon within the stratigraphic interval of interest. Alternatively, it can be defined between two reference horizons, as for example the mapped top and base of a submarine landslide or channel complex. This has the advantage of constraining the amplitude analysis to the delimited interval, without the interference of outside values.

**Coherence** is an attribute calculated by comparing the similarity between adjacent waveforms in a volume of continuity (normal reflections), converting it into a volume of discontinuity. The generated time-sliced volumes have the capacity to evidence geological discontinuities in map sections, such as faults or stratigraphic discontinuities, and are often free of interpretation bias as the use of mapped horizons is not a requirement (Brown, 2004). The coherence volumes can also be computed and sliced using a flattened interpreted horizon as a reference. This has the advantage that all the features identified in the coherence slices are guaranteed to be at identical time gaps from the fixed datum,



limiting the crossing of stratigraphic boundaries. Coherence volumes are particularly used to assess the internal architecture of the stratigraphic features identified in the seismic data.

The use of the attributes described above can be also complemented by **isochron maps**, which illustrate the time difference between the two reference horizons, providing detailed information on the thickness and lateral extent of the analysed sedimentary deposits. The combined use of attribute maps and interpretation of the geological processes is the base of seismic geomorphology, an analysis method based on the use high-resolution 3D seismic data and a valuable tool to understand the deep marine systems (Posamentier et al., 2007; Posamentier and Kolla, 2003).

#### 3.1.4 3D seismic survey parameters and time-depth conversions

The seismic volume used in this thesis covers an area of 1600 km<sup>2</sup> in the Espírito Santo basin, SE Brazil, in water depths ranging from 100 to 1800 m. The vertical extent of the survey is limited to a time depth of 4 seconds TWTT, into the top of the salt succession. Data were acquired using a dual airgun array and six, 5,700 m long streamers. Signal was sampled at 2 ms with a grid-line spacing of 12.5 m. The data were zero-phased migrated and in SEG normal polarity, i.e. increased in acoustic impedance are represented by positive amplitude reflections.

Time conversions in the specific studied intervals were estimated using the velocity profiles obtained at DSDP site 516 (Barker et al., 1983). In general, seismic velocities of 1700 m/s were used for sub-unit 3c and of 1800 m/s for sub-units 3a and 3b analysed in Chapter 6, of 2100 m/s for Unit 2 (Chapter 4) and 3100 m/s for strata at the top of Unit 1 (Chapter 5). Based on these velocities and using a computed dominant frequency of 40Hz, it is

possible to estimate the vertical resolution of the seismic data. The seismic velocity ( $v$ ) is a function of the frequency ( $f$ ) and wavelength ( $\lambda$ ), such that:

$$v = f \cdot \lambda \quad (\text{eq. 3.3})$$

As the velocity and frequency are known, it is possible to calculate the value of seismic wavelength for different depth intervals using Equation 3.1. Considering that the limit of visibility is about  $\frac{1}{4}$  of  $\lambda$  (Sheriff and Geldart, 1995; Veeken, 2007), vertical resolutions of circa 11 metres are estimated for the shallower stratigraphic levels and of 19 metres for the deeper levels in Unit 2. Considering the horizontal resolution of the seismic data, an error of 12.5 m and 0.000156 Km<sup>2</sup> is estimated for measured distances and areas, respectively.

### 3.2. Quantitative seismic analysis

A significant part of this thesis presents quantitative data for key geological features identified in the study area. Quantitative data were acquired using vertical seismic sections to assess the TWTT thickness of relevant features. To convert the time depth to true depth, first it is necessary to divide the measured time thicknesses by two, in order to obtain only the one-way time travel distance, in seconds, of the relevant geological feature. The following step consists on the multiplication of the one-way time by the velocity estimated for the stratigraphic interval of interest. The width of the studied geological features was assessed in vertical sections by multiplying the number of traces covered by the trace distance, i.e. 12.5 m. Attribute maps were used to measure the width and length, area and perimeter of the geological features of interest.



Different quantification methods were used specifically for each chapter. In Chapter 4 the study area was divided into four sub-areas, A1 to A4 (Fig. 4.1). Sub-area A1 is located at the upper slope of the Espírito Santo Basin, followed by areas A2, A3 and A4 towards the distal slope. Several measurement points, separated 1000 m and 2075 m across and along slope respectively, were defined in each sub-area to measure the thickness of MTD intervals. The collected data were used to produce various statistical plots representative of the MTDs along and across slope variations in thickness and volume. In Chapter 5, a basal MTD in Unit 2 was subdivided into three sub-regions - zone 1, zone 2 and zone 3 -, based on its relative position on the studied slope (Figure 5.1). In this chapter, the quantitative analysis focused on the morphometric properties of rafted and remnant blocks in this basal MTD. Their dimensions were measured using RMS amplitude maps. Linear regressions, when computed, were tested using residuals plots (Seber and Lee, 2003). Residuals plots are important to test how reliably a model captures the behaviour of sampled points of data (Jensen et al., 2007). In Chapter 6, the study area was sub-divided in three sub-areas, depending on the degree of confinement imposed by topography on submarine channels. A new method was devised, based on the systematic identification of channel features in successive vertical sections, followed by a spatial analysis of channel distribution. A detailed description of this method can be found in Chapter 6.

### **3.2.1. Spatial Statistics**

Spatial statistical tests were used in Chapter 6 in order to analyse the distribution patterns of the channel data. These consisted in Chi-Square tests to assess the spatial

uniformity of the data (Fig. 3.8a). The goodness-of-fit test was also used to compare the observed data with Poisson and Negative Binomial distribution models.

The **chi-square** statistic evaluates the difference between the observed and expected frequencies in each cell scaled by the expected frequency. The latter is obtained by dividing the total number of points by the number of cells. The chi-square test ( $\chi^2$ ) analyses the goodness of fit of the observed distribution to the expected uniform distribution, given by:

$$\chi^2 = \sum_{i=1}^k \frac{(O_i - E)^2}{E_i} \quad (\text{eq. 3.4})$$

Where  $O_i$  is the observed numbers of points in cell  $i$ , and  $E$  is the expected number of points (Cochran, 1952; Davis, 2002). This test is a variable with  $K-2$  degrees of freedom ( $df$ ), where  $K$  is the number of estimated parameters defining the theoretical distribution (Haschenburger and Spinelli, 2005).

A modified **Poisson** distribution (Davis, 2002) was used to test the randomness of the CP spatial distribution (Fig. 3.8b). This modified distribution analyses the density of CP in the full area to predict the probability of occurrence of  $x$  channel points per cell, calculated by

$$P(x) = e^{(-\lambda A)} \frac{(\lambda A)^x}{x!} \quad (\text{eq. 3.5})$$

where  $\lambda$  is the calculated channel point density (obtained by dividing the total number of CP,  $m$  by the total area,  $a$ ),  $x$  the number of channel points and  $A$  the area of each cell. The following step tested the goodness-of-fit of the expected Poisson model with the observed results using the chi-square test. The expected frequency for this test is obtained by

multiplying the Poisson probability by the number of cells,  $T$ . The parameters used for the Poisson model were also used to calculate the variance in CP per cell,  $s^2$ , given by

$$s^2 = \frac{\sum_{i=1}^T (x_i - m/T)^2}{T-1} \quad (\text{eq. 3.6})$$

A third test was applied to model the clustering of CP (Fig. 3.8c) in the area using a **negative binomial distribution**. In this test we consider the number of CP per cell ( $x$ ), the probability of occurrence of a CP in a cell ( $p$ ) and the degree of clustering of the data ( $k$ ) (Davis, 2002). The latter parameter is estimated by

$$k = \frac{(m/T)^2}{s^2 - (m/T)} \quad (\text{eq. 3.7})$$

Knowing  $k$ , the probability  $p$  is calculated by

$$p = \frac{(m/T)}{k} \quad (\text{eq. 3.8})$$

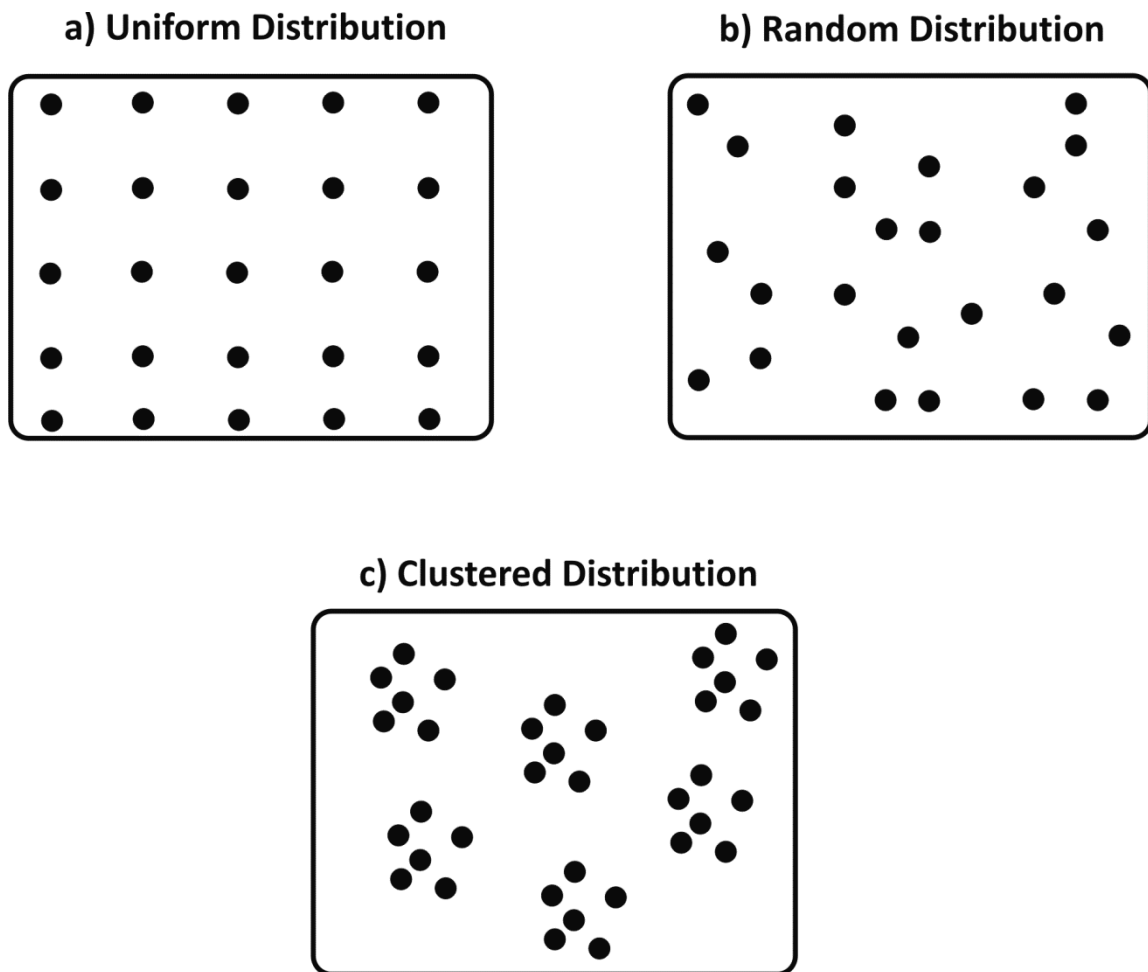
The probability of occurrence of  $r$  CP per cell is given by

$$P(0) = \frac{1}{(1+p)^k} \quad (\text{eq. 3.9})$$

and

$$P(r) = \frac{(k+r-1) \left(\frac{p}{1-p}\right)}{r} P(r-1) \quad (\text{eq. 3.10})$$

The estimated number of CP per cell is obtained by multiplying the probabilities of occurrence obtained by the number of cells. The goodness-of-fit of the binomial model to the observed results was tested using the chi-square test.



**Figure 3.8.** Representation of spatial distribution patterns. (a) Uniform distribution. (b) Random distribution. (c) Clustered distribution.

# Chapter 4

## MTD on the Espírito Santo Basin during the Palaeogene

This chapter has been published as “Gamboa, D., Alves, T., Cartwright, J., and Terrinha, P., 2010, MTD distribution on a 'passive' continental margin: The Espírito Santo Basin (SE Brazil) during the Palaeogene: *Marine and Petroleum Geology*, v. 27, p. 1311-1324.”

Note that Figure 4.10 and associated descriptive paragraphs of amplitude patterns within turbidite intervals (page X to X) are additions in the chapter in relation to the published manuscript.

## 4. MTD Distribution on the Espírito Santo Basin during the Palaeogene

### 4.1. Abstract

Mass-wasting on the Brazilian margin during the Mid-Eocene/Oligocene resulted in the accumulation of recurrent Mass Transport Deposits (MTDs) offshore Espírito Santo, SE Brazil. This chapter focuses on the characterization of a succession with stacked MTDs (Abrolhos Formation), and on the assessment of the distribution of undeformed stratigraphic packages (i.e. turbidites) with reservoir potential separating the interpreted MTDs. High-amplitude strata in less deformed areas of MTDs reflect their internal heterogeneity, as well as possible regions with a higher sand content. Separating MTDs, turbiditic intervals reach 100ms Two-Way Travel Time (TWTT), with thicker areas coincident with the flanks of growing diapirs and areas of the basin where mass-wasting is less apparent. Turbiditic strata laterally grade into, or are eroded by MTDs, with the transitional strata also influenced by the presence of diapirs. MTDs show average thickness values between 58 and 82 ms TWTT and constitute over 50% of Eocene-Oligocene strata along the basin slope. Low average accumulations of 58 ms TWTT in areas of high confinement imposed by diapirs suggest sediment accumulation upslope, and/or bypass into downslope areas. The results suggest that significant amounts of sediment derive from the northwest, and were accumulated in the middle-slope region. Interpretations of (palaeo)-slope profiles led to the establishment of a model of margin progradation by deposition of MTDs, contrasting with the retrogressive erosional margins commonly associated with these settings. This character was induced by the high sediment input into the basin associated with coastal erosion and growth of the Abrolhos volcanic plateau.

## 4.2. Introduction

Submarine mass-wasting is one of the geological processes responsible for the transfer of large amounts of sediment onto the deeper parts of continental margins (e.g. Bull et al., 2009; Frey-Martinez et al., 2005; Gee et al., 2006; Masson et al., 2006; Shipp et al., 2004). Resulting strata, commonly termed as Mass Transport Deposits (MTDs)- play an important role in shaping the seafloor (e.g. Gee et al., 2006; Moraes et al., 2007; Moscardelli et al., 2006; Moscardelli and Woods, 2008). Newly deposited MTDs can infill seafloor depressions or, instead, create new bathymetric relief that will influence later sediment distribution in a basin, controlling the geometry and lateral continuity of reservoir lithologies and stratigraphic traps (Armitage et al., 2009; Moscardelli et al., 2006; Posamentier and Kolla, 2003).

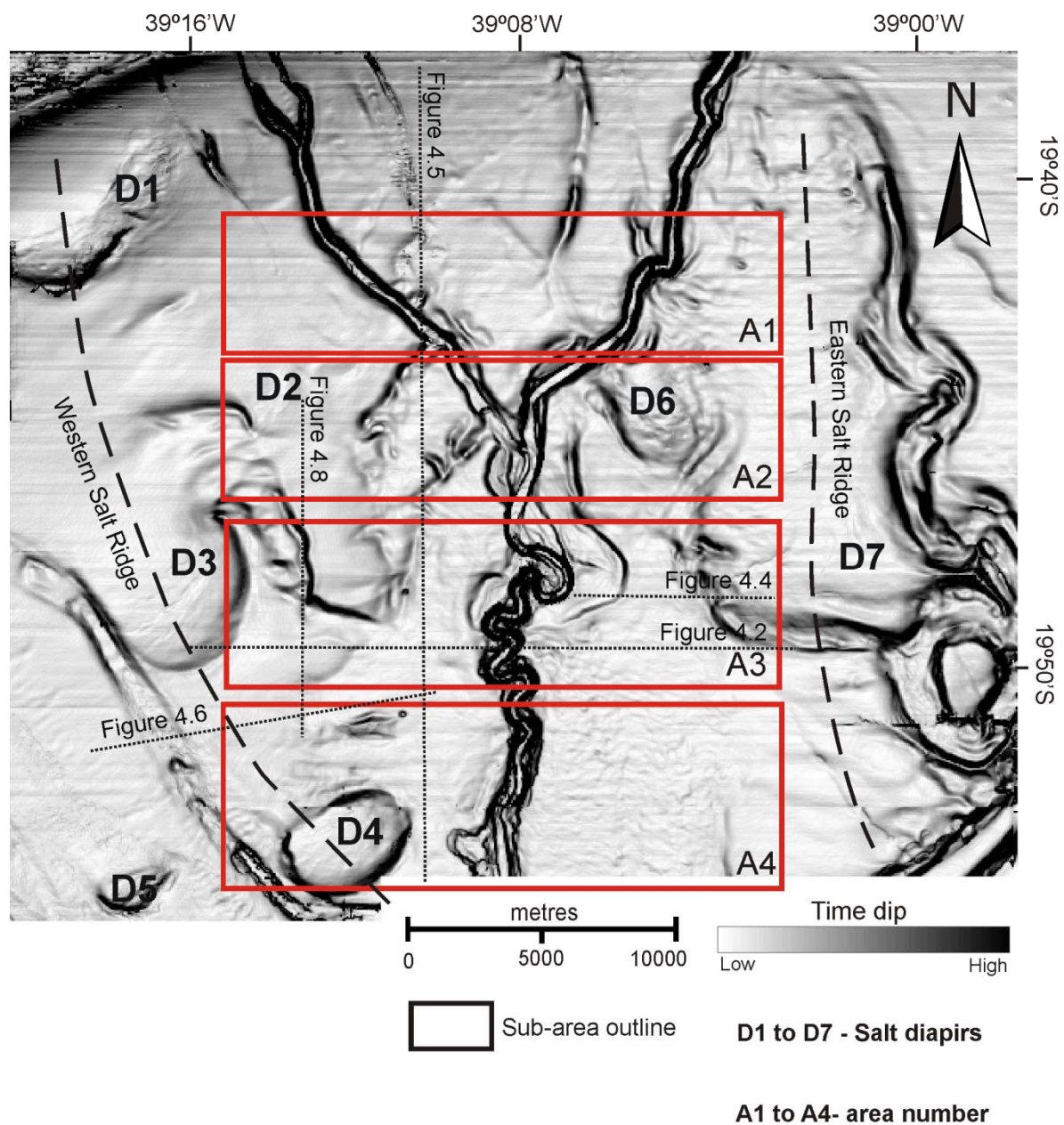
As hydrocarbon exploration moves towards deep and ultra-deep offshore basins, it is important to understand the controls mass-wasting strata can have on reservoir distribution (e.g. Jackson et al, 2010; Welbon et al., 2007). Due to the predominant mud-rich nature of MTDs, these are normally considered to have poor reservoir potential, often forming competent seal units (Moscardelli et al., 2006; Moscardelli and Wood, 2008; Posamentier, 2004; Prather, 2003). However, other lithologies are frequent within MTDs. For instance, there are cases of MTDs in the North Sea that are mostly composed of sand (Shanmugam et al., 1996) or chalk deposits (Davison, 2004), both cases presenting permeable strata with the potential to form reservoir units.

Knowing this, 3D seismic data has been useful for the identification of MTDs in hydrocarbon-rich areas as the Gulf of Mexico (e.g. Beaubouef and Abreu, 2010; Booth et al., 2003; Prather et al., 1998; Sawyer et al., 2007; Winker and Booth, 2000), West Africa (Deptuck et al., 2007; Gee et al., 2006; Heinio and Davies, 2006; Lee et al., 2004) or Brazil (Alves, 2010; Silva et al., 2010). Characterizing the limits (lateral and vertical) between stratified units and MTDs, and their relation to underlying structures, can provide insights of the distribution and compartmentalization of reservoir-prone lithologies.

This chapter aims to demonstrate the importance of mass failure processes in the construction of passive margins, and to show how resulting deposits may form critical components of reservoir plays. On the well documented Campos basin, Eocene strata similar to those in this study consists of an alternation of turbidite flows, mass-wasting and bottom-current reworked deposits that led to the development of lensoid sandy reservoirs confined by MTDs (Moraes et al., 2007). Reservoirs in the Campos Basin have very immature lithologies, reflecting a tectonically-active setting from where the sediments are derived (Fetter et al., 2009). The aim is to identify the distribution of sand prone strata in similar MTD-rich units and the control of adjacent salt structures on their deposition, also evidencing that mass-wasting in the Espírito Santo Basin led to margin growth and progradation during the Eocene-Oligocene.

The chapter focuses on a description of the seismic character and relevant features of the studied MTD succession, herein named Abrolhos Unit, by comparing two selected intervals, and by highlighting depositional changes using isochron maps and computed seismic attributes such as RMS amplitude and coherence volumes.





**Figure 4.1.** Sea-bed dip map of the 3-D seismic survey. Defined sub-areas are outlined and labelled A1 to A4. D1 to D7: Salt diapirs.

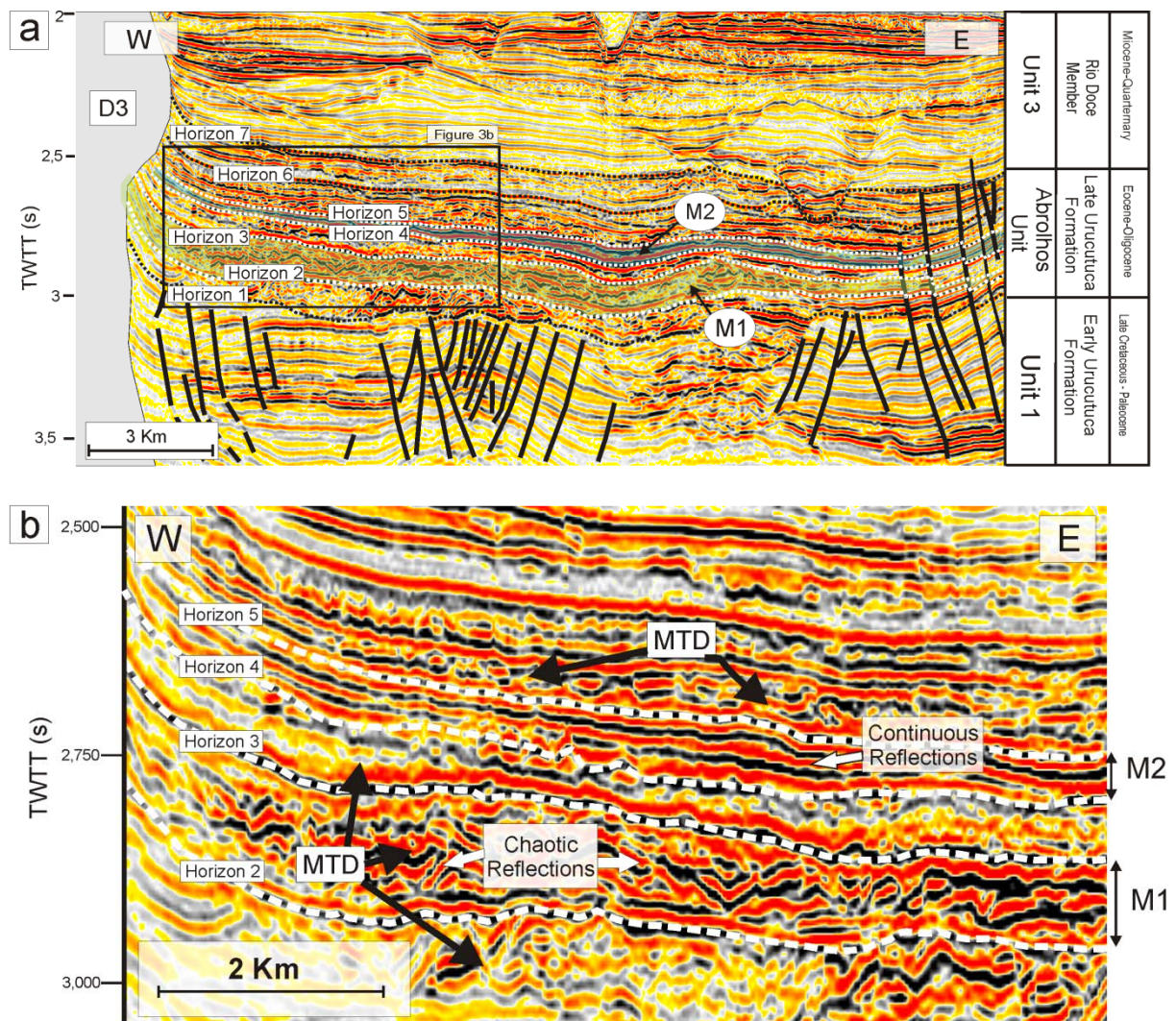
This approach is complemented by a quantitative study of along- and across-slope topographic and thickness variations in the Abrolhos Unit and by an analysis of paleo-slope curvatures of different horizons. In the discussion section, seismic facies changes related to adjacent diapir growth are discussed, as well as the control of MTDs in margin growth in the Espírito Santo Basin during the Palaeogene.

### **4.3. Results and observations**

This chapter focuses on the analysis of Unit 2, also named as the Abrolhos Unit (Fig. 4.2). The chaotic and/or transparent reflections comprise mass-transport deposits. The unit tends to thin towards downslope areas, and its base correlates with a mid-Eocene erosional surface (Fiduk et al., 2004). The higher amplitude of this unit is, according to Fiduk et al. (2004), due to the high supply of volcanoclastic material derived from the Abrolhos Plateau.

#### **4.3.1- Description of MTD intervals**

The interpretation of the several MTD intervals followed previously-established criteria, helping the identification of packages of chaotic and/or disrupted strata (e.g. Bull et al., 2009; Frey-Martinez et al., 2006; Hampton et al., 1996; Sangree and Widmier, 1977). Less chaotic MTDs were characterised by imbricated internal reflections (Frey-Martinez et al., 2006). Selected reflections on vertical seismic sections were interpreted as main boundaries of MTD intervals. The basal surface was identified as coinciding with a laterally continuous reflection that underlies chaotic reflections within MTDs (see Frey-Martinez et



**Figure 4.2.** a) Seismic section across slope representing the character of stratigraphic units. Note the faults in Unit 1 limited at the base of the Abrolhos Unit. Horizon1 to Horizon 7 represent interpreted horizons bounding defined intervals. b) Detail of seismic section to highlight the chaotic character of interval M1 and the continuous reflections of interval M2.

al., 2006). The top of the MTDs is commonly a hummocky surface covering the disrupted reflections (Sangree and Widmier, 1977). The evaluation of the stratigraphic variability within the Abrolhos Unit was made by describing two distinct intervals: M1 represents an MTD, and M2 consists of a possible sand-rich interval (Fig. 4.2). Interval M2 represents uniform, continuous poorly deformed or undeformed lithologies, whereas interval M1 represents incoherent, discontinuous MTDs.

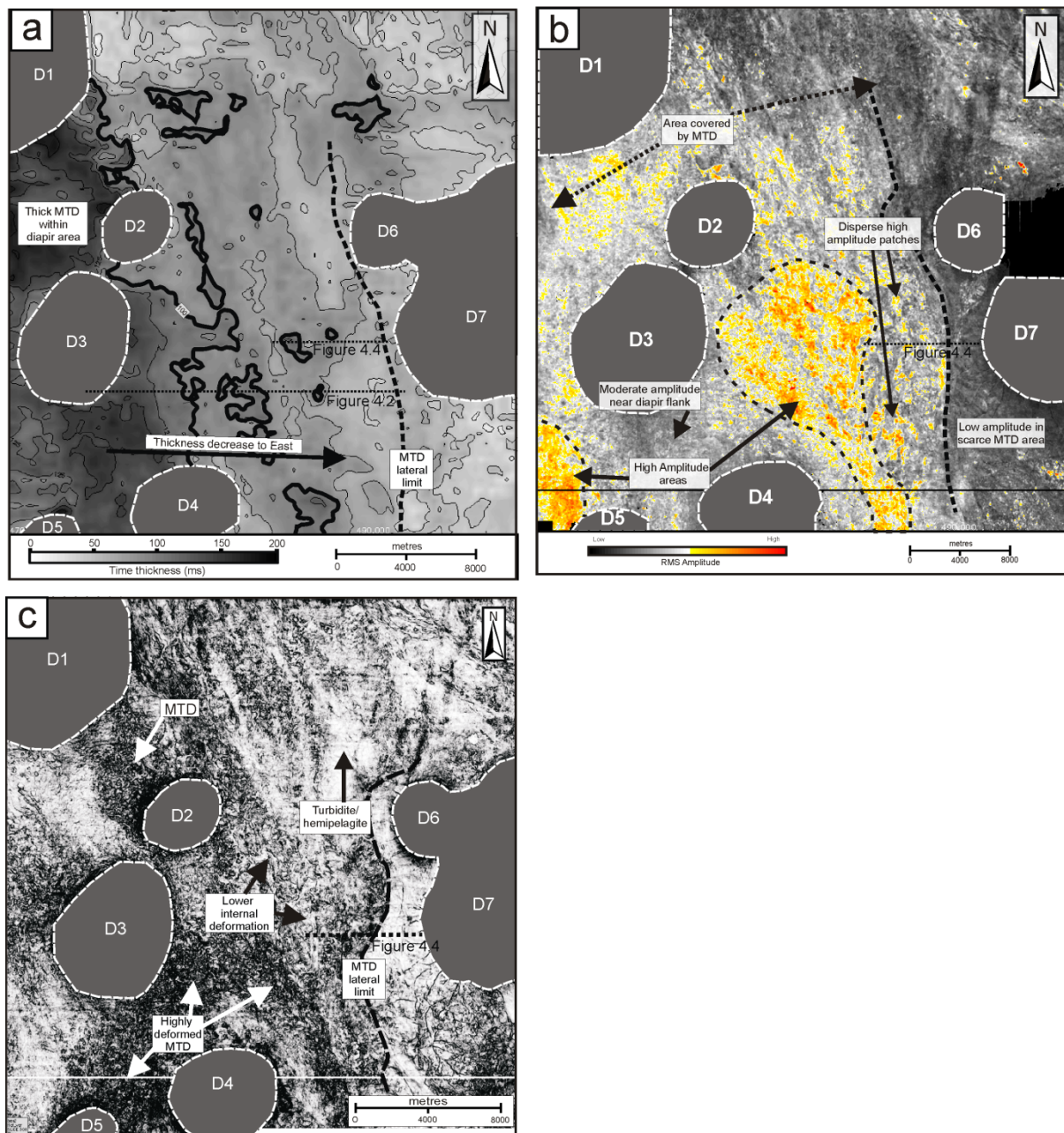
#### **4.3.1.1- Interval M1**

Interval M1 is delimited by Horizon 2 and Horizon 3. It shows chaotic and disrupted reflections on key seismic profiles (Fig. 4.2), which are clearly imaged due to their high amplitudes. Computed attribute maps for this interval are displayed in Figure 4.3.

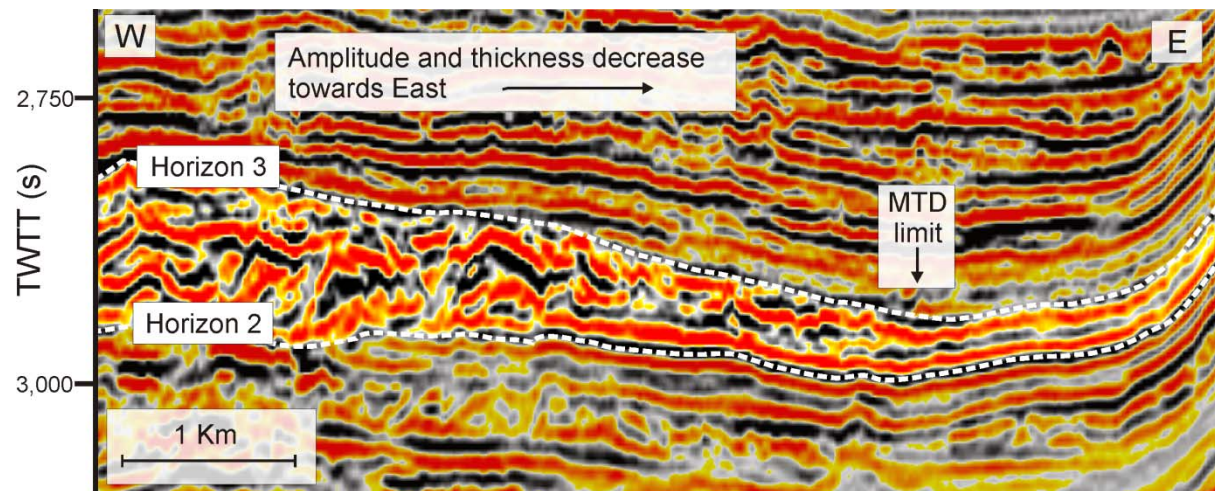
Isochron data for interval M1 show a decrease in thickness from West to East (Fig. 4.3). The largest thickness values sediment accumulations are located around diapirs D1, D2 and D3, where they reach up to 200 ms TWTT. In contrast, thin accumulations of sediment are found on the eastern limit of interval M1 with values around or below 50 ms TWTT (Figs. 4.3a and 4.4).

Lateral lithological variations were assessed using RMS amplitude maps (Fig. 4.3b). Moderate- to high-amplitude regions predominate in interval M1, with the areas with the highest amplitude found in two clusters bordering the western salt structures. In contrast, low amplitude regions are observed surrounding diapirs D6 and D7. These low amplitude areas are also coincident with the section where the thinnest (<50 ms TWTT) sediment accumulations are observed, marking the lateral limit of the MTD (Figs. 4.3a and 4.4). The





**Figure 4.3.** Attribute maps for interval M1. **a)** Isochron map of interval M1, predominantly consisting in MTDs. Note the high thickness over 100 ms TWTT in the western diapir area, represented by dark colours. Thickness of the interval gradually decreases towards the MTD limit close to the eastern salt diapirs to values below 50 ms TWTT. Contour spacing is 25 ms twtt. **b)** RMS amplitude map for interval M1. Moderate amplitudes characterize the MTDs. High amplitudes are seen in the central area of the basin, gradually decreasing to the east. Note the amplitude contrast on both flanks of diapir D3. **c)** Coherence slice across interval M1. The dark irregular patterns represent chaotic MTDs. Light colours represent lower deformation. Note the varied coherence patterns for the MTD. MTD lateral limit is marked by intersection of the coherence slice with an underlying less deformed interval.



**Figure 4.4.** Seismic section representative of the eastward thickness decrease of the MTD defined by interval M1. The overall decrease of amplitude and chaotic character of the seismic reflections follows the MTD thinning towards the salt diapirs on the Eastern section

coherence slice in Fig. 4.3c highlights the lateral heterogeneity of interval M1 shown in RMS amplitude maps. Contrasting coherence values are seen in the study area. Low coherence areas, representative of regions of larger MTD deformation, are found in the rims of diapirs, with the most significant areas located between D3 and D4. These higher deformation areas are prone in chaotic reflections (Figs. 4.2b, 4.3c and 4.4), and laterally grade into less deformed regions with larger values of coherence. This change is also coincident with a lateral increase in amplitude, as pointed out by the high-amplitude areas indicated in Figure 4.3b.

#### **4.3.1.2- Interval M2**

Interval M2 contrasts with M1 in several aspects. It occurs roughly in the middle of the Abrolhos Unit, being bounded by Horizon 4 and Horizon 5 (Figs. 4.2 and 4.5). In key seismic profiles, internal reflections within M2 are mainly sub-parallel and continuous (Fig. 4.5a and 4.5b). They are poorly deformed, although in upslope sections disrupted reflections are more common (Fig. 4.5c). The chaotic internal reflections in this interval are mainly observed towards the southwest (Fig. 4.6). Adjacent to the MTDs, there is a gradual eastward transition into high-amplitude, continuous internal reflections (Fig. 4.6b and 4.6c). Sub-horizontal reflections with poor continuity are common in the transition area between MTDs and turbidites (Fig. 4.6).

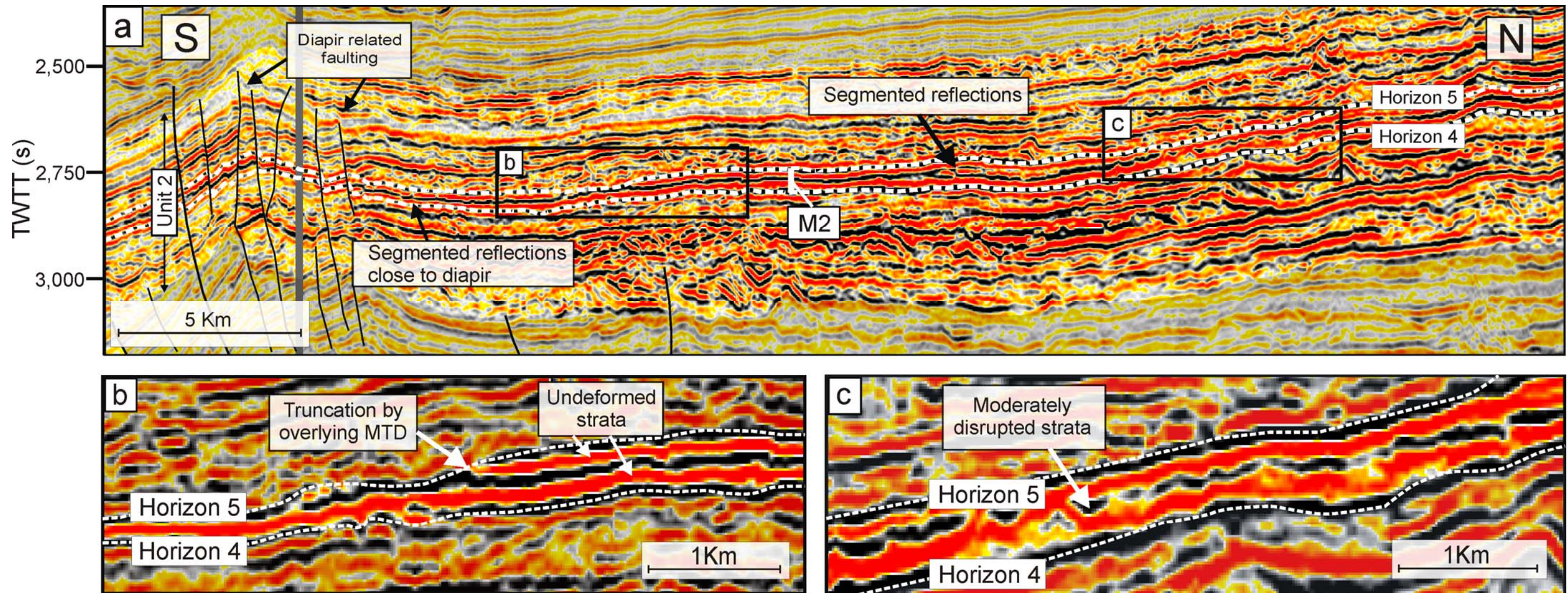
The thickness of the M2 interval is generally smaller than in M1, as shown by the isochron map (Fig. 4.7a). In M2, thicker accumulations predominate in the northwest sector of the study area, in inter-diapiric areas, suggesting predominant sediment input from the Northwest. However, M2 thins out towards the southeast, along the axis of the axial salt-

withdrawal basin. Several patches over 100 ms (TWTT) thick are found on the flanks of diapirs and in the basin axis, with two distinct patterns. On the flanks of diapirs D2 and D3 these thick patches are roughly circular, whereas within the central area they are elongated and parallel to the basin axis (Fig. 4.7a). South of diapir D3 the thickness of interval M2 is predominantly below 60 ms TWTT, coincident with MTD deposits occurring in this area (Fig. 4.6a).

The RMS amplitude map of interval M2 in Figure 8b shows an extensive NW-striking high amplitude area that stretches across most of the basin. It is relatively wider in the upslope area, surrounding diapir D2, and tends to narrow downslope. Its lateral limits are imposed by salt structures, namely diapir D4 and D7. In contrast, the upslope area is less confined by the diapirs. The extent of this high amplitude area is partially correlated with the thick sediment patch observed on the isochron map of Figure 4.7a. The area south of diapir D3 is characterized by low amplitude, increasing towards the east, concomitant with the transition from MTD strata to stratified lithologies observed on several seismic profiles (Fig. 4.6).

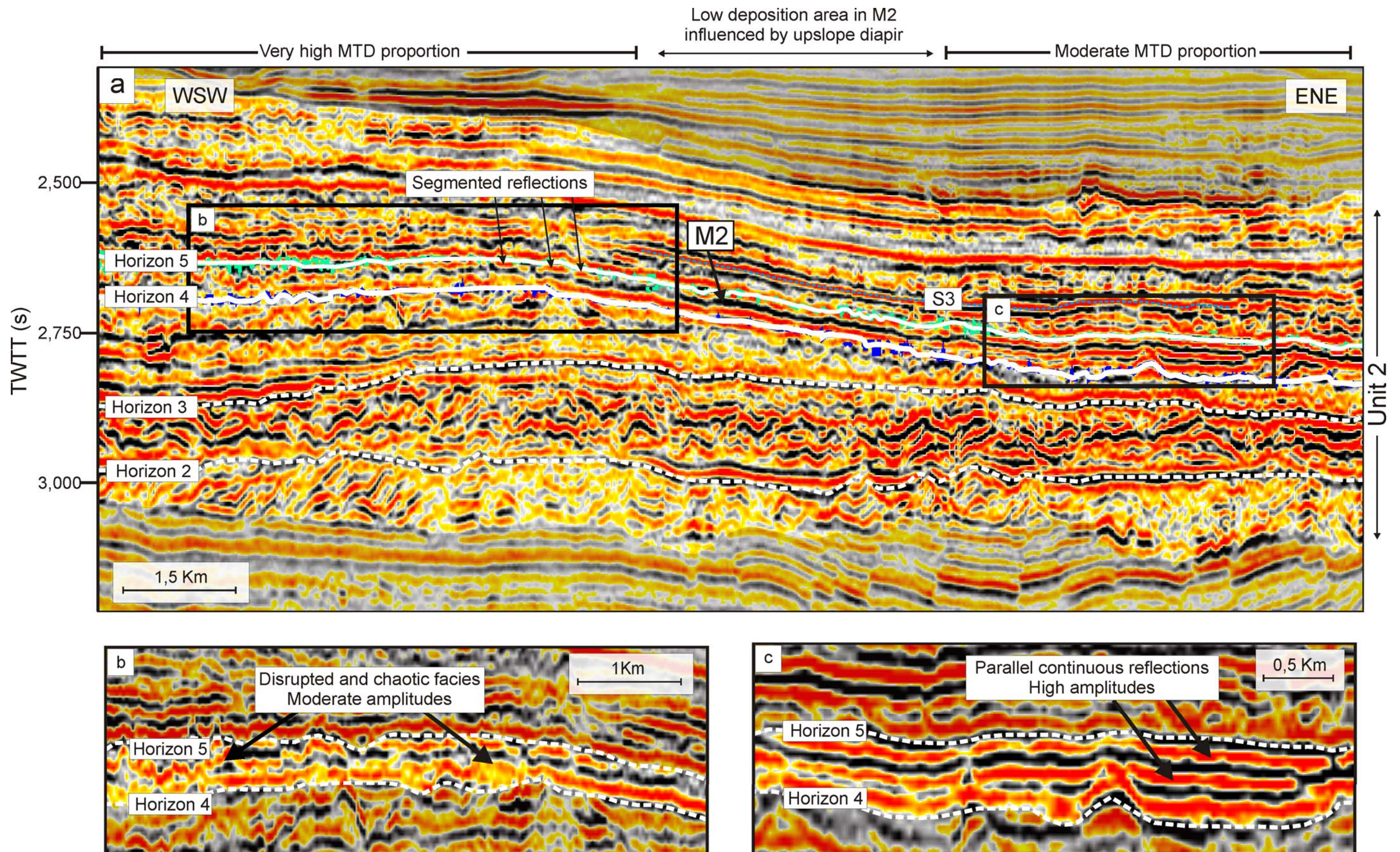
The coherence slice computed to represent this interval (Fig. 4.7c) shows that a major part of it consists of coherent, and hence less deformed, lithologies. In the centre of the salt-withdrawal basin occurs a coherent area that corresponds to continuous, stratified reflections, as seen on the seismic profiles in Figure 4.5. Lower coherence patches, characteristic of MTDs, are seen on the southern flank of diapir D3, and gradually change into regions of higher coherence towards less deformed lithologies. Within this interval there is a slump which has a different character from other MTDs seen in the Abrolhos Unit (Fig. 4.7). Instead of dark patches on coherence slices, the slump is evidenced by sharp





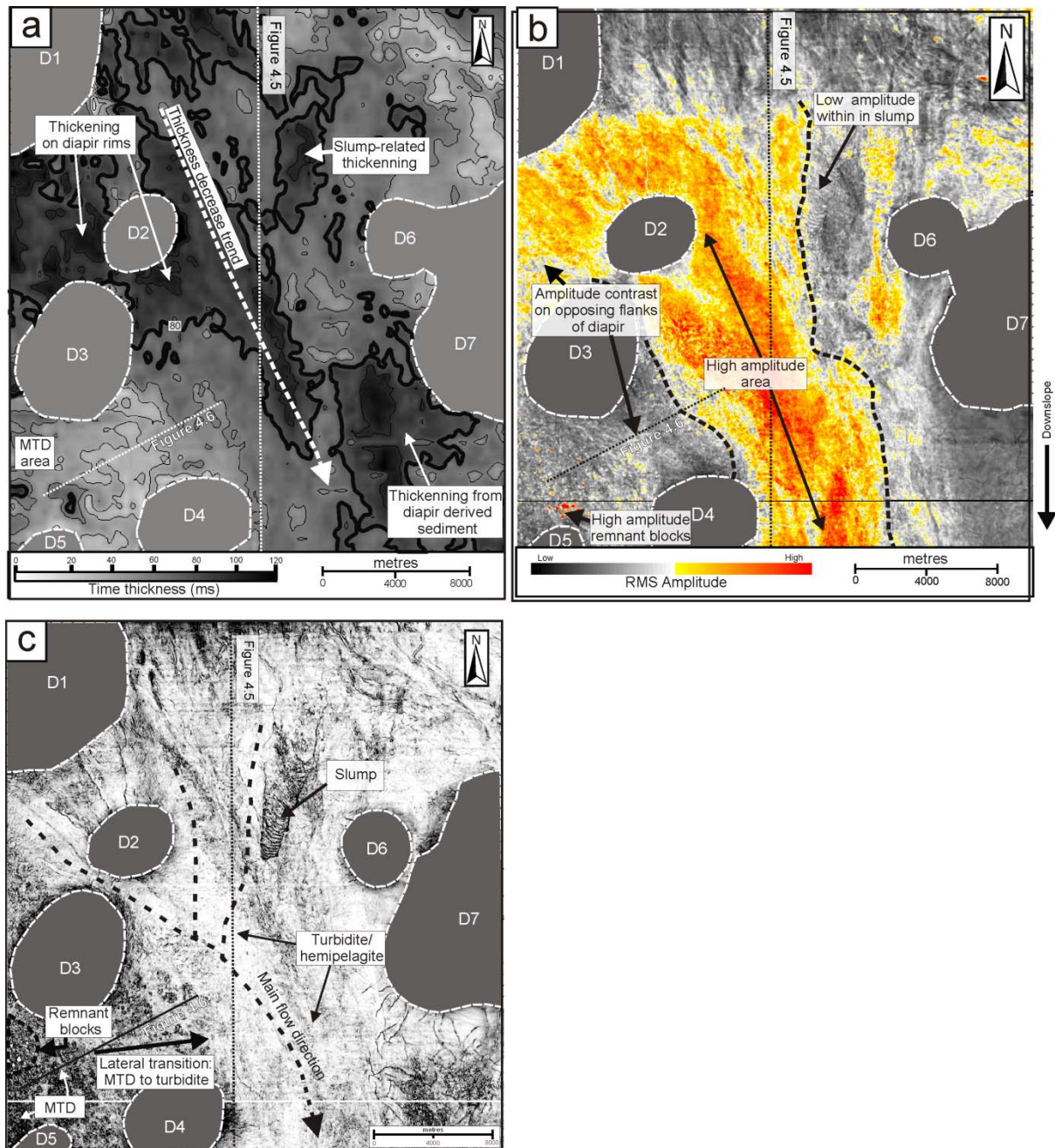
**Figure 4.5.** Vertical seismic section representative of interval M2. **a)** North-South oriented profile showing high amplitude continuous reflections of this interval. Reflector continuity is compromised close to diapir deformed areas. **b)** Detail showing the termination of continuous strata by overlying MTD flow. **c)** Detail of a section with disturbed reflectors.





**Figure 4.6.** a) Section representing the transition from MTD to continuous strata within interval M2. Note the predominant presence of MTDs in the west section of the stratigraphic succession. b) Detail of the disrupted reflections within M2. c) Detail of the continuous, less deformed strata of M2, also coincident with the thickening of the interval. Notice the segmentation of the strata on this transition area.





**Figure 4.7.** Attribute maps computed for interval M2. **a)** Isochron map for interval M2. Thicker stratigraphic accumulations over 100 ms TWTT are seen close to the diapirs and along parts of the central salt withdrawal basin. **b)** RMS amplitude map for interval M2. Very high amplitudes predominate in the centre of the basin when compared to peripheral areas. Notice the marked amplitude contrasts on the flanks of diapir D3, and the gradual amplitude decrease towards the East. **c)** Coherence slice for interval M2. Light coloured coherent patterns predominate, reflecting the continuous undeformed nature of most of its composing strata. The dark, low coherence areas correspond to areas of higher MTD deformation. Note the slump between diapirs D2 and D6, with the lateral limits and internal compression structures well evidenced by this attribute.

boundaries on its toe and lateral margins, but no clear headwall scarp. The coherence map also shows arched compressional ridges identical to features seen in Frey-Martinez et al. (2006). This slump is characterized by localized thickening in interval M2, evidenced by values above 100 ms TWTT in the isochron map (Fig. 4.7a).

#### **4.3.2- Absence of headwall scarps**

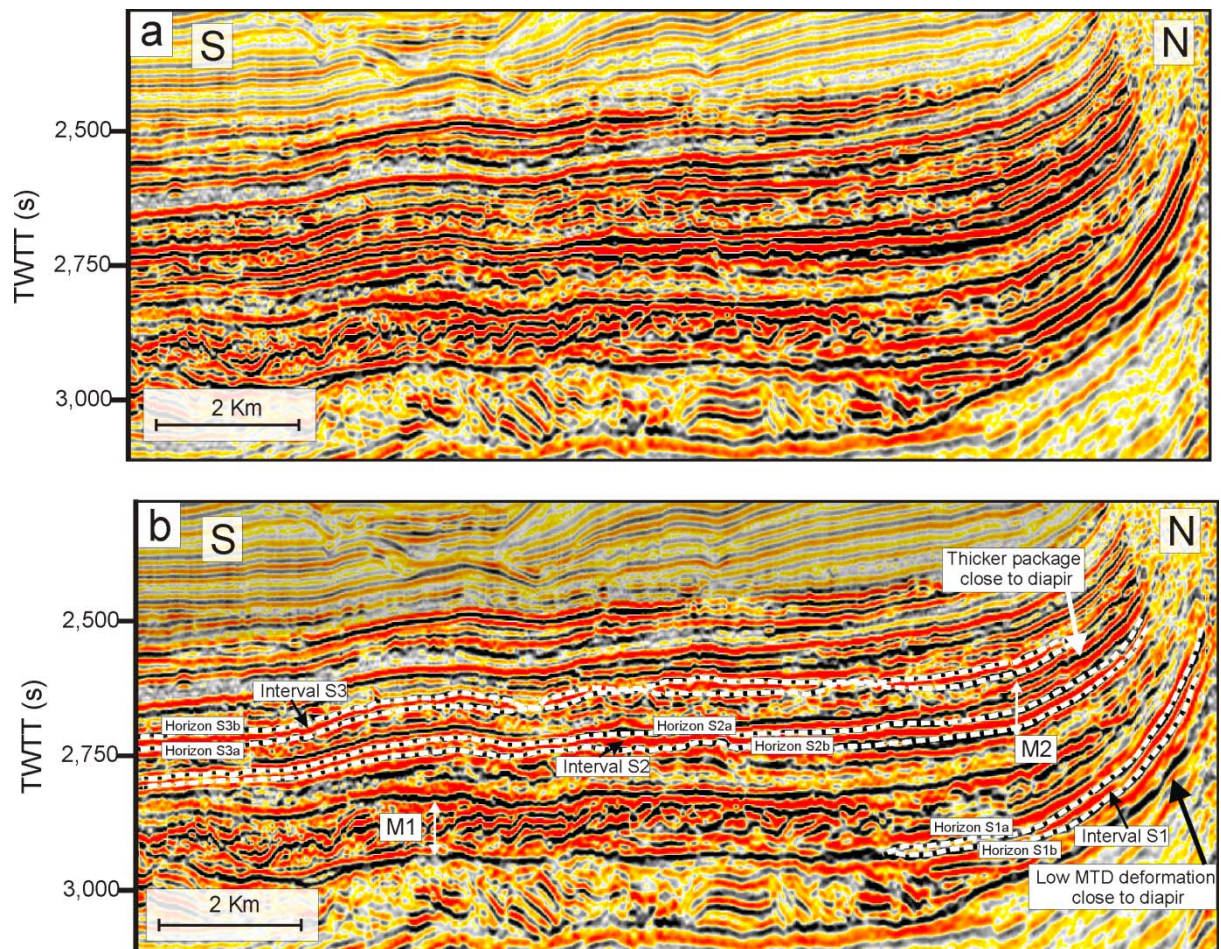
When studying MTD successions, headwall scarps are commonly present in the upper-slope areas where the seafloor acquires a steeper angle (Bull et al., 2009). Well defined scarps limit the area where chaotic reflections in MTDs contact with non-failed strata. The size of the headwall scarps is commonly related to the volume of failed material. As such, large MTDs should be related to large scarps on the slope.

In the study area, headwall scarps of MTDs seem to be absent. Any scarps observed on coherence and amplitude maps occur close to diapirs D6 and D7, marking: 1) the lateral thinning of MTDs in interval M1 and, 2) the partial intersection of the coherence slice with strata below Horizon 2 (Fig. 4.4). In addition, the profiles in Figure 4.5a do not show clear scarps upslope of any MTD strata within the area covered by the survey.

#### **4.3.3 – Distribution of stratified lithologies**

Sub-parallel (undeformed) to moderately deformed strata is observed within the Abrolhos Unit (Fig. 4.8). These were mapped on the seismic data based on their internal continuity. Continuous internal reflections at the lower half of the Abrolhos Unit are less



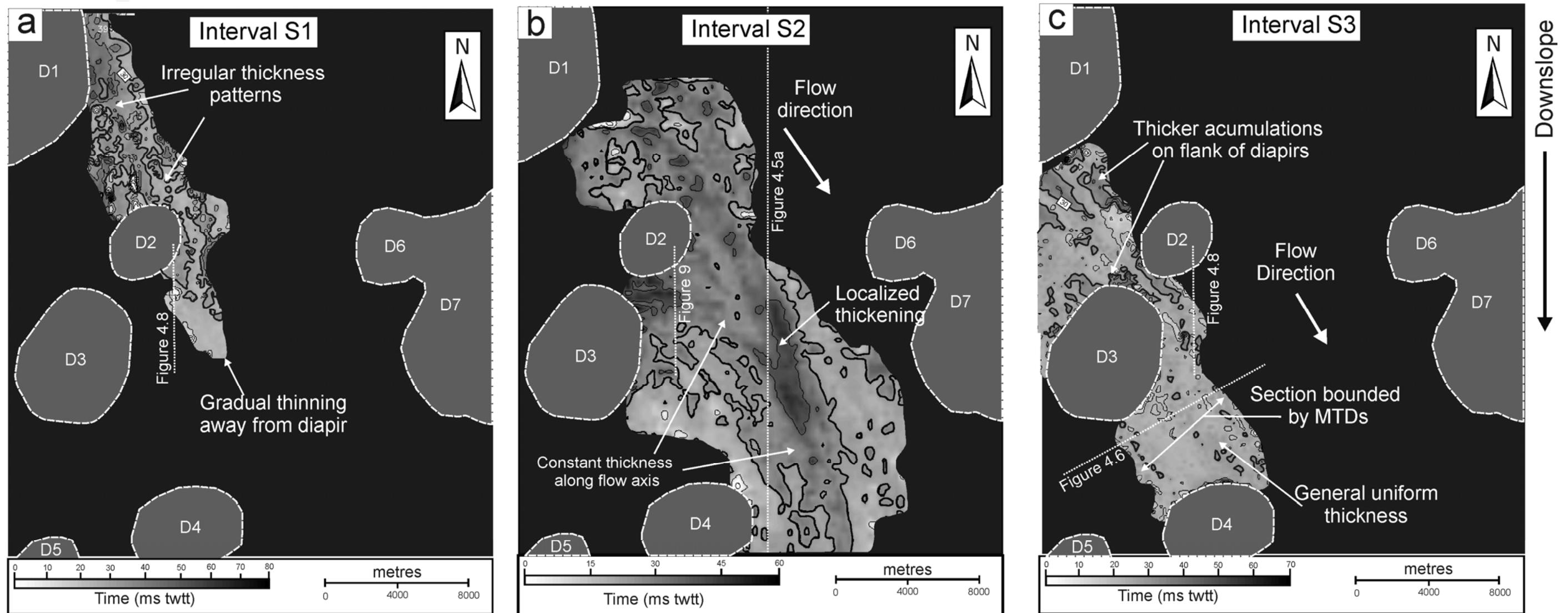


**Figure 4.8.** Uninterpreted (a) and interpreted (b) seismic section highlighting continuous strata. Solid lines highlight horizons represented in Figure 4.9. Note the higher proportion of continuous, less deformed strata above interval S2, when compared to the lower half of the Abrolhos Unit. The extent of interval S1 is limited by the MTD of interval M1, suggesting erosion by the mass-flow. Interval S2, included in interval M2, contains continuous reflections, with localized thicker packages close to the diapirs. Interval S3 is bounded by relatively thin (~40 ms TWTT) MTDs (or partially deformed strata).

extensive and gradually pinch out, limited by younger MTDs. Within interval M2, the stratified reflections are markedly continuous, forming packages of variable thickness. Thicker accumulations above 100 ms TWTT are found close to diapirs, thinning away from these until they reach values close to 80 ms TWTT (Fig. 4.8). Towards the top of the Abrolhos Unit, continuous reflections alternate with less deformed MTDs.

Figure 4.9 shows isochron data for the three selected intervals, S1, S2 and S3, shown in Figure 4.8. The lowermost S1 interval, delimited by Horizon S1a and Horizon S1b, underlies interval M1 (see position in Fig. 4.8b) and is limited to the NW sector of the study area (Fig. 4.9a). Its orientation is related to deposition on the flank of the western salt anticline, being laterally limited by an adjacent MTD (Fig. 4.8). The thicker sections of horizon S1 (above 40 ms TWTT) are related to the presence of diapirs D1 and D2, thinning to values below 30 ms TWTT circa two kilometres away from them.

The map for interval S2, defined by Horizon S2a and Horizon S2b and part of interval M2, covers a wider area than S1, with thicker sections located on the axial salt-withdrawal basin (Fig. 4.9b). The map for interval S3 shows that the relief created by the salt structures had a greater influence on its deposition than in the previous strata (Fig. 4.9c). The interval, defined by Horizon S3a and Horizon S3b, is roughly located on top of the western salt ridge. As seen in Figure 4.6a, the lateral extent of interval S3 is limited by chaotic reflections of MTDs. Diapir D3 seems to be relevant at the time of deposition of this horizon. Intervals more than 30ms TWTT thick are common, especially close to the flank of diapir D1. These thicker areas are oriented along a northwest-southeast trend. Downslope, and past diapir D3, thickness values are uniform.



**Figure 4.9.** Isochron maps of selected interval bounding continuous reflections, also representing their lateral extent. **a)** Interval S1, located below interval M1, and restricted to the NW salt structures. **b)** Interval S2, within interval M2, covering large areas in the salt withdrawal basin. Note thickening along the basin axis. **c)** Interval S3, continuous within the diapiric area. Contour spacing is 10 ms twtt in **a** and **c**, and 20ms twtt in **b**.

The amplitude pattern of the described continuous reflections shows variable degrees of lateral heterogeneity (Fig. 4.10), which is commonly associated with lateral stratigraphic variations (e.g. Brown, 2004). The most prominent feature is the presence of high amplitude patches which occur preferentially in the axial sections of the reflection. The amplitude tends to decrease towards the rims of the mapped reflection, which is particularly evident in interval S2. Nevertheless, there are cases where the lateral limit of the reflection is marked by high amplitudes, particularly in regions upslope of diapir D2. Such abrupt terminations of high-amplitude sections are interpreted to represent post-depositional erosion, especially in intervals S1 and S3 which are limited by MTDs. In contrast, the gradual amplitude decrease observed in interval S2 is concordant with gradual lateral compositional changes.

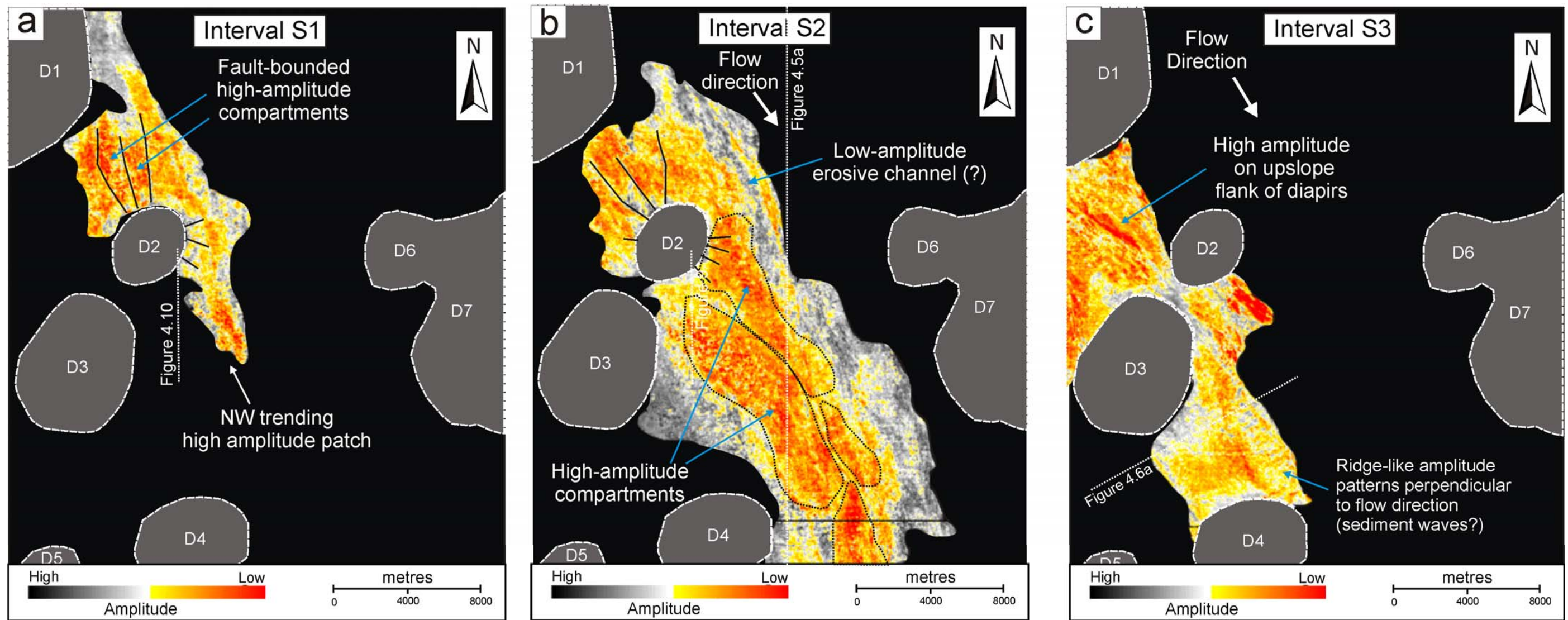
The variable amplitude patterns within the high-value region are representative of localized variations in the sediment composition and/or continuity. As such, higher amplitude homogeneity is interpreted to represent better lateral continuity, whereas amplitude variability represents lateral discontinuities imposed by the depositional architecture or faulting. The latter is particularly evidenced on the upslope flank of diapir D2, where north-trending faults with approximate lengths of 4km mark the limit of high-amplitude compartments in intervals S1 and S2. On the southeast flank of diapir D2 existing radial faults with lengths up to 2km also mark amplitude discontinuities, but subtler than the ones observed on the northern flank.

Downslope of the diapirs, the lateral amplitude variability is suggested to relate to the stratigraphic architecture. The high-amplitude patterns follow a general northwest trend and are more uniform in the axial regions. Despite this, within the central domains it is



possible to delineate distinct patches. Taking the example in interval S2, the high-amplitude areas in Figure 4.10b located at the lower half of the slope are often delimited by elongated features characterised by subtle decreases in amplitude. Other more relevant lateral amplitude heterogeneities in this interval are observed northeast of diapir D2, where a high-amplitude patch on the rim of this interval is entirely dissected by a low amplitude feature. The latter is interpreted to represent a low-amplitude channel fill that has cut through a previously laterally continuous deposit. Other alternating patterns of amplitude value are interpreted to represent syn-depositional sediment distributions, as seen in interval S3 upslope of diapir D4. Here, the alternating higher and lower amplitudes depict a ridge patterns which can be associated with the creation of sand waves created by a less confined turbidity flow that widened downslope of the confinement imposed by diapirs D2 and D3.

The high-amplitude patterns observed in Figure 4.10 are also coincident with the highest interval thicknesses (Fig. 4.9). The intervals with the most striking lateral amplitude contrasts are also the ones that exhibit a wider range of thicknesses, particularly S1 and S2. This is also partially observed in the upslope sections of interval S3, but where the thickness is relatively uniform the amplitude variations are also less pronounced. Nevertheless, it is worth mentioning that in the relatively uniform area between diapirs D3 and D4 there is a subtle trail of higher thickness patches (Fig. 4.9c) that corresponds to an elongated high-amplitude feature (Fig. 4.10c).



**Figure 4.10.** Amplitude map of the continuous reflections depicted in Figure 4.9. Lateral variations of the amplitude values are common, representative of lateral heterogeneities in the stratigraphic accumulations. The majority of the high-amplitude patches is elongated and are preferentially trending northwest to southeast. Low-amplitude features commonly separate the high-amplitude regions, either representing stratigraphic or structural (faults) discontinuities.

#### **4.4. Statistical analysis of unit variability**

The thickness of the Abrolhos Unit, as well as the relative proportions of MTDs within the unit, is variable on the studied slope. These changes were evaluated by analysing the measurements made within the four defined areas (A1 to A4 in Fig. 4.1). The produced plots represent average values of thickness and the proportion of MTDs in the study area.

##### **4.4.1- Thickness variations in the Abrolhos Unit**

Data for average thickness variations of the Abrolhos Unit are shown in Figure 4.10. Alongslope, thickness values decrease in area A1 and A2, and reach the lowest values in A2. This trend also corresponds to the highest confinement induced by salt structures. In areas A3 and A4, the main trends show a decrease in thickness into distal sections of the slope. Local variation in thickness might represent localised accumulation zones in the distal area. Across slope (Fig. 4.10b), the thickness of the Abrolhos Unit shows a decrease towards the east. The exception is a localised increase in the central area of the basin, related to thicker MTD strata within axial, hence deeper, regions of the salt withdrawal basin.

##### **4.4.2- Thickness variations of MTDs in the Abrolhos Unit**

The MTD thickness alongslope is shown in Figure 4.10c. The shaded area in the plot highlights the main values obtained, with these ranging between 61 and 69 ms TWTT. Outside this range there are three marked changes, two of them corresponding to thickness increases. The peak in area A1, where thickness reaches 79.9ms TWTT, is possibly explained by its position upslope of diapirs D2 and D6, which possibly imposed topographic barriers to

sediment derived from shallower regions. In area A2, a thickness minimum is reached (58,6ms). Within area A3, reaches the highest thickness values reached up to 82.6 ms TWTT.

Thickness values measured across the studied slope are represented in Figure 4.10d. In the figure, the maximum and minimum values for each point are plotted for each area. The values in the figure show a gradual decrease from west to east, with a local increase in the axial region, matching with area of higher MTD proportion. The minimum values in this axial region correspond to area A2, where a minimum in thickness alongslope is also recorded (Fig. 4.10c).

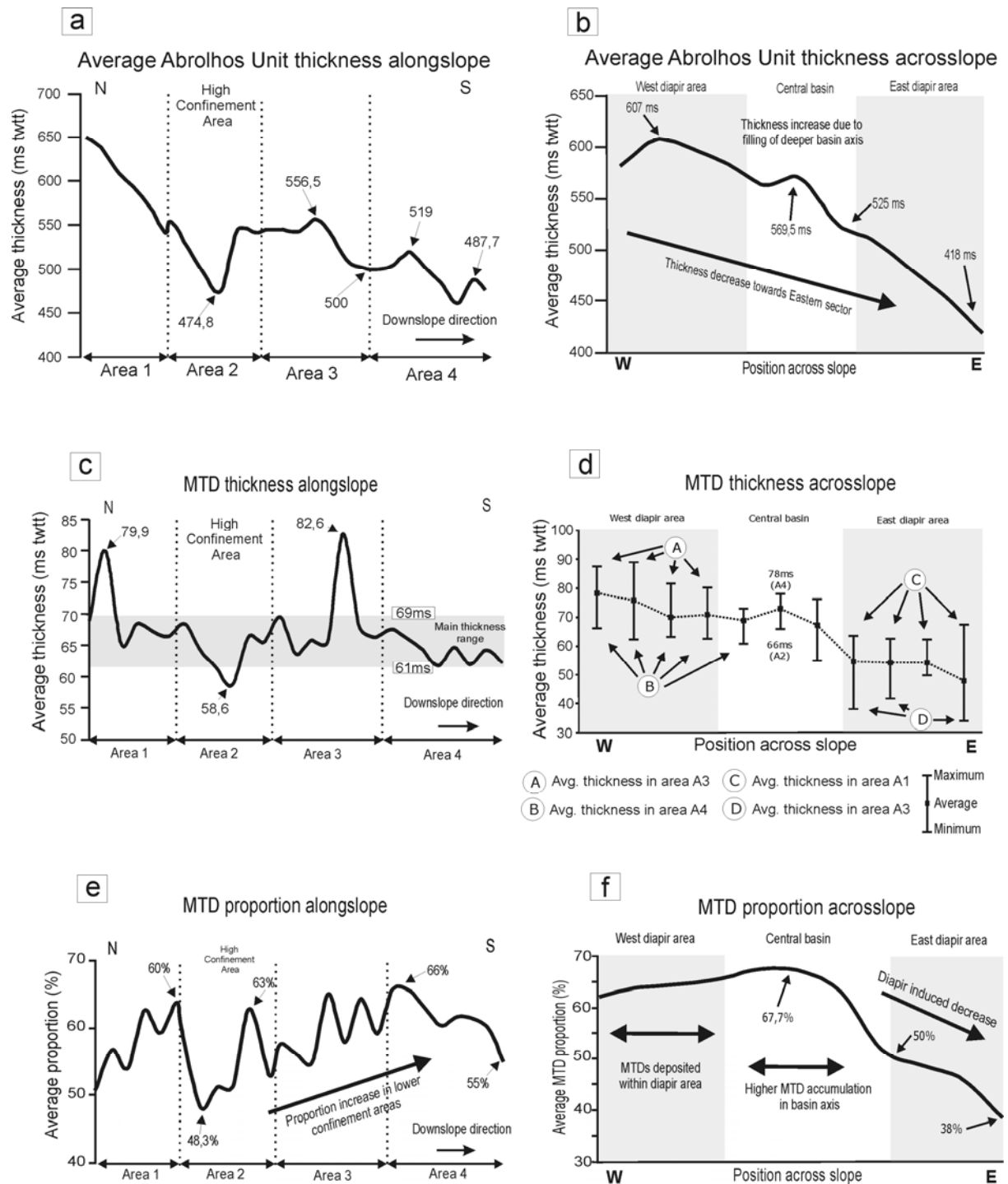
The average MTD thickness on the western diapir ridge ranges from 60 to 90 ms TWTT. The maximum values obtained for this section all correspond to area A3 (Fig. 4.10d, point A), which is also the area with the maximum MTD thickness shown in Figure 4.10c. On the eastern diapir area, the average thickness ranges between 60 and 50 ms TWTT. It should be noticed that maximum values seen here, calculated for area A1 (Fig. 4.10d, point C), are of the same range as the minimum values seen in the western diapirs (Area A4, Point B; Fig. 4.10d). Minimum values near the eastern diapirs correspond to A3, which is the area with the highest values seen in the western side (Fig. 4.10d).

Variations in MTD proportion are represented in Figures 4.10e (alongslope) and 10f (across slope). Variations alongslope are markedly sharp. Upslope, in area A1, there is an increase of up to 60% until the transition to area A2, where the lowest proportion values are reached, likely in relation to the higher confinement in this area. Between this point and the limit of area A4, the proportion follows a saw-tooth pattern until it reaches values around 65%. In area A4 the proportion of MTDs in the Abrolhos Unit decreases, but still constitutes 55% of the stratigraphic succession.

Contrasting with the irregular alongslope changes, the changes across slope are less pronounced (Fig. 4.10f). There is a slight increase from the western diapir area towards the axis of the slope, from 62% to 67.7%. Towards the east, an overall decrease is observed. At the limit of the eastern diapirs, MTDs constitute 50% of the succession, but within the diapir area the proportions decrease to 38%. MTDs constitute about twice as much of the sedimentary deposits in the western area when compared to the diapirs on the other side of the basin.

#### **4.5. Slope Profiles**

The shape of the slope profile is usually considered to be controlled by several factors related to the composition, supply rate and distribution of sediment, and to transport and resedimentation processes (e.g. Adams and Schlager, 2000). In order to compare the (palaeo) slope profiles that characterized the depositional settings in the Abrolhos Unit, we used a dip profile taken through the salt-withdrawal basin, perpendicular to the slope contours (Fig. 4.12a). Slope profiles were reconstructed by measuring the depth of 3 horizons, Horizon 2, Horizon 4 and Horizon 6 at points spaced every kilometre (referenced to a horizontal surface) along the slope, with the results plotted in distance-depth graphs (Figs 4.12b to 12d). The travel time was converted to depth assuming velocities in sediment of 2100m/s for the Abrolhos Unit. Velocities of 1800m/s and 1600m/s were used for the lower and upper parts of Unit 3 (see Figure 4.12a for delimitation), and a velocity of 1560m/s was used for the water column. The values presented do not take into account any quantification of gradient changes imposed by subsidence, faulting and/or sediment compaction.

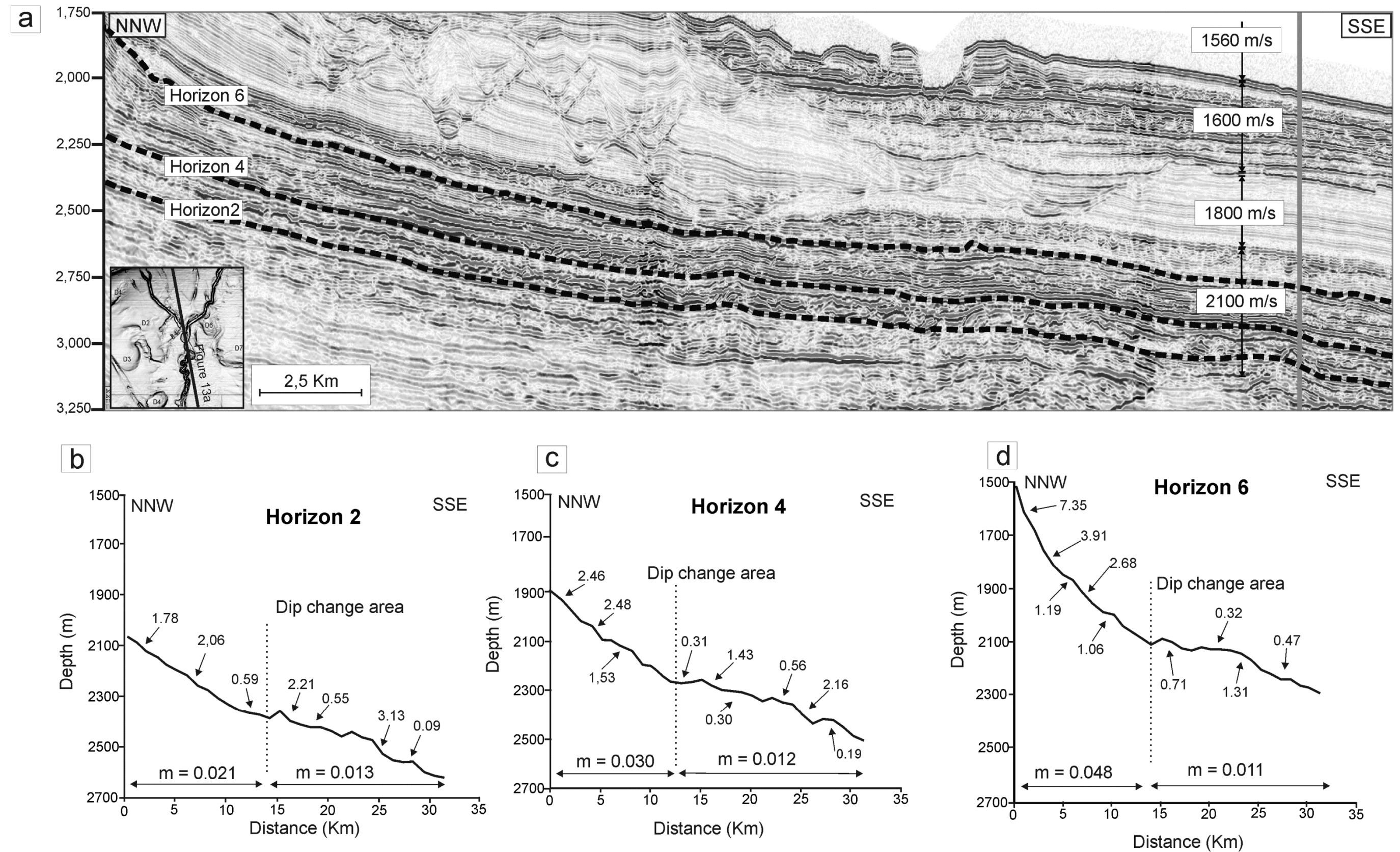


**Figure 4.11.** Graphic representation of statistical data representing variations of Abrolhos Unit and MTD thickness, and MTD proportion in the Abrolhos Unit. Plots represent variations along and across slope according to a North-South and East-West direction, respectively.

Horizon 2 has relatively low angles (Fig. 4.12b). Upslope it reaches  $\sim 2^\circ$ , decreasing to about  $0.6^\circ$  along the upper  $\sim 12$  km. This section is relatively smooth. From this point downslope, low dip angles predominate, but this part of the profile is markedly more irregular. Horizon 4 (Fig. 4.12c) has a very similar trend to Horizon 2, with the exception of higher dips upslope, reaching values up to  $2.9^\circ$ . The upper  $\sim 12$  Km also show a relatively smooth line, whereas the distal part is more irregular. The dip values in this latter are low, commonly below  $1^\circ$ , but reaching values around  $2^\circ$  at some points. Horizon 6 has higher dips of  $7^\circ$  in the upper section and gradually decreases to about  $1.3^\circ$  at  $\sim 12$ - $13$  km downslope (Fig. 4.12b). From this point downslope the trend and dip values are similar to the other horizons.

Time-depth plots show that the slopes are best fit to exponential profiles in the upper slope, changing into a linear trend from the mid-slope region towards the base of the slope (Fig. 4.12). The curvature of the upslope section in Horizon 2 is close to linear, but the same section of Horizon 6 is clearly curved. Given that the change in dip angles occurs approximately in similar regions of the slope, we calculated the slope value for each of the upper and distal sections by fitting linear trends at each. The upper slope sections show slope increases of 0.021, 0.030 and 0.048 for horizons Horizon 2, Horizon 4 and Horizon 6, respectively. The downslope sections have gradients of about 0.012/0.013 for all the horizons, showing similar values regardless of the stratigraphic level.





**Figure 4.12.** **a)** Seismic section across slope representing Horizon 2, Horizon 4 and Horizon 6. Inset shows location of seismic line. **b to d)** Plots representing the profiles of Horizon 2, Horizon 4 and Horizon 6, respectively, along with dip measurements along slope. The dip change area divides the profile in upper and lower segment, based on the dip values. “m” represents the slope value calculated for a best-fit line applied to each segment of the profile.



## 4.6. Discussion

### 4.6.1. Significance of variability in MTD-Turbidite couplets

The recognition and characterisation of the stratified reflections within MTD successions is important for hydrocarbon exploration. Their distribution in the study area is not uniform, either along- or across-slope, and was most likely controlled by slope topography. Thus, the four confinement areas defined within the study area (Fig. 4.1) reflect the influence of salt structures in MTD distribution. This is particularly shown by the topographically confined Area 2, where lower values for both MTD and Abrolhos Unit thickness were found. Considering that Area 1 is characterized by higher values for the Abrolhos Unit and MTD thicknesses, as well as higher proportions of the latter, the marked drop of the measured parameters implies that, for Area 2: a) the diapirs constituted a barrier to sediment flow with consequent accumulation upslope, and/or b) the topographically confined Area 2 corresponds to a sediment bypass area, with low sediment accumulation. The distal areas, A3 and A4, show moderate topographic confinements and an increase in MTD quantity.

An important point to consider in terms of the sediment distribution on the studied slope is the location of sediment source areas. The modern sea-floor of the basin shows that the major input point is located north of the study area (Fig. 4.1), but several features in our results indicate that during the deposition of the Abrolhos Unit there was also significant sediment input from a northwestern position. This is supported by northwest-oriented features seen in coherence slices (Figs. 4.3c and 4.7c) and amplitude maps (Figs. 4.7b), and the dispersal patterns of the continuous strata in Figures 4.9 and 4.10. The suggested diapir

flow obstruction also supports this, as this tends to occur on their northwestern flanks. In addition, our quantification of the MTDs also shows a predominance of sediment on the western regions.

Eocene and Oligocene strata in the neighbouring Campos Basin are known to constitute viable reservoirs. Fetter et al. (2009) described these reservoirs as immature and heterolithic, reflecting ongoing tectonic activity. Turbidite reservoirs in the Campos Basin mostly consist of arkoses, which include minor quartz, carbonate grains, mud intraclasts and glauconite, with minor volcanic fragments. Similar strata can be suggested for the Espírito Santo Basin, probably with relative higher amounts of volcanoclastic material derived from the Abrolhos Plateau (e.g. Fiduk et al., 2004; Mohriak, 2005). Similarly to the Campos Basin, the more continuous reservoir-prone strata appear variably intercalated with MTDs (Fig. 4.8). Middle- to lower- slope Eocene reservoirs in the Campos Basin consists of intercalations of sandy turbidites and muddy bottom-current reworked deposits (Moraes et al., 2007). These have good lateral continuity, filling depocentres created by salt growth. The turbidites are preferentially deposited along the trough axis, whereas the contourites are on the edges. In the study area, the continuous strata packages in interval M2 (Figs. 4.2 and 4.5) are an example of what has been documented in the Campos Basin, and also where the thickest accumulations are observed (Fig. 4.7a). As the studied succession is located in the upper slope, MTDs also are expected to be more prevalent, unlike the Campos lower slope where turbidites and contourites prevail.

#### **4.6.2. Influence of MTD deposition in slope profiles and margin evolution**

The occurrence of MTDs is commonly associated with erosive periods of slope evolution where retrogressive failure is common, and MTDs are considered to contribute little to margin progradation (e.g. Moreira and Carminatti, 2004; Piper et al., 2003). However, recent studies have shown that MTDs play an important role in margin construction (e.g. Boyd et al, 2010; Huppertz, 2010).

The models proposed by Adams and Schlager (2000) assume that slopes dominated by mass-wasting events have exponential profiles, due to failure upslope and decay of flow transport capacity of gravity currents towards distal areas (Kenyon and Turcotte, 1985). Prograding slopes typically have linear trends resting at a critical angle maintained by constant sediment supply (Adams and Schlager, 2000). Linear profiles have also been related to slopes with minor wasting with infrequent large failures, but when one takes place it causes the slope to acquire an exponential profile (Campbell et al., 2004).

Slopes associated with MTDs in the Espírito Santo Basin show gradually-changing exponential profiles (Fig. 4.12). The older ones have the lowest curvature, being close to linear, with curvature increasing towards younger stratigraphic intervals as seen in the profiles of Horizon 4 and Horizon 6 (Fig. 4.12a). Successive dip increases observed for the upper portions of the slope as younger strata was deposited, suggest a progressive advance of the slope located north of the study area. The advance of slopes with exponential profiles in this setting could be driven by fast rates of sedimentation in the basin (Adams and Schlager, 2000), as during the Eocene large amounts of sediment were supplied to the

Espírito Santo Basin (Bruhn and Walker, 1997). We consider that the gravitational collapse of large amounts of sediment accumulated on a narrow shelf led to the formation of a prograding wedge on the margin that included accumulation of MTDs in the basin.

The sediment supply to this specific area of the basin was complex, with main input points located north and northwest of the studied section, as suggested by the MTD distribution in the study area (Fig. 4.11) and the orientation of features in the attribute maps in Figures 4.3 and 4.7. The arcuate geometry of the basin reflects this as well focusing sediment sourced from northwestern margin areas, especially the Rio Doce, and mixed clastic/volcaniclastic material from the north (Fig. 4.1). Multiple entry points for sediment influence the sediment dispersal patterns and consequently the slope profiles.

The margin configuration was also strongly influenced by the emplacement of the Abrolhos volcanic plateau. In fact, the onset of volcanism north of the BES-2 survey extended the shelf area in over 200 km to the east (Sobreira and França, 2005), with new steep slopes contacting the deeper basin (Mohriak, 2003). Such steep margins also tend to acquire exponential profiles. Different stages for the plateau's growth imply the advance of its bordering slope, namely southwards towards our study area. Within the study area, this advance would result in increasing slope dips at successively younger stratigraphic levels, consistent with the results obtained.

## 4.7. Conclusions

The following points summarise the main conclusions from this chapter:

Mass wasting was an important process on the Brazilian Margin during the Mid-Eocene period that led to deposition of thick, up to 650 ms TWTT, MTD-rich stratigraphic units.

Thick MTD intervals with chaotic and disrupted reflections alternate with undeformed, continuous reflections related to turbidite-like strata. As stratified lithologies are relevant to the prediction of potential reservoirs within MTD-rich units (e.g. Beaubouef and Abreu, 2010), we show that potential reservoirs are thicker at the rims of diapirs when related to MTDs, but also cover significant areas of the basin at stratigraphic levels where mass-wasting is less apparent. Erosion by MTDs is shown to limit the lateral extent of the interpreted stratified strata.

MTDs deposited during the Eocene-Oligocene contributed to margin construction and progradation in the Espírito Santo Basin. High sediment input into the basin, along with the influence of salt growth and the emplacement of the Abrolhos volcanic plateau led to an unusual and complex slope growth. Thus, across-slope MTD thickness decreases from 70-80ms TWTT to 50-60ms TWTT towards the east. The average proportional thickness follows the same trend, from ~60% down to 38%. These decreasing values reflect an important sediment source northwest of the study area, and the limitation of MTD flow by the relief formed by salt diapirs in the East.

# **Chapter 5**

**Distribution and characterization of failed  
(mega) blocks along salt ridges, SE Brazil:  
Implications for vertical fluid flow on  
continental margins.**

This chapter has been published as “Gamboa, D., Alves, T., and Cartwright, J., 2011, Distribution and characterization of failed (mega) blocks along salt ridges, southeast Brazil: Implications for vertical fluid flow on continental margins: Journal of Geophysical Research, v. 116, p. B08103.”

## 5. Distribution and characterisation of failed (mega) blocks along salt ridges: Implications for vertical fluid flow

### 5.1. Abstract

Three-dimensional seismic data are used to assess the control of halokinetic structures on the distribution of blocks in a mass-transport deposit of the Espírito Santo Basin, Southeast Brazil. In contrast to what is commonly observed over growing salt structures, the thickness of the MTD-A1 is larger on top of a northwest-trending salt ridge. Emphasis was given to the statistical analysis of 172 remnant and rafted blocks identified within Eocene mass-transport deposits (MTD-A1). Three styles of block deformation are identified and scale relationships between the geometry of blocks and their relative position on the salt ridge are presented. Average block height reaches 130 m. Average block area reaches 0.43 km<sup>2</sup>, whilst 11.3% of the total area (A) investigated is covered by remnant and rafted blocks (5%<A<17%). Based on variations in block geometry (height, area, width/length ratio, orientation) and their relative distribution, we interpret that most failed strata have been remobilised by adjacent topography created during growth of the investigated salt ridge. We show that the origin of the blocks is linked to densely-spaced sets of halokinetic-related faults that deformed the pre-failure strata. The presence of underlying faults and blocks of remnant and rafted strata potentially induce sharp variations in the internal permeability of MTD-A1. Thus, the interpreted data shows that mega-blocks in MTDs can constitute viable fluid pathways on otherwise low-permeability units. This character can significantly decrease seal competence above and on the flanks of halokinetic structures.

## 5.2. Introduction

Halokinesis is triggered by loading gradients imposed by overburden rocks, with resulting deformation predominating during regional extensional events, or during shortening of pre-existing salt structures (Hudec and Jackson, 2007; Jackson et al., 1994; Jackson and Vendeville, 1994; Vendeville, 2002). In such a setting, the thickness and strength of overburden strata, sediment distribution patterns above salt, and the thickness of the original evaporitic units, together with regional and local tectonic stresses, can limit salt growth and induce geometric variability in growing salt structures (Davison et al., 1996; Dooley et al., 2009; Jackson and Hudec, 2005; Jackson et al., 1994; Schultz-Ela et al., 1993; Seni and Jackson, 1983). In Southeast Brazil this variability is expressed by a basin-ward transition from salt rollers, anticlines and pillows in proximal (extensional) regions, to salt walls, diapirs and stocks in the mid-slope region. Salt canopies and sheets occur in distal compressional regions (Davison, 2007; Demercian et al., 1993; Fiduk et al., 2004; Mohriak, 1995).

Deformation resulting from halokinesis is expressed by overburden faulting, regional folding and local subsidence, followed by gravitational collapse of flanking strata to salt structures (Davison et al., 2000a; Tripsanas et al., 2004). Over growing salt diapirs, overburden strata is commonly either thinned or completely removed by erosional processes, which accumulate eroded strata in peripheral salt-withdrawal basins (Giles and Lawton, 2002). Mass-transport deposits (or MTDs) resulting from these erosional processes are usually mud-dominated and have low exploration potential (Lee et al., 2004; Moscardelli et al., 2006; Posamentier and Kolla, 2003), except when sand-rich strata is present (Armitage et al., 2009; Beaubouef and Abreu, 2010; Davison et al., 2000b; Dunlap et al.,



2010; Moraes et al., 2007; Moscardelli and Wood, 2008; Piper et al., 1997; Shanmugam et al., 1996; Tripsanas et al., 2008). Important factors controlling the seal competence of MTDs include the presence of a strong structural fabric (including faults) in their interior, and variations in the degree of remobilization experienced by failed strata (Frey-Martínez et al., 2006). Consequently, failed submarine strata are classified into submarine “slides”, “slumps” and “debris flows” based on their degree of internal cohesion (Masson et al., 2006; Nemec, 1990). Submarine slides are composed of coherent strata with minor internal deformation. The presence of slump deposits in a MTD implies larger travel distances and internal deformation than with slides. Debris flows are characterised by presenting highly disaggregated strata and no preservation of internal strata within a cohesive matrix (Masson et al., 2006). Large blocks of remnant or rafted strata can be ubiquitous within the latter classes of submarine landslides, either close to the MTD source areas or transported to toe regions of submarine landslides through gravitational processes such as hydroplaning (Deptuck et al., 2007; Dunlap et al., 2010; Ilstad et al., 2004; Lee et al., 2004; Minisini et al., 2007; Tripsanas et al., 2008; Urgeles et al., 2007). Individual blocks are named as ‘remnant’ if left *in-situ*, or ‘rafted’ if substantially translated during slope failure. They have a wide range of sizes, from metres to hundreds of metres, but this tend to decrease with larger travel distances (Bull et al., 2009; Canals et al., 2004; Davison, 2004; Gee et al., 2006).

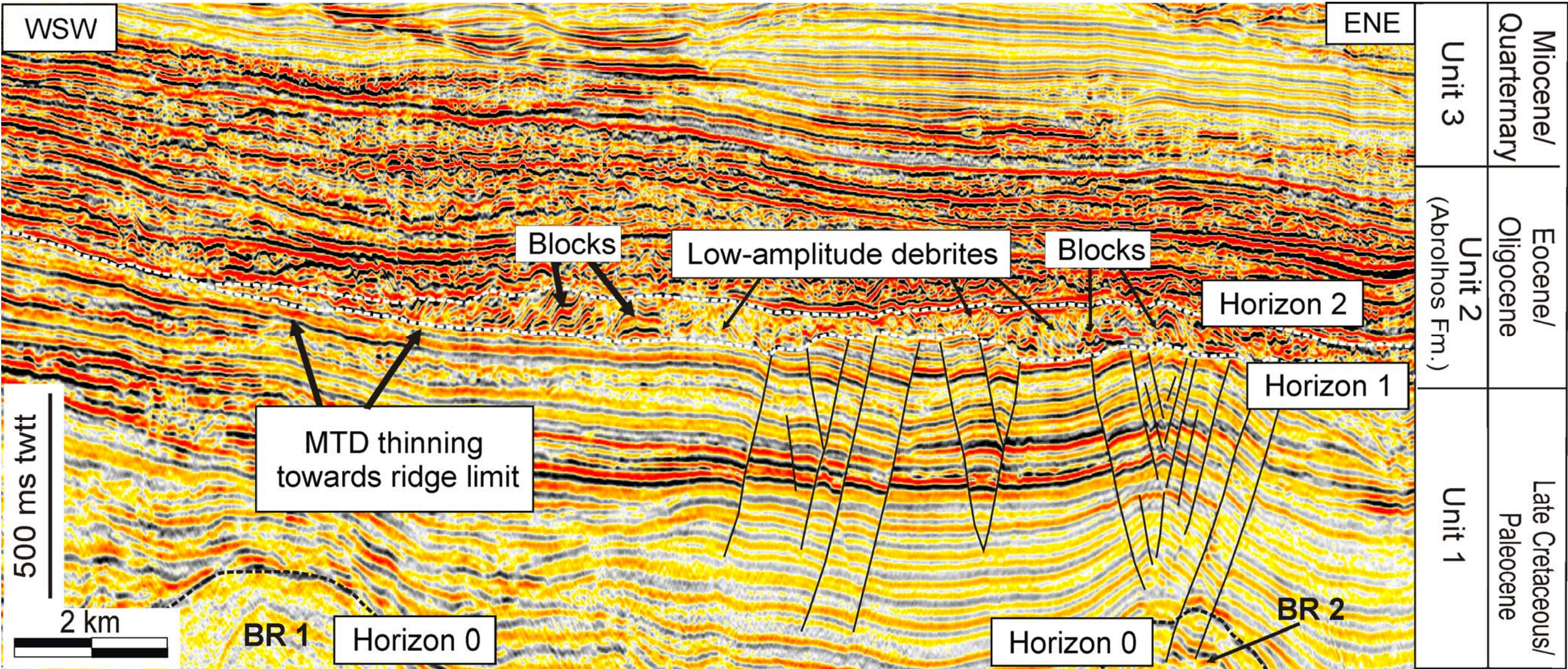
Rafted blocks have been comprehensively identified in the vicinities of salt structures, either derived from local failures (Davison et al., 2000a; Tripsanas et al., 2004) or distant (upslope) landslides (Dunlap et al., 2010; Lee et al., 2004). However, no data has been yet presented on the effect of salt diapirs on slope stability, nor the impact of such remnant/rafted strata on fluid flow has been yet assessed for a key case study. In addition,

no comprehensive reviews on the relative distribution of remnant/rafted blocks over salt structures have been attempted. In order to address these latter limitations, this work focuses on a MTD unit (MTD-A1) at the base of the Abrolhos Formation (Fig. 5.1), an important Eocene-Oligocene stratigraphic unit in the Espírito Santo Basin, Southeast Brazil (França et al., 2007). The Abrolhos Formation comprises vertically stacked MTDs intercalated with siliciclastic and volcanoclastic deposits (Fiduk et al., 2004; Gamboa et al., 2010; Mohriak, 2005). Significantly, similar units occur in the Campos basin, where Eocene sand bodies intercalated with MTDs constitute viable reservoirs (Moraes et al., 2007).

This chapter focuses on the characterisation of the internal fabric of MTD-A1 to assess the distribution of remnant/rafted blocks over salt structures which were actively growing at the start of the Eocene. We demonstrate how stratigraphic and/or structural permeable pathways for fluid flow can be present in otherwise poorly permeable MTDs. This will be primarily achieved by analysing:

- 1) The internal deformation and relative distribution of blocks above local diapir ridges, and;
- 2) The effect of underlying fault families on the generation and distribution of blocks above diapir ridges;
- 3) The relative importance of block and fault distribution to vertical fluid flow over salt structures.





**Figure 5.1.** Seismic section representing the character of the identified seismo-stratigraphic units in northern Espírito Santo Basin. Unit 1 (Late Cretaceous-Palaeogene) is characterized by low amplitude reflections. Crestal faults are present above buried salt ridges. Unit 2 is characterized by high-amplitudes and chaotic character of the seismic reflections, contrasting with the remaining units 1 and 3. MTD-A1 is the lowermost deposit identified in Unit 2, bounded by Horizon 1 and Horizon 2. This section also evidences thinning of the MTD towards the rims of the diapir ridge.



The relevant features of the basal MTD described in this chapter are made using key seismic profiles and seismic attribute maps and a quantitative analysis of block properties, aiming to discuss the occurrence of blocks and their relation to fault families in the study area, the significance of the investigated MTD-A1 as marker of halokinesis, and how the distribution of the blocks in the MTDs above the diapir ridges can influence the vertical permeability of the MTD units. Major faults similar to those identified in the study area constitute migration paths for hydrocarbons in the Campos basin, linking the Cretaceous source rocks to Cenozoic reservoirs in the basin (Guardado et al., 1989; Guardado et al., 2000; Mello et al., 1994; Mohriak et al., 1990). A similar mechanism to that identified in the Campos Basin has been suggested for the Espírito Santo Basin (Biassussi et al., 1998).

The terms “blocks” or “megablocks” *sensu* Spence and Tucker (1997) are used to describe large blocks of strata, some reaching hundreds of metres in height and width. Remnant and rafted blocks of strata are shown as partly-geometric features with high coherence and reflection strength (Fig. 5.2 and 5.3, respectively). In the study area, remnant blocks are bounded by faults propagating from underlying strata and do not show any significant disruption of strata at their base (Fig 5.3). In contrast, debrites and other mass-wasting strata are seen as low magnitude features within MTD-A1 (Fig. 5.3a and 5.3b). They comprise individual blocks embedded in low-amplitude to chaotic strata and present significant disruption of basal strata at, or adjacent to, the glide plane (Fig. 5.3). The base of the study interval is densely faulted, with developed normal faults occurring predominantly on the crest of buried salt diapirs and ridges. Their upper tips are commonly truncated by a Mid-Eocene erosive surface, with some of the faults propagating into remnant/rafted strata with MTD-A1 (Fig. 5.3c and 5.3d).

### 5.3. Studied stratigraphic interval

This chapter focuses on the lowermost seismo-stratigraphic Unit 1 and Unit 2, which are separated by the mid-Eocene erosional unconformity (Fig. 5.1). Unit 1 is characterized by low to moderate amplitude continuous reflections and the interval is densely faulted. In Unit 2 there is a predominance of high-amplitude reflections, related to the high content of volcanoclastic sediment. Packages of chaotic reflections are abundant in Unit 2 due to the abundant mass-wasting deposits. The main aim of the chapter is to investigate MTD-A1, located at the base of Unit 2, and its genetic relation with the underlying strata in Unit 1.

### 5.4. Character of the basal MTD-A1

MTD-A1 is bounded by Horizon 1 and Horizon 2 (Figs. 5.1 and 5.3), and covers about 955 Km<sup>2</sup> within the area covered by the survey (Fig. 5.4). Its base, Horizon 1, consists in an irregular, hummocky horizon marking the basal glide plane. The time-structural map of this surface (Fig. 5.4a) illustrates two distinct morphological trends. Steeper slope angles are observed in upper slope regions (average 2°) decreasing to 1° below 2900ms. This decrease in slope is related to the presence of two northwest-trending depressions along the flanks of the salt diapir ridge where the majority of the blocks are concentrated (Fig. 5.4a). On seismic profiles, the transition to these depressed areas is marked by a morphological step, which also delimits the rims of MTD-A1 (Fig. 5.5).

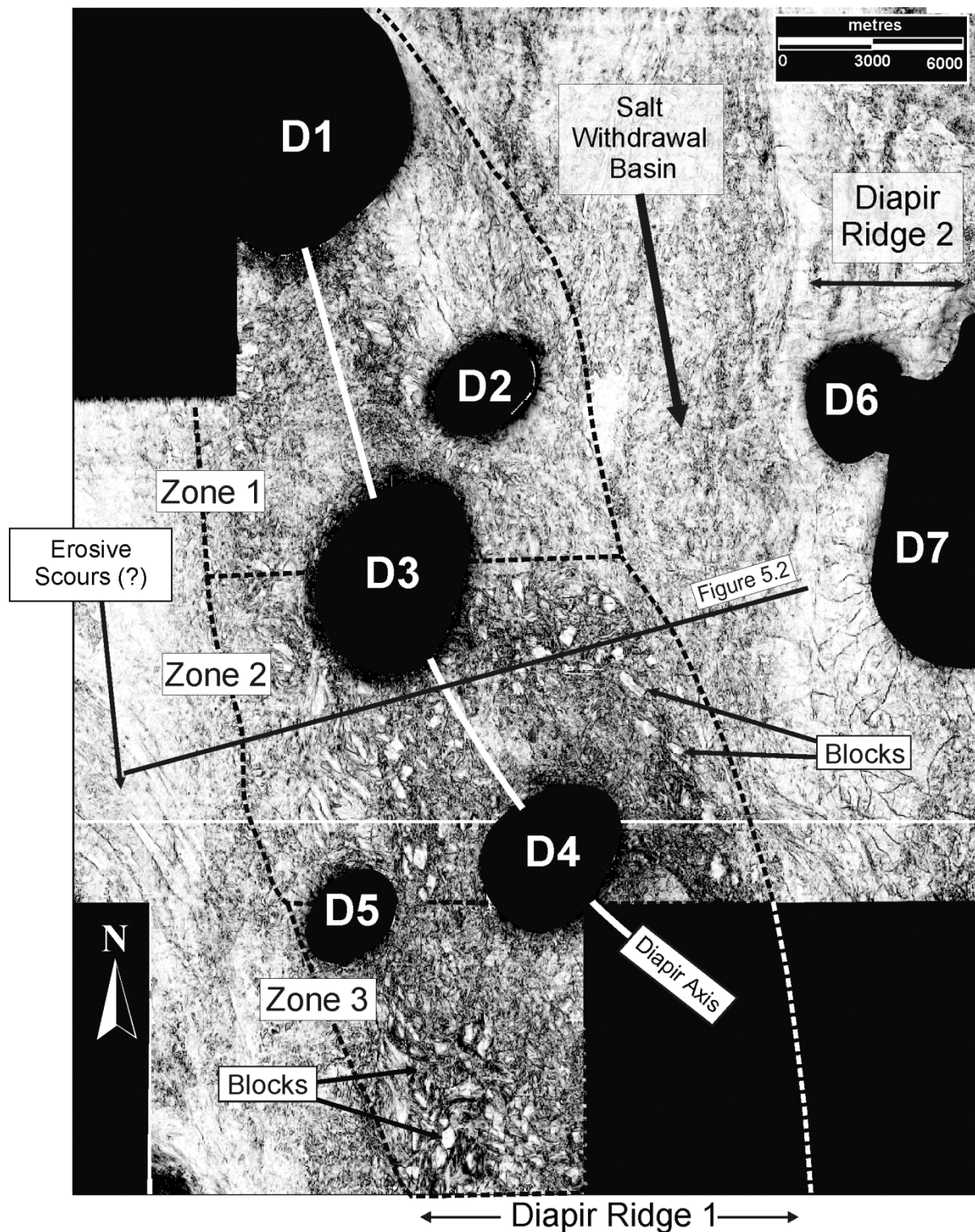
A computed isochron map shows that MTD-A1 reaches its largest thickness in the salt region along the northwest trending depressions (Fig. 5.4b). The thickness values observed here are over 75 ms twtt and reach a maximum of 175 ms twtt. Other thick

deposits in this MTD are seen on the upper slope regions northeast of diapir D2, and outside of the main study area where thickness values reach up to 200 ms twtt and no blocks are observed. Of particular relevance is that the thicker parts of MTD-A1 occur together with the regions of higher block density, over the developed salt structures (Figs. 5.3 and 5.4).

Figure 5.4c illustrates an isochron map between a Late Cretaceous horizon (Horizon 0) and Horizon 1, evidencing early relief created by halokinesis. The map shows two minor northwest-trending buried salt ridges (named BR1 and BR2) and the diapirs within the studied main diapir ridge (DR1). Diapirs D2 and D5 are located along the buried ridges BR2 and BR1, respectively. On the vicinities of the main diapir ridge focused on this study there are two axial salt withdrawal basins. On the easternmost locations of the survey there is a secondary north-trending diapir ridge (DR2) from where diapirs D6 and D7 emerge. The comparison of the latter map with the isochron map in Fig. 5.4b shows that the thicker accumulations of MTD-A1 overlie DR1.

#### **5.4.1. Internal character of the MTD**

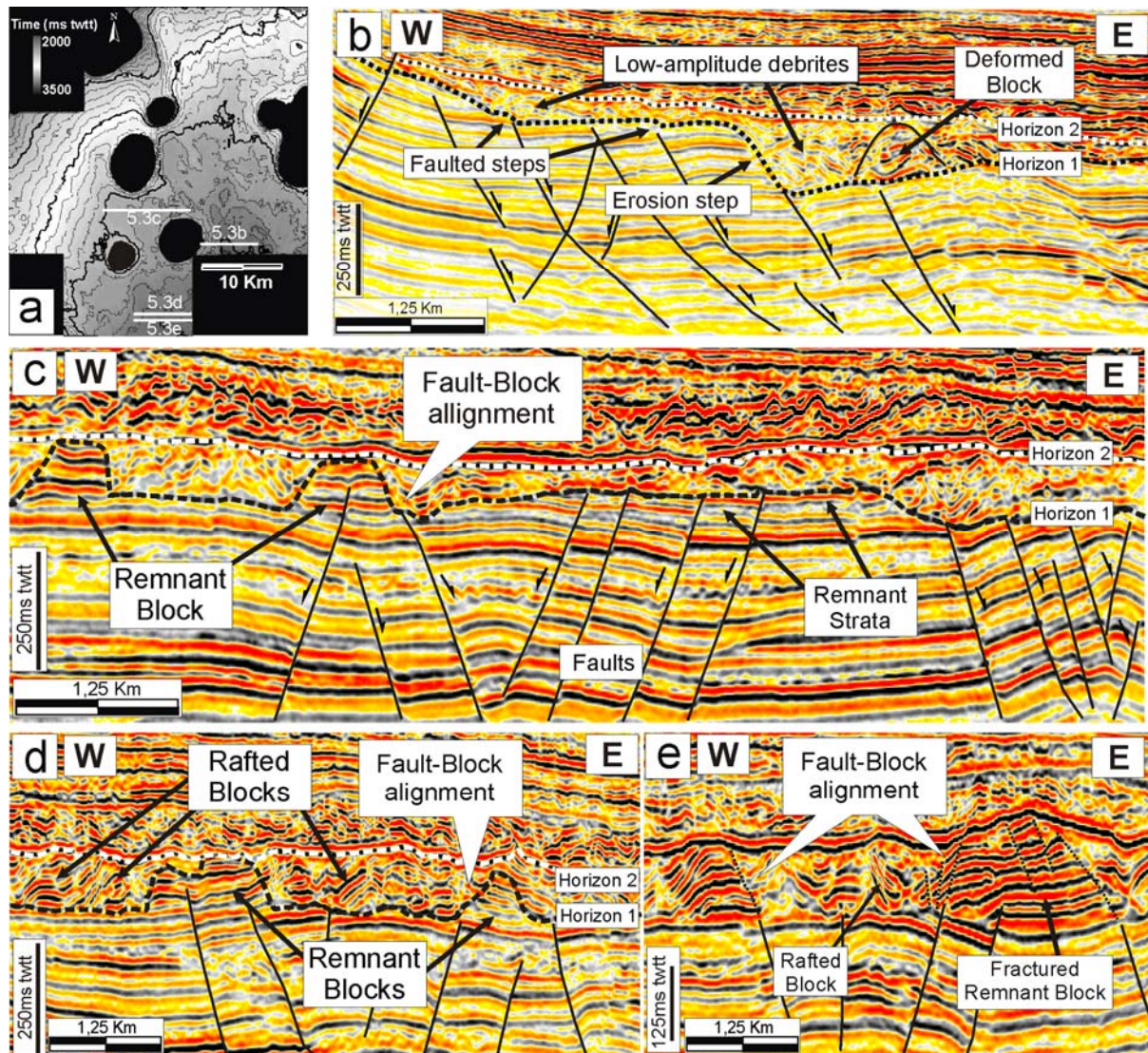
The internal character of the studied MTD is varied, with high amplitude sections grading or contacting with low to transparent amplitudes (Fig. 5.3). The identification of internal features composing MTD-A1 allows the assessment of its flow and, for the purpose of this paper, to identify elements with the potential to allow fluid percolation through the failed strata. The features interpreted on seismic data will be described in detail in the following sub-sections.



Zone 1 - Zone 3: Study Zones    D1- D7: Salt Diapirs

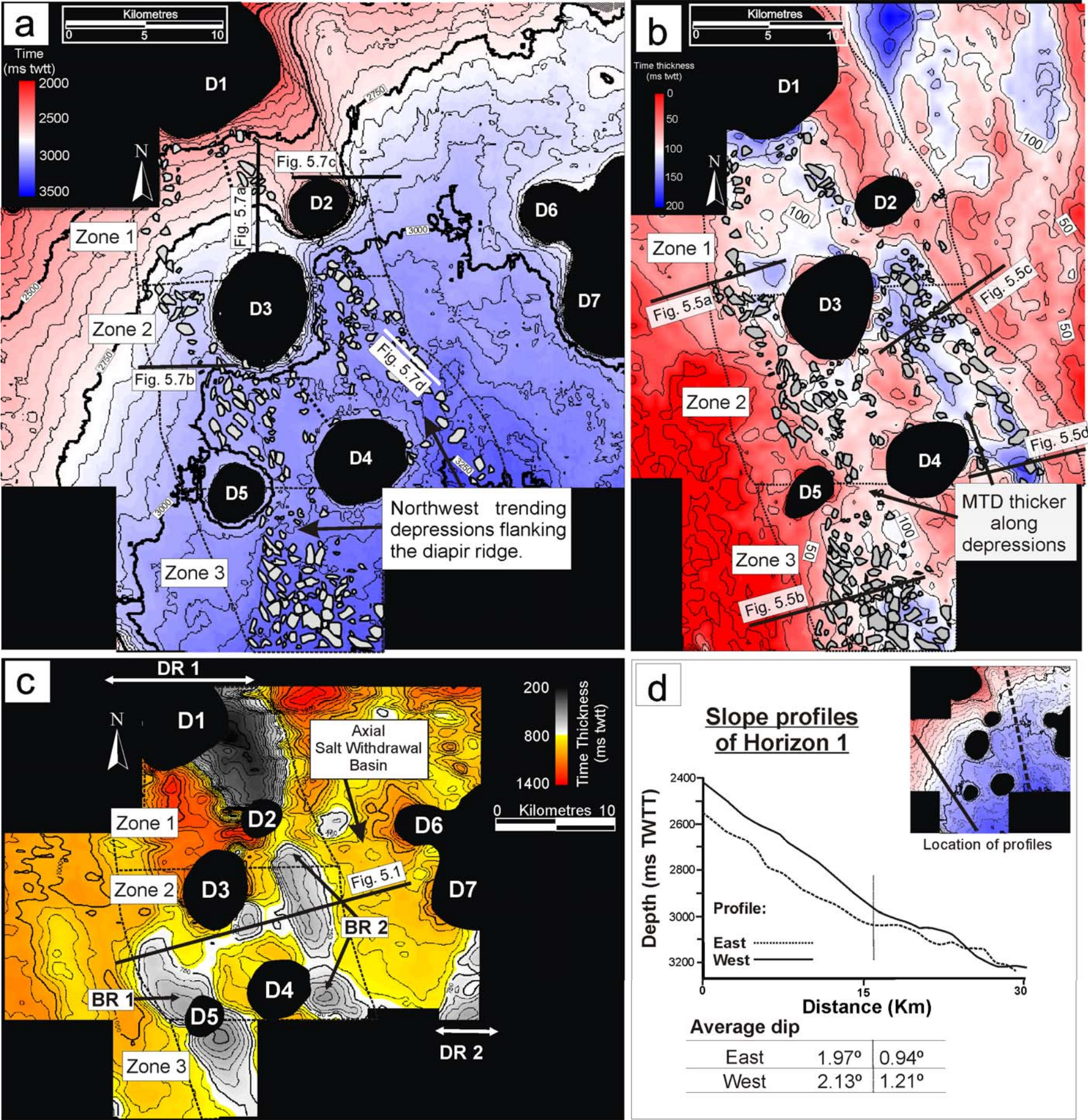
**Figure 5.2.** Coherence slice taken 20 ms TWTT above Horizon 1, intersecting the studied MTD. The studied MTD overlies a northwest-trending diapir ridge where five diapirs are present. This area was divided in three zones representative of upper, middle and lower slope, respectively. Numerous high coherence remnant/rafted blocks (light colours) are observed within the limit of Diapir Ridge 1. Blocks clusters are observed in Zone 3 and rims of Zone 2. No blocks are observed either in the salt-withdrawal basins, or the region of Diapir Ridge 2.



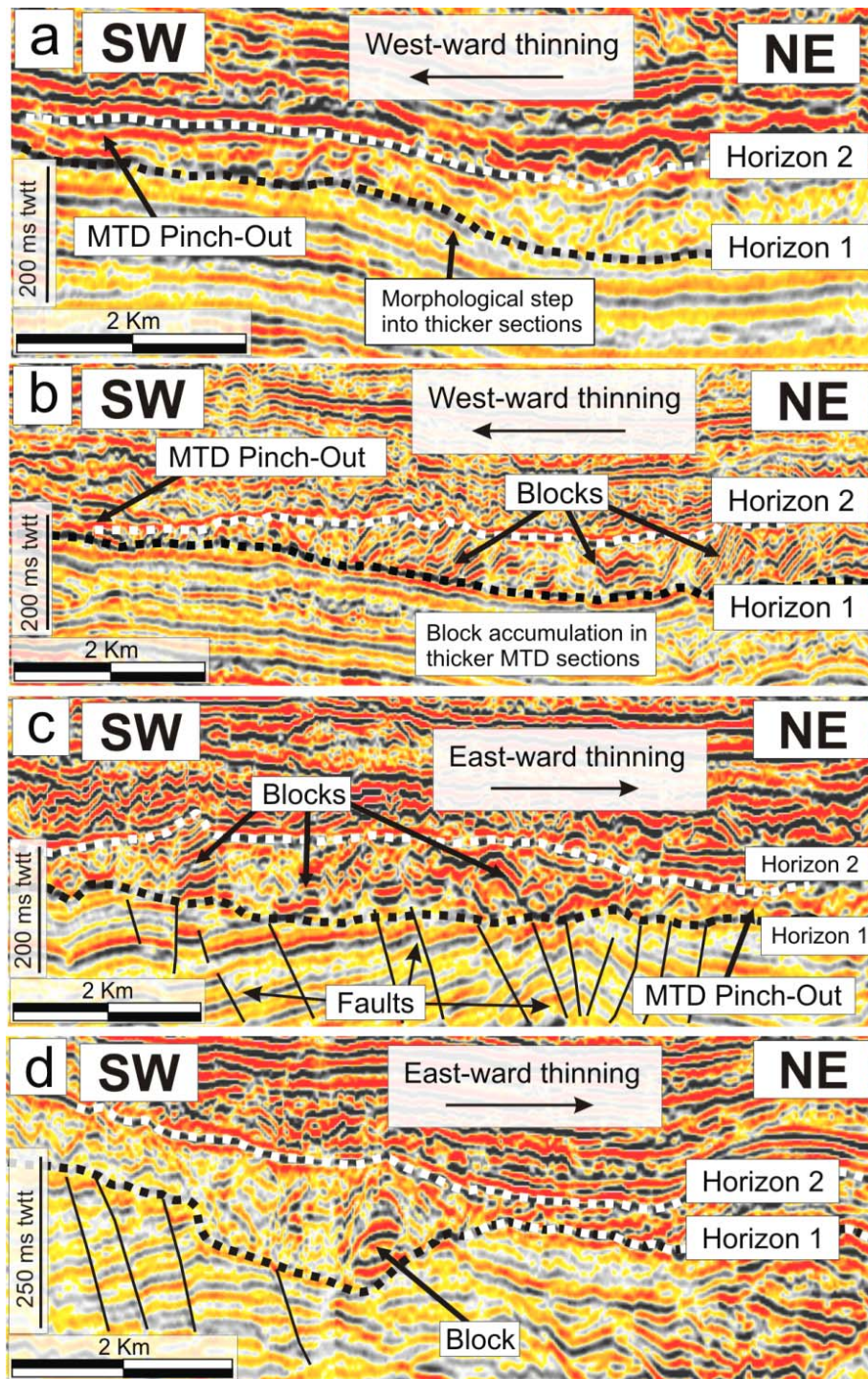


**Figure 5.3.** Seismic sections depicting the relation between faults and blocks. **a)** Map showing the location of seismic sections in this figure. **b)** Stepped profile of Horizon 1, evidencing the influence of pre-existing faults on the mass-failure. The small steps in the horizon irregular profile are due to fault activity, whereas high steps are due to remobilization of failed strata. The latter is confirmed by the height of the deformed block, similar to the height of the erosional step. **c)** section of MTD-A1 depicting the relation between faulting and remnant strata/blocks. The remnant features show evident vertical continuity with the underlying unit, limited by the erosional surface. Notice the thicker accumulations on the eastern sector underlain by faults. **d)** and **e)** illustrate in more details the link between blocks and pre-failure faults. The blocks commonly show their limits aligned with the faults, especially less deformed ones. Fractures are commonly identified within the bigger blocks. Rafted blocks show titled or folded internal reflections, implying lateral movement. Fault-block alignments are less evident in this type.









**Figure 5.5.** Seismic profiles illustrating the thinning of MTD-A1 towards the western and eastern limits. **a)** and **b)** evidence the morphological step of Horizon 1 which limits the regions of higher thickness of the MTD. **b)**, **c)** and **d)** show blocks in the morphological depressions where thicker accumulations occur. The thickness of MTD-A1 is commonly defined by the block height, and these are absent in the thinner regions.

#### 5.4.1.1. Remnant and rafted blocks

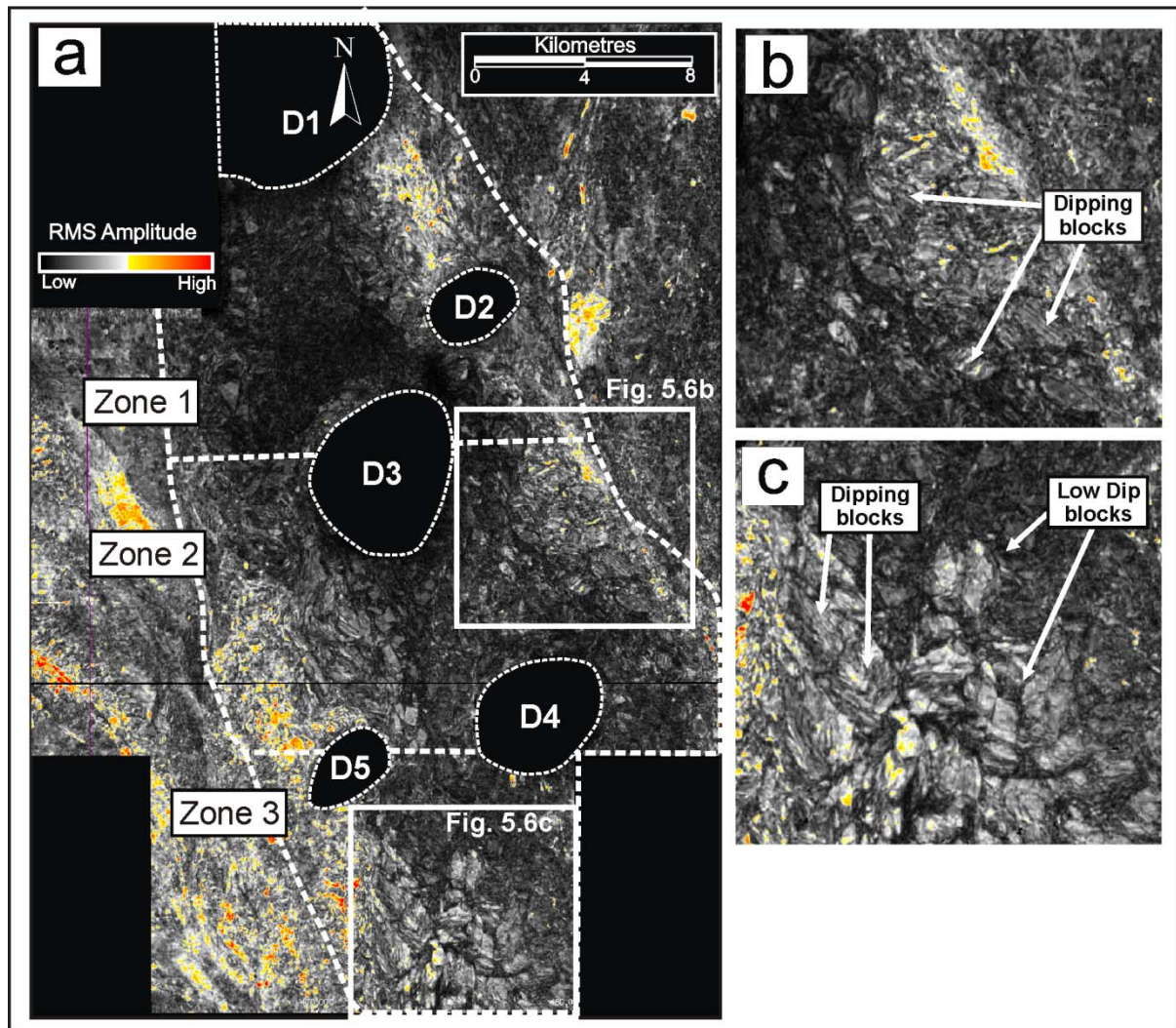
Blocks of strata within MTD-A1 were identified by the presence of moderate- to high-amplitude reflections within the low-amplitude, chaotic seismic reflections that comprise adjacent debrites (Figs. 5.1 and 5.3). The recognition of geometric features on coherence slices (Fig. 5.2) and amplitude maps (Fig. 5.6) allowed a more detailed analysis of the blocks' morphology. Remnant blocks are identified as being *in situ*, representing elements from the pre-failure strata that were not removed by erosion. Such blocks show vertical stratigraphic continuity with underlying non-MTD strata, with absence of any gliding surface, similar to the features described in Moscardelli et al. (2006) and Alves (2010). The identification of remnant features also had on account the relation between the block edges and any underlying faults. In contrast, rafted blocks are considered to have been transported downslope and commonly rest on top of the gliding surface (Horizon 1), although some are seen "floating" within the disaggregated chaotic matrix of the MTD.

The geometry of remnant and rafted blocks was assessed by combining coherence data and RMS amplitude maps (Figs. 5.2 and 6). Figure 5.2 represents a coherence slice taken 20ms above horizon H1. The chaotic sections of the MTD are represented by dark, mottled patterns. The blocks are clearly distinguished within these mottled areas as coherent sub-geometric features with sharp edges. Individual blocks are commonly in contact with each other where higher densities are observed, as in Zone 3. The majority of blocks are confined along the northwest-trending depressions observed on the diapir ridge, being practically absent away from it (Fig. 5.2 and 5.6).

Rms amplitude maps show similar results to the coherence slices (Fig. 5.6a). The map in this figure represents an interval 20 to 40 ms twtt above Horizon 1. The geometry of the remnant and rafted blocks is evidenced by moderate- to high-amplitude features with geometric to sub-geometric shape, as previously mentioned from the coherence data (Fig. 5.2). However, in contrast to coherence data, the rms amplitude map in Figure 5.6 shows that the blocks are not uniform. A significant amount of the blocks in Zone 3 are distinguished by their high amplitude values. Lower amplitude blocks also prevail in Zones 1 and 2, where they are harder to be distinguished from adjacent failed strata. Rms amplitude data can, however, highlight the presence of parallel bands inside imaged blocks, which often relate to the presence of dipping strata in the blocks (Fig. 5.6b). Such features indicate block deformation and rotation, namely stratal dip, which also provides indications to assess the transport direction of the MTD. These features are characteristic of rafted blocks.

Unless otherwise stated, the term “blocks” used in this study regards either types indistinctively of being remnant or rafted. This is used as a simplification when the block-related processes or properties are considered to be identical.



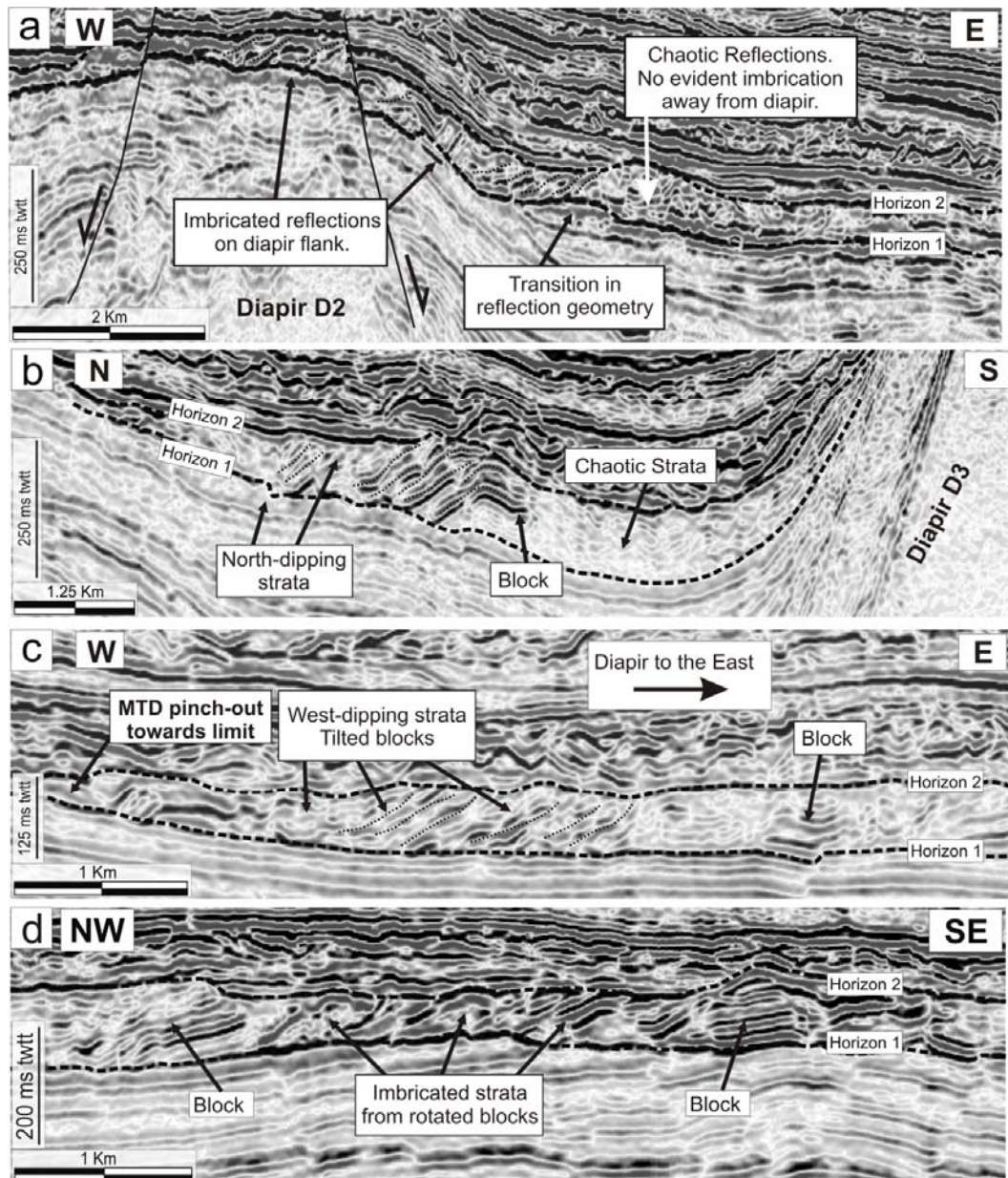


**Figure 5.6.** a) RMS (Root-Mean-Square) amplitude map of a time window within MTD-A1 between 20 and 40 ms TWTT above Horizon 1. Higher amplitudes are observed closer to the rims of the MTD, whereas the axial area of the ridge shows lower amplitudes. The blocks are evidenced by higher rms amplitude values. b) Detail of blocks with dipping internal strata evidenced by the alternations of pattern in rms amplitude. c) Detail of blocks with variable internal dip. The rms amplitude maps provides an indicator of block deformation as tilted blocks show the banded internal aspect, whereas non-tilted ones have relatively uniform amplitude patterns.

#### 5.4.1.2. Internal imbrication

Within MTD-A1 the stratal imbrications are evidenced by high-amplitude reflections dipping away and towards the observed diapirs (Fig. 5.7). The best examples are observed on the eastern flank of the main diapir ridge, on the northern flank of diapir D2 (Zone 1) (Fig. 5.7a). Strata imbrication is observed along the flank of the diapir D2. At the transition point towards the axial salt-withdrawal basin the MTD seismic character changes into the chaotic reflections with no obvious organization. These also correlate with thinner sections of the MTD, which gradually thickens as dip decreases. The section described is not related to any blocks in the coherence and rms amplitude maps, therefore it is interpreted as being related to compression resulting from movement perpendicular to salt ridge DR1.

We interpret the majority of imbricated features identified in seismic profiles as rotated rafted blocks (Fig. 5.7b). Although on key seismic profiles their character is similar to compressional features, the coherence and rms amplitude maps show a limited coverage for the higher amplitude dipping strata, being surrounded by low amplitude chaotic reflections. The blocks often dip away from the diapirs, as in Figures 7b and 7c, being bounded by normal and reverse faults (Fig. 5.3 and Section 5.3.1.3). Despite the distinct orientation in both figures, they suggest to represent collapsed blocks flowing towards the central areas of the salt ridge. Other cases also show that the rotated/imbricated blocks also occur in close association with less deformed blocks (Fig. 5.7d). This is common in the major block clusters within MTD-A1, meaning that in these sections the blocks' movement should have been more complex.



**Figure 5.7.** Seismic sections depicting internal imbrications in the MTD, used as kinematic indicators of the MTD transport direction. **a)** Seismic section north of diapir D2, showing imbrications dipping towards the diapir, indicating eastwards flow towards the salt-withdrawal basin. The evident imbrications on the top and flanks of the diapir suggest a flow collision with the chaotic masses in the salt-withdrawal basin. **b)** Section on the northern flank of diapir D3. Imbricated strata indicate southward movement of this MTD component, buttressing against the diapir. **c)** Section on the rim of MTD-A1, where imbricated blocks evidence eastwards flow of a peripheral component towards the diapir ridge **d)** Example of imbricated strata on the eastern regions of the salt ridge. This section evidences differential MTD internal flow. Rotated blocks have their movement hindered by larger, less remobilized blocks.

#### 5.4.1.3. Fault distribution and relation to failed blocks

The majority of faults in Unit 1 are truncated by the Mid-Eocene unconformity that limits the unit, with some propagation above this same surface. Propagating faults are, in the study area, related with halokinetic deformation (Alves et al., 2009), forming polygonal-shaped fault sets in Unit 1 (Figure 5.8a and 5.8b). The relation between faulting and the presence of blocks is particularly evident on the eastern section of Zone 2 and the majority of Zone 3, also coincident with the presence of underlying salt ridges (Fig. 5.8c). A quantitative comparison of the area of the blocks and the fault spacing below Horizon 1 revealed that, on average, the area of fault spacing in Zone 2 is 0.28 Km<sup>2</sup> and block area is 0.31 Km<sup>2</sup>. As for Zone 3, the average areas of fault spacing and blocks are 0.38 and 0.36 Km<sup>2</sup>, respectively. The proximity of faults and blocks, in particular remnant ones (Fig. 5.3), plus their similar trends suggest a genetic link between both features. Key seismic profiles also evidence the relation between faulting and the features present in MTD-A1 (Fig. 5.3). East of diapir D4, pre-existing faults are suggested to limit regions later deformed and evacuated by the mass-wasting event. Although Horizon 1 probably had a stepped profile due to fault offsetting, the most prominent step and consequently a section of higher MTD thickness is well delimited by one of the Palaeogene faults. The presence of a deformed rafted block with approximately the same height as the morphological step, plus the cut of several reflections in Unit 1 support the hypothesis that the irregularity of the gliding surface is equally due to tectonic and erosional processes (Fig. 5.3b).

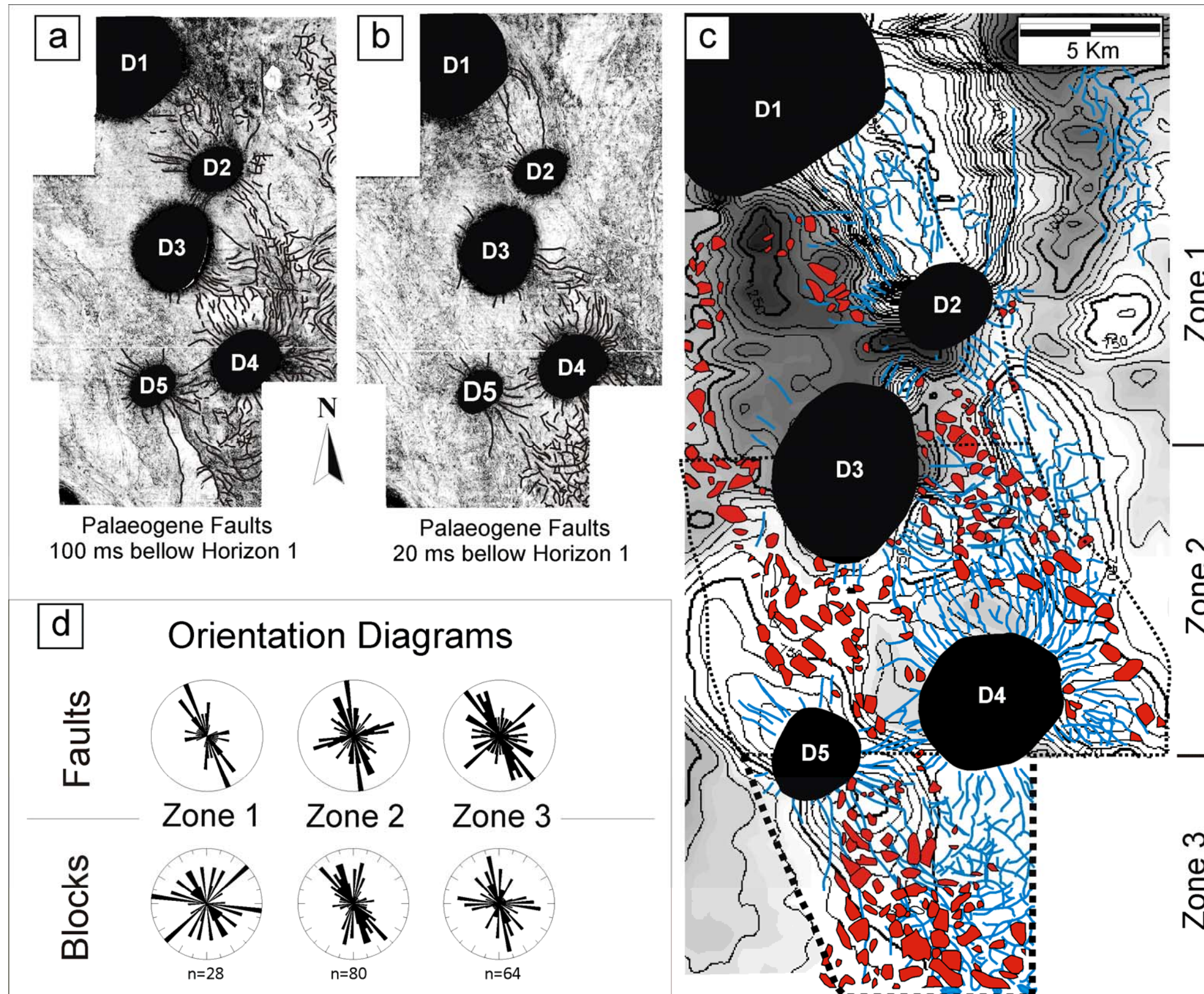
The most evident link between blocks and pre-existing faults is seen above buried salt structures in Zone 3 and Zone 2 (Figs. 5.3c and 5.3d, respectively). The limit of remnant



blocks is often aligned with the direction of underlying faults, especially in cases where blocks with sub-horizontal internal strata are observed, or where their downslope movement was hindered (Figs. 5.2 and 5.3). This character is more common in larger blocks or in locations where fractured remnant blocks with evident internal faults, but not completely broken, occur (Fig. 5.3e). In general, the regions with higher fault density are the ones with higher number, and larger sizes, of blocks.

#### **5.4.2. Peridiapiric block distribution**

This section shows the results of a quantified analysis of block characteristics and distribution. For this we considered the three zones previously mentioned in order to identify any significant statistical variations across the investigated diapir ridge. A total of 172 blocks were analysed. We measured their height, length, width, area, orientation (long axis) as well as distance from the established diapir ridge axis. The results are illustrated as graphs in Figure 5.9. The data is represented in relation of: 1) the block distance to the diapir ridge axis and 2) the position relative to the reference, i.e., East or West of the axis. The range bars in 5.9a, 5.9b and 5.9e represent the minimum, maximum and average value of the represented parameters for each zone. The block density plot (Fig. 5.9b) illustrates the number of blocks per zone identified at a given distance from the diapir ridge axis. The quantitative analysis of variations in block properties not only allows an evaluation of the origin and evolution of the MTD, as it will also characterize the possible fluid conduits through the failed strata. It should be pointed out that, due to survey limitations, in Zone 3 we can only consider the blocks west of the diapir axis. From the total, twenty eight (28) were located on Zone 1, eighty (80) on Zone 2 and sixty four (64) on Zone 3.



**Figure 5.8.** Relation between faults and blocks. **a)** Coherence map of a slice taken 100 ms TWTT bellow Horizon 1, showing the faults in Unit 1. **b)** Coherence map of a slice taken 20 ms TWTT bellow Horizon 1. These maps show important faulting of Unit 1 along the southern and eastern regions of the diapiric ridge. **c)** Map evidencing the buried salt ridges and the modern diapirs with the overlay of the faults in Unit 1 and the blocks in MTD-A1. The ridges, faults and blocks show a close relation in Zone 3 and the eastern region of Zone 2. Note how the more fractured areas correspond to the ones where block frequency is higher. **(d)** Rose diagrams with the fault and block orientation along the diapir ridge. Both features show preferential northwest trending directions.

#### 5.4.2.1. Block surface area

The total area (A) covered by the blocks is in average 11.3% over the diapir ridge. However, these values vary within the three investigated zones such as  $4.96\% < A < 17.32\%$ . The relative proportion of blocks in each sub-zone shows that these cover 4.96% (10.11  $\text{Km}^2$ ) of Zone 1, 11.60% of the area (25.17  $\text{Km}^2$ ) in Zone 2, and 17.32% (22.76  $\text{Km}^2$ ) of Zone 3. The largest block is located in Zone 2 (2.3  $\text{Km}^2$ ) and the majority of the blocks with surface area higher than 1  $\text{Km}^2$  are located in Zone 3 (Fig. 9a), but 85% of the studied blocks have areas below 0.5  $\text{Km}^2$ . Average block size is 0.4  $\text{Km}^2$ , similar in the three zones. The similar average values for the area in the three zones suggest a similar evolution for the blocks along the slope, as they should be expected to show significant variations towards downslope regions. In addition, this analysis is also important to estimate the areal extent of hypothetical fluid conduits.

#### 5.4.2.2. Block Orientation

The blocks show different long-axis orientations, as illustrated by the rose diagrams on Figure 5.8d. In Zone 1, long-axis orientations are variable and no predominant directions are evident. They predominantly occur along two northwest-trending patches away from the diapir axis. In Zone 2, there is a preferential northwest-trending orientation for the majority of the blocks. This is particularly evident on the flanks of diapir D3 where the larger blocks tend to show the long axis oriented towards northwest directions. A similar northwest trend for the majority of mapped blocks is observed in Zone 3, with a secondary West-East trend. In Zone 2 there is clear general orientation of the blocks around the flanks

of the salt diapirs which tends to be parallel to the diapir axis line, whereas in the non-pierced Zone 3 their orientation is more varied (Fig. 5.8d). The orientation of the blocks is commonly used as a diagnostic element for how far they have travelled in relation to the original location (DeBlasio et al., 2006). In this study, the blocks show a predominant northwest-trending orientation along the salt ridge, which suggests a similar dynamic and proximity to the source. Furthermore, the orientation also supports the hypothesis that Palaeogene faults and blocks are related as both features show similar trends in the rose diagrams.

#### 5.4.2.3. Block Density

Block density is shown to vary within each zone in relation to the distance to the diapir axis. The graph in Figure 5.9b shows the lowest number of block occurrences close to the centre and rims of the diapiric ridge. In essence, the majority of the blocks in MTD-A1 are within distances ranging from four to ten kilometres west of the diapir axis. In contrast, the central section registers the lowest density, especially within the first two kilometres west of the reference line. Comparing Fig. 5.9b with the isochron map for MTD-A1 in Figure 5.4b, lower block density corresponds to a thinner area in Zone 2, but in contrast it matches with some of the thickest intervals in Zone 1. On the eastern flank, most of the blocks are located within Zone 2, while the majority of them in Zone 1 are limited to an area stretching just four kilometres away from the diapir ridge axis (Fig. 5.9b). The density plot adds a quantitative aspect to the observations made in previous sections of this study about the block distribution within the MTD, especially their preferential northwest-trending accumulation flanking the axis of the diapir ridge (Fig. 5.4).

#### 5.4.2.4. Block Height

Measured blocks showed a relatively large range in height, generally limited by the thickness of MTD-A1. The majority of the blocks have heights between 100 and 180 m (Fig. 5.9c), and are preferentially clustered in two main regions. On the west flank, the majority of the blocks are located between 4 and 8 km from the salt diapir axis along the whole slope, regardless of which zone they are present. Outside this interval, the highest blocks closer to the central axis are located in Zone 2, whereas in Zone 3 tall blocks are found towards the limit of MTD-A1. The eastern side has the major agglomeration 4 km away from the axis line, with the majority of blocks in Zone 1 also occurring within this region. The highest blocks on each flank of the salt anticline are generally located within the distances previously specified, reaching heights between 200 and 250 m high. Despite having quite significant height ranges, average values around 130 m were observed for each of the three main zones.

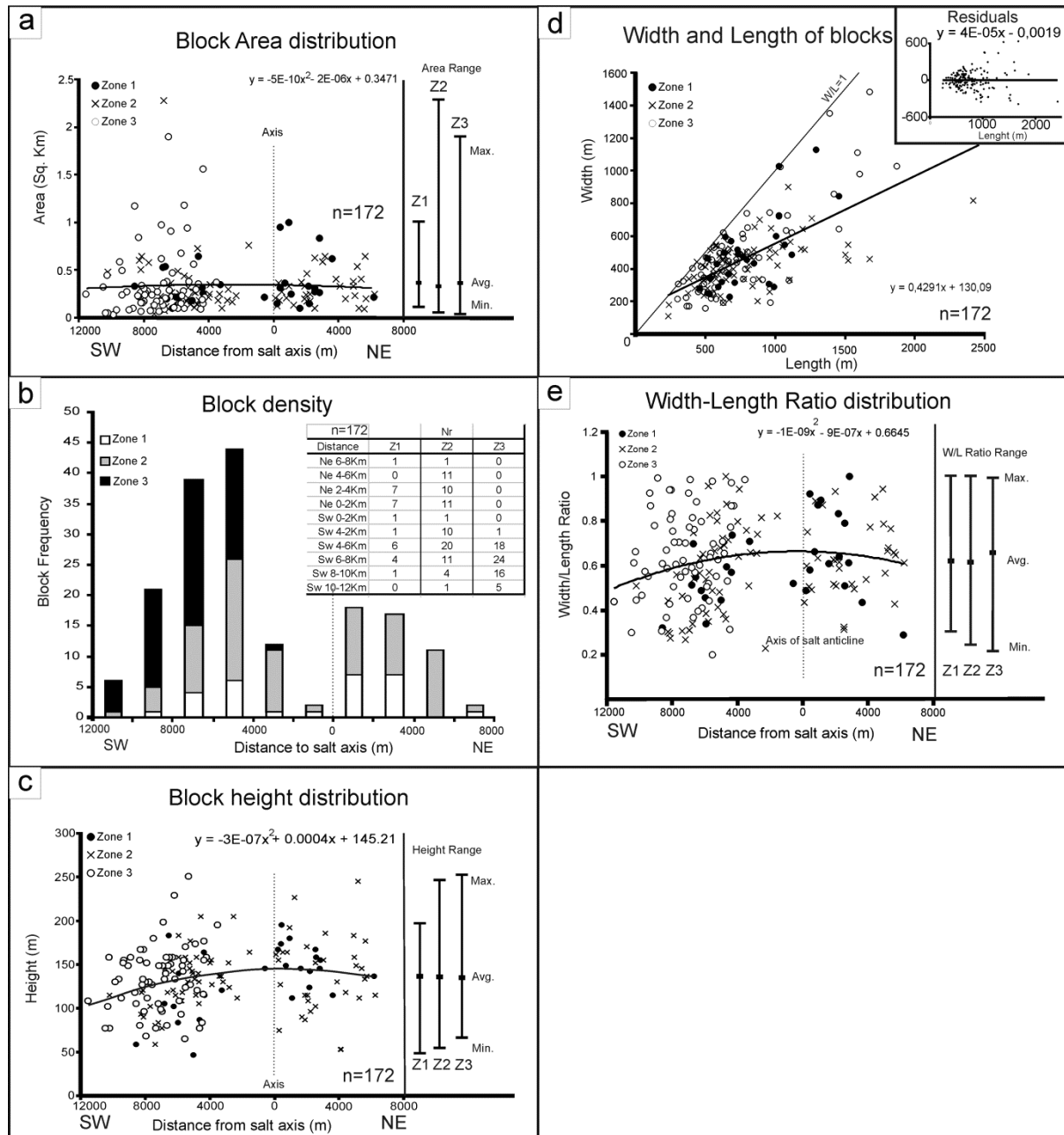
The height, as the area, is another property to take in account when assessing how far the rafted blocks have travelled as this parameter tends to decrease with distance (Alves and Cartwright, 2009; Gee et al., 2005; Laberg and Vorren, 2000). In this study the highest elements are observed in the more centralized regions of MTD-A1 which also coincide with the thickest accumulations observed in the isochron map (Fig. 5.4b). The fact that the highest elements tend to be in the central regions of the MTD also provides indications of any pre-failure relief and glide plane depth. The block height is commonly the same as the total MTD thickness, as shown in Figures 5.3 and 5.8.

#### 5.4.2.5. Width/Length Ratio

Variations in block dimensions, namely width and length, are represented in Figure 5.9d. The majority of the measurements are clustered within length values of 400 to 800 m and widths of 200 to 600 m. Outside this cluster, most of the remaining blocks have around 900 to 1200 m in length and reach up to 900 m in width, although blocks of Zone 2 have lengths up to about 2400 m. Some of the highest block width /length values are located in Zone 3, where they exceed 1000 m both in width and length. The residuals in Figure 5.9d were calculated to assess the fit of the observed values with the estimated values calculated by the linear trend. The residuals plot shows the regression against length values. The even distribution for residual values confirms the linear relation between block width and length.

Comparing the width-to-length ratio with the position within the salt ridge, there is no evident distinction between the sub-zones or the distance from the reference axis (Fig. 5.9d). The ratio values range from 0.2 to close to 1 across most of the block area in MTD-A1, except for the western limit where the ratio does not exceed 0.7. Based on the obtained values, the general shape ratio of the blocks does not seem to vary significantly along the slope, as average w/l ratios of 0.60 are seen in Zones 1 and 2, and of 0.65 in Zone 3. This aspect ratio of the blocks is commonly related to the degree of disaggregation, and consequently with their breakdown with transport (De Blasio et al., 2006). Many blocks show width/length ratios with high values, which can be interpreted as being relatively close to their source.





**Figure 5.9.** Graphic representation of the statistical data obtained from the interpreted blocks in MTD-A1, evidencing their properties in the three different zones and distance to the diapir ridge axis. Bars on right-hand side represent the minimum, maximum and average values of each parameter at a given Zone. **a)** Block area distribution in the salt ridge. **b)** Block density and their distance to the salt ridge axis. **c)** Block height. **d)** Width and length of blocks. **e)** Width-Length ratio of blocks in relation to their distance to the salt ridge axis. Blocks are distributed asymmetrically in relation to the ridge axis. The results show a general similarity of blocks alongslope, indicating similar genesis and remobilization in the three studied regions. Plotted best-fit lines represent the entire block data series, regardless of the zone.



### **5.4.3. Block deformation**

#### **5.4.3.1. Deformation styles**

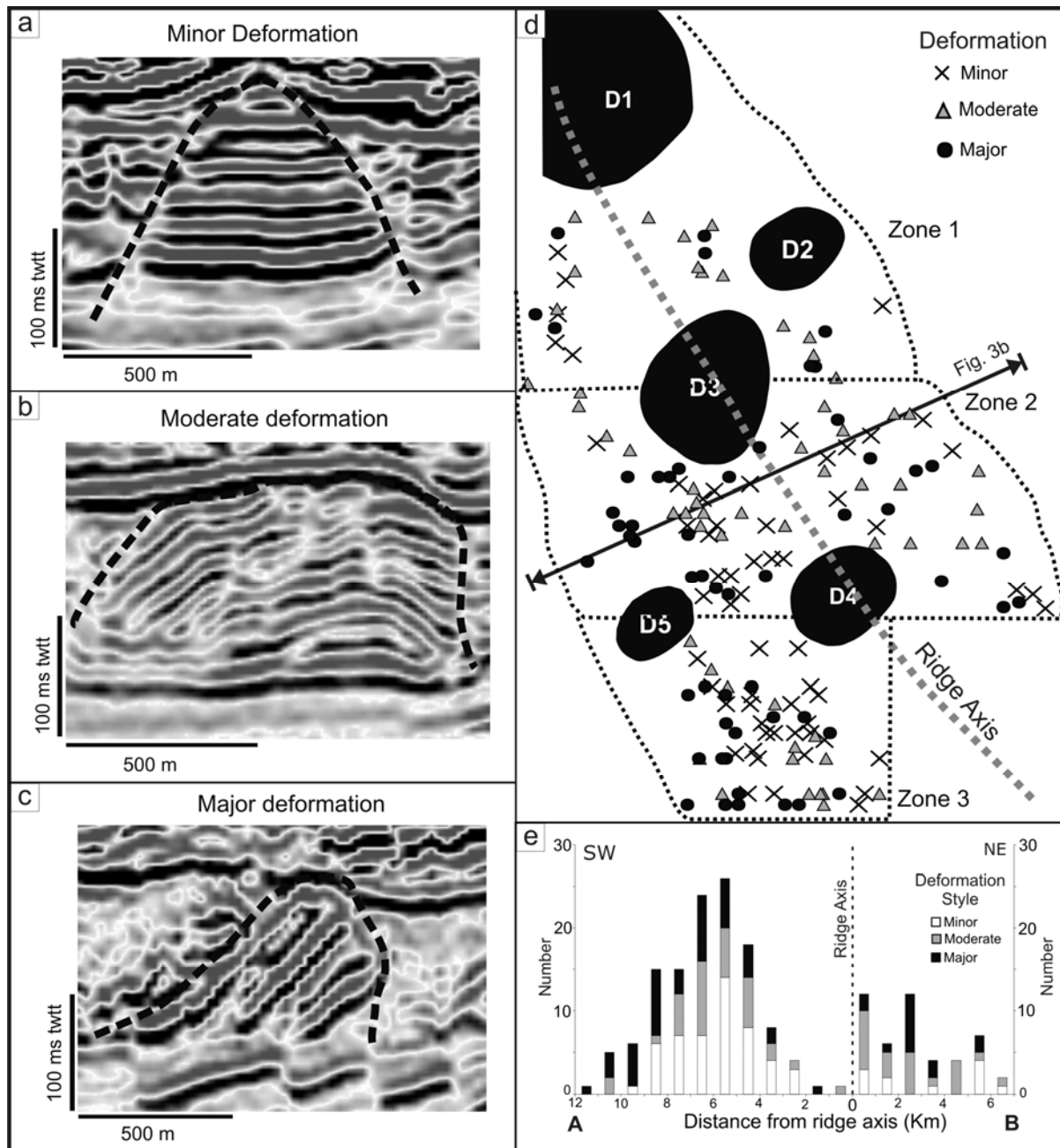
The studied remnant blocks show distinct styles of deformation. These were classified in three types, each related to a style of block deformation observed on the seismic profiles (Figure 5.10). Minor deformation blocks preserve the original stratal relations, shown by packages of parallel sub-horizontal reflections, often sub-parallel to strata present in Unit 1 (Fig. 5.10a). The moderate deformation type includes tilted blocks which show diverging dips in internal strata, as well as internal folds (Fig. 5.10b). These folds are more common in larger blocks. The folding is mostly materialised as antiforms, although some synforms are observed. Major deformation show internal strata dips over 15 degrees (Fig. 5.10c), frequently with internal folding. It is common to find blocks with major deformation in contact either with the same or the other deformation styles. Boundaries of observed blocks are well marked, and commonly coincide with faults underlying MTD-A1. Their contacts often suggest that they derive from the breakup of a larger block (Fig. 5.3e). The deformation of the blocks will imply different degrees of fracturing and folding within them, especially as smaller scale features.

#### **5.4.3.2. Quantification and distribution of deformation types**

In this section we show a quantified analysis of the different types of block deformation. Figure 10d shows the distribution of the blocks within each established zone, as well as their position in relation to the salt diapirs. The distribution is not uniform, with the three styles of block deformation commonly occurring together. The general models for

flow transformation for MTDs state that there is a gradual increase in block deformation towards the distal regions (Homza, 2004), but our results show contrasting results with different degrees of deformation occurring at the same locations. The distributions of each deformation style in relation to the axis of the main salt ridge are shown in Figure 10e. The eastern flank has fewer blocks, comprising 48 of the total 172, with the majority located in Zone 2. Moderately deformed blocks are the most common found through the extension of this flank, and these also constitute most of the ones identified in Zone 1. Blocks of minor deformation in Zone 2 show higher densities close to the diapir axis and in distances over 6 km away from it, with low occurrences in between (Fig. 5.10e).

On the western flank, the amount of blocks is much higher and their distribution is less uniform, tending to be clustered. Zone 1 has the simplest distribution with the blocks roughly aligned along a limited area. Zones 2 and 3 tend to show similar clustering and distribution trends. In each of the sub-zones blocks of minor and moderate deformation occur relatively mixed within the same locations, although in Zone 2 the latter type tends to occur further from the diapir axis (Fig. 5.10d). As for the major deformation blocks, there is an evident higher number of these towards the rims of MTD-A1, especially towards the west. Nevertheless, major deformation blocks are also found in close relation with minor deformation ones in the main clusters observed above the diapir ridge (Fig. 5.2, 5.3d, 5.5b, 5.7d and 5.10d).



**Figure 5.10.** Different styles of block deformation. **a**) Minor deformation represented by sub-horizontal internal strata. **b**) Moderate deformation with folding and low tilt of blocks. **c**) Major deformation, represented by steeply dipping strata ( $>15^\circ$ ) due to block rotation. **d**) Distribution of block deformation styles along the salt ridge. **e**) Graph of the frequency of deformation styles in relation to the distance from the ridge axis. The plot in **e**) is a projection of the blocks distribution shown in **d**), and no zone distinction is represented. Note the relatively uniform distribution of deformation styles, with the exception of the western rim of the MTD where major deformation is prevalent.

The average values for the width/length ratio, as well as the number and proportion of deformed blocks are summarized in Table 5.1. In Zone 1 the majority of blocks have moderate deformation which also corresponds to the blocks with the highest average areas and heights, but in terms of width/length ratio they are similar to the major deformation style. As for Zone 2, the proportion of each deformation style is similar. In terms of height values, the highest averages are for minor deformation, reaching up to 153m, with the remaining being around 125 m. The blocks with major deformation cover larger areas, with an average value of  $0.43 \text{ km}^2$ , nearly twice the average area of the two other types. Minor deformation blocks are the most abundant in Zone 3, representing 45.3% of the total. This is followed by major deformation blocks (31.25%) and lastly by 23.44% of the moderate style. Contrasting with the latter values, the moderately deformed blocks have the highest average values for height (91.4 m) and area ( $0.58 \text{ Km}^2$ ). As for the width/length ratios, all of them have similar values and as such relatively similar shapes

Deform.	Zone 1					Zone 2					Zone 3				
	W/L Ratio	Area (Km <sup>2</sup> )	Height (m)	Nr	%	W/L Ratio	Area (Km <sup>2</sup> )	Height (m)	Nr	%	W/L Ratio	Area (Km <sup>2</sup> )	Height (m)	Nr	%
Style 1	0.51	0.33	72.67	6	21.4%	0.64	0.26	98.92	26	32.5%	0.64	0.32	88.72	29	45.3%
Style 2	0.63	0.40	96.00	14	50.0%	0.63	0.26	80.67	27	33.8%	0.68	0.58	91.4	15	23.4%
Style 3	0.64	0.32	80.50	8	28.6%	0.54	0.43	81.11	27	33.8%	0.65	0.26	79.2	20	31.3%

**Table 5.1.** Average values of blocks properties according to style of deformation and slope zone.

## 5.5. Discussion

### 5.5.1. Halokinetic structures as triggers of slope instability

The results in this chapter show an unusual relation between MTDs and halokinetic structures, as the thickest accumulations of remnant/rafted strata occur within the region of salt growth, with MTD-A1 thinning away into the salt withdrawal basins (Fig. 5.2 and 5.5). This character contrasts with most published examples, which show accumulation and thicker deposits within salt withdrawal basins, and thinning on the rims of diapirs due to sediment removal (Alves and Cartwright, 2009; McAdoo et al., 2000; Tripsanas et al., 2004). Consequently, the principal question rising from our observations regards the origin and flow dynamics of MTD-A1. In this discussion are presented two distinct hypotheses regarding long and short travel distances of the mass-flows.

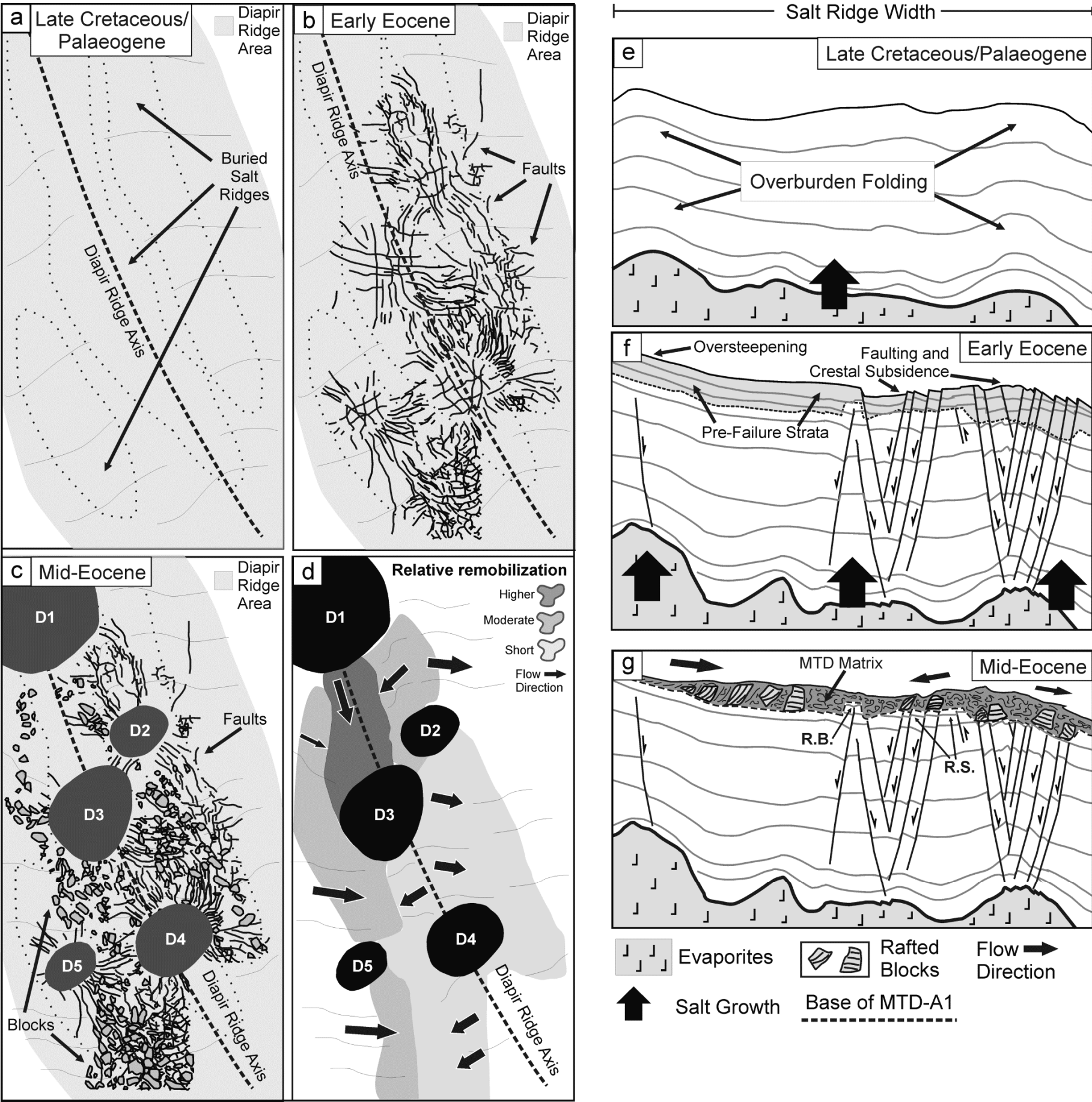
A first explanation is that MTD-A1 originated from a failure upslope from the study area, flowing southeast along a depocentre approximately coincident with the regions where the thickest accumulations (and the majority of the blocks) are observed. The blocks within the failed strata would flow and accumulate in downslope locations, as in Zone 3. This implies limited, if any, salt growth at the time of the MTD deposition. We must consider that for such long run-out the blocks would suffer size reduction and re-orientation along the extension of the flow (Alves and Cartwright, 2009; Bull et al., 2009; Homza, 2004; Laberg and Vorren, 2000). The interpreted seismic data do not support this interpretation, as block with similar geometries were observed in the three studied zones. In addition, this explanation implies that any alignment between rafted blocks and underlying faults would be aleatory. The various examples illustrated in the seismic profiles suggest a closer link

between underlying faults and remnant/rafted blocks as evidenced, for instance, by the presence of remnant strata over crestal faults (Figs. 5.2, 5.3 and 5.8).

A second explanation includes complex multi-directional remobilization of MTD-A1, with shorter travel distances involved and a localized origin for the blocks. The thickness and attribute data in Figure 5.4, depicting the location of remnant/rafted blocks, suggest a nearly mirror distribution of the MTD features relatively to the diapir axis. Statistical results confirm the latter statement as blocks cluster within specific distances to the diapir axis, and tend to show a gradual decrease in size towards the rims of the salt ridge (Fig. 5.10). This suggests remobilization of material from the central parts of the salt ridge towards its margins. Furthermore, high values of the block width-length ratio are indicative of proximity to the source regions, i.e. short remobilization distance, being this particularly evident for Zone 3 (Fig. 5.10e).

A short remobilization distance is also supported by the close spacing of blocks and their relation to underlying faults. This is particularly noted in the case of fault-bounded blocks observed on top of the ridges and in inter-diapiric areas (Fig. 5.3). Such failed blocks represent localized portions of pre-failure strata segmented into several crestal fault blocks developed above growing salt structures (Cobbold and Szatmari, 1991; Gaullier and Vendeville, 2005). In contrast, blocks not underlain by vertically-propagating faults on the western part of the salt ridge imply a different origin and further travel distances compared to the fault-related ones, but their presence above the crests of the buried ridges does not rule out a salt-related origin (Fig. 5.2 and 5.3). Blocks commonly develop in extensional domains of the MTD, whereas stratal imbrications and thrust features characterize the compressional domains (Ashabranner et al., 2010).





**Figure 5.11.** Schematic diagram with the evolution of the diapir ridge. Salt ridges developed deformed the overburden, forming a northwest-oriented relief (**a** and **e**). Early deformation and faulting of the overburden along the buried salt ridges also led to partial subsidence on the crest of the salt ridges and diapirs (**b** and **f**). Failure and deposition of MTD-A1 with numerous blocks located along the main diapir ridge. Remnant blocks/strata are limited by faults, whereas the presence of rafted blocks is not strictly dependant of underlying crestal faults (**c** and **g**). **d**) Diagram illustrating the relative movement of the MTD components. Higher remobilization is interpreted to occur in the area north of diapir D3, with convergence of flow directions. Short remobilization is interpreted to have occurred along the axis of the diapir ridge, with MTD components spreading perpendicularly to the latter. Moderate remobilization occurred predominantly along the western rim of the MTD with these components flowing eastwards, colliding with the ones in the central regions.

On the upper slope (Zone 1), the MTD imbrications evidence north-derived flows (Fig. 5.7b and 5.11d), but there is also a lateral (W-E) component derived from the collapse of strata over the upslope sections of ridge BR2 (Fig 5.7a and 5.11d). Notice also that this area is characterized by a steeper profile of Horizon 1 (Fig. 5.4d).

In the remaining zones, the flow dynamics can be estimated from the geometry of the blocks. The block rotation, orientation and proximity on western rim of zones 2 and 3 (Fig. 5.2 and 5.6) delimit an eastward-flowing compressional component of the MTD, with evidence of thrusting observed on the seismic profiles (Fig. 5.2, 5.5, 5.7c and 5.7d). The central regions of the MTD are generally correlated with extensional regimes, as shown by the dispersal and spacing of the blocks. The presence of rotated blocks close to less deformed ones may imply different downslope velocities within the flow, with the possibility of the increase of deformation being due to the collision of smaller, faster travelling blocks with larger ones with limited movement. Another possibility is that the more deformed blocks result from squeezing of softer material between less competent strata (Fig. 5.7d). The latter is also supported by published works of onshore fossil MTDs that have documented the presence of both brittle and ductile block deformation occurring close together due to contrasting sediment cementation and temporal changes (Callot et al., 2008; Odonne et al., 2011, Van der Merwe et al., 2011). This has also been associated with the block sedimentary composition, but there is no indicator that such could be the case in MTD-A1. In addition, the major deformation blocks might derive from the break-up and collapse of the flanks of larger ones.

These complex associations reveal how the classical models of intra-MTD deformation evolution may not be suitable to describe this and other complex failures.

Combining the interpretations above, and the fact that low remobilization blocks occur within the thickest sections of the MTD, we estimate the presence of a palaeo-relief developed along the diapir ridge (Fig. 5.11a and e). The morphology of the gliding surface shows some flattened or depressed regions (Fig. 5.4a) which may contradict the presence of such relief, but this is either due to erosion (Fig. 5.3c) or to limited subsidence of the faulted overburden due to the growth and eventual deflation on the crest of salt ridges (Fig. 5.11f) (e.g. Dooley et al., 2009; Jackson et al., 1994; Schultz-Ela et al., 1993). On seismic profiles this is evidenced by relatively flattened faulted sections of Horizon 1 (Fig. 5.3). Consequently, MTD-A1 is interpreted to form due to the collapse of the relief created within the diapir ridge along the MTD basal shear surface (Fig. 5.11). The differential movements observed are also concordant with the collapse of a previously folded morphology along an irregular basal surface with different dip directions. The central region of the diapir ridge shows short remobilization of the blocks, with suggested spreading and accumulation occurring perpendicularly to the axis of the main salt ridge (Fig. 5.11d). A simultaneous collapse of the northern and western limits of the MTD imply a southward and eastward flow of failed strata, with the lateral collapses also involving the formation of back-tilted blocks and collision of these with the less remobilized central masses of the MTD (Fig. 5.11g). Clustering of blocks is common within depressions created by crestal subsidence along buried salt ridges, or due to higher erosion in these deformed areas at the time of collapse (Fig. 5.3), suggesting that their limits also restricted the transport of failed features. Thus, the failure of MTD-A1 is proposed to occur by faulting and over-steepening of the overburden due to the growth of the underlying salt diapirs. This interpretation is corroborated by:

- 1) the close link between the blocks and pre-existing faults and;
- 2) the fact that the limits of the main diapir ridge are coincident with the limits of MTD-A1, particularly in regions when the failure scarps are underlain by salt ridges (Fig. 5.2 and 5.3).

Analogue failures identified in fossil MTDs show similar features to the one analysed in this work, where block and matrix deformation provide indicators to assess flow movement and delimit different components (Alves and Lourenço, 2010; Butler and McCaffrey, 2010; Callot et al., 2008; Lucente and Pini, 2003; Lucente and Pini, 2008; Odonne et al., 2011). When derived from distinct sources, often due to tectonically-influenced topographic oversteepening and failure, the components are likely to exhibit both distinct lithological compositions and bulk deformation styles (e.g. Callot et al., 2008). As the sub-seismic deformation often mimics large scale features (Callot et al., 2008), on-land slabs can be used to estimate smaller features present in submarine slide blocks. Plastic deformation features are represented by increasing fold vergence and internal strata disruption the higher the remobilization distance and shear intensity (Alves and Lourenço, 2010; Odonne et al., 2011). Faulting is also observed at multiple scales, either derived from the initial failure or developed/enhanced with remobilization (Alves and Lourenço, 2010; Lucente and Pini, 2003; Odonne et al., 2011). Increased complexity is often observed at the block base in the interface with the basal shear surfaces. The high shear stress leads to increased brecciation and soft sediment deformation at these zones of variable thickness (Alves and Lourenço, 2010), leading the formation of clastic injectites propagating upwards the failed material (block or matrix) resultant from expulsion of over-pressurized fluids within the sediment (Butler and McCaffrey, 2010; Callot et al., 2008; Odonne et al., 2011).

Nevertheless, these features are less expected to occur in remnant blocks as these were not remobilized and are not underlain by any shear surface.

The analogy between MTD-A1 and fossil landslides strengthens the importance of integrating geophysical and land based methods to improve the characterization of such deposits. While field data provides details of small to meso-scale features and complexity, seismic data allows wider-scale morphological and structural interpretations where the sole study of outcrops shows limitations.

### **5.5.2. Can blocks constitute preferential fluid-flow paths?**

The studied blocks represent strata that maintain some or most of its original cohesion and constitute potentially permeable conduits for fluid flow through MTD-A1. Lithologic or structural features below seismic resolution, as thin permeable layers or fault networks, must also be considered as these can be as efficient fluid pathways as the larger seismically-resolved features within the observed blocks.

The examples in our study show faulting not only of Unit 1 but also evidence internal fractures in blocks (Fig. 5.3). The presence of such damage zones can lead to an enhancement of the permeability potential close to faults, within or below the blocks. Considering that the blocks could form effective vertical bypass mechanisms through the MTD, the identification of the major clusters may also indicate areas with potential higher rates of leakage. The plots of block distribution show the accumulations to be located between four and eight kilometres on the western flank of the diapir axis, and in the first two kilometres on the eastern flank (Fig. 5.9).

Block height is a relevant property to take into account as it sets the vertical extension of the permeable areas. Despite the range of values, the average height is around 150m (Fig. 5.9c), which is also the average thickness of the MTD. The highest blocks show minor and moderate deformation therefore we also expect a better preservation of the internal strata along the major bypass points (Table 5.1). One of the issues that may arise is how can fluid flow through the MTD basal shear surfaces where the rafted blocks rest, which are commonly more compacted (Sawyer et al., 2009), and the erosive surface itself can form a permeability barrier (Allan et al., 2006). The remnant blocks constitute an exception as these are expected to show vertical stratigraphic continuity with the underlying strata. In this case, any permeable features within the remnant blocks are not interrupted and this can lead to the supply of fluids through, and towards the top of, the MTD. The importance of faults and blocks on the bypass of MTD basal surfaces is evidenced in our data as several amplitude anomalies are present in the studied stratigraphic units (Fig. 5.12). These anomalies are interpreted to be fluid-related as they are represented by local amplitude increases typical of bright spots (Løseth et al., 2009; Sheriff and Geldart, 1995) and occur in stratigraphic intervals with proven presence of hydrocarbons (Biassussi et al., 1998). Bright spots are frequent in the vicinity of the crestal faults developed in Palaeogene strata (Fig. 5.12a), confirming their importance in fluid flow paths in the Espírito Santo Basin (Biassussi et al., 1998). In regions of the MTD underlain by faults, but where blocks are absent, fluid accumulates along the basal surface retained by the low permeability debrites (Fig. 5.12b and c). On the contrary, when fault-bounded blocks are present they can establish vertical migration paths either through their internal strata, or along the block-debrite interface (Fig. 5.11a and e). Moreover, fault intersections are potential points for increased rates of fluid leakage (Gartrell et al., 2004; Ligtenberg, 2005).

Strikingly, in our study the higher amount of intersections is observed in Zone 3 and the eastern area of Zone 2 (Fig. 5.8). This gets additional relevance as the faulted sections of Unit 1 are predominantly located on the flanks of the developed diapirs and above the crest of buried salt diapirs and ridges, which are documented to be locations of important fluid leakage in sedimentary basins (e.g. Cartwright et al., 2007; Ligtenberg, 2005; Meldahl et al., 2001).

Taking these factors into consideration, we establish a differential permeability potential for distinct regions of the MTD (Fig. 5.12d). The highest permeability potential is observed in areas with the closer relations between the blocks and the faults, especially when the blocks are delimited or cut by faults (Fig. 5.3). This also corresponds to the sections where the block area and height have the larger values (Fig. 5.10). Regions of moderate flow potential are established to include blocks that do not show any evident relation with underlying faults, exemplified by the western limit of the MTD in Zones 1 and 2. The lowest permeability potential is expected along the diapir axis where no blocks or faults are observed (central Zone 1). In general, the faults are truncated by the erosive surface of the MTD, nevertheless, there is an exception on the northern flank of diapir D2 (Zone 1). Here major crestal faults cut through MTD-A1 and overlying strata (Fig. 7a), thus constituting a major fault-based bypass point to the strata in Unit 2. In addition, we can correlate the permeability zonation of the MTD with the different flow components discussed above. As such, the higher permeability regions are suggested to relate to the MTD sections that show lower remobilization in relation to their source, with the permeability potential tending to decrease as the transport distance increases. Furthermore, fluid expulsion can also occur at the interface between MTD components with



colliding flow behaviours (e.g. western and central regions of MTD-A1) (Lucente and Taviani, 2005). Even in the case of short-period post-depositional expulsion, resulting fluidization structures created along the contact area could allow flow of later fluids supplied to the MTD.

To summarise, the relation of the studied blocks in MTD-A1 with the Palaeogene faults in Unit 1 (Fig. 5.3) establishes a potential hydrocarbon flow mechanism through the otherwise low permeability MTDs. This provides a viable process to supply reservoir-prone lithologies above the mass-wasting products (Fig. 5.12e), also allowing for fluids to accumulate within the MTDs if the adequate lithologies are present (Beaubouef and Abreu, 2010; Galloway, 1998; Welbon et al., 2007). In fact, the internal deformation in MTD-A1 is likely to be more intense than what is observed on seismic data as faults are also commonly surrounded by sub-seismic scale damage zones (e.g. Knipe et al., 1998; Zhang et al., 2010). Outcrop- and core-based studies have also shown the degree of complex brittle and ductile deformation within MTDs and these can replicate at variable scales (Callot et al., 2008). The development of micro-fractures is common in these deposits (Tripsanas et al., 2008), especially in higher cohesion sediments. Fractures within rafted blocks commonly develop upon the initial failure (Alves and Lourenço, 2010) but the effects of shear stress during transport must also be considered, regardless of the travel distances, which can either enhance previous fracturing or develop new ones (Alves and Lourenço, 2010; Lucente and Pini, 2003). This, associated with overpressure along the basal shear zone, favours the formation of clastic injectites propagating upwards either through the heterogeneous MTD matrix or tensile fractures in the block base (Alves and Lourenço, 2010; Butler and McCaffrey, 2010; Callot et al., 2008). Clastic injectites are particularly important for smaller

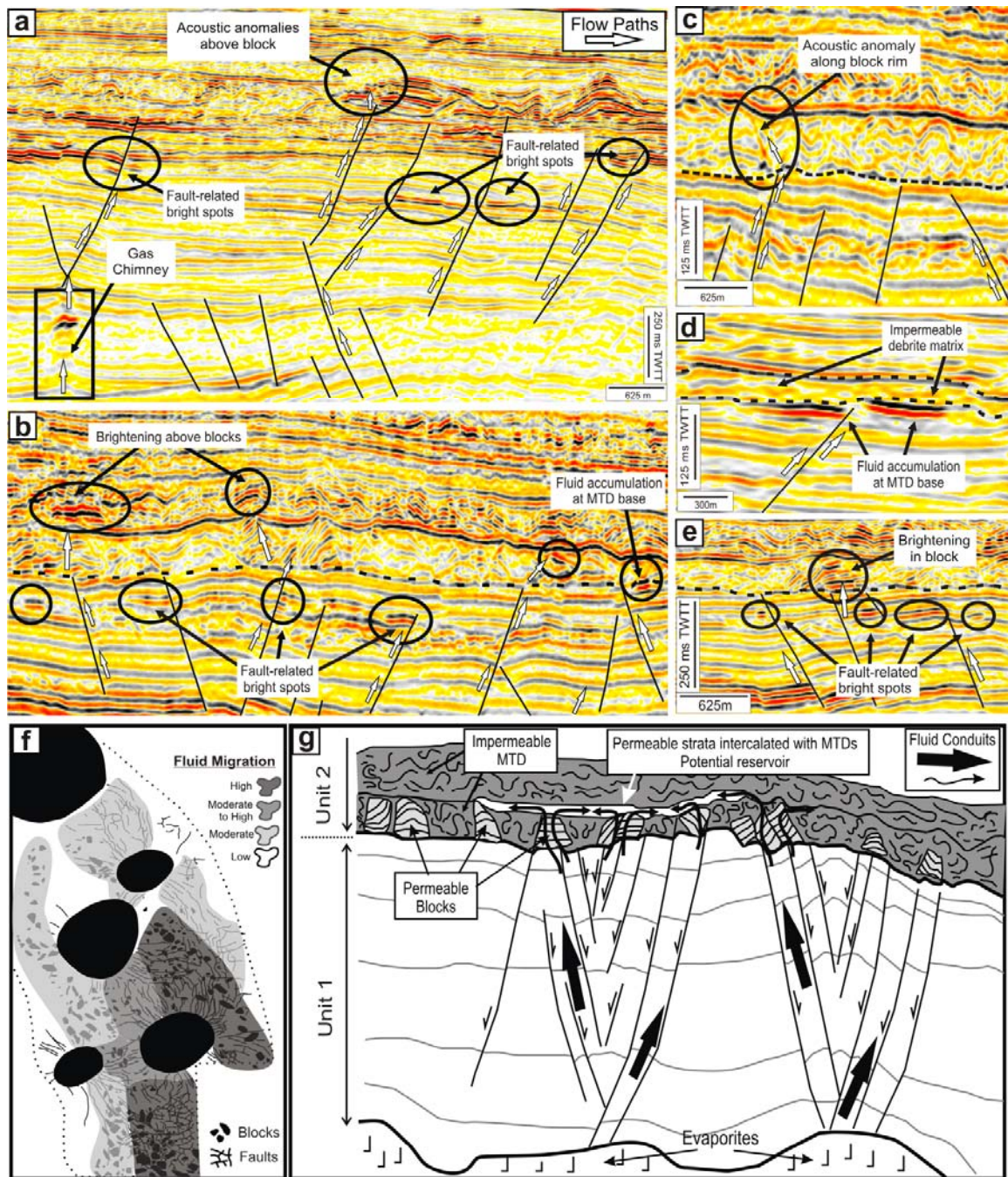
scale fluid flow within failed strata as they form good fluid conduits which can have higher permeability than their source beds (Odonne et al., 2011). Furthermore, fractures propagating on top of the blocks can also be filled by post-failure permeable clastic material (Odonne et al., 2011). The presence of sand either as a primary block component or derived from fracture filling favours the formation of permeable paths through the block strata, which can be enhanced or hindered due to variable styles of block deformation.

## **5.6. Conclusions**

The detailed analysis of the earliest Mid-Eocene mass-wasting deposit (MTD-A1) in the Espírito Santo Basin revealed a marked internal heterogeneity. Thicker accumulations of MTD-A1 are located within the region underlain by developed salt ridges and diapirs, thinning towards the salt withdrawal basin, contrasting with the more common situation of stratal thinning above growing salt structures. Several remnant/rafted blocks were identified, evidenced by sub-parallel reflections bordered by chaotic patterns in the MTD. In essence, major conclusions from this chapter include:

a) The origin of the blocks is linked to extensive arrays of halokinetic-related faults that deformed the pre-failure strata. The close relation between faults and blocks, complemented by MTD thickness maps, shows that the blocks occur close to their source area.

b) Blocks show, on average, heights of 150 m and areas of about 0.4 Km<sup>2</sup>, with these values maintained downslope, along the main ridge. This indicates similar processes and remobilisation of MTD-A1 at all slope locations. Three different styles of block deformation



**Figure 5.12.** Acoustic anomalies in the seismic data evidence the presence of fluids in the studied strata. (a to e). Faults in Unit 1 are associated with fluid migration, sourced from Late Cretaceous strata. Brightening in or above fault-bounded blocks, or the block-matrix contact suggest permeability enhancement features within the MTD. When blocks are absent, fluids are trapped underneath the impermeable debris. f) Diagram representing the fluid flow potential within MTD-A1. Areas with higher block frequency and faults have higher potential, whereas areas where no blocks or faults are observed have the lowest. Moderate potential is expected in faulted regions with fewer blocks, or where blocks show no evident relation to underlying faults. g) Schematic drawing representing fluid bypass through MTD units suggested by the close relation of faults and remnant/rafted blocks. Faults act as vertical fluid conduits in pre-failure strata. Migration through the MTD is made along permeable strata and fractures in the blocks.

were identified. Failure and collapse of a pre-Eocene northwest-trending relief generated a complex flow of the failed strata which spread along-slope in directions perpendicular to the diapir ridge axis. Relative block distribution also provides a way of dating the triggering of salt structures at the time of failure.

The heterogeneities in MTD strata shown in this chapter have implications in the assessment of the internal properties of failed strata and can constitute permeable fluid conduits, especially when in close relation with underlying faults. This is crucial when estimating seal capacity and/or fluid pathways in hydrocarbon exploration areas. The results shown for the Espírito Santo Basin in Brazil can be applied and compared to other continental margins with important mass-wasting.

# Chapter 6

## **Submarine confluence classification for topographically confined slopes**

This chapter has been published as “Gamboa, D., Alves, T.M. and Cartwright, J., 2012. A submarine channel confluence classification for topographically confined slopes. *Marine and Petroleum Geology*.

Note that sections 6.3 and 6.4.4 and Tables 6.1, 6.2 and 6.3 are available as annexes on the published manuscript. Figure 6.4 constitutes an addition to the published material in order to provide a schematic explanation of the method used.

## 6. Submarine confluence classification for topographically confined slopes

### 6.1. Abstract

High-quality 3D seismic data are used in this chapter to: a) investigate the geometry of Miocene-Holocene submarine channels in confluence regions, and b) to correlate the geometry of channel confluences with the styles of topographic confinement imposed by salt structures in the Espírito Santo Basin (SE Brazil). A new method is used to analyse geomorphic parameters of three channel intervals (sub-units 3a to 3c) and a modern channel. 5348 Channel Points (CP) are recorded on a sinusoidal slope interrupted by salt structures. In the upper-slope region, diapir confinement directly controls the location of channel confluences. These are characterised by a sharp increase in channel width and height at their junctions. Scale relationships show an increase in channel width of the order of  $1.19 < W < 1.22$  in confluence regions. Ratios of channel height between confluence and pre-confluence regions are  $1.09 < H < 1.40$ , with ratios of  $< 1$  observed in post-confluence regions. This work proves the existence of a direct relationship between topographic confinement, confluence location and relative channel distribution. The studied submarine confluences are located in regions with high confinement created by salt diapirs. The results of this work are significant, as they show clustered distribution patterns in channels, with higher channel densities being observed in pre-confluence regions. Thus, we propose a new classification for submarine confluences based on a combined analysis of channel geometry and seismic attribute data. Confluences may be symmetric or asymmetric based on the equality of the angles the tributaries bear to the post-confluence channel. Symmetric confluences can be left or right symmetric, based on whether the dominant flow path is in

the left- or right-hand tributary. Asymmetric confluences are pure asymmetric or secondary asymmetric depending on whether the dominant flow takes place along the main tributary and the post-confluence channel alignment, or along the secondary tributary which is at an angle with the main alignment.

## **6.2. Introduction**

Submarine channels are important features of deepwater continental margins. They form conduits for turbidity currents on their way towards abyssal plains (e.g. Flint and Hodgson, 2005; Mutti and Normark, 1991; Normark et al., 1993; Shepard and Marshall, 1973; Stow and Mayall, 2000). Submarine canyons show the largest thalweg heights and complex internal dynamics (Cronin et al., 2005; Shepard, 1981). Submarine channels are more common in distal slope regions where erosional and aggradational processes combine together to form meandering systems (Abreu et al., 2003; Deptuck et al., 2003; Mayall et al., 2006; McHargue et al., 2011; Pirmez et al., 2000). Nevertheless, both features are related, as submarine channels are usually developed within and at the lower reaches of submarine canyons (Shepard, 1965; Wynn et al., 2007), sharing strong analogies with sub-aerial river systems (Clark et al., 1992; Kolla, 2007; Kolla et al., 2001; Posamentier and Walker, 2006; Straub et al., 2011). The genesis and evolution of submarine channels depends on basin tectonics, climate and sea-level changes, factors that control the type, supply and deposition of sediment (Bouma, 2004; Kolla, 2007; Richards et al., 1998). In the particular case of salt-rich continental margins, the generation of accommodation space within diapir-bounded depocentres is a complex process that depends greatly on the relative subsidence of salt-withdrawal basins and on relative sediment supply to those basins (Booth et al.,



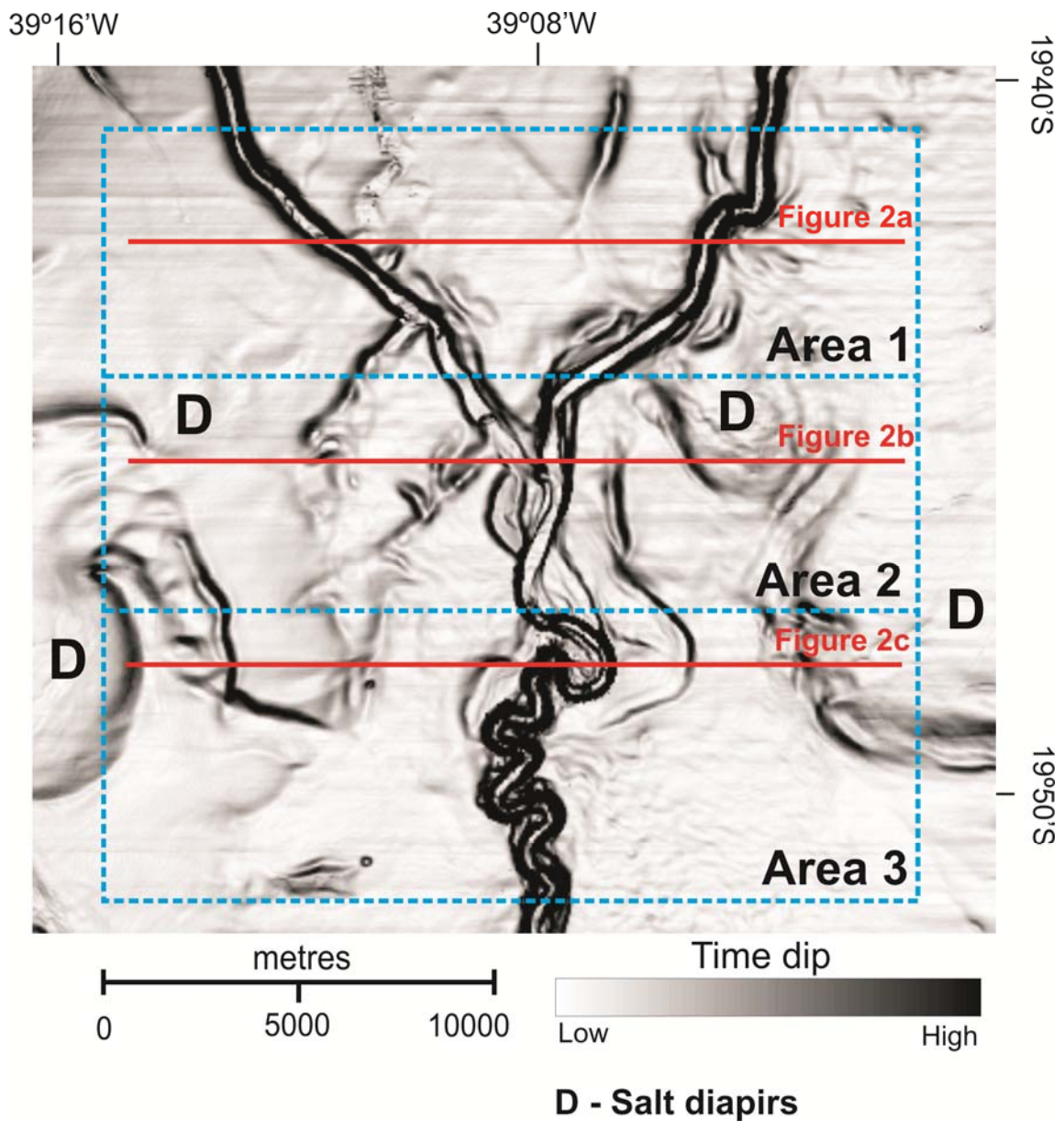
2003; Mallarino et al., 2006; Prather, 2003; Rowan et al., 2003). Rapid deformation associated with salt diapirs and faults are particularly important in deviating channel courses (Gee and Gawthorpe, 2007; Holbrook and Schumm, 1999). Intrabasinal factors such as slope topography, flow density, flow velocity and current thickness relative to topography also play an important role in shaping channel cross-section (Kolla, 2007; Mayall et al., 2010; Mohrig and Buttles, 2007; Piper and Normark, 2009; Straub et al., 2009), defining at the same time the channel equilibrium profile (Ferry et al., 2005; Hodgson et al., 2011; Holbrook and Schumm, 1999; Kneller, 2003; Pirmez et al., 2000). Despite these known concepts and the common presence of submarine confluences identified in various continental margins (e.g. Canals et al., 2000; Dalla Valle and Gamberi, 2011; Greene et al., 2002; L'Heureux et al., 2009; Mitchell, 2004; Paquet et al., 2010; Pirmez et al., 2000; Schwab et al., 2007; Straub et al., 2011; Tujino and Murakami, 2006), the geometry and processes of submarine confluences is still poorly understood when compared to their sub-aerial counterparts, and classification schemes have not been yet established. Detailed geomorphic analysis of channel segments in submarine confluence regions are still incomplete and published studies are focused on single time intervals, usually the modern seafloor. Consequently, comprehensive 4D analyses of the evolution of submarine confluence regions are still to be published.

Stream and river confluences mark the junction of two tributary branches into a single branch, at equal or unequal depths. Confluence classifications for sub-aerial settings are mainly based on channel planform geometry and downstream channels. These are classified as symmetric, with a typical 'Y'-shaped junction; or asymmetric when the post-confluence channel is aligned with the main, often larger, tributary (Best, 1987, 1988; Best

and Roy, 1991; Biron et al., 1996, 1993; Bradbrook et al., 2001; Rhoads and Kenworthy, 1995). Three morphological elements are common in regions of modern river confluences: 1) a steep face at the mouth of each tributary, 2) a central scour and 3) sediment bars in the post-confluence channel (Best, 1988). Field- and model-based studies of fluvial confluences have shown that the presence or location of these features depends on the type of confluence symmetry and magnitude of channel bed offset at tributary junctions, the junction angles and discharge ratios between two tributaries (Biron et al., 1996, 1993). The combined action of all these factors has a direct influence on the internal flow structures and associated sediment distribution at river confluences (Best, 1988; Biron et al., 2004). Fluvial studies consider relatively short time spans and analyse continuous discharges of water and/or sediment that tend to be simultaneously active, despite variable, in both active tributaries. However, seismic-based submarine channel studies involve time scales on the order of thousands of years, and the intermittence of turbidity flows in submarine channels may imply alternating periods of sediment discharge along each tributary. This may lead to sediment being transported, or deposited, during a limited time period predominantly on one (main) submarine tributary, in contrast to fluvial channels.

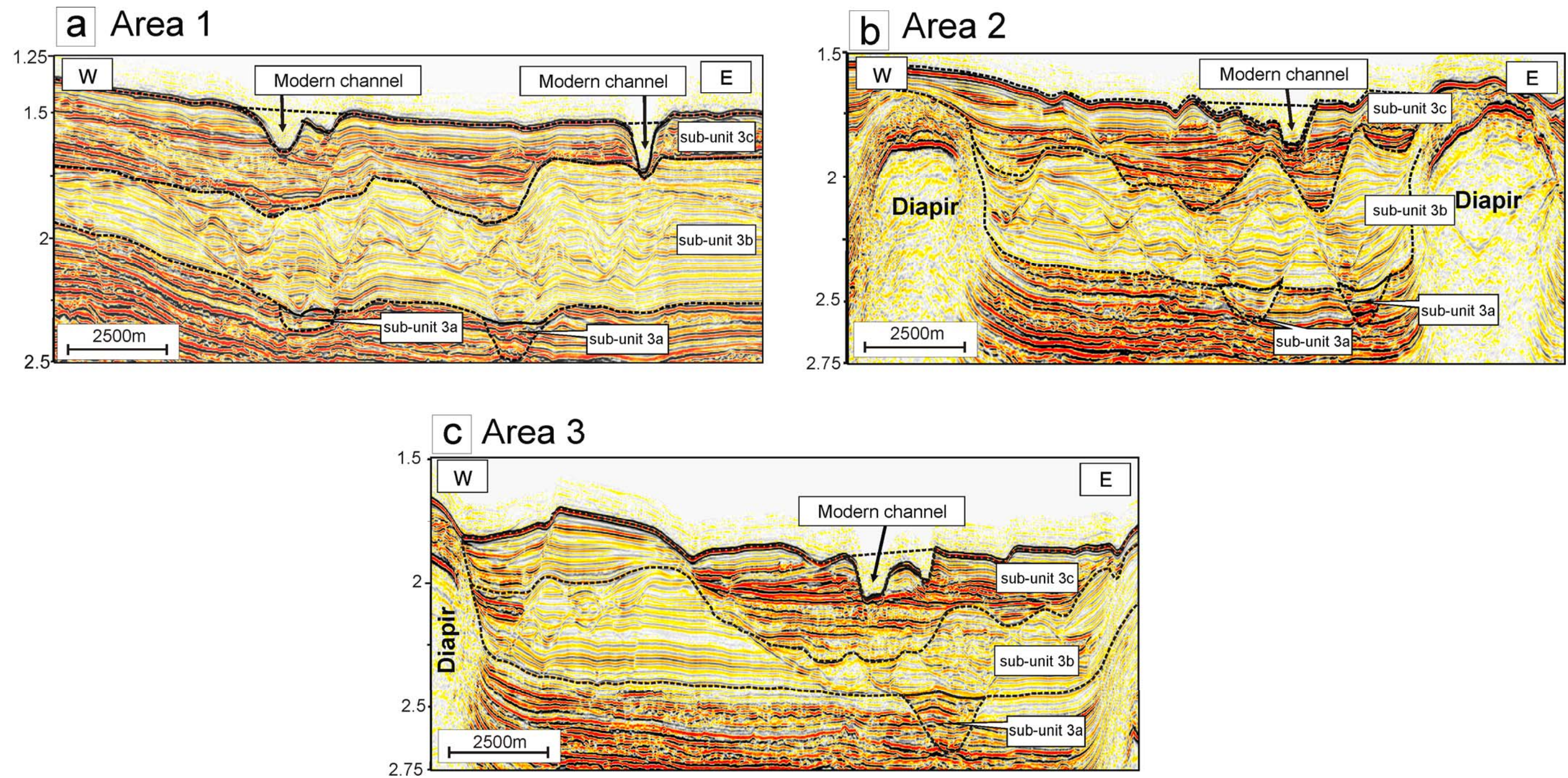
This chapter investigates the geometry of submarine channel confluences in the northern section of the Rio Doce Turbiditic System offshore SE Brazil (Schreiner et al., 2009), comparing the results obtained with data from different continental margins, including the Gulf of Mexico, US Atlantic and Pacific Margins, West Africa and the Mediterranean Sea. A quantitative analysis of the effects of salt tectonics on channel confluence and relative distribution is presented, and an analogy between submarine and fluvial systems is discussed. A new method is used to analyse the 4D distribution of submarine channels on

submarine slope settings. This method is scale-independent, survey independent, and applicable to any geophysical dataset allowing the extraction of geometrical parameters from channels. In addition, it is also flexible enough to be applied to data from distinct margins from the world where channel distribution varies significantly. The channel data obtained by this quantitative approach can be used on its own or to complement information provided by qualitative techniques for submarine channel analysis such as amplitude maps or coherence slices. In addition, accurate measurements of channel height and relative channel locations can be determined by this method whilst limiting the crossing of time lines on amplitude and coherence maps. This poses a key advantage for the characterization of submarine systems that exhibit complex erosional patterns and unclear boundaries between distinct stratigraphic units, which can be clearly identified using the proposed method. The quantification of channel morphological and spatial data is relevant to understand the organization of both submarine or sub-aerial channel systems and their controlling factors (Hajek et al., 2010; Hofmann et al., 2011; Straub et al., 2009). Thus, the method presented aims to allow a 3D statistical analysis of specific intervals of submarine slopes and to predict channel density and distribution patterns, which can help in a) the assessment of sedimentary facies distribution and consequently in b) modelling the spatial location of reservoir-prone intervals and c) risk analysis prior to drilling.



**Figure 6.1.** Sea-floor dip map of the studied slope, depicting the geometry of the modern Rio Doce Turbidite System within a salt-withdrawal basin confined by salt diapirs. The greater confinement is observed in area A2, where diapir spacing is smaller.





**Figure 6.2.** Seismic profiles representative of **a)** Area 1, **b)** Area 2 and **c)** Area 3. Three sub-units are identified, 3a, 3b, 3c and the modern channel. Sub-unit 3a and the modern channel consist in 'Y' shaped canyons located on the axis of the basin. Sub-units 3b and 3c are composed by multiple channels dispersed along width of the basin. Salt diapirs in Area 2 imposed significant topographic confinement at the mid-slope section.



The study presented in this chapter focuses on the Neogene Unit 3 where three main sub-units with vertically stacked submarine channels were identified (Figs. 6.1 and 6.2). Sub-unit 3a comprises a single channel of probable early Miocene age at its base. Sub-unit 3b (Miocene) is a low to moderate amplitude interval where multiple channels occur (Fig. 6.2). Several channels are also present in sub-unit 3c, which is characterized by high-amplitude strata of late Miocene-Quaternary age. Above sub-unit 3c the modern Rio Doce Turbidite System is emplaced (Fig. 6.2).

### **6.3. Chapter-specific Methods**

#### **6.3.1. Seismic data analysis**

The new method presented begins, in a first stage with the identification of V or U shaped erosional features on seismic data. These features are shown by onlap of seismic reflections onto the margins of channel incision surfaces and by contrasting amplitude between channel-fill and overbank deposits (Mitchum et al., 1977; Posamentier and Kolla, 2003). The geometry of submarine channels is then measured in relation to a Channel Point (CP) located at the base of the channel thalweg (Fig. 6.3). The spatial locations on the slope (X, Y, Z), the maximum channel width, height of channel and two-way travel time depth is measured and recorded for each CP.

For the purposes of this chapter, the method was systematically applied to east-west oriented seismic sections spaced 125 metres (10 lines), producing a very narrow mesh of CP and geomorphologic data. The resulting mesh can, however, be made denser (as well as the measured points integrated) in order to calculate the area and volume of interpreted

submarine channels. In a third phase, the distribution of a total of 5348 Channel Points was analysed by dividing the study area in a grid with 256 uniformly-sized cells, each covering an area of 1.56 km<sup>2</sup>. We used this grid to assess CP frequency in each uniformly-sized cell and to perform: 1) a statistical analysis of the patterns of the channel spatial distribution, and 2) a comparison of the observed data with a Poisson and a Negative Binomial probabilistic distribution (e.g. Davis, 2002) in order to identify the degree of variability in channel distribution. The final aim of these tests was to investigate channel density and clustering for specific areas of the slope. Figure 6.4 shows a simplified schematic workflow of the method described above.

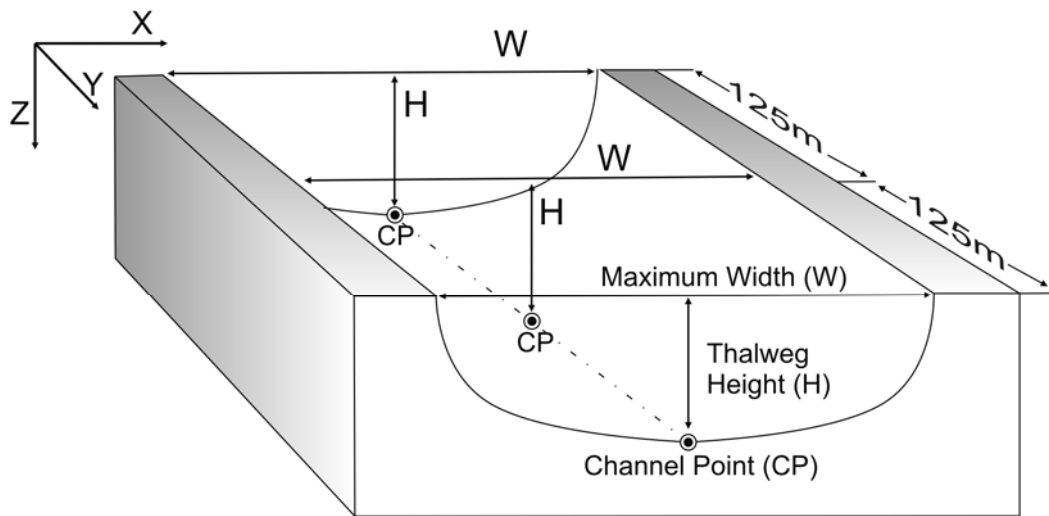
The northwest corner of a 400 km<sup>2</sup> area selected for study was set as the zero reference point, with distance increasing both southwards and eastwards to a maximum of 20 km. The study area was further divided into three sub-areas, A1 to A3, corresponding to upper, middle and lower slope regions (Fig. 6.1). This sub-division also reflects the degree of confinement imposed by the modern diapirs. Topographic confinement is higher in area A2, as shown by the smaller spacing between growing salt diapirs (Figs. 6.1 and 6.2)

### **6.3.2. Channel Spatial analysis**

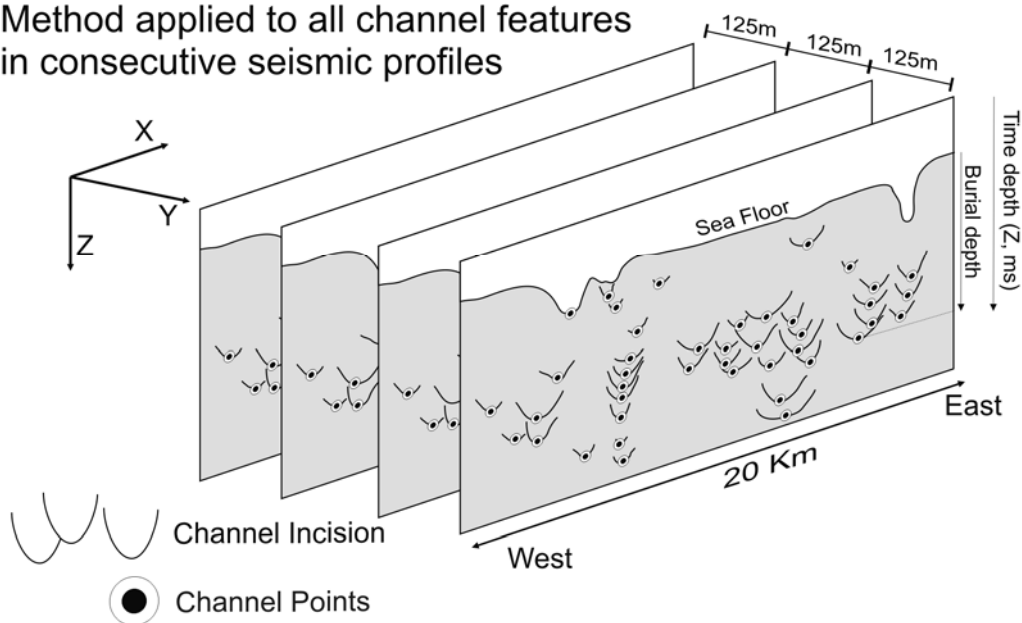
A chi-square test was used to assess how uniform is the distribution of the 5348 CPs measured, using a 256-cell grid as the base division. The goodness-of-fit of the observed distribution of CP's per cell was tested with two modelled distributions, namely a Poisson and Negative Binomial. Goodness-of-fit tests are used to assess the similarity between



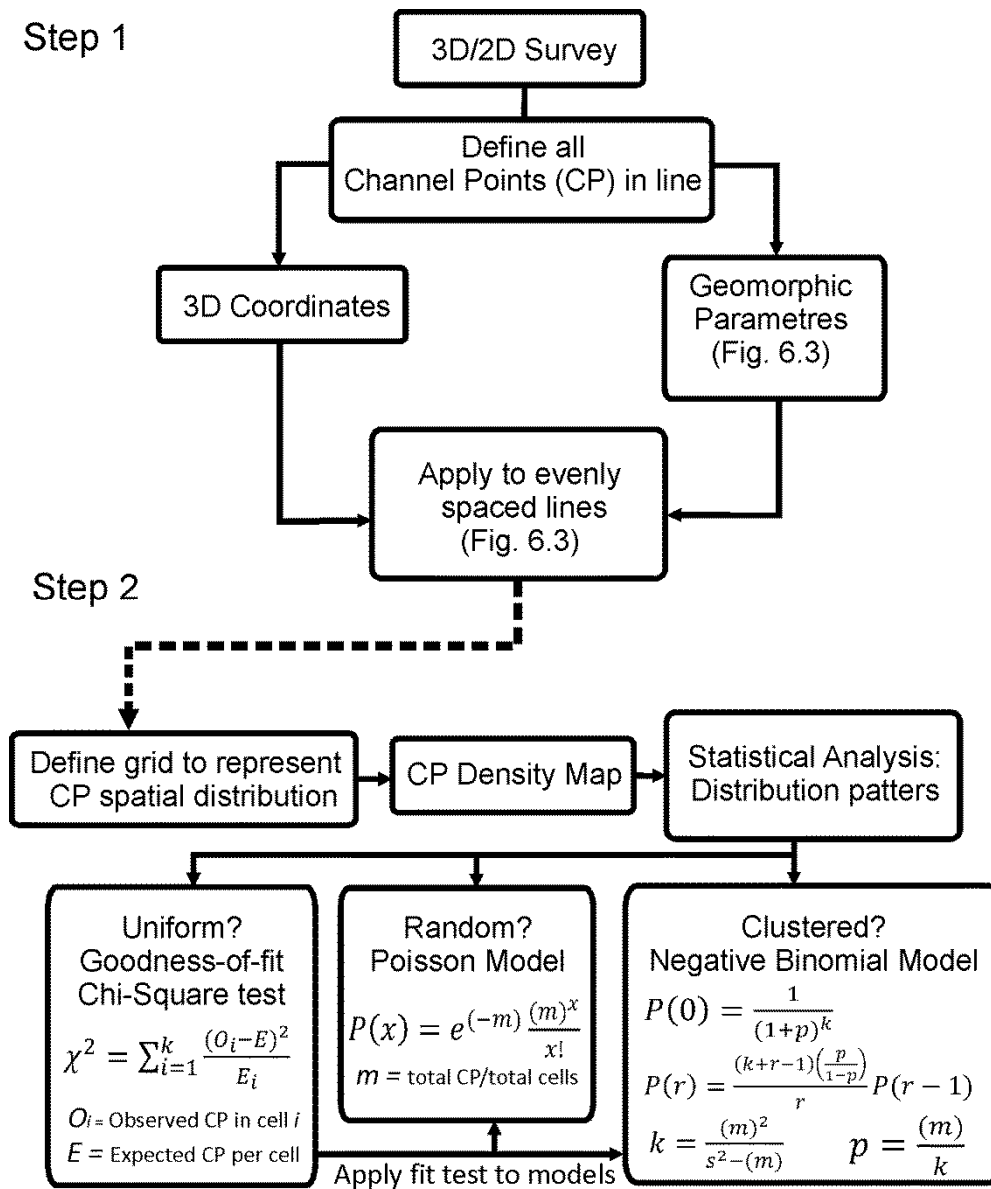
Measured parameters on a single channel



Method applied to all channel features in consecutive seismic profiles



**Figure 6.3.** Schematic representation of the channel analysis method. Channel thalweg height and width were measured from a reference Channel Point (CP) at its base. This was applied to all channel features identified on evenly spaced seismic profiles.



**Figure 6.4.** Representation of the channel analysis method workflow. Step 1 corresponds to the channel analysis and data acquisition. Step 2 is related to the statistical analysis and tests applied.

empirical data frequency and theoretical distributions (Davis, 2002; Haschenburger and Spinelli, 2005). The Poisson distribution is an indicator of random distributions, whereas the Negative Binomial is characteristic of data clustering. A more detailed description of these mathematical methods can be found in Chapter 3.

## **6.4. Results**

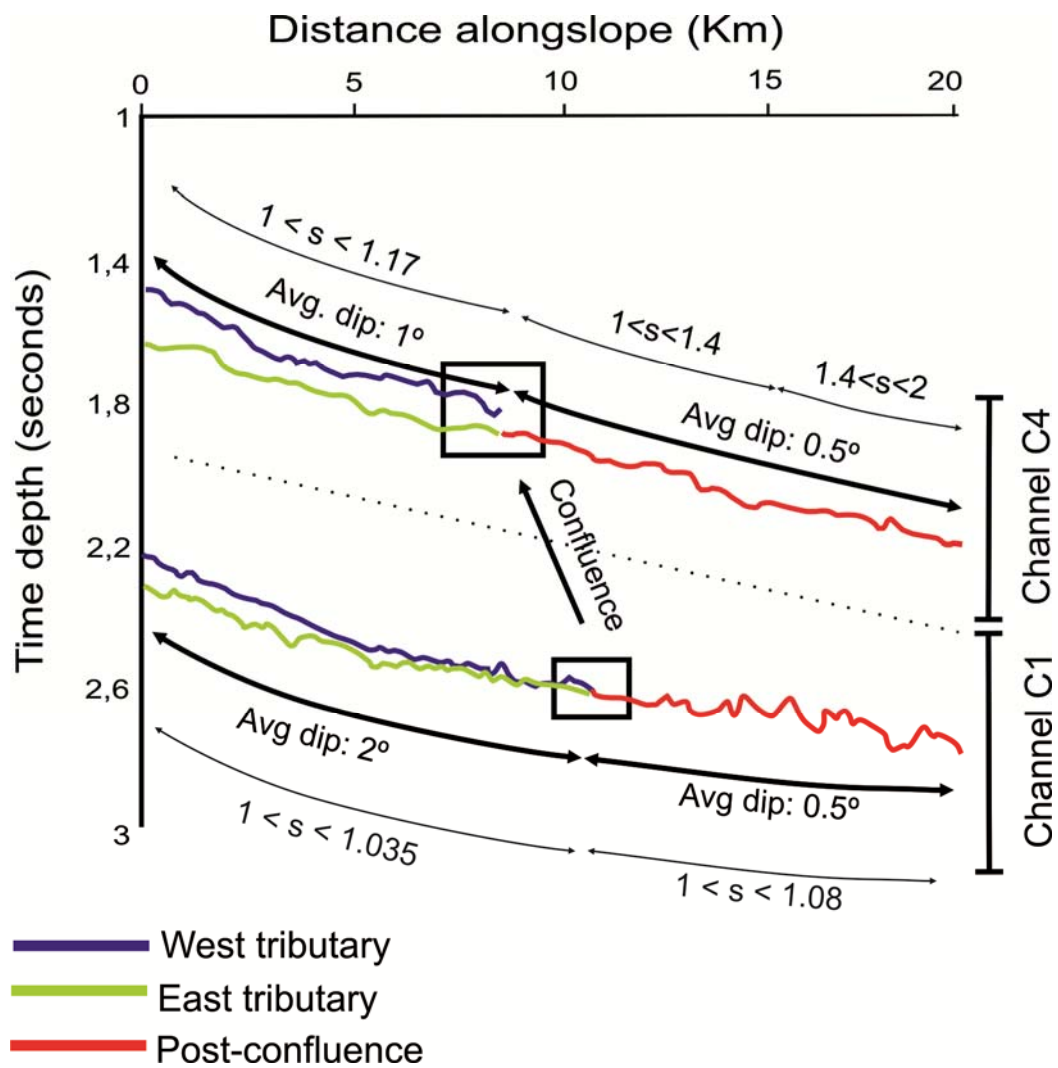
### **6.4.1 Morphology of submarine channel confluences**

This section presents a description of the geometry of channel confluences in sub-unit 3a (C1) and the modern channel (C4) (Fig. 6.2 and 6.5). Data for sub-units 3b and 3c (Fig. 6.2) are presented on the following sub-section.

#### **6.4.1.1. Channel C1 (sub-unit 3a)**

Channel C1 comprises two upper-slope tributaries, referred to as WT-1 (west tributary, sub-unit 3a) and ET-1 (east tributary, sub-unit 3a). They converge at mid-slope regions into a single main channel merging at an angle of 40 degrees (Figs. 6.6a and 6.6b).

The base of WT-1 is located at shallower depths than ET-1, but these tend to merge at equal elevations close to the confluence point (Fig. 6.6a and 6.6c). Maximum amplitude maps within the channel show the strata with the highest amplitude to be located along the eastern tributary and the main post-confluence channel (Fig. 6.6b). The average gradient in these tributaries is similar, with values of 2.14 and 2.17 degrees for WT-1 and ET-1, respectively.



**Figure 6.5.** Profiles of maximum thalweg depth, in time, of Channel C1 (sub-unit 3a) and Channel C4 (modern). Colours represent different tributaries and the post-confluence channel. Profiles indicate that tributaries join at equal levels in canyon C1, whereas in canyon C4 tributary depths are offset. Nevertheless, the eastern tributary in C4 is at a concordant level with the post-confluence channel.  $s$  = channel sinuosity.

No depth variations are observed at the junction point, with the base of the post-confluence channel being at a similar height to the upslope tributaries (Figs. 6.5. and 6.6c). The post-confluence channel is more irregular when compared with the pre-confluence tributaries, especially in the distal reaches of the studied area (Fig. 6.5). Here, steep variations in the channel profile reach localised maximum gradients of  $18^\circ$ , for a generalised gradient of  $0.5^\circ$  for the post-confluence segment.

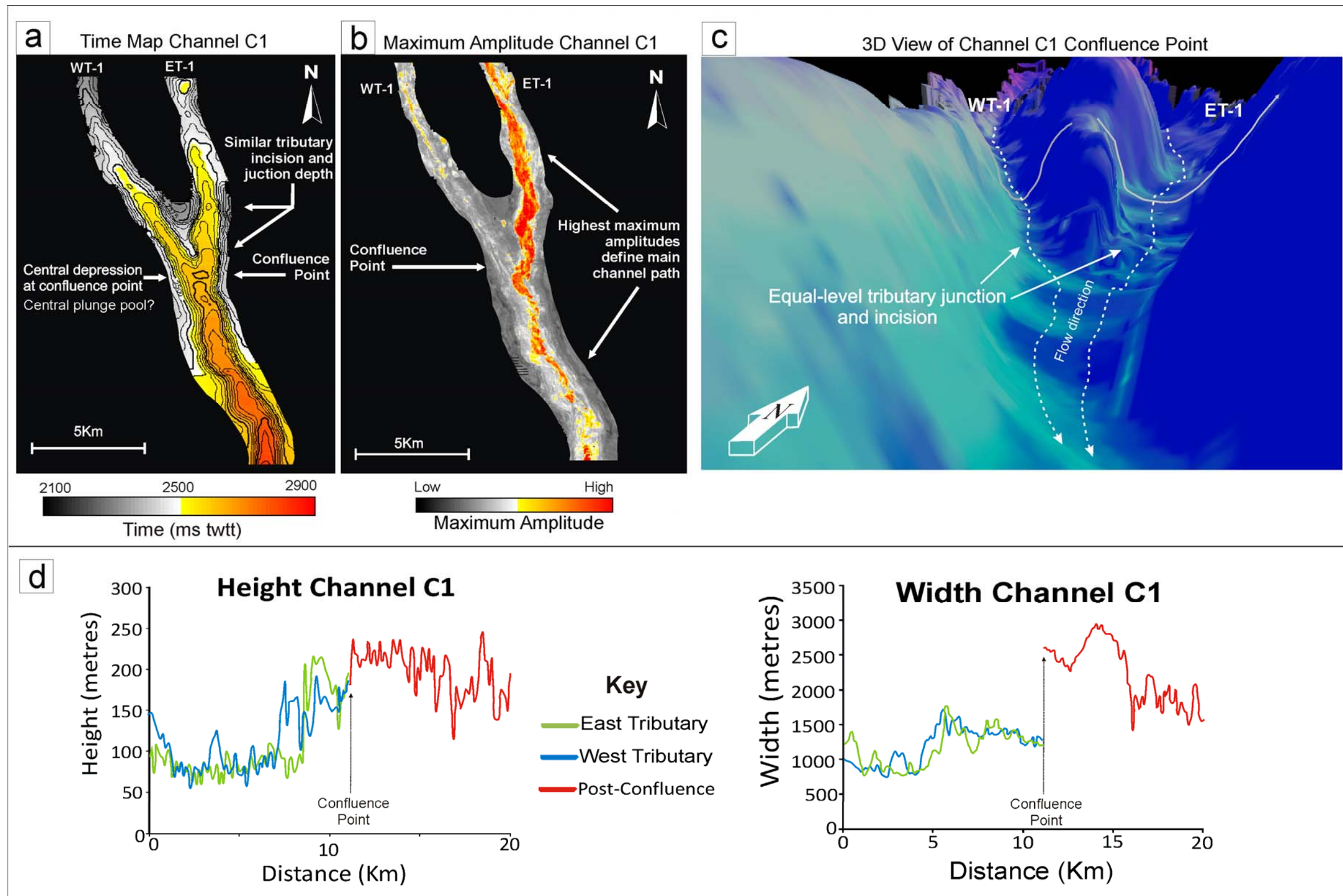
Distinct morphological trends are observed in pre- and post-confluence regions (Fig. 6.6d). In fact, the upslope tributaries have similar width and height values: width ranges between 1000 m and 1700 m, whereas height ranges from 70 m to 200 m (Fig. 6.6d). However, measured width and height do not change gradually with distance, in a downslope direction. Instead, they show a marked increase at the mid-slope region (area A2 in Fig. 6.1). Significant variations occur at confluence points, where the width of the system abruptly increases to 2500 m from an average of  $\sim 1300$  m (Fig. 6.6d). In contrast, channel height increases gradually and continuously in the confluence region, (Fig. 6.6a and 6.6c). The junction of channel C1 also shows a localised depression with a relief of 20 m at the junction point, a likely analogue to the central scours observed in river confluences (Best, 1988).

#### **6.4.1.2. Channel C4 (Modern Channel)**

Two main upslope tributaries are observed in Channel C4. They are identified as WT-4 (west tributary, Channel C4) and ET-4 (east tributary, Channel C4), joining at an angle of  $75^\circ$  (Fig. 6.7a). The western tributary has a gradient of  $1^\circ$ , although locally values up to  $5^\circ$  are observed (Fig. 6.5). ET-4 has an average gradient of  $0.7^\circ$ , with local variations that do not

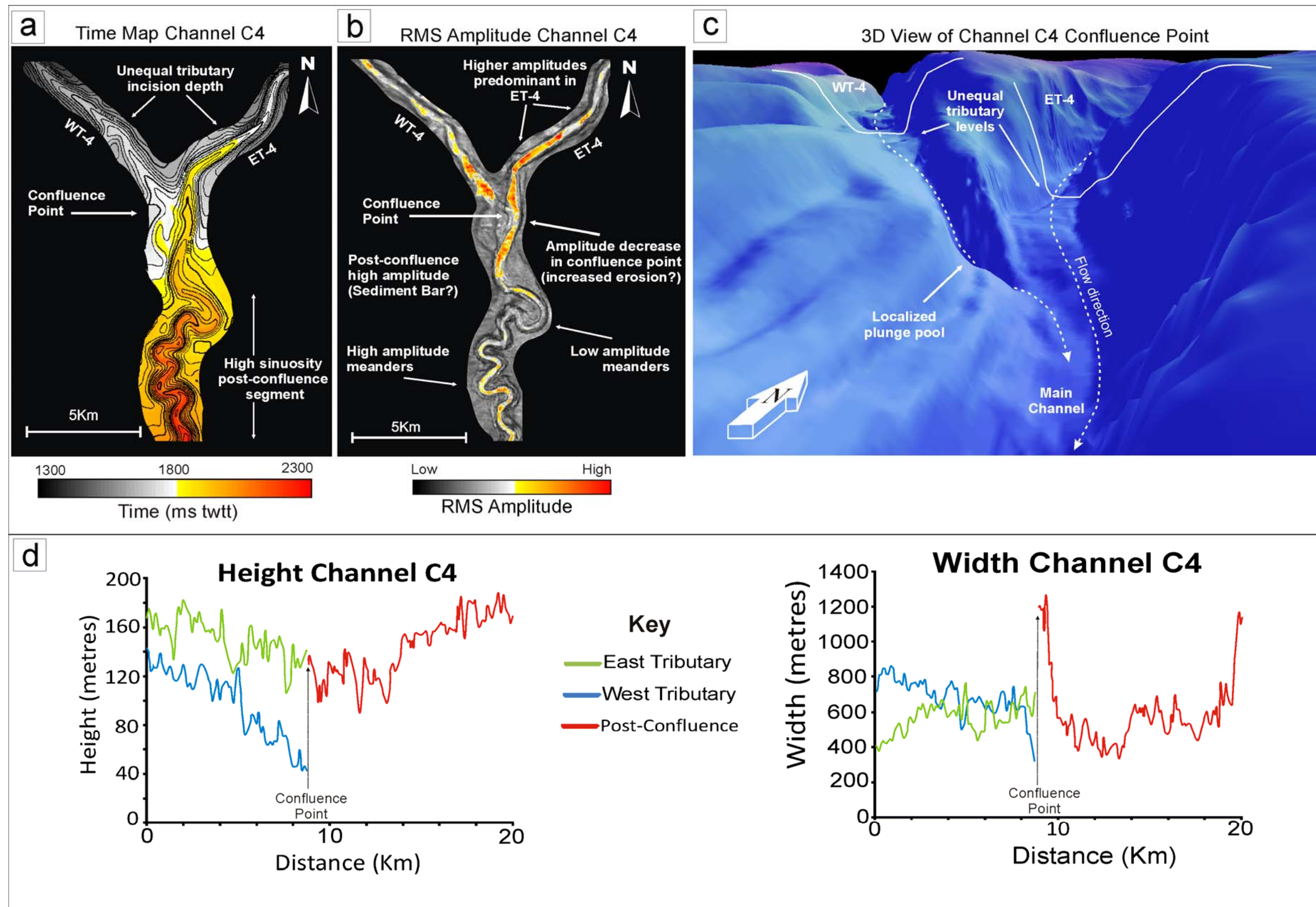
exceed  $1.4^{\circ}$ . The post-confluence branch follows a north-south trend and an average gradient of  $0.5^{\circ}$ . In contrast to sub-unit 3a, the modern channel tributaries meet at different elevations. A morphological step is observed when the western tributary (WT-4) joins the main channel (Fig. 6.7a and 6.7d). In contrast, the eastern tributary joins the post-confluence channel at a similar depth (Figs. 6.5, 6.7a and 6.7d). The width of tributary WT-4 decreases downslope, with a pronounced change from 600 m to 300 m at the vicinity of the confluence point. In contrast, the width of ET-4 tends to increase towards the junction. At the transition to the confluence point, ET-4 shows a significant increase in width, but shortly downslope of the confluence point the values decrease to the same range of values observed in the uppermost tributaries. The region where the lowest post-confluence width is observed corresponds to the segment with the highest sinuosity (Figs. 6.5 and 6.7d). Thalweg height tends to decrease towards the confluence points, with WT-4 systematically showing lower values.

At the confluence point, the difference in thalweg height of both tributaries reaches over 100 m (Fig. 6.7d). The largest thalweg heights are observed in ET-4, which occurs at the lower elevation in the confluence, having identical height values to the ones observed in the main post-confluence channel (Fig. 6.7d). In the post-confluence region, channel height increases in the mid-slope region in the segment with higher sinuosity.



**Figure 6.6.** Maps and graphical data for Channel C1. **a)** Time map of the base of channel C1. Incision depth of tributaries is identical at the junction. A central depression at the confluence point is interpreted as a plunge pool, analogous to those observed in fluvial systems. Contour spacing is 25 ms TWTT. **b)** Maximum amplitude map within channel C1. The high amplitude values along the eastern tributary and post-confluence branch suggest that these form the main channel. **c)** 3D view of the confluence geometry in channel C1. **d)** Plots of thalweg height and width variations along slope.





**Figure 6.7.** Maps and graphical data of channel C4. **a)** Time map of modern channel, which evidences unequal junctions. High sinuosity is observed at the post-confluence reaches. Contour spacing is 25 ms TWTT **b)** Rms amplitude from a 40 ms time window below the seafloor. Here, the confluence point shows a low amplitude patch, interpreted to represent sediment erosion by increase flow velocity at the junction. **c)** 3D view of the confluence geometry in channel C4. A limited plunge pool is present close to the tributary at the highest topographic level. **d)** Plots of thalweg height and width variation along slope.

### 6.4.2. Geomorphic channel parameters in relation to confluence

In summary, a clear variation of the channel dimensions influenced by tributary confluences in area A2 is only observed for channel C1 (sub-unit 3a) and the modern channel (Fig. 6.8a and 6.8d, respectively). Width values for channel C1 range from 1100 m to 1700 m in area A2, for similar values to those recorded in areas A1 and A3 (Fig. 6.8a). Data from area A2 also show an isolated cluster of points with large width and height. This cluster corresponds to the geomorphic changes at the confluence point shown in Figure 6.6. In the modern channel, areas A1 and A3 show similar channel heights, ranging from 80 m to 180 m (Fig. 6.8d). Width values observed in the modern channel generally do not exceed 900 m, being the lowest range observed in this study. In contrast, in area A2 two smaller clusters are observed (Fig. 6.8d). The cluster showing the lowest height values corresponds to the western tributary, where the thalweg height does not exceed 90 m. The second cluster is marked by the highest width values observed in area A2, which vary between 850 and 1300 m.

The analysed data show similar ranges of width and height for the numerous channel elements in sub-units 3b and 3c regardless of their slope position. This character allowed us to establish a power law relationship between the width (W) and height (H) of the kind:

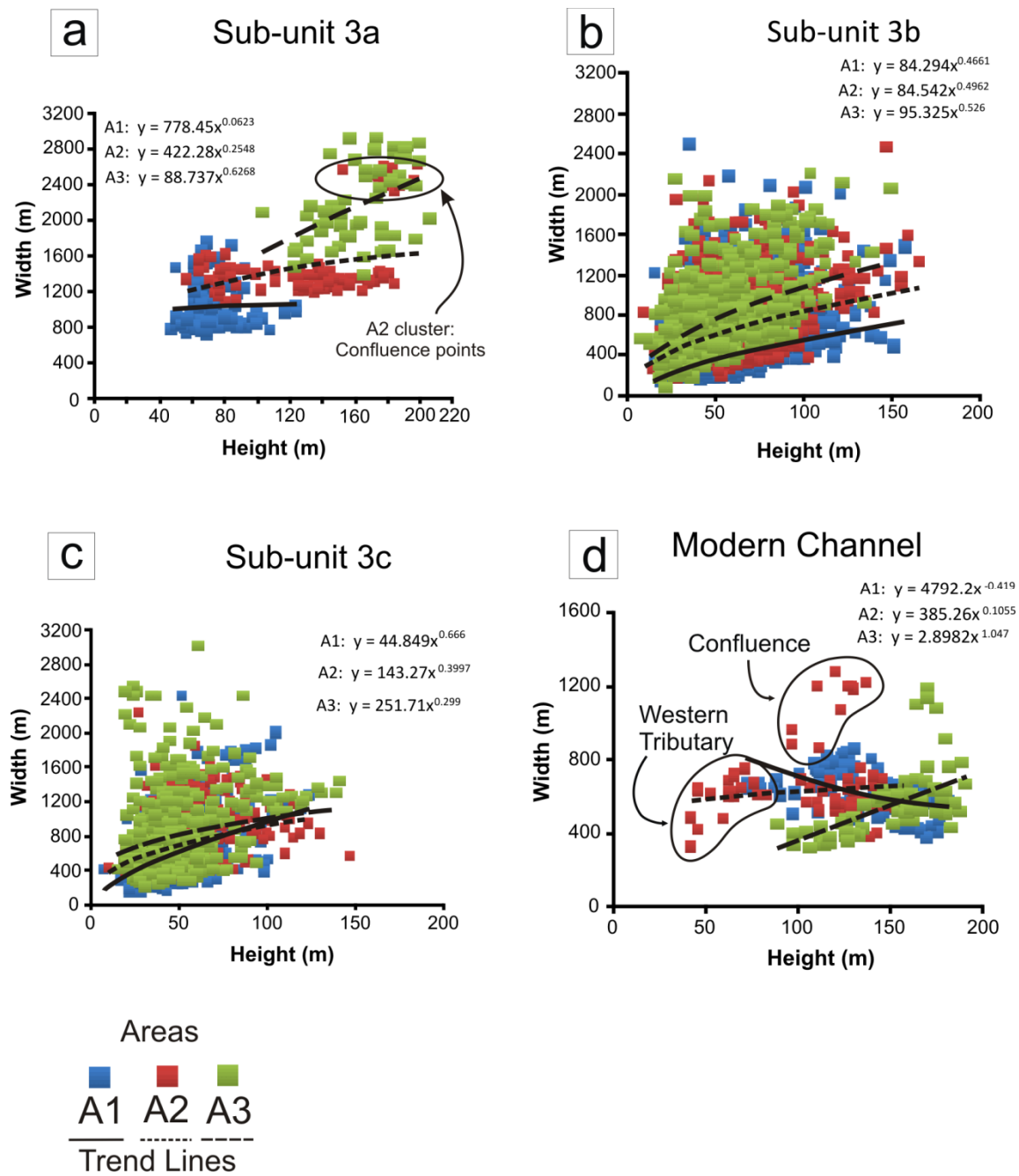
$$W = cH^a \quad (\text{eq. 6.1})$$

The results show distinct values for the constant (c) and exponent (a) (see Table 6.1). Despite the wide range in values recorded between the three areas, the data shows resembling trends for identical channel architectures. Variations of a similar order are observed in the confluence region and bordering areas of sub-unit 3a (Channel C1) and in

the modern channel. In contrast, distinct trends to these later are observed for sub-units 3b and 3c.

Sub-unit 3b shows very similar scale relationships in the three areas considered ( $84 < c < 95$ ), with  $a$  varying between 0.46 and 0.52. Sub-unit 3c, in contrast, shows an increase of the width/height ratios towards the distal slope, with  $c$  increasing from 45 in area A1 to 2523 in area A3. A reverse trend was observed for the exponent  $a$ , which decreases from 0.66 to 0.29 with distance (Table 6.1).

Ratios of channel width ( $W_r$ ) between areas A1 and A2 are on the order of  $1.19 < W_{r_{1_2}} < 1.22$ . In areas A2 and A3 these ratios show relatively higher values of  $1.31 < W_{r_{3_2}} < 1.41$ . Average ratios of channel height ( $H_r$ ) between areas A1 and A2 are in the order of  $1.09 < H_{r_{1_2}} < 1.40$ , increasing towards the confluence regions. In contrast, ratios between areas A2 and A3 of  $0.84 < H_{r_{2_3}} < 0.96$  are observed. The scale relationships presented indicate that channels in the studied slope tend to gradually widen downslope, whereas channel height increases from the upper slope towards the topographically confined confluence region, but tends to show slight decreases in the transition to lower confinement areas.



**Figure 6.8.** Scatter plots representing CP width and height in the studied stratigraphic sub-units. Data for sub-unit 3ca and Modern Channel highlight width and height variations related with the confluence region. In sub-units 3b and 3c there is no clear distinction between the different slope regions.

	Area 1		Area 2		Area 3	
Sub-unit	K	a	K	a	K	a
3a	778	0.06	422	0.25	88	0.62
3b	84	0.46	85	0.49	95	0.52
3c	45	0.66	143	0.39	2523	0.29
Modern	4792	-0.41	385	0.1	3	1.04

**Table 6.1.** Synthesis of  $c$  and  $a$  values obtained from power trend lines in the each Area/Sub-unit couplet.

### 6.4.3. Channel density and distribution

Figure 6.9 illustrates the number of CPs identified in the study area. CP number is significantly high in sub-units 3b and 3c, exceeding at least four times the number of points observed in sub-unit 3a and in the modern channel (Fig. 6.9a). The highest densities are observed in area A1, specifically in two north-northwest-trending regions adjacent to the axis of the salt-withdrawal basin where up to 90 CP per cell are observed (Fig. 6.9c). The downslope limit of the high CP density region is located in area A2. The regions proximal to salt diapirs also constitute a location with high channel density, commonly exhibiting circa 30 CP per cell. In the study area, diapir-flanking channels are represented by elements in sub-units 3b and 3c (Fig. 6.9b). Channel density and the relative location of the confluences correlate well with the presence topographic confinement in area A2 (Fig. 6.1). Relatively high channel densities are observed in the pre-confluence regions (Figs. 6.2a and 6.9c). Here, channel aggradation in a region of essential low confinement allowed the development of several channels reflecting multiple episodes of incision and fill. The largest values in density (up to 91 CP per cell) coincide, in area A1, with main tributaries (Fig. 6.9b and 6.9c). These results suggest that channels in area A1 experienced limited lateral migration and a tendency to stack vertically, a character that is associated with an aggradational behaviour (see Hodgson et al., 2011; Kneller, 2003; Pirmez et al., 2000). This behaviour is further highlighted by the limited contrast in channel height between areas A1 and A3, demonstrating similar scales of channel incision for the two regions.

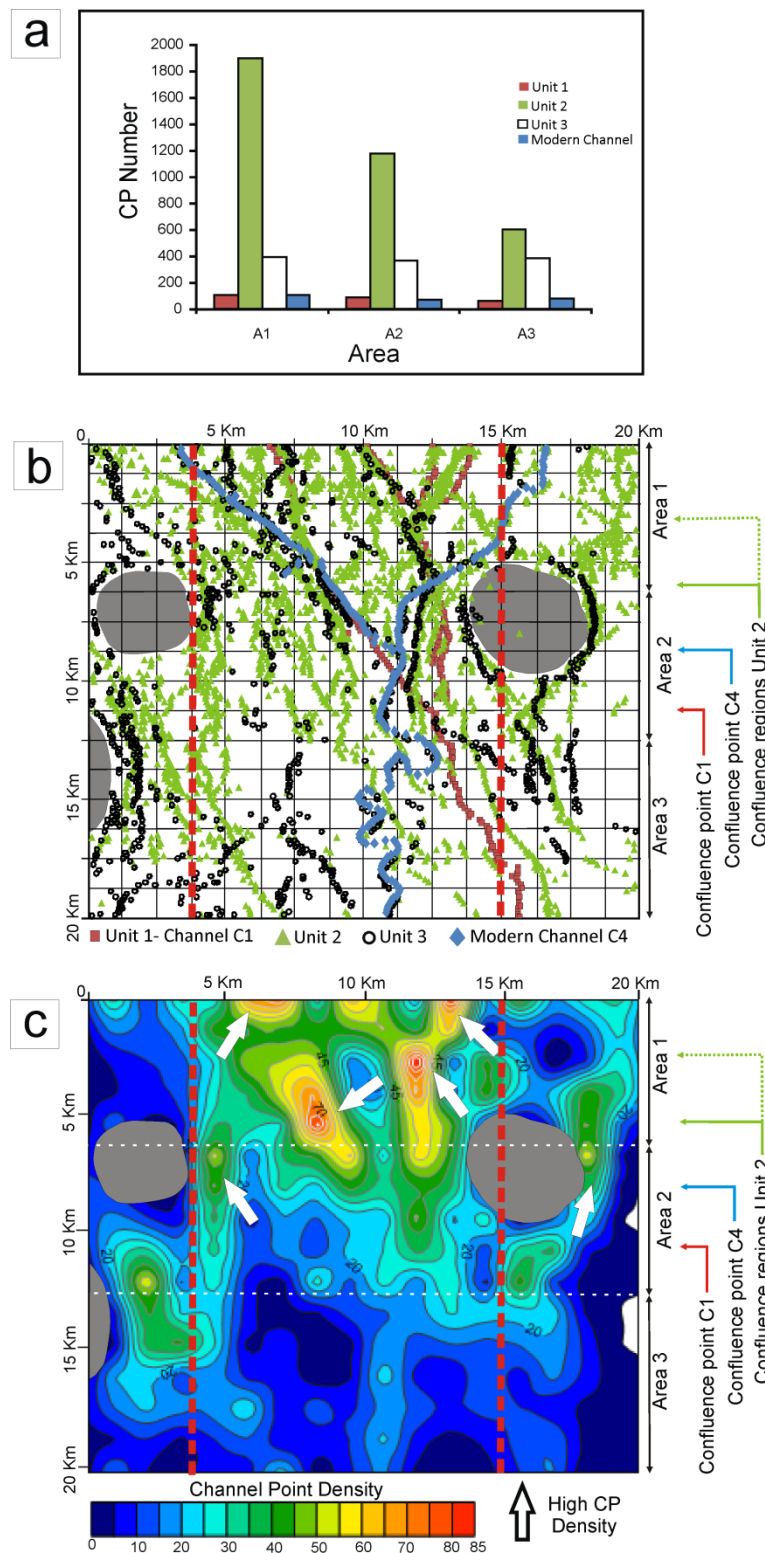
In area A2, topographic confinement is interpreted to have caused a convergence of channels and thus a decrease in their observed number (Fig. 6.9). This confinement is also

interpreted to have contributed to general sediment bypass in this region. Channel coalescence is marked by a decrease in CP numbers interpreted to result from lower sediment accumulation and increased erosion on the seafloor at bypass areas with higher confinement. A decrease in slope angle (i.e. channel bed gradient) is also observed at the main confluence area, particularly in channels C1 and C4 (Fig. 6.5).

Channel density in the post-confluence area A3 varies significantly when compared to areas A1 and A2 (Fig. 6.9c). Channels C1, C4, and several elements of sub-unit 3c precluding the incision of the modern channel, are the main features observed in area A3. They reveal a low CP number when compared with areas A1 and A2. Sub-unit 3b also shows a significantly low number of CPs in the post-confluence area A3. The highest channel densities in sub-units 3b and 3c are in fact observed around the flanks of marginal diapirs (Fig. 6.9c).

Despite the establishment of a main channel confluence zone on the slope, the analysis of the channels systems shows that confluence points are not fixed (Figs. 6.5 and 6.9b). The oldest channel C1, estimated to be of Miocene age, exhibits the southernmost confluence point. In the overlying sub-unit 3b, the main channel confluences are estimated to locate about 5000e7000 m upslope from the point observed for C1, within the lower half of area A1. As for the modern channel, its confluence point is located within area A2, showing a southward shift relatively to the confluence region of sub-unit 3b (Figs. 6.1 and 6.9). In addition, the highly sinuous post-confluence segment in the modern channel contrasts with the relatively straight tributaries, which may link the location of the modern confluence with a marked change in slope gradient (e.g. Kolla, 2007; McHargue et al., 2011; Wynn et al., 2007) (Figs. 6.1, 6.5, 6.6 and 6.7).





**Figure 6.9.** **a)** Plot illustrating the frequency of CP per sub-unit, in each area. **b)** Map representing the spatial distribution of CP in the studied area, for each sub-unit. CP distribution provides a close proxy to assess the path and orientation of the various slope channels. **c)** Map representing the density of CP per cell in the study area. High densities in the pre-confluence area are coincident with location of main tributaries. In post-confluence areas, higher densities are observed on the flanks of salt diapirs. White arrows indicate regions with higher channel densities. Dashed white lines mark the limits of zones A1, A2 and A3. Red line delimits the area of data analysed by the statistical models.

#### 6.4.4. Spatial analysis of channel distribution: a new quantitative method

The distribution patterns of CPs were assessed by using goodness-of-fit chi-square tests ( $\chi^2$ ), Poisson and Negative Binomial models. For these tests a narrower slope area was used, focused in the regions with high CP density regions (see dashed limits in Fig. 6.9c). This restricted the test to a 144 cell grid where a total of 3683 CP occurred. From these, 1892 occur in area A1, 1186 in area A2 and 605 in area A3 (Fig. 6.9a).

The simple  $\chi^2$  test is used in spatial data analysis to assess the distribution uniformity of data, based on the observed frequencies and an expected value. Note that for any chi-square test to be valid a minimum frequency of 5 CP must be present in a single cell (Davis, 2002). Thus, when this requirement was not met the low frequencies were combined in order to obtain a value equal or greater than 5.

The chi-square considers the acceptance or rejection of a distribution hypothesis ( $H_0$ ) (e.g. Davis, 2005), here stated as:

**$H_0$ :** The distribution of CP is uniform.

The test results are summarised in table 6.2. In the full area, the expected frequency for this test is of 25.5 CP per cell. The observed results show minimum and maximum CP frequencies of 0 and 90, respectively. For  $df=135$ , the critical value of chi-square at a significance level of 1% is 176. The calculated test value of  $\chi^2=5314$  greatly exceeds the critical value, thus  $H_0$  is rejected and it is concluded that CP distribution in the slope is not uniform.

Similar results are obtained when the same test is applied in each individual area. The chi-square values calculated exceed the critical values for  $H_0$  acceptance (Table 6.2a), so the CP distribution is not uniform in the defined sub-areas.

The non-uniform distribution of CP tested above does not provide any indications about their distribution patterns (Davis, 2005). To analyse if the CP are randomly distributed or follow a regular organization I compared the observed number of cells containing  $r$  CP ( $0 < r < 90$ ) with a Poisson and a negative binomial distribution model.

Figure 6.10 shows the frequencies observed in the data and the one expected from the Poisson model in the three sub-areas. Their goodness-of-fit with the observed data is analysed using a chi-square test, with a hypothesis stated as

**$H_0$ :** The distribution of CP is random in the slope

The test for the full area has 24  $df$  and a critical value of 43 for a 1% significance level. The calculated chi-square of  $1.8 \times 10^5$  greatly exceeds this, so  $H_0$  is rejected and the Poisson model is not appropriate. Channels are not randomly distributed in the study area. Likewise, the same conclusion is applied to the three areas (Table 6.2b). Chi-square values of  $2 \times 10^5$  and  $6 \times 10^4$  in areas A1 and 2, respectively, greatly exceed the critical value of 3.49 at a 1% confidence interval. The same is true for area A3, but the calculated value of 329.78 does not exceed the critical value of 3.35 in the same magnitude as in the upper slope areas. Furthermore, the graphical representation of the data (Fig. 6.10) confirms the inadequacy of this model to describe the channel distributions, as there is a significant scattering of the observed and Poisson expected frequencies. Nevertheless, the plot for area 1 shows that the model accurately predicts the occurrence of the maximum frequencies, although it fails

to predict the occurrence of the low number of cells with CP number further away from the mean value.

It is also worth mentioning that despite the lack of fit, the observed and expected Poisson frequencies in area A3 do show resemblances in the data ranges. The expected model correctly calculated the probabilities of occurrence of cells with CP frequencies between 5 and 10, but once again the major discrepancies are related to the marginal values of the sample.

The comparison of the estimated mean number of CP per cell ( $em = m/T$ ) and the variance ( $s^2$ ) also provides an indicator for the distribution patterns (Table 6.3). Calculated ratios for  $em/s^2$  lower than 1 are indicative of clustered patterns, whereas when the ratio is equal to 1 the pattern is random. Ratios exceeding one are typical of uniform patterns, but this is not expected as it has already been rejected above. The ratios obtained for the areas are all lower than 1, indicating a clustered CP distribution and confirming the inappropriate fit of the random Poisson model.

The occurrence of clustered patterns in space is commonly modelled using a negative binomial distribution (Davis, 2002). The goodness-of-fit tests of the observed frequencies and the ones expected using a negative binomial model are tested using a chi-square test, in which every considered cell class must have a minimum frequency of five elements. Thus, the test hypothesis is stated as:

**H<sub>0</sub>:** The distribution of CP is clustered in the slope

	Cells	Chi-Square value	df	Critical value (1%)	Reject Ho?
<b>Total area</b>	144	5314	135	176.1	yes
<b>Area A1</b>	45	449.8	42	105.2	yes
<b>Area A2</b>	45	343.1	42	66.2	yes
<b>Area A3</b>	54	183.48	46	71.2	yes

a) Uniform distribution test

	Cells	Chi-Square value	df	Critical value (1%)	Reject Ho?
<b>Total area</b>	144	1.79E+10	24	42.98	yes
<b>Area A1</b>	45	2.42E+05	7	3.49	yes
<b>Area A2</b>	45	6.67E+04	7	3.49	yes
<b>Area A3</b>	54	329.78	8	3.35	yes

b) Random distribution test for Poisson model

	Cells	Chi-Square value	df	Critical value (1%)	Reject Ho?
<b>Total area</b>	144	24.3	25	44	no
<b>Area A1</b>	45	5.90	7	18	no
<b>Area A2</b>	45	5.70	7	18	no
<b>Area A3</b>	54	13.97	7	21.6	no

c) Clustered distribution test for Negative Binomial model

**Table 6.2.** Summary table of the goodness-of-fit test results to the distribution models. In **a)** and **b)**, corresponding to uniform and random distribution tests, the test values exceed the critical values, hence  $H_0$  is rejected. **c)** test results are lower than the critical values, hence it is valid to consider a negative binomial distribution for the analysed channel in all areas of the slope.

The expected frequency using a negative binomial model for the full area is shown in Figure 6.10 and the results for this test are synthesised in Table 6.2c. Contrasting with the previous models, the goodness-of-fit test of the negative binomial model to the observed distributions accepts the  $H_0$  hypothesis, thus the analysed data is clustered and the negative binomial is a model accepted to describe the CP distribution in the study area. In addition, the chi-square values are accepted in tests with confidence intervals that vary from 10% to 50%, depending of the area analysed.

CP numbers show a decrease of 37% from area 1 towards the confluence area. Such a decrease is more prominent when comparing areas A2 with A3, where a 2:1 ratio in relative CP density is recorded. The results highlight the presence of non-uniform CP distributions, supported by the close fit of the expected frequencies to a negative binomial model (Fig. 6.10a). This model provides the closer approximation between the observed and expected frequencies, both in CP per cell and in the number of populated cells defined in this study, indicating a predominance of clustered patterns in the analysed data. The major limitation of this distribution, however, resides on the prediction of the low number of cells containing over 60 CP, which are prone to occur either close to confluence areas or when vertical channel stacking is predominant (Fig. 6.9).

Hence, areas of greater CP numbers show estimated mean ( $\bar{m}$ ) values significantly lower than the variance ( $s^2$ ), such as regions of larger clustering and channel connectivity on seismic data present the highest values of:

$$s^2 - (\bar{m}/t) \quad (\text{eq. 6.2})$$

This is particularly observed for Area A1, in which the calculated value in (eq. 6.2) reaches  $\sim 426$ . In contrast Area A3, where channels show limited lateral dispersion, the same value approaches 40. Thus, the larger is the observed difference between the estimated mean and the variance, the larger the potential for higher degrees of connectivity between adjacent channels.

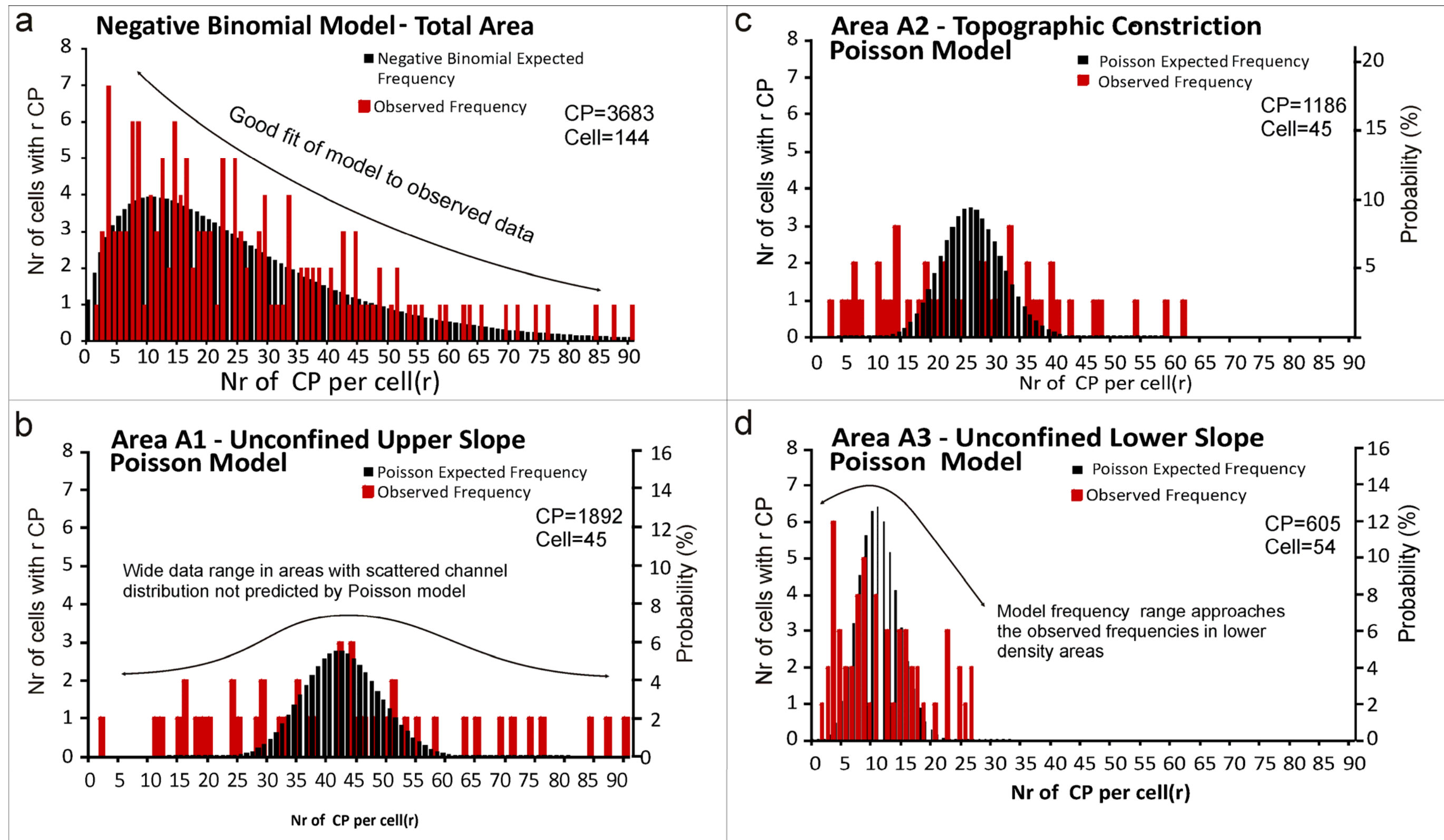
Poisson models also reveal that regions of higher connectivity present greater variations between the observed channel distributions and the calculated Poisson curves, particularly when evolving channels cross-cut older channel-levee deposits (e.g. area A2, Fig. 6.2b). The CP distribution in areas of higher channel connectivity approaches that of a normal distribution (Area 1, Fig. 6.10b), while the observed frequency is significantly scattered. This character, together with the absolute values in equation 6.2, can be used in the quantification of relative channel overlap across the continental slope.

## **6.5. Discussion**

### **6.5.1. Controls on channel clustering on submarine environments**

The results presented in this chapter are concomitant with a fit of non-random negative binomial distributions observed in geological bodies (e.g. Griffiths, 1966). Studies on the organisational patterns of fluvial channels have also shown a tendency for channel clustering which are resultant either from external factors acting on the channel organisation (Hofman et al., 2011) or from compensational stacking from autochthonous factors (Hajek et al., 2010; Straub et al., 2009). However, the clustering analysis presented here contrasts with those undertaken for fluvial channels in two aspects. First, we analyse





**Figure 6.10.** Plots illustrating the observed CP frequencies, and ones expected from distribution models. **a)** Negative Binomial distributions provide a good fit to explain the CP distribution in the slope (see also Table 6.2). **b), c)** and **d)** represent the observed and Poisson (normal) expected frequencies. The significant data scattering between the observed frequencies and the expected frequencies calculated by the Poisson distribution show that this model does not provide a good fit to describe the distribution of channels on the slope. Nevertheless, areas of higher CP density (Area A1) show an approach to normal distributions.

							Distribution Fit	
	Cell Nr	CP Nr	Estimated mean ( $em$ )	Variance ( $s^2$ )	$em-s^2$	$em/s^2$ ratio	Pattern	Negative Binomial (Clustered)
<b>Total area</b>	144	3683	25.5	394.22	368.72	0.06	Clustered	Yes
<b>Area 1</b>	45	1892	42	467.73	425.73	0.08	Clustered	Yes
<b>Area 2</b>	45	1186	26.3	220.37	194.07	0.11	Clustered	Yes
<b>Area 3</b>	54	605	11.2	51.15	39.95	0.21	Clustered	Yes

**Table 6.3.** Summary table of observed frequencies, estimated mean, variance and distribution patterns in the total and individualised areas.

the clustering of submarine channels influenced by channel confluence on variably confined tributary systems, whereas Straub et al. (2009) and Hajek et al. (2010) analyse the distributions resulting from channel avulsion in relatively undeformed sub-aerial basins. Second, the method used in this chapter is based on a map view perspective to assess the distribution patterns in distinct regions across the slope, whereas Straub et al. (2009) and Hajek et al. (2010) base their analysis on profile sections of the sedimentary sequences. Nevertheless, our methodology is also robust enough to allow the analysis of vertical profiles identical to the ones undertaken for sub-aerial channels, thus strengthening the general applicability of the tests and methods presented in this chapter to other basins and environments.

Despite these differences above, common aspects can be established between channel clustering in submarine confluences and sub-aerial avulsion environments. Channel clustering identified in river-based studies is equivalent to the high density regions identified in Figure 6.9c, with channel organisation on both environments being predominantly controlled by non-random processes. Considering that channel clusters are good indicators of the predominant sand fairways on sub-aerial settings (Hofmann et al., 2011), identifying the slope regions with higher channel density also allows an estimation of the lateral extent of the main clusters and consequently of the areas with higher probabilities for the occurrence of sand. This gains particular relevance for the assessment of compartmentalisation of stratigraphic units with distinct reservoir-prone channel clusters, with the larger spacing between them implying the higher risk of lower lateral connectivity.

In the studied slope we consider the organisation of submarine channel into clusters to be mainly derived from external factors. The distinct channel densities and architectures

observed between the different stratigraphic units, alongside their seismic character (Fig. 6.2), are indicators of external forcing on the stratigraphic arrangement of the slope tributary network (e.g. Hajek et al., 2010). However, topography resulting from diapir growth is interpreted to play an important role on channel distribution and slope drainage architecture, focusing the upslope tributaries towards the main confluence in axial regions of the salt-withdrawal basin, and also in the periphery of diapirs on the lower slope (Figs. 6.1 and 6.9). The imposition of a high diapir confinement and consequent forcing of channel confluence and coalescence is a main factor influencing the clustering styles in Areas A1, A2 and A3. In pre-confluence regions channel distribution is more widespread across the slope, with shorter distances between different clusters, although there is a predominant tendency for channels to focus on the high density areas that are correspondent with the main tributary paths of the Neogene Rio Doce Turbidite System (Fig. 6.9). Past the confluence region the channel clusters are marked by a significantly larger spacing, with distances that range from 1 to 10 km (Fig. 6.9c), thus leading to higher isolation between different clusters in areas A2 and A3. An aspect that further supports the external controls on the clustering of the studied channels is the relatively fixed position of slope channels as, shown by the high channel density regions, even in area A1 where numerous widespread channel elements are observed. This contrasts with fluvial channel clusters resultant from autogenic controls that periodically relocate to different portions of the basin (Hajek et al., 2010; Straub et al., 2009). Using the method presented in this chapter, channel clusters resulting from autogenic controls could be expected to show relatively uniform density patterns across the slope as compensating channels tend to re-occupy identical locations through time.

Shifts in the orientation of upslope tributaries, particularly from C1 and modern channels, also support the interpretation of salt-related relief as a main control on channel path. This character is exemplified by the eastern tributary of the modern channel, which shows a deviation of its path at the northern flank of a diapir located at the upslope limit of area A2 (Fig. 6.1). Salt growth is also suggested to influence the migration of the main confluence points. The confluence point in sub-unit 3a, at the base of the studied succession, is the southernmost one (Fig. 6.9b). The channel architectures on the remaining units all show a shift to the North in their confluence points, with these being generally coincident with the high confinement imposed by diapirs in area A2 (Figs. 6.5 and 6.9b).

### **6.5.2. Comparison between fluvial and submarine confluences**

The results in this chapter evidence similar confluence geometries between submarine channels and river systems. Plunge pools and avalanche faces are important elements on fluvial confluences (Best, 1988), and similar features were interpreted in the submarine channel systems in the studied slope (Figs. 6.7 and 6.7). Concordant junctions where tributaries merge at similar levels, as the one observed in channel C1 (Figs. 6.5 and 6.6c), have been observed in modern submarine canyons by Mitchell (2004), and are also considered in the general models for river-based studies (Bathurst, 1997; Best, 1987, 1988; Best and Roy, 1991; Wang et al., 1996). Nevertheless, unequal confluences are commonly observed and seem to constitute the rule in natural river systems (De Serres et al., 1999), having also been observed in submarine canyon-channel systems in the US Margin (e.g. Greene et al., 2002; Shepard and Dill, 1966) and Mediterranean Sea (e.g. Dalla Valle and Gamberi, 2011). An unequal submarine confluence is also present in the modern channel C4, where tributary depth upstream of confluence is offset by >100 m (Figs. 6.5 and 6.7).

Amplitude maps illustrative of the sedimentary fill of channel C1 (Fig. 6.6b) indicate a predominance of deposition in the eastern tributary (ET-1). The continuity of high-amplitude reflections in ET-1 in the post-confluence channel suggests that these two segments constituted the main conduit for coarse grained sediment, possibly with higher turbidite flow recurrence. Contrasting with C1, the lowest tributary of a discordant river junction tends to be continuous with the post-confluence downstream channel, with the two segments constituting the main flow channel (Biron et al., 1993; De Serres et al., 1999). Similar geometries have been observed in this submarine channel system as shown by the modern channel C4 (Fig. 6.7). The eastern tributary shows a smooth transition to the post-confluence channel, constituting the main flow paths of the modern channel, but the merging of the western tributary with the latter is marked by an abrupt drop in channel bed elevation (Figs. 6.5 and 6.7c). As a result, the junction of the western tributary with the other channel segments presents a knickpoint with an adjacent plunge pool restricted to the front of the feeder channel that does not extend through the whole width of the confluence region (Fig. 6.7c). The predominance of higher amplitude patterns along the eastern tributary and their continuity along the post-confluence segments (Fig. 6.7a) suggests that these constitute the main flow paths where coarser sediment was deposited. Strikingly, the channel portions where the lowest amplitude values are observed coincide with the tributary confluence point, including the erosive scour at the mouth of WT-4 and the adjacent upstream channel portion. Since high amplitudes are commonly associated with the accumulation of coarse sediment in channels (e.g. Pirmez et al., 2000), the lower values observed at the modern junction can be considered to represent areas of bypass of coarser sediment. The formation of scours created by flow acceleration in channels also constitutes an important process at stream confluences (e.g. Best, 1988; Christodoulou, 1993;

L'Heureux et al., 2009; Mosley, 1976). Thus, the flow dynamics identified in river confluences may have been replicated as the studied submarine channel increases in erosion at the channel junctions, forming major scours which can either extent through the whole area of equal confluences (as in channel C1, Fig. 6.6a) or limited extents restricted to knickpoints of the higher tributaries in unequal junctions (channel C4, Fig. 6.7c).

A comparison of the geomorphic parameters of confluences analysed in this study and confluences on other continental margins is summarised in Table 6.4. The nomenclature of left and right tributary is here assigned as if looking upstream into the confluence. The data obtained shows a wide range of channel width values in the vicinities of the confluences, with average values in the left and right tributaries of 2600 and 2770 m, respectively, and average confluence width values of 4734 m. The calculated ratios between the confluence width and the sum of the tributaries width also shows a significant range of values, varying between 0.53 and 1.54. The average values of this ratio equal 0.9 (Fig. 6.11). This is very approximate to the value of 1 expected in cases where the combined tributary width is equal to the one at the junction, as a result of either contemporaneous activity on, or equal evolution of both pre-confluence branches.

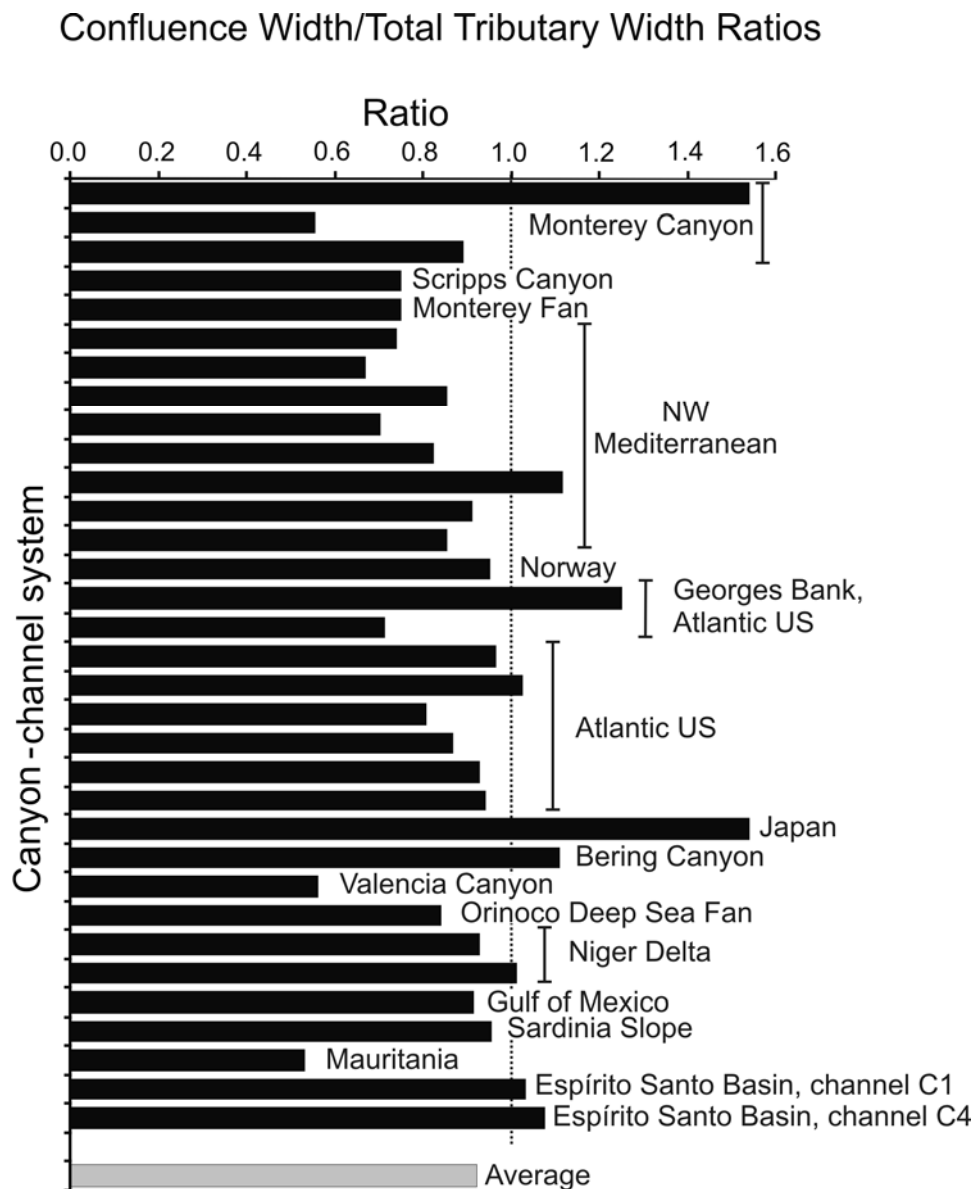
Given that the majority of the systems analysed are close to these values, there is a general tendency for submarine confluences to maintain the width relations at the tributary junctions. For this tendency to be valid, the channel height must be compensated in order to maintain the discharge equilibrium along the channel, where the sum of tributaries discharge volume equals the one at the confluence (Best, 1986; Mosley, 1976). This can be compensated by proportional decreases in channel height as the channel widens at the junctions, with the opposite occurring in the case of channel narrowing. The data obtained



in this study indicates that width-height scale relationships tend to be maintained, in particular for channel C1 where the values show the same order of greatness (Fig. 6.6). However, such proportion is not always observed, in particular when the confluence/tributary ratios are further from the proportional value of one, as in the Valencia Canyon or Monterey Canyon, for example. As these refer to major canyon systems incised on the slope, this morphological imbalance could result from their complex long-time erosion and evolution. With increasing canyon heights, the turbidity flows within it tends to be restricted to the lower thalweg levels, and only the volume of such flows could be effectively accounted for as effective discharge along the channel.

Side-wall slumping is a complementary process to the erosive flows on channel widening (Pratson and Coakley, 1996). This could explain the presence of wider tributaries, especially when one of them is the main canyon conduit. Other less certain proportions where obtained for confluences composed of several tributaries, as the Orinoco Deep Sea Fan (Ercilla et al., 2000), but the lack of detailed morphologic descriptions does not allow a correct assessment of the confluence balance.

Area	Left Tributary (t1)			Right tributary (t2)			Confluence			Confluence Angle
	Width (m)	Height (m)	Dip (deg.)	Width (m)	Height (m)	Dip (deg.)	Width (m)	Height (m)	Dip (deg.)	
Monterey Canyon	500	?	?	800	?	?	2000	?	?	65
	3540	?	?	4100	?	?	4250	?	1.8	70
	2650	?	?	2120	?	?		?		70
Scripps Canyon	28	?	?	16	?	?	33	?	?	50
Monterey Fan	1250	?	?	1250	?	?	1875	?	?	65
Hikurangi Channel NZ	4000-5000	?	4-5	?	?	?	10000	250	?	?
NW Mediterranean	1500	?	?	2550	?	?	3000	?	?	100
	500	?	?	470	?	?	650	?	?	77
	500	?	?	260	?	?	650	?	?	55
	260	?	?	310	?	?	400	?	?	40
	1900	?	?	1380	?	?	2700	?	?	50
	570	?	?	450	?	?	1140	?	?	70
	800	?	?	450	?	?	1140	?	?	70
	1140	?	?	1140	?	?	1950	?	?	75
Rockall Trough	100-500	150-300	?	100-500m	150-300	?	4500	450	?	30
Norway	326	?	?	217	?	?	516	?	?	80
Georges Bank, Atlantic US	2000	?	1	2000	?	1	5000	?	1	60
	2000	?	1	5000	?	1	5000	?	1	60
Atlantic US	200	?	?	350	?	?	530	?	?	50
	170	?	?	220	?	?	400	?	?	30
	480	?	?	400	?	?	710	?	?	25
	880	?	?	620	?	?	1300	?	?	40
	310	?	?	260	?	?	530	?	?	30
	1020	?	?	1100	?	?	2000	?	?	25
Aoga Shima Canyon, Japan	1300	?	?	1300	?	?	4000	?	?	45
Bering Canyon	9600	730		12000	800		24000	866		40
Valencia Canyon	1500	125	?	1930	150	?	1930	150	?	80
Orinoco Deep Sea Fan	42000	?	?	5500	10		40000	60	0.11 to 0.06	45
	Several tributaries: W: 2500 to 9500 m/ H:10-17m						24000	16	0.06 to 0.13	45
Niger Delta	310	?	?	465	?	?	720	?	?	80
	195	?	?	240	?	?	440	?	?	80
Gulf of Mexico	450	?	?	590	?	?	950	?	?	45
Sardinia Slope	1270	150	?	780	100	?	1960	?	?	25
Mauritania	3820	600	?	4410	600	?	4375	300	?	30
Brazil, Channel C1	1200	165	2.17	1270	158	2.14	2550	153	0.5	40
Brazil, Channel C4	410	40	1	705	140	0.7	1200	130	0.5	75



**Figure 6.11.** Plot representing the confluence-tributary width ratio observed in different margins of the world. This value is obtained by dividing the confluence width by the sum of tributary widths. Dotted line represents a width ratio equal to 1, which is expected when the confluence width is equal to the sum of tributary widths. (data from Barnes, 1992; Bellaiche, 1993; Canals et al., 2000; Cronin et al., 2005; Dalla Valle and Gamberi, *in press*; Ercilla et al., 2000; Greene et al., 2002; L'Heureux et al., 2009; McGregor, 1985; McHugh and Ryan, 2000; Mitchell, 2004; Pirmez et al., 2000; Pratson and Coakley, 1996; Scholl et al., 1970; Schwab et al., 2007; Shepard and Dill, 1966).

**Table 6.4.** (Previous page) Comparative table of channel width and height at submarine confluences from several continental margins. Left and right tributary assignment is based on the upstream tributary position in relation to the confluence.

### 6.5.2. Classification of submarine confluences

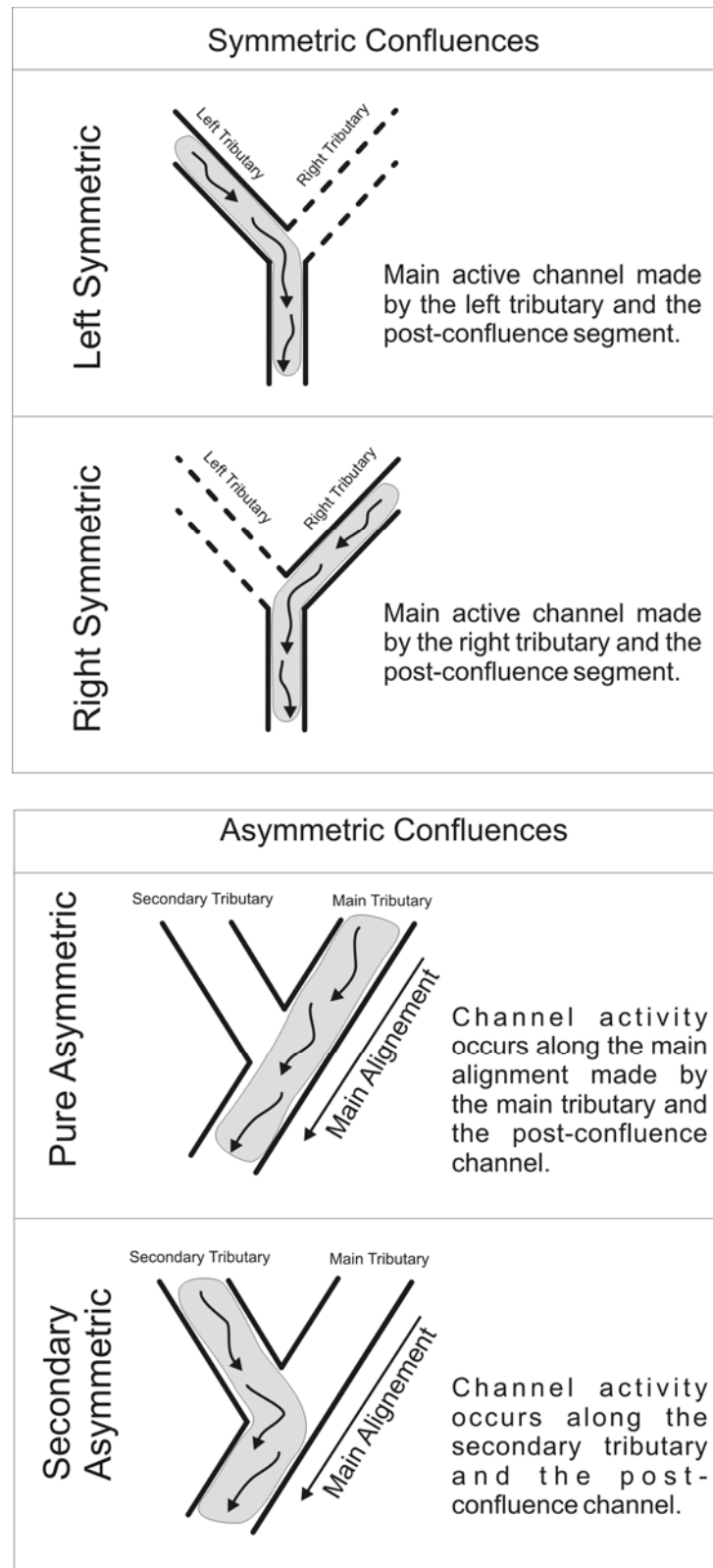
Classifications of river confluence symmetry are mainly based on channel planform geometry and on the relationship between tributary paths and downstream channels. Instead of a purely geometry-based classification, the combined concept here proposed includes both the tributary/channel geometry and patterns of sediment distribution as defining characters. These characteristics can be determined by the analysis of seismic amplitude maps for given intervals of interest, which can be aided by a quantification of specific seismic reflections or packages. The application of this analysis to buried channels has the potential to indicate either the main behaviour of the submarine confluence, or to evidence periods of alternating sediment input in the tributaries. Furthermore, this also has implications for the understanding of the distribution and continuity of reservoir-prone strata at submarine channel junctions.

In the proposed classification (Fig. 6.12), Y-shaped symmetric confluences are subdivided in left symmetric or right symmetric depending of which tributary is interpreted to show more activity. Asymmetric confluences can be divided into pure asymmetric to describe cases where the main flow occurs within the main path, i.e. the channel path made by the alignment of the major tributary and post-confluence branch. When the principal channel processes occur along the secondary tributary, these are referred to as secondary asymmetric. Given that submarine channels commonly show shifts of the main axis along their path, the proposed classification should be applied locally to each confluence point along the submarine channels. In addition, submarine channels are prone to exhibit several

tributary junctions which are not necessarily identical, and distinct confluence classifications may be applied across the whole slope.

Using the nomenclature above, the confluence of channel C1 can be classified as pure asymmetric. Despite the very similar tributary morphology, the geometry shown in Figure 6.6a suggests that the eastern tributary and the post-confluence segment form the main alignment, thus indicating an asymmetric confluence. In addition, the amplitude maps show a predominance of high-amplitude patterns (interpreted to represent coarse grained fill deposits) along the referred channel segments, indicating that these were the predominant flow and sediment deposition paths. This classification is applied to the whole vertical succession filling channel C1, but detailed analysis of limited intervals of the channel fill could provide proof of periods of time where the main sediment deposition was restricted to the western tributary and the post-confluence channel. For such periods, this would be classified as a secondary asymmetric confluence.

Similarly, the confluence of the modern channel is also classified as a pure asymmetric. The main alignment is clearly formed by the eastern tributary and the post-confluence segment, which are also the ones showing geomorphic continuity. The higher and continuous amplitude patterns related to this channel also suggest a predominance of flows in the referred segments that compose the main channel. In addition, the asymmetric character in this channel is also related to the unequal level junction of the tributaries. As the lowermost tributary is commonly levelled with the post-confluence channel, there is a tendency for these to form the main channel alignment, and to probably focus the majority of sedimentary activity in the channel. Thus, unequal tributary junctions are prone to create pure asymmetric confluences. An example of a modern secondary asymmetric confluence



**Figure 6.12.** Diagram illustrative of the submarine confluence classification. Symmetric confluences are Y-shaped and nomenclature is based on the position of the main active tributary, i.e. left or right symmetric. Asymmetric confluences are pure asymmetric if principal channel activity is along the alignment made by the main tributary and post-confluence channel. Secondary asymmetric describes cases where channel activity is not along the main alignment.

can be found in Pirmez et al. (2000). The authors describe a modern channel on the Niger Delta (channel Y) which, due to the low amplitudes, is interpreted to be inactive except downstream of the confluence with a smaller tributary. The high amplitudes predominant in the latter features show that the main channel activity takes place along the secondary tributary and the post-confluence branch. This contrasts with the modern channel in the Espírito Santo Basin described in this work, proving the validity of the proposed submarine confluence classification.

## **6.6 Conclusions**

The following points summarise the conclusions of this chapter:

The new method presented shows the maximum channel densities are coincident with the path of upper-slope tributaries. Post-confluence regions are characterized by lower channel densities.

Submarine confluence areas in the slope are strongly influenced by increasing lateral confinement. All the channel systems observed have their confluence in the vicinities of the high confinement area.

Goodness-of-fit (chi-square) and negative binomial are helpful to identify regions of channel clustering. Regions of higher channel scattering and density showing relatively higher degrees of clustering are identified in upper-slope regions. Channel clustering and channel density tends to decrease downslope.



Sharp width variations, proportional to the combined width of joining tributaries, are observed at submarine confluences. Height changes are gradual if tributaries and post-confluence branches are in equal levels. Sharp height contrasts between tributary and main channel are observed at unequal confluences.

A new classification for submarine confluences is proposed in this chapter. The identification of the main tributaries involved in the principal channel activity is based on a combined analysis of the confluence morphometry, geometry and seismic attributes. Symmetric confluences are classified as Left Symmetric or Right Symmetric, dependant of the position of the tributary with predominant activity (as observed upstream from the confluence). Asymmetric confluences are classified as Pure Asymmetric if the main flow is within the channel alignment defined by the main tributary and the post-confluence channel. Secondary Asymmetric confluences describe cases where the sedimentary flows take place along the secondary tributary, which is at an angle with the main channel alignment. On unequal junctions, the secondary tributary is present at higher elevations, being separated from the main conduit by a steep knickpoint.

Understanding the dynamics of tributary channels networks is important to assess the main conduits where reservoir-prone lithologies accumulate. In addition, the clustering patterns of submarine channels constitute indicators of the degree of slope compartmentalisation, where higher cluster isolation leads to compromised lateral connectivity between channel belts.

# **Chapter 7**

## **Summary and Discussion**

## **7. Summary and discussion**

### **7.1 Introduction and summary of major findings**

This chapter starts with a summary of the major findings of this thesis, as presented in Chapters 4, 5 and 6 (Fig. 7.1). Next, it discusses the distinct styles of compartmentalisation identified in the Espírito Santo Basin. Comparisons between the scales and styles of compartmentalisation are presented, followed by a discussion on Mass-Transport Deposits and channel architecture, and their inputs on the compartmentalisation of reservoir units. A brief outline of the data limitations and recommendations for further work are presented at the end of this chapter.

A quantitative approach was used to characterise the studied stratigraphic and structural elements, focusing on the analysis of: 1) the spatial distribution of sedimentary deposits (namely submarine channels and mass-transport deposits) and fault families, particularly in relation to adjacent salt diapirs, 2) the seismic character of successive stratigraphic successions and 3) the lateral and vertical extent of individualised sedimentary and structural features.

#### **7.1.1. Chapter 4**

The main aim of Chapter 4 was to characterise the relative distribution of MTDs and turbidites within the Eocene/Oligocene Abrolhos Unit (Fig. 7.1). The chapter was focused on a confined salt-withdrawal basin bordered by two northwest-trending diapir ridges (Fig. 4.1). The findings from Chapter 4 highlighted the contrast in internal character between MTD intervals and laterally continuous turbidites. The presence of MTDs often leads to

erosion of the underlying turbidite deposits, creating sharp lateral terminations in the latter (Fig. 4.9). Conversely, turbidite pinch-outs into MTDs can be gradual, marked by discontinuous deposits (Fig. 4.6). The relative proportion of MTDs in the Abrolhos unit is markedly variable downslope, but along-slope shows a consistent lateral decrease from over 60% to below 40% in a West-East direction (Fig. 4.11). This trend is also followed by the thickness values in the MTD. The increasing slope gradients towards the younger levels of the Abrolhos Unit are indicative of slope progradation contemporaneous with the deposition of MTDs (Fig. 4.12). Turbidites show higher degrees of compartmentalisation when the vertical proportion of MTDs in Unit 2 is larger. The presence of diapirs on slope settings can also favour the preservation of reservoir-prone strata by constituting barriers for erosive flows.

### 7.1.2. Chapter 5

Chapter 5 focuses on the lowermost MTD in the Abrolhos unit, MTD-A1 (Fig. 7.1). One particular feature of this MTD is its areal extent, which coincides with the axial region of an underlying salt diapir ridge (Figs. 5.1 and 5.4). Several failed blocks were identified within MTD-A1 (Figs. 5.2), and were classified as remnant blocks when *in-situ*, or rafted blocks when transported downslope (Fig. 5.3). Observing that fault families developed on the crest of buried salt structures delimit and cross-cut remnant blocks (Fig. 5.3), diapir-related sea-floor deformation is considered to have played a key role on the genesis of this mass-failure (Fig. 5.11). Average height of interpreted blocks reaches 150 m for an average area of 0.4 km<sup>2</sup>. These dimensions are relatively uniform over the main salt ridge (Fig. 5.9). Three styles of block deformation were established. Minor deformation is typical of remnant blocks. Rafted blocks can present minor, moderate and major deformation (Fig. 5.10). The analysis

of kinematic indicators provided by block shape and imbrications within distinct blocks led to the conclusion that MTD-A1 records a complex movement. The central masses of the MTD spread laterally in an extensional flow regime, moving perpendicularly along the axial regions of the salt ridge. This central component is estimated to have the lowest remobilisation distances, particularly in regions where remnant blocks are present. Contrastingly, peripheral masses on the western and northern sections moved towards the salt ridge axis and collided with the central masses of MTD-A1 (Fig. 5.11). Peripheral masses show evidence of internal compression, characterised by strata imbrication and unidirectional rotation of rafted blocks. Individual blocks, particularly when associated with leaking faults, can constitute viable fluid conduits through MTDs (Fig. 5.12). Significantly, the permeability potential of each MTD section is inversely proportional to its travel distance.

### **7.1.3. Chapter 6**

In chapter 6 a series of submarine channels of Miocene to Holocene age were analysed. This chapter focuses on: 1) the geometry of submarine confluences and 2) the spatial analysis of channel density in relation to confluence regions, and also to the influence of topographic confinement imposed by diapirs. A detailed geomorphic analysis of confluence points of two channels of distinct age revealed two contrasting morphologies, which are partly similar to morphologies observed in rivers (Figs. 6.6 and 6.7). In the older channel, of early Miocene age, the tributaries had similar morphologic properties and merged at the same level (Fig. 6.6.). In contrast, the Holocene channel presents an unequal confluence, where distinct tributaries merge at different levels up to an offset of 100 metres (Fig. 6.7). The channel confluences in this slope occur in regions of marked topographic confinement. A novel classification for submarine confluences is proposed in this chapter,

based on the geometric relation of the tributaries and on the introduction a temporal constrain of alternating turbiditic flows on the channel branches (Fig. 6.12). Symmetric confluences are characterised by Y-shaped junctions and, depending on the active tributary during a given turbiditic flow, are classified as left- or right-symmetric. Asymmetric confluences comprise junctions where the alignment of the larger tributary and the post-confluence channel segment constitute the main conduit onto which a secondary tributary merges at a given angle. These are considered pure asymmetric when channel activity occurs along the main channel alignment, or secondary asymmetric when channel flows take place within the secondary tributary and post-junction branch. Based on the established criteria, the confluences studied in the Miocene and Holocene channels are classified as pure asymmetric.

This chapter also presents a new quantitative method for the analysis of channel distribution on continental slopes. The analysis of channel systems in three different units reveals that their distribution is not random, following negative binomial distributions characteristic of clustered patterns (Fig. 6.10). Regions of higher channel density are indicative of preferential vertical stacking, with limited lateral migration (Fig. 6.9). Both channel density and clustering decrease downslope, being the most pronounced variations in both parameters closely related with the confluence region (Fig. 6.9c). The decreases in both density and clustering are intrinsically related to channel coalescence at the junction areas as a result of increasing topographic confinement imposed by salt diapirs.

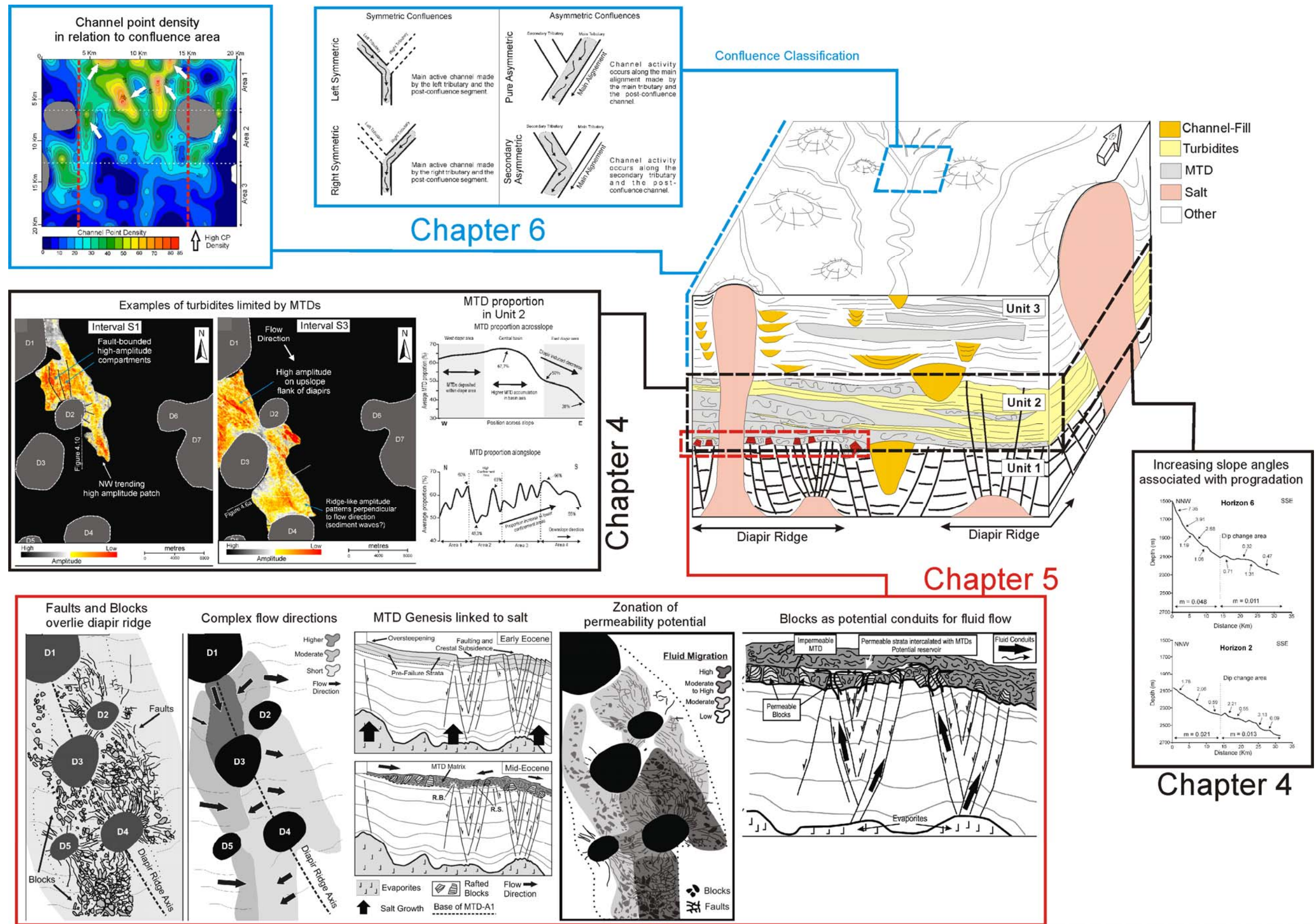


Figure 7.1. Schematic representation of the study area with a synthesis of the principal observations and results.



## 7.2. Styles and scales of compartmentalization on the Espírito Santo Basin

The first theme to be discussed is the comparison between the scales of the different styles of stratigraphic and structural compartmentalisation presented in Chapters 4, 5 and 6. After, the stratigraphic compartmentalisation styles in the Espírito Santo Basin will be presented, with particular emphasis on the impact of MTDs on reservoir intervals. The ways channel compartmentalisation varies on the Espírito Santo Basin slope will also be analysed.

Sedimentary and structural elements identified on seismic data consist of stratified turbidites (Chapter 4), MTDs (Chapters 4 and 5), channels (Chapter 6) and faults (Chapter 5). These elements show variable types of interactions depending on the seismo-stratigraphic unit in which they are included. For instance, different architectures of reservoir-prone strata are observed at different stratigraphic levels, due to their distinctive interaction with large mass-transport deposits and fault arrays. Structural compartmentalisation mainly occurs in Unit 1, a character expressed by the different fault families developed on the crests of salt structures (see Chapter 5, Fig. 5.8). In Unit 2, the compartmentalisation of potential reservoir units is predominantly stratigraphic, and the thickness and lateral continuity of turbidites is controlled by both MTDs and salt diapirs (Chapter 4). Adding to this, in the vicinity of diapirs there is also relevant structural compartmentalisation of Unit 2 (see Figs. 4.3 and 4.7).

In Unit 3 two styles of stratigraphic compartmentalisation predominate. Sub-unit 3b is characterised by the presence of widespread channel systems, whose distribution has been influenced by existing salt-related topography (Chapter 6). Sub-unit 3c also has



numerous scattered submarine channels, but these show marked variations in seismic character and depositional architecture in comparison with the underlying sub-unit 3b. In addition to the various channels observed, MTDs in sub-unit 3c observed within the salt-withdrawal basin result in stratigraphic architectures identical to those observed in Unit 2 (Fig. 2.6).

A better understanding of the scales involved in the distinct compartmentalisation styles existing in each unit can be achieved by comparing their morphometric parameters, namely width, height and length (Fig. 7.2). One issue arising from the representation of the different data series acquired is the establishment of generalist regression lines representative of the whole data sample. Each data series analysed in this thesis has its own best fit regression line. In addition, the numerous data points acquired often show great dispersion when plotted in simple x-y graphs. This leads to scattered values that do not lie strictly along a single line, thus compromising the accurate significance of regression lines applied to the data (Cowie and Scholz, 1992; Walsh and Watterson, 1988). Given the limitations on determining the best fits to the data, a simplified method to compare the range of scales involved on the several compartmentalising elements was adopted. This consists on the application of origin-intersecting linear fits on all the data series that allows the dependent variable, width (W), to be represented as a direct proportion of the independent variable height (H) (Fig. 7.2). Thus, the width-height scale relationships are present as:

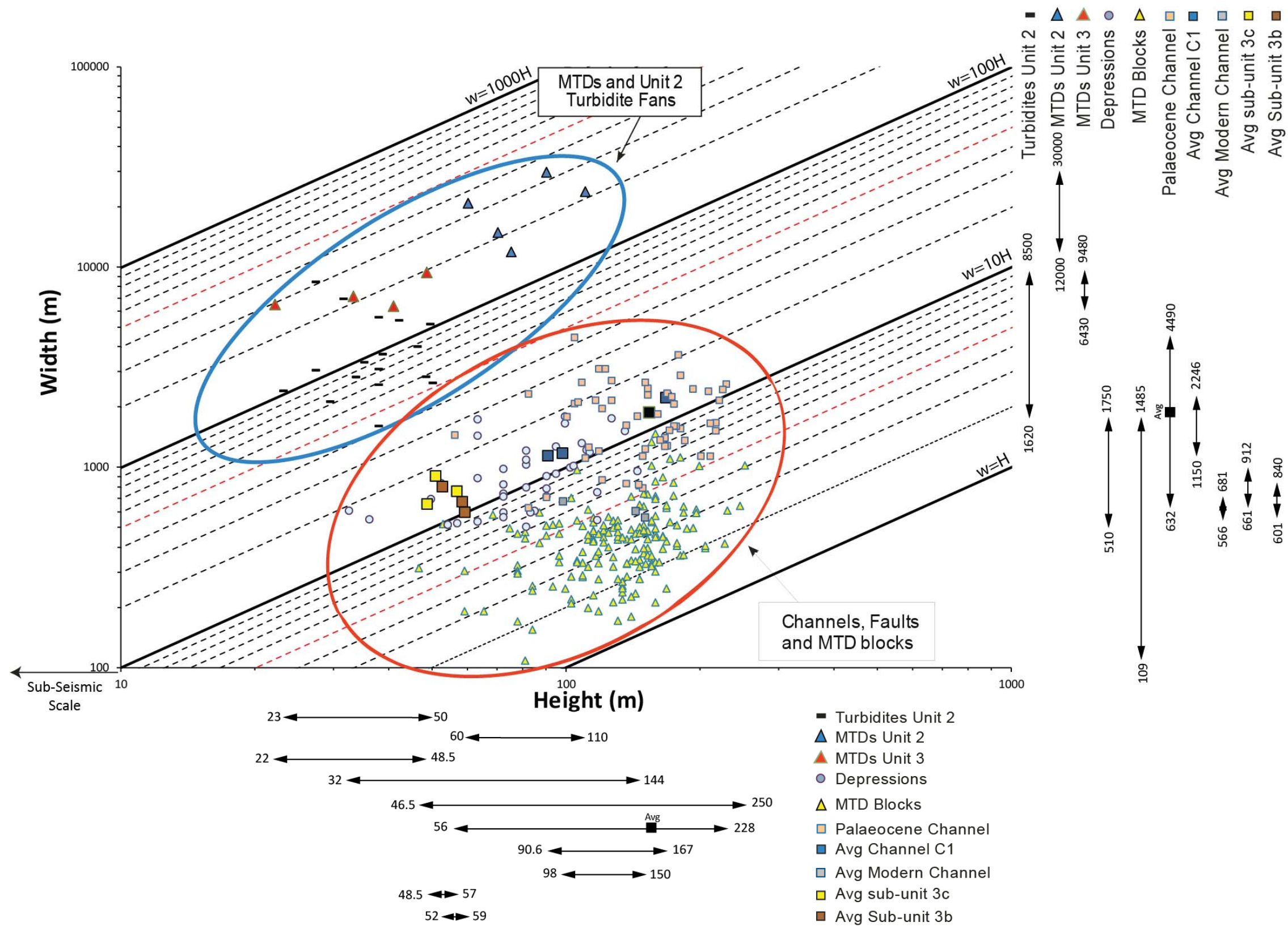
$$W = \alpha \cdot H \quad (\text{eq. 7.1})$$

where  $\alpha$  is a constant of proportionality equal to the slope of the regression line. Identically, the relations between length (L) and width (W) of the sedimentary deposits are estimated as:

$$L = \beta \cdot W \quad (\text{eq. 7.2.})$$

Based on the same principle, distinct origin-intersecting lines with variable slope values of  $\alpha$  or  $\beta$  were applied to the different data series in order to assess their maximum ( $\alpha_{\text{MAX}}$ , or  $\beta_{\text{MAX}}$ ) and minimum ( $\alpha_{\text{MIN}}$ , or  $\beta_{\text{MIN}}$ ) scaling relationships. These maximum and minimum values are used to compare the scale relationship of not only one particular type of geological feature but also between distinct ones. Log-log plots were used to represent the large ranges of values obtained.

Log-log plots of width and height of measured geological features show two distinct clusters (Fig. 7.2). The group representing the larger deposits includes MTDs identified in sub-unit 3c and Unit 2 (Abrolhos Unit), as well as turbidites within the latter unit. Heights in this cluster range from 22 m to 110 m, with widths varying between 1620 m and 30000m. The second cluster comprises channels in Units 1 and 3 and MTD blocks in Unit 2. Both groups share very similar ranges of height, as the maximum MTD thickness corresponds in fact to the size of the tallest blocks. The height of the geological features in this cluster varies between 30 and 250 m, with width varying between 110 m and 4490m. The most evident difference between both data clusters resides in the width covered by features in each distinct group. The range of sizes observed for the MTDs and associated strata, ranging between 1600 and 30000 m, is about ten times larger than the group containing channels and blocks. This relation is a direct result of the distinct scales involved



**Figure 7.2.** Plot representing the width and height of the different geological features identified in the slope. Two major dimensional groups are present. The largest values correspond to MTDs and associated turbidite intervals. The smaller dimensions correspond to channel systems and intra-MTD blocks.

in the processes that lead to the deposition of large MTDs and/or laterally extensive turbidites, in contrast to the laterally limited submarine channels.

### **7.2.1- Scale of MTD and Turbidite compartmentalization**

#### **7.2.1.1. Scale relationships between MTDs of distinct units**

The dimensions of MTDs vary within the stratigraphic unit in which they occur, with the MTDs in Unit 2 being predominantly larger than those in sub-unit 3c. The size differences are suggested to depend on the confinement imposed by the salt diapirs, which can also aid to explain the decreasing dimensions of MTDs observed. In general, scale relationships between width and height (eq. 7.1) of MTDs in Unit 2 can be explained by  $\alpha_{\text{MTD-U2}}$  values of 249, with values varying between  $150 < \alpha_{\text{MTD-U2}} < 350$  (Table 7.1). This range of bounding values is suggested to relate to a gradual tendency for MTDs to decrease in size towards the top of the stratigraphic unit. The widest MTDs in Unit 2 (up to 30000 m) are located at the lower levels of this stratigraphic interval (MTDA-1, MTD-A2 and MTD-A3). Contrastingly, the MTDs located at the upper levels of Unit 2 (Fig. 7.3) have widths as low as 12 000 m, less than half of the MTDs at the deeper levels, which can be considered to result from increasing confinement occurring during the deposition of Unit 2 (Chapter 4).

In Unit 3, the largest MTDs do not exceed widths of 9500 m, which are relatively similar to the ones of the top-most deposits in Unit 2. Such MTD sizes are identical to the general width of the modern salt-withdrawal basin in the studied area. Scale relationships obtained  $\alpha_{\text{MTD-U3}}$  values of 197.3, varying between  $150 < \alpha_{\text{MTD-U3}} < 290$  (Table 7.1). The smaller difference between the  $\alpha$  value and the minimum  $\alpha$  obtained suggests that MTDs in Unit 3

		W= $\alpha$ .H			L= $\beta$ .W		
		$\alpha$	$\alpha_{\text{Min}}$	$\alpha_{\text{Max}}$	$\beta$	$\beta_{\text{Min}}$	$\beta_{\text{Max}}$
Stratigraphic Feature	MTD Unit 3	197.0	150.0	290.0			
	MTD Unit 2	250.0	150.0	350.0			
	Turbidites Unit 2	99.6	40.0	310.0	2.9	1.1	7.0
	Paleocene Channel	11.6	5.0	45.0			
	Channel C1	12.6	5.0	30.0			
	Modern Channel (C4)	4.4	2.0	14.0			
	Avg sub-unit 3b	12.0	10.0	15.0			
	Avg sub-unit 3c	13.0	13.0	18.0			
	sub-unit 3b	10.7	3.0	80.0			
	sub-unit 3c	13.7	3.5	120.0			
	Depressions	10.9	6.0	28.0	1.5	1.0	3.0
	Blocks	3.3	1.3	10.0	1.6	1.0	5.0

**Table 7.1.** Synthesis table of the  $\alpha$  and  $\beta$  values obtained for the different depositional features.

are better represented as having width values about 150 to 197 larger than their width. The larger scale relationships are considered as less representative of this data sample.

The scale relationship between the MTDs occurring in distinct stratigraphic units can be obtained by comparing the ratios between the values of  $\alpha$  for each data series (Table 7.1). Knowing these values, both series can be compared by using:

$$\alpha_{\text{MTD-U3/MTD-U2}} = \frac{\alpha_{\text{MTD-U3}}}{\alpha_{\text{MTD-U2}}} \quad (\text{eq. 7.3})$$

Despite the evident contrasts of the general dimensions of MTDs in both stratigraphic units, the  $\alpha_{(\text{MTD-U3/MTD-U2})}$  value of 1.3 suggests a resemblance between the two series as they share scale relationships of similar order. As such, the gradual decrease in MTD size in Unit 2 and the more pronounced size difference between MTDs in Units 2 and 3 can be considered to reflect the increasing degrees of basin confinement created by the growth of salt structures during the late Palaeogene and Neogene. Considering that MTDs are often regarded as impermeable or low permeability units (Posamentier, 2004b), they can be main inducers of vertical compartmentalisation of reservoir units. Thus, understanding the scale at which MTDs occur in relation to slope confinement is relevant for the estimation of the thickness and lateral spread of the low permeability strata. Consequently, this also has implications on the vertical spacing between permeable strata.

#### **7.2.1.2. Scale relationships between MTDs and turbidites in Unit 2**

Turbidites constitute important sand-rich features in submarine slopes, thus playing a major role in the architecture of reservoirs in submarine settings. When not confined to larger channels, such deposits can spread into laterally extent turbidite fans which can in

turn have variable degrees of internal amalgamation as a result of smaller-scale events. On seismic-scale studies, the minimal vertical dimensions identifiable within the seismic facies associated with turbidites are dependant of data resolution. As such, many of the features identified in the seismic data as a single turbiditic event, with minimum thicknesses of 20 m, can in fact constitute a more complex turbiditic fan resultant from the erosion and aggradational action of successive flows. Thus, these features can have significant vertical and lateral heterogeneities which are better assessed at sub-seismic scales. Data from exposed outcrops of submarine systems provide good analogues to assess for such heterogeneities associated with the interpreted turbidite strata, which highlight the presence of metric to sub-metric beds of sandstone intercalated with shales (e.g. Beaubouef, 2004; Posamentier and Walker, 2006; Shanmugam and Moiola, 1988). In addition, metric slides and debrites are also common features identified at outcrop scale (Butler and McCaffrey, 2010; Hodgson, 2009; Van der Merwe et al., 2011), but these would be virtually impossible to identify on seismic data. Taking these considerations into account, the seismic facies identified as turbidites are not considered as uniform beds of sand. Nevertheless, for the purpose of the analysis of scale relationships between the distinct types of deposits undertaken in this thesis, the turbidites do present higher homogeneity when compared to the adjacent seismic-scale MTDs.

An evident dimensional contrast is observed between MTDs and reservoir-prone turbidites identified within Unit 2 (Fig. 7.2 and 7.3). The latter are laterally and vertically limited by the presence of the MTDs (Chapter 4). Individualised turbidite intervals identified in the seismic data have widths ranging between 1600 and 8500 m and heights between 23

and 50 m (Fig. 7.3), which fall in the thickness range of productive reservoir deposits (c. 30 metres) (Hardage et al., 1998a; Puckette and Al-Shaieb, 2003).

Scale relationships obtained using Equation 7.1 to the turbidite data show  $\alpha_{\text{turb}}$  values of 99.7, with ranges of  $40 < \alpha_{\text{turb}} < 310$  (Table 7.1). Similarly to what was observed above for the MTD data series, the slope value of the fitted regression line is closer to the minimum  $\alpha$  observed. Taking this into account, and analysing the plotted turbidite data, it is considered that the majority of turbidites can be represented by a constrained range of  $\alpha$  values varying between 60 and 120 (Fig. 7.3). The different ranges of  $\alpha$  observed between the whole and constrained samples can be related to differences in depositional or erosional processes associated with the accumulations of the turbidites.

The comparison of the width-height scale relationships between the features in Unit 2 ( $\alpha_{(\text{MTD-U2/Turb})}$ ) show that MTDs are, on average, 2.5 times larger than the turbidites. This relationship is consistent with the observed height values of both types of deposits. Nevertheless, it does not represent the width relations as accurately as the MTDs are often over 2.5 times wider than the turbidites. Taking into account that many of the turbidites are limited by MTDs (Chapter 4), erosional processes are considered to be the main factor controlling the smaller deposits, especially the ones represented by  $\alpha$  value below 120. In contrast, the turbidites with larger lateral extent, reaching values similar to MTDs (Fig. 7.3), are interpreted to suffer significantly less erosion or none at all.

#### 7.2.1.3. Scale of MTD blocks and relationship to turbidites

The presence of blocks in the mass-failures of Unit 2 is restricted to MTD-A1 (Chapter 5). The width of the blocks varies between 105 and 1500 m, being mostly



controlled by pre-existing faults and by strata disaggregation during salt movement. Block height varies between 47 and 250 m, limited by thickness of the MTD in which they are found. The scale relationships obtained for blocks show that their width is on average three times their height, with bounding  $\alpha$  values in the order of  $1 < \alpha_{\text{Blocks}} < 10$  (Table 7.1).

In terms of reservoir potential, and associated compartmentalisation, the most relevant comparison is the one between blocks and turbidites. The scale relationships of width and height of these two features ( $\alpha_{\text{Turb/Block}}$ ) show that turbidites are, on average, about 30 times larger than MTD blocks. This value is majorly a reflex of the significantly larger width associated with the turbidites (2145 m to 7000 m) although these have very limited heights (23m to 49 m) when compared to the blocks (Fig. 7.1). The smaller blocks fall in the same height values of 50 m observed for the thickest turbidites. Contrastingly, the larger blocks show heights that can reach up to 250 m, five times the maximum height of turbidites.

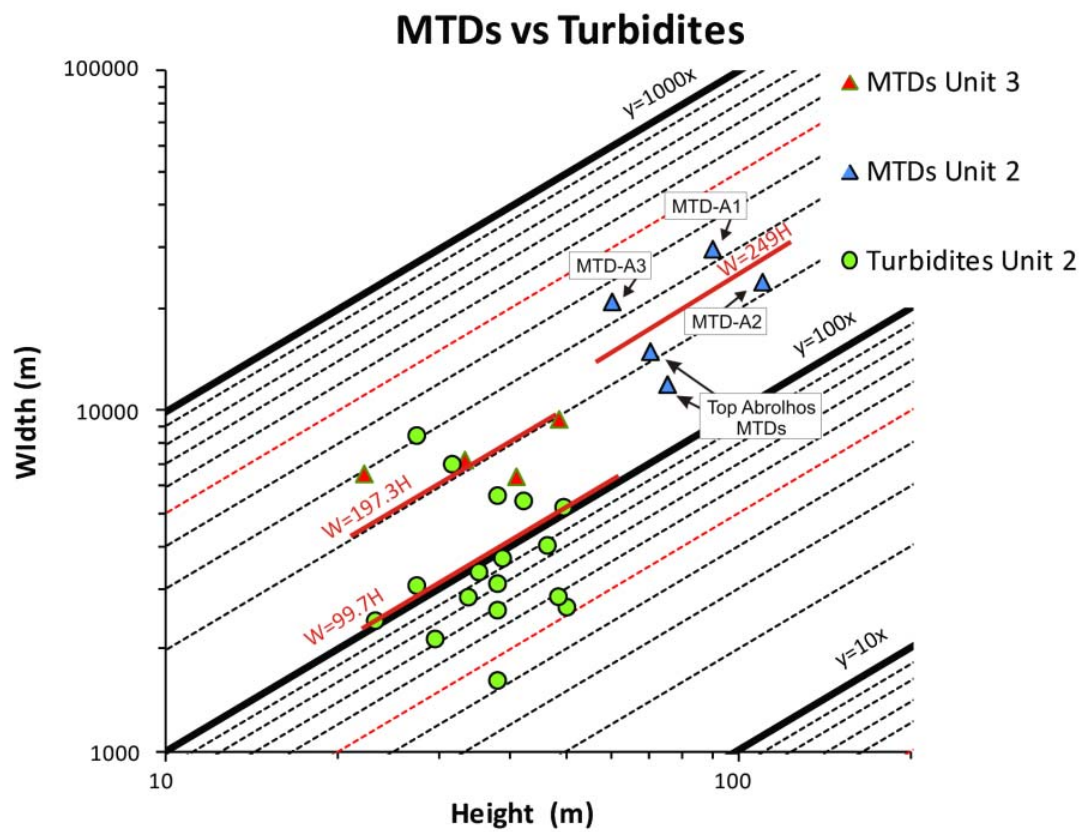
Scale relationships between the length and width of both turbidites and blocks were also estimated (Fig. 7.4), being represented as a function of  $\beta$  (eq. 7.2). The values of  $\beta$  obtained (Table 7.1) indicate that the length of turbidites is on average 2.9 times larger than their width, with variations of  $1 < \beta_{\text{Turb}} < 7$ . As for blocks, their length is estimated to be 1.6 times the width, with this varying between  $1 < \beta_{\text{Blocks}} < 5$ . The length-width relationships between these features show that, on average, turbidites are about two times larger than the blocks. Nevertheless, the ranges of  $\beta$  obtained for blocks and turbidites are fairly similar, with the maximum  $\beta$  showing a lower ratio of 1.4. Thus, the sizing relationships of blocks and turbidites can be considered to be fairly identical. Theoretically, this means that within the same range of values both the blocks and turbidites would show identical dimensions,

with a maximum difference of 40%. The major difference lies in the actual size in which these distinct features occur (Fig. 7.4). While the blocks predominantly show sizes between 100 and 1000 m for both width and length, turbidites are up to ten times larger with values between 1000 and 10000 m observed for the same parameters. From a purely dimensional perspective, if failed blocks have any viability of accumulating fluids, their reduced lateral extent constitutes the major limitation to connectivity within MTD-A1.

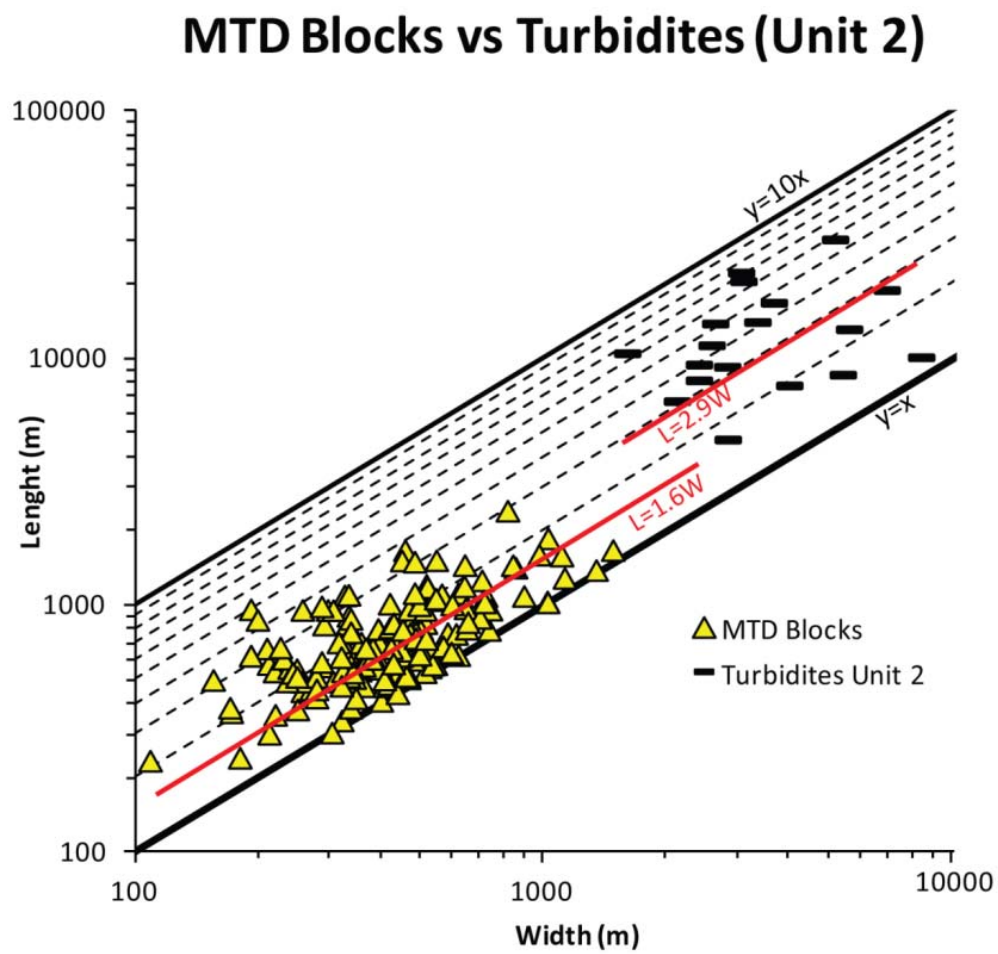
#### **7.2.1.4. Scale relationships between MTD blocks and submarine channels**

The width and height of MTD blocks tends to show identical dimensions to sections of reservoir-prone channels. The height range of the blocks, between 50 and 250 m, is equivalent to the one observed in sections of all channel systems (Fig. 7.2 and 7.5). Blocks tend to be narrower than the majority of channel sections in the Palaeocene Channel in Unit 1 and the post-confluence branch of Channel C1 (ChanC1). Despite this, blocks show width values (100 to 1000 m) of similar range to the ones of several channel sections of the Neogene units (Chapter 6) (Fig. 7.4). The general relationship of width and height between the blocks and the modern channel (MC) shows that the latter are about 30% to 40% larger. Nevertheless, some blocks exceed the maximum height observed for sections of the modern channel, and can also reach identical maximum heights (Fig. 7.5). However, these resemblances grow dimmer the as channels increase in size. Channel C1 and the Palaeocene Channel show  $\alpha$  values of 13 and 12, respectively (Fig. 7.5 and Table 7.1), which are about four times larger than the width-height scale relationships of  $\alpha=3$  obtained for the blocks.

The major contrast between these genetically distinct stratigraphic features, blocks and channels, is the length. While channels are elongated features that stretch over tenths



**Figure 7.3.** Plot representing the average width and height of MTDs in Units 2 and 3, and of turbidites in Unit 2.



**Figure 7.4.** Plot representing the width and length of blocks in MTD-A1 and of turbidites in Unit 2.

of kilometres, the blocks analysed are significantly smaller, not exceeding 2.5 km. Similarly to what was considered for turbidites, the limited dimensions of blocks comparatively to channels implies that any hydrocarbon accumulations within these would be distributed by several compartments with limited storage volume and no guaranteed connectivity.

### 7.2.2. Channel styles and compartmentalisation

In the Espírito Santo Basin, submarine channels are important features in Units 1 and 3 and their distribution is variably controlled by the presence of salt structures. The quantitative analysis of the channel systems identified in the Cenozoic stratigraphic interval reveals two predominant architectures. Smaller channels are present in sub-units 3b and 3c. These were shown to be laterally spread within the salt-withdrawal basin, focusing not only in the axial regions but also on the flanks of salt diapirs (Chapter 6, Fig. 6.9). The very high number of channel features present in these sub-units (see Chapter 6) also results on a wide range of dimensions observed (Fig. 7.5). As a consequence, the scale relationships of channels in these units also show great variability. The linear regression lines indicate that the width of channels in sub-unit 3b is about 11 times the height, but  $\alpha$  is highly variable with value ranges of  $3 < \alpha_{3b} < 80$  (Fig. 7.5a). Similar scales were determined for sub-unit 3c with fitted  $\alpha_{3c}$  values of 13.7 but the magnitude of variability is larger ( $4 < \alpha_{3b} < 120$ ) (Fig. 7.5b and Table 7.1). Nevertheless, the highest data point densities can be constrained within narrower ranges of  $\alpha$  values, such that the scale relationships for each unit can be expressed by  $4 < \alpha_{3b} < 30$  and  $4 < \alpha_{3c} < 40$ .

Contrasting with the previous sub-units, channels in Unit 1 (Palaeocene Channel), sub-unit 3a (Channel C1) and the modern sea-floor are predominantly located in the axial

regions of the salt-withdrawal basin, with no relevant expression on its marginal areas. The comparison of width and height ranges between these larger submarine channels indicates a close resemblance between the Palaeocene Channel (ChanPal) and Channel C1 (Fig. 7.5c). This resemblance is further confirmed by the best fit regression lines, with  $\alpha$  values of 11.6 and 12.6 for the Palaeocene and C1 channels, respectively (Table 7.1). The scale relationships obtained for the buried (C1 and Palaeocene) axial channels are about of 3 to 3.25 times larger than ones obtained for the modern channel. This channel is characterised by a much smaller widths and heights, with  $\alpha$  values of 4 varying between  $2 < \alpha_{MC} < 14$  (Figure 7.5c and Table 7.1). These differences in scale between the modern and buried channels may be related to their stage of development. The buried ones present the maximum dimensions achieved before being filled by sediment, whereas the modern channel is still evolving as part of a major channel system set.

The simplest approach to assess relations between the axial and widespread channel systems is by comparing their average sizes and dimensional relations. The axial channels are larger, with average width and heights that are two to three times the size of channels in widespread systems. Nevertheless, all the buried channel systems can be explained by identical scaling relationships. Except for the modern channel, the average channel sizes can all be fitted along lines with slope values ( $\alpha$ ) of 12 or 13 (Fig. 7.5d). Such scale relationships can constitute an indicator of general channel evolution trends with time in the studied slope. As such, it is suggested that when slope channel systems become inactive their width is about 12 to 13 larger than the height. Furthermore, data from Channel C1 also suggests that linear scale relationships are valid for the size prediction of pre- and post-confluence channel segments in submarine slopes. The same is not considered to be valid for active

channels since these have not reached their largest dimensions or these modern conduits only constitute only a portion of larger channel complexes in development, as mentioned above.

Considering that the thickness of productive channel-fill sands is often in the order of 5 to 30 m, the accommodation potential on the distinct channel systems is proportional to their scale. The larger the features the higher the potential to accumulate multiple permeable intervals, but this is also accompanied with a variable probability of occurrence of low permeability layers that constitute vertical flow barriers (Mayall et al., 2006; Slatt and Weimer, 2001). If channel size scale relationships are similar, submarine slope dynamics and processes should be determining factors controlling the size to which channels can develop. As such, conditions focusing flows to limited slope regions are prone to generate larger channels. When submarine conditions favour sediment aggradation and flow scattering across the slope, as suggested to be the case for sub-units 3b and 3c (Chapter 6), more numerous, smaller channels will tend to develop. Consequently, the compartmentalisation degree of channel-bearing reservoir units must be complemented with an analysis of channel distribution. This has been shown to vary in the Cenozoic strata of the studied basin (Chapter 6). In general, the larger axial channels will tend to be geographically limited but may imply more heterogeneous fill, thus increasing the risk of vertical compartmentalisation within the main channel body. The lateral extent of the channel-fill sand bodies will dictate the degree of lateral compartmentalisation within the channels, thus connectivity within these larger conduits will be dependant of intra-channel processes. Contrastingly, the widespread distribution of the smaller non-axial channels in the basin, particularly in the upslope sections, leads to increased lateral compartmentalisation within reservoir units due

to the spacing between the individual bodies. Given the higher number of features identified, sub-units 3b and 3c are considered to have higher degrees of compartmentalisation due to the scatter of relatively small bodies in the three dimensions. Nevertheless, this can be mitigated by the observed incision and vertical stacking of channels (Figs. 6.2 and 6.7), leading to increase connectivity. This is more likely to take place in the high density areas which have been identified (Fig. 6.9).

### 7.2.3- Scale of fault-bounded compartments

The dimensions of fault-bounded compartments are controlled by the spacing between faults, their length, and interactions between different fault orientations. Faulting of the stratigraphic units in the Espírito Santo Basin is intrinsically related to halokinesis. In the studied successions, faults are more expressive in Unit 1 (Figs. 5.3 and 5.8) and are distinguished in two distinct families of crestal faults and synclinal faults (Alves et al 2009). The assessment of the scale relationships between the two fault families was based on the relation between fault spacing (S) and fault throw (T) as a function of a constant of proportionality  $\gamma$ , such that:

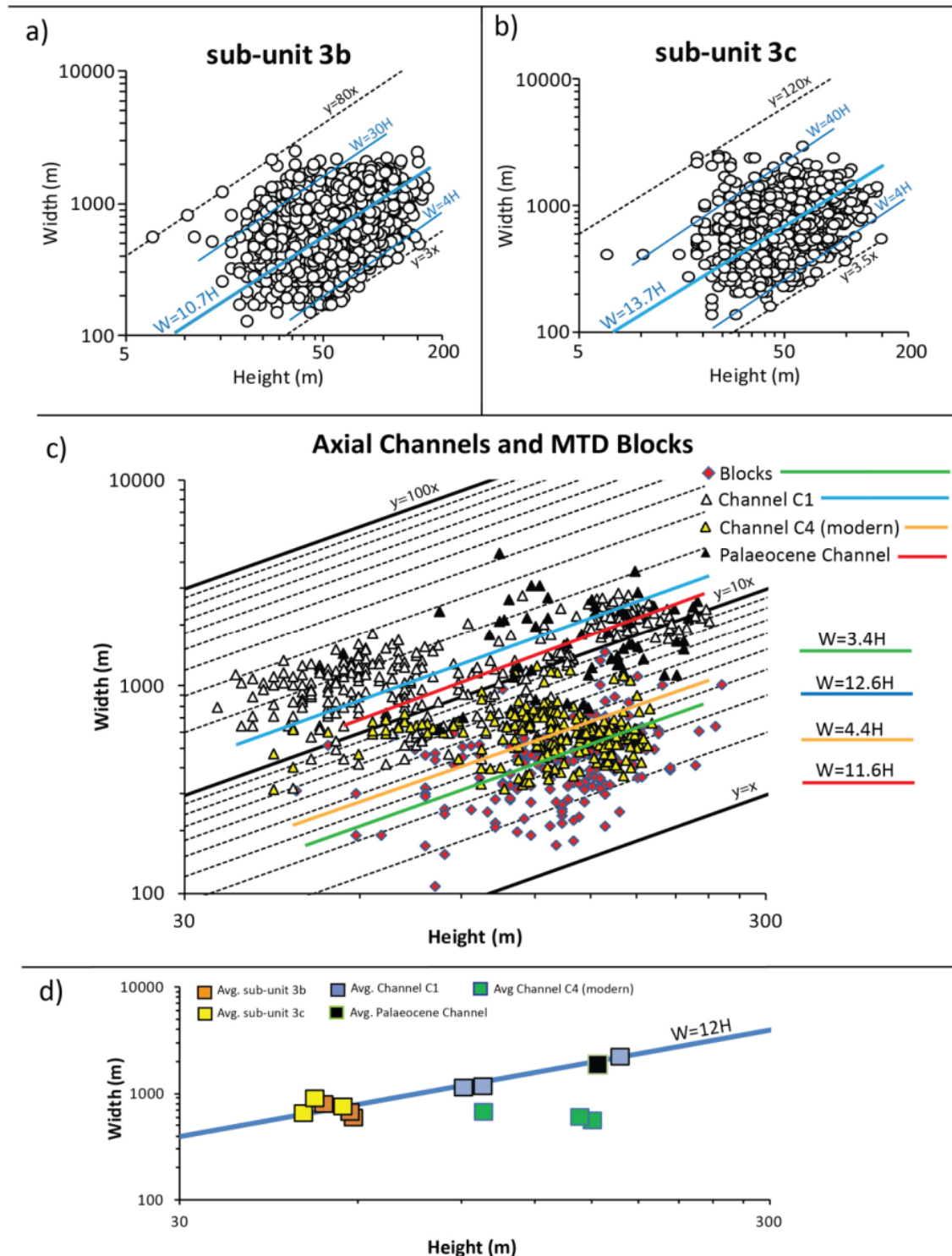
$$S = \gamma \cdot T \quad (\text{eq. 7.4})$$

Similarly, scale relationships between the fault length (L) and spacing (S) were also calculated as a function of  $\eta$ :

$$L = \eta \cdot S$$

The connectivity between individual fault-bounded compartments is dependent of the fault throw and permeability (Hooper, 1991; Knipe et al., 1998). The primary impact of





**Figure 7.5.** Plots of channel data. (a) and (b) show the width and height of the numerous channel sections measured in sub-units 3b and 3c. (c) Width and height of measured sections of the Palaeocene Channel, Channel C1 and the modern channel. Blocks in MTD-A1 are also represented for comparison with the dimensions of channel sections. Regression lines of each data series are colour-coded for clearer distinction. (d) Average width and height of the distinct channels systems. The buried systems show identical scale relationships where, on average, channel width is about 12 times the height.

the fault throw on connectivity resides on the offset of permeable strata on both sides of fault (Jolley et al., 2007). The larger throws will lead to increased offsets between individualised beds of permeable strata, which can compromise lateral connectivity, although it can also favour the contact between permeable intervals of different levels. Large fault throws can have a role in the flow potential if the displacement induces higher smearing of the fault gouge and increased permeability baffling (James, 1997; Jolley et al., 2007). On the Espírito Santo Basin, crestal faults have average throws of 122 m, about 1.5 times larger than synclinal ones with 83 m (Table 7.2). As the larger throws are related to crestal faults, permeable strata cut by them are prone to present higher offsets between adjacent compartments, favouring accumulations at stratigraphic levels further apart. On the opposite situation, the lower throw values of the synclinal faults also lead to lower vertical offsets between adjacent compartments, which can favour connectivity across faults and decrease the impact of compartmentalisation.

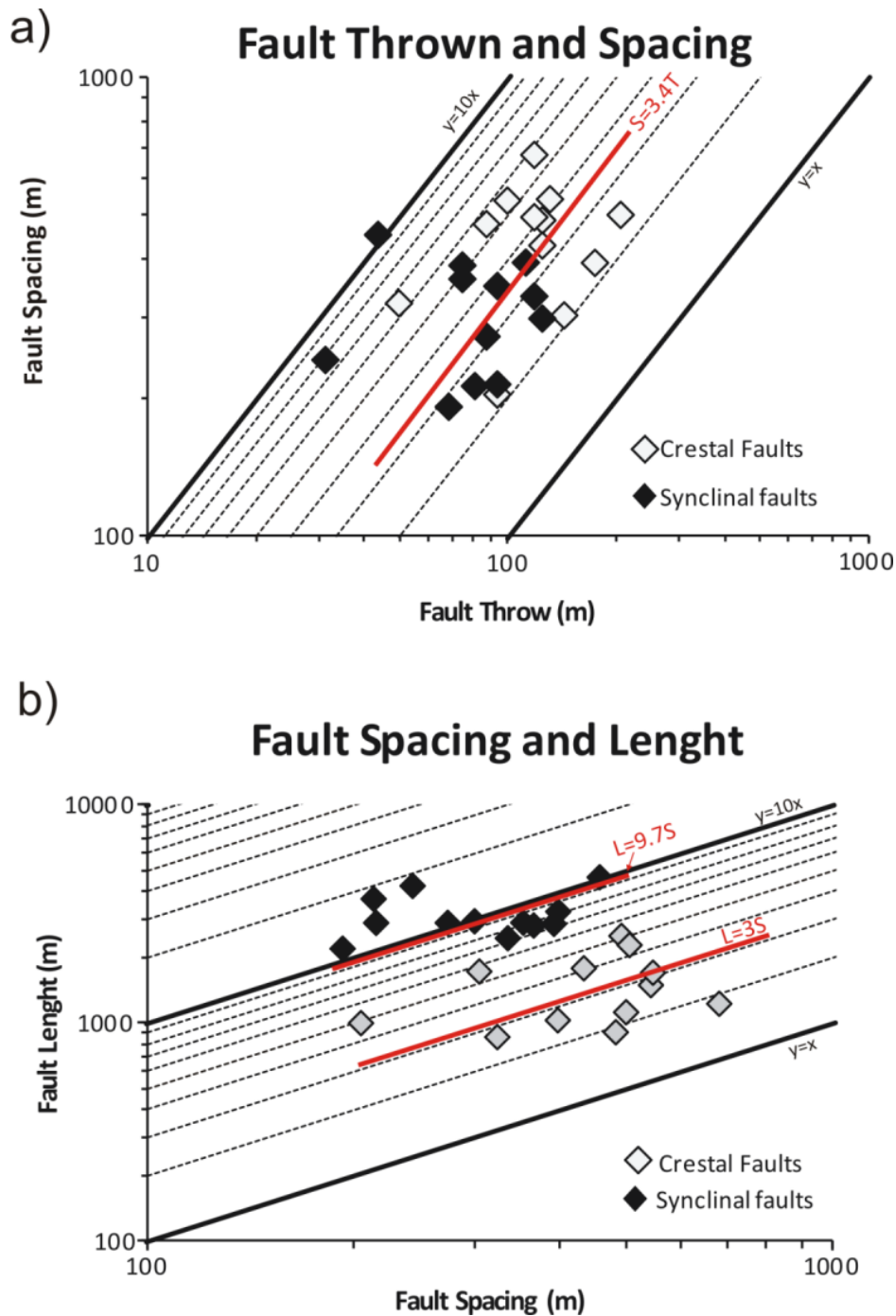
Throw values of the analysed faults are also related to their spacing, which will ultimately control the width of any fault bounded compartments (Fig. 7.6a). Throw-spacing relationships for both fault families can be explained by identical regression lines with slope values ( $\gamma$ ) of 3.4 for crestal faults and synclinal faults (Table 7.2). Nevertheless, the higher  $\gamma_{\text{MAX}}$  of the synclinal faults indicates that their spacing can be up to 10.5 times the throw, while the crestal faults only show a relationship of 6.5 (Fig. 7.6, Table 7.2.). Thus, as the synclinal faults have potentially higher spacing, they are prone to delimit wider fault-bounded compartments. The third control on size of this style of compartmentalisation is the length of the faults. Unlike the spacing, which shows similar scale relationships and size ranges for both fault families (Fig. 7.6a), the lengths of synclinal faults are on average twice

the ones of crestal faults (Table 7.2 and Fig. 7.6b). Consequently, the fault length-spacing scaling relationships between the two fault families are not identical to the ones for spacing and throw. While the length of synclinal faults is about 9.7 times their spacing, with values varying between  $7.3 < \eta_{\text{syncl}} < 17.5$ , the length of crestal faults is about 3 times their spacing. Furthermore, this does not exceed a maximum  $\eta$  of 5.5 (Table 7.2). As such synclinal faults are likely to delimit compartments three to four times larger than crestal faults. Furthermore, these scale relationships indicate that the largest compartments created by crestal faults may not reach the size of the smaller ones delimited by synclinal faults.

To summarise, the degree of structural compartmentalisation on this slope is higher on the vicinities of the diapirs and salt ridges due to the genesis of crestal faults and it tends to decrease towards the axial regions of salt-withdrawal basins where synclinal faults are present. This gains particular relevance as synclinal faults located towards the axial regions of the main salt-withdrawal basin bound the main Palaeocene channel units and compartmentalise reservoir-prone channel overbank strata (Alves et al., 2009).

Faults	Average (units in m)			$S=\gamma.T$			$L=\eta.W$		
	Length (L)	Throw (T)	Spacing (S)	$\gamma$	$\gamma_{Min}$	$\gamma_{Max}$	$\eta$	$\eta_{Min}$	$\eta_{Max}$
Crestal	1478.2	121.9	449.5	3.5	2.0	6.5	3.1	1.8	5.5
Synclinal	3161.9	83.2	310.7	3.4	2.3	10.5	9.6	7.3	17.5

**Table 7.2.** Table representing the average length, throw and spacing, and the constants  $\gamma$  and  $\eta$  that represent the scale relationships of the families of crestal and synclinal faults



**Figure 7.6.** (a) Plot with throw and spacing of the crestal and synclinal faults. Both families have identical scale relationships of these parameters. (b) Plot representing length and spacing of the two fault families. Synclinal faults are prone to delimit larger compartments when compared to crestal ones.

### 7.3. Can MTDs be reservoirs?

The general conception of MTDs on hydrocarbon plays is that they are low porosity and low permeability mud-dominated sealing units, inducing both vertical and lateral compartmentalisation between adjacent drainage units (Larue and Hovadik, 2006; Posamentier, 2004a; Posamentier, 2004b; Weimer, 1990). Nevertheless, mass-flow deposits show a wide range of compositional and architectural heterogeneities that directly influence their capacity to act as reservoirs (Dykstra et al., 2011; Meckel III, 2011; Weimer and Shipp, 2004). Such variability can be considered to create an internal compartmentalisation of the MTDs with distinct fluid flow and/or retention properties. The primary factor controlling this is the proportion of clastic material within the mass-failure. Various studies have shown that MTDs often include coarse-grained material as a main component or can have variable amounts of sand derived from either the original protolith at the source region or incorporated from eroded lithologies like turbidites (Dykstra et al., 2011; Haughton et al., 2003; Hogg, 2003; Meckel III, 2011; Meckel III et al., 2011; Taylor et al., 2003; Welbon et al., 2007). Shelf-derived MTDs are prone to include higher amounts of clastic material, particularly if the mass-failure is linked to periods of tectonic instability and erosion of the margin. In such cases, coarser-grained MTDs are expected in upper slope settings, although shelf-derived failures are also able to flow for long distances and deposit sand further into distal regions of the basin (Haughton et al., 2003). With exception of the lowermost MTD-A1, the MTDs in the Abrolhos Unit are interpreted to have a significant proportion of material sourced from further upslope and shelf regions (Chapter 4), and as such they can include coarser fractions being transported further into the basin. This hypothesis is

strengthened by the generalised high seismic amplitudes observed in Unit 2, either related to MTDs or turbiditic strata, which are commonly considered indicators of coarser lithologies (Hardage et al., 1998b; Hart, 2008). Furthermore, documented margin uplift of the Brazilian margin and erosion during the Eocene-Oligocene allied to volcanic activity in the same period resulted in a rapid input of high volumes of siliciclastic and volcanoclastic material into the basin (Fiduk et al., 2004; França et al., 2007; Mohriak, 2005), thus increasing the probability of coarser fractions being present in the MTDs. Contrasting with shelf derived MTDs, the ones generated in the distal domains are most likely to include sand in their composition only if related to failure of coarser fractions of channel-levee complexes or submarine fan lobes. As these constitute important reservoirs in deep-offshore domains, any related MTDs have the potential to accumulate hydrocarbons, particularly if resultant from the collapse of intra-channel sand accumulations (Labourdette, 2007; Meckel III et al., 2011). The main issue regarding MTDs as reservoirs resides in the connectivity between porous strata within. Considering that this is compromised as deformation in the MTD increases, less remobilised sections are considered to have the highest potential to constitute reservoirs, particularly if remnant blocks are present (Cossey and Jacobs, 1992; Gibbons et al., 2003; Stuart, 2003; Taylor et al., 2003; Welbon et al., 2007).

#### **7.4. Does channel compartmentalization change alongslope?**

##### **7.4.1. Channel distribution**

Submarine channels constitute important reservoirs in deepwater settings being characterised by large dimensional ranges, in addition to variable architectures and degrees of confinement. These characteristics of submarine channels systems have been

demonstrated to vary along slope, conditioning the sediment distribution patterns into the distal domains (Deptuck et al., 2007; Mayall et al., 2010; Posamentier, 2004b; Prather, 2003). One key parameter in channel reservoir studies and compartmentalisation assessment is the degree of channel amalgamation, strictly related to the connectivity between sand deposits (Labourdette, 2007; Slatt and Weimer, 2001). Channel amalgamation reflects the channel spatial distribution (vertical and horizontal), which is ultimately dependant of the accommodation space controlled by topography and sea-level (Ainsworth, 2010; Clark et al., 1996; Posamentier, 2004b). As these change during the history of the basin, the conditions of each evolutionary stage are reflected in the architecture of contemporaneous channel systems, resulting not only in a lateral but also vertical change of slope channel compartmentalisation styles.

The channel systems identified at the different stratigraphic levels in the Espírito Santo Basin constitute examples of such variability. As shown in Chapter 6, the spatial distribution of channels is a function of the relative number of features identified in each unit. Large-sized ones, as the modern channel and channel C1 (Figs. 6.5 and 6.6), tend to be the major gravity-flow reservoir element present at their stratigraphic level, with the same being observed for the Palaeogene canyon (Fig. 2.6). In terms of the large-scale reservoir units, these conduits act as a major stratigraphic compartment for sediment accumulation that is relatively localised and does not show significant lateral migration to other slope regions. Intra-channel compartmentalisation of reservoir strata will be dependant of the spatial dispersion of sand-fill deposits, but this will be contained within the major incision. The degree of lateral and vertical compartmentalisation is higher the larger the channels



are, as there is more accommodation space available for distinct lithologies to accumulate through time.

Contrastingly, stratigraphic intervals marked by smaller, linear channel features as in sub-unit 3b tend to develop numerous channel elements. These are found scattered through the lateral extent of the salt-confined basin (Fig. 6.9), thus leading to increased lateral compartmentalisation within the unit. Despite this lateral scatter, areas with high channel densities are observed (Fig. 6.9c). These indicate preferential points for channel (re-) incision, particularly when vertical stacking and less significant lateral migration takes place, thus increasing the vertical connectivity potential between compartments at different levels. Furthermore, channel complexes with numerous, small elements have less available space for sediment to accumulate. This potentially favours higher homogeneity, or amalgamation of channel deposits, decreasing the internal compartmentalisation of any permeable filling lithologies.

Regardless of the style or size, all channel systems analysed in the Espírito Santo Basin were shown to be topographically controlled by growing salt structures, with particular relevance for the creation of specific confluence points at high confinement areas (Chapter 6). The distribution patterns of channels show different responses upslope and downslope of the topographic constrain areas, which can be useful as indicators of the compartmentalisation potential in different slope sections. In upper slope domains channel density is higher and, despite the overall clustering, the models show an approximation to random distribution patterns (Chapter 6). The assessment of channel positions is therefore more uncertain, with a high probability for the occurrence of smaller channel compartments in the interfluvies of the major paths highlighted by high channel densities (Fig. 6.9), with the

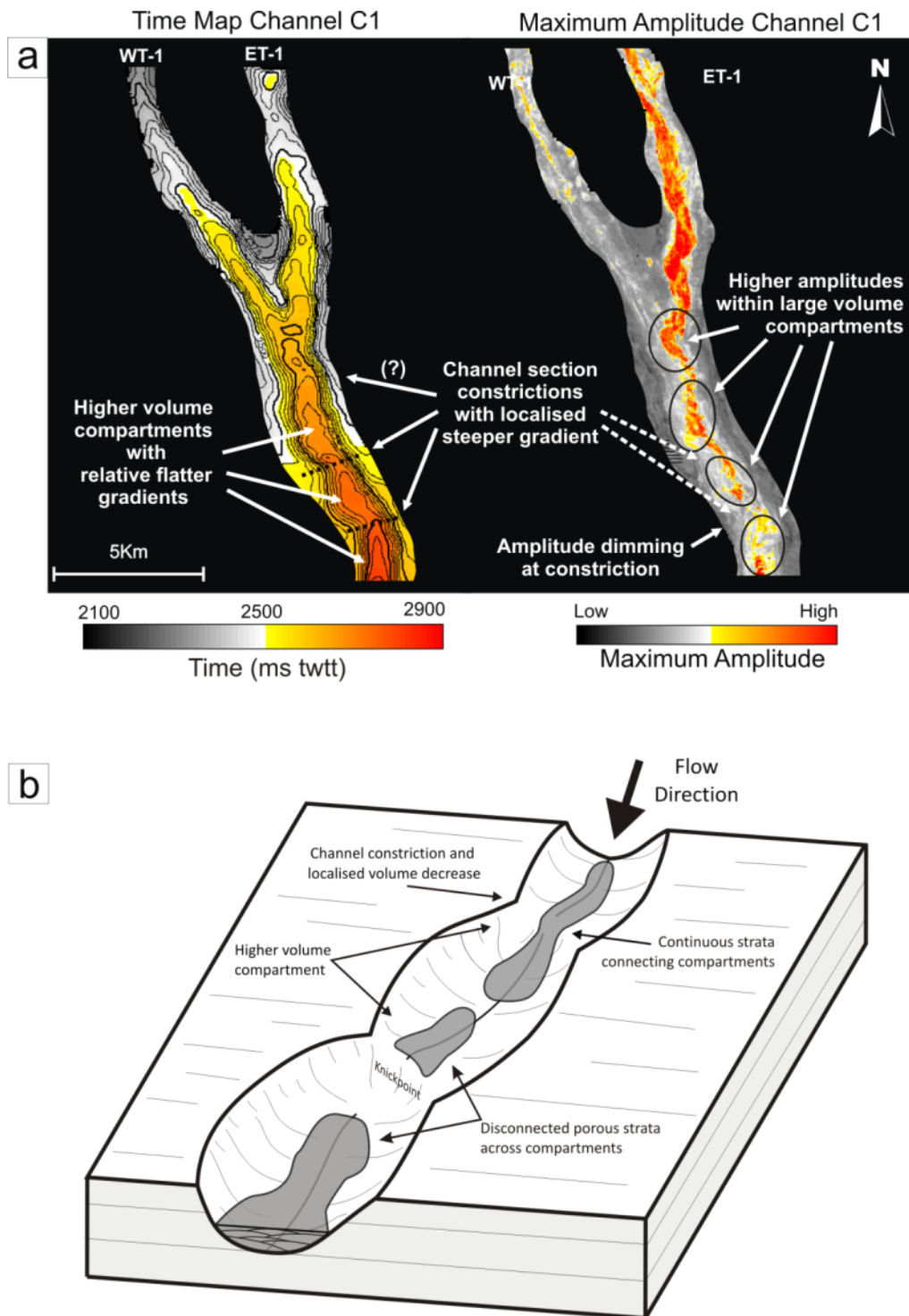
risk of limited lateral connection. As the channels evolve downslope, they tend to coalesce and widen, particularly when influenced by increased slope confinement. This also leads to increased channel clustering and spatial limitation of their distribution, not only within the high-confinement regions but also on less confined slope sections immediately downslope. This creates focused locations within the total width of the basin where laterally isolated channel complexes tend to develop. Consequently, the distribution of these reservoir-prone stratigraphic features and flow units becomes more predictable. As these channels may tend to stack vertically, the nature of sediment composition can be the main factor to induce vertical compartmentalisation. Nevertheless, recurrent cut phases can erode any low permeability strata and favour vertical connectivity (McKie et al., 2010).

#### **7.4.2. Changes in channel accommodation space**

Data from the channels studied in Chapter 6 highlight the presence of pronounced height variations, with these being coincident with localised decreases in channel width (Figs. 6.4, 6.5 and 6.6). Although such irregularities are observed along the whole channel, the studied examples in the Espírito Santo Basin (particular channel C1, Chapter 6) show the most pronounced thalweg irregularities towards the distal sections (Fig. 7.7). These irregularities are characterised by abrupt increases in channel profile gradient, and consequent formation of knickpoints (Heiniö and Davies, 2007; Howard et al., 1994; Mitchell, 2006). In addition, the localised decreases in width and height of the channel section are ultimately expressed as volumetric changes within the sediment conduit envelope, particularly when smaller, low volume sections are present. These reduced volume sections can result in morphological constrictions that, when coincident with the location of knickpoints, are able to influence the depositional or erosional character of

sediment flows. The presence of knickpoints induces the formation of localised steps with increased gradients. Hydraulic jumps that take place at these points induce localised sediment erosion due to flow acceleration, but also this can also induce the deposition of coarse material downdip as the gradient and current energy decrease (Komar, 1971; Mitchell, 2006). The along-channel volumetric variations can also contribute to such variations in flow energy and influence the locations of sediment accumulation or erosion. Thus, sections marked by lower volume are prone to constitute locations of flow acceleration and low or no deposition, especially if associated with knickpoints.

At the transition to larger volume sections, the resultant decrease in relative confinement leads to an energy decrease and favour the deposition of the coarser sediment fractions. An example of this can be observed in Figure 7.7. The time map showing the base of channel C1 shows such morphological variations of the channel section. These are characterised by flatter regions where channel widens, followed by steeper gradients at the narrowing points (Fig. 7.7a). Contrasting this with the maximum amplitude map, higher values are coincident with the wider channel sections, complemented by dimming at the narrower, steeper constrictions immediately down-stream (Fig. 7.7a). Such character illustrates heterogeneities in sediment accumulation along the channel and preferential deposition/preservation on lower gradient sections adjacent to knickpoints. This agrees with the concept that coarser sediment deposition is likely to occur upstream of knickpoints, with these marking localised erosion and downstream remobilisation (Heiniö and Davies, 2007). Furthermore, the scours created in the vicinities of knickpoints can also be filled by coarse grained material, from sand to conglomerate clasts, creating laterally limited intra-channel



**Figure 7.7.** (a) Time and maximum amplitude maps of Channel C1. The time map shows that several morphological constrictions along the channel path, being better evidenced at downslope locations. The amplitude map shows that these constrictions bound channel sections, or compartments, with higher amplitude values, interpreted to represent higher amounts of coarse-grained sediment. (b) Schematic representation of the effect of morphologic constrictions within channels on the formation of higher volume compartments, and on sediment distribution. Constrictions are associated with sharp knickpoints are prone to compromise connectivity between compartments.

compartments with increased permeability (Ardies et al., 2003; Brunt et al., 2007). Thus, uneven and/or discontinuous accumulations of porous strata can be found along the channels, with the large volume channel sections acting as preferential compartments for the accumulation of reservoir-prone lithologies. If the existing knickpoints' height exceeds the thickness of strata immediately downslope, the updip continuity is compromised and the sand bodies are isolated. In case the sediment thickness overcomes the knickpoints' offset, the porous strata is prone to be connected, although baffling may occur if finer material is present at the constriction (Fig. 7.8b).

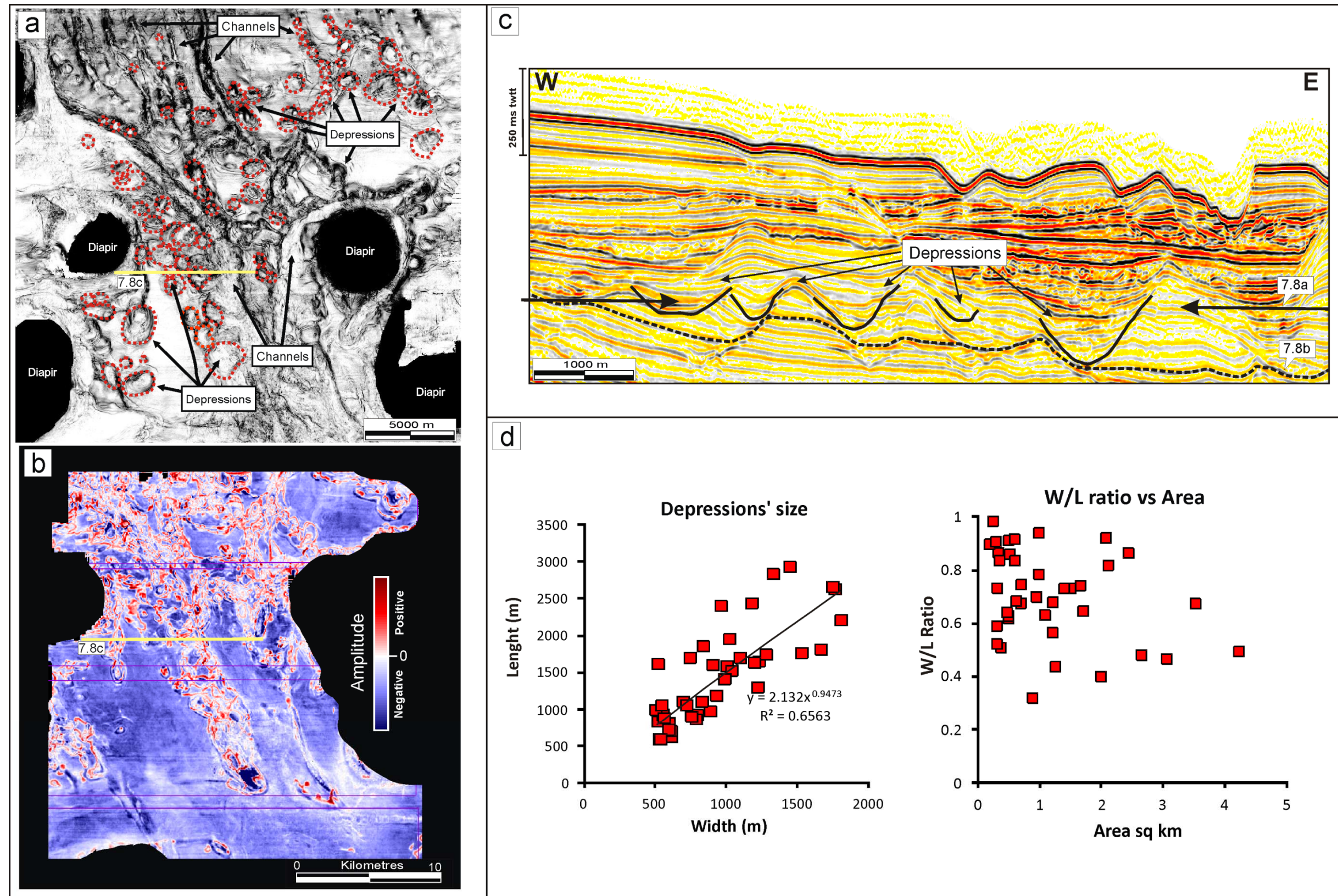
#### **7.4.3. Morphological depressions as isolated compartments**

Several circular to elongated depressions associated with the channel systems have been identified in sub-unit 3b (Fig. 7.8). Such Submarine channel-related morphological depressions have been increasingly observed in different continental margins, being described as resultant from flow erosion, channel-fill or fluid escape processes (Fildani et al., 2006; Heiniö and Davies, 2009; Jobe et al., 2011; Maier et al., 2011). In sub-unit 3b various alignments of pronounced morphological depressions have been identified, being preferentially located on the upper slope sections of the salt-withdrawal basin (Fig. 7.8a and b). Several of these depression alignments are genetically related to filling submarine channels (Heiniö and Davies, 2009). Nevertheless, not all the depression trails are associated with channel features, as suggested by isolated ones showing no evidence of such structures underlying them, nor any clear connecting path to adjacent depressions. The genetic contrasts between the types of depressions will not be discussed here, but these are shown to influence the dimension of such features. Depressions not underlain by channels are

generally larger than channel-confined ones, with maximum width, length and height of the previous reaching up to 2200 m, 4800 m and 170 m, respectively (Fig. 7.8c and d). These are double of the maximum values of 850 m, 1062 m and 64 m for the respective parameters for channel-related depressions obtained by Heiniö and Davies (2009). The height of the depressions ranges between 30 and 170 m, and width between 500 and 2200 m (Figs. 7.2). These values are comparable to various channel features analysed in the basin, with the majority of the depression-related data being coincident with the sizes observed for sections of the larger axial channels and also MTD blocks. The main contrast between these depressions and the submarine channels is the limited length of the previous (Fig. 7.8a). While channels tend to be continuous for over tenths of kilometres, crossing the whole survey, the depressions have lengths comprehended between 500 and 3000 m, with the majority being below 1500 m (Fig. 7.8 d).

The limited length greatly increases the compartmentalisation potential associated with the depressions. In essence, each morphological depression acts as an isolated laterally closed compartment (*sensu* Larue and Hovadik, 2006) within the stratigraphic successions in which they are found. The larger the depressions are, the higher the volume of sediment trapped within. A major issue in reservoir units where such isolated features are present is the heterogeneity of sediment fill and connectivity among them. Like in channels, larger depressions have higher probabilities of having a heterogeneous channel fill with alternations of coarse and fine lithologies. On amplitude maps, these depressions evidence a concentric pattern of alternating high and low values (Fig. 7.8b), similar to the amplitude variations identified in point bars created by sinuous submarine channels (Abreu et al., 2003; Dykstra and Kneller, 2009). These amplitude variations reflect lateral lithological





**Figure 7.8.** Circular to elongated depressions in sub-unit 3b. (a) Coherence slice with several depressions evidenced by red dashed lines. Depressions upslope are smaller and aligned with channels. Depressions at mid-slope position are larger and have higher spacing. (b) amplitude map highlighting ring-shaped amplitude patterns associated with the depression. (c) Seismic profile representing the Neogene units in the study area. Depressions cannot be easily distinguished from channels on vertical sections. (d) Plots representing dimensional data from the morphological depressions.

contrasts within the sinuous channel complexes and often delimit stratigraphic compartments. Likewise, the amplitude patterns are likely to represent alternating types of sedimentary fill in a bowl-shaped depocentre with limited connection to any surrounding areas. The connectivity between these features is likely to depend on their spatial density. As such, the upslope regions can have better connection between these enclosed compartments as, despite the general smaller size, they are numerous and in close contact with each other. In addition, the upslope area is also where the depressions have a closer relation with channels therefore the lateral isolation between the compartments may be decreased. The opposite is observed on distal regions where spacing between depressions increases as they grow larger in size. In these sections the depressions may form completely isolated compartments with very poor connection to any adjacent features.

### **7.5. Primary and secondary controls of halokinesis on reservoir compartmentalisation**

The growth of salt structures in the Espírito Santo Basin was shown to play important controls on the deformation of the stratigraphic successions analysed in this thesis, as well as on the architecture of the depositional systems. The combined interaction between these factors ultimately dictates the size and geometry of compartments within the reservoir units. Proof of diachronous salt growth throughout the Cenozoic is presented by several features on the studied succession. Palaeocene strata in Unit 1 evidences differential salt growth with the presence of rising diapirs and deeply buried salt ridges (Fig. 2.6). Crestal faults developed on top of these ridges, resultant from salt movement, induced a strong structural compartmentalisation in Unit 1. Furthermore, halokinetic structures developed in



the early Cenozoic where shown to influence the depositional features in Unit 2, namely by controlling the genesis and location of blocks in MTD-A1 (Chapter 5), controlling the depositional paths of turbidite fans and inducing an increasing confinement of the salt-withdrawal basin (Chapter 4, see also Unit 2 MTD dimensions illustrated in Fig. 7.2). Furthermore, the rise of salt diapirs is also shown to influence the preservation of turbidites from erosive MTDs (Fig. 4.10c). Evidence of recent salt growth is shown by the channel distribution patterns in Unit 3, with diapir-created topography forcing the main channel paths into a main confluence point coincident with the area with the higher diapir confinement (Chapter 6). Modern growth of the salt structures is shown by the diapir relief on the sea-floor (Fig. 2.5).

Taking these factors into consideration, halokinesis can be considered to exert two distinct controls on reservoir strata within the unit's mega-compartments, here denominated as 1) primary and 2) secondary, depending on the temporal relation between salt growth and the genetic affinity of the compartments.

1) The **primary control** regards the structural deformation of reservoir units resultant from salt movement. This is essentially represented by the development of faults and folds surrounding growing salt structures, which can compromise the lateral connectivity of permeable strata within reservoir units. Faults are the most relevant feature to be considered on the structural compartmentalisation induced by salt growth, as if impermeable ones are present the reservoir units tend to be highly compartmentalised. Crestal faults developing above salt structures are prone to create numerous closed compartments (e.g. Fig. 5.8). The shape and orientation of such compartments is predominantly defined by the control that the salt bodies, i.e. ridges or diapirs, exert on the

geometry of the overlying faults. Radial faults present on the flanks of salt structures are also important compartmentalising features (see diapir D5 in Fig. 5.8, and also Stewart, 2006). Radial faults are likely to create open compartments, thus inducing a lower compartmentalisation of the diapir-flanking strata when compared to crestal ones. Nevertheless, compartmentalisation is higher if compartments bounded by radial faults are affected by concentric faults present around the diapir (e.g. North Sea, Stewart, 2006), with consequent decrease in compartment size and connectivity.

The geometry, extent and connectivity of impermeable salt bodies control the large-scale compartmentalisation of offshore basins. The growth of salt ridges can create laterally isolated sub-basins that constitute mega-compartments with limited lateral connectivity. Isolation is more effective when large, continuous ridges presenting limited points of stratigraphic connection between adjacent basins are present. In contrast, regions marked by diapir alignments (e.g. the Diapir Ridge 1 analysed in this thesis) are prone to have numerous connectivity points between adjacent withdrawal basins. Although not analysed in this study, salt canopies are important features in the distal Espírito Santo Basin (Fiduk et al., 2004), as well in other salt basins (e.g. Gulf of Mexico, Hudec and Jackson, 2006 or West Africa, Cramez and Jackson, 2000). These induce important vertical compartmentalisation of reservoir units, particularly when isolating different generations of withdrawal mini-basins (Pilcher et al., 2011).

2) The **secondary** controls regard the influence that topography resultant from salt deformation has on the extent and connectivity of permeable units.

Topography resultant from salt growth creates conduits that variably confine the turbiditic flows (Chapters 4 and 6, see also Clark and Cartwright, 2011; Mayall et al., 2006),

thus influencing the accommodation space created on the slope (e.g. Prather, 2003). This, alongside the amount of sediment supplied to the basin, will control the degree of vertical and lateral amalgamation of the reservoir-prone strata (Ainsworth, 2011). In such cases, the distribution and amalgamation of permeable strata is dependant of the amount and extent of the topographic confinement. When higher confinements are imposed, the sediment deposition is constrained in narrower areas with low accommodation space, forcing flows to coalesce (see for example the confluences in Chapter 6). Such increase in confinement is able to induce the amalgamation of the sedimentary deposits, which can allow a better connectivity between distinct sedimentary bodies and compensate for limited lateral extents, with the high amalgamation areas being often coincident with the areas of topographic constrain. Decreases in flow energy past the constriction points can lead to lateral spreading of the flows, particularly in turbidite fans (see Fig. 4.10), inducing lower sand body amalgamation and consequently decreased lateral connectivity of permeable strata. On a different perspective, topography created by salt growth also constitutes barriers to erosive flows. This is particularly relevant when the new topography is able to contain the downslope movement of destructive MTDs, allowing the preservation of continuous, reservoir-prone strata on the erosional shadow regions (e.g. Fig. 4.10c). The extension of the preserved compartments is therefore proportional to lateral extent of the barrier. When diapirs are present the preserved sections are likely to be smaller, but extensive salt ridges can be effective barriers for MTDs and impede their flow to adjacent salt-withdrawal basins downslope.

Strata failure is a common occurrence on the flanks and crests of salt structures (Chapter 5) and also controls the compartmentalisation of surrounding reservoir units. Such

consideration is particularly valid when the genesis of MTDs, and any related remnant/rafted strata, is genetically linked to halokinesis (see Chapter 5). Also, in case the MTDs derived from the crests have low permeability there may be a decrease in the spatial connectivity of permeable strata present at the periphery of salt structures.

On a more dynamic perspective, these secondary controls must be taken into account as a response to salt growth. As this takes place, gravity flows must re-adjust to the new slope morphology, thus changing their flow positions and influencing the depositional architecture of the sedimentary structures (Clark and Cartwright, 2011). This ultimately influences the degree of compartmentalisation of potential reservoir units.

In essence, the influence of halokinesis on the compartmentalisation of reservoir strata is based on the alternation or synchronicity of the primary and secondary controls established here. Salt growth induces the deformation of pre-existing strata and genesis of predominantly structural compartments, with coeval sedimentary responses. On quiescent periods the sedimentary systems re-arrange and adapt to the new topographic conditions, only to be subjected to deformation resultant from younger growth phases. Ultimately, this leads to a high probability of mixed compartmentalisation styles to be present in reservoir strata flanking or overlying salt structures.

### **7.6. Limitations of this research**

The work produced for this thesis benefited from the high quality of the 3D seismic data which, allied to a very low number of artefacts, allowed a very good visualisation and interpretation of the facies and structures present in the studied stratigraphic intervals. The major limitations reside on the geographical coverage and the

minimum scales possible to be obtained from the 3D seismic dataset. Despite the fair geographical data coverage, the assessment of the true extent of geological features (channel systems, MTDs or halokinetic structures) is compromised, implying that the quantitative studies undertaken may be unable to represent the geological reality in its fullness. The other major constrain in this research is the minimum resolution available from the 3D seismic data. Although the lateral resolution of the data is about 12.5 metres, this can be considered sufficient for the general assessment of the lateral extent of the stratigraphic/structural features or compartments at the scales required for deep-marine exploration. The major limitation resides on the vertical scale of the analysed features. The seismic resolution was about 10 metres at the shallower units to about 19 metres in the deeper stratigraphic levels. Although this is still sufficient to highlight features at the limit of seismic resolution on attribute maps, there are strong limitations on the visualisation of geological features at a sub-seismic scale that can have important small-scale controls on the compartmentalisation of reservoir strata. Such is expected to influence the correct assessment of intra-channel facies variations and/or the detailed assessment of small fault and fractures networks, and consequently their impact of the fluid flow paths in the reservoir strata.

This research would also have greatly benefited from the availability of well data, but such was not the case. The information provided by wells would have allowed a more detailed characterisation of the composition and age of the stratigraphic units analysed, minimising the errors from the literature-based assumptions undertaken. The availability of well data would also have allowed a more detailed characterisation of the composition and thickness of reservoir-prone units, particularly at sub-seismic scales, especially when

complex and heterogeneous sediment sources (siliciclastic, volcanoclastic, carbonated) have been identified to supply this basin. Furthermore, sonic velocity logs across the studied stratigraphic units would also have been important for the decrease in error of the quantification of the thickness and gradients of the stratigraphic features undertaken in this thesis.

### **7.7. Further Work**

The work developed in this thesis provided a number of answers to better understand reservoir compartmentalisation on offshore continental margins, but many other open questions remain. One key subject in this thesis focused on the impact of MTDs on the compartmentalisation of reservoir strata in deep-marine basins. Following the methods applied here, it would be valuable for the understanding of deepwater submarine slope systems, and reservoir units within, to assess the overall distribution and proportions of MTDs within relevant stratigraphic successions, and understand how these deposits contribute to the margin evolution during specific periods of time. These studies would benefit from a wide availability of high-quality datasets in order to understand the full extent of the stratigraphic architectures, which are often underestimated due to the limited size of the 3D seismic volumes. This would take advantage from a wider scale study applied to many other geographical locations, useful for the understanding of not only well studied margins but with relevant applications to new exploration frontiers where high quality 3D seismic datasets have been increasingly acquired.

This thesis also evidenced a close link between the internal architecture of MTDs and deformation imposed by salt structures. Although it is known that salt growth is a common

cause for slope failure, it is suggested that further detailed studies should be undertaken to better understand: 1) what are the main conditioning factors for the occurrence and location of slope failures related to halokinesis, and 2) how do these influence the internal architecture of heterogeneous MTDs. These studies would greatly benefit from additional information provided by well data. Despite the high costs involved in deep-offshore drilling, the increasing interest of the scientific and exploration communities on of submarine landslides does provide a window of opportunity to deepen our understanding on the impact of such deposits on the margin architecture and fluid flow within the stratigraphic sequences.

Submarine channel confluences were a subject analysed in this thesis which are still poorly studied in scientific literature. To surpass this knowledge gap, it is suggested that further work on the detailed morphological analysis of submarine channel junctions of different world margins should be undertaken. Given the growing number of high-quality 3D datasets available that provide increased resolution of deeper stratigraphic levels, it would be possible to study submarine confluences not only within shallower units but also older channel systems. These studies would have to be further complemented by the understanding of flow and sedimentary dynamics at channel confluences, to which the use of analogue and computer-based models can provide valuable aids. These may provide valuable insights in the sediment distribution patterns within submarine channels, with particular relevance for the continuity and connectivity of reservoir strata.

The morphological depressions that were briefly analysed in this thesis have been gaining relevance in submarine systems, as these can influence the depositional processes in

slope systems. Further work is still required to fully understand the dynamic processes that lead to their genesis, and what is the role of the basin morphology in their distribution.

The considerations above would be relevant for a multi-scale understanding of the compartmentalisation of flow units related to the interaction of the varied stratigraphic and structural processes, and resultant sedimentary architectures, which take place in deepwater settings.



# Chapter 8

## Conclusions

## 8. Conclusions

This chapter presents the conclusions of this thesis. The main integrated conclusions drawn from this study are firstly presented, followed by summarised conclusions of each results chapter.

### 8.1. Main conclusions

- The use of high-quality 3D seismic data provides detailed information on multi-scale types of compartmentalisation affecting reservoir units, being only limited by its resolution. Seismic attributes provide detailed information for the outline of stratigraphic and structural compartments.
- MTDs are important features on stratigraphic compartmentalisation. Their erosive potential and erosional relief are major controls on the extent of turbidite strata. The degree of heterogeneity of MTDs increases their reservoir potential, particularly if associated with permeable underlying structures.
- Channel distribution is a key factor on the compartmentalisation of reservoir units. Systems with large channels (canyons) tend to focus on the central regions of salt-withdrawal basins, whereas on sub-units with numerous smaller channels these are laterally scattered across the basin. The presence of channel confluence regions is a key control on the density and distribution patterns of channels, which is controlled by existing topographic confinement.

- Halokinesis induces a primary structural compartmentalisation by faulting and folding reservoir units, followed by a secondary stratigraphic compartmentalisation resultant from the re-adjustment of the stratigraphic architectures to new salt-related topography. MTDs with genetic links to salt structures can be considered an intermediate result from primary and secondary factors. Structural compartments tend to be smaller than stratigraphically controlled compartments.
- The establishment of scale relations is a useful method to analyse trends in the dimensional proportionality of the different compartmentalising features. In addition, it allows the comparison of relations between distinct compartmentalisation features or styles.

## 8.2. Conclusions from Chapter 4

- Mass wasting was an important process on the Brazilian Margin during the Mid-Eocene period that led to deposition of thick, up to 650 ms TWTT, MTD-rich stratigraphic units.
- Thick MTD intervals alternate with stratified turbidites. As stratified lithologies are relevant to the prediction of potential reservoirs within MTD-rich units (e.g. Beaubouef and Abreu, 2010), we show that potential reservoirs are thicker at the rims of diapirs when related to MTDs, but also cover significant areas of the basin at stratigraphic levels where mass-wasting is less apparent. Erosion by MTDs is shown to limit the lateral extent of the interpreted stratified strata.
- MTDs deposited during the Eocene-Oligocene contributed to margin construction and progradation in the Espírito Santo Basin. High sediment input into the basin, along with

the influence of salt growth and the emplacement of the Abrolhos volcanic plateau led to an unusual and complex slope growth. Thus, across-slope MTD thickness decreases from 70-80ms TWTT to 50-60ms TWTT towards the east. The average proportional thickness follows the same trend, from ~60% down to 38%. These decreasing values reflect an important sediment source northwest of the study area, and the limitation of MTD flow by the relief formed by salt diapirs in the East.

### 8.3. Conclusions from Chapter 5

- The detailed analysis of the earliest Mid-Eocene mass-wasting deposit (MTD-A1) in the Espírito Santo Basin revealed a marked internal heterogeneity.
- Thicker accumulations of MTD-A1 are located within the region underlain by developed salt ridges and diapirs, thinning towards the salt withdrawal basin, contrasting with the more common situation of stratal thinning above growing salt structures. Several remnant/rafted blocks were identified, evidenced by sub-parallel reflections bordered by chaotic patterns in the MTD.
- The origin of the blocks is linked to extensive arrays of halokinetic-related faults that deformed the pre-failure strata. The close relation between faults and blocks, complemented by MTD thickness maps, shows that the blocks occur close to their source area.
- Blocks show, on average, heights of 150 m and areas of about 0.4 Km<sup>2</sup>, with these values maintained downslope, along the main ridge. This indicates similar processes and remobilisation of MTD-A1 at all slope locations. Three different styles of block

deformation were identified. Failure and collapse of a pre-Eocene northwest-trending relief generated a complex flow of the failed strata which spread along-slope in directions perpendicular to the diapir ridge axis. Relative block distribution also provides a way of dating the triggering of salt structures at the time of failure.

- The heterogeneities in MTD strata shown in this chapter have implications in the assessment of the internal properties of failed strata and can constitute permeable fluid conduits, especially when in close relation with underlying faults. This is crucial when estimating seal capacity and/or fluid pathways in hydrocarbon exploration areas. The results shown for the Espírito Santo Basin in Brazil can be applied and compared to other continental margins with important mass-wasting.

#### **8.4. Conclusions from Chapter 6**

- The new method presented shows the maximum channel densities are coincident with the path of upper-slope tributaries. Post-confluence regions are characterized by lower channel densities.
- Submarine confluence areas in the slope are strongly influenced by increasing lateral confinement. All the channel systems observed have their confluence in the vicinities of the high confinement area.
- Goodness-of-fit (chi-square) and negative binomial are helpful to identify regions of channel clustering. Regions of higher channel scattering and density showing relatively higher degrees of clustering are identified in upper-slope regions. Channel clustering and channel density tends to decrease downslope.

- Sharp width variations, proportional to the combined width of joining tributaries, are observed at submarine confluences. Height changes are gradual if tributaries and post-confluence branches are in equal levels. Sharp height contrasts between tributary and main channel are observed at unequal confluences.
- A new classification for submarine confluences is proposed in this chapter. The identification of the main tributaries involved in the principal channel activity is based on a combined analysis of the confluence morphometry, geometry and seismic attributes. Symmetric confluences are classified as Left Symmetric or Right Symmetric, dependant of the position of the tributary with predominant activity (as observed upstream from the confluence). Asymmetric confluences are classified as Pure Asymmetric if the main flow is within the channel alignment defined by the main tributary and the post-confluence channel. Secondary Asymmetric confluences describe cases where the sedimentary flows take place along the secondary tributary, which is at an angle with the main channel alignment. On unequal junctions, the secondary tributary is present at higher elevations, being separated from the main conduit by a steep knickpoint.
- Understanding the dynamics of tributary channels networks is important to assess the main conduits where reservoir-prone lithologies accumulate. In addition, the clustering patterns of submarine channels constitute indicators of the degree of slope compartmentalisation, where higher cluster isolation leads to compromised lateral connectivity between channel belts.

# References

## References

- Abreu, V., Sullivan, M., Pirmez, C. and Mohrig, D., 2003. Lateral accretion packages (LAPs): an important reservoir element in deep water sinuous channels. *Marine and Petroleum Geology*, 20(6-8): 631-648.
- Adams, E.W., Morsilli, M., Schlager, W., Keim, L. and van Hoek, T., 2002. Quantifying the geometry and sediment fabric of linear slopes: examples from the Tertiary of Italy (Southern Alps and Gargano Promontory). *Sedimentary Geology*, 154(1-2): 11-30.
- Adams, E.W. and Schlager, W., 2000. Basic Types of Submarine Slope Curvature. *Journal of Sedimentary Research*, 70(4): 814-828.
- Adeogba, A.A., McHargue, T.R. and Graham, S.A., 2005. Transient fan architecture and depositional controls from near-surface 3-D seismic data, Niger Delta continental slope. *AAPG Bulletin*, 89(5): 627.
- Ainsworth, R.B., 2005. Sequence stratigraphic-based analysis of reservoir connectivity: influence of depositional architecture - a case study from a marginal marine depositional setting. *Petroleum Geoscience*, 11: 257-276.
- Ainsworth, R.B., 2006. Sequence stratigraphic-based analysis of reservoir connectivity: influence of sealing faults a case study from a marginal marine depositional setting. *Petroleum Geoscience*, 12: 127-141.
- Ainsworth, R.B., 2010. Prediction of stratigraphic compartmentalization in marginal marine reservoirs. In: S.J. Jolley, Q.J. Fisher, R.B. Ainsworth, P. Vrolijk and S. Delisle (Eds.), *Reservoir Compartmentalization*. Geological Society Special Publication, Vol 347, pp. 199-218.
- Al-Shaieb, Z., Puckette, J.O., Abdalla, A.A. and Ely, P.B., 1994a. Megacompartement complex in the Anadarko basin: a completely sealed overpressured phenomenon. In: P.J. Ortoleva (Ed.), *Basin Compartments and Seals*. AAPG Memoir 61, pp. 55-68.
- Al-Shaieb, Z., Puckette, J.O., Abdalla, A.A. and Ely, P.B., 1994b. Three levels of compartmentation within the overpressured interval of the Anadarko Basin. In: P.J. Ortoleva (Ed.), *Basin Compartments and Seals*. AAPG Memoir 61, pp. 69-83.
- Algar, S., Milton, C., Upshall, H., Roestenburg, J. and Crevello, P., 2011. Mass-transport deposits of the deepwater northwestern Borneo margin (Malaysia)- characterisation



- from seismic-reflection, borehole, and core data with implications for hydrocarbon exploration and exploitation. In: C. Shipp, P. Weimer and H. Posamentier (Eds.), Mass-transport deposits in deepwater settings. SEPM Special Publications 96, pp. 351-366.
- Allan, J.R., Sun, S.Q. and Trice, R., 2006a. The deliberate search for stratigraphic and subtle combination traps: where are we now? Geological Society, London, Special Publications, 254(1): 57-103.
- Allan, J.R., Sun, S.Q. and Trice, R. (Eds.), 2006b. The deliberate search for stratigraphic and subtle combination traps: where are we now? Geological Society Special Publications, 254. Geological Society London, 57-103 pp.
- Allen, P.A. and Allen, J.R., 2005. Basin analysis: principles and applications. Wiley-Blackwell, 550 pp.
- Alsop, G., Brown, J., Davison, I. and Gibling, M., 2000. The geometry of drag zones adjacent to salt diapirs. *Journal of the Geological Society*, 157(5): 1019.
- Alsop, G.I., 1996. Physical modelling of fold and fracture geometries associated with salt diapirism. In: G.I. Alsop, D. Blundell and I. Davison (Eds.), *Salt Tectonics*. vol 100, Geological Society, London, Special Publications, pp. 227-241.
- Alves, T.M., 2010. 3D Seismic examples of differential compaction in mass-transport deposits and their effect on post-failure strata. *Marine Geology*, 271(3-4): 212-224.
- Alves, T.M., Cartwright, J. and Davies, R.J., 2009. Faulting of salt-withdrawal basins during early halokinesis: Effects on the Paleogene Rio Doce Canyon system (Espírito Santo Basin, Brazil). *AAPG Bulletin*, 93(5): 617-652.
- Alves, T.M. and Cartwright, J.A., 2009. Volume balance of a submarine landslide in the Espírito Santo Basin, offshore Brazil: Quantifying seafloor erosion, sediment accumulation and depletion. *Earth and Planetary Science Letters*, 288(3-4): 572-580.
- Alves, T.M. and Lourenço, S.D.N., 2010. Geomorphologic features related to gravitational collapse: Submarine landsliding to lateral spreading on a Late Miocene-Quaternary slope (SE Crete, eastern Mediterranean). *Geomorphology*, 123(1-2): 13-33.
- Ardies, G.W., Dalrymple, R.W. and Zaitlin, B.A., 2003. Structural and intrinsic fluvial controls on the geomorphology of an integrated, incised-valley network in the Lower Cretaceous of southern Alberta, Canada, AAPG Annual Meeting, Salt Lake City, Utah, May 11-14.

- Armitage, D.A., Romans, B.W., Covault, J.A. and Graham, S.A., 2009. The Influence of Mass-Transport-Deposit Surface Topography on the Evolution of Turbidite Architecture: The Sierra Contreras, Tres Pasos Formation (Cretaceous), Southern Chile. *Journal of Sedimentary Research*, 79(5): 287-301.
- Arzola, R.G., Wynn, R.B., Lastras, G., Masson, D.G. and Weaver, P.P.E., 2008. Sedimentary features and processes in the Nazaré and Setúbal submarine canyons, west Iberian margin. *Marine Geology*, 250(1-2): 64-88.
- Ashabrunner, L.B., Tripsanas, E.K. and Shipp, R.C., 2010. Multi-direction flow in a Mass-Transport Deposit, Santos Basin, offshore Brazil. In: D.C. Mosher et al. (Eds.), *Submarine Mass Movements and Their Consequences*. Springer, pp. 247-255.
- Baas, J.H. and Best, J.L., 2002. Turbulence modulation in clay-rich sediment-laden flows and some implications for sediment deposition. *Journal of Sedimentary Research*, 72: 336-340.
- Baas, J.H., McCaffrey, W.D. and Knipe, R.J., 2005. The deep-water architecture knowledge base: Towards an objective comparison of deep-marine sedimentary systems. *Petroleum Geoscience*, 11(4): 309-320.
- Babonneau, N., Savoye, B., Cremer, M. and Bez, M. (Eds.), 2004. Multiple terraces within the deep incised Zaire Valley (ZaiAngo Project): Are they confined levees? *Confined Turbidite Systems*. Geological Society Special Publication, Vol 222, 91-114 pp.
- Babonneau, N., Savoye, B., Cremer, M. and Klein, B., 2002. Morphology and architecture of the present canyon and channel system of the Zaire deep-sea fan. *Marine and Petroleum Geology*, 19(4): 445-467.
- Bacciotti, F., D'Amore, K. and Seguin, J., 2011. 4D Seismic Integrated to Dynamic Modeling Revealed a Late Stage Development Opportunity in the West Brae Field, 73rd EAGE Conference and Exhibition, Vienna, Austria, 23-26 May, 2011.
- Bacon, M., Simm, R. and Redshaw, T., 2003. 3-D seismic interpretation. Cambridge Univ Pr, 209 pp.
- Barker, P.F., Buffler, R.T. and Gambôa, L.A., 1983. A seismic reflection study of the Rio Grande Rise. In: P.F. Barker, R.L. Carlson and D.A. Hohnson (Eds.), *Initial Reports of the Deep Sea Drilling Program*, Washington, D.C., Government Printing Office, pp. 953-976.

- Barnes, P.M., 1992. Mid-bathyal current scours and sediment drifts adjacent to the Hikurangi deep-sea turbidite channel, eastern New Zealand: Evidence from echo character mapping. *Marine Geology*, 106(3-4): 169-187.
- Bathurst, J.C., 1997. Environmental River Flow Hydraulics. In: C.R. Thorne, R.D. Hey and M.D. Newson (Eds.), *Applied Fluvial Geomorphology for River Engineering and Management*. John Wiley and Sons Ltd, pp. 69-93.
- Baudon, C. and Cartwright, J., 2008. The kinematics of reactivation of normal faults using high resolution throw mapping. *Journal of Structural Geology*, 30(8): 1072-1084.
- Beaubouef, R.T., 2004. Deep-water leveed-channel complexes of the Cerro Toro Formation, Upper Cretaceous, southern Chile. *AAPG Bulletin*, 88(11): 1471-1500.
- Beaubouef, R.T. and Abreu, V., 2010. MTCs of the Brazos-Trinity Slope System; Thoughts on the Sequence Stratigraphy of MTCs and Their Possible Roles in Shaping Hydrocarbon Traps. In: D.C. Mosher et al. (Eds.), *Submarine Mass Movements and Their Consequences*. Springer, pp. 475-490.
- Beaubouef, R.T. and Friedmann, J.S., 2000. High resolution seismic/sequence stratigraphic framework for the evolution of Pleistocene intra slope basins, western Gulf of Mexico: Depositional models and reservoir analogs, Deepwater Reservoirs of the World, GCSSEPM Foundation 20th Annual Research Conference, pp. 40-60.
- Bellaiche, G., 1993. Sedimentary mechanisms and underlying tectonic structures of the northwestern Mediterranean margin, as revealed by comprehensive bathymetric and seismic surveys. *Marine Geology*, 112(1-4): 89-108.
- Best, J.L., 1986. The morphology of river channel confluences. *Progress in Physical Geography*, 10(2): 157-174.
- Best, J.L., 1987. Flow dynamics at river channel confluences: implications for sediment transport and bed morphology. *Recent developments in fluvial sedimentology*, 39: 27-35.
- Best, J.L., 1988. Sediment transport and bed morphology at river channel confluences. *Sedimentology*, 35(3): 481-498.
- Best, J.L. and Roy, A.G., 1991. Mixing-layer distortion at the confluence of channels of different depth. *Nature*, 350: 411-413.
- Bhullar, A.G., Karlsen, D.A., Holm, K., Backer-Owe, K. and Le Tran, K., 1998. Petroleum geochemistry of the Frøy field and Rind discovery, Norwegian Continental Shelf.

- Implications for reservoir characterization, compartmentalization and basin scale hydrocarbon migration patterns in the region. *Organic Geochemistry*, 29(1-3): 735-768.
- Biassussi, A.S., D'Avila, R.S.F., Guirro, A.C. and Silva, J.G.R., 1998. Urucutuca-Urucutuca(?) Petroleum System, Espírito Santo Basin, Brazil, AAPG International Conference and Exhibition, Rio de Janeiro, Brazil.
- Biddle, K.T. and Wielchowsky, C.C., 1994. Hydrocarbon traps. In: L.B. Magoon and W.G. Dow (Eds.), *The petroleum system -from source to trap*. AAPG Memoir 60, pp. 219-235.
- Biron, P., Best, J.L. and Roy, A.G., 1996. Effects of Bed Discordance on Flow Dynamics at Open Channel Confluences. *Journal of Hydraulic Engineering*, 122(12): 676-682.
- Biron, P., Roy, A.È.G., Best, J.L. and Boyer, C.J., 1993. Bed morphology and sedimentology at the confluence of unequal depth channels. *Geomorphology*, 8(2-3): 115-129.
- Biron, P.M., Ramamurthy, A.S. and Han, S., 2004. Three-Dimensional Numerical Modeling of Mixing at River Confluences. *Journal of Hydraulic Engineering*, 130(3): 243-253.
- Booth, J.R., Dean, M.C., DuVernay, A.E. and Styzen, M.J., 2003. Paleo-bathymetric controls on the stratigraphic architecture and reservoir development of confined fans in the Auger Basin: central Gulf of Mexico slope. *Marine and Petroleum Geology*, 20(6-8): 563-586.
- Bouma, A.H., 2004. Key controls on the characteristics of turbidite systems. In: S.A. Lomas and P. Joseph (Eds.), *Confined Turbidite Systems*. Geological Society of London, Special Publication, 222, pp. 9-22.
- Bouma, A.H., Kuenen, P. and Shepard, F.P., 1962. *Sedimentology of some flysch deposits: a graphic approach to facies interpretation*, 168. Elsevier Amsterdam.
- Boyd, R. et al., 2010. Southeast Australia: A Cenozoic Continental Margin Dominated by Mass Transport. In: D.C. Mosher et al. (Eds.), *Submarine Mass Movements and Their Consequences*. Springer Netherlands, pp. 491-502.
- Bradbrook, K.F., Lane, S.N., Richards, K.S., Biron, P.M. and Roy, A.G., 2001. Role of Bed Discordance at Asymmetrical River Confluences. *Journal of Hydraulic Engineering*, 127(5): 351-368.
- Bradley, J.S. and Powley, D.E., 1994. Pressure compartments in sedimentary basins: a review. In: P.J. Ortoleva (Ed.), *Basin Compartments and Seals*. Am. Assoc. of Petrol. Geologists Memoir, pp. 3–26.

- Brown, A.R., 2004. Interpretation of Three-Dimensional Seismic Data, sixth ed. AAPG Memoir, 42. American Association of Petroleum Geologists, Tulsa.
- Bruhn, C.H.L. and Walker, R.G., 1997. Internal architecture and sedimentary evolution of coarse-grained, turbidite channel-levee complexes, early eocene Regência canyon, Espírito Santo Basin, Brazil. *Sedimentology*, 44(1): 17-46.
- Brun, J.-P. and Fort, X., 2011. Salt tectonics at passive margins: Geology versus models. *Marine and Petroleum Geology*, 28(6): 1123-1145.
- Brun, J.P. and Fort, X., 2004. Compressional salt tectonics (Angolan margin). *Tectonophysics*, 382(3-4): 129-150.
- Brunt, R.L. and McCaffrey, W.D., 2007. Heterogeneity of fill within an incised channel: The Oligocene Grès du Champsaur, SE France. *Marine and Petroleum Geology*, 24(6-9): 529-539.
- Bull, S., Cartwright, J. and Huuse, M., 2009. A review of kinematic indicators from mass-transport complexes using 3D seismic data. *Marine and Petroleum Geology*, 26(7): 1132-1151.
- Bünz, S., Mienert, J., Bryn, P. and Berg, K., 2005. Fluid flow impact on slope failure from 3D seismic data: a case study in the Storegga Slide. *Basin Research*, 17(1): 109-122.
- Butler, R.W.H. and McCaffrey, W.D., 2010. Structural evolution and sediment entrainment in mass-transport complexes: outcrop studies from Italy. *Journal of the Geological Society*, 167(3): 617-631.
- Caine, J.S., Evans, J.P. and Forster, C.B., 1996. Fault zone architecture and permeability structure. *Geology*, 24(11): 1025.
- Callot, P., Odonne, F. and Sempere, T., 2008. Liquefaction and soft-sediment deformation in a limestone megabreccia: The Ayabacas giant collapse, Cretaceous, southern Peru. *Sedimentary Geology*, 212(1-4): 49-69.
- Campbell, D.C. and Mosher, D.C., 2010. Middle to Late Miocene slope failure and the generation of a regional unconformity beneath the Western Scotian Slope, eastern Canada. In: D.C. Mosher et al. (Eds.), *Submarine Mass Movements and Their Consequences. Advances in Natural and Technological Hazards Research*, Vol 28. Springer.

- Campbell, D.C., Shimeld, J.W., Mosher, D.C. and Piper, D.J.W., 2004. Relationships between sediment mass-failure modes and magnitudes in the evolution of the Scotian Slope, offshore Nova Scotia, Offshore Technology Conference, Houston, Texas.
- Canals, M., Casamor, J.L., Urgeles, R., Lastras, G. and Calafat, A.M., 2000. The Ebro Continental Margin, Western Mediterranean Sea: Interplay Between Canyon-Channel Systems and Mass Wasting Processes, Deepwater Reservoirs of the World, GCSSEPM Foundation 20th Annual Research Conference, pp. 152-174.
- Canals, M. et al., 2004. Slope failure dynamics and impacts from seafloor and shallow sub-seafloor geophysical data: case studies from the COSTA project. *Marine Geology*, 213(1-4): 9-72.
- Cartwright, J., Huuse, M. and Aplin, A., 2007. Seal bypass systems. *AAPG Bulletin*, 91(8): 1141-1166.
- Carvajal, C., Steel, R. and Petter, A., 2009. Sediment supply: The main driver of shelf-margin growth. *Earth-Science Reviews*, 96(4): 221-248.
- Chang, H.K., Kowsmann, R.O., Figueiredo, A.M.F. and Bender, A., 1992. Tectonics and stratigraphy of the East Brazil Rift system: an overview. *Tectonophysics*, 213(1-2): 97-138.
- Chapin, M. et al., 2002. Integrated seismic and subsurface characterization of Bonga Field, offshore Nigeria. *The Leading Edge*, 21(11): 1125.
- Chilingar, G.V., Buryakovsky, L.A., Eremenko, N.A. and Gorfunkel, M.V., 2005. *Geology and geochemistry of oil and gas*, 52. Elsevier Science, 370 pp.
- Christodoulou, G.C., 1993. Incipient Hydraulic Jump at Channel Junctions. *Journal of Hydraulic Engineering*, 119(3): 409-423.
- Chuparova, E. et al. (Eds.), 2010. Integration of time-lapse geochemistry with well logging and seismic to monitor dynamic reservoir fluid communication: Auger field case-study, deep water Gulf of Mexico. *Reservoir Compartmentalization*, 347. Geological Society Special Publication, Vol 347, 55-70 pp.
- Clark, I.R. and Cartwright, J.A., 2009. Interactions between submarine channel systems and deformation in deepwater fold belts: Examples from the Levant Basin, Eastern Mediterranean sea. *Marine and Petroleum Geology*, 26(8): 1465-1482.
- Clark, I.R. and Cartwright, J.A., 2011. Key controls on submarine channel development in structurally active settings. *Marine and Petroleum Geology*, 28(7): 1333-1349.

- Clark, J.D., Kenyon, N.H. and Pickering, K.T., 1992. Quantitative analysis of the geometry of submarine channels: Implications for the classification of submarine fans. *Geology*, 20(7): 633-636.
- Clark, J.D. and Pickering, K.T., 1996. Architectural elements and growth patterns of submarine channels; application to hydrocarbon exploration. *AAPG Bulletin*, 80(2): 194-221.
- Clark, M.S., Beckley, L.M., Crebs, T.J. and Singleton, M.T., 1996. Tectono-eustatic controls on reservoir compartmentalisation and quality -- an example from the Upper Miocene of the San Joaquin basin, California. *Marine and Petroleum Geology*, 13(5): 475-491.
- Cobbold, P.R., Meisling, K.E. and Mount, V.S., 2001. Reactivation of an obliquely rifted margin, Campos and Santos basins, southeastern Brazil. *AAPG Bulletin*, 85(11): 1925-1944.
- Cobbold, P.R. and Szatmari, P., 1991. Radial gravitational gliding on passive margins. *Tectonophysics*, 188(3-4): 249-289.
- Cochran, W.G., 1952. The  $\chi^2$  test of goodness of fit. *The Annals of Mathematical Statistics*, 23(3): 315-345.
- Coleman, J.M. and Prior, D.B., 1988. Mass Wasting on Continental Margins. *Annual Review of Earth and Planetary Sciences*, 16(1): 101-119.
- Cossey, S.P.J. and Jacobs, R.E., 1992. Oligocene Hackberry Formation of southwest Louisiana: sequence stratigraphy, sedimentology, and hydrocarbon potential. *AAPG Bulletin*, 76(5): 589-606.
- Covault, J.A. and Graham, S.A., 2010. Submarine fans at all sea-level stands: Tectono-morphologic and climatic controls on terrigenous sediment delivery to the deep sea. *Geology*, 38(10): 939-942.
- Cowie, P.A. and Scholz, C.H., 1992. Physical explanation for the displacement-length relationship of faults using a post-yield fracture mechanics model. *Journal of Structural Geology*, 14(10): 1133-1148.
- Cramez, C. and Jackson, M.P.A., 2000. Superposed deformation straddling the continental-oceanic transition in deep-water Angola. *Marine and Petroleum Geology*, 17(10): 1095-1109.

- Cronin, B.T. et al., 2005. Morphology, evolution and fill: Implications for sand and mud distribution in filling deep-water canyons and slope channel complexes. *Sedimentary Geology*, 179(1-2): 71-97.
- Cunha, L.B. et al., 2001. A multi-scale approach to improve reservoir characterization and forecasting: the Albacora Field deep-water offshore Brazil study. *Petroleum Geoscience*, 7: 17-23.
- Dalla Valle, G. and Gamberi, F., *in press*. Slope channel formation, evolution and backfilling in a wide shelf, passive continental margin (Northeastern Sardinia slope, Central Tyrrhenian Sea). *Marine Geology*, In Press, Corrected Proof.
- Davis, J.C., 2002. *Statistics and Data Analysis in Geology*, 3rd Edition. Wiley, New York.
- Davison, I., 1999. Tectonics and hydrocarbon distribution along the Brazilian South Atlantic margin. In: N.R. Cameron, R.H. Bate and V.S. Clure (Eds.), *The oil and gas habitats of the South Atlantic*. Geological Society London Special Publications 153, pp. 133-151.
- Davison, I., 2004. Bathymetric control on Paleocene gravity flows around salt domes in the Central Graben, North Sea. In: P.J. Post et al. (Eds.), *Salt-sediment interactions and hydrocarbon prospectivity: Concepts, applications, and case studies for the 21st century*. GCSSEPM 24th Annual Research Conference, pp. 1031-144.
- Davison, I., 2007. Geology and tectonics of the South Atlantic Brazilian salt basins. In: A.C. Ries, R.W.H. Butler and R.H. Graham (Eds.), *Deformation of the Continental Crust: The Legacy of Mike Coward*. Geological Society London, Special Publications 272, pp. 345-359.
- Davison, I., Alsop, G.I., Evans, N.G. and Safaricz, M., 2000a. Overburden deformation patterns and mechanisms of salt diapir penetration in the Central Graben, North Sea. *Marine and Petroleum Geology*, 17(5): 601-618.
- Davison, I. et al., 2000b. Geometry and late-stage structural evolution of Central Graben salt diapirs, North Sea. *Marine and Petroleum Geology*, 17(4): 499-522.
- Davison, I., Alsop, I. and Blundell, D., 1996. Salt tectonics: some aspects of deformation mechanics. Alsop, G. I., Blundell, D. J. & Davison, I. (eds), 1996, *Salt Tectonics*, Geological Society, London, Special Publications 1996, 100: 1-10.
- De Blasio, F.V., Engvik, L.E. and Elverhøi, A., 2006. Sliding of outrunner blocks from submarine landslides. *Geophysical Research Letters*, 33(L06614).



- De Serres, B., Roy, A.G., Biron, P.M. and Best, J.L., 1999. Three-dimensional structure of flow at a confluence of river channels with discordant beds. *Geomorphology*, 26(4): 313-335.
- de Souza, R.S., de Ros, L.F. and Morad, S., 1995. Dolomite diagenesis and porosity preservation in lithic reservoirs; Carmopolis Member, Sergipe-Alagoas Basin, northeastern Brazil. *AAPG Bulletin*, 79(5): 725-748.
- Demercian, S., Szatmari, P. and Cobbold, P.R., 1993. Style and pattern of salt diapirs due to thin-skinned gravitational gliding, Campos and Santos basins, offshore Brazil. *Tectonophysics*, 228(3-4): 393-433.
- Demyttenaere, R., Tromp, J.P., Ibrahim, A. and Allman-Ward, P., 2000. Brunei Deep Water Exploration: From Sea Floor Images and Shallow Seismic Analogue to Depositional Models in a Slope Turbidite Setting. In: P. Weimer et al. (Eds.), *Deep-Water Reservoirs of the World*, December 3-6, Houston Texas.
- Deptuck, M.E., Mosher, D.C., Campbell, D.C., Hughes-Clarke, J.E. and Noseworthy, D., 2007a. Alongslope variations in mass failures and relationships to major Plio-Pleistocene morphological elements, SW Labrador Sea. In: V. Lykousis, D. Sakellariou and J. Locat (Eds.), *Submarine Mass Movements and Their Consequences*. Springer, pp. 37-45.
- Deptuck, M.E., Steffens, G.S., Barton, M. and Pirmez, C., 2003. Architecture and evolution of upper fan channel-belts on the Niger Delta slope and in the Arabian Sea. *Marine and Petroleum Geology*, 20(6-8): 649-676.
- Deptuck, M.E., Sylvester, Z., Pirmez, C. and O'Byrne, C., 2007b. Migration-aggradation history and 3-D seismic geomorphology of submarine channels in the Pleistocene Benin-major Canyon, western Niger Delta slope. *Marine and Petroleum Geology*, 24(6-9): 406-433.
- Dias, J.L., 2005. Tectonica, estratigrafia e sedimentacao no Andar Aptiano da margem leste brasileira. *Boletim de Geociencias da Petrobras*, 13(1): 7-25.
- Dooley, T.P., Jackson, M.P.A. and Hudec, M.R., 2009. Inflation and deflation of deeply buried salt stocks during lateral shortening. *Journal of Structural Geology*, 31(6): 582-600.
- Dunlap, D.B., Wood, L.J., Weisenberger, C. and Jabour, H., 2010. Seismic geomorphology of offshore Morocco's east margin, Safi Haute Mer area. *AAPG Bulletin*, 94(5): 615-642.
- Duval, B., Cramez, C. and Jackson, M.P.A., 1992. Raft tectonics in the Kwanza Basin, Angola. *Marine and Petroleum Geology*, 9(4): 389-404.

- Dykstra, M. et al., 2011. Mass-transport deposits: combining outcrop studies and seismic forward modeling to understand lithofacies distributions, deformation, and their seismic stratigraphic expression. In: C. Shipp, P. Weimer and H. Posamentier (Eds.), Mass-transport deposits in deepwater settings. SEPM Special Publication 96, pp. 293-310.
- Dykstra, M. and Kneller, B., 2009. Lateral accretion in a deep-marine channel complex: implications for channellized flow processes in turbidity currents. *Sedimentology*, 56(5): 1411-1432.
- Ercilla, G., Alonso, B. and Baraza, J., 2000. High resolution morpho-sedimentary characteristics of the distal Orinoco Turbidite System, Deepwater Reservoirs of the World, GCSSEPM Foundation 20th Annual Research Conference, pp. 374-388.
- Eschard, R., 2001. Geological factors controlling sediment transport from platform to deep basin: a review. *Marine and Petroleum Geology*, 18(4): 487-490.
- Eschard, R., Albouy, E., Gaumet, F. and Ayub, A., 2004. Comparing the depositional architecture of basin floor fans and slope fans in the Pab Sandstone, Maastrichtian, Pakistan. In: S.A. Lomas and P. Joseph (Eds.), *Confined Turbidite Systems*. Geological Society Special Publication, Vol 222, pp. 159-185.
- Fainstein, R. and Summerhayes, C.P., 1982. Structure and origin of marginal banks off Eastern Brazil. *Marine Geology*, 46(3-4): 199-215.
- Ferry, J.N., Mulder, T., Parize, O. and Raillard, S., 2005. Concept of equilibrium profile in deep-water turbidite system: effects of local physiographic changes on the nature of sedimentary process and the geometries of deposits. In: D.M. Hodgson and S.S. Flint (Eds.), *Submarine Slope System*. Geological Society of London, Special Publications, 244, pp. 181-193.
- Fetter, M., De Ros, L.F. and Bruhn, C.H.L., 2009. Petrographic and seismic evidence for the depositional setting of giant turbidite reservoirs and the paleogeographic evolution of Campos Basin, offshore Brazil. *Marine and Petroleum Geology*, 26(6): 824-853.
- Fiduk, J.C., Brush, E.R., Anderson, L.E., Gibbs, P.B. and Rowan, M.G., 2004. Salt deformation, magmatism, and hydrocarbon prospectivity in the Espirito Santo Basin, offshore Brazil. In: P.J. Post et al. (Eds.), *Salt-sediment interactions and hydrocarbon prospectivity: Concepts, applications, and case studies for the 21st century*. GCSSEPM 24th Annual Research Conference, pp. 370-392.

- Fildani, A., Normark, W.R., Kostic, S. and Parker, G., 2006. Channel formation by flow stripping: large-scale scour features along the Monterey East Channel and their relation to sediment waves. *Sedimentology*, 53(6): 1265-1287.
- Flint, S.S. and Hodgson, D.M., 2005a. Submarine slope systems: Processes and products. *Geological Society Special Publication*(244): 1-6.
- Flint, S.S. and Hodgson, D.M., 2005b. Submarine slope systems: processes and products. In: D.M. Hodgson and S.S. Flint (Eds.), *Submarine Slope Systems*. Geological Society of London, Special Publications, 244, pp. 1-6.
- Flint, S.S. et al., 2011. Depositional architecture and sequence stratigraphy of the Karoo basin floor to shelf edge succession, Laingsburg depocentre, South Africa. *Marine and Petroleum Geology*, 28(3): 658-674.
- Fort, X., Brun, J.-P. and Chauvel, F., 2004. Salt tectonics on the Angolan margin, synsedimentary deformation processes, pp. 1523-1544.
- França, R.L., Del Rey, A.C., Tagliari, C.V., Brandão, J.R. and Fontanelli, P.R., 2007. Bacia de Espírito Santo. *Boletim de Geociencias da Petrobras*, 15(2): 501-509.
- Frey-Martínez, J., Bertoni, C., Gérard, J. and Matías, H., 2011. Processes of submarine slope failure and fluid migration on the Ebro Continental Margin: implications for offshore exploration and development. In: C. Shipp, P. Weimer and H. Posamentier (Eds.), *Mass-transport deposits in deepwater settings*. SEPM Special Publication 96, pp. 181-198.
- Frey-Martinez, J., Cartwright, J. and Hall, B., 2005. 3D seismic interpretation of slump complexes: examples from the continental margin of Israel. *Basin Research*, 17(1): 83-108.
- Frey-Martínez, J., Cartwright, J. and James, D., 2006. Frontally confined versus frontally emergent submarine landslides: A 3D seismic characterisation. *Marine and Petroleum Geology*, 23(5): 585-604.
- Gafeira, J., Bulat, J. and Evans, D., 2007. The southern flank of the Storegga Slide: imaging and geomorphological analysis using 3D Seismic. In: V. Lykousis, D. Sakellariou and J. Locat (Eds.), *Submarine Mass Movements And Their Consequences*. Springer, pp. 57-66.
- Galloway, W.E., 1998. Siliciclastic slope and base-of-slope depositional systems; component facies, stratigraphic architecture and classification. *AAPG Bulletin*, 82(4): 569-595.

- Gamboa, D., Alves, T. and Cartwright, J., 2011a. Distribution and characterization of failed (mega) blocks along salt ridges, southeast Brazil: Implications for vertical fluid flow on continental margins. *Journal of Geophysical Research*, 116(B8): B08103.
- Gamboa, D., Alves, T., Cartwright, J. and Terrinha, P., 2010. MTD distribution on a 'passive' continental margin: The Espírito Santo Basin (SE Brazil) during the Palaeogene. *Marine and Petroleum Geology*, 27(7): 1311-1324.
- Gamboa, D., Alves, T.M. and Cartwright, J. (Eds.), 2011b. Seismic-Scale Rafted and Remnant Blocks over Salt Ridges in the Espírito Santo Basin, Brazil. *Submarine Mass Movements and Their Consequences*. Springer, 629-638 pp.
- Gartrell, A., Zhang, Y., Lisk, M. and Dewhurst, D., 2004. Fault intersections as critical hydrocarbon leakage zones: integrated field study and numerical modelling of an example from the Timor Sea, Australia. *Marine and Petroleum Geology*, 21(9): 1165-1179.
- Garziglia, S., Migeon, S., Ducassou, E., Loncke, L. and Mascle, J., 2008. Mass-transport deposits on the Rosetta province (NW Nile deep-sea turbidite system, Egyptian margin): Characteristics, distribution, and potential causal processes. *Marine Geology*, 250(3-4): 180-198.
- Gaullier, V. and Vendeville, B.C., 2005. Salt tectonics driven by sediment progradation: Part II--Radial spreading of sedimentary lobes prograding above salt. *AAPG Bulletin*, 89(8): 1081-1089.
- Gee, M.J.R. and Gawthorpe, R.L., 2006. Submarine channels controlled by salt tectonics: Examples from 3D seismic data offshore Angola. *Marine and Petroleum Geology*, 23(4): 443-458.
- Gee, M.J.R. and Gawthorpe, R.L., 2007. Early evolution of submarine channels offshore Angola revealed by three-dimensional seismic data. In: R.J. Davies, H. Posamentier, L. Wood and J. Cartwright (Eds.), *Seismic Geomorphology*. Geological Society of London, Special Publications, 277, pp. 223-235.
- Gee, M.J.R., Gawthorpe, R.L., Bakke, K. and Friedmann, S.J., 2007. Seismic Geomorphology and Evolution of Submarine Channels from the Angolan Continental Margin. *Journal of Sedimentary Research*, 77(5): 433-446.
- Gee, M.J.R., Gawthorpe, R.L. and Friedmann, J.S., 2005. Giant striations at the base of a submarine landslide. *Marine Geology*, 214(1-3): 287-294.

- Gee, M.J.R., Gawthorpe, R.L. and Friedmann, S.J., 2006. Triggering and Evolution of a Giant Submarine Landslide, Offshore Angola, Revealed by 3D Seismic Stratigraphy and Geomorphology. *Journal of Sedimentary Research*, 76(1): 9-19.
- Gibbons, K.A., Jourdan, C.A. and Hesthammer, J., 2003. The Statfjord Field, Blocks 33/9, 33/12 Norwegian sector, Blocks 211/24, 211/25 UK sector, Northern North Sea. Geological Society, London, *Memoirs*, 20(1): 335-353.
- Giles, K.A. and Lawton, T.F., 2002. Halokinetic sequence stratigraphy adjacent to the El Papalote diapir, northeastern Mexico. *AAPG Bulletin*, 86(5): 823-840.
- Godo, T.J., 2006. Identification of stratigraphic traps with subtle seismic amplitude effects in Miocene channel/levee sand systems, NE Gulf of Mexico. Geological Society, London, *Special Publications*, 254(1): 127-151.
- Greene, H.G., Maher, N.M. and Paull, C.K., 2002. Physiography of the Monterey Bay National Marine Sanctuary and implications about continental margin development. *Marine Geology*, 181(1-3): 55-82.
- Griffiths, J.C., 1966. Exploration for Natural Resources. *Operations Research*, 14(2): 189.
- Guardado, L.R., Gamboa, L.A.P. and Luchesi, C.F. (Eds.), 1989. Petroleum geology of the Campos Basin, a model for a producing Atlantic-type basin. *Divergent/Passive Margin Basins*, 48. *Am. Assoc. Pet. Geol. Mem.*, 3-79 pp.
- Guardado, L.R., Spadini, A.R., Brandão, J.S.L. and Mello, M.R. (Eds.), 2000. Petroleum System of the Campos Basin, Brazil. *Petroleum systems of South Atlantic margins*, AAPG Memoir 73, 317-324 pp.
- Hajek, E.A., Heller, P.L. and Sheets, B.A., 2010. Significance of channel-belt clustering in alluvial basins. *Geology*, 38(6): 535-538.
- Hampton, M.A., Lee, H.J. and Locat, J., 1996. Submarine Landslides. *Review of Geophysics*, 34(1): 33-59.
- Hardage, B.A., Pendleton, V.M., Simmons, J.J.L., Stubbs, B.A. and Uszynski, B.J., 1998a. 3-D instantaneous frequency used as a coherency/continuity parameter to interpret reservoir compartment boundaries across an area of complex turbidite deposition. *Geophysics*, 63(5): 1520-1531.
- Hardage, B.A., Simmons, J.J.L., Pendleton, V.M., Stubbs, B.A. and Uszynski, B.J., 1998b. 3-D seismic imaging and interpretation of Brushy Canyon slope and basin thin-bed reservoirs, northwest Delaware Basin. *Geophysics*, 63(5): 1507-1519.

- Hart, B., 2008. Stratigraphically significant attributes. *The Leading Edge*, 27: 320-324.
- Hart, B.S., 1999. Definition of subsurface stratigraphy, structure and rock properties from 3-D seismic data. *Earth-Science Reviews*, 47(3-4): 189-218.
- Haschenburger, J.K. and Spinelli, J.J., 2005. Assessing the goodness-of-fit of statistical distributions when data are grouped. *Mathematical geology*, 37(3): 261-276.
- Haughton, P.D.W., Barker, S.P. and McCaffrey, W.D., 2003. 'Linked' debrites in sand-rich turbidite systems - origin and significance. *Sedimentology*, 50(3): 459-482.
- Heinio, P. and Davies, R.J., 2006. Degradation of compressional fold belts: Deep-water Niger Delta. *AAPG Bulletin*, 90(5): 753-770.
- Heiniö, P. and Davies, R.J., 2007. Knickpoint migration in submarine channels in response to fold growth, western Niger Delta. *Marine and Petroleum Geology*, 24(6-9): 434-449.
- Heiniö, P. and Davies, R.J., 2009. Trails of depressions and sediment waves along submarine channels on the continental margin of Espirito Santo Basin, Brazil. *Geological Society of America Bulletin*, 121(5-6): 698-711.
- Hernández-Molina, F., Llave, E. and Stow, D., 2008. Continental slope contourites. *Developments in Sedimentology*, 60: 379-408.
- Hey, R.D., 1997. Stable River Morphology. In: C.R. Thorne, R.D. Hey and M.D. Newson (Eds.), *Applied Fluvial Geomorphology for River Engineering and Management*. John Wiley & Sons, Ltd, pp. 223-236.
- Hodgson, D.M., 2009. Distribution and origin of hybrid beds in sand-rich submarine fans of the Tanqua depocentre, Karoo Basin, South Africa. *Marine and Petroleum Geology*, 26(10): 1940-1956.
- Hodgson, D.M., Di Celma, C.N., Brunt, R.L. and Flint, S.S., 2011. Submarine slope degradation and aggradation and the stratigraphic evolution of channel–levee systems. *Journal of the Geological Society*, 168(3): 625-628.
- Hofmann, M.H., Wroblewski, A. and Boyd, R., 2011. Mechanisms Controlling the Clustering of Fluvial Channels and the Compensational Stacking of Cluster Belts. *Journal of Sedimentary Research*, 81(9): 670-685.
- Hogg, A.J.C., 2003. The Montrose, Arbroath and Arkwright Fields, Blocks 22/17, 22/23a, UK North Sea. *Geological Society, London, Memoirs*, 20(1): 611-616.
- Holbrook, J. and Schumm, S.A., 1999. Geomorphic and sedimentary response of rivers to tectonic deformation: a brief review and critique of a tool for recognizing subtle

- epeirogenic deformation in modern and ancient settings. *Tectonophysics*, 305(1-3): 287-306.
- Homza, T.X., 2004. A structural interpretation of the Fish Creek Slide (Lower Cretaceous), northern Alaska. *AAPG Bulletin*, 88(3): 265-278.
- Hooper, E.C.D., 1991. Fluid Migration along Growth Faults in Compacting Sediments. *Journal of Petroleum Geology*, 14: 161-180.
- Howard, A.D., Dietrich, W.E. and Seidl, M.A., 1994. Modeling fluvial erosion on regional to continental scales. *Journal of Geophysical Research*, 99(B7): 13,971-13,986.
- Hudec, M.R. and Jackson, M.P.A., 2006. Advance of allochthonous salt sheets in passive margins and orogens. *AAPG Bulletin*, 90(10): 1535-1564.
- Hudec, M.R. and Jackson, M.P.A., 2007. Terra infirma: Understanding salt tectonics. *Earth-Science Reviews*, 82(1-2): 1-28.
- Huppertz, T.J., Piper, D.J.W., Mosher, D.C. and Jenner, K., 2010. The Significance of Mass-Transport Deposits for the Evolution of a Proglacial Continental Slope. In: D.C. Mosher et al. (Eds.), *Submarine Mass Movements and Their Consequences*. Springer Netherlands, pp. 631-641.
- Hurst, A., Verstralen, I., Cronin, B. and Hartley, A., 1999. Sand-rich fairways in deep-water clastic reservoirs: genetic units, capturing uncertainty, and a new approach to reservoir modeling. *AAPG Bulletin*, 83: 1096-1118.
- Ilstad, T. et al., 2004a. On the frontal dynamics and morphology of submarine debris flows. *Marine Geology*, 213(1-4): 481-497.
- Ilstad, T., Elverhøi, A., Issler, D. and Marr, J.G., 2004b. Subaqueous debris flow behaviour and its dependence on the sand/clay ratio: a laboratory study using particle tracking. *Marine Geology*, 213(1-4): 415-438.
- Jackson, C.A.L. and Johnson, H.D., 2009. Sustained turbidity currents and their interaction with debrite-related topography; Labuan Island, offshore NW Borneo, Malaysia. *Sedimentary Geology*, 219(1-4): 77-96.
- Jackson, M.P.A. and Hudec, M.R., 2005. Stratigraphic record of translation down ramps in a passive-margin salt detachment. *Journal of Structural Geology*, 27(5): 889-911.
- Jackson, M.P.A., Vendeville, B. and Schultz-Ela, D.D., 1994. Structural Dynamics of Salt Systems. *Annual Review of Earth and Planetary Sciences*, 22: 93-117.

- Jackson, M.P.A. and Vendeville, B.C., 1994. Regional extension as a geologic trigger for diapirism. *Geological Society of America Bulletin*, 106(1): 57-73.
- Jahn, F., Cook, M. and Graham, M., 2003. *Hydrocarbon exploration and production*. Elsevier Science, 384 pp.
- James, D., 1997. Discussion on a model for the structure and development of fault zones. *Journal of the Geological Society*, 154(2): 366-368.
- Jensen, J.L., Corbett, P.W.M., Lake, L.W. and Goggin, D.J., 2007. *Statistics for Petroleum Geologists and Geoscientists, Handbook of Petroleum Exploration and Productin, 2. Handbook of Petroleum Exploration and Productin, 2*. Elsevier, 339 pp.
- Jobe, Z.R., Lowe, D.R. and Uchytíl, S.J., 2011. Two fundamentally different types of submarine canyons along the continental margin of Equatorial Guinea. *Marine and Petroleum Geology*, 28(3): 843-860.
- Jolley, S.J., Barr, D., Walsh, J.J. and Knipe, R.J., 2007a. Structurally complex reservoirs: an introduction. *Geological Society, London, Special Publications*, 292(1): 1-24.
- Jolley, S.J. et al., 2007b. Faulting and fault sealing in production simulation models: Brent Province, northern North Sea. *Petroleum Geoscience*, 13: 321-340.
- Jolley, S.J., Fisher, Q.J. and Ainsworth, R.B. (Eds.), 2010. Reservoir compartmentalization: an introduction. *Reservoir Compartmentalization*, 347. Geological Society Special Publication, Vol 347, NP pp.
- Kane, I.A. and Hodgson, D.M., 2011. Sedimentological criteria to differentiate submarine channel levee subenvironments: Exhumed examples from the Rosario Fm. (Upper Cretaceous) of Baja California, Mexico, and the Fort Brown Fm. (Permian), Karoo Basin, S. Africa. *Marine and Petroleum Geology*, 28(3): 807-823.
- Kane, I.A., Kneller, B.C., Dykstra, M., Kassem, A. and McCaffrey, W.D., 2007. Anatomy of a submarine channel-levee: An example from Upper Cretaceous slope sediments, Rosario Formation, Baja California, Mexico. *Marine and Petroleum Geology*, 24(6-9): 540-563.
- Kearey, P., Brooks, M. and Hill, I., 2002. *An introduction to geophysical exploration*. Wiley-Blackwell, 268 pp.
- Kendrick, J.W., 1998. Turbidite reservoir architecture in the Gulf of Mexico - insights from field development, EAGE/AAPG 3rd Research Symposium on Developing and Managing Turbidite Reservoirs, 3-9 October 1998, Almería, Spain.



- Kennett, J.P., 1982. *Marine Geology*. Prentice-Hall, Englewood Cliffs, NJ.
- Kenyon, P.M. and Turcotte, D.L., 1985. Morphology of a delta prograding by bulk sediment transport. *Geological Society of America Bulletin*, 96(11): 1457-1465.
- Kneller, B., 2003. The influence of flow parameters on turbidite slope channel architecture. *Marine and Petroleum Geology*, 20(6-8): 901-910.
- Knipe, R.J., 1997. Juxtaposition and seal diagrams to help analyze fault seals in hydrocarbon reservoirs. *AAPG Bulletin*, 81(2): 187-195.
- Knipe, R.J., Jones, G. and Fisher, Q.J., 1998. Faulting, fault sealing and fluid flow in hydrocarbon reservoirs: an introduction. In: G. Jones, Q.J. Fisher and R.J. Knipe (Eds.), *Faulting, Fault Sealing and Fluid Flow in Hydrocarbon Reservoirs*. Geological Society, London, Special Publications, 147, pp. vii-xxi.
- Kolla, V., 2007. A review of sinuous channel avulsion patterns in some major deep-sea fans and factors controlling them. *Marine and Petroleum Geology*, 24(6-9): 450-469.
- Kolla, V., Bourges, P., Urruty, J.M. and Safa, P., 2001. Evolution of deep-water Tertiary sinuous channels offshore Angola (west Africa) and implications for reservoir architecture. *American Association of Petroleum Geologists Bulletin*, 85(8): 1373-1405.
- Komar, P.D., 1971. Hydraulic Jumps in Turbidity Currents. *Geological Society of America Bulletin*, 82(6): 1477-1488.
- Kroon, D., Zachos, J.C. and Party, L.S., 2007. Leg 208 synthesis: Cenozoic climate cycles and excursions. In: D. Kroon, J.C. Zachos and C. Richter (Eds.), *Proceedings ODP, Scientific Results, 208*. College Station, TX (Ocean Drilling Program), pp. 1-55.
- L'Heureux, J.-S., Hansen, L. and Longva, O., 2009. Development of the submarine channel in front of the Nidelva River, Trondheimsfjorden, Norway. *Marine Geology*, 260(1-4): 30-44.
- Laberg, J.S. and Vorren, T.O., 2000. The Trænadjupet Slide, offshore Norway -- morphology, evacuation and triggering mechanisms. *Marine Geology*, 171(1-4): 95-114.
- Labourdet, R., 2007. Integrated three-dimensional modeling approach of stacked turbidite channels. *AAPG Bulletin*, 91(11): 1603.
- Labourdet, R., 2011. Stratigraphy and static connectivity of braided fluvial deposits of the lower Escanilla Formation, south central Pyrenees, Spain. *AAPG Bulletin*, 95(4): 585-617.

- Labourdette, R. et al., 2006. Three-dimensional modelling of stacked turbidite channels in West Africa: impact on dynamic reservoir simulations. *Petroleum Geoscience*, 12: 335-345.
- Larue, D.K. and Hovadik, J., 2006. Connectivity of channelized reservoirs: a modelling approach. *Petroleum Geoscience*, 12: 291-308.
- Lastras, G. et al., 2002. Seafloor imagery from the BIG'95 debris flow, western Mediterranean. *Geology*, 30(10): 871-874.
- Lee, C., Nott, J.A. and Keller, F.B., 2004. Seismic expression of the Cenozoic Mass Transport Complexes, deepwater Tarfaya-Agadir Basin, offshore Morocco, Offshore Technology Conference, Houston, Texas.
- Lee, G.H. and Watkins, J.S., 1996. Bryant Canyon fan system: an unconfined, large river-sourced system in the northwestern Gulf of Mexico. *AAPG Bulletin-American Association of Petroleum Geologists*, 80(3): 340-358.
- Lee, Y. and Deming, D., 2002. Overpressures in the Anadarko basin, southwestern Oklahoma: Static or dynamic? *AAPG Bulletin*, 86(1): 145.
- Leeder, M., 1999. *Sedimentology and sedimentary basins: from turbulence to tectonics*. Wiley-Blackwell.
- Leyden, R., Asmus, H., Zembruski, S. and Bryan, G., 1976. South Atlantic diapiric structures. *AAPG Bulletin*, 60(2): 196-212.
- Ligtenberg, J.H., 2005. Detection of fluid migration pathways in seismic data: implications for fault seal analysis. *Basin Research*, 17(1): 141-153.
- Lima, C., 2003. Ongoing compression across South American plate: observations, numerical modelling and some implications for petroleum geology. In: M. Ameen (Ed.), *Fracture and In-Situ Stress Characterization of Hydrocarbon Reservoirs*. Geological Society, London, Special Publications, pp. 87-100.
- Løseth, H., Gading, M. and Wensaas, L., 2009. Hydrocarbon leakage interpreted on seismic data. *Marine and Petroleum Geology*, 26(7): 1304-1319.
- Love, F. et al., 2005. Northern Espírito Santo basin canyon models ancient sand transport. *Offshore*, March 2005: 74-78.
- Lucente, C.C. and Pini, G.A., 2003. Anatomy and emplacement mechanism of a large submarine slide within a Miocene foredeep in the northern Apennines, Italy: A field perspective. *American Journal of Science*, 303(7): 565-602.

- Lucente, C.C. and Pini, G.A., 2008. Basin-wide mass-wasting complexes as markers of the Oligo-Miocene foredeep-accretionary wedge evolution in the Northern Apennines, Italy. *Basin Research*, 20(1): 49-71.
- Lucente, C.C. and Taviani, M., 2005. Chemosynthetic communities as fingerprints of submarine sliding-linked hydrocarbon seepage, Miocene deep-sea strata of the Tuscan-Romagna Apennines, Italy. *Palaeogeography, Palaeoclimatology, Palaeoecology*, 227(1-3): 176-190.
- Maier, K.L. et al., 2011. The elusive character of discontinuous deep-water channels: New insights from Lucia Chica channel system, offshore California. *Geology*, 39(4): 327-330.
- Mallarino, G., Beaubouef, R.T., Droxler, A.W., Abreu, V. and Labeyrie, L., 2006. Sea level influence on the nature and timing of a minibasin sedimentary fill (northwestern slope of the Gulf of Mexico). *AAPG Bulletin*, 90(7): 1089-1119.
- Martín-Chivelet, J., Fregenal-Martínez, M.A. and Chacón, B., 2008. Traction Structures in Contourites. In: M. Rebesco and A. Camerlenghi (Eds.), *Developments in Sedimentology*. Elsevier, pp. 157-182.
- Martinsen, O.J., 1994. Mass movements. In: A. Maltman (Ed.), *The Geological Deformation of Sediments*. Chapman & Hall, London, pp. 127-165.
- Martinsen, O.J. and Bakken, B., 1990. Extensional and compressional zones in slumps and slides in the Namurian of County Clare, Ireland. *Journal of the Geological Society of London*, 147: 153-164.
- Masson, D., Wynn, R.B. and Talling, P.J., 2010. Large landslides on passive continental margins: processes, hypotheses and outstanding questions. In: D.C. Mosher et al. (Eds.), *Submarine Mass Movements and Their Consequences. Advances in Natural and Technological Hazards Research*. Springer.
- Masson, D.G., Harbitz, C.B., Wynn, R.B., Pedersen, G. and Løvholt, F., 2006. Submarine landslides: Processes, triggers and hazard prediction. *Philosophical Transactions: Mathematical, Physical and Engineering Sciences (Series A)*, 364(1845): 2009-2039.
- Mayall, M., Jones, E. and Casey, M., 2006. Turbidite channel reservoirs--Key elements in facies prediction and effective development. *Marine and Petroleum Geology*, 23(8): 821-841.

- Mayall, M. et al., 2010. The response of turbidite slope channels to growth-induced seabed topography. *AAPG Bulletin*, 94(7): 1011-1030.
- Mayall, M. and Stewart, I., 2000. The architecture of turbidite slope channels, Deepwater Reservoirs of the World, GCSSEPM Foundation 20th Annual Research Conference, pp. 578–586.
- McAdoo, B.G., Pratson, L.F. and Orange, D.L., 2000. Submarine landslide geomorphology, US continental slope. *Marine Geology*, 169(1-2): 103-136.
- McBride, B.C., Rowan, M.G. and Weimer, P., 1998. The evolution of allochthonous salt systems, northern Green Canyon and Ewing Bank (offshore Louisiana), northern Gulf of Mexico. *AAPG Bulletin*, 82(5B): 1013-1036.
- McGregor, B.A., 1985. Role of submarine canyons in shaping the rise between Lydonia and Oceanographer canyons, Georges Bank. *Marine Geology*, 62(3-4): 277-293.
- McHargue, T. et al., 2011. Architecture of turbidite channel systems on the continental slope: Patterns and predictions. *Marine and Petroleum Geology*, 28(3): 728-743.
- McHugh, C.M.G. and Ryan, W.B.F., 2000. Sedimentary features associated with channel overbank flow: examples from the Monterey Fan. *Marine Geology*, 163(1-4): 199-215.
- McKie, T., Jolley, S.J. and Kristensen, M.B., 2010. Stratigraphic and structural compartmentalization of dryland fluvial reservoirs: Triassic Heron Cluster, Central North Sea. In: S.J. Jolley, Q.J. Fisher, R.B. Ainsworth, P. Vrolijk and S. Delisle (Eds.), *Reservoir Compartmentalization*. Geological Society Special Publication, Vol 347, pp. 165-198.
- Meckel III, L.D., 2011. Reservoir characteristics and classification of sand-prone submarine mass-transport deposits. In: C. Shipp, P. Weimer and H. Posamentier (Eds.), *Mass-transport deposits in deepwater settings*. SEPM Special Publication 96, pp. 423-450.
- Meckel III, L.D. et al., 2011. Reservoir characterization of sand-prone mass-transport deposits within slope canyons. In: C. Shipp, P. Weimer and H. Posamentier (Eds.), *Mass-transport deposits in deepwater settings*. SEPM Special Publication 96, pp. 391-422.
- Meldahl, P., Heggland, R., Bril, B. and de Groot, P., 2001. Identifying faults and gas chimneys using multiattributes and neural networks. *The Leading Edge*, 20(5): 474-482.

- Mello, M.R., Mohriak, W.U., Koutsoukos, E.A.M. and Bacoccoli, G., 1994. Selected petroleum systems in Brazil, AAPG Memoir, 60, pp. 499-512.
- Milani, E.J., Brandão, J.A.S.L., Zalán, P.V. and Gamboa, L.A.P., 2001. Petróleo na Margin Continental Brasileira: Geologia, Exploração, Resultados e Perspectivas. Brazilian Journal of Geophysics, 18(3): 352-396.
- Milkov, A.V. et al., 2007. Compartmentalization and time-lapse geochemical reservoir surveillance of the Horn Mountain oil field, deep-water Gulf of Mexico. AAPG Bulletin, 91(6): 847.
- Minisini, D., Trincardi, F., Asioli, A., Canu, M. and Foglini, F., 2007. Morphologic variability of exposed mass-transport deposits on the eastern slope of Gela Basin (Sicily channel). Basin Research, 19(2): 217-240.
- Mitchell, N.C., 2004. Form of submarine erosion from confluences in Atlantic USA continental slope Canyons. Am J Sci, 304(7): 590-611.
- Mitchell, N.C., 2006. Morphologies of knickpoints in submarine canyons. Geological Society of America Bulletin, 118(5-6): 589-605.
- Mitchum, R.M., Jr., Vail, P.R. and Sangree, J.B., 1977a. Seismic stratigraphy and global changes of sea level, part 6: Stratigraphic interpretation of seismic reflection patterns in depositional sequences. In: C.E. Payton (Ed.), Seismic stratigraphy - applications to hydrocarbon exploration. AAPG Memoir 26, Tulsa, Ok, pp. 117-133.
- Mitchum, R.M., Jr., Vail, P.R. and Thompson, S., 1977b. Seismic Stratigraphy and Global Changes of Sea Level, Part 2: The Depositional Sequence as a Basic Unit for Stratigraphic Analysis. In: C.E. Payton (Ed.), Seismic stratigraphy - applications to hydrocarbon exploration. AAPG Memoir 26, Tulsa, pp. 53-62.
- Modica, C.J. and Brush, E.R., 2004. Postrift sequence stratigraphy, paleogeography, and fill history of the deep-water Santos Basin, offshore southeast Brazil. AAPG Bulletin, 88(7): 923-945.
- Mohriak, W.U., 1995. Salt tectonics structural styles: contrasts and similarities between the South Atlantic and the Gulf of Mexico. In: C.J. Travis et al. (Eds.), Salt, Sediment and Hydrocarbons, Gulf Coast Section of the Society of Economic Paleontologists and Mineralogists ( GCSSEPM Foundation), 16th Annual Research Conference, Houston, Texas, pp. 177-191.

- Mohriak, W.U., 2003. Bacias sedimentares da margem continental Brasileira. In: L.A. Bizzi, C. Schobbenhaus, R.M. Vidotti and J.H. Goncalves (Eds.), *Geologia, Tectonica e Recursos Minerais do Brasil*. CPRM, Brasilia, pp. 87-165.
- Mohriak, W.U., 2004. Recursos energéticos associados a ativação tectônica Mesozóica-Cenozóica da América do Sul. In: V. Mantesso-Neto, A. Bartoreli, C.D.R. Carneiro and B.B. Brito Neves (Eds.), *Geologia do Continente Sul-Americano: Evolução da Obra de Fernando Marques de Almeida*, São Paulo, pp. 293-319.
- Mohriak, W.U., 2005. Interpretação geológica e geofísica da Bacia do Espírito Santo e da região de Abrolhos: Petrografia, datação radiométrica e visualização sísmica das rochas vulcânicas. *Boletim de Geociencias da Petrobras*, 14(1): 133-142.
- Mohriak, W.U., Mello, M.R., Dewey, J.F. and Maxwell, J.R. (Eds.), 1990. *Petroleum Geology of the Campos Basin, offshore Brazil. Classic Petroleum Provinces*. Geological Society, London, 119-141 pp.
- Mohriak, W.U., Nemcok, M. and Enciso, G., 2008. South Atlantic divergen margin evolution: rift-borded uplift and salt tectonics in the basins of Southeastern Brazil. In: R.J. Pankhurst, R.A.J. Trouw, B.B. Brito Neves and M.J. de Wit (Eds.), *West Gondwana pre-Cenozoic correlations across the South Atlantic region*. Geological Society London, Special Publications 294, pp. 365-398.
- Mohriak, W.U., Rabelo, J.H.L., De Matos, R.D. and De Barros, M.C., 1995. Deep seismic reflection profiling of sedimentary basins offshore Brazil: geological objectives and preliminary results in the Sergipe Basin. *Journal of Geodynamics*, 20(4): 515-539.
- Moraes, M.A.S., Maciel, W.B., Braga, M.S.S. and Viana, A.R., 2007. Bottom-current reworked Palaeocene-Eocene deep-water reservoirs of the Campos Basin, Brazil. In: A.R. Viana and M. Rebesco (Eds.), *Economic and Palaeoceanographic Significant of Contourite Deposits*. Geological Society London, Special Publications, 276, pp. 81-94.
- Moreira, J.L.P. and Carminatti, M., 2004. Sistemas deposicionais de talude e de bacia no Eoceno da Bacia de Santos. *Boletim de Geociencias da Petrobras*, 12(1): 73-87.
- Moscardelli, L. and Wood, L., 2008. New classification system for mass transport complexes in offshore Trinidad. *Basin Research*, 20(1): 73-98.
- Moscardelli, L., Wood, L. and Mann, P., 2006. Mass-transport complexes and associated processes in the offshore area of Trinidad and Venezuela. *AAPG Bulletin*, 90(7): 1059-1088.

- Mosley, M.P., 1976. An Experimental Study of Channel Confluences. *Journal of Geology*, 84: 535-562.
- Mulder, T. and Cochonat, P., 1996. Classification of offshore mass movements. *Journal of Sedimentary Research*, 66(1): 43-57.
- Mutti, E. and Normark, W.B., 1991. An integrated approach to the study of turbidite systems. In: P. Weimer and M.H. Link (Eds.), *Seismic facies and sedimentary processes of submarine fans and turbidite systems*. Springer-Verlag, New York, pp. 75-106.
- Naruse, H. and Otsubo, M., 2011. Heterogeneity of internal structures in a mass-transport deposit, Upper Cretaceous to Paleocene Akkeshi Formation, Hokkaido Island, northern Japan. In: C. Shipp, P. Weimer and H. Posamentier (Eds.), *Mass-transport deposits in deepwater settings*. SEPM Special Publication, pp. 279-290.
- Nelson, C.H., Escutia, C., Damuth, J.E. and Twichell Jr., D.C., 2011. Interplay of mass-transport and turbidite-system deposits in different active tectonic and passive continental margin settings: external and local controlling factors. In: C. Shipp, P. Weimer and H. Posamentier (Eds.), *Mass-transport deposits in deepwater settings*. SEPM Special Publication 96, pp. 39-67.
- Nemec, W., 1990. Aspects of sediment movement on steep delta slopes. *Special Publication of the International Association of Sedimentologists*, 10, 29–73 pp.
- Nissen, S.E., Haskell, N.L., Steiner, C.T. and Coterill, K.L., 1999. Debris flow outrunner blocks, glide tracks, and pressure ridges identified on the Nigerian continental slope using 3-D seismic coherency. *The Leading Edge*, 18(5): 595-599.
- Normark, W.R., 1970. Growth patterns of deep-sea fans. *AAPG Bulletin*, 54(11): 2170-2195.
- Normark, W.R., 1978. Fan valleys, channels, and depositional lobes on modern submarine fans: characters for recognition of sandy turbidite environments. *AAPG Bulletin*, 62(6): 912-931.
- Normark, W.R. and Piper, D.J.W., 1969. Deep-Sea Fan-Valleys, Past and Present. *Geological Society of America Bulletin*, 80(9): 1859-1866.
- Normark, W.R., Posamentier, H. and Mutti, E., 1993. Turbidite systems: State of the art and future directions. *Reviews of Geophysics*, 31(2): 91-116.
- Odonne, F. et al., 2011. Soft-sediment deformation from submarine sliding: Favourable conditions and triggering mechanisms in examples from the Eocene Sobrarbe delta

- (Ainsa, Spanish Pyrenees) and the mid-Cretaceous Ayabacas Formation (Andes of Peru). *Sedimentary Geology*, 235(3-4): 234-248.
- Ojeda, H.A.O., 1982. Structural framework, stratigraphy, and evolution of Brazilian marginal basins. *AAPG Bulletin*, 66(6): 732-749.
- Ortoleva, P.J., 1994. Basin compartmentation: definitions and mechanisms. In: P.J. Ortoleva (Ed.), *Basin Compartments and Seals*. AAPG Memoir 61, pp. 39-51.
- Ouchi, S., 1985. Response of alluvial rivers to slow active tectonic movement. *Geological Society of America Bulletin*, 96(4): 504-515.
- Paquet, F. et al., 2010. Buried fluvial incisions as a record of Middle-Late Miocene eustasy fall on the Armorican Shelf (Bay of Biscay, France). *Marine Geology*, 268(1-4): 137-151.
- Peakall, J., Amos, K.J., Keevil, G.M., William Bradbury, P. and Gupta, S., 2007. Flow processes and sedimentation in submarine channel bends. *Marine and Petroleum Geology*, 24(6-9): 470-486.
- Permanyer, A., Rebufa, C. and Kister, J., 2007. Reservoir compartmentalization assessment by using FTIR spectroscopy. *Journal of Petroleum Science and Engineering*, 58(3-4): 464-471.
- Pilcher, R.S., Kilsdonk, B. and Trude, J., 2011. Primary basins and their boundaries in the deep-water northern Gulf of Mexico: Origin, trap types, and petroleum system implications. *AAPG Bulletin*, 95(2): 219-240.
- Piper, D.J.W., 1970. Transport and deposition of Holocene sediment on La Jolla Deep Sea Fan, California. *Marine Geology*, 8(3-4): 211-227.
- Piper, D.J.W. and McCall, C., 2003. A synthesis of the distribution of submarine mass movements on the eastern Canadian margin. In: J. Locat and J. Mienert (Eds.), *Submarine mass movements and their consequences*. Kluwer, Dordrecht, pp. 291-298.
- Piper, D.J.W. and Normark, W.R., 2009. Processes That Initiate Turbidity Currents and Their Influence on Turbidites: A Marine Geology Perspective. *Journal of Sedimentary Research*, 79(6): 347-362.
- Piper, D.J.W. et al., 1997. Mass transport deposits of the Amazon Fan. In: R.D. Flood, D.J.W. Piper, A. Klaus and L.C. Peterson (Eds.), *Proc. ODP Sci. Results*, 155. Ocean Drilling Program,, College Station, TX., pp. 109-146.



- Pirmez, C., Beaubouef, R.T., Friedmann, S.J. and Mohrig, D.C., 2000. Equilibrium profile and baselevel in submarine channels: examples from Late Pleistocene systems and implications for the architecture of deepwater reservoirs, Deepwater Reservoirs of the World, GCSSEPM Foundation 20th Annual Research Conference, pp. 782–805.
- Pirmez, C. and Imran, J., 2003. Reconstruction of turbidity currents in Amazon Channel. *Marine and Petroleum Geology*, 20(6-8): 823-849.
- Posamentier, H., 2004a. Stratigraphy and geomorphology of deep-water mass transport complexes based on 3D seismic data, Offshore Technology Conference, Houston, TX.
- Posamentier, H. and Martinsen, O.J., 2011. The character and genesis of submarine mass-transport deposits: insights from outcrop and 3D seismic data. In: C. Shipp, P. Weimer and H. Posamentier (Eds.), *Mass-transport deposits in deepwater settings*. SEPM Special Publication 96, pp. 7-38.
- Posamentier, H. and Walker, R.G., 2006. Deep water turbidites and submarine fans. In: H. Posamentier and R.G. Walker (Eds.), *Facies Models Revisited - SEPM Special Publication*. SEPM (Society for Sedimentary Geology), Tulsa, Oklahoma, U.S.A., pp. 397-520.
- Posamentier, H.W., 2003. Depositional elements associated with a basin floor channel-levee system: case study from the Gulf of Mexico. *Marine and Petroleum Geology*, 20(6-8): 677-690.
- Posamentier, H.W., 2004b. Seismic Geomorphology: Imaging Elements of Depositional Systems from Shelf to Deep Basin Using 3D Seismic Data: Implications for Exploration and Development. In: R.J. Davies, J. Cartwright, S.A. Stewart, M. Lappin and J.R. Underhill (Eds.), *Geological Society, London, Memoirs*, Vol 29, pp. 11-24.
- Posamentier, H.W. and Allen, G.P., 1993. Variability of the sequence stratigraphic model: effects of local basin factors. *Sedimentary Geology*, 86(1-2): 91-109.
- Posamentier, H.W., Davies, R.J., Cartwright, J.A. and Wood, L., 2007. Seismic geomorphology - an overview. *Geological Society, London, Special Publications*, 277(1): 1-14.
- Posamentier, H.W. and Kolla, V., 2003. Seismic Geomorphology and Stratigraphy of Depositional Elements in Deep-Water Settings. *Journal of Sedimentary Research*, 73(3): 367-388.
- Prather, B.E., 2003. Controls on reservoir distribution, architecture and stratigraphic trapping in slope settings. *Marine and Petroleum Geology*, 20(6-8): 529-545.

- Prather, B.E., Booth, J.R., Steffens, G.S. and Craig, P.A., 1998. Classification, lithologic calibration, and stratigraphic succession of seismic facies of intraslope basins, deep-water Gulf of Mexico. *AAPG Bulletin*, 82(5A): 701-728.
- Pratson, L.F. and Coakley, B.J., 1996. A model for the headward erosion of submarine canyons induced by downslope-eroding sediment flows. *Geological Society of America Bulletin*, 108(2): 225.
- Pratson, L.F. et al., 2007. Seascape evolution on clastic continental shelves and slopes. In: C.A. Nittrouer et al. (Eds.), *Continental Margin Sedimentation*. Special Publication Nr 37, International Association of Sedimentologists, Wiley Online Library, pp. 339-380.
- Puckette, J. and Al-Shaieb, Z., 2003. Naturally underpressured reservoirs: applying the compartment concept to the safe disposal of liquid waste. *search and discovery article*, 40071.
- Rahimpour-Bonab, H., 2007. A procedure for appraisal of a hydrocarbon reservoir continuity and quantification of its heterogeneity. *Journal of Petroleum Science and Engineering*, 58(1-2): 1-12.
- Ramon, J.C. and Fajardo, A., 2006. Sedimentology, sequence stratigraphy, and reservoir architecture of the Eocene Mirador Formation, Cupiagua field, Llanos Foothills, Colombia. In: P.M. Harris and L.J. Weber (Eds.), *Giant hydrocarbon reservoirs of the world: From rocks to reservoir characterization and modeling*. AAPG Memoir 88, pp. 433-469.
- Reading, H.G. and Richards, M., 1994. Turbidite systems in deep-water basin margins classified by grain size and feeder system. *AAPG Bulletin*, 78(5): 792-822.
- Rhoads, B.L. and Kenworthy, S.T., 1995. Flow structure at an asymmetrical stream confluence. *Geomorphology*, 11(4): 273-293.
- Richards, F.W., Vrolijk, P.J., Gordon, J.D. and Miller, B.R., 2010. Reservoir connectivity analysis of a complex combination trap: Terra Nova Field, Jeanne d'Arc Basin, Newfoundland, Canada. In: S.J. Jolley, Q.J. Fisher, R.B. Ainsworth, P. Vrolijk and S. Delisle (Eds.), *Reservoir Compartmentalization*. Geological Society Special Publication, Vol 347, pp. 333-355.
- Richards, M. and Bowman, M., 1998. Submarine fans and related depositional systems ii: variability in reservoir architecture and wireline log character. *Marine and Petroleum Geology*, 15(8): 821-839.

- Richards, M., Bowman, M. and Reading, H., 1998. Submarine-fan systems i: characterization and stratigraphic prediction. *Marine and Petroleum Geology*, 15(7): 689-717.
- Richardson, S.E.J., Davies, R.J., Allen, M.B. and Grant, S.F., 2011. Structure and evolution of mass transport deposits in the South Caspian Basin, Azerbaijan. *Basin Research*: no-no.
- Rowan, M.G., Jackson, M.P.A. and Trudgill, B.D., 1999. Salt-related fault families and fault welds in the northern Gulf of Mexico. *AAPG Bulletin*, 83(9): 1454-1484.
- Rowan, M.G., Lawton, T.F., Giles, K.A. and Ratliff, R.A., 2003. Near-salt deformation in La Popa basin, Mexico, and the northern Gulf of Mexico: A general model for passive diapirism. *AAPG Bulletin*, 87(5): 733-756.
- Rowan, M.G. and Weimer, P., 1998. Salt-sediment interaction, northern Green Canyon and Ewing Bank (offshore Louisiana), northern Gulf of Mexico. *AAPG Bulletin*, 82(5B): 1055-1082.
- Sangree, J.B. and Widmier, J.M., 1977. Seismic stratigraphy and global changes of sea level, part 9: Seismic interpretation of clastic depositional facies, Seismic stratigraphy - applications to hydrocarbon exploration. *AAPG Memoir* 26, pp. 165-184.
- Sawyer, D.E., Flemings, P.B., Dugan, B. and Germaine, J.T., 2009. Retrogressive failures recorded in mass transport deposits in the Ursa Basin, Northern Gulf of Mexico. *Journal of Geophysical Research*, 114.
- Sawyer, D.E., Flemings, P.B., Shipp, R.C. and Winker, C.D., 2007. Seismic geomorphology, lithology, and evolution of the late Pleistocene Mars-Ursa turbidite region, Mississippi Canyon area, northern Gulf of Mexico. *AAPG Bulletin*, 91(2): 215-234.
- Scholl, D.W., Buffington, E.C., Hopkins, D.M. and Alpha, T.R., 1970. The structure and origin of the large submarine canyons of the Bering Sea. *Marine Geology*, 8(3-4): 187-210.
- Schultz-Ela, D.D., 2003. Origin of drag folds bordering salt diapirs. *AAPG Bulletin*, 87(5): 757-780.
- Schultz-Ela, D.D., Jackson, M.P.A. and Vendeville, B.C., 1993. Mechanics of active salt diapirism. *Tectonophysics*, 228(3-4): 275-312.
- Schwab, A.M., Tremblay, S. and Hurst, A., 2007. Seismic expression of turbidity-current and bottom-current processes on the Northern Mauritanian continental slope. In: R.J. Davies, H. Posamentier, L. Wood and J. Cartwright (Eds.), *Seismic Geomorphology*. Geological Society of London, Special Publications, 277, pp. 237-252.

- Scott, E.D. et al., 2010. Sedimentological control of fluid flow in deep marine turbidite reservoirs: Pierce Field, UK Central North Sea. In: S.J. Jolley, Q.J. Fisher, R.B. Ainsworth, P. Vrolijk and S. Delisle (Eds.), *Reservoir Compartmentalization*. Geological Society Special Publication, Vol 347, pp. 113-132.
- Seber, G.A.F. and Lee, A.J., 2003. *Linear Regression Analysis*. Wiley Series in Probability and Statistics, 569 pp.
- Selley, R.C., 1998. *Elements of petroleum geology*. WH Freeman and Company, New York, NY, 470 pp.
- Seni, S.J. and Jackson, M.P.A., 1983a. Evolution of salt structures, East Texas diapir province; Part 1, Sedimentary record of halokinesis. *AAPG Bulletin*, 67(8): 1219-1244.
- Seni, S.J. and Jackson, M.P.A., 1983b. Evolution of salt structures, East Texas diapir province; Part 2, Patterns and rates of halokinesis. *AAPG Bulletin*, 67(8): 1245-1274.
- Shanmugam, G., 2006. *Deep-water processes and facies models: Implications for sandstone petroleum reservoirs*, 5. Elsevier Science, 476 pp.
- Shanmugam, G. et al., 1996. Slump and debris-flow dominated basin-floor fans in the North Sea: an evaluation of conceptual sequence-stratigraphical models based on conventional core data. In: S.P. Hesselbo and D.N. Parkinson (Eds.), *Sequence Stratigraphy in British Geology*. Geological Society London, Special Publications 103, pp. 145-176.
- Shanmugam, G. and Moiola, R.J., 1988. Submarine fans: Characteristics, models, classification, and reservoir potential. *Earth-Science Reviews*, 24(6): 383-428.
- Shepard, F.P., 1965. Types of submarine valleys. *AAPG Bulletin*, 49(3): 304.
- Shepard, F.P., 1981. Submarine canyons; multiple causes and long-time persistence. *AAPG Bulletin*, 65(6): 1062-1077.
- Shepard, F.P. and Dill, R.F., 1966. *Submarine canyons and other sea valleys*. Rand McNally and Company, Chicago, 381 pp.
- Shepard, F.P. and Emery, K.O., 1973. Congo Submarine Canyon and Fan Valley. *AAPG Bulletin*, 57(9): 1679-1691.
- Shepard, F.P. and Marshall, N.F., 1973. Currents Along Floors of Submarine Canyons. *AAPG Bulletin*, 57(2): 244-264.
- Sheriff, R.E. and Geldart, L.P., 1995. *Exploration Seismology*. Cambridge University Press, second edition, 628 pp.

- Shipp, C., Nott, J.A. and Newlin, J.A., 2004. Physical characteristics and impact of mass transport complexes on deepwater jetted conductors and suction anchor piles, Offshore Technology Conference, Houston, Texas.
- Silva, C.G. et al., 2010. Megaslides in the Foz do Amazonas Basin, Brazilian Equatorial Margin. In: D.C. Mosher et al. (Eds.), Submarine Mass Movements and Their Consequences. Springer Netherlands, pp. 581-592.
- Skene, K.I., Piper, D.J.W. and Hill, P.S., 2002. Quantitative analysis of variations in depositional sequence thickness from submarine channel levees. *Sedimentology*, 49(6): 1411-1430.
- Slatt, R.M. (Ed.), 2006. Stratigraphic Reservoir Characterization for Petroleum Geologists, Geophysicists and Engineers. Handbook of Petroleum Exploration and Production, Volume 6, Volume 6. Elsevier, 478 pp.
- Slatt, R.M., Eslinger, E.V. and Van Dyke, S.K., 2009. Acoustic and petrophysical properties of a clastic deepwater depositional system from lithofacies to architectural elements' scales. *Geophysics*, 74(2): WA35-WA50.
- Slatt, R.M. and Weimer, P., 1999. Turbidite systems Part 2: Subseismic-scale reservoir characteristics. *The Leading Edge*, 18(5): 562-567.
- Slatt, R.M. and Weimer, P., 2001. Styles of compartmentalization of deepwater (turbidite) reservoirs and associated performance issues, Rock the Foundation Convention, June 18-21, Canadian Society of Petroleum Geologists.
- Smith, R., 2004a. Silled sub-basins to connected tortuous corridors: Sediment distribution systems on topographically complex sub-aqueous slopes. In: S.A. Lomas and P. Joseph (Eds.), Confined Turbidite Systems. Geological Society of London, Special Publication, 222, pp. 23-43.
- Smith, R., 2004b. Turbidite systems influenced by structurally induced topography in the multi-sourced Welsh Basin. In: S.A. Lomas and P. Joseph (Eds.), Confined Turbidite Systems. Geological Society of London, Special Publication, 222, pp. 209-228.
- Snedden, J. et al., 2007. Reservoir Connectivity: Definitions, Strategies, and Applications, International Petroleum Technology Conference, Dubai.
- Sobreira, J.F.F. and França, R.L., 2005. A tectono-magmatic model for the Abrolhos Volcanic Complex region. *Boletim de Geociencias da Petrobras*, 14(1): 143-147.

- Solheim, A., Bryn, P., Sejrup, H.P., Mienert, J. and Berg, K., 2005. Ormen Lange- an integrated study for the safe development of a deep-water gas field within the Storegga Slide Complex, NE Atlantic continental margin; executive summary. *Marine and Petroleum Geology*, 22(1-2): 1-9.
- Spence, G.H. and Tucker, M.E., 1997. Genesis of limestone megabreccias and their significance in carbonate sequence stratigraphic models: a review. *Sedimentary Geology*, 112(3-4): 163-193.
- Sprague, A. et al., 2005. Integrated slope channel depositional models: The key to successful prediction of reservoir presence and quality in offshore west Africa Veracruz, CIPM, cuarto E-Exitep 2005, February 20 e 23, 2005, Veracruz, Mexico, pp. 1-13.
- Stewart, S.A., 2006. Implications of passive salt diapir kinematics for reservoir segmentation by radial and concentric faults. *Marine and Petroleum Geology*, 23(8): 843-853.
- Stow, D., Reading, H.G. and Collinson, J.D., 1996. Deep Seas. In: H.G. Reading (Ed.), *Sedimentary Environments: Processes, Facies and Stratigraphy*. Blackwell, Oxford, pp. 395-453.
- Stow, D.A.V., Alam, M. and Piper, D.J.W., 1984. Sedimentology of the Halifax Formation, Nova Scotia: Lower Palaeozoic fine-grained turbidites. In: D.A.V. Stow and D.J.W. Piper (Eds.), *Fine-grained sediments: Deep-water processes and facies*. Geological Society, London, Special Publications 15, pp. 127-144.
- Stow, D.A.V. and Johansson, M., 2000. Deep-water massive sands: nature, origin and hydrocarbon implications. *Marine and Petroleum Geology*, 17(2): 145-174.
- Stow, D.A.V. and Mayall, M., 2000. Deep-water sedimentary systems: New models for the 21st century. *Marine and Petroleum Geology*, 17(2): 125-135.
- Straub, K.M., Mohrig, D. and Pirmez, C., 2011. Architecture of an aggradational tributary submarine-channel network on the continental slope offshore Brunei Darussalam, Application of Seismic Geomorphology Principles to Continental Slope and Base-of-slope Systems: Case Studies from Seafloor and Near-Seafloor Analogues Society for Sedimentary Geology.
- Straub, K.M., Paola, C., Mohrig, D., Wolinsky, M.A. and George, T., 2009. Compensational Stacking of Channelized Sedimentary Deposits. *Journal of Sedimentary Research*, 79(9): 673-688.

- Stuart, I.A., 2003. The Armada development, UK Central North Sea: The Fleming, Drake and Hawkins Gas-Condensate Fields. *Geological Society, London, Memoirs*, 20(1): 139-151.
- Sweet, M.L. and Sumpter, L.T., 2007. Genesis field, Gulf of Mexico: Recognizing reservoir compartments on geologic and production time scales in deep-water reservoirs. *AAPG Bulletin*, 91(12): 1701.
- Sylvester, Z., Pirmez, C. and Cantelli, A., 2011. A model of submarine channel-levee evolution based on channel trajectories: Implications for stratigraphic architecture. *Marine and Petroleum Geology*, 28(3): 716-727.
- Taghavi, A.A., rk, A. and Emadi, M.A., 2006. Sequence stratigraphically controlled diagenesis governs reservoir quality in the carbonate Dehloran Field, southwest Iran. *Petroleum Geoscience*, 12: 115-126.
- Taylor, S.R., Almond, J., Arnott, S., Kemshell, D. and Taylor, D., 2003. The Brent Field, Block 211/29, UK North Sea. *Geological Society, London, Memoirs*, 20(1): 233-250.
- Tripsanas, E.K., Bryant, W.R. and Phaneuf, B.A., 2004. Slope-instability processes caused by salt movements in a complex deep-water environment, Bryant Canyon area, northwest Gulf of Mexico. *AAPG Bulletin*, 88(6): 801-823.
- Tripsanas, E.K., Piper, D.J.W., Jenner, K.A. and Bryant, W.R., 2008. Submarine mass-transport facies: new perspectives on flow processes from cores on the eastern North American margin. *Sedimentology*, 55(1): 97-136.
- Trudgill, B.D., 2011. Evolution of salt structures in the northern Paradox Basin: controls on evaporite deposition, salt wall growth and supra-salt stratigraphic architecture. *Basin Research*, 23(2): 208-238.
- Trudgill, B.D. et al., 1999. The Perdido fold belt, northwestern deep Gulf of Mexico; Part 1, Structural geometry, evolution and regional implications. *AAPG Bulletin*, 83(1): 88-113.
- TuJino, T. and Murakami, F., 2006. Changes in planview geometry and erosion-deposition patterns along a channel-levee complex in the southern corner of the Kurile Basin, Okhotsk Sea. *Marine Geology*, 230(1-2): 127-146.
- Urgeles, R., Locat, J. and Dugan, B., 2007. Recursive failure of the Gulf of Mexico continental slope: timing and causes. In: V. Lykousis, D. Sakellariou and J. Locat (Eds.), *Submarine Mass Movements and Their Consequences*. Springer, pp. 209-219.

- Van Der Merwe, W.C., Hodgson, D.M. and Flint, S.S., 2011. Origin and terminal architecture of a submarine slide: a case study from the Permian Vischkuil Formation, Karoo Basin, South Africa. *Sedimentology*, 58(7): 2012-2038.
- Van Hulten, F.F.N., 2010. Geological factors effecting compartmentalization of Rotliegend gas fields in the Netherlands. In: S.J. Jolley, Q.J. Fisher, R.B. Ainsworth, P. Vrolijk and S. Delisle (Eds.), *Reservoir Compartmentalization*. Geological Society Special Publication, Vol 347, pp. 301-315.
- Varnes, D.J., 1978. Slope movement types and processes. Transportation Research Board Special Report(176).
- Veeken, P.C.H., 2007. Seismic stratigraphy, basin analysis and reservoir characterisation, 37. Elsevier Science, 509 pp.
- Vendeville, B., 2002. A new interpretation of Trusheim's classic model of salt-diapir growth. *Gulf Coast Association of Geological Societies Transactions*, 52: 943-952.
- Vendeville, B.C., 2005. Salt tectonics driven by sediment progradation: Part I--Mechanics and kinematics. *AAPG Bulletin*, 89(8): 1071-1079.
- Vendeville, B.C. and Jackson, M.P.A., 1992a. The fall of diapirs during thin-skinned extension. *Marine and Petroleum Geology*, 9(4): 354-371.
- Vendeville, B.C. and Jackson, M.P.A., 1992b. The rise of diapirs during thin-skinned extension. *Marine and Petroleum Geology*, 9(4): 331-353.
- Walsh, J.J. and Watterson, J., 1988. Analysis of the relationship between displacements and dimensions of faults. *Journal of Structural Geology*, 10(3): 239-247.
- Wang, K.H., Cleveland, T.G., Fitzgerald, S. and Ren, X., 1996. Hydrodynamic flow modeling at confluence of two streams. *Journal of Engineering Mechanics*, 122: 994.
- Weaver, P.P.E., Wynn, R.B., Kenyon, N.H. and Evans, J., 2000. Continental margin sedimentation, with special reference to the north-east Atlantic margin. *Sedimentology*, 47(SUPPL. 1): 239-256.
- Weimer, P., 1990. Sequence stratigraphy, facies geometries, and depositional history of the Mississippi Fan, Gulf of Mexico. *AAPG Bulletin*, 74(4): 425-453.
- Weimer, P. and Shipp, C., 2004. Mass transport complex: musing on the past uses and suggestions for future directions, Offshore Technology Conference, Houston, Texas.
- Weimer, P. and Slatt, R.M., 2004. Petroleum systems of deepwater settings, 7. Soc of Exploration Geophysicists.



- Weimer, P., Slatt, R.M., Dromgoole, P., Bowman, M. and Leonard, A., 2000. Developing and Managing Turbidite Reservoirs: Case Histories and Experiences: Results of the 1998 EAGE/AAPG Research Conference. AAPG Bulletin, 84(4): 453-465.
- Welbon, A.I.F., Brockbank, P.J., Brunsden, D. and Olsen, T.S., 2007. Characterizing and producing from reservoirs in landslides: challenges and opportunities. In: S.J. Jolley, D. Barr, J.J. Walsh and R.J. Knipe (Eds.), Structurally Complex Reservoirs. Geological Society London, Special Publications 292, pp. 49-74.
- Winker, C.D. and Booth, J.R., 2000. Sedimentary Dynamics of the Salt-Dominated Continental Slope, Gulf of Mexico: Integration of observations from the seafloor, near-surface and deep subsurface, Deepwater Reservoirs of the World, GCSSEPM Foundation 20th Annual Research Conference.
- Wonham, J.P., Cyrot, M., Nguyen, T., Louhouamou, J. and Ruau, O., 2010. Integrated approach to geomodelling and dynamic simulation in a complex mixed siliciclastic–carbonate reservoir, N'Kossa field, Offshore Congo. In: S.J. Jolley, Q.J. Fisher, R.B. Ainsworth, P. Vrolijk and S. Delisle (Eds.), Reservoir Compartmentalization. Geological Society Special Publication, Vol 347, pp. 133-163.
- Wynn, R.B., Cronin, B.T. and Peakall, J., 2007. Sinuous deep-water channels: Genesis, geometry and architecture. Marine and Petroleum Geology, 24(6-9): 341-387.
- Wynn, R.B., Kenyon, N.H., Masson, D.G., Stow, D.A.V. and Weaver, P.P.E., 2002. Characterization and recognition of deep-water channel-lobe transition zones. Am. Assoc. Petrol. Geol. Bull., 86: 1441-1462.
- Yilmaz, Ö., 2001. Seismic data analysis, Vol. II. Investigations in Geophysics No. 10. Society of Exploration Geophysicists.
- Zhang, L. et al., 2010. Quantitative evaluation of synsedimentary fault opening and sealing properties using hydrocarbon connection probability assessment. AAPG Bulletin, 94(9): 1379-1399.

# Annexes

## **A1. Seismic acquisition and processing parameters of BES-2 survey**

### **Acquisition parameters**

Vessel: CGG Harmattan

Source: Airgun Dual

Shotpoint Interval: 25 m flip-flop

CMP xline: 25 metres

Group spacing: 12.5 m

Streamers: 6 x 5700 m

Record length: 8.0 sec

Sample interval: 2ms

Nominal fold: 56

### **Processing Sequence**

Reformat from SEG D

Navigation/seismic merge

Resample from 2 ms to 4 ms with anti-alias filter

Spherical divergence correction

“SPARN” – signal preserving attenuation of random noise and swell noise

Zero phase conversion using modelled far field signature

Q phase only compensation (referenced to water bottom)

FX shotpoint interpolation and radon multiple attenuation

3D Kirchhoff Bin centring DMO

3D V(c) pre-stack time migration using Stolt algorithm

0.5 Km grid Final velocity analysis

Full offset stack

Post stack demigration

Crossline FX trace interpolation

Zhimming Li steep dip one pass 3D time migration

### **Final Product**

Raw stack in SEG Y format

Raw migration in SEG Y format

Final stacking velocities in VelTape format

Final migration velocities in VelTape format

Migrated bin centre positions in UKOOA P1/90 format

Final report

## A2. Supplementary data for Chapter 4

Table A.1. Table with thickness of MTDs identified at each measuring point.

		inline	5640	5474	5308	5142	4976	4810	4644	4478	4312	4146	3980
		xline	Individual MTD thickness at each measurement point										
A1	7800		64	54	88	106	48	48	62	48	32	48	34
			76	78	38	42	36	26	32	52	38	42	40
			128	76	26	22	54	60	66	54	34	46	68
			88	38	84	82	42	72	26	66	50	104	80
				124	152	128	96	162	162		130		
	7720						138						
			88	52	60	120	78	46	68	68	26	144	122
			30	28	86	28	90	36	70	120	72	30	74
			30	58	56	26	28	104	80	106	38	52	94
			86	66	86	80	32	184	162		96	104	
	7640		68	32	144	144	94				140		
				120			150						
			44	48	76	120	50	48	44	52	50	40	106
			42	52	84	40	70	46	38	32	16	74	76
			38	42	66	54	50	32	69	18	60	26	78
	7560		108	68	90	60	186	64	168	102	48	52	
			24	110	46	126		178		80	54	82	
			56		102						44		
			18	44	36	82	86	152	86	32	40	22	138
			58	66	96	38	78	34	56	60	26	22	38
	7480		38	86	36	70	38	34	18	18	65	60	32
			106	116	56	124	30	62	52	112	31	62	88
			68	112	84		82	28	196	84	56	30	
					154		126	62			62	72	
								156			90		
	7400		82	70	52	34	78	74	96	12	22	72	100
			48	50	44	64	40	38	63	42	88	88	24
			78	58	66	36	22	90	34	102	112	112	44
			54	38	30	32	44	56	58	86	88		50
				54	34	76	78	148	106				
A2	7372		56	94	152	132							
			58	130									
			72										
			88	116	42	46	48	80	68	16	72	60	36
			62	38	34	74	42	44	34	44	62	64	76
			56	34	62	50	42	24	32	98	104	30	32
			124	80	32	46	32	74	44	88	94	78	54
				104	36	38	84	30	142			66	
					96	102	130	52					
					142	132		138					
			44	144	63	46	50	50	60	62	72	40	48
	7372		74	144	47	46	42	22	54	36	24	56	36
			56		26	32	30	80	20	96	32	92	48
			126		42	20	34	58	78	84	94	68	58
			98		60	84	82	132	36		146		
					134	142	144		136				

	7282	44	38	72	72	50	52		52	12	
		126		24	32	48	40	36		54	50
			84	40	54	76	38				52
			96	44	74	66	46				
				38	148	112	86				
			88								
			172								
	7202		54	96	52	70	50		46	44	
			52	42	72	24	34		32		
			42	66	40	70	34				
			66	46	36	76	58				
		108	34	80	136	78					
			72	136							
			66								
			50								
	7122		57	88	62	72	64		26	44	
			26	14	86	40	24		32		
			70	24	44	38	38				
			50	64	32	76	36				
		74	104	76	112	108					
		68	56	112							
			58								
	7042	38	36	56	90	82	28	70	46	58	
		76	90	92	64	114	74	30	72	52	
		60	40	32	26	26	32	32	46	58	
		86	52	66	48	42	28	46			
		80	94	66	80	56	96	104			
		106	104	116	74	120					
					132						
	6942	116	34	50	80	68	56	36	32	46	
		44	56	56	86	108	28	26	24	62	
		74	28	44	50	44	40	48	64	24	
			64	76	78	78	30	92	56		
			104	98	120	126	74				
		130			106						
A3	6893		62	44	74	76	74	60	58	14	
			74	46	72	94	66	26	28	40	
			136	40	40	38	30	62	20	64	
			156	122	120	42	78	112	44		
				100	102	74	130		20		
					134						
	6813		66	28	72	80	62	76	34	30	
			64	76	78	48	24	24	20	46	
			124	58	36	36	42	88	24	32	
			152	92	86	86	40	106	32	26	
				118	102	102	82		56		
						110		24			
6733		84	66	72	88	60	62	30	50		
		90	84	78	34	62	26	22	4		
		128	110	68	36	30	82	24	36		
		132	100	90	24	98	62	42	30		

				50	74	132		62			
					88			30			
	6653	52	78	100	88	88	60	26			
		42	60	88	38	44	44	58			
		66	98	60	40	96	36	46			
		126	116	82	30	86	104	46			
		118		106	50		76				
					90						
					100						
	6573	58	58	54	84	88	76	72	34		
		30	84	62	62	44	26	36	48		
		64	90	82	40	52	68	28	26		
		134	130	114	94	68	90	56	64		
		132			120	104		34	34		
	6493	58	38	56	78	86	80	36	40		
		40	66	92	30	46	54	46	74		
		66	80	68	62	40	18	24	76		
		118	92	86	76	40	112	56	32		
		104	120	110	86	80	78	22			
					90	132					
	6413	26	52	52	70	74	106	68	52	30	38
		80	34	52	68	74	48	36	32	42	42
		130	64	70	80	42	48	38	48	24	62
		114	132	96	104	90	74	42	50	54	70
			86	138	106	106	118	70	36	56	
								88			
A4	6339	78	52	40	48	74	98	86	50	58	40
		84	48	46	40	24	60	48	44	72	60
		140	66	50	62	86	52	82	36	32	66
		102	142	62	62	40	74	40	50	54	76
			66	106	78	96	110	70	46	68	
				108	114	104		112	26		
	6259	56	22	50	74	82	76	92	56	64	44
		30	52	60	56	36	56	118	96	74	50
		86	22	46	50	92	54	64	36	32	46
		138	62	42	52	110	72	66	46	22	66
		108	146	94	74		118	102	38	60	
			72	94	108				58	60	
	6179	32	32	20	48	34	76	90	66	56	44
		88	40	24	56	72	70	66	74	78	40
		92	38	119	36	48	108	40	36	64	60
		138	66	42	32	68	72	82	52	38	42
		104	120	22	74	102	106	100	46		66
			90	104	106				54		
				94							
	6099	38	38			38	50	76	88	52	60
		100	24			74	68	56	74	88	52
		86	30			24	54	24	44	50	56
		134	30			70	76	70	62	58	48
		98	68			106	104	86	54	46	
			94								
			78								

	6019	44		56	78	98	92	34	48	48
		68		104	90	54	50	70	46	26
		28		32	26	36	36	82	60	30
		46		66	90	90	52		66	48
		134		90	132	88	52			
		106					62			
	5939	88		46	70	78	88	20	54	60
		102		34	64	92	60	36	26	60
		38		62	18	34	62	60	58	32
		56		18	82	118	58	34	36	
		128		70	122	64	44			
		84		96						
	5859	70		24	96	86	96	26	50	50
		80		38	62	34	104	38	34	42
		40		46	92	34	32	18	52	100
		38		58	138	92	64	48	76	
		124		64		101	64	74		
		94								
	5793	92	44	30	80	78	78	54	52	34
		96	38	56	14	60	162	58	30	30
		32		24	52	24	48	34	46	40
		28		44	88	104	68		66	114
		132		58	94	86	70			
		94								

Table A.2. Unit 2 thickness at each measuring point.

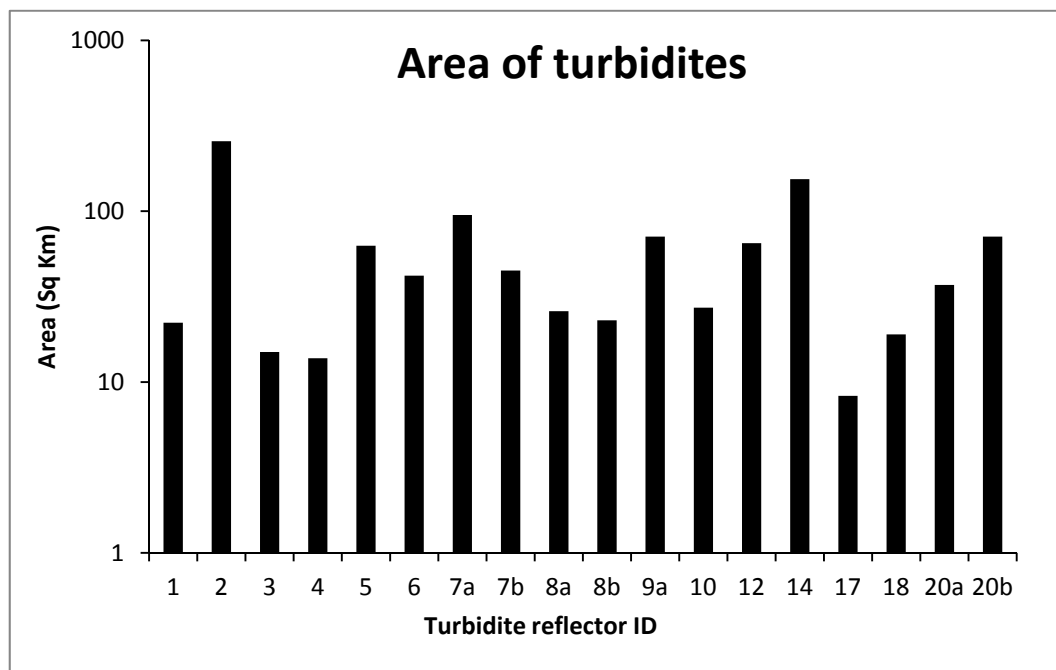
inline	5640	5474	5308	5142	4976	4810	4644	4478	4312	4146	3980	
xline	Unit Thickness (ms twtt)											
7800	558	639	578	632	656	682	730	692	682	660	648	A1
7720	614	610	652	636	678	646	714	662	636	598	574	
7640	624	590	622	592	656	640	660	610	614	540	566	
7560	608	608	642	558	618	646	658	604	482	530	580	
7480	590	614	616	578	608	634	526	548	560	553	462	
7400	592	578	612	612	526	594	490	546	542	474	394	
7372	612	564	624	634	536	566	504	637	580	466	376	A2
7282	464		606	666	546	594	510			438	358	
7202			608	640	580	562	520			346	200	
7122			622	622	588	450	482			252	308	
7042	598	698	608	610	608	506	360	444	466			
6942	478	660	618	604	590	548	444	478	458			
6893		674	614	602	596	552	412	436	472			A3
6813		684	608	566	582	564	424	474	460			
6733		660	580	540	578	540	492	492	460			
6653		648	604	578	570	534	502	460				
6573		616	592	562	552	562	506	468	476			
6493		556	574	570	498	592	500	340	456			
6413	540	542	576	550	544	580	514	410	452	442	366	A4
6339	582	534	534	532	546	556	520	454	456	436	348	
6259	576	512	512	532	548	530	536	490	476	446	382	
6179	632	594	560	548	564	528	536	482	448	428	390	
6099	606	572			530	556	498	510	446	422	382	
6019	598				482	562	536	482	432	408	380	
5939	594				476	532	524	470	310	386	394	
5859	582				476	574	542	530	362	404	432	
5793	596			454	478	546	538	490	368	402	412	
avg	581.26	607.65	598.27	583.39	563.33	569.48	525.11	508.71	482.35	454.26	418.53	

Average Unit Thickness per crossline											
	5640	5474	5308	5142	4976	4810	4644	4478	4312	4146	3980
A1	597.67	606.50	620.33	601.33	623.67	640.33	629.67	610.33	586.00	559.17	537.33
A2	538.00	640.67	614.33	629.33	574.67	537.67	470.00	519.67	501.33	375.50	310.50
A3	540.00	625.71	592.57	566.86	560.00	560.57	478.57	440.00	462.67	442.00	366.00
A4	595.75	553.00	535.33	516.50	512.50	548.00	528.75	488.50	412.25	416.50	390.00

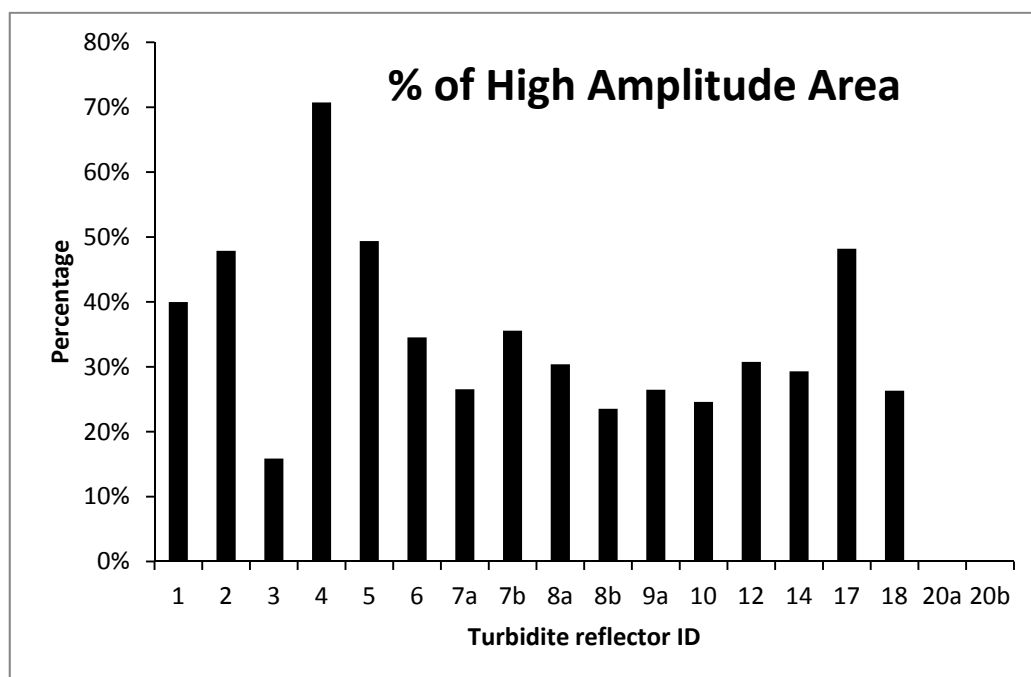


Table A.3. Percentage of MTDs in Unit 2 at each measuring point.

	inline	5640	5474	5308	5142	4976	4810	4644	4478	4312	4146	3980		
	xline	MTD percentage at each measurement point											average	
A1	7800	64%	58%	67%	60%	63%	54%	48%	32%	42%	36%	34%	50.7%	Average MTD proportion downslope (N-S orientation)
	7720	49%	58%	66%	63%	70%	57%	53%	44%	58%	55%	51%	56.8%	
	7640	50%	54%	75%	68%	54%	58%	48%	47%	44%	51%	46%	54.0%	
	7560	47%	70%	72%	56%	71%	82%	62%	51%	77%	51%	51%	62.7%	
	7480	44%	74%	73%	68%	65%	64%	68%	44%	55%	49%	47%	59.3%	
	7400	56%	64%	73%	80%	72%	74%	65%	45%	61%	63%	50%	63.9%	
A2	7372	65%	51%	60%	58%	71%	60%	76%	44%	63%	55%	51%	59.5%	
	7282	37%		40%	73%	73%	58%	51%			24%	32%	48.3%	
	7202			53%	74%	72%	67%	49%			23%	22%	51.2%	
	7122			55%	66%	70%	75%	56%			23%	14%	51.4%	
	7042	57%	60%	68%	70%	87%	75%	78%	37%	36%			63.0%	
	6942	49%	63%	52%	69%	72%	61%	45%	37%	29%			53.0%	
A3	6893		64%	57%	68%	77%	68%	63%	39%	25%			57.6%	
	6813		59%	61%	66%	60%	64%	69%	40%	29%			56.2%	
	6733		66%	62%	66%	60%	71%	47%	43%	26%			55.0%	
	6653		62%	58%	75%	76%	82%	64%	38%				65.2%	
	6573		68%	61%	56%	72%	63%	51%	48%	43%			57.9%	
	6493		69%	69%	62%	85%	58%	68%	54%	49%			64.4%	
	6413	65%	68%	71%	78%	71%	68%	67%	53%	46%	48%	19%	59.3%	
A4	6339	69%	70%	77%	76%	78%	71%	84%	56%	62%	56%	25%	65.8%	
	6259	73%	73%	75%	78%	58%	71%	82%	67%	66%	46%	32%	65.7%	
	6179	72%	65%	76%	64%	57%	82%	71%	68%	53%	43%	43%	63.1%	
	6099	75%	63%			59%	63%	63%	63%	66%	51%	40%	60.4%	
	6019	71%				72%	74%	68%	71%	43%	54%	40%	61.8%	
	5939	84%				68%	67%	74%	66%	48%	45%	39%	61.4%	
	5859	77%				48%	68%	64%	68%	56%	52%	44%	59.7%	
	5793	80%			18%	44%	60%	65%	87%	40%	48%	53%	55.0%	
		Average MTD proportion- slope strike (W-E orientation)												
		62%	64%	65%	66%	68%	67%	63%	52%	49%	46%	39%		



**Figure A.1.** Plot representing the area of individual turbidites in Unit 2.



**Figure A.2.** Plot representing the percentage of high-amplitude areas in relation to the total area of individual turbidites in Unit 2.

## A3. Supplementary data for Chapter 5

Table A.4. Table with block measurement data and deformation style.

Nr	Zone	Area (sq Km)	Length (metres)	Width (metres)	Height (metres)	W/L Ratio	Deformation style
1	1	0.22	663.69	576.17	107.10	0.87	1
2	1	0.94	1868.53	1029.35	170.10	0.55	1
3	1	0.09	579.43	213	107.10	0.37	2
4	1	0.08	302.62	213.68	86.10	0.71	3
5	1	0.07	342.37	321.69	86.10	0.94	3
6	1	0.03	369.39	172.52	88.20	0.47	3
7	1	0.05	361	221	69.30	0.61	3
8	1	0.24	770.4	336.17	73.50	0.44	3
9	1	1.56	1391	1350	105.00	0.97	2
10	1	0.56	1028.01	727.86	117.60	0.71	1
11	1	0.10	566.55	285.49	73.50	0.50	3
12	1	1.90	1675.37	1484.06	107.10	0.89	2
13	1	0.21	629.34	478.48	54.60	0.76	2
14	1	0.97	1037.99	1024.66	134.40	0.99	2
15	1	0.84	1076.95	632.25	113.40	0.59	1
16	1	0.27	663.69	517.56	100.80	0.78	1
17	1	0.09	449.36	257.67	90.30	0.57	3
18	1	0.05	385.76	171.19	52.50	0.44	2
19	1	0.38	629.34	620.55	132.30	0.99	1
20	1	0.23	544.71	356.14	105.00	0.65	2
21	1	0.13	457.44	270.67	90.30	0.59	2
22	1	0.31	773.01	584.06	46.20	0.76	1
23	1	0.50	796	738	102.90	0.93	3
24	1	0.59	1120	620	75.60	0.55	3
25	1	0.45	1091.11	724.07	107.10	0.66	2
26	1	0.32	1098.01	326.63	52.50	0.30	3
27	1	0.47	767.07	612.76	155.40	0.80	1
28	1	0.08	306	304	107.10	0.99	1
29	1	0.16	561.68	528.5	65.10	0.94	1
30	1	0.29	841.37	332.19	101.85	0.39	2
31	1	0.38	802.08	503.66	86.10	0.63	1
32	1	1.18	1591.52	1111.07	115.50	0.70	2
33	1	0.30	745.26	488.42	81.90	0.66	3
34	1	0.36	605.24	492.63	94.50	0.81	1
35	1	0.11	540.07	220.31	90.30	0.41	1
36	1	0.62	961.74	744.34	100.80	0.77	1
37	1	0.17	492.16	345.04	71.40	0.70	1
38	1	0.22	666.45	445.27	54.60	0.67	3

Nr	Zone	Area (sq Km)	Length (metres)	Width (metres)	Height (metres)	W/L Ratio	Deformation style
39	1	0.28	965.06	192.59	44.10	0.20	1
40	1	0.13	492.16	306.38	52.50	0.62	1
41	1	1.17	1605.02	978.33	71.40	0.61	3
42	1	0.10	411.05	402.04	84.00	0.98	3
43	1	0.38	841.37	478.48	100.80	0.57	3
44	1	0.68	1456.5	643.38	100.80	0.44	1
45	1	0.91	1422.64	857	107.10	0.60	2
46	1	0.27	654.66	374.32	100.80	0.57	1
47	1	0.34	804.36	650.8	113.40	0.81	1
48	1	0.09	499.55	155.78	56.70	0.31	1
49	1	0.06	552.23	249.55	67.20	0.45	1
50	1	0.24	787.39	398.03	102.90	0.51	3
51	1	0.24	617.59	536.67	105.00	0.87	3
52	1	0.35	882.28	469.3	52.50	0.53	1
53	1	0.18	506.74	469.78	65.10	0.93	3
54	1	0.28	726.91	439.06	88.20	0.60	2
55	1	0.23	908.36	334.25	105.00	0.37	1
56	1	0.10	626.43	192.58	79.80	0.31	3
57	1	0.25	623.13	439.06	75.60	0.70	2
58	1	0.16	558	239.24	90.30	0.43	1
59	1	0.19	471.25	364.4	78.75	0.77	1
60	1	0.24	664.73	365.65	121.80	0.55	1
61	1	0.17	545.55	453.93	88.20	0.83	2
62	1	0.15	492	256	63.00	0.52	1
63	1	0.15	470.76	408.81	119.70	0.87	3
64	2	0.15	616.11	392.82	96.60	0.64	1
65	2	0.23	701	398.03	100.80	0.57	3
66	2	0.07	242	181	94.50	0.75	1
67	2	0.09	379.18	250.46	90.30	0.66	1
68	2	0.21	526.33	441.14	102.90	0.84	1
69	2	0.20	536.67	513.56	73.50	0.96	3
70	2	0.53	973.33	646.92	165.90	0.66	1
71	2	0.23	671.59	436.44	77.70	0.65	3
72	2	0.10	670	210.75	69.30	0.31	3
73	2	0.12	514.01	278.18	79.80	0.54	3
74	2	0.35	578.15	545.55	86.10	0.94	3
75	2	0.31	633.69	507.28	98.70	0.80	1
76	2	0.15	670.22	382.78	79.80	0.57	1
77	2	0.37	830.96	469.3	96.60	0.56	3
78	2	0.21	602.58	480.87	102.90	0.80	1
79	2	0.48	1050.48	534.96	77.70	0.51	3
80	2	0.18	558	366.28	102.90	0.66	1
81	2	0.25	650.81	332.19	92.40	0.51	1

Nr	Zone	Area (sq Km)	Length (metres)	Width (metres)	Height (metres)	W/L Ratio	Deformation style
82	2	0.65	1211.98	518	119.70	0.43	3
83	2	0.33	890.54	701	107.10	0.79	2
84	2	0.33	680	524.59	35.70	0.77	2
85	2	0.25	594	365	65.10	0.61	2
86	2	0.21	514	457.44	111.30	0.89	2
87	2	0.65	1674	459.44	60.90	0.27	3
88	2	0.50	1520.64	451.4	81.90	0.30	3
89	2	0.14	385.76	338.34	71.40	0.88	2
90	2	0.41	1016.6	421.5	119.70	0.41	1
91	2	0.23	882.8	338.34	107.10	0.38	3
92	2	0.13	480.87	419.43	153.30	0.87	1
93	2	0.23	874.19	200	75.60	0.23	2
94	2	0.30	642.3	475.12	84.00	0.74	1
95	2	0.18	555.12	398.03	138.60	0.72	1
96	2	0.17	508.63	345.04	94.50	0.68	2
97	2	0.12	421.5	348.34	98.70	0.83	1
98	2	0.58	1263.85	708.73	69.30	0.56	3
99	2	0.60	1183.7	521.08	63.00	0.44	3
100	2	0.37	665.76	500	50.40	0.75	3
101	2	0.18	581.31	440.62	92.40	0.76	2
102	2	0.27	623.86	449.87	90.30	0.72	2
103	2	0.44	961.74	469.3	107.10	0.49	2
104	2	0.49	1196.2	641.95	123.90	0.54	2
105	2	0.30	1104.45	334.25	79.80	0.30	3
106	2	0.41	855.93	655.01	98.70	0.77	2
107	2	0.46	1109.83	564.93	77.70	0.51	3
108	2	0.11	608.63	231.46	77.70	0.38	2
109	2	0.19	707.44	358.7	86.10	0.51	1
110	2	0.72	1523.5	548.06	88.20	0.36	1
111	2	0.25	569.77	364.4	105.00	0.64	1
112	2	0.14	441.14	440.62	94.50	1.00	2
113	2	0.59	1057	545.55	105.00	0.52	2
114	2	0.37	848.68	515.34	60.90	0.61	2
115	2	0.17	501.38	408.81	138.60	0.82	1
116	2	0.14	492.16	236.35	96.60	0.48	3
117	2	2.28	2418.67	819.03	98.70	0.34	3
118	2	0.10	423.67	279	88.20	0.66	3
119	2	0.17	719.31	478.48	88.20	0.67	3
120	2	0.26	837	291.05	73.50	0.35	3
121	2	0.25	719	440.62	77.70	0.61	2
122	2	0.40	959.11	514.45	88.20	0.54	3
123	2	0.27	803.22	394.57	111.30	0.49	2
124	2	0.26	655.01	451.4	107.10	0.69	1

Nr	Zone	Area (sq Km)	Length (metres)	Width (metres)	Height (metres)	W/L Ratio	Deformation style
125	2	0.62	1504	485.13	102.90	0.32	3
126	2	0.17	574.97	338.34	65.10	0.59	3
127	2	0.33	792.03	501.38	130.20	0.63	1
128	2	0.20	515.34	334.25	92.40	0.65	1
129	2	0.27	671.92	424.74	81.90	0.63	2
130	2	0.33	778.91	487.96	77.70	0.63	1
131	2	0.13	541.76	323.82	105.00	0.60	2
132	2	0.76	1092.15	898.73	111.30	0.82	3
133	2	0.12	626.43	192.58	39.90	0.31	1
134	2	0.04	235.38	109.1	54.60	0.46	2
135	2	0.64	1002.99	497.71	126.00	0.50	1
136	2	0.18	608.26	380.99	73.50	0.63	2
137	2	0.20	778.91	338.34	109.20	0.43	1
138	2	0.10	473	321	75.60	0.68	1
139	2	0.24	576.1	536.67	115.50	0.93	3
140	2	0.38	635	599	123.90	0.94	2
141	2	0.20	517.26	469	79.80	0.91	2
142	2	0.29	959.11	257.67	56.70	0.27	2
143	2	0.19	814.82	422.04	58.80	0.52	2
144	2	0.23	959.11	297.28	52.50	0.31	2
145	3	0.33	956.96	306.38	39.90	0.32	2
146	3	0.84	1028.42	1027.34	105.00	1.00	2
147	3	0.30	632.25	499	107.10	0.79	3
148	3	0.15	534.96	342	96.60	0.64	3
149	3	0.27	846.52	430.63	113.40	0.51	2
150	3	0.20	671.58	368.15	123.90	0.55	1
151	3	0.54	1028.9	719.32	94.50	0.70	1
152	3	0.27	771.53	472.7	98.70	0.61	2
153	3	0.62	1121.32	485.13	77.70	0.43	3
154	3	0.33	682.4	569.77	84.00	0.83	2
155	3	0.21	534	243.9	56.70	0.46	1
156	3	0.52	1066	546.8	71.40	0.51	3
157	3	0.13	675.66	227.47	94.50	0.34	2
158	3	0.22	991.28	287.09	92.40	0.29	1
159	3	0.18	708.73	315.94	31.50	0.45	1
160	3	1.00	1292.79	1129.86	121.80	0.87	2
161	3	0.31	645.15	596.09	132.30	0.92	2
162	3	0.31	796.35	453.42	111.30	0.57	2
163	3	0.15	514.01	250	113.40	0.49	2
164	3	0.37	736.3	487.96	100.80	0.66	3
165	3	0.64	1009.36	599.54	58.80	0.59	1
166	3	0.25	517.56	462.92	75.60	0.89	3
167	3	0.95	1455.24	844.08	117.60	0.58	2

Nr	Zone	Area (sq Km)	Length (metres)	Width (metres)	Height (metres)	W/L Ratio	Deformation style
168	3	0.26	582.1	430	77.70	0.74	3
169	3	0.10	457.44	279	98.70	0.61	2
170	3	0.21	617.59	320.61	98.70	0.52	2
171	3	0.35	731.3	517.56	81.90	0.71	2
172	3	0.10	590.3	287.09	69.30	0.49	3

**Table A.5.** Table with location, size, perpendicular distance to salt ridge axis and deformation style of the studied blocks. Negative distances are indicative of westward position in relation to the ridge axis, positive distance values are eastward positions.

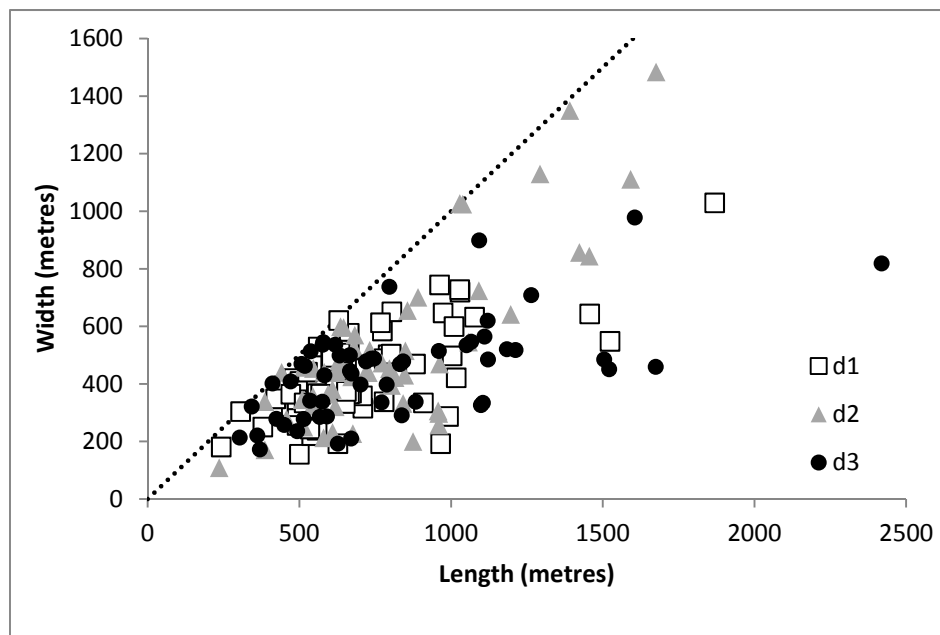
Inline	Crossline	Area (sq Km)	W/L Ratio	Height (m)	Distance to salt axis (m)	Deformation Style
7092	5218	0.22	0.29	136.4	6168	1
6983	5402	0.62	0.43	114.7	3624	3
6787	5367	0.84	1.00	155	2853	2
6960	5454	0.27	0.61	145.7	2818	2
6833	5437	0.30	0.79	158.1	2563	3
6885	5442	0.27	0.51	167.4	2552	2
6837	5451	0.15	0.64	142.6	2212	3
7010	5540	0.33	0.83	124	2171	2
7439	5770	0.10	0.61	145.7	1614	2
7390	5796	0.25	0.89	111.6	1099	3
7222	5736	1.00	0.87	179.8	941	2
7316	5794	0.37	0.66	148.8	718	3
7238	5802	0.31	0.92	195.3	425	2
7390	5860	0.95	0.58	173.6	418	2
7257	5816	0.15	0.49	167.4	195	2
7470	5976	0.21	0.52	145.7	-576	2
7474	6216	0.35	0.71	120.9	-3275	2
7402	6271	0.26	0.74	114.7	-4335	3
7241	6216	0.31	0.57	164.3	-4372	2
7320	6271	0.64	0.59	86.8	-4651	1
7203	6246	0.18	0.45	46.5	-5028	1
7082	6274	0.13	0.34	139.5	-5949	2
7059	6272	0.21	0.46	83.7	-5967	1
7000	6280	0.10	0.49	102.3	-6233	3
6885	6224	0.20	0.55	182.9	-6557	1
6938	6278	0.54	0.70	139.5	-6686	1
7059	6344	0.52	0.51	105.4	-6810	3
6764	6368	0.33	0.32	58.9	-8579	2
5861	4728	0.09	0.66	133.3	5608	1
6387	4904	0.25	0.61	114.7	6225	2
6472	4990	0.20	0.65	136.4	5697	1
6036	4825	0.65	0.43	176.7	5630	3
6224	4910	0.41	0.77	145.7	5411	2
6606	5086	0.10	0.68	111.6	5261	1
5876	4782	0.53	0.66	244.9	5176	1
5823	4774	0.23	0.57	148.8	5042	3
6082	4894	0.33	0.79	158.1	4933	2
6631	5128	0.38	0.94	182.9	4920	2
6631	5178	0.20	0.91	117.8	4420	2
6082	4958	0.33	0.77	52.7	4113	2



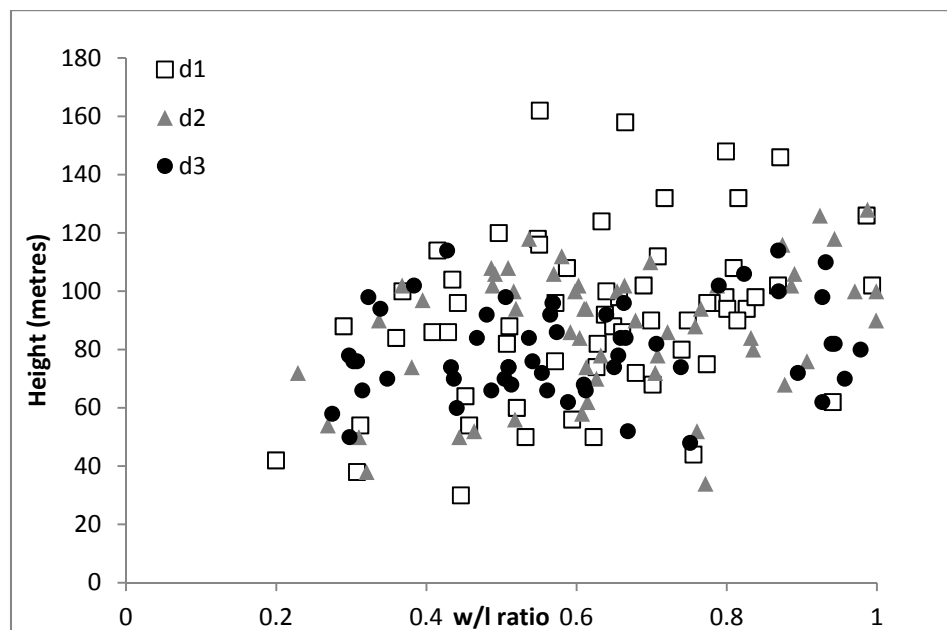
6387	5110	0.40	0.54	130.2	3878	3
6537	5254	0.64	0.50	186	3157	1
6330	5158	0.59	0.52	155	3036	2
6407	5056	0.62	0.32	151.9	2529	3
5916	5026	0.10	0.31	102.3	2523	3
6082	5126	0.25	0.61	96.1	2244	2
6441	5258	0.17	0.59	96.1	2244	3
6560	5346	0.18	0.63	108.5	2084	2
6224	5200	0.46	0.51	114.7	2045	3
6606	5364	0.24	0.93	170.5	2004	3
6664	5406	0.19	0.52	86.8	1906	2
6486	5332	0.33	0.63	114.7	1904	1
6330	5286	0.37	0.61	89.9	1704	2
6147	5236	0.13	0.87	226.3	1233	1
6441	5398	0.33	0.63	192.2	931	1
6082	5242	0.21	0.89	164.3	801	2
6387	5406	0.27	0.49	164.3	531	2
6269	5364	0.19	0.51	127.1	380	1
6202	5340	0.37	0.75	74.4	292	3
6486	5482	0.13	0.60	155	242	2
6560	5520	0.20	0.43	161.2	112	1
6486	5616	0.76	0.82	164.3	-1534	3
6155	5534	0.23	0.23	111.6	-2296	2
6330	5646	0.17	0.82	204.6	-2537	1
6155	5594	0.30	0.74	124	-2787	1
6013	5540	0.18	0.66	151.9	-2835	1
6361	5716	0.10	0.66	130.2	-3187	3
6013	5576	0.25	0.51	136.4	-3316	1
6209	5674	0.18	0.76	136.4	-3430	2
5939	5598	0.35	0.94	127.1	-3888	3
6300	5764	0.25	0.64	155	-3930	1
6001	5634	0.21	0.80	151.9	-3998	1
6155	5756	0.18	0.72	204.6	-4571	1
6117	5740	0.14	0.88	105.4	-4671	2
6269	5800	0.72	0.36	130.2	-4690	1
6312	5830	0.14	1.00	139.5	-4720	2
6397	5878	0.26	0.69	158.1	-4818	3
6255	5822	0.11	0.38	114.7	-4870	2
6209	5798	0.27	0.72	133.3	-4930	2
6155	5808	0.17	0.68	139.5	-5071	2
6330	5878	0.14	0.48	142.6	-5101	1
6117	5780	0.41	0.41	176.7	-5200	1
5939	5710	0.31	0.80	145.7	-5241	1
5861	5678	0.21	0.84	151.9	-5264	1
6361	5908	0.17	0.67	130.2	-5373	3
6209	5856	0.44	0.49	158.1	-5521	2

6155	5850	0.12	0.83	145.7	-5674	1
5939	5750	0.15	0.57	117.8	-5717	1
5861	5718	0.20	0.96	108.5	-5758	3
6361	5944	0.26	0.35	108.5	-5803	3
6209	5896	0.49	0.54	182.9	-5915	2
6117	5848	0.23	0.38	158.1	-5935	3
5885	5758	0.23	0.65	114.7	-6105	3
6476	6038	0.27	0.63	120.9	-6287	2
5939	5804	0.37	0.56	142.6	-6333	3
5933	5836	0.12	0.54	117.8	-6634	3
5851	5798	0.07	0.75	139.5	-6693	1
6360	6045	2.28	0.34	145.7	-6770	3
6723	6198	0.23	0.31	77.5	-6952	2
6663	6202	0.29	0.27	83.7	-7188	2
6536	6112	0.04	0.46	80.6	-7369	2
6504	6146	0.12	0.31	58.9	-7385	1
6155	6030	0.58	0.56	102.3	-7705	3
6085	6022	0.65	0.27	89.9	-8127	3
6110	6038	0.50	0.30	120.9	-8162	3
6209	6092	0.30	0.30	117.8	-8237	3
6155	6072	0.60	0.44	93	-8246	3
6001	6176	0.48	0.51	114.7	-10211	3
5797	4688	0.15	0.52	93	-5782	1
5159	5228	0.38	0.99	195.3	-3527	1
4959	4971	0.22	0.87	158.1	-4222	1
5805	4824	0.15	0.87	176.7	-4351	3
5007	5228	1.56	0.97	155	-4352	2
5627	5490	0.19	0.77	116.25	-4400	1
5430	5426	0.09	0.31	83.7	-4489	1
5466	5450	0.35	0.53	77.5	-4619	1
5269	5388	0.30	0.66	120.9	-4799	3
5007	5274	0.56	0.71	173.6	-4901	1
5240	5406	0.38	0.63	127.1	-5190	1
4959	5294	0.94	0.55	251.1	-5310	1
5257	5436	1.18	0.70	170.5	-5501	2
5336	5472	0.10	0.98	124	-5521	3
5310	5460	0.28	0.20	65.1	-5536	1
5159	5400	0.23	0.65	155	-5632	2
5817	5710	0.15	0.64	142.6	-5684	1
5393	5514	0.68	0.44	148.8	-5721	1
5007	5358	0.10	0.50	108.5	-5876	3
5269	5502	0.11	0.41	133.3	-6155	1
5174	5472	0.47	0.80	229.4	-6212	1
5393	5566	0.91	0.60	158.1	-6324	2
5209	5502	0.29	0.39	150.35	-6433	2
5007	5410	1.90	0.89	158.1	-6493	2

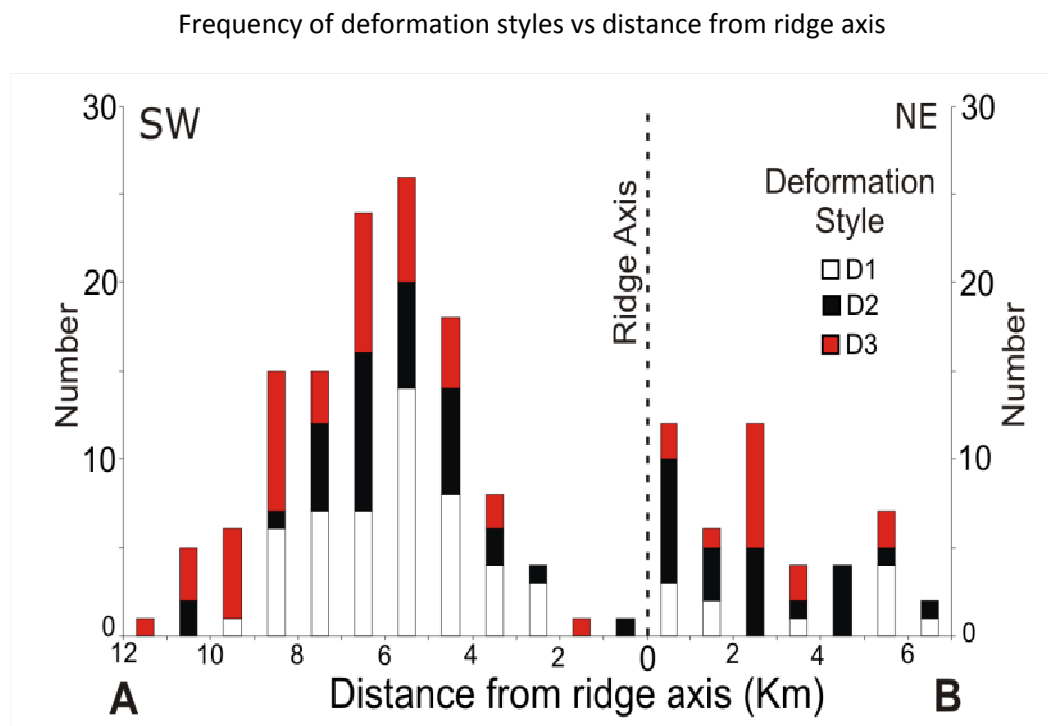
5336	5572	0.38	0.57	148.8	-6593	3
5007	5418	0.21	0.76	80.6	-6647	2
4959	5408	0.09	0.37	158.1	-6709	2
5269	5450	0.36	0.81	139.5	-6746	1
5159	5508	0.13	0.59	133.3	-6805	2
5007	5456	0.97	0.99	198.4	-6904	2
5269	5568	0.62	0.77	148.8	-6924	1
5466	5642	0.18	0.93	96.1	-6975	3
5430	5640	0.06	0.45	99.2	-7055	1
5393	5648	0.27	0.57	148.8	-7167	1
5269	5594	0.17	0.70	105.4	-7209	1
5310	5610	0.13	0.62	77.5	-7345	1
5627	5616	0.24	0.55	179.8	-7505	1
4959	5488	0.08	0.71	127.1	-7568	3
5466	5720	0.28	0.60	130.2	-7759	2
5540	5774	0.25	0.70	111.6	-7862	2
5430	5728	0.24	0.51	151.9	-7923	3
5159	5622	0.31	0.76	68.2	-7956	1
5659	5840	0.17	0.83	130.2	-7998	2
5191	5638	0.16	0.94	96.1	-8078	1
5393	5726	0.34	0.81	167.4	-8120	1
5584	5818	0.16	0.43	133.3	-8148	1
4959	5534	0.07	0.94	127.1	-8176	3
5007	5568	0.84	0.59	167.4	-8307	1
5269	5696	0.22	0.67	80.6	-8338	3
5466	5770	0.23	0.37	155	-8341	1
5310	5724	1.17	0.61	105.4	-8576	3
5466	5794	0.10	0.31	117.8	-8657	3
5180	5695	0.08	0.99	158.1	-8909	1
5007	5654	0.27	0.78	148.8	-9062	1
5430	5848	0.24	0.87	155	-9329	3
5159	5726	0.50	0.93	151.9	-9354	3
5159	5738	0.59	0.55	111.6	-9482	3
5007	5684	0.09	0.57	133.3	-9653	3
4959	5684	0.03	0.47	130.2	-9873	3
5007	5738	0.05	0.44	77.5	-10220	2
5159	5810	0.45	0.66	158.1	-10254	2
4959	5728	0.05	0.61	102.3	-10338	3
5159	5814	0.32	0.30	77.5	-10483	3
4959	5850	0.24	0.44	108.5	-11549	3



**Figure A.3.** Plot representing width and length of deformed blocks. D1=low deformation, D2=moderate deformation, D3= Major deformation.



**Figure A.4.** Plot with height and W/L ratio of deformed blocks. D1=low deformation, D2=moderate deformation, D3= Major deformation.



**Figure A.5.** Plot representing the frequency of variably deformed blocks and the distance from the diapir ridge axis. D1=low deformation, D2=moderate deformation, D3= Major deformation.

## A4. Supplementary data for Chapter 6

**Table A.6.** Table with location, area and unit ID, and morphometric parameters of each CP identified in the Neogene stratigraphic units.

(N-S)	X (E-W)	Area	Unit	Width (m)	Height (m)	Depth (mbsl)	Burial depth (m)	W/H ratio
1	1304	1	3a (C1)	950	71,40	1899,8	792,2	13,31
1	1002	1	3a (C1)	1300	86,70	1861,96	768,4	14,99
1	726	1	3a (C1)	1150	59,50	1806,82	742,9	19,33
1	1200	1	3a (C1)	700	71,40	1849,16	669,8	9,80
10	1308	1	3a (C1)	1350	76,50	1904,34	790,5	17,65
10	1010	1	3a (C1)	1175	93,50	1873,02	770,1	12,57
10	728	1	3a (C1)	1075	64,60	1808,24	741,2	16,64
10	1200	1	3a (C1)	600	68,00	1845,92	649,4	8,82
20	1014	1	3a (C1)	1200	115,60	1896,26	787,1	10,38
20	1310	1	3a (C1)	650	51,00	1895,7	780,3	12,75
20	742	1	3a (C1)	1075	59,50	1816,04	741,2	18,07
20	1204	1	3a (C1)	450	56,10	1841,54	634,1	8,02
30	1308	1	3a (C1)	650	83,30	1922,34	800,7	7,80
30	1022	1	3a (C1)	1250	110,50	1895,7	780,3	11,31
30	748	1	3a (C1)	1625	68,00	1825,12	737,8	23,90
30	1206	1	3a (C1)	425	66,30	1853,58	647,7	6,41
40	1308	1	3a (C1)	975	88,40	1923,62	797,3	11,03
40	1028	1	3a (C1)	1175	95,20	1894,86	770,1	12,34
40	758	1	3a (C1)	1500	69,70	1834,04	751,4	21,52
40	1204	1	3a (C1)	575	73,10	1855,14	647,7	7,87
50	1308	1	3a (C1)	900	100,30	1925,18	797,3	8,97
50	1030	1	3a (C1)	1225	102,00	1894,3	763,3	12,01
50	750	1	3a (C1)	1425	74,80	1840,42	753,1	19,05
50	1202	1	3a (C1)	575	74,80	1865,2	656,2	7,69
60	1203	1	3a (C1)	925	102,00	1949,58	855,7	9,07
60	1044	1	3a (C1)	1250	95,20	1887,5	756,5	13,13
60	750	1	3a (C1)	1250	76,50	1851,92	741,2	16,34
60	1198	1	3a (C1)	675	96,90	1886,16	683,4	6,97
70	1304	1	3a (C1)	1375	139,40	1955,22	821,1	9,86
70	1048	1	3a (C1)	1225	68,00	1888,36	748	18,01
70	766	1	3a (C1)	1575	77,35	1839,32	720,8	20,36
70	1200	1	3a (C1)	725	113,90	1906,14	698,7	6,37
80	1298	1	3a (C1)	1100	113,90	1934,68	799	9,66
80	1056	1	3a (C1)	1175	88,40	1901,12	751,4	13,29
80	768	1	3a (C1)	1275	69,70	1848,68	720,8	18,29
80	1202	1	3a (C1)	625	108,80	1909,38	719,1	5,74
90	1290	1	3a (C1)	1200	124,10	1956,36	816	9,67
90	1064	1	3a (C1)	1375	69,70	1901,54	756,5	19,73
90	776	1	3a (C1)	1050	73,10	1856,32	737,8	14,36
90	1208	1	3a (C1)	650	105,40	1918,02	729,3	6,17
100	1292	1	3a (C1)	1175	105,40	1937,52	795,6	11,15

(N-S)	X (E-W)	Area	Unit	Width (m)	Height (m)	Depth (mbsl)	Burial depth (m)	W/H ratio
100	1066	1	3a (C1)	1150	74,80	1909,06	753,1	15,37
100	1208	1	3a (C1)	450	96,90	1913,62	732,7	4,64
100	776	1	3a (C1)	950	61,20	1852,36	727,6	15,52
110	1286	1	3a (C1)	1050	103,70	1937,52	795,6	10,13
110	1070	1	3a (C1)	1350	44,20	1912,18	753,1	30,54
110	1206	1	3a (C1)	675	86,70	1904,24	751,4	7,79
110	778	1	3a (C1)	800	56,10	1857,46	732,7	14,26
120	1190	1	3a (C1)	1100	115,60	1950,56	802,4	9,52
120	1076	1	3a (C1)	1050	71,40	1921,4	751,4	14,71
120	1194	1	3a (C1)	575	76,50	1927,08	744,6	7,52
120	782	1	3a (C1)	950	47,60	1857,6	734,4	19,96
130	1276	1	3a (C1)	950	115,60	1951,98	800,7	8,22
130	1082	1	3a (C1)	1550	66,30	1924,66	753,1	23,38
130	1192	1	3a (C1)	600	74,80	1924,75	735,25	8,02
130	794	1	3a (C1)	1175	44,20	1859,88	724,2	26,58
140	1274	1	3a (C1)	900	117,30	1961,48	802,4	7,67
140	1090	1	3a (C1)	1200	52,70	1928,78	746,3	22,77
140	794	1	3a (C1)	1200	54,40	1878,58	742,9	22,06
140	1192	1	3a (C1)	750	103,70	1924,54	732,7	7,23
150	1268	1	3a (C1)	900	127,50	1977,92	812,6	7,06
150	1096	1	3a (C1)	1100	39,10	1929,76	758,2	28,13
150	790	1	3a (C1)	900	59,50	1883,68	748	15,13
150	1184	1	3a (C1)	725	95,20	1932,76	737,8	7,62
160	1264	1	3a (C1)	800	100,30	1950,72	785,4	7,98
160	800	1	3a (C1)	800	74,80	1922,22	780,3	10,70
160	1098	1	3a (C1)	1025	42,50	1934,44	758,2	24,12
160	1178	1	3a (C1)	625	79,90	1934,18	736,1	7,82
170	1260	1	3a (C1)	975	115,60	1963,9	793,9	8,43
170	1102	1	3a (C1)	1325	57,80	1939,4	761,6	22,92
170	796	1	3a (C1)	1125	79,90	1906,5	759,9	14,08
170	1174	1	3a (C1)	525	74,80	1934,46	739,5	7,02
180	1256	1	3a (C1)	925	91,80	1972,12	799	10,08
180	1104	1	3a (C1)	1350	56,10	1940,54	756,5	24,06
180	800	1	3a (C1)	925	73,10	1910,48	751,4	12,65
180	1172	1	3a (C1)	500	54,40	1932,2	731	9,19
190	1238	1	3a (C1)	1100	68,00	1964,06	776,9	16,18
190	1112	1	3a (C1)	850	57,80	1951,46	756,5	14,71
190	804	1	3a (C1)	750	66,30	1916,72	751,4	11,31
200	1156	1	3a (C1)	1425	137,70	2018,2	809,2	10,35
200	796	1	3a (C1)	750	59,50	1918	748	12,61
210	1164	1	3a (C1)	1425	130,90	2036,9	827,9	10,89
210	800	1	3a (C1)	800	34,00	1901,44	717,4	23,53
220	1160	1	3a (C1)	1600	134,30	2041,58	827,9	11,91
220	794	1	3a (C1)	850	45,90	1906,26	719,1	18,52
230	1158	1	3a (C1)	1725	122,40	2038,6	829,6	14,09
230	796	1	3a (C1)	800	52,70	1912,24	697	15,18
240	1154	1	3a (C1)	1475	130,90	2040,44	833	11,27
240	798	1	3a (C1)	650	45,05	1915,22	695,3	14,43

(N-S)	X (E-W)	Area	Unit	Width (m)	Height (m)	Depth (mbsl)	Burial depth (m)	W/H ratio
250	1158	1	3a (C1)	1350	110,50	2021,46	810,9	12,22
250	802	1	3a (C1)	725	45,90	1918,86	739,5	15,80
260	1146	1	3a (C1)	1225	74,80	2004,46	793,9	16,38
260	808	1	3a (C1)	850	54,40	1928,36	741,2	15,63
270	1146	1	3a (C1)	975	76,50	2007,58	793,9	12,75
270	806	1	3a (C1)	750	54,40	1931,06	736,1	13,79
280	1144	1	3a (C1)	975	71,40	2003,36	761,6	13,66
280	808	1	3a (C1)	575	49,30	1933,48	727,6	11,66
290	1152	1	3a (C1)	900	71,40	2003,2	778,6	12,61
290	810	1	3a (C1)	725	52,70	1939,44	724,2	13,76
300	1148	1	3a (C1)	925	90,10	2015,24	792,2	10,27
300	818	1	3a (C1)	900	39,10	1940,72	720,8	23,02
310	1160	1	3a (C1)	875	47,60	1982,94	759,9	18,38
310	816	1	3a (C1)	1025	47,60	1946,96	720,8	21,53
320	1164	1	3a (C1)	800	71,40	2001,5	776,9	11,20
320	822	1	3a (C1)	1050	40,80	1948,68	703,8	25,74
330	1166	1	3a (C1)	900	49,30	1996,12	768,4	18,26
330	830	1	3a (C1)	825	42,50	1955,06	705,5	19,41
340	1182	1	3a (C1)	975	40,80	1987,06	753,1	23,90
340	834	1	3a (C1)	725	42,50	1959,78	668,1	17,06
350	1182	1	3a (C1)	850	47,60	1992,6	744,6	17,86
350	836	1	3a (C1)	750	52,70	1967,04	642,6	14,23
360	1180	1	3a (C1)	1125	42,50	1989,2	741,2	26,47
360	840	1	3a (C1)	650	56,10	1968,6	642,6	11,59
370	1188	1	3a (C1)	1150	36,55	1983,14	705,5	31,46
370	838	1	3a (C1)	800	47,60	1972,16	629	16,81
380	1186	1	3a (C1)	1050	44,20	1993,08	693,6	23,76
380	842	1	3a (C1)	975	56,10	1977,68	639,2	17,38
390	1182	1	3a (C1)	1225	52,70	1997,62	691,9	23,24
390	850	1	3a (C1)	625	51,00	1980,78	657,9	12,25
400	1180	1	3a (C1)	1275	51,00	2005,98	698,7	25,00
400	854	1	3a (C1)	1050	44,20	1983,3	688,5	23,76
410	1182	1	3a (C1)	1300	61,20	2008,38	708,9	21,24
410	860	1	3a (C1)	1000	52,70	1993,78	702,1	18,98
420	1190	1	3a (C1)	1275	57,80	2012,24	680	22,06
420	864	1	3a (C1)	1825	62,90	1993,12	656,2	29,01
430	1190	1	3a (C1)	1125	59,50	2018,06	674,9	18,91
430	870	1	3a (C1)	1025	45,90	1998,08	659,6	22,33
440	1188	1	3a (C1)	1550	61,20	2026,28	680	25,33
440	878	1	3a (C1)	950	52,70	2004,46	661,3	18,03
450	1196	1	3a (C1)	1375	61,20	2029,84	666,4	22,47
450	878	1	3a (C1)	850	57,80	2012,26	661,3	14,71
460	890	1	3a (C1)	1050	49,30	2001,78	647,7	21,30
460	1196	1	3a (C1)	1450	59,50	2027,78	603,5	24,37
470	892	1	3a (C1)	1150	47,60	2001,78	647,7	24,16
470	1192	1	3a (C1)	1075	73,10	2035,56	622,2	14,71
480	900	1	3a (C1)	1125	45,90	2005,18	651,1	24,51
480	1196	1	3a (C1)	1700	69,70	2032,46	603,5	24,39



(N-S)	X (E-W)	Area	Unit	Width (m)	Height (m)	Depth (mbsl)	Burial depth (m)	W/H ratio
490	900	1	3a (C1)	1300	62,90	2006,74	651,1	20,67
490	1200	1	3a (C1)	1475	74,80	2029,34	603,5	19,72
500	910	1	3a (C1)	1525	54,40	2004,6	663	28,03
500	1204	1	3a (C1)	1500	79,90	2036,68	635,8	18,77
510	1210	2	3a (C1)	1325	71,40	2040,12	734,4	18,56
510	914	2	3a (C1)	1300	49,30	2012,5	702,1	26,37
520	1214	2	3a (C1)	1375	64,60	2038,84	737,8	21,28
520	920	2	3a (C1)	1625	59,50	2023,18	661,3	27,31
530	1216	2	3a (C1)	1300	64,60	2039,12	741,2	20,12
530	932	2	3a (C1)	1175	57,80	2032,78	702,1	20,33
540	1224	2	3a (C1)	1425	59,50	2047,62	749,7	23,95
540	934	2	3a (C1)	1600	81,60	2032,2	714	19,61
550	1226	2	3a (C1)	1525	61,20	2053,86	749,7	24,92
550	934	2	3a (C1)	2050	91,80	2033,36	690,2	22,33
560	1230	2	3a (C1)	1325	56,10	2052,44	751,4	23,62
560	936	2	3a (C1)	2800	113,90	2027,28	673,2	24,58
570	1234	2	3a (C1)	1225	51,00	2057,12	751,4	24,02
570	942	2	3a (C1)	2425	132,60	2025,26	705,5	18,29
580	1232	2	3a (C1)	1225	61,20	2059,1	756,5	20,02
580	950	2	3a (C1)	1800	108,80	2030,7	657,9	16,54
590	1234	2	3a (C1)	1150	61,20	2058,82	753,1	18,79
590	958	2	3a (C1)	1675	103,70	2031,14	644,3	16,15
600	1236	2	3a (C1)	1075	54,40	2058,4	748	19,76
600	968	2	3a (C1)	1800	127,50	2036,38	651,1	14,12
600	1232	2	3a (C1)	550	54,40	1957,68	642,6	10,11
610	1236	2	3a (C1)	1050	54,40	2056,42	742,9	19,30
610	1234	2	3a (C1)	325	45,90	1972,7	654,5	7,08
610	986	2	3a (C1)	2150	151,30	2026,18	640,9	14,21
620	1238	2	3a (C1)	975	49,30	2051,18	736,1	19,78
620	1230	2	3a (C1)	450	49,30	1979,36	659,6	9,13
620	988	2	3a (C1)	2200	163,20	2034,96	652,8	13,48
630	1240	2	3a (C1)	850	52,70	2058,26	746,3	16,13
630	992	2	3a (C1)	2175	176,80	2054,08	676,6	12,30
630	1222	2	3a (C1)	800	74,80	2002,04	669,8	10,70
640	1244	2	3a (C1)	425	59,50	2064,06	759,9	7,14
640	1008	2	3a (C1)	2200	175,10	2047,28	669,8	12,56
640	956	2	3a (C1)	850	81,60	1948,1	583,1	10,42
650	1248	2	3a (C1)	875	69,70	2076,26	756,5	12,55
650	1220	2	3a (C1)	475	85,00	2015,5	681,7	5,59
650	1020	2	3a (C1)	2200	180,20	2050,98	657,9	12,21
660	1246	2	3a (C1)	825	76,50	2082,34	773,5	10,78
660	1026	2	3a (C1)	2175	183,60	2063,58	678,3	11,85
660	1218	2	3a (C1)	625	79,90	2009,42	664,7	7,82
670	1242	2	3a (C1)	850	71,40	2074,14	749,7	11,90
670	1218	2	3a (C1)	600	98,60	2028,26	685,1	6,09
670	1028	2	3a (C1)	2050	175,10	2067,12	683,4	11,71
680	1240	2	3a (C1)	900	68,00	2069,3	766,7	13,24
680	1028	2	3a (C1)	1950	176,80	2064	683,4	11,03

(N-S)	X (E-W)	Area	Unit	Width (m)	Height (m)	Depth (mbsl)	Burial depth (m)	W/H ratio
680	1216	2	3a (C1)	450	71,40	2008,86	657,9	6,30
690	1240	2	3a (C1)	1000	66,30	2063,22	749,7	15,08
690	1038	2	3a (C1)	1975	171,70	2070,94	691,9	11,50
690	1212	2	3a (C1)	550	76,50	2012,56	646	7,19
700	1236	2	3a (C1)	1150	52,70	2065,06	753,1	21,82
700	1040	2	3a (C1)	2175	163,20	2061,6	673,2	13,33
700	1210	2	3a (C1)	625	81,60	2010,3	637,5	7,66
710	1228	2	3a (C1)	1125	56,10	2071,16	751,4	20,05
710	1048	2	3a (C1)	2100	168,30	2069,52	693,6	12,48
710	1206	2	3a (C1)	600	85,00	2018,96	629	7,06
720	1228	2	3a (C1)	1250	71,40	2084,62	763,3	17,51
720	1054	2	3a (C1)	2025	168,30	2074,52	659,6	12,03
720	1200	2	3a (C1)	725	78,20	2013,42	637,5	9,27
730	1216	2	3a (C1)	1200	56,10	2080,52	751,4	21,39
730	1062	2	3a (C1)	2075	173,40	2083,3	671,5	11,97
740	1224	2	3a (C1)	1225	56,10	2082,22	753,1	21,84
740	1068	2	3a (C1)	1200	112,20	2081,04	663	10,70
740	1200	2	3a (C1)	800	59,50	1995	622,2	13,45
750	1220	2	3a (C1)	1250	59,50	2076,98	746,3	21,01
750	1074	2	3a (C1)	1050	88,40	2076,96	632,4	11,88
760	1226	2	3a (C1)	1175	51,00	2076,58	722,5	23,04
760	1080	2	3a (C1)	1350	100,30	2081,78	634,1	13,46
770	1222	2	3a (C1)	1275	47,60	2078,42	725,9	26,79
770	1088	2	3a (C1)	1375	127,50	2080,64	639,2	10,78
780	1222	2	3a (C1)	1250	59,50	2086,2	744,6	21,01
780	1094	2	3a (C1)	1450	134,30	2080,1	613,7	10,80
790	1230	2	3a (C1)	1100	68,00	2083,12	707,2	16,18
790	1104	2	3a (C1)	1325	137,70	2078,7	596,7	9,62
800	1230	2	3a (C1)	1125	64,60	2081,3	685,1	17,41
800	1110	2	3a (C1)	1425	125,80	2077,12	615,4	11,33
810	1238	2	3a (C1)	950	57,80	2095,56	744,6	16,44
810	1116	2	3a (C1)	1400	136,00	2087,42	664,7	10,29
820	1234	2	3a (C1)	1050	37,40	2092,16	741,2	28,07
820	1116	2	3a (C1)	1425	136,00	2082,32	659,6	10,48
830	1238	2	3a (C1)	925	49,30	2091,55	714,85	18,76
830	1132	2	3a (C1)	1475	132,60	2074,54	640,9	11,12
840	1242	2	3a (C1)	650	39,10	2090,06	715,7	16,62
840	1134	2	3a (C1)	1250	110,50	2068,86	647,7	11,31
840	1218	2	3a (C1)	962,5	49,30	2023,38	606,9	19,52
850	1242	2	3a (C1)	650	37,40	2098	717,4	17,38
850	1138	2	3a (C1)	1275	136,00	2087,98	671,5	9,38
850	1214	2	3a (C1)	525	71,40	2037,96	632,4	7,35
860	1242	2	3a (C1)	725	39,10	2097,7	732,7	18,54
860	1164	2	3a (C1)	1325	136,00	2086,28	669,8	9,74
860	1216	2	3a (C1)	650	69,70	2055,1	651,1	9,33
870	1164	2	3a (C1)	1925	124,10	2085,58	661,3	15,51
880	1170	2	3a (C1)	2225	141,10	2088,98	664,7	15,77
890	1176	2	3a (C1)	1975	147,90	2091,4	656,2	13,35

(N-S)	X (E-W)	Area	Unit	Width (m)	Height (m)	Depth (mbsl)	Burial depth (m)	W/H ratio
900	1196	2	3a (C1)	2275	158,10	2110,1	674,9	14,39
910	1212	2	3a (C1)	2375	168,3	2112,8	669,8	14,11
920	1206	2	3a (C1)	2550	147,9	2100,9	657,9	17,24
930	1204	2	3a (C1)	2550	161,5	2102,46	657,9	15,79
940	1212	2	3a (C1)	2625	163,2	2102,74	661,3	16,08
950	1210	2	3a (C1)	2825	173,4	2111,1	668,1	16,29
960	1206	2	3a (C1)	2500	170	2108,12	669,8	14,71
970	1216	2	3a (C1)	2475	156,4	2105,3	654,5	15,82
980	1224	2	3a (C1)	2375	185,3	2120,16	683,4	12,82
990	1216	2	3a (C1)	2400	168,3	2113,08	673,2	14,26
1000	1226	2	3a (C1)	2275	170	2115,22	661,3	13,38
1010	1242	3	3a (C1)	2425	180,20	2126,7	668,1	13,46
1020	1256	3	3a (C1)	2325	175,10	2117,2	666,4	13,28
1030	1252	3	3a (C1)	2275	161,50	2114,08	666,4	14,09
1040	1260	3	3a (C1)	2200	180,20	2128,24	686,8	12,21
1050	1256	3	3a (C1)	2300	168,30	2129,8	686,8	13,67
1060	1260	3	3a (C1)	2175	173,40	2134,9	691,9	12,54
1070	1252	3	3a (C1)	2150	178,50	2139,72	693,6	12,04
1080	1258	3	3a (C1)	2300	183,60	2142	683,4	12,53
1090	1258	3	3a (C1)	2425	188,70	2142,56	690,2	12,85
1100	1256	3	3a (C1)	2275	176,80	2138,88	683,4	12,87
1110	1258	3	3a (C1)	2000	170,00	2147,52	693,6	11,76
1120	1252	3	3a (C1)	2250	166,60	2141,28	693,6	13,51
1130	1260	3	3a (C1)	2200	170,00	2146,82	685,1	12,94
1140	1258	3	3a (C1)	2250	159,80	2141,16	673,2	14,08
1150	1266	3	3a (C1)	2225	158,10	2140,88	669,8	14,07
1160	1268	3	3a (C1)	2175	181,90	2157,18	678,3	11,96
1170	1278	3	3a (C1)	2075	187,00	2154,2	680	11,10
1180	1278	3	3a (C1)	2475	176,80	2160,42	698,7	14,00
1190	1276	3	3a (C1)	2350	175,95	2143,27	689,35	13,36
1200	1280	3	3a (C1)	2375	183,60	2150,92	697	12,94
1210	1278	3	3a (C1)	2300	173,40	2142	683,4	13,26
1220	1284	3	3a (C1)	2400	187,00	2156,18	685,1	12,83
1230	1294	3	3a (C1)	2500	190,40	2164,12	686,8	13,13
1240	1304	3	3a (C1)	2275	181,90	2169,22	691,9	12,51
1250	1312	3	3a (C1)	2150	149,60	2139,9	657,9	14,37
1260	1306	3	3a (C1)	2200	161,50	2165,4	683,4	13,62
1270	1338	3	3a (C1)	2175	167,45	2171,36	680	12,99
1280	1342	3	3a (C1)	2000	167,45	2157,05	667,25	11,94
1290	1358	3	3a (C1)	1775	165,75	2178,87	685,95	10,71
1300	1366	3	3a (C1)	1750	155,55	2164,92	668,1	11,25
1310	1360	3	3a (C1)	1850	164,05	2163,15	665,55	11,28
1320	1364	3	3a (C1)	1825	156,40	2185,11	685,95	11,67
1330	1366	3	3a (C1)	1875	172,55	2186,6	685,1	10,87
1340	1366	3	3a (C1)	1775	165,75	2190,85	689,35	10,71
1350	1372	3	3a (C1)	1925	149,60	2193,76	686,8	12,87
1360	1376	3	3a (C1)	2025	155,55	2189,3	680	13,02
1370	1370	3	3a (C1)	2025	124,10	2157,36	642,6	16,32

(N-S)	X (E-W)	Area	Unit	Width (m)	Height (m)	Depth (mbsl)	Burial depth (m)	W/H ratio
1380	1386	3	3a (C1)	2575	187,85	2184,28	666,4	13,71
1390	1388	3	3a (C1)	2700	153,00	2181,45	660,45	17,65
1400	1394	3	3a (C1)	2725	156,40	2183,36	664,7	17,42
1410	1378	3	3a (C1)	2875	166,60	2180,39	657,05	17,26
1420	1410	3	3a (C1)	2525	172,55	2190,45	665,55	14,63
1430	1448	3	3a (C1)	2400	202	779	662,15	11,88
1440	1448	3	3a (C1)	2300	192	781	663,85	11,98
1450	1446	3	3a (C1)	2175	231	809	687,65	9,42
1460	1432	3	3a (C1)	2125	197	777	660,45	10,79
1470	1444	3	3a (C1)	2400	236	815	692,75	10,17
1480	1448	3	3a (C1)	2100	239	814	691,9	8,79
1490	1456	3	3a (C1)	2225	226	809	687,65	9,85
1500	1460	3	3a (C1)	2225	204	781	663,85	10,91
1510	1448	3	3a (C1)	2275	171,7	2199,54	652,8	13,25
1520	1450	3	3a (C1)	2175	181,05	2216,12	664,7	12,01
1530	1452	3	3a (C1)	2100	173,4	2217,68	664,7	12,11
1540	1450	3	3a (C1)	1875	203,15	2236,38	683,4	9,23
1550	1450	3	3a (C1)	1750	192,95	2232,77	677,45	9,07
1560	1455	3	3a (C1)	1725	203,15	2243,33	682,55	8,49
1570	1448	3	3a (C1)	1925	204	2245,24	686,8	9,44
1580	1448	3	3a (C1)	2050	205,7	2242,27	679,15	9,97
1590	1448	3	3a (C1)	1950	218,45	2251,2	683,4	8,93
1600	1450	3	3a (C1)	1900	211,65	2244,47	677,45	8,98
1610	1458	3	3a (C1)	2000	209,95	2248,51	679,15	9,53
1620	1456	3	3a (C1)	1975	209,1	2251,7	680	9,45
1630	1452	3	3a (C1)	2100	222,7	2258,22	683,4	9,43
1640	1450	3	3a (C1)	2050	221	2255,53	679,15	9,28
1650	1458	3	3a (C1)	2100	220,15	2253,62	674,9	9,54
1660	1458	3	3a (C1)	2125	216,75	2254,83	670,65	9,80
1670	1450	3	3a (C1)	2150	215,05	2249,87	667,25	10,00
1680	1458	3	3a (C1)	2300	221,85	2262,83	682,55	10,37
1690	1460	3	3a (C1)	2275	215,9	2260,64	674,9	10,54
1700	1470	3	3a (C1)	2050	223,55	2267,3	680	9,17
1710	1470	3	3a (C1)	1900	215,05	2259,23	667,25	8,84
1720	1470	3	3a (C1)	1975	203,15	2350,18	688,5	9,72
1730	1474	3	3a (C1)	1825	198,9	2246,34	652,8	9,18
1740	1484	3	3a (C1)	2100	201,45	2251,37	657,05	10,42
1750	1478	3	3a (C1)	2050	181,9	2238,91	638,35	11,27
1760	1492	3	3a (C1)	2200	200,6	2256,97	658,75	10,97
1770	1485	3	3a (C1)	2025	198,9	2253,65	646,85	10,18
1790	1486	3	3a (C1)	2050	198,05	2256,41	651,95	10,35
1800	1490	3	3a (C1)	1975	181,9	2246,99	641,75	10,86
1810	1498	3	3a (C1)	1950	177,65	2249,97	640,05	10,98
1820	1504	3	3a (C1)	1850	184,45	2249,34	632,4	10,03
1830	1504	3	3a (C1)	1875	192,95	2254,58	639,2	9,72
1840	1514	3	3a (C1)	1875	179,35	2244,95	626,45	10,45
1850	1514	3	3a (C1)	1775	173,4	2249,2	630,7	10,24
1860	1512	3	3a (C1)	1925	172,55	2254,09	633,25	11,16

(N-S)	X (E-W)	Area	Unit	Width (m)	Height (m)	Depth (mbsl)	Burial depth (m)	W/H ratio
1870	1516	3	3a (C1)	1875	184,45	2253,24	632,4	10,17
1880	1516	3	3a (C1)	1800	172,55	2253,6	627,3	10,43
1890	1522	3	3a (C1)	1800	179,35	2253,46	625,6	10,04
1900	1524	3	3a (C1)	1750	174,25	2254,6	620,5	10,04
1910	1538	3	3a (C1)	1825	192,95	2278,54	646	9,46
1920	1542	3	3a (C1)	1750	223,55	2311,62	678,3	7,83
1930	1542	3	3a (C1)	1850	228,65	2315,31	675,75	8,09
1940	1546	3	3a (C1)	1900	231,2	2322,25	684,25	8,22
1950	1548	3	3a (C1)	2150	198,9	2281,95	640,05	10,81
1960	1546	3	3a (C1)	1925	234,6	2323,32	678,3	8,21
1970	1540	3	3a (C1)	2050	199,75	2283,3	637,5	10,26
1980	1538	3	3a (C1)	1950	198,9	2279,48	629	9,80
2000	1546	3	3a (C1)	2050	191,25	2285,29	633,25	10,72
1	2550	1	3b	758,09	137,70	1397,68	472,60	5,51
1	2725	1	3b	554,70	98,60	1440,34	498,10	5,63
1	3750	1	3b	258,86	44,20	1456,66	487,90	5,86
1	3850	1	3b	221,88	52,70	1398,44	425,00	4,21
1	4200	1	3b	258,86	32,30	1501,30	518,50	8,01
1	5650	1	3b	295,84	69,70	1574,86	426,70	4,24
1	6700	1	3b	184,90	52,70	1624,74	596,70	3,51
1	7500	1	3b	203,39	39,10	1567,24	523,60	5,20
1	7525	1	3b	221,88	45,90	1602,38	552,50	4,83
1	7600	1	3b	295,84	51,00	1544,86	498,10	5,80
1	7625	1	3b	406,78	54,40	1478,56	431,80	7,48
1	7650	1	3b	425,27	66,30	1450,08	408,00	6,41
1	8850	1	3b	184,90	57,80	1652,68	595,00	3,20
1	8850	1	3b	184,90	47,60	1605,22	549,10	3,88
1	9475	1	3b	480,74	39,10	1445,72	374,00	12,30
1	9625	1	3b	166,41	62,90	1642,36	564,40	2,65
1	9650	1	3b	388,29	66,30	1554,10	477,70	5,86
1	9700	1	3b	591,68	71,40	1505,08	431,80	8,29
1	11525	1	3b	591,68	34,00	1281,26	195,50	17,40
1	11575	1	3b	462,25	66,30	1568,28	479,40	6,97
1	11700	1	3b	258,86	51,00	1668,44	578,00	5,08
1	11700	1	3b	517,72	69,70	1629,62	542,30	7,43
1	12525	1	3b	369,80	49,30	1564,46	470,90	7,50
1	12575	1	3b	332,82	42,50	1666,32	571,20	7,83
1	12575	1	3b	536,21	62,90	1513,04	414,80	8,52
1	15000	1	3b	351,31	45,90	1648,26	484,50	7,65
1	15100	1	3b	554,70	40,80	1594,58	419,90	13,60
1	16200	1	3b	647,15	86,70	1603,44	489,60	7,46
1	16225	1	3b	499,23	78,20	1577,80	462,40	6,38
1	16250	1	3b	277,35	57,80	1734,90	627,30	4,80
1	16300	1	3b	610,17	78,20	1547,48	435,20	7,80
1	16300	1	3b	610,17	66,30	1518,44	404,60	9,20
1	16300	1	3b	499,23	52,70	1448,88	336,60	9,47
1	16450	1	3b	332,82	68,00	1634,46	525,30	4,89

(N-S)	X (E-W)	Area	Unit	Width (m)	Height (m)	Depth (mbsl)	Burial depth (m)	W/H ratio
1	16625	1	3b	295,84	57,80	1666,62	555,90	5,12
1	17725	1	3b	776,58	45,90	1493,12	343,40	16,92
1	17900	1	3b	684,13	57,80	1536,02	409,70	11,84
1	18600	1	3b	443,76	45,90	1563,12	397,80	9,67
1	19150	1	3b	1220,34	51,00	1624,86	351,90	23,93
1	21050	1	3b	721,11	61,20	1593,22	498,10	11,78
1	21200	1	3b	628,66	35,70	1648,60	564,40	17,61
1	21850	1	3b	979,97	52,70	1690,28	578,00	18,60
1	22100	1	3b	425,27	49,30	1668,74	562,70	8,63
1	22275	1	3b	869,03	76,50	1600,88	496,40	11,36
125	2675	1	3b	1220,34	134,30	1382,54	440,30	9,09
125	2875	1	3b	739,60	74,80	1410,32	455,60	9,89
125	3275	1	3b	665,64	39,10	1163,56	187,00	17,02
125	3750	1	3b	277,35	56,10	1404,82	426,70	4,94
125	3850	1	3b	277,35	54,40	1436,98	457,30	5,10
125	5650	1	3b	369,80	64,60	1592,86	436,90	5,72
125	6575	1	3b	406,78	61,20	1704,78	678,30	6,65
125	7550	1	3b	277,35	49,30	1565,98	508,30	5,63
125	7550	1	3b	406,78	51,00	1529,28	479,40	7,98
125	7575	1	3b	184,90	40,80	1612,58	562,70	4,53
125	7575	1	3b	203,39	34,00	1133,32	85,00	5,98
125	7675	1	3b	480,74	79,90	1475,16	428,40	6,02
125	8400	1	3b	351,31	42,50	1539,34	487,90	8,27
125	8500	1	3b	406,78	66,30	1662,16	615,40	6,14
125	8625	1	3b	388,29	44,20	1590,20	537,20	8,78
125	8725	1	3b	277,35	59,50	1739,94	688,50	4,66
125	8875	1	3b	240,37	34,00	1530,14	470,90	7,07
125	9525	1	3b	517,72	52,70	1474,34	399,50	9,82
125	9650	1	3b	166,41	54,40	1645,62	566,10	3,06
125	9650	1	3b	443,76	66,30	1535,12	455,60	6,69
125	11575	1	3b	406,78	57,80	1576,36	482,80	7,04
125	11700	1	3b	388,29	62,90	1622,40	530,40	6,17
125	11750	1	3b	240,37	47,60	1682,04	591,60	5,05
125	11750	1	3b	443,76	57,80	1514,74	416,50	7,68
125	12550	1	3b	536,21	69,70	1600,88	496,40	7,69
125	12550	1	3b	536,21	83,30	1514,18	409,70	6,44
125	12600	1	3b	369,80	57,80	1750,64	574,60	6,40
125	15050	1	3b	332,82	68,00	1699,70	521,90	4,89
125	15200	1	3b	443,76	59,50	1620,96	418,20	7,46
125	15250	1	3b	369,80	45,90	1541,06	338,30	8,06
125	15800	1	3b	388,29	57,80	1393,92	275,40	6,72
125	16100	1	3b	462,25	74,80	1451,72	333,20	6,18
125	16125	1	3b	369,80	96,90	1625,40	510,00	3,82
125	16150	1	3b	647,15	68,00	1469,42	358,70	9,52
125	16200	1	3b	332,82	76,50	1734,06	617,10	4,35
125	16275	1	3b	425,27	49,30	1498,04	384,20	8,63
125	16325	1	3b	406,78	74,80	1644,10	528,70	5,44
125	16325	1	3b	443,76	108,80	1623,42	504,90	4,08

(N-S)	X (E-W)	Area	Unit	Width (m)	Height (m)	Depth (mbsl)	Burial depth (m)	W/H ratio
125	16450	1	3b	351,31	81,60	1625,40	510,00	4,31
125	17650	1	3b	684,13	23,80	1486,90	324,70	28,74
125	17775	1	3b	647,15	52,70	1208,36	68,00	12,28
125	17800	1	3b	573,19	44,20	1519,74	382,50	12,97
125	17925	1	3b	684,13	68,00	1552,74	423,30	10,06
125	18975	1	3b	628,66	59,50	1540,28	272,00	10,57
125	19225	1	3b	906,01	52,70	1611,12	336,60	17,19
125	20800	1	3b	480,74	44,20	1630,48	533,80	10,88
125	20975	1	3b	1127,89	100,30	1593,22	498,10	11,25
125	21725	1	3b	979,97	54,40	1682,62	579,70	18,01
125	22025	1	3b	536,21	71,40	1670,44	564,40	7,51
125	22275	1	3b	832,05	64,60	1586,00	486,20	12,88
250	2725	1	3b	1072,42	85,00	1356,20	404,60	12,62
250	3000	1	3b	1053,93	91,80	1409,90	450,50	11,48
250	3125	1	3b	258,86	45,90	1141,02	178,50	5,64
250	5700	1	3b	369,80	57,80	1573,88	414,80	6,40
250	6600	1	3b	110,94	20,40	1568,22	535,50	5,44
250	7575	1	3b	166,41	44,20	1624,62	576,30	3,76
250	7575	1	3b	203,39	44,20	1583,68	533,80	4,60
250	7575	1	3b	314,33	37,40	1115,62	59,50	8,40
250	7625	1	3b	425,27	74,80	1525,46	470,90	5,69
250	7700	1	3b	591,68	66,30	1461,28	411,40	8,92
250	8450	1	3b	369,80	74,80	1584,68	527,00	4,94
250	8500	1	3b	295,84	44,20	1673,22	617,10	6,69
250	8625	1	3b	573,19	68,00	1525,60	472,60	8,43
250	8675	1	3b	425,27	73,10	1745,90	685,10	5,82
250	8800	1	3b	184,90	52,70	1688,10	627,30	3,51
250	8825	1	3b	277,35	64,60	1556,50	487,90	4,29
250	9525	1	3b	369,80	40,80	1475,62	396,10	9,06
250	9625	1	3b	462,25	27,20	1116,64	34,00	16,99
250	9650	1	3b	184,90	54,40	1658,94	576,30	3,40
250	9675	1	3b	369,80	56,10	1513,02	433,50	6,59
250	9750	1	3b	332,82	54,40	1547,88	459,00	6,12
250	10525	1	3b	480,74	57,80	1605,56	442,00	8,32
250	10650	1	3b	480,74	78,20	1605,26	511,70	6,15
250	10675	1	3b	369,80	45,90	1542,50	450,50	8,06
250	11675	1	3b	332,82	68,00	1579,20	479,40	4,89
250	11725	1	3b	443,76	69,70	1648,48	544,00	6,37
250	11750	1	3b	184,90	44,20	1687,58	583,10	4,18
250	11775	1	3b	610,17	79,90	1526,08	421,60	7,64
250	12450	1	3b	499,23	64,60	1634,32	523,60	7,73
250	12450	1	3b	369,80	73,10	1516,46	399,50	5,06
250	12675	1	3b	351,31	56,10	1688,58	576,30	6,26
250	14975	1	3b	351,31	69,70	1748,02	559,30	5,04
250	15100	1	3b	369,80	62,90	1686,56	476,00	5,88
250	15175	1	3b	388,29	73,10	1651,28	445,40	5,31
250	15850	1	3b	332,82	49,30	1397,46	280,50	6,75
250	16050	1	3b	591,68	110,50	1645,80	530,40	5,35

(N-S)	X (E-W)	Area	Unit	Width (m)	Height (m)	Depth (mbsl)	Burial depth (m)	W/H ratio
250	16100	1	3b	425,27	71,40	1488,98	368,90	5,96
250	16450	1	3b	462,25	57,80	1727,12	608,60	8,00
250	17675	1	3b	462,25	34,00	1198,18	39,10	13,60
250	17750	1	3b	721,11	35,70	1514,24	353,60	20,20
250	17775	1	3b	554,70	47,60	1216,16	68,00	11,65
250	17875	1	3b	869,03	78,20	1562,96	414,80	11,11
250	17875	1	3b	554,70	61,20	1243,92	102,00	9,06
250	18175	1	3b	443,76	51,00	1588,42	477,70	8,70
250	19125	1	3b	832,05	37,40	1602,06	321,30	22,25
250	20725	1	3b	665,64	69,70	1626,52	523,60	9,55
250	20900	1	3b	832,05	98,60	1603,42	508,30	8,44
250	21775	1	3b	924,50	40,80	1671,72	561,00	22,66
250	21825	1	3b	684,13	49,30	1636,72	533,80	13,88
250	22200	1	3b	813,56	61,20	1580,34	474,30	13,29
375	2850	1	3b	1090,91	74,80	1353,42	86,70	14,58
375	3075	1	3b	758,09	49,30	1405,38	433,50	15,38
375	3150	1	3b	795,07	52,70	1419,12	448,80	15,09
375	5750	1	3b	332,82	47,60	1557,88	391,00	6,99
375	6650	1	3b	240,37	40,80	1595,86	549,10	5,89
375	7525	1	3b	295,84	44,20	1569,66	515,10	6,69
375	7600	1	3b	184,90	47,60	1612,44	561,00	3,88
375	7675	1	3b	443,76	83,30	1544,30	491,30	5,33
375	7700	1	3b	536,21	90,10	1493,02	436,90	5,95
375	8525	1	3b	258,86	39,10	1679,46	617,10	6,62
375	8650	1	3b	480,74	64,60	1575,90	515,10	7,44
375	8650	1	3b	517,72	74,80	1521,36	459,00	6,92
375	8900	1	3b	203,39	51,00	1647,16	584,80	3,99
375	9500	1	3b	351,31	39,10	1495,46	409,70	8,98
375	9700	1	3b	203,39	57,80	1671,98	583,10	3,52
375	9750	1	3b	406,78	61,20	1567,86	474,30	6,65
375	9800	1	3b	314,33	40,80	1539,10	447,10	7,70
375	10500	1	3b	536,21	76,50	1551,00	459,00	7,01
375	10650	1	3b	369,80	73,10	1577,92	482,80	5,06
375	10725	1	3b	499,23	83,30	1627,36	533,80	5,99
375	11725	1	3b	369,80	66,30	1583,74	477,70	5,58
375	11800	1	3b	295,84	57,80	1691,84	578,00	5,12
375	11825	1	3b	388,29	64,60	1635,88	523,60	6,01
375	11825	1	3b	647,15	59,50	1504,70	389,30	10,88
375	11925	1	3b	462,25	56,10	1552,72	442,00	8,24
375	12175	1	3b	406,78	44,20	1431,18	311,10	9,20
375	12450	1	3b	369,80	69,70	1635,04	513,40	5,31
375	12450	1	3b	314,33	39,10	1528,22	409,70	8,04
375	12525	1	3b	388,29	37,40	1243,90	120,70	10,38
375	12675	1	3b	314,33	85,00	1718,06	593,30	3,70
375	13475	1	3b	221,88	23,80	1423,52	312,80	9,32
375	14875	1	3b	351,31	47,60	1732,14	555,90	7,38
375	14925	1	3b	369,80	45,90	1761,32	588,20	8,06
375	14975	1	3b	277,35	39,10	1765,44	581,40	7,09



(N-S)	X (E-W)	Area	Unit	Width (m)	Height (m)	Depth (mbsl)	Burial depth (m)	W/H ratio
375	15125	1	3b	425,27	52,70	1680,00	510,00	8,07
375	15225	1	3b	443,76	62,90	1652,98	447,10	7,06
375	15400	1	3b	295,84	47,60	1615,58	409,70	6,22
375	15825	1	3b	277,35	85,00	1786,20	663,00	3,26
375	15850	1	3b	850,54	62,90	1406,40	275,40	13,52
375	15975	1	3b	425,27	52,70	1661,82	535,50	8,07
375	15975	1	3b	573,19	47,60	1488,84	367,20	12,04
375	16075	1	3b	406,78	68,00	1616,20	493,00	5,98
375	16075	1	3b	369,80	62,90	1561,66	436,90	5,88
375	16150	1	3b	314,33	27,20	1532,62	406,30	11,56
375	16150	1	3b	406,78	56,10	1461,78	341,70	7,25
375	17675	1	3b	573,19	28,90	1503,92	323,00	19,83
375	17775	1	3b	517,72	59,50	1204,84	44,20	8,70
375	17825	1	3b	425,27	62,90	1222,12	64,60	6,76
375	17850	1	3b	702,62	86,70	1581,54	413,10	8,10
375	17875	1	3b	443,76	83,30	1250,98	130,90	5,33
375	19125	1	3b	462,25	28,90	1594,84	309,40	15,99
375	20775	1	3b	850,54	103,70	1622,42	511,70	8,20
375	21675	1	3b	942,99	47,60	1664,36	547,40	19,81
375	21825	1	3b	517,72	49,30	1560,66	443,70	10,50
375	21900	1	3b	536,21	45,90	1643,82	525,30	11,68
375	22075	1	3b	665,64	52,70	1579,78	467,50	12,63
500	3025	1	3b	1608,63	95,20	1393,06	416,50	16,90
500	3525	1	3b	1775,04	102,00	1453,00	462,40	17,40
500	4425	1	3b	480,74	45,90	1530,94	518,50	10,47
500	5975	1	3b	517,72	35,70	1445,90	338,30	14,50
500	7600	1	3b	277,35	52,70	1627,32	571,20	5,26
500	7625	1	3b	406,78	42,50	1572,64	513,40	9,57
500	7650	1	3b	369,80	76,50	1557,34	498,10	4,83
500	7650	1	3b	647,15	100,30	1509,60	448,80	6,45
500	8350	1	3b	332,82	42,50	1465,40	404,60	7,83
500	8575	1	3b	351,31	68,00	1685,98	620,50	5,17
500	8650	1	3b	554,70	96,90	1546,44	479,40	5,72
500	8825	1	3b	203,39	34,00	1642,22	562,70	5,98
500	9700	1	3b	314,33	54,40	1678,92	591,60	5,78
500	9725	1	3b	369,80	62,90	1557,10	457,30	5,88
500	10225	1	3b	462,25	45,90	1516,30	416,50	10,07
500	10400	1	3b	462,25	102,00	1759,54	661,30	4,53
500	10450	1	3b	480,74	44,20	1519,98	423,30	10,88
500	10500	1	3b	517,72	51,00	1547,18	450,50	10,15
500	10625	1	3b	517,72	73,10	1570,56	469,20	7,08
500	10825	1	3b	573,19	71,40	1601,02	498,10	8,03
500	11775	1	3b	573,19	71,40	1574,54	460,70	8,03
500	11800	1	3b	184,90	59,50	1701,76	584,80	3,11
500	11875	1	3b	258,86	68,00	1648,50	525,30	3,81
500	11925	1	3b	258,86	44,20	1664,36	547,40	5,86
500	11950	1	3b	480,74	78,20	1509,66	392,70	6,15
500	12500	1	3b	332,82	56,10	1645,10	521,90	5,93

(N-S)	X (E-W)	Area	Unit	Width (m)	Height (m)	Depth (mbsl)	Burial depth (m)	W/H ratio
500	12750	1	3b	314,33	56,10	1690,58	562,70	5,60
500	12775	1	3b	295,84	51,00	1719,34	589,90	5,80
500	15000	1	3b	332,82	57,80	1756,78	589,90	5,76
500	15150	1	3b	388,29	54,40	1635,28	421,60	7,14
500	15775	1	3b	332,82	85,00	1783,66	651,10	3,92
500	15850	1	3b	406,78	56,10	1661,96	537,20	7,25
500	15900	1	3b	665,64	76,50	1420,42	294,10	8,70
500	15925	1	3b	314,33	57,80	1561,66	436,90	5,44
500	15975	1	3b	517,72	64,60	1509,10	385,90	8,01
500	16025	1	3b	406,78	88,40	1626,12	499,80	4,60
500	16075	1	3b	406,78	79,90	1587,44	465,80	5,09
500	16550	1	3b	258,86	44,20	1734,78	606,90	5,86
500	17875	1	3b	536,21	47,60	1525,18	334,90	11,26
500	17925	1	3b	591,68	90,10	1591,60	421,60	6,57
500	20750	1	3b	832,05	107,10	1622,28	510,00	7,77
500	21200	1	3b	739,60	45,90	1496,62	385,90	16,11
500	21675	1	3b	850,54	90,10	1660,40	537,20	9,44
500	21850	1	3b	480,74	74,80	1577,10	453,90	6,43
625	3400	1	3b	1238,83	100,30	1437,98	450,50	12,35
625	3700	1	3b	1719,57	120,70	1472,56	472,60	14,25
625	5250	1	3b	388,29	47,60	1539,20	486,20	8,16
625	5375	1	3b	295,84	49,30	1506,34	447,10	6,00
625	5425	1	3b	240,37	34,00	1474,90	406,30	7,07
625	5975	1	3b	388,29	34,00	1451,34	290,70	11,42
625	7225	1	3b	406,78	40,80	1728,76	666,40	9,97
625	7375	1	3b	221,88	30,60	1198,22	134,30	7,25
625	7625	1	3b	314,33	52,70	1626,62	562,70	5,96
625	7650	1	3b	240,37	32,30	1579,16	516,80	7,44
625	7725	1	3b	536,21	100,30	1551,68	486,20	5,35
625	8625	1	3b	221,88	42,50	1688,68	615,40	5,22
625	8650	1	3b	332,82	42,50	1532,00	455,60	7,83
625	9700	1	3b	351,31	57,80	1674,26	572,90	6,08
625	9875	1	3b	351,31	28,90	1127,28	30,60	12,16
625	9925	1	3b	240,37	40,80	1166,38	69,70	5,89
625	9975	1	3b	166,41	42,50	1222,20	122,40	3,92
625	10025	1	3b	443,76	74,80	1518,00	418,20	5,93
625	10475	1	3b	665,64	117,30	1772,58	668,10	5,67
625	10800	1	3b	517,72	61,20	1570,00	462,40	8,46
625	11825	1	3b	184,90	47,60	1703,18	583,10	3,88
625	11825	1	3b	425,27	47,60	1568,60	445,40	8,93
625	11875	1	3b	369,80	74,80	1672,44	550,80	4,94
625	11900	1	3b	388,29	52,70	1626,40	503,20	7,37
625	12025	1	3b	480,74	74,80	1519,30	396,10	6,43
625	12500	1	3b	332,82	49,30	1637,74	508,30	6,75
625	12850	1	3b	129,43	42,50	1743,14	613,70	3,05
625	12900	1	3b	480,74	71,40	1695,12	561,00	6,73
625	14925	1	3b	314,33	47,60	1741,66	538,90	6,60
625	15775	1	3b	406,78	95,20	1774,02	647,70	4,27

(N-S)	X (E-W)	Area	Unit	Width (m)	Height (m)	Depth (mbsl)	Burial depth (m)	W/H ratio
625	15850	1	3b	554,70	73,10	1642,42	508,30	7,59
625	15850	1	3b	295,84	78,20	1498,20	367,20	3,78
625	15850	1	3b	665,64	73,10	1426,94	297,50	9,11
625	15875	1	3b	443,76	56,10	1610,68	482,80	7,91
625	15950	1	3b	425,27	45,90	1567,90	436,90	9,27
625	17625	1	3b	517,72	34,00	1513,42	324,70	15,23
625	17975	1	3b	480,74	54,40	1581,26	409,70	8,84
625	20625	1	3b	628,66	74,80	1603,86	494,70	8,40
625	20675	1	3b	610,17	45,90	1628,80	513,40	13,29
625	21425	1	3b	1368,26	56,10	1648,64	527,00	24,39
625	21675	1	3b	480,74	40,80	1604,16	479,40	11,78
625	21775	1	3b	517,72	47,60	1517,74	396,10	10,88
625	21900	1	3b	554,70	47,60	1545,22	426,70	11,65
750	3375	1	3b	314,33	32,30	1137,94	141,10	9,73
750	3600	1	3b	924,50	100,30	1457,40	459,00	9,22
750	4075	1	3b	1368,26	90,10	1503,74	491,30	15,19
750	5950	1	3b	314,33	40,80	1522,34	338,30	7,70
750	6000	1	3b	462,25	57,80	1486,50	300,90	8,00
750	6025	1	3b	351,31	57,80	1559,60	374,00	6,08
750	7700	1	3b	184,90	54,40	1635,56	557,60	3,40
750	7700	1	3b	388,29	64,60	1567,98	494,70	6,01
750	8725	1	3b	258,86	34,00	1688,12	608,60	7,61
750	8750	1	3b	369,80	64,60	1607,94	525,30	5,72
750	9700	1	3b	147,92	49,30	1684,62	566,10	3,00
750	9750	1	3b	295,84	71,40	1591,26	474,30	4,14
750	9950	1	3b	351,31	52,70	1524,38	419,90	6,67
750	10025	1	3b	647,15	52,70	1460,92	350,20	12,28
750	10425	1	3b	573,19	91,80	1766,06	664,70	6,24
750	11900	1	3b	203,39	45,90	1705,60	574,60	4,43
750	11900	1	3b	721,11	45,90	1462,78	334,90	15,71
750	11925	1	3b	295,84	57,80	1656,44	527,00	5,12
750	11975	1	3b	684,13	100,30	1560,96	428,40	6,82
750	12525	1	3b	351,31	42,50	1634,06	501,50	8,27
750	12950	1	3b	277,35	40,80	1761,14	623,90	6,80
750	12950	1	3b	536,21	44,20	1677,84	540,60	12,13
750	14800	1	3b	351,31	47,60	1640,20	462,40	7,38
750	15125	1	3b	166,41	49,30	1708,66	498,10	3,38
750	15775	1	3b	554,70	81,60	1628,96	496,40	6,80
750	15775	1	3b	795,07	68,00	1424,40	285,60	11,69
750	15800	1	3b	499,23	100,30	1784,94	647,70	4,98
750	15825	1	3b	406,78	59,50	1567,76	435,20	6,84
750	15850	1	3b	406,78	76,50	1498,06	365,50	5,32
750	17800	1	3b	628,66	39,10	1526,74	334,90	16,08
750	18075	1	3b	351,31	25,50	1562,14	385,90	13,78
750	18700	1	3b	979,97	54,40	1593,54	464,10	18,01
750	21800	1	3b	536,21	40,80	1526,38	406,30	13,14
875	2900	1	3b	443,76	25,50	1265,14	283,90	17,40
875	3425	1	3b	332,82	25,50	1207,50	209,10	13,05

(N-S)	X (E-W)	Area	Unit	Width (m)	Height (m)	Depth (mbsl)	Burial depth (m)	W/H ratio
875	3675	1	3b	702,62	51,00	1443,52	442,00	13,78
875	4125	1	3b	1423,73	110,50	1520,18	501,50	12,88
875	5950	1	3b	388,29	51,00	1535,64	367,20	7,61
875	5950	1	3b	536,21	49,30	1501,94	317,90	10,88
875	6000	1	3b	295,84	52,70	1597,28	414,80	5,61
875	6000	1	3b	314,33	57,80	1563,28	380,80	5,44
875	8075	1	3b	295,84	47,60	1619,84	537,20	6,22
875	8650	1	3b	295,84	74,80	1515,72	428,40	3,96
875	8800	1	3b	369,80	73,10	1600,72	513,40	5,06
875	9725	1	3b	221,88	66,30	1687,60	564,40	3,35
875	9725	1	3b	314,33	51,00	1440,96	316,20	6,16
875	9750	1	3b	258,86	59,50	1606,00	482,80	4,35
875	9750	1	3b	332,82	56,10	1549,90	426,70	5,93
875	9800	1	3b	351,31	49,30	1519,86	402,90	7,13
875	10450	1	3b	554,70	64,60	1738,02	627,30	8,59
875	10600	1	3b	388,29	25,50	1504,98	392,70	15,23
875	11850	1	3b	332,82	57,80	1646,24	516,80	5,76
875	11850	1	3b	739,60	59,50	1483,04	353,60	12,43
875	11975	1	3b	221,88	44,20	1707,16	574,60	5,02
875	12000	1	3b	425,27	59,50	1611,82	477,70	7,15
875	12025	1	3b	425,27	62,90	1572,30	433,50	6,76
875	12150	1	3b	369,80	51,00	1611,98	406,30	7,25
875	12625	1	3b	314,33	27,20	1635,20	496,40	11,56
875	12900	1	3b	462,25	44,20	1653,62	511,70	10,46
875	13075	1	3b	425,27	62,90	1782,96	642,60	6,76
875	14925	1	3b	554,70	68,00	1691,80	482,80	8,16
875	15700	1	3b	388,29	59,50	1673,02	538,90	6,53
875	15725	1	3b	684,13	52,70	1428,08	292,40	12,98
875	15750	1	3b	388,29	64,60	1543,26	402,90	6,01
875	15750	1	3b	406,78	39,10	1470,16	329,80	10,40
875	15800	1	3b	499,23	78,20	1771,48	635,80	6,38
875	15800	1	3b	610,17	83,30	1631,66	491,30	7,32
875	15825	1	3b	499,23	78,20	1585,90	447,10	6,38
875	17850	1	3b	610,17	52,70	1534,96	340,00	11,58
875	18675	1	3b	887,52	35,70	1569,88	442,00	24,86
875	20550	1	3b	480,74	68,00	1604,44	482,80	7,07
875	20750	1	3b	314,33	32,30	1552,44	438,60	9,73
875	21725	1	3b	499,23	52,70	1583,76	459,00	9,47
875	22125	1	3b	295,84	37,40	1560,24	438,60	7,91
1000	4600	1	3b	1405,24	100,30	1541,30	511,70	14,01
1000	5925	1	3b	351,31	61,20	1552,92	387,60	5,74
1000	6050	1	3b	258,86	68,00	1590,76	411,40	3,81
1000	6725	1	3b	332,82	28,90	1524,96	408,00	11,52
1000	7100	1	3b	351,31	40,80	1210,42	130,90	8,61
1000	8075	1	3b	480,74	74,80	1642,66	549,10	6,43
1000	8650	1	3b	591,68	62,90	1507,80	408,00	9,41
1000	8825	1	3b	388,29	79,90	1611,64	513,40	4,86
1000	9725	1	3b	554,70	71,40	1556,28	428,40	7,77

(N-S)	X (E-W)	Area	Unit	Width (m)	Height (m)	Depth (mbsl)	Burial depth (m)	W/H ratio
1000	9725	1	3b	314,33	51,00	1525,82	399,50	6,16
1000	9750	1	3b	425,27	68,00	1596,94	467,50	6,25
1000	9775	1	3b	203,39	56,10	1692,28	564,40	3,63
1000	9950	1	3b	702,62	49,30	1481,90	358,70	14,25
1000	10450	1	3b	388,29	45,90	1727,26	610,30	8,46
1000	11425	1	3b	517,72	28,90	1462,36	329,80	17,91
1000	11850	1	3b	591,68	47,60	1507,98	372,30	12,43
1000	11950	1	3b	425,27	34,00	1534,90	396,10	12,51
1000	11975	1	3b	166,41	45,90	1720,48	584,80	3,63
1000	12000	1	3b	369,80	54,40	1633,36	493,00	6,80
1000	12025	1	3b	480,74	79,90	1618,06	477,70	6,02
1000	12100	1	3b	388,29	73,10	1597,80	459,00	5,31
1000	12725	1	3b	647,15	51,00	1648,38	504,90	12,69
1000	13025	1	3b	351,31	54,40	1831,84	686,80	6,46
1000	13150	1	3b	351,31	64,60	1795,72	646,00	5,44
1000	13375	1	3b	258,86	30,60	1586,76	438,60	8,46
1000	13575	1	3b	147,92	23,80	1447,92	306,00	6,22
1000	14875	1	3b	462,25	28,90	1669,70	460,70	15,99
1000	15575	1	3b	758,09	66,30	1422,00	275,40	11,43
1000	15675	1	3b	665,64	78,20	1628,54	491,30	8,51
1000	15675	1	3b	499,23	86,70	1517,48	374,00	5,76
1000	15750	1	3b	591,68	73,10	1592,70	453,90	8,09
1000	15800	1	3b	499,23	78,20	1566,78	423,30	6,38
1000	16075	1	3b	443,76	73,10	1767,38	623,90	6,07
1000	17925	1	3b	499,23	39,10	1519,22	338,30	12,77
1000	18775	1	3b	942,99	66,30	1575,88	401,20	14,22
1000	20400	1	3b	536,21	59,50	1608,12	489,60	9,01
1000	20625	1	3b	554,70	49,30	1553,30	430,10	11,25
1000	20700	1	3b	628,66	34,00	1645,10	521,90	18,49
1000	21750	1	3b	813,56	98,60	1584,76	452,20	8,25
1000	22125	1	3b	406,78	52,70	1539,28	411,40	7,72
1125	4675	1	3b	1497,69	86,70	1541,60	496,40	17,27
1125	6000	1	3b	221,88	45,90	1561,66	436,90	4,83
1125	6675	1	3b	351,31	37,40	1251,56	119,00	9,39
1125	6775	1	3b	425,27	71,40	1601,62	467,50	5,96
1125	8125	1	3b	591,68	73,10	1637,28	540,60	8,09
1125	8250	1	3b	369,80	45,90	1689,42	586,50	8,06
1125	8575	1	3b	591,68	51,00	1510,92	408,00	11,60
1125	8800	1	3b	351,31	83,30	1649,06	532,10	4,22
1125	9725	1	3b	221,88	45,90	1701,76	584,80	4,83
1125	9750	1	3b	628,66	107,10	1586,46	453,90	5,87
1125	9850	1	3b	388,29	66,30	1527,22	416,50	5,86
1125	11825	1	3b	1146,38	95,20	1531,64	394,40	12,04
1125	12000	1	3b	277,35	54,40	1717,94	572,90	5,10
1125	12000	1	3b	425,27	68,00	1668,64	523,60	6,25
1125	12075	1	3b	443,76	73,10	1638,46	498,10	6,07
1125	12150	1	3b	517,72	64,60	1596,96	448,80	8,01
1125	12875	1	3b	499,23	57,80	1610,70	464,10	8,64

(N-S)	X (E-W)	Area	Unit	Width (m)	Height (m)	Depth (mbsl)	Burial depth (m)	W/H ratio
1125	13050	1	3b	258,86	52,70	1831,84	686,80	4,91
1125	13175	1	3b	462,25	66,30	1792,88	649,40	6,97
1125	14375	1	3b	462,25	37,40	1625,60	455,60	12,36
1125	14650	1	3b	221,88	30,60	1660,20	459,00	7,25
1125	15500	1	3b	388,29	42,50	1474,56	326,40	9,14
1125	15550	1	3b	813,56	52,70	1428,80	282,20	15,44
1125	15575	1	3b	332,82	49,30	1711,42	569,50	6,75
1125	15600	1	3b	351,31	59,50	1523,86	375,70	5,90
1125	15625	1	3b	610,17	73,10	1643,00	496,40	8,35
1125	15700	1	3b	443,76	61,20	1568,34	423,30	7,25
1125	15725	1	3b	480,74	69,70	1606,02	464,10	6,90
1125	18525	1	3b	1090,91	61,20	1548,96	377,40	17,83
1125	20325	1	3b	554,70	62,90	1624,70	501,50	8,82
1125	20575	1	3b	499,23	54,40	1563,08	435,20	9,18
1125	20725	1	3b	517,72	49,30	1631,22	504,90	10,50
1125	20925	1	3b	462,25	47,60	1655,02	528,70	9,71
1125	21050	1	3b	443,76	54,40	1675,56	550,80	8,16
1125	21825	1	3b	684,13	79,90	1574,42	440,30	8,56
1250	5150	1	3b	850,54	66,30	1563,42	515,10	12,83
1250	6650	1	3b	443,76	105,40	1602,26	399,50	4,21
1250	7625	1	3b	647,15	76,50	1527,48	438,60	8,46
1250	8175	1	3b	517,72	81,60	1660,24	554,20	6,34
1250	8275	1	3b	388,29	47,60	1792,84	686,80	8,16
1250	8375	1	3b	628,66	52,70	1710,82	600,10	11,93
1250	8575	1	3b	499,23	35,70	1498,46	389,30	13,98
1250	8900	1	3b	295,84	47,60	1642,84	513,40	6,22
1250	9450	1	3b	406,78	86,70	1790,74	661,30	4,69
1250	9700	1	3b	351,31	57,80	1562,80	431,80	6,08
1250	10875	1	3b	277,35	30,60	1693,70	562,70	9,06
1250	11975	1	3b	684,13	40,80	1531,36	391,00	16,77
1250	12000	1	3b	351,31	52,70	1719,50	572,90	6,67
1250	12025	1	3b	480,74	88,40	1685,92	544,00	5,44
1250	12025	1	3b	517,72	79,90	1627,56	479,40	6,48
1250	12100	1	3b	425,27	66,30	1663,26	515,10	6,41
1250	12525	1	3b	314,33	27,20	1464,08	312,80	11,56
1250	12925	1	3b	499,23	42,50	1600,08	448,80	11,75
1250	13125	1	3b	388,29	64,60	1796,00	649,40	6,01
1250	15425	1	3b	979,97	24,70	1437,88	278,80	39,67
1250	15475	1	3b	758,09	62,90	1748,26	600,10	12,05
1250	15500	1	3b	573,19	66,30	1491,70	345,10	8,65
1250	15575	1	3b	536,21	54,40	1511,96	363,80	9,86
1250	15625	1	3b	554,70	73,10	1688,48	537,20	7,59
1250	15625	1	3b	425,27	64,60	1573,16	425,00	6,58
1250	15650	1	3b	647,15	71,40	1618,78	467,50	9,06
1250	18375	1	3b	462,25	32,30	1526,72	353,60	14,31
1250	20375	1	3b	721,11	71,40	1632,50	501,50	10,10
1250	20650	1	3b	758,09	78,20	1564,92	438,60	9,69
1250	20950	1	3b	665,64	42,50	1653,46	528,70	15,66

(N-S)	X (E-W)	Area	Unit	Width (m)	Height (m)	Depth (mbsl)	Burial depth (m)	W/H ratio
1250	21725	1	3b	610,17	71,40	1574,56	442,00	8,55
1250	22300	1	3b	628,66	47,60	1684,92	550,80	13,21
1375	3275	1	3b	462,25	37,40	1404,72	387,60	12,36
1375	4625	1	3b	425,27	42,50	1451,36	404,60	10,01
1375	5175	1	3b	1312,79	102,00	1557,48	499,80	12,87
1375	5400	1	3b	554,70	51,00	1613,30	552,50	10,88
1375	6675	1	3b	240,37	64,60	1598,30	389,30	3,72
1375	6775	1	3b	277,35	44,20	1679,76	469,20	6,27
1375	8250	1	3b	258,86	20,40	1608,96	499,80	12,69
1375	8325	1	3b	332,82	40,80	1800,78	688,50	8,16
1375	8450	1	3b	314,33	45,90	1649,20	533,80	6,85
1375	8525	1	3b	573,19	56,10	1705,30	589,90	10,22
1375	8975	1	3b	314,33	40,80	1609,70	470,90	7,70
1375	9350	1	3b	314,33	51,00	1746,26	613,70	6,16
1375	9375	1	3b	314,33	62,90	1498,06	365,50	5,00
1375	9625	1	3b	591,68	62,90	1554,44	425,00	9,41
1375	10875	1	3b	221,88	44,20	1725,72	591,60	5,02
1375	12025	1	3b	221,88	54,40	1748,12	598,40	4,08
1375	12025	1	3b	776,58	81,60	1627,56	479,40	9,52
1375	12050	1	3b	684,13	102,00	1693,86	545,70	6,71
1375	12175	1	3b	351,31	47,60	1669,64	516,80	7,38
1375	13125	1	3b	332,82	47,60	1785,52	635,80	6,99
1375	15300	1	3b	573,19	40,80	1467,06	311,10	14,05
1375	15350	1	3b	979,97	61,20	1431,22	273,70	16,01
1375	15550	1	3b	388,29	64,60	1686,64	533,80	6,01
1375	15575	1	3b	443,76	81,60	1557,30	402,90	5,44
1375	15600	1	3b	554,70	57,80	1610,28	459,00	9,60
1375	15625	1	3b	184,90	57,80	1729,42	579,70	3,20
1375	17775	1	3b	869,03	74,80	1624,00	493,00	11,62
1375	20700	1	3b	684,13	69,70	1554,72	428,40	9,82
1375	21550	1	3b	591,68	27,20	1656,30	525,30	21,75
1375	21725	1	3b	517,72	49,30	1552,60	421,60	10,50
1375	22225	1	3b	1164,87	66,30	1775,04	567,80	17,57
1375	22425	1	3b	425,27	40,80	1672,60	533,80	10,42
1500	2950	1	3b	480,74	34,00	1252,42	243,10	14,14
1500	5450	1	3b	332,82	37,40	1604,10	535,50	8,90
1500	5550	1	3b	1127,89	98,60	1570,24	503,20	11,44
1500	6375	1	3b	1257,32	49,30	1467,26	389,30	25,50
1500	6875	1	3b	258,86	39,10	1676,08	462,40	6,62
1500	7300	1	3b	277,35	42,50	1745,40	622,20	6,53
1500	7775	1	3b	369,80	47,60	1642,68	530,40	7,77
1500	8375	1	3b	499,23	100,30	1807,46	674,90	4,98
1500	8425	1	3b	295,84	49,30	1680,24	550,80	6,00
1500	8475	1	3b	554,70	62,90	1612,10	481,10	8,82
1500	8725	1	3b	351,31	56,10	1717,94	572,90	6,26
1500	9575	1	3b	480,74	51,00	1705,60	574,60	9,43
1500	9600	1	3b	573,19	57,80	1549,20	418,20	9,92
1500	9725	1	3b	332,82	44,20	1615,36	482,80	7,53

(N-S)	X (E-W)	Area	Unit	Width (m)	Height (m)	Depth (mbsl)	Burial depth (m)	W/H ratio
1500	10850	1	3b	314,33	54,40	1745,70	606,90	5,78
1500	11025	1	3b	240,37	37,40	1696,12	554,20	6,43
1500	11825	1	3b	628,66	54,40	1622,18	470,90	11,56
1500	12075	1	3b	480,74	93,50	1739,06	583,10	5,14
1500	12150	1	3b	795,07	49,30	1543,56	387,60	16,13
1500	13425	1	3b	665,64	32,30	1602,36	438,60	20,61
1500	14675	1	3b	203,39	51,00	1778,78	572,90	3,99
1500	14675	1	3b	425,27	32,30	1619,26	416,50	13,17
1500	15300	1	3b	443,76	39,10	1461,98	287,30	11,35
1500	15475	1	3b	536,21	98,60	1565,24	404,60	5,44
1500	15650	1	3b	406,78	119,00	1723,62	566,10	3,42
1500	19000	1	3b	628,66	52,70	1588,32	306,00	11,93
1500	20425	1	3b	1220,34	96,90	1618,34	481,10	12,59
1500	20800	1	3b	647,15	57,80	1559,12	425,00	11,20
1500	21725	1	3b	536,21	37,40	1524,42	382,50	14,34
1500	21750	1	3b	443,76	42,50	1674,16	533,80	10,44
1625	3100	1	3b	721,11	56,10	1407,84	387,60	12,85
1625	5550	1	3b	1312,79	56,10	1523,78	450,50	23,40
1625	5675	1	3b	665,64	61,20	1588,10	511,70	10,88
1625	5750	1	3b	1312,79	39,10	1462,02	382,50	33,58
1625	5900	1	3b	406,78	39,10	1628,34	545,70	10,40
1625	6375	1	3b	221,88	42,50	1643,44	482,80	5,22
1625	8525	1	3b	499,23	78,20	1676,84	547,40	6,38
1625	9100	1	3b	462,25	66,30	1548,24	387,60	6,97
1625	9600	1	3b	591,68	54,40	1541,98	406,30	10,88
1625	9775	1	3b	295,84	56,10	1708,44	571,20	5,27
1625	10400	1	3b	240,37	44,20	1671,18	535,50	5,44
1625	10700	1	3b	221,88	47,60	1774,88	639,20	4,66
1625	10825	1	3b	758,09	40,80	1526,12	384,20	18,58
1625	10875	1	3b	332,82	69,70	1740,32	598,40	4,78
1625	10875	1	3b	758,09	45,90	1529,38	385,90	16,52
1625	11000	1	3b	240,37	32,30	1634,36	486,20	7,44
1625	11275	1	3b	240,37	54,40	1715,54	562,70	4,42
1625	11925	1	3b	314,33	37,40	1658,32	493,00	8,40
1625	12075	1	3b	388,29	54,40	1709,04	540,60	7,14
1625	12125	1	3b	277,35	45,90	1751,68	584,80	6,04
1625	12125	1	3b	665,64	56,10	1614,26	450,50	11,87
1625	12325	1	3b	536,21	54,40	1552,50	382,50	9,86
1625	13450	1	3b	480,74	40,80	1644,44	476,00	11,78
1625	13750	1	3b	277,35	17,00	1617,68	435,20	16,31
1625	14600	1	3b	536,21	51,00	1598,86	396,10	10,51
1625	14825	1	3b	351,31	35,70	1564,85	305,15	9,84
1625	15150	1	3b	351,31	22,10	1451,22	270,30	15,90
1625	15250	1	3b	295,84	34,00	1765,86	586,50	8,70
1625	15375	1	3b	647,15	59,50	1513,82	348,50	10,88
1625	15400	1	3b	462,25	57,80	1571,34	402,90	8,00
1625	15475	1	3b	665,64	42,50	1636,36	472,60	15,66
1625	15525	1	3b	647,15	69,70	1700,96	537,20	9,28



(N-S)	X (E-W)	Area	Unit	Width (m)	Height (m)	Depth (mbsl)	Burial depth (m)	W/H ratio
1625	15525	1	3b	406,78	44,20	1624,46	460,70	9,20
1625	15700	1	3b	351,31	56,10	1850,56	686,80	6,26
1625	18275	1	3b	554,70	54,40	1513,60	289,00	10,20
1625	19250	1	3b	536,21	45,90	1570,20	275,40	11,68
1625	20450	1	3b	1257,32	73,10	1590,28	462,40	17,20
1625	20525	1	3b	813,56	54,40	1627,12	493,00	14,96
1625	21675	1	3b	554,70	74,80	1687,20	540,60	7,42
1625	22175	1	3b	536,21	54,40	1624,02	474,30	9,86
1625	22275	1	3b	998,46	69,70	1726,86	586,50	14,33
1625	22300	1	3b	610,17	35,70	1559,56	411,40	17,09
1625	22450	1	3b	647,15	73,10	1661,70	515,10	8,85
1750	5800	1	3b	1571,65	68,00	1541,78	460,70	23,11
1750	5875	1	3b	813,56	68,00	1605,82	518,50	11,96
1750	5900	1	3b	1405,24	44,20	1466,70	382,50	31,79
1750	5975	1	3b	517,72	49,30	1624,38	535,50	10,50
1750	6075	1	3b	314,33	52,70	1672,12	584,80	5,96
1750	6575	1	3b	388,29	42,50	1255,26	239,70	9,14
1750	7300	1	3b	351,31	51,00	1750,18	528,70	6,89
1750	7625	1	3b	332,82	42,50	1642,96	533,80	7,83
1750	7875	1	3b	314,33	52,70	1739,58	627,30	5,96
1750	8050	1	3b	425,27	71,40	1553,86	436,90	5,96
1750	8550	1	3b	221,88	56,10	1693,70	562,70	3,96
1750	8875	1	3b	443,76	45,90	1528,40	374,00	9,67
1750	9050	1	3b	369,80	66,30	1594,84	442,00	5,58
1750	9800	1	3b	295,84	51,00	1659,42	525,30	5,80
1750	9975	1	3b	277,35	59,50	1737,20	598,40	4,66
1750	10500	1	3b	277,35	49,30	1679,96	547,40	5,63
1750	10650	1	3b	869,03	59,50	1525,42	375,70	14,61
1750	10800	1	3b	369,80	66,30	1747,26	606,90	5,58
1750	10950	1	3b	702,62	59,50	1603,90	457,30	11,81
1750	11025	1	3b	351,31	44,20	1690,88	547,40	7,95
1750	11450	1	3b	443,76	47,60	1633,66	477,70	9,32
1750	11650	1	3b	295,84	68,00	1662,70	508,30	4,35
1750	11725	1	3b	388,29	59,50	1672,34	511,70	6,53
1750	11950	1	3b	369,80	61,20	1695,58	528,70	6,04
1750	12075	1	3b	443,76	59,50	1704,36	540,60	7,46
1750	12175	1	3b	425,27	64,60	1763,44	595,00	6,58
1750	12175	1	3b	536,21	68,00	1721,08	554,20	7,89
1750	12400	1	3b	573,19	56,10	1588,06	416,50	10,22
1750	12825	1	3b	573,19	49,30	1540,32	367,20	11,63
1750	13525	1	3b	684,13	83,30	1681,28	506,60	8,21
1750	13750	1	3b	517,72	39,10	1613,14	436,90	13,24
1750	15100	1	3b	277,35	34,00	1463,54	287,30	8,16
1750	15200	1	3b	277,35	39,10	1768,26	596,70	7,09
1750	15200	1	3b	499,23	62,90	1528,42	355,30	7,94
1750	15325	1	3b	332,82	49,30	1570,64	394,40	6,75
1750	15400	1	3b	406,78	64,60	1683,26	511,70	6,30
1750	15450	1	3b	240,37	59,50	1819,82	654,50	4,04

(N-S)	X (E-W)	Area	Unit	Width (m)	Height (m)	Depth (mbsl)	Burial depth (m)	W/H ratio
1750	15475	1	3b	406,78	52,70	1631,12	465,80	7,72
1750	15625	1	3b	480,74	47,60	1738,08	571,20	10,10
1750	19175	1	3b	758,09	62,90	1576,86	280,50	12,05
1750	21750	1	3b	536,21	57,80	1677,16	513,40	9,28
1750	22275	1	3b	369,80	66,30	1617,36	469,20	5,58
1750	22325	1	3b	1109,40	73,10	1719,50	572,90	15,18
1875	4925	1	3b	443,76	47,60	1523,92	452,20	9,32
1875	5000	1	3b	369,80	45,90	1530,16	452,20	8,06
1875	6150	1	3b	517,72	57,80	1661,08	564,40	8,96
1875	6150	1	3b	813,56	85,10	1599,88	503,20	9,56
1875	7300	1	3b	277,35	28,90	1747,14	586,50	9,60
1875	7300	1	3b	536,21	49,30	1652,44	421,60	10,88
1875	8050	1	3b	443,76	54,40	1557,26	440,30	8,16
1875	8500	1	3b	369,80	64,60	1695,54	566,10	5,72
1875	8675	1	3b	443,76	54,40	1635,64	482,80	8,16
1875	9025	1	3b	536,21	62,90	1552,20	397,80	8,52
1875	9825	1	3b	369,80	68,00	1688,90	542,30	5,44
1875	9975	1	3b	240,37	62,90	1748,96	608,60	3,82
1875	10575	1	3b	1164,87	59,50	1503,40	146,20	19,58
1875	10675	1	3b	924,50	79,90	1606,88	455,60	11,57
1875	10750	1	3b	277,35	39,10	1726,02	576,30	7,09
1875	10950	1	3b	906,01	61,20	1637,34	484,50	14,80
1875	11300	1	3b	554,70	83,30	1653,78	494,70	6,66
1875	11525	1	3b	573,19	88,40	1662,00	499,80	6,48
1875	11650	1	3b	591,68	79,90	1684,10	521,90	7,41
1875	12050	1	3b	776,58	73,10	1701,82	528,70	10,62
1875	12100	1	3b	610,17	90,10	1759,14	239,70	6,77
1875	12625	1	3b	906,01	62,90	1553,78	379,10	14,40
1875	12675	1	3b	610,17	62,90	1604,64	428,40	9,70
1875	13525	1	3b	332,82	61,20	1735,96	564,40	5,44
1875	13625	1	3b	462,25	49,30	1659,46	487,90	9,38
1875	15200	1	3b	462,25	71,40	1524,46	345,10	6,47
1875	15350	1	3b	517,72	45,90	1779,18	596,70	11,28
1875	15350	1	3b	462,25	69,70	1575,74	399,50	6,63
1875	15400	1	3b	499,23	51,00	1630,84	462,40	9,79
1875	15475	1	3b	388,29	73,10	1831,30	661,30	5,31
1875	15475	1	3b	665,64	79,90	1727,46	555,90	8,33
1875	15475	1	3b	406,78	49,30	1681,70	511,70	8,25
1875	19050	1	3b	665,64	44,20	1559,16	255,00	15,06
1875	20500	1	3b	1275,81	86,70	1601,20	462,40	14,72
1875	20875	1	3b	591,68	54,40	1571,88	428,40	10,88
1875	21800	1	3b	942,99	52,70	1676,46	504,90	17,89
1875	22225	1	3b	536,21	78,20	1613,68	462,40	6,86
1875	22250	1	3b	1183,36	88,40	1714,40	567,80	13,39
2000	3400	1	3b	610,17	20,40	1268,88	234,60	29,91
2000	4275	1	3b	480,74	52,70	1456,62	392,70	9,12
2000	4600	1	3b	314,33	32,30	1483,26	413,10	9,73
2000	4975	1	3b	406,78	44,20	1528,60	452,20	9,20

(N-S)	X (E-W)	Area	Unit	Width (m)	Height (m)	Depth (mbsl)	Burial depth (m)	W/H ratio
2000	6175	1	3b	961,48	86,70	1594,22	491,30	11,09
2000	6200	1	3b	369,80	42,50	1660,94	562,70	8,70
2000	6475	1	3b	869,03	62,90	1619,02	508,30	13,82
2000	7000	1	3b	406,78	51,00	1740,70	508,30	7,98
2000	8200	1	3b	240,37	52,70	1789,46	664,70	4,56
2000	8525	1	3b	554,70	88,40	1717,80	571,20	6,27
2000	8625	1	3b	480,74	37,40	1628,70	474,30	12,85
2000	9100	1	3b	517,72	64,60	1573,74	413,10	8,01
2000	9800	1	3b	425,27	66,30	1685,50	538,90	6,41
2000	10000	1	3b	258,86	28,90	1737,64	584,80	8,96
2000	10400	1	3b	850,54	59,50	1520,04	367,20	14,29
2000	10700	1	3b	684,13	66,30	1541,72	384,20	10,32
2000	10725	1	3b	351,31	34,00	1688,06	532,10	10,33
2000	10800	1	3b	850,54	56,10	1579,40	425,00	15,16
2000	11725	1	3b	332,82	54,40	1737,66	566,10	6,12
2000	12075	1	3b	665,64	110,50	1810,62	637,50	6,02
2000	12375	1	3b	314,33	40,80	1746,02	572,90	7,70
2000	12725	1	3b	591,68	83,30	1624,90	447,10	7,10
2000	12825	1	3b	1146,38	51,00	1480,12	299,20	22,48
2000	12925	1	3b	813,56	79,90	1563,42	382,50	10,18
2000	13450	1	3b	425,27	28,90	1756,08	581,40	14,72
2000	13475	1	3b	166,41	23,80	1785,40	615,40	6,99
2000	13600	1	3b	443,76	52,70	1699,56	520,20	8,42
2000	14300	1	3b	184,90	32,30	1809,36	622,20	5,72
2000	14825	1	3b	277,35	42,50	1454,08	248,20	6,53
2000	15150	1	3b	462,25	40,80	1502,50	324,70	11,33
2000	15225	1	3b	554,70	74,80	1571,92	391,00	7,42
2000	15300	1	3b	702,62	66,30	1626,46	447,10	10,60
2000	15325	1	3b	813,56	93,50	1700,12	527,00	8,70
2000	15525	1	3b	277,35	45,90	1853,26	681,70	6,04
2000	18950	1	3b	573,19	40,80	1555,32	265,20	14,05
2000	20400	1	3b	776,58	69,70	1583,34	453,90	11,14
2000	21125	1	3b	887,52	54,40	1524,56	384,20	16,31
2000	21200	1	3b	425,27	44,20	1616,66	460,70	9,62
2000	21925	1	3b	406,78	49,30	1660,14	515,10	8,25
2000	22150	1	3b	554,70	68,00	1582,94	430,10	8,16
2000	22250	1	3b	1331,28	85,00	1695,42	545,70	15,66
2125	3475	1	3b	684,13	39,10	1287,88	238,00	17,50
2125	4200	1	3b	351,31	30,60	1217,34	158,10	11,48
2125	4350	1	3b	425,27	39,10	1459,60	391,00	10,88
2125	5000	1	3b	462,25	45,90	1521,10	436,90	10,07
2125	6450	1	3b	258,86	40,80	1661,54	532,10	6,34
2125	6500	1	3b	961,48	125,80	1628,10	504,90	7,64
2125	8250	1	3b	499,23	49,30	1581,64	452,20	10,13
2125	9100	1	3b	443,76	66,30	1589,46	433,50	6,69
2125	9775	1	3b	314,33	68,00	1712,14	559,30	4,62
2125	10000	1	3b	332,82	76,50	1789,06	640,90	4,35
2125	10300	1	3b	443,76	74,80	1632,24	479,40	5,93

(N-S)	X (E-W)	Area	Unit	Width (m)	Height (m)	Depth (mbsl)	Burial depth (m)	W/H ratio
2125	10300	1	3b	647,15	66,30	1540,16	384,20	9,76
2125	11675	1	3b	295,84	52,70	1730,16	550,80	5,61
2125	11950	1	3b	258,86	52,70	1794,90	617,10	4,91
2125	12150	1	3b	573,19	83,30	1842,22	661,30	6,88
2125	12375	1	3b	277,35	42,50	1808,50	630,70	6,53
2125	12475	1	3b	480,74	76,50	1713,02	532,10	6,28
2125	12550	1	3b	351,31	35,70	1673,78	491,30	9,84
2125	12800	1	3b	425,27	71,40	1649,84	465,80	5,96
2125	12900	1	3b	869,03	103,70	1588,78	406,30	8,38
2125	13600	1	3b	425,27	81,60	1721,52	540,60	5,21
2125	14300	1	3b	166,41	47,60	1815,74	623,90	3,50
2125	14875	1	3b	258,86	30,60	1442,88	244,80	8,46
2125	15200	1	3b	536,21	73,10	1560,02	379,10	7,34
2125	15225	1	3b	684,13	52,70	1622,64	438,60	12,98
2125	15250	1	3b	295,84	52,70	1821,68	639,20	5,61
2125	15400	1	3b	573,19	81,60	1709,76	530,40	7,02
2125	15725	1	3b	388,29	68,00	1727,74	559,30	5,71
2125	15900	1	3b	277,35	74,80	1805,52	632,40	3,71
2125	16450	1	3b	258,86	25,50	1445,68	278,80	10,15
2125	18750	1	3b	924,50	61,20	1538,28	285,60	15,11
2125	19725	1	3b	499,23	39,10	1509,12	367,20	12,77
2125	21200	1	3b	647,15	39,10	1526,98	375,70	16,55
2125	21225	1	3b	610,17	45,90	1608,86	460,70	13,29
2125	21850	1	3b	462,25	54,40	1620,34	467,50	8,50
2125	21950	1	3b	536,21	57,80	1671,62	521,90	9,28
2125	22075	1	3b	1164,87	76,50	1681,54	528,70	15,23
2125	22125	1	3b	721,11	52,70	1557,30	402,90	13,68
2250	4800	1	3b	610,17	51,00	1502,26	416,50	11,96
2250	6575	1	3b	1146,38	74,80	1567,32	448,80	15,33
2250	6650	1	3b	610,17	64,60	1626,12	499,80	9,45
2250	6875	1	3b	277,35	32,30	1748,70	586,50	8,59
2250	6875	1	3b	499,23	42,50	1681,02	484,50	11,75
2250	6875	1	3b	906,01	78,20	1645,00	482,80	11,59
2250	7275	1	3b	425,27	52,70	1736,46	494,70	8,07
2250	7475	1	3b	425,27	34,00	1460,36	210,80	12,51
2250	8425	1	3b	480,74	115,60	1799,96	659,60	4,16
2250	8525	1	3b	684,13	68,00	1592,42	450,50	10,06
2250	9950	1	3b	499,23	85,00	1714,98	555,90	5,87
2250	10025	1	3b	314,33	100,30	1818,54	657,90	3,13
2250	10350	1	3b	813,56	98,60	1636,92	479,40	8,25
2250	10350	1	3b	573,19	64,60	1529,54	368,90	8,87
2250	10450	1	3b	480,74	73,10	1606,18	447,10	6,58
2250	11475	1	3b	425,27	68,00	1679,72	506,60	6,25
2250	11675	1	3b	332,82	68,00	1732,14	555,90	4,89
2250	12175	1	3b	665,64	74,80	1811,62	630,70	8,90
2250	12525	1	3b	554,70	52,70	1696,16	516,80	10,53
2250	12800	1	3b	388,29	37,40	1738,24	554,20	10,38
2250	12825	1	3b	665,64	91,80	1656,50	470,90	7,25

(N-S)	X (E-W)	Area	Unit	Width (m)	Height (m)	Depth (mbsl)	Burial depth (m)	W/H ratio
2250	12950	1	3b	832,05	64,60	1563,14	379,10	12,88
2250	13600	1	3b	406,78	91,80	1745,46	566,10	4,43
2250	15075	1	3b	499,23	28,90	1483,10	297,50	17,27
2250	15100	1	3b	573,19	76,50	1566,12	377,40	7,49
2250	15175	1	3b	573,19	39,10	1611,02	430,10	14,66
2250	15250	1	3b	573,19	85,00	1700,70	515,10	6,74
2250	15325	1	3b	258,86	64,60	1828,34	644,30	4,01
2250	15850	1	3b	406,78	100,30	1776,34	600,10	4,06
2250	15950	1	3b	314,33	44,20	1665,70	487,90	7,11
2250	20050	1	3b	554,70	42,50	1533,20	394,40	13,05
2250	21175	1	3b	573,19	51,00	1538,74	385,90	11,24
2250	21300	1	3b	684,13	52,70	1613,68	462,40	12,98
2250	21900	1	3b	240,37	54,40	1621,20	459,00	4,42
2250	22050	1	3b	314,33	49,30	1552,34	399,50	6,38
2250	22125	1	3b	1460,71	81,60	1672,62	515,10	17,90
2375	4775	1	3b	591,68	61,20	1512,32	425,00	9,67
2375	5175	1	3b	443,76	54,40	1471,10	379,10	8,16
2375	6725	1	3b	1016,95	83,30	1572,28	452,20	12,21
2375	6850	1	3b	536,21	78,20	1646,54	501,50	6,86
2375	7175	1	3b	499,23	25,50	1740,40	523,60	19,58
2375	7275	1	3b	388,29	57,80	1730,18	532,10	6,72
2375	8400	1	3b	499,23	139,40	1810,46	654,50	3,58
2375	8600	1	3b	721,11	42,50	1581,80	435,20	16,97
2375	9975	1	3b	462,25	90,10	1741,20	571,20	5,13
2375	10050	1	3b	240,37	62,90	1845,32	680,00	3,82
2375	10275	1	3b	462,25	61,20	1640,04	479,40	7,55
2375	10375	1	3b	314,33	54,40	1600,94	440,30	5,78
2375	11850	1	3b	351,31	35,70	1646,30	460,70	9,84
2375	12275	1	3b	462,25	64,60	1813,18	630,70	7,16
2375	12725	1	3b	573,19	51,00	1779,62	583,10	11,24
2375	12825	1	3b	332,82	47,60	1653,10	467,50	6,99
2375	13075	1	3b	887,52	100,30	1602,10	416,50	8,85
2375	13325	1	3b	517,72	59,50	1843,50	657,90	8,70
2375	13675	1	3b	462,25	62,90	1725,78	535,50	7,35
2375	13675	1	3b	369,80	37,40	1596,58	406,30	9,89
2375	13700	1	3b	517,72	71,40	1668,12	479,40	7,25
2375	14650	1	3b	443,76	71,40	1489,64	282,20	6,22
2375	14900	1	3b	554,70	71,40	1818,44	618,80	7,77
2375	14900	1	3b	499,23	76,50	1576,76	374,00	6,53
2375	15000	1	3b	351,31	54,40	1638,24	438,60	6,46
2375	15275	1	3b	517,72	79,90	1714,44	530,40	6,48
2375	16075	1	3b	499,23	83,30	1685,68	503,20	5,99
2375	16500	1	3b	480,74	32,30	1456,74	280,50	14,88
2375	18400	1	3b	388,29	28,90	1568,38	385,90	13,44
2375	18450	1	3b	351,31	39,10	1519,92	346,80	8,98
2375	20325	1	3b	1312,79	52,70	1547,52	397,80	24,91
2375	21350	1	3b	924,50	62,90	1626,86	470,90	14,70
2375	22075	1	3b	1442,22	59,50	1656,90	494,70	24,24

(N-S)	X (E-W)	Area	Unit	Width (m)	Height (m)	Depth (mbsl)	Burial depth (m)	W/H ratio
2500	4325	1	3b	887,52	57,80	1458,62	379,10	15,36
2500	4700	1	3b	332,82	42,50	1512,74	430,10	7,83
2500	7025	1	3b	998,46	105,40	1656,46	508,30	9,47
2500	7250	1	3b	610,17	57,80	1750,30	549,10	10,56
2500	7500	1	3b	443,76	44,20	1704,02	460,70	10,04
2500	8275	1	3b	369,80	32,30	1561,98	402,90	11,45
2500	8425	1	3b	369,80	107,10	1828,46	664,70	3,45
2500	8525	1	3b	702,62	40,80	1580,40	418,20	17,22
2500	9825	1	3b	406,78	54,40	1648,56	469,20	7,48
2500	10050	1	3b	369,80	95,20	1849,44	673,20	3,88
2500	10050	1	3b	443,76	73,10	1721,80	544,00	6,07
2500	10100	1	3b	499,23	71,40	1646,86	467,50	6,99
2500	10300	1	3b	628,66	81,60	1598,82	433,50	7,70
2500	10350	1	3b	665,64	52,70	1512,26	348,50	12,63
2500	11825	1	3b	406,78	35,70	1717,42	528,70	11,39
2500	11825	1	3b	369,80	34,00	1666,56	479,40	10,88
2500	12250	1	3b	425,27	57,80	1789,82	593,30	7,36
2500	12825	1	3b	425,27	54,40	1621,94	430,10	7,82
2500	13150	1	3b	388,29	47,60	1604,52	408,00	8,16
2500	13250	1	3b	499,23	81,60	1852,72	656,20	6,12
2500	13675	1	3b	499,23	105,40	1687,96	493,00	4,74
2500	14700	1	3b	462,25	40,80	1492,34	277,10	11,33
2500	14775	1	3b	203,39	44,20	1865,48	659,60	4,60
2500	14925	1	3b	499,23	64,60	1812,64	605,20	7,73
2500	14975	1	3b	332,82	40,80	1743,50	542,30	8,16
2500	14975	1	3b	517,72	57,80	1561,60	360,40	8,96
2500	15000	1	3b	425,27	81,60	1650,14	450,50	5,21
2500	15125	1	3b	369,80	85,00	1688,24	496,40	4,35
2500	16150	1	3b	499,23	120,70	1714,30	528,70	4,14
2500	17650	1	3b	443,76	27,20	1561,46	226,10	16,31
2500	18425	1	3b	388,29	45,90	1572,32	414,80	8,46
2500	20575	1	3b	906,01	54,40	1544,98	385,90	16,65
2500	21550	1	3b	1016,95	59,50	1624,74	464,10	17,09
2500	21850	1	3b	1294,30	47,60	1650,10	487,90	27,19
2625	4050	1	3b	795,07	54,40	1461,46	375,70	14,62
2625	4525	1	3b	536,21	35,70	1490,08	401,20	15,02
2625	5900	1	3b	406,78	40,80	1549,04	435,20	9,97
2625	6575	1	3b	998,46	34,00	1520,72	394,40	29,37
2625	7200	1	3b	721,11	91,80	1662,44	486,20	7,86
2625	7200	1	3b	887,52	68,00	1579,26	423,30	13,05
2625	7275	1	3b	536,21	64,60	1782,44	598,40	8,30
2625	7325	1	3b	554,70	59,50	1726,24	503,20	9,32
2625	8450	1	3b	610,17	40,80	1566,54	382,50	14,96
2625	9975	1	3b	462,25	57,80	1651,26	464,10	8,00
2625	10050	1	3b	314,33	34,00	1733,14	549,10	9,25
2625	10100	1	3b	332,82	117,30	1866,58	691,90	2,84
2625	10125	1	3b	517,72	64,60	1629,86	450,50	8,01
2625	10175	1	3b	443,76	44,20	1597,84	421,60	10,04

(N-S)	X (E-W)	Area	Unit	Width (m)	Height (m)	Depth (mbsl)	Burial depth (m)	W/H ratio
2625	10225	1	3b	554,70	52,70	1511,84	343,40	10,53
2625	10275	1	3b	665,64	71,40	1581,54	413,10	9,32
2625	10700	1	3b	295,84	32,30	1637,36	465,80	9,16
2625	11750	1	3b	443,76	35,70	1554,22	365,50	12,43
2625	12200	1	3b	443,76	47,60	1749,16	554,20	9,32
2625	12925	1	3b	351,31	30,60	1732,02	535,50	11,48
2625	13000	1	3b	314,33	44,20	1788,26	593,30	7,11
2625	13400	1	3b	554,70	85,00	1867,88	669,80	6,53
2625	14425	1	3b	462,25	27,20	1356,48	142,80	16,99
2625	14675	1	3b	425,27	66,30	1877,10	668,10	6,41
2625	14700	1	3b	425,27	79,90	1878,10	661,30	5,32
2625	14775	1	3b	332,82	59,50	1790,12	578,00	5,59
2625	14875	1	3b	314,33	61,20	1737,98	532,10	5,14
2625	14875	1	3b	351,31	64,60	1557,92	353,60	5,44
2625	14900	1	3b	369,80	59,50	1736,14	528,70	6,22
2625	14900	1	3b	332,82	57,80	1562,25	349,35	5,76
2625	14925	1	3b	388,29	71,40	1782,04	574,60	5,44
2625	14950	1	3b	314,33	51,00	1607,06	419,90	6,16
2625	14975	1	3b	295,84	32,30	1595,46	392,70	9,16
2625	15075	1	3b	277,35	47,60	1643,48	445,40	5,83
2625	15075	1	3b	314,33	52,70	1643,20	442,00	5,96
2625	15125	1	3b	277,35	27,20	1810,08	612,00	10,20
2625	15175	1	3b	462,25	71,40	1677,62	481,10	6,47
2625	15175	1	3b	684,13	73,10	1679,04	479,40	9,36
2625	16175	1	3b	610,17	102,00	1730,88	540,60	5,98
2625	16200	1	3b	277,35	39,10	1472,62	283,90	7,09
2625	16250	1	3b	388,29	66,30	1693,90	508,30	5,86
2625	16500	1	3b	573,19	54,40	1552,52	363,80	10,54
2625	17575	1	3b	702,62	54,40	1586,68	248,20	12,92
2625	17800	1	3b	517,72	37,40	1555,10	205,70	13,84
2625	20500	1	3b	887,52	47,60	1546,82	389,30	18,65
2625	21600	1	3b	942,99	57,80	1627,58	460,70	16,31
2625	21825	1	3b	1442,22	68,00	1648,68	489,60	21,21
2750	3800	1	3b	480,74	42,50	1453,38	372,30	11,31
2750	5700	1	3b	277,35	30,60	1538,98	426,70	9,06
2750	6550	1	3b	739,60	37,40	1525,40	394,40	19,78
2750	7175	1	3b	536,21	61,20	1765,70	603,50	8,76
2750	7250	1	3b	406,78	39,10	1682,86	487,90	10,40
2750	7325	1	3b	536,21	62,90	1650,26	470,90	8,52
2750	7450	1	3b	351,31	47,60	1710,24	479,40	7,38
2750	7500	1	3b	388,29	32,30	1574,64	367,20	12,02
2750	7725	1	3b	332,82	51,00	1608,42	341,70	6,53
2750	7850	1	3b	332,82	35,70	1528,80	265,20	9,32
2750	9900	1	3b	462,25	52,70	1643,76	448,80	8,77
2750	9925	1	3b	369,80	44,20	1695,62	491,30	8,37
2750	10025	1	3b	351,31	40,80	1785,70	600,10	8,61
2750	10050	1	3b	406,78	64,60	1620,36	448,80	6,30
2750	10075	1	3b	203,39	56,10	1857,38	674,90	3,63

(N-S)	X (E-W)	Area	Unit	Width (m)	Height (m)	Depth (mbsl)	Burial depth (m)	W/H ratio
2750	10175	1	3b	425,27	54,40	1588,78	406,30	7,82
2750	10275	1	3b	573,19	64,60	1507,60	329,80	8,87
2750	10325	1	3b	665,64	62,90	1579,56	408,00	10,58
2750	11775	1	3b	480,74	47,60	1577,46	382,50	10,10
2750	12175	1	3b	739,60	56,10	1737,12	540,60	13,18
2750	13050	1	3b	369,80	42,50	1778,92	574,60	8,70
2750	13275	1	3b	1035,44	96,90	1600,42	396,10	10,69
2750	13325	1	3b	332,82	61,20	1845,08	639,20	5,44
2750	13600	1	3b	332,82	47,60	1829,92	625,60	6,99
2750	13800	1	3b	554,70	83,30	1673,24	465,80	6,66
2750	13900	1	3b	184,90	37,40	1873,42	661,30	4,94
2750	14575	1	3b	388,29	64,60	1881,22	661,30	6,01
2750	14825	1	3b	739,60	81,60	1779,50	562,70	9,06
2750	14900	1	3b	591,68	64,60	1720,84	513,40	9,16
2750	14975	1	3b	462,25	69,70	1695,20	486,20	6,63
2750	14975	1	3b	573,19	57,80	1625,22	413,10	9,92
2750	17650	1	3b	776,58	61,20	1609,64	261,80	12,69
2750	17725	1	3b	795,07	64,60	1566,58	212,50	12,31
2750	20750	1	3b	1146,38	57,80	1550,36	394,40	19,83
2750	21800	1	3b	1164,87	85,00	1651,52	486,20	13,70
2875	3250	1	3b	166,41	20,40	1150,48	85,00	8,16
2875	6200	1	3b	1238,83	54,40	1500,46	375,70	22,77
2875	7150	1	3b	351,31	68,00	1782,98	623,90	5,17
2875	7500	1	3b	462,25	37,40	1486,20	316,20	12,36
2875	7525	1	3b	517,72	68,00	1755,26	552,50	7,61
2875	7550	1	3b	869,03	85,00	1652,24	476,00	10,22
2875	7600	1	3b	462,25	54,40	1701,56	506,60	8,50
2875	8900	1	3b	388,29	61,20	1852,58	654,50	6,34
2875	9375	1	3b	295,84	42,50	1481,26	294,10	6,96
2875	9700	1	3b	647,15	35,70	1347,98	134,30	18,13
2875	9900	1	3b	351,31	59,50	1727,90	542,30	5,90
2875	10000	1	3b	277,35	35,70	1851,72	663,00	7,77
2875	10025	1	3b	406,78	54,40	1655,08	472,60	7,48
2875	10075	1	3b	406,78	39,10	1493,30	307,70	10,40
2875	10100	1	3b	462,25	47,60	1598,56	411,40	9,71
2875	10175	1	3b	258,86	42,50	1774,92	601,80	6,09
2875	10250	1	3b	610,17	56,10	1572,20	394,40	10,88
2875	11825	1	3b	517,72	78,20	1618,82	430,10	6,62
2875	12150	1	3b	684,13	49,30	1725,50	532,10	13,88
2875	13025	1	3b	573,19	42,50	1724,80	523,60	13,49
2875	13075	1	3b	554,70	59,50	1573,36	370,60	9,32
2875	13075	1	3b	554,70	49,30	1564,86	362,10	11,25
2875	13550	1	3b	517,72	54,40	1620,82	416,50	9,52
2875	13750	1	3b	1127,89	47,60	1491,20	282,20	23,70
2875	13900	1	3b	443,76	96,90	1791,96	581,40	4,58
2875	13925	1	3b	388,29	51,00	1651,00	442,00	7,61
2875	13975	1	3b	295,84	62,90	1880,64	673,20	4,70
2875	14375	1	3b	573,19	35,70	1414,28	200,60	16,06



(N-S)	X (E-W)	Area	Unit	Width (m)	Height (m)	Depth (mbsl)	Burial depth (m)	W/H ratio
2875	14525	1	3b	332,82	78,20	1887,88	666,40	4,26
2875	14600	1	3b	258,86	35,70	1379,58	158,10	7,25
2875	14650	1	3b	425,27	71,40	1590,80	374,00	5,96
2875	14800	1	3b	462,25	62,90	1660,64	445,40	7,35
2875	14900	1	3b	573,19	88,40	1810,38	596,70	6,48
2875	14925	1	3b	406,78	76,50	1723,12	503,20	5,32
2875	16450	1	3b	647,15	64,60	1747,04	547,40	10,02
2875	16550	1	3b	166,41	35,70	1555,64	363,80	4,66
2875	16575	1	3b	536,21	68,00	1667,70	474,30	7,89
2875	16625	1	3b	517,72	57,80	1603,24	411,40	8,96
2875	16675	1	3b	480,74	62,90	1810,22	613,70	7,64
2875	16775	1	3b	776,58	40,80	1477,16	282,20	19,03
2875	17675	1	3b	665,64	88,40	1599,72	255,00	7,53
2875	20350	1	3b	702,62	27,20	1491,44	323,00	25,83
2875	20925	1	3b	536,21	28,90	1566,10	396,10	18,55
2875	21750	1	3b	961,48	73,10	1647,42	474,30	13,15
3000	6525	1	3b	443,76	44,20	1569,46	436,90	10,04
3000	7175	1	3b	147,92	28,90	1754,50	600,10	5,12
3000	7450	1	3b	924,50	64,60	1558,72	401,20	14,31
3000	7625	1	3b	332,82	69,70	1780,32	591,60	4,78
3000	7625	1	3b	684,13	61,20	1653,68	455,60	11,18
3000	7725	1	3b	425,27	59,50	1709,22	504,90	7,15
3000	8975	1	3b	314,33	64,60	1857,14	634,10	4,87
3000	9825	1	3b	184,90	56,10	1805,30	572,90	3,30
3000	9850	1	3b	369,80	68,00	1742,78	552,50	5,44
3000	9925	1	3b	184,90	51,00	1859,24	659,60	3,63
3000	10025	1	3b	573,19	93,50	1677,46	498,10	6,13
3000	10075	1	3b	314,33	44,20	1773,66	586,50	7,11
3000	10125	1	3b	684,13	93,50	1621,50	443,70	7,32
3000	11800	1	3b	536,21	69,70	1655,52	459,00	7,69
3000	11925	1	3b	665,64	56,10	1604,66	409,70	11,87
3000	12775	1	3b	536,21	56,10	1672,10	470,90	9,56
3000	13000	1	3b	406,78	39,10	1734,44	527,00	10,40
3000	13900	1	3b	480,74	59,50	1737,70	528,70	8,08
3000	14250	1	3b	573,19	88,40	1895,66	685,10	6,48
3000	14600	1	3b	351,31	59,50	1600,30	375,70	5,90
3000	14675	1	3b	536,21	47,60	1640,96	414,80	11,26
3000	14800	1	3b	480,74	66,30	1678,64	455,60	7,25
3000	14850	1	3b	480,74	74,80	1773,98	552,50	6,43
3000	14875	1	3b	388,29	59,50	1731,62	511,70	6,53
3000	16475	1	3b	850,54	83,30	1765,32	561,00	10,21
3000	16575	1	3b	591,68	71,40	1720,26	525,30	8,29
3000	16600	1	3b	406,78	66,30	1687,96	493,00	6,14
3000	16725	1	3b	258,86	27,20	1791,38	593,30	9,52
3000	16750	1	3b	610,17	61,20	1631,58	433,50	9,97
3000	16775	1	3b	628,66	39,10	1573,64	374,00	16,08
3000	17700	1	3b	221,88	45,90	1449,00	91,80	4,83
3000	17825	1	3b	665,64	91,80	1597,88	251,60	7,25

(N-S)	X (E-W)	Area	Unit	Width (m)	Height (m)	Depth (mbsl)	Burial depth (m)	W/H ratio
3000	20350	1	3b	647,15	30,60	1494,56	323,00	21,15
3000	21125	1	3b	795,07	54,40	1571,92	391,00	14,62
3000	21825	1	3b	813,56	51,00	1650,40	472,60	15,95
3000	21950	1	3b	850,54	34,00	1600,96	421,60	25,02
3000	22100	1	3b	998,46	32,30	1509,58	334,90	30,91
3125	6350	1	3b	665,64	78,20	1575,42	433,50	8,51
3125	6650	1	3b	721,11	35,70	1485,60	346,80	20,20
3125	7725	1	3b	443,76	96,90	1756,08	581,40	4,58
3125	7725	1	3b	406,78	57,80	1661,16	489,60	7,04
3125	7825	1	3b	573,19	66,30	1812,04	635,80	8,65
3125	7850	1	3b	517,72	68,00	1725,20	547,40	7,61
3125	8000	1	3b	517,72	61,20	1610,48	404,60	8,46
3125	8150	1	3b	277,35	37,40	1662,06	443,70	7,42
3125	8325	1	3b	536,21	40,80	1534,60	278,80	13,14
3125	9000	1	3b	332,82	59,50	1851,92	608,60	5,59
3125	9575	1	3b	203,39	62,90	1300,12	64,60	3,23
3125	9900	1	3b	314,33	73,10	1777,78	579,70	4,30
3125	10025	1	3b	462,25	74,80	1646,86	467,50	6,18
3125	10050	1	3b	332,82	51,00	1730,74	538,90	6,53
3125	10050	1	3b	388,29	52,70	1690,64	506,60	7,37
3125	10125	1	3b	499,23	49,30	1590,62	409,70	10,13
3125	10475	1	3b	258,86	56,10	1692,62	511,70	4,61
3125	11825	1	3b	499,23	59,50	1663,60	462,40	8,39
3125	11875	1	3b	425,27	57,80	1665,30	464,10	7,36
3125	12000	1	3b	573,19	39,10	1588,80	387,60	14,66
3125	12725	1	3b	406,78	40,80	1624,50	423,30	9,97
3125	12750	1	3b	536,21	45,90	1674,80	465,80	11,68
3125	12900	1	3b	702,62	44,20	1726,36	523,60	15,90
3125	13100	1	3b	240,37	49,30	1569,68	363,80	4,88
3125	13600	1	3b	573,19	71,40	1664,60	455,60	8,03
3125	13700	1	3b	536,21	37,40	1579,46	368,90	14,34
3125	14000	1	3b	425,27	52,70	1731,04	523,60	8,07
3125	14325	1	3b	832,05	98,60	1893,82	681,70	8,44
3125	14575	1	3b	332,82	54,40	1622,54	399,50	6,12
3125	14725	1	3b	517,72	64,60	1688,98	467,50	8,01
3125	14825	1	3b	443,76	49,30	1746,64	523,60	9,00
3125	14950	1	3b	184,90	32,30	1812,08	598,40	5,72
3125	16075	1	3b	221,88	25,50	1481,28	275,40	8,70
3125	16675	1	3b	480,74	93,50	1738,54	538,90	5,14
3125	16775	1	3b	628,66	59,50	1644,76	442,00	10,57
3125	16775	1	3b	462,25	47,60	1597,30	396,10	9,71
3125	17450	1	3b	369,80	49,30	1732,46	389,30	7,50
3125	17725	1	3b	517,72	68,00	1579,60	238,00	7,61
3125	17750	1	3b	554,70	66,30	1647,16	319,60	8,37
3125	21175	1	3b	832,05	30,60	1456,46	277,10	27,19
3125	21200	1	3b	610,17	47,60	1566,96	387,60	12,82
3125	21675	1	3b	443,76	61,20	1633,54	457,30	7,25
3125	21700	1	3b	610,17	25,50	1668,96	489,60	23,93

(N-S)	X (E-W)	Area	Unit	Width (m)	Height (m)	Depth (mbsl)	Burial depth (m)	W/H ratio
3250	5075	1	3b	388,29	37,40	1434,72	316,20	10,38
3250	5500	1	3b	332,82	34,00	1481,34	351,90	9,79
3250	6250	1	3b	758,09	52,70	1566,50	419,90	14,39
3250	6275	1	3b	443,76	39,10	1449,20	302,60	11,35
3250	6500	1	3b	499,23	45,90	1490,44	329,80	10,88
3250	7550	1	3b	314,33	59,50	1784,82	627,30	5,28
3250	7775	1	3b	702,62	90,10	1643,88	469,20	7,80
3250	7900	1	3b	314,33	47,60	1790,80	605,20	6,60
3250	7925	1	3b	499,23	96,90	1747,02	566,10	5,15
3250	8200	1	3b	351,31	27,20	1659,96	418,20	12,92
3250	9000	1	3b	388,29	37,40	1839,22	549,10	10,38
3250	9950	1	3b	203,39	74,80	1800,02	603,50	2,72
3250	10025	1	3b	647,15	108,80	1726,34	542,30	5,95
3250	10025	1	3b	702,62	100,30	1647,72	459,00	7,01
3250	10125	1	3b	665,64	78,20	1627,46	440,30	8,51
3250	12025	1	3b	332,82	32,30	1633,00	431,80	10,30
3250	12025	1	3b	554,70	45,90	1592,06	389,30	12,08
3250	12650	1	3b	277,35	47,60	1664,04	448,80	5,83
3250	12750	1	3b	351,31	35,70	1608,22	396,10	9,84
3250	13075	1	3b	406,78	44,20	1562,46	351,90	9,20
3250	13725	1	3b	591,68	81,60	1667,58	453,90	7,25
3250	14200	1	3b	887,52	85,00	1893,82	681,70	10,44
3250	14225	1	3b	425,27	35,70	1802,16	591,60	11,91
3250	14425	1	3b	406,78	69,70	1627,78	406,30	5,84
3250	14675	1	3b	610,17	103,70	1732,90	508,30	5,88
3250	16000	1	3b	147,92	22,10	1482,70	273,70	6,69
3250	16725	1	3b	499,23	76,50	1728,20	527,00	6,53
3250	16800	1	3b	536,21	52,70	1610,62	406,30	10,17
3250	16850	1	3b	295,84	59,50	1679,18	481,10	4,97
3250	17150	1	3b	295,84	57,80	1772,28	550,80	5,12
3250	17325	1	3b	480,74	91,80	1854,20	598,40	5,24
3250	17375	1	3b	332,82	61,20	1691,48	384,20	5,44
3250	17450	1	3b	332,82	42,50	1793,66	450,50	7,83
3250	17500	1	3b	462,25	62,90	1753,96	442,00	7,35
3250	17700	1	3b	480,74	61,20	1564,00	238,00	7,86
3250	17775	1	3b	369,80	23,80	1504,38	158,10	15,54
3250	17800	1	3b	480,74	62,90	1635,70	294,10	7,64
3250	20525	1	3b	369,80	35,70	1527,72	346,80	10,36
3250	21275	1	3b	906,01	49,30	1461,70	283,90	18,38
3250	21500	1	3b	554,70	59,50	1577,16	397,80	9,32
3250	21625	1	3b	406,78	69,70	1646,86	467,50	5,84
3250	21750	1	3b	628,66	35,70	1711,46	532,10	17,61
3375	6225	1	3b	480,74	35,70	1586,62	436,90	13,47
3375	6275	1	3b	684,13	52,70	1555,02	413,10	12,98
3375	7225	1	3b	536,21	37,40	1565,66	409,70	14,34
3375	7850	1	3b	647,15	57,80	1618,10	440,30	11,20
3375	7975	1	3b	665,64	45,90	1792,36	605,20	14,50
3375	8100	1	3b	665,64	95,20	1741,64	557,60	6,99

(N-S)	X (E-W)	Area	Unit	Width (m)	Height (m)	Depth (mbsl)	Burial depth (m)	W/H ratio
3375	8200	1	3b	554,70	52,70	1674,52	462,40	10,53
3375	9000	1	3b	147,92	47,60	1356,30	45,90	3,11
3375	9975	1	3b	314,33	73,10	1777,78	579,70	4,30
3375	10025	1	3b	388,29	56,10	1703,26	508,30	6,92
3375	10075	1	3b	536,21	62,90	1662,18	464,10	8,52
3375	10150	1	3b	517,72	66,30	1633,70	440,30	7,81
3375	11425	1	3b	369,80	28,90	1610,76	408,00	12,80
3375	12250	1	3b	406,78	25,50	1574,64	367,20	15,95
3375	12850	1	3b	684,13	62,90	1678,20	469,20	10,88
3375	12850	1	3b	388,29	35,70	1601,28	387,60	10,88
3375	13800	1	3b	480,74	62,90	1665,46	447,10	7,64
3375	14200	1	3b	721,11	88,40	1893,26	674,90	8,16
3375	14650	1	3b	369,80	73,10	1734,32	506,60	5,06
3375	16775	1	3b	517,72	74,80	1711,92	499,80	6,92
3375	16775	1	3b	628,66	59,50	1619,70	402,90	10,57
3375	17075	1	3b	240,37	56,10	1771,42	559,30	4,28
3375	17325	1	3b	425,27	98,60	1848,82	589,90	4,31
3375	17550	1	3b	517,72	81,60	1770,30	413,10	6,34
3375	17750	1	3b	406,78	52,70	1624,92	295,80	7,72
3375	21550	1	3b	1331,28	32,30	1441,16	261,80	41,22
3375	21650	1	3b	462,25	78,20	1648,00	462,40	5,91
3375	21700	1	3b	869,03	40,80	1722,66	535,50	21,30
3500	6175	1	3b	332,82	40,80	1586,34	433,50	8,16
3500	7300	1	3b	443,76	37,40	1563,54	402,90	11,87
3500	7650	1	3b	369,80	44,20	1756,78	589,90	8,37
3500	7900	1	3b	517,72	51,00	1614,90	382,50	10,15
3500	8175	1	3b	480,74	54,40	1809,94	610,30	8,84
3500	8200	1	3b	554,70	81,60	1747,46	552,50	6,80
3500	8250	1	3b	739,60	64,60	1676,06	481,10	11,45
3500	9025	1	3b	295,84	83,30	1641,62	328,10	3,55
3500	10075	1	3b	647,15	98,60	1708,80	499,80	6,56
3500	10100	1	3b	332,82	81,60	1819,86	617,10	4,08
3500	10200	1	3b	739,60	86,70	1646,04	438,60	8,53
3500	10375	1	3b	184,90	57,80	1879,92	683,40	3,20
3500	12025	1	3b	388,29	39,10	1545,60	336,60	9,93
3500	12900	1	3b	758,09	105,40	1682,46	464,10	7,19
3500	12900	1	3b	480,74	62,90	1628,34	413,10	7,64
3500	13950	1	3b	480,74	51,00	1657,10	440,30	9,43
3500	14125	1	3b	351,31	61,20	1859,54	644,30	5,74
3500	14425	1	3b	462,25	90,10	1749,90	525,30	5,13
3500	14450	1	3b	369,80	54,40	1695,22	467,50	6,80
3500	14475	1	3b	425,27	51,00	1571,12	343,40	8,34
3500	14525	1	3b	388,29	51,00	1620,14	389,30	7,61
3500	14750	1	3b	554,70	54,40	1843,26	617,10	10,20
3500	15825	1	3b	277,35	44,20	1646,48	425,00	6,27
3500	16050	1	3b	295,84	28,90	1497,16	278,80	10,24
3500	16800	1	3b	499,23	71,40	1650,68	476,00	6,99
3500	16950	1	3b	443,76	71,40	1695,78	474,30	6,22

(N-S)	X (E-W)	Area	Unit	Width (m)	Height (m)	Depth (mbsl)	Burial depth (m)	W/H ratio
3500	17325	1	3b	665,64	74,80	1805,78	521,90	8,90
3500	17475	1	3b	388,29	56,10	1723,84	360,40	6,92
3500	17500	1	3b	480,74	56,10	1763,22	402,90	8,57
3500	21600	1	3b	499,23	59,50	1632,70	447,10	8,39
3500	21750	1	3b	1035,44	71,40	1758,08	567,80	14,50
3500	21750	1	3b	1867,49	57,80	1454,06	266,90	32,31
3625	5600	1	3b	425,27	42,50	1587,88	452,20	10,01
3625	6300	1	3b	258,86	25,50	1560,84	408,00	10,15
3625	8250	1	3b	610,17	83,30	1743,06	555,90	7,32
3625	8275	1	3b	425,27	73,10	1812,34	620,50	5,82
3625	8475	1	3b	869,03	88,40	1661,60	476,00	9,83
3625	8900	1	3b	295,84	73,10	1797,52	554,20	4,05
3625	10100	1	3b	887,52	124,10	1694,22	474,30	7,15
3625	10150	1	3b	240,37	64,60	1823,56	605,20	3,72
3625	10275	1	3b	240,37	54,40	1741,82	521,90	4,42
3625	10350	1	3b	258,86	44,20	1872,30	647,70	5,86
3625	12875	1	3b	776,58	79,90	1664,04	448,80	9,72
3625	13000	1	3b	573,19	54,40	1614,46	396,10	10,54
3625	14225	1	3b	536,21	57,80	1656,68	435,20	9,28
3625	14400	1	3b	443,76	54,40	1692,38	470,90	8,16
3625	14450	1	3b	480,74	113,90	1783,34	552,50	4,22
3625	17000	1	3b	739,60	91,80	1671,84	448,80	8,06
3625	17375	1	3b	758,09	85,00	1788,52	482,80	8,92
3625	17475	1	3b	591,68	98,60	1740,56	374,00	6,00
3625	21525	1	3b	924,50	34,00	1710,76	523,60	27,19
3625	21675	1	3b	1294,30	73,10	1785,70	600,10	17,71
3625	21675	1	3b	979,97	59,50	1498,26	311,10	16,47
3625	21850	1	3b	887,52	88,40	1632,28	442,00	10,04
3625	22375	1	3b	684,13	61,20	1668,54	484,50	11,18
3750	4850	1	3b	277,35	18,70	1235,26	110,50	14,83
3750	5500	1	3b	517,72	44,20	1601,62	467,50	11,71
3750	8425	1	3b	776,58	37,40	1679,18	481,10	20,76
3750	8475	1	3b	573,19	90,10	1750,72	554,20	6,36
3750	8475	1	3b	1035,44	74,80	1652,26	457,30	13,84
3750	8575	1	3b	499,23	93,50	1844,22	647,70	5,34
3750	8950	1	3b	314,33	59,50	1803,92	537,20	5,28
3750	9150	1	3b	942,99	78,20	1534,76	261,80	12,06
3750	9350	1	3b	610,17	35,70	1375,86	56,10	17,09
3750	10025	1	3b	758,09	102,00	1646,62	426,70	7,43
3750	10150	1	3b	295,84	59,50	1825,98	596,70	4,97
3750	10200	1	3b	332,82	44,20	1687,42	467,50	7,53
3750	10300	1	3b	258,86	66,30	1759,82	532,10	3,90
3750	12975	1	3b	924,50	73,10	1645,20	428,40	12,65
3750	12975	1	3b	554,70	45,90	1601,00	384,20	12,08
3750	13950	1	3b	332,82	32,30	1500,14	277,10	10,30
3750	14075	1	3b	906,01	40,80	1459,20	234,60	22,21
3750	14300	1	3b	591,68	40,80	1659,66	433,50	14,50
3750	14325	1	3b	462,25	73,10	1727,94	504,90	6,32

(N-S)	X (E-W)	Area	Unit	Width (m)	Height (m)	Depth (mbsl)	Burial depth (m)	W/H ratio
3750	14450	1	3b	351,31	62,90	1802,46	576,30	5,59
3750	14525	1	3b	536,21	62,90	1595,34	372,30	8,52
3750	14575	1	3b	221,88	56,10	1822,72	595,00	3,96
3750	16950	1	3b	647,15	34,00	1578,34	355,30	19,03
3750	17050	1	3b	850,54	74,80	1661,38	416,50	11,37
3750	17400	1	3b	739,60	59,50	1777,68	540,60	12,43
3750	17450	1	3b	517,72	79,90	1744,24	380,80	6,48
3750	17500	1	3b	240,37	52,70	1697,18	358,70	4,56
3750	21275	1	3b	1137,14	35,70	1445,28	255,00	31,85
3750	21375	1	3b	388,29	34,00	1773,80	588,20	11,42
3750	21425	1	3b	443,76	37,40	1613,86	426,70	11,87
3750	21550	1	3b	1164,87	59,50	1737,82	549,10	19,58
3750	21725	1	3b	906,01	90,10	1814,46	627,30	10,06
3750	21825	1	3b	906,01	98,60	1674,78	484,50	9,19
3875	6325	1	3b	499,23	40,80	1542,00	387,60	12,24
3875	8525	1	3b	536,21	54,40	1813,06	610,30	9,86
3875	8525	1	3b	591,68	69,70	1738,40	537,20	8,49
3875	8575	1	3b	758,09	42,50	1694,48	496,40	17,84
3875	8625	1	3b	721,11	61,20	1656,80	455,60	11,78
3875	9950	1	3b	628,66	73,10	1628,36	394,40	8,60
3875	10200	1	3b	351,31	71,40	1679,78	450,50	4,92
3875	10275	1	3b	240,37	52,70	1841,28	612,00	4,56
3875	10350	1	3b	314,33	79,90	1769,88	540,60	3,93
3875	12950	1	3b	591,68	78,20	1648,18	426,70	7,57
3875	14275	1	3b	591,68	100,30	1730,78	501,50	5,90
3875	14450	1	3b	462,25	113,90	1841,28	612,00	4,06
3875	14600	1	3b	517,72	66,30	1587,84	357,00	7,81
3875	17225	1	3b	1183,36	93,50	1625,04	316,20	12,66
3875	17375	1	3b	1016,95	86,70	1750,76	384,20	11,73
3875	21125	1	3b	665,64	42,50	1736,26	549,10	15,66
3875	21375	1	3b	499,23	54,40	1773,38	583,10	9,18
3875	21575	1	3b	776,58	74,80	1645,74	453,90	10,38
3875	21725	1	3b	813,56	100,30	1829,48	639,20	8,11
3875	21800	1	3b	443,76	66,30	1709,06	521,90	6,69
3875	22100	1	3b	573,19	61,20	1766,86	579,70	9,37
4000	6350	1	3b	554,70	51,00	1644,58	477,70	10,88
4000	6375	1	3b	702,62	35,70	1596,84	428,40	19,68
4000	8650	1	3b	554,70	54,40	1818,02	613,70	10,20
4000	8700	1	3b	869,03	62,90	1661,48	455,60	13,82
4000	8725	1	3b	647,15	96,90	1761,64	554,20	6,68
4000	8775	1	3b	979,97	59,50	1588,24	380,80	16,47
4000	10000	1	3b	647,15	68,00	1614,08	353,60	9,52
4000	10275	1	3b	332,82	32,30	1813,66	579,70	10,30
4000	10275	1	3b	388,29	61,20	1668,88	431,80	6,34
4000	10375	1	3b	314,33	71,40	1766,06	532,10	4,40
4000	10400	1	3b	388,29	59,50	1857,44	618,80	6,53
4000	12925	1	3b	665,64	83,30	1673,12	445,40	7,99
4000	12925	1	3b	702,62	69,70	1602,42	382,50	10,08

(N-S)	X (E-W)	Area	Unit	Width (m)	Height (m)	Depth (mbsl)	Burial depth (m)	W/H ratio
4000	14050	1	3b	869,03	44,20	1536,56	302,60	19,66
4000	14250	1	3b	721,11	129,20	1754,86	528,70	5,58
4000	14450	1	3b	536,21	96,90	1822,72	595,00	5,53
4000	14525	1	3b	702,62	39,10	1574,52	346,80	17,97
4000	17250	1	3b	850,54	90,10	1627,30	324,70	9,44
4000	17425	1	3b	573,19	122,40	1733,06	358,70	4,68
4000	20150	1	3b	443,76	28,90	1437,50	236,30	15,36
4000	21000	1	3b	258,86	35,70	1697,88	499,80	7,25
4000	21100	1	3b	536,21	35,70	1743,92	547,40	15,02
4000	21350	1	3b	425,27	151,30	1776,50	583,10	2,81
4000	21550	1	3b	739,60	98,60	1670,96	476,00	7,50
4000	21675	1	3b	480,74	52,70	1701,70	508,30	9,12
4000	21725	1	3b	554,70	81,60	1830,06	627,30	6,80
4000	22175	1	3b	610,17	98,60	1768,00	574,60	6,19
4125	6425	1	3b	684,13	73,10	1663,14	494,70	9,36
4125	6450	1	3b	739,60	52,70	1607,18	440,30	14,03
4125	7800	1	3b	462,25	44,20	1669,54	477,70	10,46
4125	8725	1	3b	610,17	71,40	1669,28	455,60	8,55
4125	8825	1	3b	684,13	129,20	1763,20	554,20	5,30
4125	8950	1	3b	332,82	56,10	1814,20	605,20	5,93
4125	9250	1	3b	942,99	57,80	1538,70	290,70	16,31
4125	10050	1	3b	628,66	100,30	1617,08	333,20	6,27
4125	10225	1	3b	536,21	95,20	1658,72	384,20	5,63
4125	10375	1	3b	425,27	78,20	1692,12	448,80	5,44
4125	10400	1	3b	332,82	66,30	1780,80	540,60	5,02
4125	10475	1	3b	425,27	85,00	1897,82	654,50	5,00
4125	12925	1	3b	610,17	69,70	1722,70	498,10	8,75
4125	12925	1	3b	702,62	90,10	1673,12	445,40	7,80
4125	14250	1	3b	1793,53	81,60	1639,12	411,40	21,98
4125	14275	1	3b	665,64	110,50	1763,08	533,80	6,02
4125	14325	1	3b	517,72	62,90	1766,90	542,30	8,23
4125	14325	1	3b	1109,40	52,70	1554,26	328,10	21,05
4125	14400	1	3b	517,72	93,50	1824,28	595,00	5,54
4125	16025	1	3b	443,76	34,00	1514,20	258,40	13,05
4125	16400	1	3b	536,21	51,00	1609,66	375,70	10,51
4125	16525	1	3b	406,78	49,30	1669,16	435,20	8,25
4125	17350	1	3b	758,09	71,40	1610,10	229,50	10,62
4125	17375	1	3b	628,66	86,70	1733,64	346,80	7,25
4125	17475	1	3b	573,19	76,50	1689,30	300,90	7,49
4125	20025	1	3b	665,64	40,80	1457,48	251,60	16,31
4125	20700	1	3b	277,35	44,20	1643,34	443,70	6,27
4125	20850	1	3b	314,33	62,90	1690,66	487,90	5,00
4125	20975	1	3b	388,29	40,80	1748,60	547,40	9,52
4125	21200	1	3b	240,37	42,50	1762,62	566,10	5,66
4125	21450	1	3b	739,60	100,30	1691,22	494,70	7,37
4125	21650	1	3b	277,35	56,10	1733,30	532,10	4,94
4125	21750	1	3b	684,13	78,20	1811,92	615,40	8,75
4125	21900	1	3b	388,29	71,40	1724,80	523,60	5,44

(N-S)	X (E-W)	Area	Unit	Width (m)	Height (m)	Depth (mbsl)	Burial depth (m)	W/H ratio
4125	22000	1	3b	480,74	68,00	1744,34	552,50	7,07
4250	6450	1	3b	776,58	85,00	1649,40	479,40	9,14
4250	7975	1	3b	591,68	66,30	1718,56	523,60	8,92
4250	8150	1	3b	480,74	39,10	1563,16	360,40	12,30
4250	8825	1	3b	721,11	83,30	1699,88	486,20	8,66
4250	8975	1	3b	721,11	90,10	1766,32	554,20	8,00
4250	9425	1	3b	1072,42	37,40	1536,46	263,50	28,67
4250	10275	1	3b	480,74	79,90	1632,42	311,10	6,02
4250	10400	1	3b	462,25	61,20	1779,82	528,70	7,55
4250	10400	1	3b	610,17	91,80	1700,20	452,20	6,65
4250	10525	1	3b	517,72	91,80	1931,68	686,80	5,64
4250	11300	1	3b	258,86	40,80	1485,40	268,60	6,34
4250	12450	1	3b	480,74	40,80	1613,90	389,30	11,78
4250	12475	1	3b	480,74	45,90	1390,92	163,20	10,47
4250	12950	1	3b	979,97	146,20	1732,62	504,90	6,70
4250	14300	1	3b	684,13	96,90	1761,52	533,80	7,06
4250	14350	1	3b	425,27	69,70	1815,78	586,50	6,10
4250	14400	1	3b	887,52	66,30	1662,50	430,10	13,39
4250	14475	1	3b	221,88	69,70	1898,66	664,70	3,18
4250	15950	1	3b	554,70	37,40	1550,18	297,50	14,83
4250	16075	1	3b	462,25	66,30	1630,64	384,20	6,97
4250	17250	1	3b	869,03	68,00	1610,80	238,00	12,78
4250	17250	1	3b	314,33	88,40	1481,90	93,50	3,56
4250	17275	1	3b	1201,85	93,50	1731,50	358,70	12,85
4250	17275	1	3b	1053,93	15,30	1652,58	290,70	68,88
4250	18925	1	3b	721,11	56,10	1651,70	450,50	12,85
4250	20325	1	3b	610,17	57,80	1486,80	285,60	10,56
4250	20550	1	3b	406,78	51,00	1549,56	346,80	7,98
4250	20975	1	3b	416,03	102,00	1731,32	527,00	4,08
4250	21300	1	3b	406,78	40,80	1683,86	481,10	9,97
4250	21300	1	3b	850,54	54,40	1651,70	450,50	15,63
4250	21525	1	3b	647,15	56,10	1709,36	506,60	11,54
4250	21700	1	3b	647,15	90,10	1736,84	537,20	7,18
4250	21800	1	3b	795,07	88,40	1792,80	591,60	8,99
4375	5625	1	3b	221,88	40,80	1287,86	124,10	5,44
4375	6375	1	3b	610,17	44,20	1618,24	442,00	13,80
4375	8000	1	3b	758,09	76,50	1753,84	554,20	9,91
4375	9025	1	3b	665,64	64,60	1763,06	552,50	10,30
4375	9025	1	3b	1072,42	110,50	1704,84	489,60	9,71
4375	9075	1	3b	554,70	88,40	1868,18	654,50	6,27
4375	9100	1	3b	1294,30	51,00	1594,90	385,90	25,38
4375	9975	1	3b	869,03	34,00	1391,60	57,80	25,56
4375	10250	1	3b	499,23	86,70	1628,60	302,60	5,76
4375	10275	1	3b	628,66	54,40	1667,70	341,70	11,56
4375	10350	1	3b	425,27	61,20	1730,86	426,70	6,95
4375	10375	1	3b	240,37	45,90	1779,46	467,50	5,24
4375	10550	1	3b	517,72	81,60	1916,84	639,20	6,34
4375	10575	1	3b	425,27	56,10	1836,38	552,50	7,58



(N-S)	X (E-W)	Area	Unit	Width (m)	Height (m)	Depth (mbsl)	Burial depth (m)	W/H ratio
4375	12625	1	3b	369,80	35,70	1659,24	428,40	10,36
4375	13050	1	3b	684,13	88,40	1726,82	491,30	7,74
4375	14175	1	3b	369,80	79,90	1713,50	481,10	4,63
4375	14400	1	3b	536,21	110,50	1799,92	564,40	4,85
4375	14525	1	3b	351,31	64,60	1889,18	644,30	5,44
4375	14575	1	3b	832,05	49,30	1632,90	392,70	16,88
4375	16075	1	3b	499,23	56,10	1654,44	408,00	8,90
4375	17125	1	3b	684,13	51,00	1606,00	217,60	13,41
4375	17400	1	3b	961,48	81,60	1702,76	312,80	11,78
4375	17975	1	3b	610,17	51,00	1790,00	557,60	11,96
4375	18050	1	3b	610,17	59,50	1843,84	605,20	10,25
4375	19100	1	3b	536,21	69,70	1705,96	503,20	7,69
4375	19675	1	3b	295,84	32,30	1657,24	442,00	9,16
4375	20375	1	3b	628,66	74,80	1771,70	562,70	8,40
4375	20400	1	3b	554,70	37,40	1453,94	246,50	14,83
4375	20600	1	3b	351,31	30,60	1475,76	265,20	11,48
4375	20650	1	3b	517,72	57,80	1557,36	346,80	8,96
4375	20775	1	3b	702,62	25,50	1735,86	525,30	27,55
4375	21175	1	3b	813,56	83,30	1688,96	486,20	9,77
4375	21575	1	3b	258,86	56,10	1791,52	595,00	4,61
4375	21650	1	3b	369,80	40,80	1719,70	518,50	9,06
4500	5900	1	3b	388,29	32,30	1504,76	333,20	12,02
4500	6800	1	3b	573,19	49,30	1514,54	338,30	11,63
4500	7325	1	3b	573,19	25,50	1554,50	368,90	22,48
4500	7725	1	3b	425,27	27,20	1583,98	385,90	15,63
4500	7875	1	3b	776,58	90,10	1761,92	557,60	8,62
4500	7950	1	3b	499,23	66,30	1741,66	538,90	7,53
4500	8025	1	3b	221,88	28,90	1321,48	115,60	7,68
4500	9075	1	3b	647,15	86,70	1850,90	634,10	7,46
4500	9075	1	3b	610,17	71,40	1770,44	547,40	8,55
4500	9175	1	3b	998,46	73,10	1692,24	469,20	13,66
4500	10300	1	3b	369,80	66,30	1628,04	295,80	5,58
4500	10400	1	3b	610,17	110,50	1759,08	428,40	5,52
4500	10625	1	3b	351,31	71,40	1828,64	496,40	4,92
4500	10650	1	3b	388,29	83,30	1940,54	623,90	4,66
4500	10650	1	3b	295,84	27,20	1863,74	562,70	10,88
4500	12350	1	3b	443,76	37,40	1635,58	406,30	11,87
4500	12775	1	3b	758,09	34,00	1384,98	147,90	22,30
4500	13050	1	3b	979,97	107,10	1734,90	494,70	9,15
4500	13250	1	3b	406,78	47,60	1765,50	525,30	8,55
4500	13900	1	3b	388,29	35,70	1555,12	319,60	10,88
4500	14150	1	3b	554,70	40,80	1629,78	392,70	13,60
4500	14375	1	3b	1220,34	59,50	1564,06	314,50	20,51
4500	14425	1	3b	240,37	42,50	1827,56	578,00	5,66
4500	14425	1	3b	665,64	100,30	1790,16	540,60	6,64
4500	14450	1	3b	1035,44	85,00	1660,68	408,00	12,18
4500	14600	1	3b	314,33	95,20	1912,14	657,90	3,30
4500	14875	1	3b	240,37	32,30	1638,86	389,30	7,44

(N-S)	X (E-W)	Area	Unit	Width (m)	Height (m)	Depth (mbsl)	Burial depth (m)	W/H ratio
4500	15725	1	3b	406,78	32,30	1386,72	112,20	12,59
4500	15975	1	3b	480,74	64,60	1666,92	408,00	7,44
4500	16550	1	3b	240,37	37,40	1633,24	340,00	6,43
4500	16825	1	3b	258,86	37,40	1598,20	217,60	6,92
4500	16850	1	3b	591,68	95,80	1835,50	447,10	6,18
4500	17325	1	3b	813,56	64,60	1699,76	333,20	12,59
4500	17400	1	3b	443,76	37,40	1670,26	334,90	11,87
4500	17550	1	3b	536,21	61,20	1771,84	564,40	8,76
4500	17875	1	3b	758,09	57,80	1800,90	576,30	13,12
4500	18050	1	3b	684,13	79,90	1864,26	606,90	8,56
4500	18275	1	3b	258,86	45,90	1752,62	501,50	5,64
4500	19150	1	3b	665,64	85,00	1723,42	487,90	7,83
4500	19675	1	3b	369,80	68,00	1691,38	477,70	5,44
4500	20250	1	3b	813,56	64,60	1793,38	579,70	12,59
4500	20350	1	3b	499,23	61,20	1724,82	504,90	8,16
4500	20600	1	3b	443,76	51,00	1582,30	365,50	8,70
4500	20675	1	3b	480,74	27,20	1431,98	226,10	17,67
4500	20725	1	3b	425,27	51,00	1489,64	282,20	8,34
4500	20750	1	3b	388,29	32,30	1537,24	329,80	12,02
4500	21200	1	3b	776,58	64,60	1667,00	465,80	12,02
4500	21850	1	3b	554,70	96,90	1770,84	571,20	5,72
4500	22500	1	3b	499,23	39,10	1615,58	409,70	12,77
4625	4650	1	3b	813,56	44,20	1510,68	367,20	18,41
4625	5625	1	3b	869,03	47,60	1556,60	394,40	18,26
4625	6675	1	3b	443,76	45,90	1648,56	469,20	9,67
4625	6850	1	3b	684,13	37,40	1515,68	333,20	18,29
4625	6875	1	3b	758,09	45,90	1520,78	338,30	16,52
4625	7425	1	3b	536,21	40,80	1692,92	496,40	13,14
4625	7550	1	3b	480,74	64,60	1624,78	426,70	7,44
4625	7775	1	3b	702,62	71,40	1771,56	561,00	9,84
4625	8075	1	3b	351,31	37,40	1824,26	613,70	9,39
4625	8775	1	3b	258,86	51,00	1738,98	525,30	5,08
4625	8775	1	3b	776,58	52,70	1647,04	431,80	14,74
4625	9200	1	3b	665,64	78,20	1785,46	559,30	8,51
4625	9225	1	3b	406,78	61,20	1862,10	637,50	6,65
4625	9350	1	3b	665,64	68,00	1746,08	516,80	9,79
4625	9350	1	3b	665,64	52,70	1697,20	472,60	12,63
4625	10225	1	3b	166,41	39,10	1610,34	270,30	4,26
4625	10425	1	3b	462,25	117,30	1763,20	421,60	3,94
4625	10550	1	3b	258,86	54,40	1928,66	593,30	4,76
4625	10725	1	3b	203,39	54,40	1865,44	564,40	3,74
4625	12375	1	3b	425,27	45,90	1661,94	423,30	9,27
4625	13125	1	3b	536,21	61,20	1728,24	489,60	8,76
4625	14425	1	3b	665,64	59,50	1803,20	547,40	11,19
4625	14425	1	3b	443,76	86,70	1764,38	511,70	5,12
4625	14575	1	3b	1146,38	149,60	1673,30	409,70	7,66
4625	14600	1	3b	240,37	76,50	1905,08	629,00	3,14
4625	16600	1	3b	157,17	61,20	1644,82	253,30	2,57

(N-S)	X (E-W)	Area	Unit	Width (m)	Height (m)	Depth (mbsl)	Burial depth (m)	W/H ratio
4625	17375	1	3b	499,23	90,10	1706,50	396,10	5,54
4625	17550	1	3b	425,27	90,10	1805,70	596,70	4,72
4625	18075	1	3b	554,70	78,20	1871,32	635,80	7,09
4625	18150	1	3b	240,37	34,00	1675,42	416,50	7,07
4625	18225	1	3b	258,86	68,00	1724,44	462,40	3,81
4625	18350	1	3b	332,82	49,30	1763,52	520,20	6,75
4625	18675	1	3b	332,82	37,40	1667,72	455,60	8,90
4625	18900	1	3b	462,25	54,40	1834,32	622,20	8,50
4625	19075	1	3b	314,33	57,80	1706,12	486,20	5,44
4625	19225	1	3b	277,35	40,80	1752,30	535,50	6,80
4625	19250	1	3b	351,31	28,90	1620,84	397,80	12,16
4625	19700	1	3b	314,33	49,30	1679,34	464,10	6,38
4625	20100	1	3b	258,86	35,70	1682,60	465,80	7,25
4625	20325	1	3b	443,76	57,80	1837,30	620,50	7,68
4625	20375	1	3b	499,23	79,90	1754,00	537,20	6,25
4625	20525	1	3b	388,29	40,80	1580,88	367,20	9,52
4625	20700	1	3b	591,68	64,60	1524,50	307,70	9,16
4625	20825	1	3b	758,09	59,50	1674,38	460,70	12,74
4625	21250	1	3b	351,31	27,20	1724,52	520,20	12,92
4625	21750	1	3b	369,80	52,70	1765,18	559,30	7,02
4625	22475	1	3b	443,76	62,90	1642,36	431,80	7,06
4750	5775	1	3b	610,17	54,40	1577,72	404,60	11,22
4750	6475	1	3b	332,82	34,00	1627,88	445,40	9,79
4750	6700	1	3b	536,21	73,10	1689,22	508,30	7,34
4750	6950	1	3b	425,27	49,30	1608,62	419,90	8,63
4750	6950	1	3b	628,66	37,40	1530,70	345,10	16,81
4750	7525	1	3b	702,62	49,30	1705,82	501,50	14,25
4750	7600	1	3b	462,25	71,40	1639,52	435,20	6,47
4750	7700	1	3b	832,05	68,00	1769,58	555,90	12,24
4750	8525	1	3b	425,27	56,10	1643,36	425,00	7,58
4750	9025	1	3b	369,80	49,30	1818,04	595,00	7,50
4750	9350	1	3b	610,17	61,20	1864,68	557,60	9,97
4750	9350	1	3b	406,78	47,60	1874,44	635,80	8,55
4750	9475	1	3b	739,60	64,60	1742,12	506,60	11,45
4750	10425	1	3b	406,78	56,10	1649,30	307,70	7,25
4750	10475	1	3b	536,21	96,90	1740,68	394,40	5,53
4750	10625	1	3b	314,33	57,80	1938,02	593,30	5,44
4750	10700	1	3b	221,88	59,50	1859,40	510,00	3,73
4750	12100	1	3b	573,19	73,10	1693,12	442,00	7,84
4750	12350	1	3b	628,66	57,80	1667,74	436,90	10,88
4750	13175	1	3b	647,15	69,70	1723,28	486,20	9,28
4750	13350	1	3b	388,29	44,20	1662,66	413,10	8,78
4750	14275	1	3b	887,52	78,20	1772,06	491,30	11,35
4750	14475	1	3b	314,33	51,00	1837,24	544,00	6,16
4750	14500	1	3b	739,60	96,90	1747,56	459,00	7,63
4750	14600	1	3b	332,82	61,20	1890,80	588,20	5,44
4750	14775	1	3b	721,11	42,50	1642,18	334,90	16,97
4750	16575	1	3b	665,64	34,00	1566,20	170,00	19,58

(N-S)	X (E-W)	Area	Unit	Width (m)	Height (m)	Depth (mbsl)	Burial depth (m)	W/H ratio
4750	16650	1	3b	332,82	34,00	1510,24	115,60	9,79
4750	16825	1	3b	850,54	49,30	1620,60	224,40	17,25
4750	17425	1	3b	462,25	83,30	1728,36	510,00	5,55
4750	17525	1	3b	573,19	73,10	1801,18	579,70	7,84
4750	18050	1	3b	499,23	76,50	1856,58	627,30	6,53
4750	18050	1	3b	462,25	52,70	1789,60	533,80	8,77
4750	18350	1	3b	480,74	86,70	1742,98	498,10	5,54
4750	18975	1	3b	462,25	69,70	1835,60	618,80	6,63
4750	19075	1	3b	295,84	49,30	1682,88	469,20	6,00
4750	19225	1	3b	277,35	37,40	1726,52	506,60	7,42
4750	20325	1	3b	425,27	74,80	1845,80	629,00	5,69
4750	20350	1	3b	776,58	96,90	1760,24	537,20	8,01
4750	20500	1	3b	332,82	47,60	1585,98	372,30	6,99
4750	20675	1	3b	906,01	62,90	1524,64	309,40	14,40
4750	21025	1	3b	443,76	76,50	1662,90	453,90	5,80
4750	21250	1	3b	332,82	69,70	1699,88	486,20	4,78
4750	21625	1	3b	425,27	62,90	1752,86	542,30	6,76
4875	5850	1	3b	499,23	45,90	1574,04	397,80	10,88
4875	6725	1	3b	462,25	69,70	1716,86	521,90	6,63
4875	7075	1	3b	702,62	73,10	1638,52	442,00	9,61
4875	7400	1	3b	573,19	37,40	1311,98	113,90	15,33
4875	7600	1	3b	462,25	49,30	1719,42	515,10	9,38
4875	7600	1	3b	277,35	52,70	1622,38	416,50	5,26
4875	7975	1	3b	702,62	86,70	1793,24	578,00	8,10
4875	8375	1	3b	332,82	23,80	1709,52	489,60	13,98
4875	8450	1	3b	517,72	69,70	1657,96	431,80	7,43
4875	9300	1	3b	425,27	54,40	1683,92	425,00	7,82
4875	9500	1	3b	184,90	59,50	1852,22	593,30	3,11
4875	9500	1	3b	647,15	45,90	1789,04	527,00	14,10
4875	9500	1	3b	480,74	40,80	1756,06	467,50	11,78
4875	9500	1	3b	739,60	81,60	1717,94	440,30	9,06
4875	9975	1	3b	517,72	59,50	1620,68	282,20	8,70
4875	10550	1	3b	184,90	25,50	1759,10	409,70	7,25
4875	10550	1	3b	425,27	64,60	1715,16	387,60	6,58
4875	10625	1	3b	388,29	61,70	1872,86	521,90	6,29
4875	10625	1	3b	277,35	32,30	1803,44	455,60	8,59
4875	10850	1	3b	184,90	45,90	1393,32	40,80	4,03
4875	10875	1	3b	184,90	34,00	1870,28	547,40	5,44
4875	12175	1	3b	721,11	108,80	1728,10	487,90	6,63
4875	13250	1	3b	647,15	59,50	1717,34	470,90	10,88
4875	13900	1	3b	351,31	52,70	1724,44	462,40	6,67
4875	14200	1	3b	425,27	37,40	1686,92	404,60	11,37
4875	14350	1	3b	1016,95	95,20	1755,24	438,60	10,68
4875	14450	1	3b	554,70	49,30	1821,68	506,60	11,25
4875	14700	1	3b	351,31	49,30	1866,44	557,60	7,13
4875	14700	1	3b	1220,34	42,50	1583,54	266,90	28,71
4875	14875	1	3b	813,56	45,90	1643,30	348,50	17,72
4875	16250	1	3b	277,35	42,50	1554,58	161,50	6,53

(N-S)	X (E-W)	Area	Unit	Width (m)	Height (m)	Depth (mbsl)	Burial depth (m)	W/H ratio
4875	16500	1	3b	406,78	44,20	1685,20	289,00	9,20
4875	16800	1	3b	924,50	45,90	1634,20	238,00	20,14
4875	18925	1	3b	591,68	78,20	1828,52	608,60	7,57
4875	20300	1	3b	795,07	98,60	1760,52	540,60	8,06
4875	20325	1	3b	499,23	86,70	1850,76	632,40	5,76
4875	20600	1	3b	702,62	86,70	1551,70	334,90	8,10
4875	20825	1	3b	979,97	74,80	1576,92	357,00	13,10
4875	20825	1	3b	554,70	37,40	1461,32	241,40	14,83
4875	21300	1	3b	425,27	86,70	1711,64	496,40	4,91
4875	21700	1	3b	332,82	30,60	1711,92	499,80	10,88
5000	5700	1	3b	628,66	49,30	1670,52	489,60	12,75
5000	6750	1	3b	554,70	64,60	1732,58	542,30	8,59
5000	7125	1	3b	739,60	103,70	1657,36	462,40	7,13
5000	7550	1	3b	425,27	44,20	1698,46	487,90	9,62
5000	8075	1	3b	1201,85	88,40	1790,12	578,00	13,60
5000	8375	1	3b	739,60	110,50	1662,92	435,20	6,69
5000	9425	1	3b	295,84	54,40	1682,08	421,60	5,44
5000	9625	1	3b	776,58	85,00	1789,36	493,00	9,14
5000	9650	1	3b	314,33	59,50	1874,64	581,40	5,28
5000	9650	1	3b	462,25	42,50	1714,02	392,70	10,88
5000	9675	1	3b	480,74	44,20	1742,78	419,90	10,88
5000	10075	1	3b	388,29	52,70	1667,56	340,00	7,37
5000	10625	1	3b	203,39	61,20	1853,88	499,80	3,32
5000	10700	1	3b	517,72	54,40	1739,98	385,90	9,52
5000	10800	1	3b	277,35	59,50	1945,82	593,30	4,66
5000	11000	1	3b	314,33	32,30	1884,88	554,20	9,73
5000	12175	1	3b	647,15	39,10	1765,78	528,70	16,55
5000	12275	1	3b	351,31	35,70	1807,72	564,40	9,84
5000	12275	1	3b	554,70	68,00	1708,84	462,40	8,16
5000	12725	1	3b	480,74	54,40	1660,24	421,60	8,84
5000	13225	1	3b	591,68	35,70	1693,40	445,40	16,57
5000	13875	1	3b	277,35	54,40	1737,48	469,20	5,10
5000	14125	1	3b	462,25	45,90	1781,28	489,60	10,07
5000	14200	1	3b	351,31	47,60	1700,26	396,10	7,38
5000	14450	1	3b	832,05	64,60	1816,16	496,40	12,88
5000	14700	1	3b	240,37	34,00	1878,04	584,80	7,07
5000	14800	1	3b	536,21	78,20	1774,36	462,40	6,86
5000	14875	1	3b	1053,93	74,80	1646,16	326,40	14,09
5000	15075	1	3b	314,33	32,30	1673,62	375,70	9,73
5000	16025	1	3b	258,86	34,00	1542,40	146,20	7,61
5000	16650	1	3b	813,56	45,90	1647,92	272,00	17,72
5000	16925	1	3b	795,07	45,90	1593,64	238,00	17,32
5000	18875	1	3b	554,70	59,50	1817,88	612,00	9,32
5000	20200	1	3b	1053,93	71,40	1746,24	499,80	14,76
5000	20350	1	3b	499,23	81,60	1826,26	600,10	6,12
5000	20525	1	3b	591,68	56,10	1529,04	306,00	10,55
5000	20725	1	3b	702,62	74,80	1547,46	321,30	9,39
5000	20775	1	3b	906,01	98,60	1581,46	355,30	9,19

(N-S)	X (E-W)	Area	Unit	Width (m)	Height (m)	Depth (mbsl)	Burial depth (m)	W/H ratio
5000	20825	1	3b	628,66	34,00	1481,72	261,80	18,49
5000	21225	1	3b	443,76	61,20	1694,36	476,00	7,25
5000	21825	1	3b	961,48	54,40	1742,52	530,40	17,67
5000	22050	1	3b	517,72	35,70	1689,40	472,60	14,50
5125	6750	1	3b	573,19	64,60	1732,30	538,90	8,87
5125	7575	1	3b	443,76	42,50	1707,10	498,10	10,44
5125	8125	1	3b	887,52	88,40	1784,04	561,00	10,04
5125	8325	1	3b	628,66	93,50	1664,90	440,30	6,72
5125	8425	1	3b	758,09	88,40	1651,84	452,20	8,58
5125	9575	1	3b	369,80	39,10	1832,32	503,20	9,46
5125	9675	1	3b	573,19	74,80	1785,86	450,50	7,66
5125	9675	1	3b	573,19	68,00	1702,84	370,60	8,43
5125	9800	1	3b	443,76	39,10	1883,04	550,80	11,35
5125	10000	1	3b	295,84	40,80	1746,60	428,40	7,25
5125	10150	1	3b	351,31	42,50	1683,84	367,20	8,27
5125	10175	1	3b	813,56	44,20	1650,00	316,20	18,41
5125	10687,5	1	3b	295,84	64,60	1866,34	518,50	4,58
5125	10750	1	3b	332,82	32,30	1788,14	440,30	10,30
5125	10900	1	3b	406,78	73,10	1704,84	357,00	5,56
5125	11950	1	3b	462,25	49,30	1662,50	430,10	9,38
5125	11950	1	3b	351,31	22,10	1591,24	360,40	15,90
5125	12175	1	3b	610,17	69,70	1797,52	554,20	8,75
5125	12200	1	3b	702,62	74,80	1697,50	457,30	9,39
5125	12275	1	3b	517,72	44,20	1850,50	610,30	11,71
5125	13225	1	3b	480,74	52,70	1696,10	440,30	9,12
5125	13750	1	3b	332,82	54,40	1728,00	448,80	6,12
5125	14000	1	3b	610,17	64,60	1761,02	470,90	9,45
5125	14200	1	3b	499,23	35,70	1674,48	367,20	13,98
5125	14675	1	3b	499,23	37,40	1830,88	523,60	13,35
5125	14900	1	3b	462,25	61,20	1772,24	455,60	7,55
5125	15275	1	3b	295,84	32,30	1676,06	348,50	9,16
5125	15675	1	3b	240,37	28,90	1768,02	423,30	8,32
5125	16050	1	3b	221,88	25,50	1545,24	142,80	8,70
5125	16950	1	3b	887,52	85,00	1617,92	343,40	10,44
5125	18875	1	3b	647,15	56,10	1794,24	571,20	11,54
5125	19500	1	3b	388,29	56,10	1778,96	537,20	6,92
5125	20150	1	3b	924,50	85,00	1738,44	499,80	10,88
5125	20350	1	3b	499,23	61,20	1786,46	552,50	8,16
5125	20525	1	3b	517,72	64,60	1524,66	290,70	8,01
5125	20750	1	3b	425,27	56,10	1574,52	346,80	7,58
5125	21125	1	3b	332,82	78,20	1719,58	498,10	4,26
5125	21550	1	3b	425,27	51,00	1655,26	436,90	8,34
5125	21700	1	3b	406,78	44,20	1752,44	537,20	9,20
5125	22175	1	3b	776,58	54,40	1773,70	549,10	14,28
5125	22450	1	3b	628,66	49,30	1594,76	384,20	12,75
5250	3175	1	3b	813,56	47,60	1516,90	385,90	17,09
5250	3475	1	3b	832,05	49,30	1542,12	408,00	16,88
5250	5825	1	3b	332,82	37,40	1600,40	414,80	8,90

(N-S)	X (E-W)	Area	Unit	Width (m)	Height (m)	Depth (mbsl)	Burial depth (m)	W/H ratio
5250	6675	1	3b	480,74	62,90	1725,36	530,40	7,64
5250	7175	1	3b	758,09	71,40	1644,34	436,90	10,62
5250	7400	1	3b	277,35	35,70	1590,94	375,70	7,77
5250	8225	1	3b	998,46	73,10	1782,20	557,60	13,66
5250	8300	1	3b	647,15	79,90	1648,90	416,50	8,10
5250	9875	1	3b	665,64	74,80	1776,78	453,90	8,90
5250	10125	1	3b	1090,91	96,90	1699,86	372,30	11,26
5250	10225	1	3b	443,76	86,70	1692,06	372,30	5,12
5250	10825	1	3b	277,35	44,20	1791,26	440,30	6,27
5250	10925	1	3b	388,29	71,40	1733,74	385,90	5,44
5250	10950	1	3b	221,88	45,90	1393,88	47,60	4,83
5250	11675	1	3b	776,58	34,00	1608,68	363,80	22,84
5250	11950	1	3b	517,72	45,90	1642,24	411,40	11,28
5250	12075	1	3b	554,70	25,50	1578,64	340,00	21,75
5250	12125	1	3b	351,31	40,80	1784,20	544,00	8,61
5250	12125	1	3b	647,15	59,50	1687,44	448,80	10,88
5250	12200	1	3b	425,27	61,20	1884,64	646,00	6,95
5250	12300	1	3b	351,31	34,00	1838,32	595,00	10,33
5250	13200	1	3b	369,80	39,10	1680,38	419,90	9,46
5250	13525	1	3b	406,78	37,40	1886,10	606,90	10,88
5250	13925	1	3b	702,62	59,50	1733,54	440,30	11,81
5250	14675	1	3b	536,21	59,50	1577,58	270,30	9,01
5250	14825	1	3b	443,76	59,50	1639,78	324,70	7,46
5250	14875	1	3b	369,80	37,40	1901,18	562,70	9,89
5250	16325	1	3b	610,17	66,30	1724,00	476,00	9,20
5250	16375	1	3b	314,33	30,60	1582,84	258,40	10,27
5250	16625	1	3b	795,07	39,10	1649,10	362,10	20,33
5250	18800	1	3b	499,23	52,70	1772,70	555,90	9,47
5250	20050	1	3b	869,03	52,70	1690,14	443,70	16,49
5250	20450	1	3b	517,72	44,20	1771,44	540,60	11,71
5250	20525	1	3b	443,76	52,70	1484,14	253,30	8,42
5250	20575	1	3b	517,72	42,50	1640,54	409,70	12,18
5250	20775	1	3b	517,72	83,30	1586,56	360,40	6,22
5250	20800	1	3b	388,29	56,10	1495,32	275,40	6,92
5250	21125	1	3b	221,88	35,70	1700,88	479,40	6,22
5250	21550	1	3b	462,25	52,70	1675,66	457,30	8,77
5250	21700	1	3b	462,25	57,80	1697,90	481,10	8,00
5250	21950	1	3b	684,13	44,20	1730,34	515,10	15,48
5250	22325	1	3b	813,56	40,80	1558,64	343,40	19,94
5250	22425	1	3b	684,13	49,30	1585,70	368,90	13,88
5375	3175	1	3b	1109,40	45,90	1511,80	380,80	24,17
5375	5925	1	3b	406,78	52,70	1602,10	416,50	7,72
5375	6200	1	3b	832,05	56,10	1564,28	374,00	14,83
5375	6650	1	3b	554,70	81,60	1715,02	518,50	6,80
5375	7250	1	3b	721,11	57,80	1640,24	425,00	12,48
5375	7825	1	3b	554,70	52,70	1726,52	506,60	10,53
5375	8300	1	3b	554,70	73,10	1637,56	411,40	7,59
5375	8400	1	3b	739,60	62,90	1793,40	561,00	11,76

(N-S)	X (E-W)	Area	Unit	Width (m)	Height (m)	Depth (mbsl)	Burial depth (m)	W/H ratio
5375	9850	1	3b	536,21	39,10	1792,30	263,50	13,71
5375	10025	1	3b	869,03	76,50	1779,88	472,60	11,36
5375	10175	1	3b	1275,81	158,10	1752,94	467,50	8,07
5375	10925	1	3b	351,31	73,10	1725,10	375,70	4,81
5375	10975	1	3b	295,84	51,00	1859,12	506,60	5,80
5375	11550	1	3b	406,78	39,10	1591,28	323,00	10,40
5375	11800	1	3b	462,25	47,60	1726,98	474,30	9,71
5375	12050	1	3b	924,50	73,10	1656,42	413,10	12,65
5375	13500	1	3b	332,82	42,50	1906,08	622,20	7,83
5375	13775	1	3b	406,78	51,00	1808,48	516,80	7,98
5375	13800	1	3b	536,21	44,20	1728,72	438,60	12,13
5375	14950	1	3b	295,84	44,20	1895,94	555,90	6,69
5375	15025	1	3b	647,15	88,40	1800,18	453,90	7,32
5375	15350	1	3b	517,72	35,70	1740,56	374,00	14,50
5375	16325	1	3b	647,15	64,60	1736,40	418,20	10,02
5375	16400	1	3b	406,78	62,90	1832,24	578,00	6,47
5375	19350	1	3b	406,78	51,00	1754,74	508,30	7,98
5375	20375	1	3b	702,62	47,60	1637,14	406,30	14,76
5375	20400	1	3b	425,27	52,70	1783,34	552,50	8,07
5375	20825	1	3b	665,64	83,30	1579,90	355,30	7,99
5375	21525	1	3b	758,09	76,50	1690,54	467,50	9,91
5375	22400	1	3b	443,76	49,30	1558,08	336,60	9,00
5500	6350	1	3b	647,15	54,40	1565,42	368,90	11,90
5500	6625	1	3b	517,72	78,20	1709,36	506,60	6,62
5500	7275	1	3b	499,23	59,50	1627,36	401,20	8,39
5500	7950	1	3b	795,07	61,20	1734,74	511,70	12,99
5500	8275	1	3b	554,70	59,50	1620,00	387,60	9,32
5500	8525	1	3b	499,23	37,40	1785,90	545,70	13,35
5500	9200	1	3b	425,27	34,00	1808,80	482,80	12,51
5500	9275	1	3b	406,78	54,40	1697,30	379,10	7,48
5500	10125	1	3b	480,74	52,70	1790,06	501,50	9,12
5500	10275	1	3b	721,11	73,10	1734,80	455,60	9,86
5500	10975	1	3b	277,35	35,70	1702,58	348,50	7,77
5500	11075	1	3b	258,86	64,60	1893,12	540,60	4,01
5500	11800	1	3b	369,80	37,40	1489,70	226,10	9,89
5500	11875	1	3b	573,19	74,80	1725,14	470,90	7,66
5500	12000	1	3b	739,60	51,00	1629,36	387,60	14,50
5500	12275	1	3b	351,31	64,60	1871,90	623,90	5,44
5500	13575	1	3b	332,82	66,30	1947,16	666,40	5,02
5500	13725	1	3b	314,33	66,30	1751,38	467,50	4,74
5500	13750	1	3b	295,84	54,40	1829,02	538,90	5,44
5500	13800	1	3b	462,25	61,20	1688,06	399,50	7,55
5500	14700	1	3b	480,74	34,00	1633,86	290,70	14,14
5500	15025	1	3b	388,29	37,40	1662,92	302,60	10,38
5500	15075	1	3b	536,21	129,20	1838,30	481,10	4,15
5500	15150	1	3b	443,76	44,20	1747,36	380,80	10,04
5500	16050	1	3b	591,68	51,00	1748,26	467,50	11,60
5500	16125	1	3b	406,78	83,30	1862,44	584,80	4,88



(N-S)	X (E-W)	Area	Unit	Width (m)	Height (m)	Depth (mbsl)	Burial depth (m)	W/H ratio
5500	16850	1	3b	591,68	42,50	1548,00	346,80	13,92
5500	19625	1	3b	536,21	51,00	1755,16	513,40	10,51
5500	19700	1	3b	332,82	51,00	1747,80	499,80	6,53
5500	19875	1	3b	425,27	51,00	1523,54	277,10	8,34
5500	20375	1	3b	480,74	68,00	1836,62	593,30	7,07
5500	20375	1	3b	647,15	59,50	1625,26	375,70	10,88
5500	20725	1	3b	573,19	66,30	1583,60	343,40	8,65
5500	20875	1	3b	425,27	57,80	1720,16	486,20	7,36
5500	21625	1	3b	388,29	69,70	1625,66	399,50	5,57
5625	6025	1	3b	406,78	40,80	1310,42	113,90	9,97
5625	6275	1	3b	610,17	56,10	1566,28	360,40	10,88
5625	6725	1	3b	480,74	59,50	1698,32	486,20	8,08
5625	7225	1	3b	425,27	32,30	1608,66	382,50	13,17
5625	8225	1	3b	647,15	64,60	1607,96	374,00	10,02
5625	8275	1	3b	647,15	59,50	1752,74	521,90	10,88
5625	9150	1	3b	240,37	42,50	1645,74	321,30	5,66
5625	9225	1	3b	536,21	59,50	1820,84	496,40	9,01
5625	9350	1	3b	499,23	47,60	1697,44	380,80	10,49
5625	10175	1	3b	517,72	61,20	1787,22	504,90	8,46
5625	10325	1	3b	702,62	52,70	1733,38	457,30	13,33
5625	10600	1	3b	314,33	32,30	1704,84	357,00	9,73
5625	10625	1	3b	388,29	35,70	1662,28	370,60	10,88
5625	11150	1	3b	2144,84	35,70	1880,94	525,30	60,08
5625	11675	1	3b	388,29	35,70	1614,24	336,60	10,88
5625	11825	1	3b	295,84	44,20	1496,20	248,20	6,69
5625	11925	1	3b	240,37	35,70	1704,58	467,50	6,73
5625	12150	1	3b	406,78	62,90	1887,34	640,90	6,47
5625	12950	1	3b	332,82	49,30	1887,78	627,30	6,75
5625	13250	1	3b	277,35	32,30	1813,00	533,80	8,59
5625	13700	1	3b	351,31	45,90	1729,28	445,40	7,65
5625	13725	1	3b	258,86	37,40	1817,96	537,20	6,92
5625	14275	1	3b	406,78	47,60	1716,30	382,50	8,55
5625	14950	1	3b	554,70	52,70	1528,64	149,60	10,53
5625	15025	1	3b	388,29	57,80	1663,66	273,70	6,72
5625	15050	1	3b	517,72	73,10	1764,98	348,50	7,08
5625	15125	1	3b	406,78	45,90	1792,18	375,70	8,86
5625	15150	1	3b	462,25	61,20	1850,26	436,90	7,55
5625	16075	1	3b	517,72	56,10	1767,94	498,10	9,23
5625	19975	1	3b	277,35	45,90	1529,92	278,80	6,04
5625	20450	1	3b	406,78	62,90	1840,88	588,20	6,47
5625	20525	1	3b	499,23	81,60	1665,62	430,10	6,12
5625	20825	1	3b	240,37	52,70	1764,08	527,00	4,56
5625	21600	1	3b	462,25	71,40	1623,96	397,80	6,47
5750	6475	1	3b	536,21	44,20	1546,74	331,50	12,13
5750	6650	1	3b	499,23	66,30	1626,08	404,60	7,53
5750	6750	1	3b	536,21	49,30	1680,34	457,30	10,88
5750	7075	1	3b	536,21	57,80	1450,28	221,00	9,28
5750	8025	1	3b	591,68	51,00	1662,78	433,50	11,60

(N-S)	X (E-W)	Area	Unit	Width (m)	Height (m)	Depth (mbsl)	Burial depth (m)	W/H ratio
5750	8075	1	3b	665,64	51,00	1602,72	367,20	13,05
5750	8525	1	3b	665,64	49,30	1741,84	503,20	13,50
5750	10275	1	3b	499,23	56,10	1793,88	510,00	8,90
5750	10350	1	3b	647,15	59,50	1731,40	452,20	10,88
5750	10475	1	3b	240,37	52,70	1898,14	620,50	4,56
5750	10575	1	3b	332,82	49,30	1713,62	368,90	6,75
5750	10625	1	3b	517,72	56,10	1681,68	397,80	9,23
5750	11175	1	3b	795,07	52,70	1853,88	499,80	15,09
5750	11275	1	3b	499,23	51,00	1865,62	528,70	9,79
5750	11400	1	3b	425,27	74,80	1773,50	470,90	5,69
5750	11550	1	3b	314,33	40,80	1653,08	353,60	7,70
5750	11775	1	3b	369,80	42,50	1617,94	324,70	8,70
5750	13100	1	3b	536,21	62,90	1918,54	640,90	8,52
5750	13550	1	3b	314,33	49,30	1702,08	418,20	6,38
5750	14275	1	3b	536,21	57,80	1748,32	411,40	9,28
5750	14700	1	3b	554,70	61,20	1600,60	227,80	9,06
5750	15150	1	3b	425,27	52,70	1802,96	374,00	8,07
5750	15200	1	3b	406,78	54,40	1752,10	324,70	7,48
5750	20150	1	3b	369,80	45,90	1533,34	263,50	8,06
5750	20500	1	3b	406,78	61,20	1819,34	572,90	6,65
5750	20525	1	3b	591,68	93,50	1679,22	443,70	6,33
5750	20725	1	3b	332,82	39,10	1767,90	535,50	8,51
5750	20850	1	3b	369,80	49,30	1724,70	484,50	7,50
5750	20925	1	3b	295,84	32,30	1581,04	350,20	9,16
5875	6600	1	3b	388,29	44,20	1623,82	396,10	8,78
5875	6750	1	3b	443,76	54,40	1687,00	462,40	8,16
5875	6775	1	3b	721,11	54,40	1566,44	343,40	13,26
5875	7725	1	3b	665,64	59,50	1380,72	153,00	11,19
5875	8075	1	3b	480,74	69,70	1684,60	452,20	6,90
5875	8175	1	3b	462,25	64,60	1614,76	380,80	7,16
5875	8425	1	3b	480,74	37,40	1732,36	482,80	12,85
5875	9325	1	3b	573,19	91,80	1853,56	533,80	6,24
5875	10475	1	3b	147,92	52,70	1919,54	634,10	2,81
5875	10525	1	3b	739,60	47,60	1596,54	311,10	15,54
5875	11300	1	3b	351,31	61,20	1783,44	459,00	5,74
5875	11375	1	3b	332,82	35,70	1885,32	540,60	9,32
5875	12575	1	3b	462,25	25,50	1619,60	363,80	18,13
5875	12750	1	3b	295,84	32,30	1712,40	448,80	9,16
5875	13275	1	3b	369,80	52,70	1923,64	646,00	7,02
5875	13275	1	3b	406,78	57,80	1845,44	567,80	7,04
5875	13525	1	3b	295,84	39,10	1733,96	445,40	7,57
5875	13550	1	3b	425,27	54,40	1663,26	382,50	7,82
5875	14300	1	3b	628,66	69,70	1767,60	418,20	9,02
5875	14350	1	3b	351,31	49,30	1711,08	357,00	7,13
5875	14700	1	3b	517,72	66,30	1604,62	181,90	7,81
5875	14875	1	3b	351,31	47,60	1671,92	241,40	7,38
5875	15300	1	3b	388,29	47,60	1848,86	419,90	8,16
5875	15300	1	3b	443,76	47,60	1686,80	384,20	9,32

(N-S)	X (E-W)	Area	Unit	Width (m)	Height (m)	Depth (mbsl)	Burial depth (m)	W/H ratio
5875	15425	1	3b	314,33	37,40	1719,66	290,70	8,40
5875	16000	1	3b	721,11	44,20	1777,58	501,50	16,31
5875	16225	1	3b	462,25	79,90	1853,76	612,00	5,79
5875	20575	1	3b	462,25	52,70	1794,26	552,50	8,77
5875	20600	1	3b	610,17	115,60	1701,18	464,10	5,28
6000	6675	1	3b	462,25	115,60	1698,62	470,90	4,00
6000	8150	1	3b	388,29	73,10	1687,58	450,50	5,31
6000	8150	1	3b	517,72	56,10	1616,32	380,80	9,23
6000	9375	1	3b	554,70	78,20	1857,94	549,10	7,09
6000	9575	1	3b	628,66	39,10	1613,28	306,00	16,08
6000	10425	1	3b	628,66	68,00	1817,26	528,70	9,25
6000	10475	1	3b	462,25	54,40	1677,86	389,30	8,50
6000	10525	1	3b	443,76	45,90	1778,02	487,90	9,67
6000	10525	1	3b	684,13	44,20	1733,96	445,40	15,48
6000	10575	1	3b	314,33	86,70	1934,56	646,00	3,63
6000	10850	1	3b	425,27	54,40	1724,54	368,90	7,82
6000	11550	1	3b	295,84	42,50	1722,68	384,20	6,96
6000	12100	1	3b	314,33	44,20	1880,12	629,00	7,11
6000	13425	1	3b	351,31	61,20	1709,02	426,70	5,74
6000	14150	1	3b	258,86	28,90	1653,72	285,60	8,96
6000	14375	1	3b	295,84	37,40	1689,02	297,50	7,91
6000	14400	1	3b	480,74	40,80	1741,86	351,90	11,78
6000	14750	1	3b	573,19	62,90	1610,86	181,90	9,11
6000	14950	1	3b	369,80	32,30	1661,86	232,90	11,45
6000	15050	1	3b	369,80	22,10	1692,60	265,20	16,73
6000	15350	1	3b	388,29	51,00	1728,84	326,40	7,61
6000	15925	1	3b	924,50	59,50	1860,18	576,30	15,54
6000	17100	1	3b	332,82	61,20	1880,98	620,50	5,44
6000	20500	1	3b	295,84	59,50	1545,92	302,60	4,97
6000	20600	1	3b	480,74	144,50	1731,22	487,90	3,33
6000	20725	1	3b	277,35	47,60	1778,82	535,50	5,83
6125	6700	1	3b	240,37	56,10	1710,66	484,50	4,28
6125	6725	1	3b	332,82	54,40	1651,02	423,30	6,12
6125	6900	1	3b	351,31	39,10	1596,62	368,90	8,98
6125	8050	1	3b	332,82	32,30	1587,28	350,20	10,30
6125	8125	1	3b	739,60	73,10	1670,02	426,70	10,12
6125	8250	1	3b	554,70	37,40	1620,58	375,70	14,83
6125	9675	1	3b	610,17	61,20	1697,28	397,80	9,97
6125	10500	1	3b	351,31	45,90	1673,90	379,10	7,65
6125	10600	1	3b	499,23	62,90	1787,80	493,00	7,94
6125	10625	1	3b	332,82	56,10	1917,98	634,10	5,93
6125	10650	1	3b	554,70	39,10	1727,02	436,90	14,19
6125	11350	1	3b	277,35	42,50	1918,34	562,70	6,53
6125	11500	1	3b	295,84	42,50	1726,52	374,00	6,96
6125	12275	1	3b	369,80	35,70	1827,34	518,50	10,36
6125	12975	1	3b	240,37	39,10	1726,72	452,20	6,15
6125	13025	1	3b	388,29	49,30	1842,88	574,60	7,88
6125	13025	1	3b	277,35	23,80	1677,42	402,90	11,65

(N-S)	X (E-W)	Area	Unit	Width (m)	Height (m)	Depth (mbsl)	Burial depth (m)	W/H ratio
6125	13475	1	3b	369,80	78,20	1716,10	436,90	4,73
6125	13525	1	3b	388,29	57,80	1779,72	489,60	6,72
6125	15225	1	3b	628,66	40,80	1728,32	414,80	15,41
6125	15600	1	3b	647,15	52,70	1773,66	453,90	12,28
6125	15875	1	3b	832,05	61,20	1867,68	591,60	13,60
6125	20525	1	3b	406,78	42,50	1751,06	501,50	9,57
6125	20550	1	3b	443,76	108,80	1716,92	465,80	4,08
6125	20550	1	3b	388,29	69,70	1564,06	314,50	5,57
6250	6675	1	3b	277,35	64,60	1739,14	508,30	4,29
6250	6725	1	3b	462,25	86,70	1669,58	440,30	5,33
6250	6925	1	3b	425,27	51,00	1611,36	377,40	8,34
6250	7700	1	3b	295,84	47,60	1610,52	367,20	6,22
6250	8875	1	3b	443,76	59,50	1713,86	409,70	7,46
6250	9050	1	3b	314,33	37,40	1757,78	450,50	8,40
6250	9350	1	3b	443,76	61,20	1836,54	535,50	7,25
6250	9675	1	3b	739,60	100,30	1743,32	445,40	7,37
6250	10100	1	3b	258,86	34,00	1741,34	440,30	7,61
6250	10500	1	3b	258,86	42,50	1673,90	379,10	6,09
6250	10700	1	3b	332,82	62,90	1933,28	649,40	5,29
6250	10700	1	3b	499,23	52,70	1787,94	494,70	9,47
6250	11025	1	3b	776,58	73,10	1810,66	467,50	10,62
6250	11050	1	3b	406,78	35,70	1867,90	518,50	11,39
6250	12325	1	3b	425,27	49,30	1856,20	584,80	8,63
6250	12675	1	3b	480,74	35,70	1679,96	414,80	13,47
6250	12775	1	3b	480,74	52,70	1798,82	532,10	9,12
6250	13125	1	3b	887,52	79,90	1858,90	579,70	11,11
6250	13500	1	3b	425,27	35,70	1787,66	491,30	11,91
6250	13775	1	3b	554,70	40,80	1925,60	537,20	13,60
6250	14700	1	3b	647,15	61,20	1599,96	163,20	10,57
6250	14775	1	3b	351,31	47,60	1833,98	409,70	7,38
6250	15125	1	3b	406,78	56,10	1731,18	392,70	7,25
6250	15325	1	3b	536,21	47,60	1792,76	496,40	11,26
6250	15700	1	3b	924,50	85,00	1879,58	603,50	10,88
6250	20550	1	3b	369,80	62,90	1560,38	307,70	5,88
6250	20675	1	3b	295,84	51,00	1725,42	474,30	5,80
6250	20850	1	3b	240,37	35,70	1763,10	515,10	6,73
6375	6725	2	3b	277,35	47,60	1650,74	419,90	5,83
6375	6775	2	3b	369,80	78,20	1744,24	513,40	4,73
6375	6975	2	3b	369,80	52,70	1611,22	375,70	7,02
6375	7875	2	3b	536,21	49,30	1610,52	367,20	10,88
6375	8975	2	3b	462,25	62,90	1714,56	418,20	7,35
6375	9350	2	3b	443,76	79,90	1843,20	540,60	5,55
6375	9575	2	3b	832,05	112,20	1746,72	448,80	7,42
6375	9625	2	3b	258,86	34,00	1784,12	486,20	7,61
6375	10450	2	3b	240,37	40,80	1683,82	385,90	5,89
6375	10675	2	3b	314,33	52,70	1728,30	433,50	5,96
6375	10750	2	3b	332,82	45,90	1778,60	476,00	7,25
6375	10850	2	3b	314,33	73,10	1945,76	649,40	4,30

(N-S)	X (E-W)	Area	Unit	Width (m)	Height (m)	Depth (mbsl)	Burial depth (m)	W/H ratio
6375	11025	2	3b	388,29	52,70	1748,42	450,50	7,37
6375	11150	2	3b	369,80	61,20	1891,54	559,30	6,04
6375	11300	2	3b	277,35	62,90	1805,58	443,70	4,41
6375	12550	2	3b	573,19	47,60	1684,50	413,10	12,04
6375	12725	2	3b	369,80	59,50	1757,32	482,80	6,22
6375	13350	2	3b	536,21	39,10	1867,98	576,30	13,71
6375	13475	2	3b	480,74	52,70	1825,42	457,30	9,12
6375	13900	2	3b	499,23	54,40	1928,48	496,40	9,18
6375	14725	2	3b	499,23	56,10	1655,00	282,20	8,90
6375	14875	2	3b	258,86	40,80	1852,38	443,70	6,34
6375	15050	2	3b	369,80	47,60	1734,26	430,10	7,77
6375	15275	2	3b	573,19	62,90	1801,26	504,90	9,11
6375	15775	2	3b	536,21	91,80	1883,56	595,00	5,84
6375	16025	2	3b	240,37	28,90	1651,36	370,60	8,32
6375	16175	2	3b	277,35	37,40	1601,92	319,60	7,42
6375	20575	2	3b	332,82	59,50	1727,98	467,50	5,59
6375	20600	2	3b	388,29	68,00	1568,32	309,40	5,71
6375	20700	2	3b	480,74	69,70	1665,36	408,00	6,90
6375	20875	2	3b	314,33	49,30	1789,88	537,20	6,38
6500	6750	2	3b	351,31	90,10	1745,52	510,00	3,90
6500	6750	2	3b	295,84	71,40	1650,32	414,80	4,14
6500	6900	2	3b	258,86	40,80	1658,54	419,90	6,34
6500	6950	2	3b	258,86	44,20	1618,02	382,50	5,86
6500	9075	2	3b	351,31	56,10	1787,38	487,90	6,26
6500	9400	2	3b	961,48	88,40	1697,70	402,90	10,88
6500	9575	2	3b	979,97	110,50	1766,98	467,50	8,87
6500	9625	2	3b	776,58	54,40	1848,44	547,40	14,28
6500	10825	2	3b	351,31	51,00	1786,10	491,30	6,89
6500	10925	2	3b	813,56	54,40	1726,32	428,40	14,96
6500	10950	2	3b	425,27	81,60	1948,60	646,00	5,21
6500	11175	2	3b	332,82	64,60	1888,00	554,20	5,15
6500	11300	2	3b	351,31	47,60	1796,52	428,40	7,38
6500	12550	2	3b	591,68	73,10	1718,64	448,80	8,09
6500	12925	2	3b	628,66	61,20	1780,70	501,50	10,27
6500	13575	2	3b	647,15	69,70	1857,76	452,20	9,28
6500	14000	2	3b	610,17	49,30	1910,50	467,50	12,38
6500	14950	2	3b	462,25	57,80	1730,72	425,00	8,00
6500	15025	2	3b	388,29	69,70	1947,90	637,50	5,57
6500	15225	2	3b	628,66	69,70	1801,82	511,70	9,02
6500	15550	2	3b	351,31	42,50	1917,56	629,00	8,27
6500	15725	2	3b	739,60	57,80	1871,66	583,10	12,80
6500	16425	2	3b	258,86	52,70	1628,28	336,60	4,91
6500	20575	2	3b	314,33	52,70	1709,00	445,40	5,96
6500	20700	2	3b	388,29	74,80	1661,82	402,90	5,19
6500	20850	2	3b	295,84	81,60	1811,98	559,30	3,63
6625	6725	2	3b	332,82	61,20	1736,60	496,40	5,44
6625	6725	2	3b	221,88	56,10	1665,76	431,80	3,96
6625	6925	2	3b	369,80	62,90	1607,26	365,50	5,88

(N-S)	X (E-W)	Area	Unit	Width (m)	Height (m)	Depth (mbsl)	Burial depth (m)	W/H ratio
6625	8675	2	3b	332,82	42,50	1698,58	375,70	7,83
6625	9050	2	3b	369,80	42,50	1781,56	493,00	8,70
6625	9325	2	3b	591,68	56,10	1707,62	409,70	10,55
6625	9525	2	3b	425,27	52,70	1773,78	474,30	8,07
6625	9800	2	3b	628,66	56,10	1865,30	562,70	11,21
6625	10925	2	3b	277,35	37,40	1797,58	498,10	7,42
6625	11025	2	3b	721,11	54,40	1741,34	440,30	13,26
6625	11100	2	3b	480,74	61,20	1946,48	639,20	7,86
6625	11150	2	3b	406,78	61,20	1869,28	554,20	6,65
6625	11175	2	3b	573,19	52,70	1681,84	380,80	10,88
6625	11375	2	3b	332,82	51,00	1805,30	440,30	6,53
6625	12600	2	3b	314,33	52,70	1736,36	455,60	5,96
6625	12975	2	3b	351,31	54,40	1782,82	508,30	6,46
6625	13625	2	3b	869,03	86,70	1849,30	406,30	10,02
6625	14675	2	3b	665,64	88,40	1635,96	316,20	7,53
6625	14875	2	3b	443,76	49,30	1738,94	430,10	9,00
6625	15250	2	3b	462,25	64,60	1809,76	513,40	7,16
6625	15525	2	3b	573,19	49,30	1855,94	562,70	11,63
6625	20550	2	3b	351,31	56,10	1717,36	452,20	6,26
6625	20775	2	3b	443,76	78,20	1657,72	391,00	5,67
6625	20850	2	3b	295,84	54,40	1796,26	538,90	5,44
6750	6775	2	3b	295,84	56,10	1666,62	423,30	5,27
6750	6800	2	3b	425,27	47,60	1722,72	479,40	8,93
6750	6925	2	3b	388,29	54,40	1588,70	348,50	7,14
6750	8650	2	3b	369,80	57,80	1708,50	382,50	6,40
6750	9300	2	3b	573,19	64,60	1707,90	413,10	8,87
6750	9575	2	3b	998,46	93,50	1742,76	438,60	10,68
6750	9825	2	3b	721,11	71,40	1870,12	564,40	10,10
6750	11100	2	3b	591,68	68,00	1741,20	438,60	8,70
6750	11175	2	3b	610,17	59,50	1803,68	496,40	10,25
6750	11200	2	3b	332,82	73,10	1960,96	625,60	4,55
6750	11200	2	3b	443,76	71,40	1871,02	518,50	6,22
6750	12575	2	3b	388,29	51,00	1724,88	448,80	7,61
6750	12950	2	3b	425,27	47,60	1777,16	496,40	8,93
6750	13775	2	3b	1016,95	74,80	1849,84	431,80	13,60
6750	14525	2	3b	739,60	62,90	1630,44	306,00	11,76
6750	14575	2	3b	443,76	42,50	1678,74	362,10	10,44
6750	14800	2	3b	388,29	45,90	1738,38	423,30	8,46
6750	15125	2	3b	554,70	45,90	1797,02	491,30	12,08
6750	15500	2	3b	536,21	79,90	1874,36	578,00	6,71
6750	16000	2	3b	314,33	28,90	1613,42	307,70	10,88
6750	20500	2	3b	332,82	71,40	1723,60	452,20	4,66
6750	20675	2	3b	406,78	62,90	1562,52	295,80	6,47
6750	20725	2	3b	425,27	96,90	1670,18	409,70	4,39
6750	20900	2	3b	295,84	71,40	1789,32	530,40	4,14
6750	21825	2	3b	351,31	47,60	1615,90	375,70	7,38
6750	22225	2	3b	332,82	44,20	1645,22	409,70	7,53
6875	6775	2	3b	295,84	61,20	1729,10	481,10	4,83

(N-S)	X (E-W)	Area	Unit	Width (m)	Height (m)	Depth (mbsl)	Burial depth (m)	W/H ratio
6875	6800	2	3b	258,86	52,70	1647,92	404,60	4,91
6875	6875	2	3b	406,78	52,70	1595,22	351,90	7,72
6875	6925	2	3b	406,78	45,90	1543,80	295,80	8,86
6875	7050	2	3b	277,35	40,80	1672,44	418,20	6,80
6875	8650	2	3b	388,29	61,20	1709,06	389,30	6,34
6875	9025	2	3b	332,82	34,00	1763,86	467,50	9,79
6875	9425	2	3b	425,27	34,00	1710,74	409,70	12,51
6875	9725	2	3b	684,13	52,70	1864,46	552,50	12,98
6875	9875	2	3b	388,29	49,30	1713,16	401,20	7,88
6875	10400	2	3b	406,78	93,50	1769,96	465,80	4,35
6875	10575	2	3b	277,35	32,30	1904,12	598,40	8,59
6875	11125	2	3b	351,31	40,80	1807,08	499,80	8,61
6875	11175	2	3b	314,33	32,30	1866,48	520,20	9,73
6875	11225	2	3b	924,50	81,60	1727,46	423,30	11,33
6875	11525	2	3b	369,80	44,20	1759,68	397,80	8,37
6875	11525	2	3b	332,82	37,40	1674,82	314,50	8,90
6875	12525	2	3b	351,31	42,50	1734,82	436,90	8,27
6875	12850	2	3b	332,82	56,10	1894,18	610,30	5,93
6875	12900	2	3b	314,33	49,30	1784,10	504,90	6,38
6875	14575	2	3b	573,19	62,90	1678,18	355,30	9,11
6875	14675	2	3b	406,78	47,60	1738,24	421,60	8,55
6875	15050	2	3b	610,17	40,80	1805,38	498,10	14,96
6875	15275	2	3b	610,17	64,60	1872,24	571,20	9,45
6875	20650	2	3b	332,82	59,50	1701,64	431,80	5,59
6875	20775	2	3b	425,27	61,20	1560,68	292,40	6,95
6875	20825	2	3b	351,31	54,40	1646,38	385,90	6,46
6875	20875	2	3b	443,76	52,70	1792,44	530,40	8,42
6875	21000	2	3b	240,37	45,90	1742,00	486,20	5,24
6875	21125	2	3b	221,88	39,10	1708,00	452,20	5,67
6875	21200	2	3b	258,86	49,30	1666,78	406,30	5,25
6875	21775	2	3b	277,35	40,80	1622,70	382,50	6,80
6875	22425	2	3b	665,64	79,90	1670,86	436,90	8,33
7000	6725	2	3b	314,33	56,10	1637,72	394,40	5,60
7000	6825	2	3b	277,35	44,20	1703,60	455,60	6,27
7000	6900	2	3b	314,33	37,40	1591,12	340,00	8,40
7000	7975	2	3b	462,25	34,00	1730,84	445,40	13,60
7000	8725	2	3b	369,80	51,00	1705,22	399,50	7,25
7000	8975	2	3b	351,31	40,80	1754,66	450,50	8,61
7000	9825	2	3b	499,23	42,50	1859,50	549,10	11,75
7000	10450	2	3b	425,27	64,60	1769,68	462,40	6,58
7000	10625	2	3b	369,80	40,80	1903,98	596,70	9,06
7000	11250	2	3b	462,25	51,00	1871,86	528,70	9,06
7000	11325	2	3b	739,60	56,10	1807,96	472,60	13,18
7000	12375	2	3b	351,31	40,80	1703,68	380,80	8,61
7000	12450	2	3b	369,80	56,10	1791,64	482,80	6,59
7000	12650	2	3b	406,78	37,40	1813,44	520,20	10,88
7000	12850	2	3b	277,35	37,40	1752,38	460,70	7,42
7000	13350	2	3b	480,74	49,30	1810,64	486,20	9,75

(N-S)	X (E-W)	Area	Unit	Width (m)	Height (m)	Depth (mbsl)	Burial depth (m)	W/H ratio
7000	14150	2	3b	425,27	44,20	1791,58	406,30	9,62
7000	14575	2	3b	499,23	71,40	1691,50	365,50	6,99
7000	14675	2	3b	314,33	56,10	1756,80	438,60	5,60
7000	14975	2	3b	480,74	51,00	1810,20	499,80	9,43
7000	15125	2	3b	665,64	57,80	1873,24	564,40	11,52
7000	20675	2	3b	295,84	57,80	1694,42	419,90	5,12
7000	20825	2	3b	869,03	47,60	1633,36	360,40	18,26
7000	20950	2	3b	379,05	51,00	1792,44	530,40	7,43
7000	21000	2	3b	295,84	45,90	1738,18	477,70	6,45
7000	21175	2	3b	277,35	44,20	1653,18	392,70	6,27
7000	21925	2	3b	554,70	79,90	1638,00	397,80	6,94
7125	6675	2	3b	240,37	44,20	1661,10	413,10	5,44
7125	6750	2	3b	314,33	44,20	1713,24	459,00	7,11
7125	6825	2	3b	314,33	56,10	1615,20	367,20	5,60
7125	8150	2	3b	573,19	42,50	1734,12	428,40	13,49
7125	8550	2	3b	388,29	42,50	1612,30	294,10	9,14
7125	9000	2	3b	406,78	47,60	1722,50	419,90	8,55
7125	9700	2	3b	979,97	35,70	1674,06	362,10	27,45
7125	9875	2	3b	702,62	66,30	1860,78	545,70	10,60
7125	10200	2	3b	295,84	34,00	1626,46	314,50	8,70
7125	10425	2	3b	240,37	20,40	1812,04	503,20	11,78
7125	10450	2	3b	480,74	69,70	1757,50	447,10	6,90
7125	11325	2	3b	628,66	73,10	1740,36	428,40	8,60
7125	11425	2	3b	480,74	45,90	1800,46	457,30	10,47
7125	12375	2	3b	351,31	39,10	1749,90	392,70	8,98
7125	12525	2	3b	295,84	51,00	1706,94	382,50	5,80
7125	12550	2	3b	332,82	59,50	1793,78	470,90	5,59
7125	14525	2	3b	425,27	52,70	1695,46	375,70	8,07
7125	14550	2	3b	721,11	71,40	1640,92	319,60	10,10
7125	14600	2	3b	388,29	39,10	1746,18	423,30	9,93
7125	14925	2	3b	554,70	39,10	1806,10	487,90	14,19
7125	15275	2	3b	647,15	54,40	1867,72	554,20	11,90
7125	20625	2	3b	443,76	64,60	1677,14	399,50	6,87
7125	20925	2	3b	406,78	54,40	1791,46	518,50	7,48
7125	20925	2	3b	369,80	51,00	1601,48	333,20	7,25
7125	21000	2	3b	388,29	34,00	1738,62	464,10	11,42
7125	22050	2	3b	610,17	76,50	1631,06	389,30	7,98
7250	6700	2	3b	221,88	59,50	1669,04	414,80	3,73
7250	6875	2	3b	295,84	54,40	1613,22	362,10	5,44
7250	6875	2	3b	610,17	54,40	1566,90	311,10	11,22
7250	6950	2	3b	258,86	52,70	1748,38	487,90	4,91
7250	7350	2	3b	369,80	56,10	1667,36	394,40	6,59
7250	8175	2	3b	443,76	44,20	1765,72	452,20	10,04
7250	9150	2	3b	425,27	49,30	1728,60	418,20	8,63
7250	9375	2	3b	1201,85	44,20	1668,54	351,90	27,19
7250	9925	2	3b	554,70	40,80	1840,52	527,00	13,60
7250	11325	2	3b	702,62	71,40	1733,42	419,90	9,84
7250	11375	2	3b	351,31	37,40	1919,32	574,60	9,39



(N-S)	X (E-W)	Area	Unit	Width (m)	Height (m)	Depth (mbsl)	Burial depth (m)	W/H ratio
7250	11375	2	3b	517,72	59,50	1888,74	525,30	8,70
7250	11550	2	3b	739,60	78,20	1818,90	453,90	9,46
7250	13400	2	3b	369,80	52,70	1760,94	413,10	7,02
7250	14475	2	3b	480,74	69,70	1702,12	380,80	6,90
7250	14575	2	3b	295,84	37,40	1750,00	431,80	7,91
7250	14950	2	3b	628,66	39,10	1801,42	487,90	16,08
7250	14975	2	3b	702,62	74,80	1889,68	574,60	9,39
7250	20675	2	3b	388,29	69,70	1692,16	411,40	5,57
7250	20950	2	3b	443,76	78,20	1793,58	525,30	5,67
7250	20950	2	3b	351,31	69,70	1634,06	368,90	5,04
7250	21075	2	3b	221,88	52,70	1716,08	455,60	4,21
7375	6525	2	3b	573,19	54,40	1475,24	221,00	10,54
7375	6675	2	3b	314,33	103,70	1687,32	428,40	3,03
7375	6850	2	3b	647,15	62,90	1571,72	312,80	10,29
7375	6900	2	3b	425,27	81,60	1775,30	511,70	5,21
7375	7325	2	3b	425,27	69,70	1688,50	385,90	6,10
7375	8075	2	3b	795,07	61,20	1566,26	246,50	12,99
7375	8250	2	3b	480,74	42,50	1782,44	465,80	11,31
7375	9075	2	3b	369,80	56,10	1712,74	396,10	6,59
7375	9325	2	3b	1312,79	42,50	1649,56	329,80	30,89
7375	9850	2	3b	647,15	34,00	1811,06	491,30	19,03
7375	10750	2	3b	517,72	39,10	1840,52	527,00	13,24
7375	11350	2	3b	647,15	49,30	1712,74	396,10	13,13
7375	11400	2	3b	351,31	51,00	1886,18	532,10	6,89
7375	11525	2	3b	721,11	90,10	1821,26	501,50	8,00
7375	11650	2	3b	240,37	49,30	1930,28	537,20	4,88
7375	12600	2	3b	351,31	28,90	1678,92	326,40	12,16
7375	12675	2	3b	369,80	54,40	1762,64	414,80	6,80
7375	13400	2	3b	517,72	44,20	1743,68	374,00	11,71
7375	14450	2	3b	721,11	81,60	1639,22	317,90	8,84
7375	14475	2	3b	499,23	62,90	1707,08	384,20	7,94
7375	14850	2	3b	221,88	52,70	1929,64	605,20	4,21
7375	14875	2	3b	591,68	40,80	1811,34	494,70	14,50
7375	15125	2	3b	554,70	74,80	1881,04	564,40	7,42
7375	20775	2	3b	295,84	45,90	1668,08	384,20	6,45
7375	20800	2	3b	425,27	78,20	1573,02	290,70	5,44
7375	20975	2	3b	332,82	42,50	1759,44	489,60	7,83
7375	21075	2	3b	277,35	47,60	1793,30	521,90	5,83
7375	21075	2	3b	258,86	52,70	1718,64	448,80	4,91
7500	6675	2	3b	332,82	64,60	1701,06	443,70	5,15
7500	6850	2	3b	351,31	66,30	1766,38	498,10	5,30
7500	6875	2	3b	369,80	52,70	1624,14	362,10	7,02
7500	6900	2	3b	647,15	61,20	1575,12	316,20	10,57
7500	8650	2	3b	647,15	45,90	1811,62	498,10	14,10
7500	8700	2	3b	573,19	47,60	1726,48	411,40	12,04
7500	9250	2	3b	795,07	78,50	1612,44	295,80	10,13
7500	11275	2	3b	702,62	64,60	1732,86	413,10	10,88
7500	11550	2	3b	332,82	59,50	1903,58	572,90	5,59

(N-S)	X (E-W)	Area	Unit	Width (m)	Height (m)	Depth (mbsl)	Burial depth (m)	W/H ratio
7500	11700	2	3b	628,66	76,50	1822,54	498,10	8,22
7500	14600	2	3b	314,33	51,00	1781,60	455,60	6,16
7500	15200	2	3b	480,74	68,00	1890,04	635,80	7,07
7500	15400	2	3b	536,21	85,00	1943,80	625,60	6,31
7500	16725	2	3b	221,88	39,10	1369,62	56,10	5,67
7500	20750	2	3b	351,31	62,90	1662,84	377,40	5,59
7500	20775	2	3b	314,33	47,60	1804,64	527,00	6,60
7500	21100	2	3b	295,84	64,60	1740,88	472,60	4,58
7625	6650	2	3b	351,31	62,90	1693,70	430,10	5,59
7625	6800	2	3b	425,27	61,20	1637,74	375,70	6,95
7625	6800	2	3b	684,13	51,00	1569,60	306,00	13,41
7625	6825	2	3b	388,29	57,80	1752,64	482,80	6,72
7625	7225	2	3b	462,25	61,20	1705,10	379,10	7,55
7625	8550	2	3b	610,17	51,00	1829,48	506,60	11,96
7625	8600	2	3b	665,64	61,20	1747,88	425,00	10,88
7625	9300	2	3b	813,56	47,60	1654,24	329,80	17,09
7625	10475	2	3b	406,78	42,50	1813,90	487,90	9,57
7625	11450	2	3b	887,52	54,40	1733,72	404,60	16,31
7625	11525	2	3b	332,82	52,70	1903,28	588,20	6,32
7625	11625	2	3b	795,07	45,90	1844,50	518,50	17,32
7625	11700	2	3b	573,19	76,50	1817,86	498,10	7,49
7625	13300	2	3b	443,76	62,90	1702,74	331,50	7,06
7625	13375	2	3b	554,70	37,40	1750,70	307,70	14,83
7625	14425	2	3b	554,70	88,40	1733,72	404,60	6,27
7625	14425	2	3b	813,56	61,20	1636,82	307,70	13,29
7625	14650	2	3b	295,84	59,50	1788,54	464,10	4,97
7625	15150	2	3b	665,64	88,40	1898,76	571,20	7,53
7625	20750	2	3b	314,33	76,50	1665,40	370,60	4,11
7625	21025	2	3b	314,33	64,60	1747,26	474,30	4,87
7625	21100	2	3b	240,37	42,50	1681,24	411,40	5,66
7750	6625	2	3b	295,84	59,50	1708,30	436,90	4,97
7750	6775	2	3b	425,27	42,50	1631,94	362,10	10,01
7750	6775	2	3b	702,62	10,20	1516,34	246,50	68,88
7750	6800	2	3b	258,86	35,70	1745,70	474,30	7,25
7750	6800	2	3b	702,62	54,40	1580,66	307,70	12,92
7750	7225	2	3b	443,76	54,40	1692,36	357,00	8,16
7750	8650	2	3b	684,13	57,80	1840,12	503,20	11,84
7750	8675	2	3b	591,68	61,20	1777,36	442,00	9,67
7750	9325	2	3b	628,66	78,20	1694,76	367,20	8,04
7750	9575	2	3b	184,90	34,00	1650,70	324,70	5,44
7750	10450	2	3b	813,56	56,10	1842,80	516,80	14,50
7750	11450	2	3b	813,56	61,20	1747,74	423,30	13,29
7750	11725	2	3b	684,13	79,90	1822,54	498,10	8,56
7750	11775	2	3b	739,60	61,20	1882,74	566,10	12,08
7750	13300	2	3b	406,78	40,80	1654,74	260,10	9,97
7750	13350	2	3b	314,33	57,80	1795,58	379,10	5,44
7750	13375	2	3b	277,35	40,80	1867,70	440,30	6,80
7750	14450	2	3b	795,07	125,80	1711,76	384,20	6,32

(N-S)	X (E-W)	Area	Unit	Width (m)	Height (m)	Depth (mbsl)	Burial depth (m)	W/H ratio
7750	15125	2	3b	554,70	107,10	1913,64	581,40	5,18
7750	16000	2	3b	332,82	59,50	1749,84	448,80	5,59
7750	20750	2	3b	314,33	85,00	1676,88	377,40	3,70
7750	20750	2	3b	351,31	66,30	1571,20	268,60	5,30
7750	21025	2	3b	295,84	42,50	1732,82	450,50	6,96
7750	21675	2	3b	369,80	68,00	1726,14	464,10	5,44
7875	6500	2	3b	369,80	62,90	1706,88	438,60	5,88
7875	6750	2	3b	517,72	57,80	1647,10	375,70	8,96
7875	6800	2	3b	388,29	39,10	1729,84	452,20	9,93
7875	6800	2	3b	702,62	62,90	1597,66	324,70	11,17
7875	7150	2	3b	332,82	32,30	1687,26	351,90	10,30
7875	8575	2	3b	591,68	49,30	1769,44	421,60	12,00
7875	8800	2	3b	887,52	73,10	1848,76	513,40	12,14
7875	8850	2	3b	351,31	37,40	1458,32	129,20	9,39
7875	9300	2	3b	739,60	110,50	1747,46	419,90	6,69
7875	9800	2	3b	314,33	32,30	1615,00	289,00	9,73
7875	10500	2	3b	887,52	68,00	1876,24	544,00	13,05
7875	11200	2	3b	924,50	35,70	1656,38	317,90	25,90
7875	11375	2	3b	776,58	62,90	1740,66	413,10	12,35
7875	11750	2	3b	665,64	54,40	1863,20	537,20	12,24
7875	11775	2	3b	832,05	66,30	1816,88	486,20	12,55
7875	13350	2	3b	388,29	74,80	1692,30	280,50	5,19
7875	13425	2	3b	499,23	78,20	1809,18	392,70	6,38
7875	14450	2	3b	795,07	136,00	1708,36	380,80	5,85
7875	14650	2	3b	425,27	61,20	1781,04	448,80	6,95
7875	15050	2	3b	628,66	68,00	1877,94	545,70	9,25
7875	15150	2	3b	443,76	62,90	1921,72	584,80	7,06
7875	20775	2	3b	388,29	74,80	1696,44	387,60	5,19
7875	21075	2	3b	591,68	59,50	1756,18	487,90	9,94
7875	21550	2	3b	332,82	57,80	1718,92	452,20	5,76
8000	6450	2	3b	184,90	39,10	1747,68	479,40	4,73
8000	6500	2	3b	388,29	64,60	1703,20	431,80	6,01
8000	6600	2	3b	832,05	61,20	1590,30	311,10	13,60
8000	6650	2	3b	795,07	32,30	1531,08	255,00	24,62
8000	6725	2	3b	425,27	62,90	1646,68	370,60	6,76
8000	7200	2	3b	277,35	39,10	1675,90	365,50	7,09
8000	8650	2	3b	702,62	54,40	1755,42	402,90	12,92
8000	8850	2	3b	610,17	64,60	1850,32	513,40	9,45
8000	9325	2	3b	684,13	96,90	1761,06	433,50	7,06
8000	9875	2	3b	351,31	54,40	1639,94	307,70	6,46
8000	10025	2	3b	258,86	57,80	1738,68	408,00	4,48
8000	10575	2	3b	869,03	74,80	1898,20	564,40	11,62
8000	11725	2	3b	499,23	62,90	1901,48	547,40	7,94
8000	11775	2	3b	591,68	51,00	1802,46	443,70	11,60
8000	11800	2	3b	573,19	40,80	1844,40	479,40	14,05
8000	13325	2	3b	388,29	74,80	1708,88	292,40	5,19
8000	13425	2	3b	351,31	66,30	1800,00	357,00	5,30
8000	14700	2	3b	351,31	62,90	1791,24	459,00	5,59

(N-S)	X (E-W)	Area	Unit	Width (m)	Height (m)	Depth (mbsl)	Burial depth (m)	W/H ratio
8000	15050	2	3b	776,58	88,40	1891,12	554,20	8,78
8000	16150	2	3b	369,80	45,90	1709,18	409,70	8,06
8000	18175	2	3b	610,17	62,90	1756,24	431,80	9,70
8000	20775	2	3b	258,86	69,70	1591,76	272,00	3,71
8000	20825	2	3b	295,84	64,60	1683,98	368,90	4,58
8000	21125	2	3b	388,29	69,70	1757,74	487,90	5,57
8000	21425	2	3b	258,86	54,40	1692,00	428,40	4,76
8125	6500	2	3b	240,37	47,60	1765,96	493,00	5,05
8125	6600	2	3b	610,17	100,30	1709,72	435,20	6,08
8125	7650	2	3b	314,33	37,40	1686,70	345,10	8,40
8125	8550	2	3b	443,76	37,40	1742,94	402,90	11,87
8125	8900	2	3b	610,17	78,20	1849,32	520,20	7,80
8125	9300	2	3b	554,70	62,90	1772,82	443,70	8,82
8125	9475	2	3b	647,15	79,90	1735,14	402,90	8,10
8125	10575	2	3b	906,01	79,90	1918,18	579,70	11,34
8125	11450	2	3b	573,19	51,00	1761,20	435,20	11,24
8125	11650	2	3b	628,66	68,00	1886,48	516,80	9,25
8125	11825	2	3b	665,64	47,60	1804,88	435,20	13,98
8125	13450	2	3b	443,76	51,00	1773,08	333,20	8,70
8125	14650	2	3b	369,80	51,00	1763,76	428,40	7,25
8125	15050	2	3b	721,11	102,00	1889,42	552,50	7,07
8125	20725	2	3b	277,35	74,80	1702,12	380,80	3,71
8125	21100	2	3b	369,80	66,30	1793,16	520,20	5,58
8125	21375	2	3b	332,82	56,10	1680,96	408,00	5,93
8250	6425	2	3b	332,82	35,70	1753,20	489,60	9,32
8250	6550	2	3b	869,03	132,60	1730,26	457,30	6,55
8250	6775	2	3b	979,97	30,60	1532,92	258,40	32,03
8250	6850	2	3b	369,80	39,10	1772,78	481,10	9,46
8250	7200	2	3b	258,86	51,00	1713,30	402,90	5,08
8250	7700	2	3b	314,33	59,50	1701,84	377,40	5,28
8250	8475	2	3b	388,29	42,50	1747,04	414,80	9,14
8250	9000	2	3b	665,64	81,60	1851,60	510,00	8,16
8250	9325	2	3b	406,78	62,90	1766,02	436,90	6,47
8250	9625	2	3b	351,31	32,30	1718,28	387,60	10,88
8250	10200	2	3b	295,84	25,50	1824,82	487,90	11,60
8250	10575	2	3b	776,58	81,60	1920,32	567,80	9,52
8250	11475	2	3b	573,19	62,90	1772,56	421,60	9,11
8250	11500	2	3b	665,64	34,00	1701,02	348,50	19,58
8250	11700	2	3b	776,58	93,50	1882,94	511,70	8,31
8250	11850	2	3b	795,07	61,20	1807,86	433,50	12,99
8250	11975	2	3b	499,23	86,70	1954,90	589,90	5,76
8250	13425	2	3b	443,76	52,70	1719,24	285,60	8,42
8250	14600	2	3b	277,35	40,80	1768,58	430,10	6,80
8250	14950	2	3b	758,09	78,20	1890,84	550,80	9,69
8250	15450	2	3b	628,66	32,30	1777,36	442,00	19,46
8250	16025	2	3b	258,86	47,60	1716,84	408,00	5,44
8250	20700	2	3b	332,82	59,50	1732,12	442,00	5,59
8250	20875	2	3b	388,29	56,10	1683,82	385,90	6,92

(N-S)	X (E-W)	Area	Unit	Width (m)	Height (m)	Depth (mbsl)	Burial depth (m)	W/H ratio
8250	21075	2	3b	443,76	71,40	1803,69	553,35	6,22
8375	6325	2	3b	443,76	44,20	1762,98	494,70	10,04
8375	6475	2	3b	850,54	122,40	1732,24	462,40	6,95
8375	6725	2	3b	480,74	49,30	1797,14	511,70	9,75
8375	6725	2	3b	942,99	30,60	1534,48	258,40	30,82
8375	7200	2	3b	295,84	54,40	1720,52	414,80	5,44
8375	9050	2	3b	702,62	69,70	1854,28	523,60	10,08
8375	9400	2	3b	425,27	47,60	1745,34	413,10	8,93
8375	10025	2	3b	480,74	44,20	1756,54	416,50	10,88
8375	10300	2	3b	351,31	30,60	1724,66	389,30	11,48
8375	10625	2	3b	702,62	83,30	1913,52	561,00	8,43
8375	11575	2	3b	573,19	66,30	1779,24	408,00	8,65
8375	11675	2	3b	554,70	61,20	1862,40	489,60	9,06
8375	11900	2	3b	795,07	51,00	1807,14	443,70	15,59
8375	13150	2	3b	240,37	23,80	1700,10	280,50	10,10
8375	13475	2	3b	480,74	73,10	1752,50	348,50	6,58
8375	13550	2	3b	369,80	62,90	1816,96	411,40	5,88
8375	14475	2	3b	499,23	49,30	1755,26	419,90	10,13
8375	15000	2	3b	739,60	81,60	1889,14	549,10	9,06
8375	15400	2	3b	517,72	51,00	1795,36	452,20	10,15
8375	20750	2	3b	332,82	47,60	1713,28	421,60	6,99
8375	20950	2	3b	351,31	61,20	1776,60	489,60	5,74
8500	2575	2	3b	1386,75	117,30	1569,40	360,40	11,82
8500	6200	2	3b	1053,93	122,40	1739,74	477,70	8,61
8500	6575	2	3b	1275,81	40,80	1536,60	265,20	31,27
8500	6775	2	3b	517,72	62,90	1797,28	513,40	8,23
8500	7250	2	3b	332,82	54,40	1717,96	421,60	6,12
8500	7325	2	3b	295,84	30,60	1692,74	399,50	9,67
8500	8500	2	3b	388,29	37,40	1729,34	389,30	10,38
8500	9000	2	3b	591,68	49,30	1849,04	516,80	12,00
8500	9425	2	3b	388,29	39,10	1734,58	396,10	9,93
8500	10125	2	3b	702,62	83,30	1803,86	460,70	8,43
8500	10275	2	3b	536,21	85,00	1773,40	431,80	6,31
8500	10575	2	3b	832,05	85,00	1908,14	552,50	9,79
8500	11725	2	3b	813,56	96,90	1868,64	489,60	8,40
8500	13500	2	3b	554,70	68,00	1752,40	309,40	8,16
8500	13525	2	3b	295,84	71,40	1843,62	413,10	4,14
8500	14500	2	3b	480,74	42,50	1757,96	414,80	11,31
8500	14900	2	3b	758,09	122,40	1926,40	584,80	6,19
8500	15425	2	3b	536,21	51,00	1767,88	421,60	10,51
8500	16450	2	3b	517,72	81,60	1612,44	295,80	6,34
8500	20725	2	3b	425,27	79,90	1575,30	280,50	5,32
8500	20775	2	3b	369,80	76,50	1680,26	399,50	4,83
8500	20825	2	3b	314,33	69,70	1761,30	474,30	4,51
8625	2650	2	3b	961,48	83,30	1596,74	389,30	11,54
8625	6175	2	3b	1183,36	125,80	1748,52	489,60	9,41
8625	6700	2	3b	1035,44	45,90	1542,54	280,50	22,56
8625	6800	2	3b	499,23	49,30	1788,64	503,20	10,13

(N-S)	X (E-W)	Area	Unit	Width (m)	Height (m)	Depth (mbsl)	Burial depth (m)	W/H ratio
8625	7250	2	3b	369,80	68,00	1721,64	428,40	5,44
8625	8575	2	3b	425,27	35,70	1731,04	391,00	11,91
8625	9075	2	3b	702,62	73,10	1508,34	168,30	9,61
8625	9175	2	3b	425,27	35,70	1850,46	515,10	11,91
8625	9750	2	3b	332,82	28,90	1856,42	511,70	11,52
8625	10225	2	3b	406,78	51,00	1815,20	465,80	7,98
8625	10350	2	3b	610,17	73,10	1765,76	414,80	8,35
8625	10725	2	3b	758,09	51,00	1885,20	520,20	14,86
8625	11550	2	3b	240,37	49,30	1789,32	397,80	4,88
8625	11750	2	3b	573,19	78,20	1852,22	460,70	7,33
8625	12150	2	3b	258,86	39,10	1791,54	443,70	6,62
8625	13525	2	3b	480,74	71,40	1849,20	367,20	6,73
8625	13550	2	3b	462,25	47,60	1766,46	290,70	9,71
8625	13575	2	3b	240,37	49,30	1908,28	421,60	4,88
8625	14500	2	3b	388,29	47,60	1770,72	418,20	8,16
8625	14875	2	3b	850,54	93,50	1903,46	552,50	9,10
8625	15375	2	3b	462,25	32,30	1772,40	438,60	14,31
8625	20625	2	3b	425,27	98,60	1615,82	317,90	4,31
8625	20675	2	3b	351,31	52,70	1667,24	374,00	6,67
8625	20725	2	3b	388,29	61,20	1746,72	448,80	6,34
8750	2775	2	3b	1201,85	112,20	1609,92	397,80	10,71
8750	6000	2	3b	1201,85	49,30	1665,36	408,00	24,38
8750	6375	2	3b	1016,95	73,10	1746,54	484,50	13,91
8750	7325	2	3b	369,80	79,90	1729,58	430,10	4,63
8750	8800	2	3b	702,62	73,10	1757,82	413,10	9,61
8750	9775	2	3b	425,27	71,40	1873,00	523,60	5,96
8750	10325	2	3b	499,23	66,30	1838,58	484,50	7,53
8750	10425	2	3b	314,33	39,10	1763,36	404,60	8,04
8750	11800	2	3b	776,58	69,70	1848,22	487,90	11,14
8750	11900	2	3b	1016,95	62,90	1770,72	418,20	16,17
8750	13500	2	3b	517,72	49,30	1765,90	283,90	10,50
8750	13525	2	3b	406,78	59,50	1830,64	350,20	6,84
8750	14425	2	3b	573,19	37,40	1760,52	408,00	15,33
8750	14900	2	3b	813,56	78,20	1891,44	520,20	10,40
8750	15250	2	3b	388,29	22,10	1766,78	389,30	17,57
8750	16750	2	3b	554,70	78,20	1616,84	292,40	7,09
8750	20550	2	3b	536,21	64,60	1569,92	272,00	8,30
8750	20600	2	3b	351,31	54,40	1679,00	384,20	6,46
8750	20625	2	3b	480,74	61,20	1741,34	440,30	7,86
8875	2875	2	3b	1257,32	90,10	1633,02	413,10	13,95
8875	6350	2	3b	1090,91	61,20	1746,40	482,80	17,83
8875	7275	2	3b	314,33	86,70	1744,46	440,30	3,63
8875	8850	2	3b	665,64	34,00	1677,36	326,40	19,58
8875	8900	2	3b	813,56	66,30	1755,70	406,30	12,27
8875	9050	2	3b	332,82	35,70	1822,84	482,80	9,32
8875	9825	2	3b	443,76	49,30	1868,34	504,90	9,00
8875	10325	2	3b	499,23	69,70	1838,02	477,70	7,16
8875	11800	2	3b	684,13	74,80	1845,52	493,00	9,15

(N-S)	X (E-W)	Area	Unit	Width (m)	Height (m)	Depth (mbsl)	Burial depth (m)	W/H ratio
8875	11850	2	3b	647,15	42,50	1768,88	414,80	15,23
8875	13500	2	3b	462,25	76,50	1811,06	358,70	6,04
8875	13800	2	3b	610,17	28,90	1747,88	292,40	21,11
8875	14000	2	3b	314,33	59,50	1852,44	387,60	5,28
8875	14475	2	3b	517,72	34,00	1766,76	408,00	15,23
8875	20550	2	3b	351,31	62,90	1681,84	380,80	5,59
8875	20625	2	3b	480,74	79,90	1755,64	462,40	6,02
9000	3050	2	3b	610,17	54,40	1649,46	423,30	11,22
9000	5100	2	3b	406,78	52,70	1720,60	472,60	7,72
9000	6400	2	3b	758,09	52,70	1735,22	460,70	14,39
9000	6600	2	3b	554,70	37,40	1809,46	528,70	14,83
9000	7250	2	3b	388,29	59,50	1766,14	457,30	6,53
9000	7400	2	3b	369,80	40,80	1710,18	402,90	9,06
9000	8850	2	3b	887,52	100,30	1758,96	408,00	8,85
9000	9050	2	3b	369,80	39,10	1837,44	489,60	9,46
9000	10250	2	3b	961,48	51,00	1876,56	510,00	18,85
9000	10550	2	3b	610,17	45,90	1826,84	455,60	13,29
9000	11050	2	3b	462,25	44,20	1802,62	426,70	10,46
9000	11825	2	3b	536,21	100,30	1863,80	506,60	5,35
9000	11900	2	3b	1035,44	39,10	1726,80	377,40	26,48
9000	14150	2	3b	314,33	40,80	1840,78	416,50	7,70
9000	14500	2	3b	610,17	66,30	1782,20	425,00	9,20
9000	14875	2	3b	721,11	69,70	1891,86	525,30	10,35
9000	16800	2	3b	240,37	49,30	1717,86	382,50	4,88
9000	16875	2	3b	443,76	95,20	1619,40	285,60	4,66
9000	16925	2	3b	295,84	45,90	1811,92	482,80	6,45
9000	20300	2	3b	610,17	52,70	1565,26	253,30	11,58
9000	20375	2	3b	425,27	88,40	1678,58	379,10	4,81
9000	20500	2	3b	499,23	71,40	1773,22	467,50	6,99
9125	3275	2	3b	665,64	62,90	1676,10	443,70	10,58
9125	4550	2	3b	295,84	47,60	1793,70	545,70	6,22
9125	4800	2	3b	776,58	57,80	1710,68	465,80	13,44
9125	6350	2	3b	665,64	51,00	1724,60	445,40	13,05
9125	6675	2	3b	369,80	52,70	1849,42	559,30	7,02
9125	7150	2	3b	406,78	47,60	1787,82	474,30	8,55
9125	7275	2	3b	443,76	34,00	1757,22	443,70	13,05
9125	7400	2	3b	425,27	81,60	1731,58	416,50	5,21
9125	8750	2	3b	942,99	98,60	1758,10	416,50	9,56
9125	9000	2	3b	499,23	62,90	1856,56	513,40	7,94
9125	10400	2	3b	998,46	57,80	1867,50	494,70	17,27
9125	11975	2	3b	813,56	39,10	1735,02	382,50	20,81
9125	14500	2	3b	480,74	62,90	1792,12	431,80	7,64
9125	14850	2	3b	684,13	57,80	1879,66	528,70	11,84
9125	16950	2	3b	517,72	73,10	1642,78	304,30	7,08
9125	20350	2	3b	499,23	81,60	1677,32	363,80	6,12
9125	20450	2	3b	388,29	71,40	1752,40	442,00	5,44
9250	2850	2	3b	591,68	40,80	1777,82	542,30	14,50
9250	3300	2	3b	1016,95	54,40	1685,46	443,70	18,69

(N-S)	X (E-W)	Area	Unit	Width (m)	Height (m)	Depth (mbsl)	Burial depth (m)	W/H ratio
9250	4825	2	3b	832,05	39,10	1701,76	452,20	21,28
9250	6200	2	3b	869,03	47,60	1721,06	440,30	18,26
9250	6625	2	3b	517,72	68,00	1874,50	579,70	7,61
9250	7050	2	3b	591,68	59,50	1790,94	474,30	9,94
9250	7275	2	3b	443,76	59,50	1758,36	438,60	7,46
9250	7350	2	3b	517,72	52,70	1748,02	426,70	9,82
9250	7450	2	3b	499,23	59,50	1705,66	385,90	8,39
9250	8800	2	3b	721,11	124,10	1802,44	462,40	5,81
9250	9050	2	3b	462,25	68,00	1856,00	506,60	6,80
9250	10350	2	3b	758,09	59,50	1866,40	462,40	12,74
9250	10550	2	3b	869,03	51,00	1800,50	419,90	17,04
9250	12000	2	3b	758,09	113,90	1875,84	520,20	6,66
9250	14475	2	3b	295,84	45,90	1858,00	493,00	6,45
9250	14500	2	3b	591,68	90,10	1803,46	436,90	6,57
9250	16175	2	3b	425,27	59,50	1877,52	540,60	7,15
9250	16350	2	3b	554,70	57,80	1732,88	394,40	9,60
9250	17025	2	3b	517,72	57,80	1655,82	311,10	8,96
9250	17125	2	3b	351,31	56,10	1817,74	477,70	6,26
9250	20250	2	3b	480,74	83,30	1700,56	380,80	5,77
9250	20275	2	3b	351,31	59,50	1770,82	457,30	5,90
9375	3175	2	3b	1127,89	61,20	1657,42	406,30	18,43
9375	4775	2	3b	924,50	45,90	1686,32	435,20	20,14
9375	6450	2	3b	517,72	69,70	1656,18	372,30	7,43
9375	6600	2	3b	462,25	59,50	1870,10	583,10	7,77
9375	7075	2	3b	647,15	83,30	1783,58	460,70	7,77
9375	7300	2	3b	351,31	42,50	1754,26	426,70	8,27
9375	7375	2	3b	536,21	52,70	1704,40	370,60	10,17
9375	8725	2	3b	795,07	81,60	1781,20	431,80	9,74
9375	8800	2	3b	979,97	62,90	1703,00	353,60	15,58
9375	9100	2	3b	591,68	62,90	1866,90	525,30	9,41
9375	10000	2	3b	647,15	35,70	1642,94	287,30	18,13
9375	10300	2	3b	536,21	56,10	1854,22	447,10	9,56
9375	10550	2	3b	702,62	54,40	1784,52	377,40	12,92
9375	11975	2	3b	906,01	90,10	1863,10	498,10	10,06
9375	12025	2	3b	1053,93	54,40	1742,54	379,10	19,37
9375	14425	2	3b	462,25	45,90	1867,50	494,70	10,07
9375	14525	2	3b	684,13	74,80	1808,00	435,20	9,15
9375	16025	2	3b	665,64	51,00	1872,70	538,90	13,05
9375	16450	2	3b	517,72	64,60	1749,60	408,00	8,01
9375	17150	2	3b	517,72	68,00	1844,52	499,80	7,61
9375	17250	2	3b	665,64	47,60	1635,28	289,00	13,98
9375	19925	2	3b	832,05	74,80	1563,16	227,80	11,12
9375	20025	2	3b	499,23	66,30	1829,06	501,50	7,53
9375	20200	2	3b	406,78	64,60	1747,88	425,00	6,30
9375	20300	2	3b	406,78	69,70	1652,68	329,80	5,84
9500	2850	2	3b	1016,95	40,80	1787,88	550,80	24,93
9500	3625	2	3b	554,70	49,30	1754,90	491,30	11,25
9500	6625	2	3b	499,23	64,60	1875,34	589,90	7,73



(N-S)	X (E-W)	Area	Unit	Width (m)	Height (m)	Depth (mbsl)	Burial depth (m)	W/H ratio
9500	7025	2	3b	591,68	83,30	1799,86	487,90	7,10
9500	7200	2	3b	536,21	51,00	1750,30	416,50	10,51
9500	7275	2	3b	628,66	45,90	1698,16	370,60	13,70
9500	7675	2	3b	314,33	35,70	1608,64	268,60	8,80
9500	8725	2	3b	998,46	88,40	1717,74	362,10	11,29
9500	8850	2	3b	1164,87	98,60	1765,90	416,50	11,81
9500	9125	2	3b	647,15	73,10	1871,30	521,90	8,85
9500	10300	2	3b	665,64	71,40	1689,44	302,60	9,32
9500	10600	2	3b	628,66	81,60	1772,20	360,40	7,70
9500	11950	2	3b	1053,93	57,80	1736,90	348,50	18,23
9500	12075	2	3b	739,60	98,60	1851,57	471,75	7,50
9500	14375	2	3b	536,21	78,20	1871,90	491,30	6,86
9500	14450	2	3b	702,62	69,70	1804,18	426,70	10,08
9500	16425	2	3b	536,21	85,00	1770,00	428,40	6,31
9500	17250	2	3b	499,23	85,00	1844,10	494,70	5,87
9500	17375	2	3b	591,68	73,10	1728,78	382,50	8,09
9500	17375	2	3b	832,05	59,50	1636,42	283,90	13,98
9500	19925	2	3b	499,23	96,90	1825,66	498,10	5,15
9500	20000	2	3b	739,60	68,00	1697,46	362,10	10,88
9625	4375	2	3b	721,11	52,70	1623,84	377,40	13,68
9625	6125	2	3b	684,13	47,60	1635,36	346,80	14,37
9625	6500	2	3b	776,58	37,40	1846,16	557,60	20,76
9625	6850	2	3b	295,84	35,70	1889,80	595,00	8,29
9625	7000	2	3b	647,15	88,40	1809,48	510,00	7,32
9625	7200	2	3b	832,05	95,20	1754,52	448,80	8,74
9625	8775	2	3b	1035,44	119,00	1770,72	418,20	8,70
9625	9075	2	3b	388,29	37,40	1661,50	304,30	10,38
9625	9175	2	3b	684,13	79,90	1867,76	516,80	8,56
9625	10325	2	3b	536,21	62,90	1693,82	317,90	8,52
9625	10600	2	3b	573,19	56,10	1752,66	331,50	10,22
9625	11575	2	3b	369,80	42,50	1882,50	525,30	8,70
9625	11700	2	3b	628,66	59,50	1846,52	486,20	10,57
9625	12125	2	3b	647,15	69,70	1818,94	416,50	9,28
9625	14450	2	3b	573,19	86,70	1878,28	493,00	6,61
9625	14550	2	3b	684,13	51,00	1794,98	409,70	13,41
9625	16025	2	3b	610,17	54,40	1875,96	540,60	11,22
9625	16025	2	3b	166,41	32,30	1707,24	367,20	5,15
9625	16450	2	3b	332,82	47,60	1742,94	402,90	6,99
9750	3475	2	3b	702,62	40,80	1806,74	552,50	17,22
9750	4650	2	3b	739,60	45,90	1647,50	399,50	16,11
9750	6575	2	3b	517,72	27,20	1837,80	550,80	19,03
9750	7025	2	3b	1035,44	110,50	1813,30	518,50	9,37
9750	7050	2	3b	1238,83	79,90	1745,30	450,50	15,50
9750	8700	2	3b	1090,91	90,10	1750,46	399,50	12,11
9750	9025	2	3b	961,48	81,60	1707,82	355,30	11,78
9750	9200	2	3b	369,80	34,00	1852,60	503,20	10,88
9750	10575	2	3b	462,25	45,90	1732,40	312,80	10,07
9750	11525	2	3b	610,17	40,80	1899,08	537,20	14,96

(N-S)	X (E-W)	Area	Unit	Width (m)	Height (m)	Depth (mbsl)	Burial depth (m)	W/H ratio
9750	11525	2	3b	721,11	51,00	1848,22	487,90	14,14
9750	12125	2	3b	665,64	68,00	1807,04	404,60	9,79
9750	12550	2	3b	314,33	34,00	1908,60	520,20	9,25
9750	14125	2	3b	1016,95	120,70	1727,12	343,40	8,43
9750	14300	2	3b	332,82	66,30	1946,42	562,70	5,02
9750	14450	2	3b	536,21	56,10	1796,96	414,80	9,56
9750	14575	2	3b	647,15	79,90	1883,52	499,80	8,10
9750	17425	2	3b	628,66	105,40	1843,40	486,20	5,96
9750	17550	2	3b	702,62	62,90	1741,54	385,90	11,17
9750	17850	2	3b	721,11	37,40	1620,42	260,10	19,28
9750	19800	2	3b	628,66	68,00	1775,52	438,60	9,25
9875	3325	2	3b	388,29	51,00	1794,70	538,90	7,61
9875	3750	2	3b	406,78	45,90	1823,46	566,10	8,86
9875	4000	2	3b	369,80	28,90	1607,42	348,50	12,80
9875	4500	2	3b	591,68	68,00	1662,94	416,50	8,70
9875	5025	2	3b	610,17	40,80	1824,74	562,70	14,96
9875	5175	2	3b	462,25	45,90	1715,80	452,20	10,07
9875	6400	2	3b	610,17	57,80	1735,94	450,50	10,56
9875	6525	2	3b	351,31	32,30	1834,40	547,40	10,88
9875	6775	2	3b	1349,77	159,80	1815,28	523,60	8,45
9875	8975	2	3b	795,07	71,40	1721,56	370,60	11,14
9875	11475	2	3b	610,17	34,00	1915,52	547,40	17,95
9875	11550	2	3b	739,60	71,40	1880,10	515,10	10,36
9875	12225	2	3b	2107,86	147,90	1815,08	445,40	14,25
9875	14350	2	3b	591,68	73,10	1800,94	406,30	8,09
9875	14375	2	3b	443,76	64,60	1960,88	567,80	6,87
9875	14900	2	3b	1460,71	64,60	1892,74	498,10	22,61
10000	3900	2	3b	462,25	51,00	1830,84	561,00	9,06
10000	4025	2	3b	443,76	49,30	1599,64	329,80	9,00
10000	4500	2	3b	591,68	64,60	1672,58	419,90	9,16
10000	5150	2	3b	887,52	64,60	1851,80	588,20	13,74
10000	6450	2	3b	887,52	76,50	1746,14	460,70	11,60
10000	6775	2	3b	1331,28	124,10	1822,08	530,40	10,73
10000	6975	2	3b	776,58	37,40	1683,68	384,20	20,76
10000	9125	2	3b	628,66	62,90	1716,46	365,50	9,99
10000	11425	2	3b	573,19	56,10	1876,56	510,00	10,22
10000	11475	2	3b	906,01	85,00	1936,06	569,50	10,66
10000	12125	2	3b	1516,18	76,50	1800,20	435,20	19,82
10000	14200	2	3b	776,58	83,30	1806,32	414,80	9,32
10000	15400	2	3b	1516,18	90,10	1912,72	513,40	16,83
10000	17525	2	3b	924,50	156,40	1834,06	467,50	5,91
10000	18775	2	3b	628,66	71,40	1789,30	416,50	8,80
10000	19450	2	3b	906,01	49,30	1726,40	353,60	18,38
10000	19450	2	3b	351,31	62,90	1677,94	314,50	5,59
10000	19600	2	3b	332,82	37,40	1800,76	442,00	8,90
10000	20175	2	3b	314,33	35,70	1783,74	443,70	8,80
10125	3450	2	3b	425,27	56,10	1662,26	389,30	7,58
10125	3950	2	3b	499,23	51,00	1843,04	557,60	9,79

(N-S)	X (E-W)	Area	Unit	Width (m)	Height (m)	Depth (mbsl)	Burial depth (m)	W/H ratio
10125	4575	2	3b	462,25	45,90	1675,98	423,30	10,07
10125	4575	2	3b	462,25	49,30	1673,86	416,50	9,38
10125	5100	2	3b	721,11	32,30	1832,12	557,60	22,33
10125	6450	2	3b	573,19	51,00	1752,94	467,50	11,24
10125	6575	2	3b	462,25	37,40	1841,50	538,90	12,36
10125	6775	2	3b	776,58	52,70	1807,22	501,50	14,74
10125	10725	2	3b	388,29	44,20	1755,44	384,20	8,78
10125	10775	2	3b	406,78	44,20	1808,00	435,20	9,20
10125	11450	2	3b	721,11	78,20	1951,08	581,40	9,22
10125	11500	2	3b	536,21	51,00	1866,36	499,80	10,51
10125	11950	2	3b	295,84	22,10	1845,68	476,00	13,39
10125	12150	2	3b	591,68	61,20	1812,02	389,30	9,67
10125	14450	2	3b	554,70	73,10	1782,82	375,70	7,59
10125	15475	2	3b	1386,75	96,90	1930,44	520,20	14,31
10125	17325	2	3b	480,74	56,10	1740,28	370,60	8,57
10125	17600	2	3b	258,86	47,60	1890,88	513,40	5,44
10125	17600	2	3b	536,21	85,00	1838,46	464,10	6,31
10125	19025	2	3b	684,13	56,10	1800,78	423,30	12,19
10125	19125	2	3b	739,60	51,00	1776,70	396,10	14,50
10125	19400	2	3b	721,11	45,90	1728,38	358,70	15,71
10125	19525	2	3b	591,68	54,40	1686,30	321,30	10,88
10125	20200	2	3b	425,27	32,30	1792,38	453,90	13,17
10125	20525	2	3b	184,90	34,00	1826,92	513,40	5,44
10250	3975	2	3b	369,80	51,00	1840,08	540,60	7,25
10250	5050	2	3b	721,11	37,40	1830,42	555,90	19,28
10250	6050	2	3b	869,03	42,50	1704,64	411,40	20,45
10250	6525	2	3b	480,74	44,20	1751,82	453,90	10,88
10250	6650	2	3b	425,27	64,60	1871,82	566,10	6,58
10250	6875	2	3b	1053,93	69,70	1791,64	482,80	15,12
10250	6925	2	3b	721,11	64,60	1696,58	389,30	11,16
10250	9675	2	3b	721,11	59,50	1718,20	329,80	12,12
10250	10750	2	3b	499,23	71,40	1831,52	455,60	6,99
10250	10825	2	3b	443,76	42,50	1772,30	399,50	10,44
10250	11425	2	3b	832,05	81,60	1941,02	572,90	10,20
10250	11850	2	3b	314,33	28,90	1861,26	494,70	10,88
10250	12050	2	3b	591,68	68,00	1816,56	387,60	8,70
10250	14375	2	3b	665,64	56,10	1768,94	358,70	11,87
10250	15325	2	3b	758,09	37,40	1824,18	423,30	20,27
10250	15425	2	3b	1312,79	90,10	1932,70	528,70	14,57
10250	17025	2	3b	388,29	35,70	1648,48	278,80	10,88
10250	17400	2	3b	462,25	74,80	1760,26	385,90	6,18
10250	17600	2	3b	480,74	68,00	1832,94	453,90	7,07
10250	18925	2	3b	665,64	56,10	1685,18	307,70	11,87
10250	19050	2	3b	906,01	51,00	1824,16	442,00	17,76
10250	19100	2	3b	795,07	61,20	1802,48	425,00	12,99
10250	19150	2	3b	942,99	23,80	1725,84	346,80	39,62
10375	3525	2	3b	351,31	49,30	1724,74	447,10	7,13
10375	4050	2	3b	406,78	28,90	1809,92	496,40	14,08

(N-S)	X (E-W)	Area	Unit	Width (m)	Height (m)	Depth (mbsl)	Burial depth (m)	W/H ratio
10375	5075	2	3b	1257,32	66,30	1784,66	511,70	18,96
10375	5900	2	3b	869,03	47,60	1710,30	423,30	18,26
10375	6475	2	3b	480,74	43,35	1743,89	442,85	11,09
10375	6675	2	3b	388,29	51,00	1863,62	542,30	7,61
10375	6825	2	3b	536,21	42,50	1696,02	382,50	12,62
10375	7100	2	3b	499,23	34,00	1651,26	331,50	14,68
10375	7175	2	3b	536,21	52,70	1803,98	481,10	10,17
10375	9350	2	3b	610,17	42,50	1653,30	280,50	14,36
10375	9725	2	3b	850,54	71,40	1741,30	345,10	11,91
10375	10875	2	3b	499,23	68,00	1855,46	481,10	7,34
10375	11425	2	3b	758,09	69,70	1939,46	572,90	10,88
10375	11825	2	3b	443,76	56,10	1863,24	499,80	7,91
10375	12100	2	3b	776,58	78,20	1821,90	433,50	9,93
10375	13200	2	3b	369,80	42,50	1943,56	452,20	8,70
10375	14400	2	3b	869,03	83,30	1786,22	379,10	10,43
10375	15225	2	3b	1460,71	47,60	1821,06	423,30	30,69
10375	15400	2	3b	1479,20	79,90	1926,32	527,00	18,51
10375	17425	2	3b	499,23	69,70	1772,02	396,10	7,16
10375	17425	2	3b	480,74	69,70	1770,46	396,10	6,90
10375	17625	2	3b	499,23	56,10	1829,40	448,80	8,90
10375	17775	2	3b	277,35	62,90	1899,24	520,20	4,41
10375	18825	2	3b	647,15	45,90	1679,80	299,20	14,10
10375	18975	2	3b	702,62	40,80	1846,40	465,80	17,22
10375	19100	2	3b	739,60	68,00	1810,42	426,70	10,88
10375	19275	2	3b	758,09	30,60	1732,92	357,00	24,77
10375	19525	2	3b	573,19	52,70	1710,96	336,60	10,88
10500	4125	2	3b	388,29	59,50	1832,16	520,20	6,53
10500	4525	2	3b	721,11	40,80	1703,90	440,30	17,67
10500	5000	2	3b	1072,42	79,90	1796,42	521,90	13,42
10500	5875	2	3b	795,07	37,40	1696,56	408,00	21,26
10500	6700	2	3b	480,74	68,00	1869,00	550,80	7,07
10500	6850	2	3b	684,13	68,00	1675,20	357,00	10,06
10500	7100	2	3b	1035,44	127,50	1811,36	476,00	8,12
10500	9800	2	3b	1072,42	120,70	1785,36	387,60	8,89
10500	9925	2	3b	887,52	88,40	1755,04	360,40	10,04
10500	10950	2	3b	647,15	81,60	1858,30	477,70	7,93
10500	11375	2	3b	647,15	56,10	1918,36	544,00	11,54
10500	11750	2	3b	554,70	47,60	1850,50	477,70	11,65
10500	12100	2	3b	721,11	69,70	1814,94	443,70	10,35
10500	14150	2	3b	795,07	30,60	1699,52	292,40	25,98
10500	14450	2	3b	961,48	90,10	1795,86	382,50	10,67
10500	15325	2	3b	1664,10	44,20	1826,16	428,40	37,65
10500	15400	2	3b	1275,81	81,60	1926,46	528,70	15,63
10500	17500	2	3b	425,27	69,70	1773,86	399,50	6,10
10500	17800	2	3b	517,72	57,80	1832,80	452,20	8,96
10500	18900	2	3b	702,62	45,90	1864,68	479,40	15,31
10500	18900	2	3b	1127,89	42,50	1769,20	380,80	26,54
10500	18950	2	3b	813,56	35,70	1820,06	430,10	22,79

(N-S)	X (E-W)	Area	Unit	Width (m)	Height (m)	Depth (mbsl)	Burial depth (m)	W/H ratio
10500	19150	2	3b	1201,85	57,80	1696,66	314,50	20,79
10500	19225	2	3b	832,05	52,70	1747,66	365,50	15,79
10500	20100	2	3b	314,33	47,60	1764,46	436,90	6,60
10500	20150	2	3b	314,33	54,40	1709,36	374,00	5,78
10625	3300	2	3b	388,29	37,40	1411,66	130,90	10,38
10625	3325	2	3b	758,09	44,20	1720,78	436,90	17,15
10625	4025	2	3b	554,70	51,00	1648,26	351,90	10,88
10625	4225	2	3b	388,29	44,20	1828,76	516,80	8,78
10625	4275	2	3b	351,31	34,00	1417,20	122,40	10,33
10625	4550	2	3b	573,19	85,00	1730,68	462,40	6,74
10625	5150	2	3b	1238,83	95,20	1792,74	515,10	13,01
10625	5575	2	3b	462,25	52,70	1739,34	453,90	8,77
10625	6775	2	3b	480,74	47,60	1875,80	557,60	10,10
10625	6825	2	3b	1127,89	78,20	1660,60	350,20	14,42
10625	7125	2	3b	1238,83	147,90	1822,98	484,50	8,38
10625	7325	2	3b	610,17	62,90	1778,64	438,60	9,70
10625	9075	2	3b	721,11	39,10	1657,84	278,80	18,44
10625	9800	2	3b	979,97	136,00	1823,76	418,20	7,21
10625	9900	2	3b	813,56	102,00	1793,72	394,40	7,98
10625	11000	2	3b	591,68	59,50	1865,38	487,90	9,94
10625	11200	2	3b	591,68	35,70	1897,54	518,50	16,57
10625	11750	2	3b	573,19	51,00	1833,36	459,00	11,24
10625	12200	2	3b	684,13	44,20	1791,00	418,20	15,48
10625	12225	2	3b	1479,20	81,60	1742,98	365,50	18,13
10625	14250	2	3b	869,03	61,20	1704,34	294,10	14,20
10625	14475	2	3b	1035,44	61,20	1759,32	336,60	16,92
10625	15325	2	3b	1664,10	28,90	1813,28	404,60	57,58
10625	15475	2	3b	1312,79	79,90	1914,98	521,90	16,43
10625	17575	2	3b	536,21	66,30	1768,20	387,60	8,09
10625	17950	2	3b	517,72	59,50	1828,96	462,40	8,70
10625	18300	2	3b	332,82	47,60	1770,74	399,50	6,99
10625	18850	2	3b	480,74	68,00	1825,30	436,90	7,07
10625	18875	2	3b	795,07	39,10	1863,12	479,40	20,33
10625	19100	2	3b	1072,42	78,20	1713,80	333,20	13,71
10625	19325	2	3b	388,29	35,70	1758,00	377,40	10,88
10750	3225	2	3b	554,70	49,30	1720,94	419,90	11,25
10750	3425	2	3b	1201,85	49,30	1638,18	362,10	24,38
10750	3875	2	3b	295,84	34,00	1787,08	503,20	8,70
10750	4600	2	3b	480,74	39,10	1721,08	421,60	12,30
10750	5075	2	3b	906,01	45,90	1765,68	489,60	19,74
10750	5500	2	3b	499,23	56,10	1740,90	453,90	8,90
10750	6775	2	3b	295,84	35,70	1866,60	540,60	8,29
10750	7225	2	3b	1146,38	103,70	1826,10	484,50	11,05
10750	7300	2	3b	721,11	61,20	1783,88	445,40	11,78
10750	8075	2	3b	314,33	37,40	1663,64	292,40	8,40
10750	9750	2	3b	702,62	141,10	1842,04	431,80	4,98
10750	9775	2	3b	369,80	25,50	1874,62	467,50	14,50
10750	9850	2	3b	832,05	130,90	1809,60	397,80	6,36

(N-S)	X (E-W)	Area	Unit	Width (m)	Height (m)	Depth (mbsl)	Burial depth (m)	W/H ratio
10750	11000	2	3b	684,13	76,50	1866,24	479,40	8,94
10750	11150	2	3b	425,27	27,20	1895,28	510,00	15,63
10750	12825	2	3b	480,74	52,70	1813,44	387,60	9,12
10750	14450	2	3b	739,60	59,50	1764,70	345,10	12,43
10750	15150	2	3b	1183,36	32,30	1823,44	452,20	36,64
10750	15450	2	3b	1109,40	52,70	1900,66	518,50	21,05
10750	16425	2	3b	295,84	52,70	1886,20	513,40	5,61
10750	17250	2	3b	369,80	32,30	1589,70	209,10	11,45
10750	17550	2	3b	406,78	44,20	1769,48	384,20	9,20
10750	17700	2	3b	351,31	35,70	1782,80	394,40	9,84
10750	17975	2	3b	443,76	47,60	1826,72	435,20	9,32
10750	18775	2	3b	628,66	57,80	1826,86	436,90	10,88
10750	18850	2	3b	702,62	37,40	1863,98	470,90	18,79
10750	18925	2	3b	832,05	39,10	1748,80	360,40	21,28
10750	18975	2	3b	942,99	54,40	1712,68	319,60	17,33
10750	20175	2	3b	129,43	28,90	1866,04	533,80	4,48
10750	22000	2	3b	406,78	30,60	1559,56	278,80	13,29
10875	3300	2	3b	462,25	68,00	1730,84	445,40	6,80
10875	3500	2	3b	1201,85	54,40	1628,98	345,10	22,09
10875	3625	2	3b	314,33	32,30	1803,66	515,10	9,73
10875	3850	2	3b	314,33	34,00	1793,32	503,20	9,25
10875	4050	2	3b	332,82	39,10	1699,12	401,20	8,51
10875	5300	2	3b	628,66	27,20	1751,52	469,20	23,11
10875	5525	2	3b	480,74	61,20	1735,80	448,80	7,86
10875	6825	2	3b	258,86	40,80	1876,38	545,70	6,34
10875	7175	2	3b	906,01	81,60	1824,40	482,80	11,10
10875	7575	2	3b	240,37	32,30	1756,70	399,50	7,44
10875	8100	2	3b	332,82	42,50	1668,04	289,00	7,83
10875	9800	2	3b	998,46	156,40	1836,94	426,70	6,38
10875	9875	2	3b	443,76	61,20	1806,20	394,40	7,25
10875	9900	2	3b	314,33	37,40	1880,28	479,40	8,40
10875	11075	2	3b	369,80	47,60	1837,52	414,80	7,77
10875	11125	2	3b	739,60	81,60	1872,48	479,40	9,06
10875	11800	2	3b	462,25	45,90	1785,34	406,30	10,07
10875	12825	2	3b	499,23	81,60	1849,00	421,60	6,12
10875	14200	2	3b	610,17	52,70	1752,96	316,20	11,58
10875	14325	2	3b	295,84	32,30	1786,24	360,40	9,16
10875	15500	2	3b	1053,93	54,40	1879,12	503,20	19,37
10875	15850	2	3b	979,97	23,80	1838,32	462,40	41,18
10875	16400	2	3b	369,80	40,80	1887,76	513,40	9,06
10875	17650	2	3b	203,39	32,30	1758,86	368,90	6,30
10875	18125	2	3b	369,80	42,50	1832,68	431,80	8,70
10875	18625	2	3b	906,01	54,40	1877,16	479,40	16,65
10875	18750	2	3b	739,60	51,00	1829,56	431,80	14,50
10875	18875	2	3b	813,56	44,20	1756,74	362,10	18,41
10875	18975	2	3b	979,97	45,90	1690,58	297,50	21,35
10875	21925	2	3b	369,80	27,20	1587,76	299,20	13,60
11000	3400	2	3b	554,70	64,60	1744,16	455,60	8,59

(N-S)	X (E-W)	Area	Unit	Width (m)	Height (m)	Depth (mbsl)	Burial depth (m)	W/H ratio
11000	3600	2	3b	1183,36	64,60	1641,74	348,50	18,32
11000	3925	2	3b	332,82	44,20	1802,68	503,20	7,53
11000	4100	2	3b	499,23	66,30	1704,94	396,10	7,53
11000	4825	2	3b	517,72	44,20	1854,08	578,00	11,71
11000	5525	2	3b	499,23	52,70	1708,04	414,80	9,47
11000	6875	2	3b	480,74	42,50	1872,98	542,30	11,31
11000	7175	2	3b	850,54	108,80	1834,04	486,20	7,82
11000	7575	2	3b	388,29	39,10	1759,82	399,50	9,93
11000	8100	2	3b	351,31	54,40	1676,40	295,80	6,46
11000	9825	2	3b	1127,89	166,60	1844,86	447,10	6,77
11000	9900	2	3b	277,35	37,40	1893,02	501,50	7,42
11000	11200	2	3b	499,23	52,70	1873,90	477,70	9,47
11000	11925	2	3b	610,17	51,00	1815,66	433,50	11,96
11000	11950	2	3b	647,15	51,00	1929,70	549,10	12,69
11000	12875	2	3b	462,25	71,40	1865,58	433,50	6,47
11000	14300	2	3b	554,70	61,20	1765,98	341,70	9,06
11000	14425	2	3b	499,23	42,50	1806,36	377,40	11,75
11000	14450	2	3b	480,74	69,70	1862,60	435,20	6,90
11000	15600	2	3b	869,03	39,10	1871,06	481,10	22,23
11000	15800	2	3b	1035,44	51,00	1837,48	452,20	20,30
11000	18625	2	3b	776,58	54,40	1883,54	481,10	14,28
11000	18650	2	3b	776,58	56,10	1827,44	425,00	13,84
11000	18675	2	3b	1146,38	93,50	1599,64	197,20	12,26
11000	18725	2	3b	795,07	40,80	1761,42	362,10	19,49
11000	18950	2	3b	795,07	61,20	1724,86	334,90	12,99
11000	20025	2	3b	332,82	39,10	1881,78	535,50	8,51
11000	21725	2	3b	332,82	42,50	1650,10	355,30	7,83
11125	3525	2	3b	573,19	88,40	1753,38	453,90	6,48
11125	3875	2	3b	351,31	45,90	1810,76	506,60	7,65
11125	4500	2	3b	517,72	52,70	1770,42	433,50	9,82
11125	4600	2	3b	332,82	42,50	1746,76	411,40	7,83
11125	4625	2	3b	406,78	49,30	1712,46	392,70	8,25
11125	5475	2	3b	332,82	35,70	1679,00	384,20	9,32
11125	6900	2	3b	425,27	30,60	1871,28	540,60	13,90
11125	7000	2	3b	499,23	42,50	1728,06	392,70	11,75
11125	7175	2	3b	832,05	98,60	1827,38	481,10	8,44
11125	8275	2	3b	295,84	40,80	1654,16	272,00	7,25
11125	10000	2	3b	1053,93	142,80	1817,80	421,60	7,38
11125	11275	2	3b	295,84	37,40	1883,10	494,70	7,91
11125	11875	2	3b	573,19	35,70	1920,50	532,10	16,06
11125	12900	2	3b	406,78	85,00	1890,58	396,10	4,79
11125	14325	2	3b	480,74	47,60	1766,00	323,00	10,10
11125	14575	2	3b	573,19	85,00	1870,96	442,00	6,74
11125	15650	2	3b	869,03	40,80	1862,58	453,90	21,30
11125	15775	2	3b	942,99	40,80	1826,88	418,20	23,11
11125	16525	2	3b	277,35	34,00	1944,72	561,00	8,16
11125	17800	2	3b	351,31	35,70	1779,84	377,40	9,84
11125	18375	2	3b	462,25	44,20	1623,72	224,40	10,46

(N-S)	X (E-W)	Area	Unit	Width (m)	Height (m)	Depth (mbsl)	Burial depth (m)	W/H ratio
11125	18400	2	3b	1035,44	69,70	1895,86	498,10	14,86
11125	18475	2	3b	684,13	64,60	1837,92	438,60	10,59
11125	18700	2	3b	758,09	27,20	1752,64	350,20	27,87
11125	18750	2	3b	573,19	37,40	1719,76	329,80	15,33
11250	2600	2	3b	462,25	42,50	1457,24	78,20	10,88
11250	3525	2	3b	517,72	69,70	1738,94	430,10	7,43
11250	3750	2	3b	1146,38	30,60	1623,62	317,90	37,46
11250	4075	2	3b	314,33	49,30	1818,56	506,60	6,38
11250	4525	2	3b	462,25	40,80	1776,94	436,90	11,33
11250	4625	2	3b	332,82	56,10	1746,06	402,90	5,93
11250	5350	2	3b	314,33	42,50	1861,04	567,80	7,40
11250	6900	2	3b	369,80	49,30	1886,44	554,20	7,50
11250	6975	2	3b	776,58	44,20	1662,04	329,80	17,57
11250	7000	2	3b	462,25	34,00	1733,58	402,90	13,60
11250	7200	2	3b	776,58	79,90	1821,30	464,10	9,72
11250	8175	2	3b	332,82	37,40	1649,64	255,00	8,90
11250	9900	2	3b	1072,42	124,10	1813,28	404,60	8,64
11250	11825	2	3b	998,46	30,60	1897,98	504,90	32,63
11250	12900	2	3b	499,23	83,30	1904,34	392,70	5,99
11250	14300	2	3b	425,27	42,50	1782,02	328,10	10,01
11250	14575	2	3b	536,21	62,90	1873,94	440,30	8,52
11250	15750	2	3b	869,03	49,30	1831,16	394,40	17,63
11250	16150	2	3b	388,29	40,80	1879,42	487,90	9,52
11250	16450	2	3b	369,80	49,30	1961,02	569,50	7,50
11250	17775	2	3b	314,33	34,00	1783,52	384,20	9,25
11250	18325	2	3b	1109,40	68,00	1896,86	491,30	16,31
11250	18400	2	3b	684,13	64,60	1837,36	431,80	10,59
11250	18425	2	3b	351,31	51,00	1624,72	217,60	6,89
11250	18900	2	3b	813,56	49,30	1717,06	334,90	16,50
11250	19975	2	3b	147,92	54,40	1922,02	569,50	2,72
11250	21600	2	3b	369,80	37,40	1623,60	336,60	9,89
11375	3650	2	3b	406,78	71,40	1758,64	442,00	5,70
11375	3800	2	3b	1294,30	51,00	1621,50	311,10	25,38
11375	3825	2	3b	665,64	49,30	1689,78	382,50	13,50
11375	3950	2	3b	832,05	35,70	1570,50	260,10	23,31
11375	4225	2	3b	369,80	37,40	1830,18	515,10	9,89
11375	4500	2	3b	240,37	34,00	1813,78	467,50	7,07
11375	4600	2	3b	591,68	49,30	1775,12	414,80	12,00
11375	4625	2	3b	480,74	37,40	1751,88	397,80	12,85
11375	4675	2	3b	332,82	47,60	1724,40	367,20	6,99
11375	5275	2	3b	314,33	37,40	1857,64	564,40	8,40
11375	6950	2	3b	443,76	40,80	1753,28	414,80	10,88
11375	6975	2	3b	499,23	47,60	1889,56	554,20	10,49
11375	7075	2	3b	573,19	51,00	1676,92	340,00	11,24
11375	7225	2	3b	369,80	74,80	1826,96	476,00	4,94
11375	7425	2	3b	332,82	47,60	1779,10	406,30	6,99
11375	8225	2	3b	314,33	34,00	1624,86	219,30	9,25
11375	9925	2	3b	979,97	107,10	1789,34	379,10	9,15



(N-S)	X (E-W)	Area	Unit	Width (m)	Height (m)	Depth (mbsl)	Burial depth (m)	W/H ratio
11375	10550	2	3b	240,37	34,00	1837,08	428,40	7,07
11375	10775	2	3b	573,19	47,60	1884,68	476,00	12,04
11375	11450	2	3b	388,29	32,30	1862,14	467,50	12,02
11375	11525	2	3b	425,27	45,90	1792,58	399,50	9,27
11375	11975	2	3b	739,60	42,50	1892,46	494,70	17,40
11375	12950	2	3b	499,23	59,50	1912,70	399,50	8,39
11375	13050	2	3b	480,74	74,80	1880,96	374,00	6,43
11375	14300	2	3b	536,21	51,00	1791,24	326,40	10,51
11375	14300	2	3b	628,66	49,30	1713,18	249,90	12,75
11375	14650	2	3b	591,68	61,20	1873,66	436,90	9,67
11375	15675	2	3b	850,54	47,60	1827,90	392,70	17,87
11375	16150	2	3b	351,31	56,10	1907,06	501,50	6,26
11375	17700	2	3b	499,23	40,80	1784,10	372,30	12,24
11375	18150	2	3b	906,01	66,30	1901,40	489,60	13,67
11375	18325	2	3b	684,13	64,60	1840,48	431,80	10,59
11375	18450	2	3b	277,35	32,30	1629,96	224,40	8,59
11375	18725	2	3b	998,46	73,10	1585,04	190,40	13,66
11375	18750	2	3b	721,11	30,60	1764,96	367,20	23,57
11375	18775	2	3b	684,13	54,40	1723,44	336,60	12,58
11375	21600	2	3b	406,78	56,10	1636,36	340,00	7,25
11500	3650	2	3b	554,70	66,30	1761,90	443,70	8,37
11500	3775	2	3b	869,03	62,90	1689,08	374,00	13,82
11500	4225	2	3b	443,76	61,20	1847,76	520,20	7,25
11500	4500	2	3b	647,15	59,50	1787,42	450,50	10,88
11500	4775	2	3b	314,33	49,30	1737,44	374,00	6,38
11500	5075	2	3b	240,37	34,00	1695,16	391,00	7,07
11500	6750	2	3b	721,11	51,00	1698,30	372,30	14,14
11500	7000	2	3b	388,29	42,50	1882,06	538,90	9,14
11500	7275	2	3b	1257,32	105,40	1801,46	450,50	11,93
11500	10050	2	3b	869,03	81,60	1769,80	350,20	10,65
11500	10675	2	3b	702,62	68,00	1894,46	481,10	10,33
11500	11875	2	3b	850,54	54,40	1883,82	484,50	15,63
11500	12975	2	3b	647,15	83,30	1911,00	397,80	7,77
11500	14325	2	3b	758,09	45,90	1718,56	258,40	16,52
11500	14600	2	3b	665,64	56,10	1873,52	435,20	11,87
11500	16200	2	3b	443,76	51,00	1917,70	498,10	8,70
11500	18075	2	3b	942,99	52,70	1899,28	482,80	17,89
11500	18275	2	3b	924,50	52,70	1828,58	419,90	17,54
11500	18625	2	3b	924,50	35,70	1770,36	357,00	25,90
11500	18875	2	3b	776,58	64,60	1733,64	346,80	12,02
11500	20000	2	3b	425,27	66,30	1781,20	431,80	6,41
11625	3675	2	3b	536,21	59,50	1752,84	428,40	9,01
11625	4225	2	3b	462,25	52,70	1869,44	537,20	8,77
11625	4575	2	3b	665,64	73,10	1783,32	438,60	9,11
11625	4775	2	3b	406,78	61,20	1753,74	382,50	6,65
11625	4950	2	3b	443,76	34,00	1874,28	520,20	13,05
11625	7175	2	3b	221,88	15,30	1858,26	515,10	14,50
11625	7225	2	3b	1053,93	83,30	1798,76	455,60	12,65

(N-S)	X (E-W)	Area	Unit	Width (m)	Height (m)	Depth (mbsl)	Burial depth (m)	W/H ratio
11625	10050	2	3b	998,46	44,20	1757,20	329,80	22,59
11625	10450	2	3b	591,68	64,60	1831,00	411,40	9,16
11625	10650	2	3b	684,13	86,70	1920,38	511,70	7,89
11625	11875	2	3b	795,07	54,40	1875,32	476,00	14,62
11625	13000	2	3b	758,09	103,70	1904,48	394,40	7,31
11625	14625	2	3b	702,62	61,20	1868,14	426,70	11,48
11625	15375	2	3b	721,11	44,20	1804,42	334,90	16,31
11625	16150	2	3b	610,17	68,00	1922,56	462,40	8,97
11625	17525	2	3b	388,29	42,50	1778,72	363,80	9,14
11625	18025	2	3b	887,52	71,40	1907,36	486,20	12,43
11625	18050	2	3b	554,70	49,30	1831,28	414,80	11,25
11625	18600	2	3b	1072,42	52,70	1734,78	341,70	20,35
11625	18675	2	3b	887,52	30,60	1774,46	368,90	29,00
11625	19975	2	3b	369,80	39,10	1781,92	421,60	9,46
11750	3700	2	3b	536,21	62,90	1756,82	419,90	8,52
11750	3750	2	3b	369,80	22,10	1782,60	448,80	16,73
11750	4275	2	3b	406,78	56,10	1884,60	550,80	7,25
11750	4475	2	3b	314,33	37,40	1838,56	503,20	8,40
11750	4575	2	3b	517,72	45,90	1787,84	455,60	11,28
11750	4900	2	3b	388,29	51,00	1746,80	374,00	7,61
11750	5150	2	3b	425,27	42,50	1873,26	545,70	10,01
11750	7150	2	3b	203,39	52,70	1886,04	530,40	3,86
11750	7200	2	3b	1164,87	96,90	1799,04	459,00	12,02
11750	10400	2	3b	647,15	64,60	1826,18	409,70	10,02
11750	10450	2	3b	351,31	40,80	1872,36	459,00	8,61
11750	10600	2	3b	795,07	86,70	1915,14	504,90	9,17
11750	10925	2	3b	314,33	34,00	1857,76	452,20	9,25
11750	11775	2	3b	480,74	28,90	1838,06	440,30	16,63
11750	13000	2	3b	869,03	127,50	1905,76	391,00	6,82
11750	14325	2	3b	443,76	54,40	1818,72	357,00	8,16
11750	14600	2	3b	702,62	66,30	1863,48	408,00	10,60
11750	15325	2	3b	499,23	44,20	1795,34	338,30	11,29
11750	16175	2	3b	665,64	71,40	1927,10	460,70	9,32
11750	17475	2	3b	351,31	56,10	1807,62	392,70	6,26
11750	18000	2	3b	942,99	69,70	1893,48	469,20	13,53
11750	18200	2	3b	1035,44	61,20	1842,48	418,20	16,92
11750	18575	2	3b	869,03	34,00	1775,60	363,80	25,56
11875	4050	2	3b	1183,36	79,90	1765,60	431,80	14,81
11875	4225	2	3b	702,62	62,90	1871,00	537,20	11,17
11875	5175	2	3b	536,21	39,10	1861,40	496,40	13,71
11875	6950	2	3b	462,25	45,90	1750,02	413,10	10,07
11875	7125	2	3b	240,37	39,10	1884,34	528,70	6,15
11875	7275	2	3b	1238,83	105,40	1796,94	433,50	11,75
11875	10200	2	3b	832,05	51,00	1720,78	304,30	16,31
11875	10375	2	3b	628,66	78,20	1841,20	421,60	8,04
11875	10550	2	3b	832,05	102,00	1917,12	510,00	8,16
11875	11625	2	3b	591,68	45,90	1795,84	401,20	12,89
11875	13125	2	3b	979,97	130,90	1906,62	382,50	7,49

(N-S)	X (E-W)	Area	Unit	Width (m)	Height (m)	Depth (mbsl)	Burial depth (m)	W/H ratio
11875	14700	2	3b	721,11	52,70	1852,58	389,30	13,68
11875	16100	2	3b	684,13	68,00	1920,44	455,60	10,06
11875	17475	2	3b	406,78	62,90	1803,80	384,20	6,47
11875	18050	2	3b	887,52	66,30	1894,76	465,80	13,39
11875	18275	2	3b	887,52	44,20	1821,46	314,50	20,08
11875	18500	2	3b	1201,85	51,00	1741,04	323,00	23,57
11875	18700	2	3b	1164,87	40,80	1770,80	343,40	28,55
12000	3775	2	3b	351,31	39,10	1773,56	414,80	8,98
12000	4025	2	3b	1331,28	61,20	1741,94	409,70	21,75
12000	4150	2	3b	425,27	37,40	1908,40	574,60	11,37
12000	4425	2	3b	388,29	40,80	1867,60	533,80	9,52
12000	4550	2	3b	332,82	30,60	1834,60	493,00	10,88
12000	6425	2	3b	1812,02	47,60	1571,92	258,40	38,07
12000	6825	2	3b	536,21	56,10	1691,08	360,40	9,56
12000	6925	2	3b	554,70	47,60	1753,56	418,20	11,65
12000	7175	2	3b	1275,81	76,50	1790,56	431,80	16,68
12000	10000	2	3b	369,80	37,40	1740,34	314,50	9,89
12000	10400	2	3b	684,13	56,10	1831,14	413,10	12,19
12000	10675	2	3b	869,03	74,80	1871,80	452,20	11,62
12000	11725	2	3b	869,03	54,40	1805,20	401,20	15,97
12000	13175	2	3b	1016,95	124,10	1898,70	362,10	8,19
12000	14275	2	3b	240,37	62,90	1866,76	391,00	3,82
12000	14650	2	3b	887,52	49,30	1833,60	367,20	18,00
12000	16125	2	3b	684,13	51,00	1901,46	433,50	13,41
12000	17775	2	3b	536,21	54,40	1811,32	380,80	9,86
12000	18000	2	3b	850,54	68,00	1893,06	464,10	12,51
12000	18475	2	3b	1608,63	98,60	1776,90	341,70	16,31
12125	3400	2	3b	406,78	51,00	1476,94	90,10	7,98
12125	3700	2	3b	536,21	40,80	1570,14	198,90	13,14
12125	3825	2	3b	554,70	45,90	1641,40	268,60	12,08
12125	4075	2	3b	406,78	61,20	1884,76	533,80	6,65
12125	4450	2	3b	351,31	34,00	1860,38	521,90	10,33
12125	5200	2	3b	480,74	59,50	1800,78	423,30	8,08
12125	6775	2	3b	610,17	34,00	1742,66	399,50	17,95
12125	6800	2	3b	554,70	51,00	1702,98	372,30	10,88
12125	7050	2	3b	1460,71	66,30	1773,12	428,40	22,03
12125	10075	2	3b	480,74	32,30	1741,90	314,50	14,88
12125	10575	2	3b	813,56	66,30	1850,98	426,70	12,27
12125	11775	2	3b	739,60	39,10	1845,58	436,90	18,92
12125	13300	2	3b	961,48	125,80	1914,56	384,20	7,64
12125	14700	2	3b	887,52	35,70	1826,52	357,00	24,86
12125	16125	2	3b	721,11	44,20	1888,70	430,10	16,31
12125	17875	2	3b	758,09	59,50	1879,04	445,40	12,74
12125	18375	2	3b	536,21	32,30	1816,00	380,80	16,60
12125	18525	2	3b	1331,28	83,30	1775,06	338,30	15,98
12250	3950	2	3b	536,21	51,00	1728,52	360,40	10,51
12250	5000	2	3b	758,09	45,90	1881,78	535,50	16,52
12250	5150	2	3b	258,86	34,00	1853,74	498,10	7,61

(N-S)	X (E-W)	Area	Unit	Width (m)	Height (m)	Depth (mbsl)	Burial depth (m)	W/H ratio
12250	5275	2	3b	628,66	76,50	1803,60	438,60	8,22
12250	5450	2	3b	406,78	37,40	1726,04	425,00	10,88
12250	6625	2	3b	1442,22	39,10	1581,84	265,20	36,89
12250	6675	2	3b	554,70	39,10	1730,18	399,50	14,19
12250	6725	2	3b	517,72	47,60	1699,86	372,30	10,88
12250	7150	2	3b	1460,71	62,90	1763,20	421,60	23,22
12250	10225	2	3b	647,15	56,10	1762,72	340,00	11,54
12250	10550	2	3b	776,58	74,80	1838,94	413,10	10,38
12250	11750	2	3b	721,11	45,90	1876,32	469,20	15,71
12250	12875	2	3b	480,74	51,00	1830,00	418,20	9,43
12250	13375	2	3b	758,09	86,70	1902,96	357,00	8,74
12250	14550	2	3b	813,56	34,00	1826,38	355,30	23,93
12250	16225	2	3b	924,50	69,70	1890,26	430,10	13,26
12250	17575	2	3b	406,78	39,10	1818,68	394,40	10,40
12250	17900	2	3b	1035,44	66,30	1867,14	433,50	15,62
12250	18375	2	3b	850,54	40,80	1815,86	379,10	20,85
12250	18400	2	3b	1719,57	95,20	1770,10	334,90	18,06
12375	4325	2	3b	369,80	35,70	1901,60	567,80	10,36
12375	4575	2	3b	240,37	22,10	1830,06	494,70	10,88
12375	4850	2	3b	369,80	34,00	1891,56	540,60	10,88
12375	4925	2	3b	369,80	17,00	1836,88	482,80	21,75
12375	5275	2	3b	536,21	20,40	1871,16	520,20	26,28
12375	5275	2	3b	702,62	79,90	1805,42	460,70	8,79
12375	5525	2	3b	499,23	45,90	1719,38	419,90	10,88
12375	6700	2	3b	388,29	34,00	1687,96	360,40	11,42
12375	7100	2	3b	1405,24	81,60	1745,20	411,40	17,22
12375	7600	2	3b	610,17	30,60	1668,58	314,50	19,94
12375	10575	2	3b	462,25	30,60	1808,34	382,50	15,11
12375	11675	2	3b	647,15	45,90	1882,84	472,60	14,10
12375	12600	2	3b	406,78	56,10	1873,50	453,90	7,25
12375	13650	2	3b	702,62	93,50	1910,18	368,90	7,51
12375	14125	2	3b	517,72	34,00	1845,86	307,70	15,23
12375	15125	2	3b	480,74	30,60	1837,54	396,10	15,71
12375	16125	2	3b	961,48	73,10	1891,68	428,40	13,15
12375	17475	2	3b	425,27	42,50	1803,10	375,70	10,01
12375	17900	2	3b	998,46	52,70	1844,90	409,70	18,95
12375	18350	2	3b	499,23	45,90	1809,34	375,70	10,88
12375	18625	2	3b	887,52	27,20	1761,88	329,80	32,63
12375	19525	2	3b	295,84	45,90	1749,92	374,00	6,45
12375	19625	2	3b	295,84	25,50	1800,50	419,90	11,60
12500	4000	2	3b	554,70	54,40	1760,68	391,00	10,20
12500	4250	2	3b	369,80	45,90	1869,04	513,40	8,06
12500	5300	2	3b	425,27	34,00	1879,46	583,10	12,51
12500	10550	2	3b	425,27	25,50	1903,82	481,10	16,68
12500	11575	2	3b	924,50	105,40	1892,76	479,40	8,77
12500	11700	2	3b	573,19	34,00	1928,60	516,80	16,86
12500	13725	2	3b	942,99	102,00	1917,98	368,90	9,25
12500	15050	2	3b	665,64	42,50	1859,64	418,20	15,66

(N-S)	X (E-W)	Area	Unit	Width (m)	Height (m)	Depth (mbsl)	Burial depth (m)	W/H ratio
12500	17500	2	3b	462,25	39,10	1789,36	360,40	11,82
12500	17925	2	3b	554,70	45,90	1832,72	394,40	12,08
12500	18375	2	3b	536,21	32,30	1800,56	363,80	16,60
12500	18475	2	3b	1146,38	28,90	1766,84	333,20	39,67
12500	19575	2	3b	332,82	69,70	1789,04	394,40	4,78
12625	3975	3	3b	499,23	40,80	1757,42	389,30	12,24
12625	4050	3	3b	406,78	49,30	1876,56	510,00	8,25
12625	5200	3	3b	628,66	59,50	1775,52	438,60	10,57
12625	6700	3	3b	480,74	40,80	1732,30	406,30	11,78
12625	7175	3	3b	536,21	34,00	1701,72	357,00	15,77
12625	11725	3	3b	906,01	98,60	1909,20	489,60	9,19
12625	13800	3	3b	628,66	95,20	1918,80	397,80	6,60
12625	15025	3	3b	610,17	57,80	1883,58	443,70	10,56
12625	16350	3	3b	591,68	34,00	1903,72	442,00	17,40
12625	18275	3	3b	684,13	32,30	1736,38	304,30	21,18
12625	18325	3	3b	1053,93	23,80	1807,22	368,90	44,28
12750	4100	3	3b	295,84	32,30	1793,70	413,10	9,16
12750	4175	3	3b	425,27	34,00	1871,46	504,90	12,51
12750	4650	3	3b	665,64	42,50	1866,18	535,50	15,66
12750	5350	3	3b	573,19	44,20	1754,82	433,50	12,97
12750	6125	3	3b	665,64	25,50	1942,44	40,80	26,10
12750	6675	3	3b	591,68	49,30	1723,94	399,50	12,00
12750	11575	3	3b	832,05	90,10	1897,16	476,00	9,23
12750	12275	3	3b	869,03	98,60	1939,80	520,20	8,81
12750	13875	3	3b	739,60	71,40	1904,72	435,20	10,36
12750	15050	3	3b	591,68	52,70	1889,24	455,60	11,23
12750	16175	3	3b	647,15	34,00	1907,40	448,80	19,03
12750	16500	3	3b	406,78	39,10	1861,22	399,50	10,40
12750	18350	3	3b	813,56	37,40	1736,24	302,60	21,75
12750	18375	3	3b	702,62	17,00	1787,24	353,60	41,33
12750	18475	3	3b	628,66	30,60	1765,14	331,50	20,54
12750	19550	3	3b	332,82	34,00	1850,68	442,00	9,79
12875	4175	3	3b	406,78	37,40	1865,24	486,20	10,88
12875	5150	3	3b	166,41	32,30	1885,34	521,90	5,15
12875	5275	3	3b	425,27	25,50	1749,34	385,90	16,68
12875	5275	3	3b	573,19	37,40	1713,36	346,80	15,33
12875	6075	3	3b	517,72	45,90	2000,04	683,40	11,28
12875	6575	3	3b	665,64	57,80	1716,72	387,60	11,52
12875	6750	3	3b	1849,00	27,20	1577,60	251,60	67,98
12875	7525	3	3b	499,23	28,90	1668,30	311,10	17,27
12875	11500	3	3b	721,11	62,90	1885,12	462,40	11,46
12875	11850	3	3b	591,68	49,30	1917,84	499,80	12,00
12875	12550	3	3b	536,21	61,20	1943,50	508,30	8,76
12875	13825	3	3b	1590,14	71,40	1911,24	438,60	22,27
12875	15125	3	3b	776,58	47,60	1878,06	433,50	16,31
12875	16500	3	3b	628,66	54,40	1878,66	402,90	11,56
12875	18400	3	3b	721,11	34,00	1790,22	351,90	21,21
12875	18850	3	3b	295,84	23,80	1859,50	416,50	12,43

(N-S)	X (E-W)	Area	Unit	Width (m)	Height (m)	Depth (mbsl)	Burial depth (m)	W/H ratio
12875	19450	3	3b	240,37	30,60	1864,58	440,30	7,86
12875	19575	3	3b	443,76	40,80	1773,78	341,70	10,88
13000	4175	3	3b	332,82	52,70	1867,10	470,90	6,32
13000	5300	3	3b	406,78	27,20	1760,06	440,30	14,96
13000	6225	3	3b	295,84	23,80	1974,26	654,50	12,43
13000	6425	3	3b	832,05	73,10	1737,26	409,70	11,38
13000	7525	3	3b	499,23	51,00	1697,06	338,30	9,79
13000	11675	3	3b	906,01	62,90	1880,16	459,00	14,40
13000	12100	3	3b	1072,42	93,50	1917,42	494,70	11,47
13000	12800	3	3b	351,31	59,50	1935,16	482,80	5,90
13000	14025	3	3b	979,97	103,70	1922,58	443,70	9,45
13000	15200	3	3b	665,64	62,90	1881,16	452,20	10,58
13000	16600	3	3b	499,23	57,80	1897,08	418,20	8,64
13000	18875	3	3b	147,92	37,40	1898,46	453,90	3,96
13000	19525	3	3b	277,35	42,50	1866,42	443,70	6,53
13125	4150	3	3b	388,29	40,80	1852,66	447,10	9,52
13125	4600	3	3b	351,31	35,70	1765,54	355,30	9,84
13125	5225	3	3b	147,92	18,70	1892,42	532,10	7,91
13125	5225	3	3b	480,74	32,30	1692,54	321,30	14,88
13125	5325	3	3b	406,78	35,70	1763,92	411,40	11,39
13125	6300	3	3b	443,76	39,10	1989,42	668,10	11,35
13125	6375	3	3b	295,84	28,90	1900,18	569,50	10,24
13125	6525	3	3b	869,03	37,40	1681,30	355,30	23,24
13125	6550	3	3b	776,58	112,20	1789,96	462,40	6,92
13125	7375	3	3b	73,96	22,10	1894,26	535,50	3,35
13125	7550	3	3b	554,70	78,20	1727,38	365,50	7,09
13125	11700	3	3b	850,54	79,90	1875,92	445,40	10,65
13125	12275	3	3b	1072,42	76,50	1917,14	491,30	14,02
13125	14000	3	3b	850,54	102,00	1930,80	448,80	8,34
13125	15250	3	3b	554,70	39,10	1861,60	309,40	14,19
13125	16575	3	3b	536,21	71,40	1904,66	358,70	7,51
13125	18400	3	3b	499,23	35,70	1755,94	314,50	13,98
13125	18875	3	3b	499,23	30,60	1782,30	331,50	16,31
13125	19550	3	3b	369,80	52,70	1811,18	379,10	7,02
13250	4200	3	3b	443,76	59,50	1852,24	442,00	7,46
13250	4250	3	3b	684,13	61,20	1755,06	341,70	11,18
13250	5400	3	3b	332,82	39,10	1765,16	445,40	8,51
13250	6300	3	3b	443,76	35,70	1978,52	649,40	12,43
13250	6375	3	3b	684,13	42,50	1721,68	391,00	16,10
13250	6525	3	3b	517,72	71,40	1803,00	469,20	7,25
13250	6525	3	3b	832,05	51,00	1682,86	355,30	16,31
13250	7575	3	3b	628,66	73,10	1706,56	340,00	8,60
13250	11800	3	3b	832,05	64,60	1864,30	436,90	12,88
13250	12200	3	3b	942,99	64,60	1904,68	472,60	14,60
13250	13975	3	3b	869,03	93,50	1921,68	357,00	9,29
13250	15300	3	3b	499,23	51,00	1870,94	328,10	9,79
13250	16625	3	3b	702,62	79,90	1916,34	443,70	8,79
13250	17925	3	3b	795,07	40,80	1821,96	377,40	19,49

(N-S)	X (E-W)	Area	Unit	Width (m)	Height (m)	Depth (mbsl)	Burial depth (m)	W/H ratio
13250	19175	3	3b	665,64	39,10	1817,56	380,80	17,02
13375	4125	3	3b	388,29	40,80	1854,50	450,50	9,52
13375	4150	3	3b	443,76	42,50	1813,28	404,60	10,44
13375	4250	3	3b	665,64	47,60	1757,74	355,30	13,98
13375	5450	3	3b	462,25	61,20	1770,84	438,60	7,55
13375	6475	3	3b	499,23	22,10	1973,42	644,30	22,59
13375	6550	3	3b	517,72	66,30	1765,32	428,40	7,81
13375	7525	3	3b	499,23	56,10	1684,88	323,00	8,90
13375	12250	3	3b	610,17	81,60	1882,58	450,50	7,48
13375	14075	3	3b	739,60	95,20	1925,80	350,20	7,77
13375	15525	3	3b	499,23	45,90	1884,16	431,80	10,88
13375	16650	3	3b	536,21	69,70	1923,14	450,50	7,69
13375	19200	3	3b	499,23	66,30	1852,70	409,70	7,53
13500	4225	3	3b	684,13	64,60	1835,94	433,50	10,59
13500	5050	3	3b	369,80	54,40	1797,66	423,30	6,80
13500	5375	3	3b	166,41	27,20	1899,60	581,40	6,12
13500	5525	3	3b	591,68	85,00	1804,40	486,20	6,96
13500	6525	3	3b	517,72	40,80	1736,28	397,80	12,69
13500	6525	3	3b	443,76	45,90	1676,78	338,30	9,67
13500	7500	3	3b	573,19	47,60	1679,36	312,80	12,04
13500	12625	3	3b	850,54	52,70	1893,56	394,40	16,14
13500	14100	3	3b	721,11	79,90	1910,10	311,10	9,03
13500	15650	3	3b	684,13	54,40	1898,34	433,50	12,58
13500	16750	3	3b	517,72	93,50	1916,92	431,80	5,54
13500	19275	3	3b	628,66	59,50	1855,96	411,40	10,57
13625	4175	3	3b	536,21	61,20	1836,80	425,00	8,76
13625	5450	3	3b	591,68	27,20	1738,96	411,40	21,75
13625	5550	3	3b	462,25	73,10	1825,66	498,10	6,32
13625	6150	3	3b	647,15	30,60	1620,54	280,50	21,15
13625	6500	3	3b	443,76	51,00	1686,42	341,70	8,70
13625	6675	3	3b	462,25	39,10	1988,18	634,10	11,82
13625	7575	3	3b	573,19	49,30	1707,42	331,50	11,63
13625	12675	3	3b	961,48	62,90	1923,02	430,10	15,29
13625	14125	3	3b	647,15	90,10	1928,24	323,00	7,18
13625	15200	3	3b	166,41	37,40	1590,60	30,60	4,45
13625	15675	3	3b	628,66	64,60	1910,52	448,80	9,73
13625	16750	3	3b	499,23	69,70	1930,38	443,70	7,16
13625	19250	3	3b	554,70	62,90	1853,14	396,10	8,82
13750	4175	3	3b	332,82	30,60	1834,82	419,90	10,88
13750	4275	3	3b	536,21	40,80	1782,68	374,00	13,14
13750	5425	3	3b	443,76	42,50	1896,68	527,00	10,44
13750	5600	3	3b	517,72	88,40	1842,52	513,40	5,86
13750	6200	3	3b	425,27	37,40	1616,72	272,00	11,37
13750	6775	3	3b	351,31	25,50	1694,94	331,50	13,78
13750	6825	3	3b	443,76	40,80	1987,76	629,00	10,88
13750	7550	3	3b	628,66	73,10	1758,14	379,10	8,60
13750	12900	3	3b	961,48	100,30	1963,66	487,90	9,59
13750	14125	3	3b	573,19	64,60	1901,16	316,20	8,87

(N-S)	X (E-W)	Area	Unit	Width (m)	Height (m)	Depth (mbsl)	Burial depth (m)	W/H ratio
13750	16850	3	3b	425,27	61,20	1918,20	428,40	6,95
13750	19300	3	3b	517,72	64,60	1874,54	409,70	8,01
13875	4075	3	3b	369,80	39,10	1850,98	426,70	9,46
13875	4250	3	3b	554,70	56,10	1769,52	346,80	9,89
13875	5300	3	3b	591,68	39,10	1900,70	481,10	15,13
13875	5325	3	3b	388,29	23,80	1673,14	294,10	16,31
13875	5525	3	3b	591,68	42,50	1768,58	430,10	13,92
13875	5700	3	3b	536,21	81,60	1850,04	510,00	6,57
13875	6775	3	3b	628,66	44,20	1713,22	345,10	14,22
13875	6825	3	3b	517,72	56,10	2005,20	632,40	9,23
13875	7475	3	3b	795,07	134,30	1849,52	465,80	5,92
13875	12875	3	3b	1460,71	113,90	1966,92	489,60	12,82
13875	14075	3	3b	425,27	57,80	1891,40	292,40	7,36
13875	15800	3	3b	536,21	40,80	1898,62	436,90	13,14
13875	16850	3	3b	517,72	81,60	1937,46	453,90	6,34
13875	19350	3	3b	591,68	81,60	1898,48	435,20	7,25
14000	4025	3	3b	314,33	44,20	1832,84	414,80	7,11
14000	4325	3	3b	536,21	39,10	1800,70	365,50	13,71
14000	5325	3	3b	610,17	49,30	1898,86	477,70	12,38
14000	5425	3	3b	369,80	27,20	1693,10	328,10	13,60
14000	5600	3	3b	480,74	28,90	1759,66	416,50	16,63
14000	5750	3	3b	499,23	86,70	1856,56	513,40	5,76
14000	6500	3	3b	702,62	37,40	1708,12	340,00	18,79
14000	6925	3	3b	406,78	35,70	1992,74	613,70	11,39
14000	7400	3	3b	1146,38	129,20	1866,24	479,40	8,87
14000	12875	3	3b	1220,34	103,70	1966,22	481,10	11,77
14000	14225	3	3b	573,19	45,90	1873,10	297,50	12,49
14000	16850	3	3b	813,56	73,10	1928,54	440,30	11,13
14000	19275	3	3b	628,66	79,90	1891,40	425,00	7,87
14125	3975	3	3b	332,82	44,20	1830,16	401,20	7,53
14125	4325	3	3b	499,23	34,00	1798,58	358,70	14,68
14125	5300	3	3b	684,13	44,20	1895,74	477,70	15,48
14125	5375	3	3b	369,80	22,10	1704,14	348,50	16,73
14125	5675	3	3b	406,78	47,60	1791,54	443,70	8,55
14125	5725	3	3b	332,82	57,80	1863,08	516,80	5,76
14125	6525	3	3b	573,19	39,10	1701,60	336,60	14,66
14125	6925	3	3b	517,72	37,40	1992,74	613,70	13,84
14125	12850	3	3b	1294,30	110,50	1961,54	481,10	11,71
14125	14250	3	3b	443,76	32,30	1876,64	302,60	13,74
14125	16925	3	3b	850,54	91,80	1944,54	464,10	9,27
14125	19375	3	3b	665,64	83,30	1889,42	419,90	7,99
14250	3925	3	3b	277,35	37,40	1873,22	450,50	7,42
14250	4775	3	3b	795,07	57,80	1818,56	374,00	13,76
14250	5425	3	3b	554,70	44,20	1914,42	515,10	12,55
14250	5450	3	3b	554,70	56,10	1725,84	346,80	9,89
14250	5675	3	3b	369,80	61,20	1802,32	442,00	6,04
14250	5775	3	3b	295,84	54,40	1859,98	498,10	5,44
14250	6525	3	3b	480,74	45,90	1699,48	329,80	10,47



(N-S)	X (E-W)	Area	Unit	Width (m)	Height (m)	Depth (mbsl)	Burial depth (m)	W/H ratio
14250	6900	3	3b	443,76	35,70	1986,94	600,10	12,43
14250	7400	3	3b	1220,34	139,40	1856,74	477,70	8,75
14250	12875	3	3b	1294,30	113,90	1964,66	481,10	11,36
14250	14275	3	3b	610,17	64,60	1888,26	311,10	9,45
14250	14775	3	3b	517,72	35,70	1994,08	421,60	14,50
14250	16900	3	3b	665,64	84,15	1946,38	467,50	7,91
14250	19325	3	3b	591,68	74,80	1904,72	435,20	7,91
14375	4000	3	3b	443,76	13,60	1824,34	406,30	32,63
14375	4950	3	3b	684,13	62,90	1846,60	411,40	10,88
14375	5525	3	3b	628,66	45,90	1918,84	493,00	13,70
14375	5650	3	3b	443,76	40,80	1732,54	314,50	10,88
14375	5750	3	3b	314,33	61,20	1801,94	399,50	5,14
14375	5800	3	3b	295,84	44,20	1855,50	443,70	6,69
14375	6600	3	3b	443,76	37,40	1667,46	300,90	11,87
14375	6675	3	3b	591,68	27,20	1595,64	224,40	21,75
14375	6950	3	3b	554,70	39,10	1989,48	612,00	14,19
14375	12800	3	3b	1257,32	110,50	1962,96	479,40	11,38
14375	14375	3	3b	628,66	86,70	1907,06	368,90	7,25
14375	16950	3	3b	628,66	81,60	1943,40	469,20	7,70
14375	19400	3	3b	665,64	91,80	1897,50	423,30	7,25
14500	3900	3	3b	369,80	37,40	1822,64	404,60	9,89
14500	4950	3	3b	647,15	74,80	1863,60	428,40	8,65
14500	5650	3	3b	517,72	71,40	1765,02	311,10	7,25
14500	5675	3	3b	813,56	32,30	1912,20	469,20	25,19
14500	5875	3	3b	351,31	62,90	1859,76	438,60	5,59
14500	6825	3	3b	628,66	32,30	1605,56	231,20	19,46
14500	6850	3	3b	554,70	34,00	1659,96	285,60	16,31
14500	6900	3	3b	702,62	32,30	1998,12	622,20	21,75
14500	7250	3	3b	1220,34	105,40	1816,08	438,60	11,58
14500	7975	3	3b	369,80	27,20	1994,64	561,00	13,60
14500	12875	3	3b	1257,32	110,50	1967,08	472,60	11,38
14500	14500	3	3b	573,19	66,30	1888,14	423,30	8,65
14500	17000	3	3b	739,60	95,20	1950,76	482,80	7,77
14500	19400	3	3b	573,19	73,10	1902,04	421,60	7,84
14625	4175	3	3b	369,80	42,50	1818,96	397,80	8,70
14625	5025	3	3b	702,62	73,10	1870,12	431,80	9,61
14625	5375	3	3b	295,84	30,60	1656,80	190,40	9,67
14625	5725	3	3b	499,23	59,50	1750,58	287,30	8,39
14625	5875	3	3b	813,56	39,10	1923,40	472,60	20,81
14625	5900	3	3b	314,33	42,50	1853,84	404,60	7,40
14625	6775	3	3b	739,60	49,30	1628,52	244,80	15,00
14625	6850	3	3b	647,15	40,80	1993,74	606,90	15,86
14625	7150	3	3b	795,07	47,60	1798,24	411,40	16,70
14625	7625	3	3b	462,25	45,90	1751,78	358,70	10,07
14625	12900	3	3b	1590,14	107,10	1963,44	428,40	14,85
14625	14650	3	3b	961,48	56,10	1872,98	409,70	17,14
14625	17025	3	3b	702,62	98,60	1950,48	479,40	7,13
14625	19450	3	3b	591,68	86,70	1917,34	436,90	6,82

(N-S)	X (E-W)	Area	Unit	Width (m)	Height (m)	Depth (mbsl)	Burial depth (m)	W/H ratio
14750	3900	3	3b	573,19	49,30	1844,88	428,40	11,63
14750	5075	3	3b	388,29	27,20	1563,70	120,70	14,28
14750	5100	3	3b	554,70	59,50	1864,60	421,60	9,32
14750	5525	3	3b	295,84	35,70	1657,94	185,30	8,29
14750	5950	3	3b	758,09	32,30	1931,20	472,60	23,47
14750	6475	3	3b	406,78	23,80	1740,76	319,60	17,09
14750	6950	3	3b	388,29	27,20	1996,74	586,50	14,28
14750	7075	3	3b	721,11	45,90	1774,32	367,20	15,71
14750	7550	3	3b	332,82	35,70	1730,40	326,40	9,32
14750	9725	3	3b	665,64	47,60	1662,48	183,60	13,98
14750	13225	3	3b	1479,20	108,80	1974,44	353,60	13,60
14750	15025	3	3b	795,07	52,70	1882,62	413,10	15,09
14750	17100	3	3b	684,13	83,30	1940,00	465,80	8,21
14750	19325	3	3b	739,60	54,40	1817,90	328,10	13,60
14750	19425	3	3b	517,72	74,80	1921,88	435,20	6,92
14875	3925	3	3b	536,21	56,10	1844,46	423,30	9,56
14875	4275	3	3b	998,46	85,00	1726,88	302,60	11,75
14875	5125	3	3b	665,64	66,30	1870,72	401,20	10,04
14875	6125	3	3b	554,70	37,40	1934,60	476,00	14,83
14875	6950	3	3b	480,74	34,00	1995,92	557,60	14,14
14875	13275	3	3b	1534,67	103,70	1969,92	336,60	14,80
14875	15325	3	3b	758,09	49,30	1885,88	414,80	15,38
14875	17125	3	3b	702,62	90,10	1950,06	474,30	7,80
14875	19500	3	3b	721,11	73,10	1924,86	433,50	9,86
15000	3875	3	3b	684,13	69,70	1852,96	431,80	9,82
15000	5375	3	3b	1109,40	71,40	1842,80	384,20	15,54
15000	5475	3	3b	887,52	42,50	1894,94	430,10	20,88
15000	6200	3	3b	665,64	32,30	1934,46	474,30	20,61
15000	6950	3	3b	869,03	39,10	1999,34	542,30	22,23
15000	7100	3	3b	443,76	40,80	1699,16	231,20	10,88
15000	13325	3	3b	1257,32	91,80	1975,02	341,70	13,70
15000	15400	3	3b	1109,40	56,10	1884,02	430,10	19,78
15000	17175	3	3b	591,68	76,50	1948,50	474,30	7,73
15000	19400	3	3b	554,70	44,20	1991,02	498,10	12,55
15000	19425	3	3b	406,78	45,90	1892,56	401,20	8,86
15000	19525	3	3b	332,82	30,60	1926,00	428,40	10,88
15125	3850	3	3b	832,05	51,00	1863,58	447,10	16,31
15125	3925	3	3b	573,19	42,50	1805,78	389,30	13,49
15125	4625	3	3b	388,29	27,20	1773,92	343,40	14,28
15125	6350	3	3b	517,72	30,60	1939,84	482,80	16,92
15125	7025	3	3b	721,11	47,60	2004,74	532,10	15,15
15125	13375	3	3b	1349,77	96,90	1973,74	477,70	13,93
15125	15375	3	3b	665,64	28,90	1881,90	423,30	23,03
15125	17175	3	3b	610,17	88,40	1963,10	481,10	6,90
15125	19450	3	3b	332,82	23,80	1990,74	494,70	13,98
15125	19625	3	3b	758,09	83,30	1956,74	460,70	9,10
15250	3875	3	3b	647,15	42,50	1804,36	391,00	15,23
15250	4000	3	3b	869,03	56,10	1870,38	453,90	15,49

(N-S)	X (E-W)	Area	Unit	Width (m)	Height (m)	Depth (mbsl)	Burial depth (m)	W/H ratio
15250	5600	3	3b	1127,89	88,40	1880,76	428,40	12,76
15250	6400	3	3b	536,21	32,30	1939,70	481,10	16,60
15250	7050	3	3b	665,64	54,40	2001,48	530,40	12,24
15250	13425	3	3b	1516,18	102,00	1976,02	467,50	14,86
15250	15450	3	3b	795,07	37,40	1881,62	419,90	21,26
15250	17200	3	3b	684,13	90,10	1962,82	477,70	7,59
15250	19650	3	3b	832,05	86,70	1960,28	465,80	9,60
15375	3975	3	3b	499,23	32,30	1793,74	375,70	15,46
15375	5375	3	3b	684,13	90,10	1830,46	385,90	7,59
15375	5750	3	3b	813,56	103,70	1894,78	447,10	7,85
15375	6475	3	3b	499,23	39,10	1938,22	406,30	12,77
15375	7150	3	3b	721,11	52,70	2001,34	528,70	13,68
15375	13450	3	3b	1220,34	90,10	1975,32	459,00	13,54
15375	17275	3	3b	462,25	79,90	1969,62	484,50	5,79
15375	19475	3	3b	369,80	28,90	1997,82	504,90	12,80
15375	19500	3	3b	942,99	44,20	1857,20	47,60	21,33
15375	19675	3	3b	665,64	66,30	1951,64	455,60	10,04
15500	4150	3	3b	832,05	49,30	1889,22	474,30	16,88
15500	5700	3	3b	1016,95	110,50	1899,74	450,50	9,20
15500	6450	3	3b	536,21	40,80	1940,12	486,20	13,14
15500	7275	3	3b	647,15	37,40	1996,80	530,40	17,30
15500	13400	3	3b	1368,26	95,20	1981,96	482,80	14,37
15500	17300	3	3b	443,76	71,40	1964,24	476,00	6,22
15500	19675	3	3b	906,01	91,80	1958,30	460,70	9,87
15625	3575	3	3b	406,78	49,30	1763,42	348,50	8,25
15625	3650	3	3b	295,84	35,70	1842,04	431,80	8,29
15625	5825	3	3b	1127,89	112,20	1905,40	462,40	10,05
15625	6575	3	3b	536,21	35,70	1943,66	491,30	15,02
15625	13600	3	3b	1442,22	96,90	1988,02	518,50	14,88
15625	17350	3	3b	499,23	76,50	1958,86	467,50	6,53
15625	19725	3	3b	832,05	112,20	1980,40	482,80	7,42
15750	3500	3	3b	554,70	88,40	1795,72	380,80	6,27
15750	5925	3	3b	1312,79	112,20	1907,24	465,80	11,70
15750	6600	3	3b	517,72	34,00	1939,12	493,00	15,23
15750	7275	3	3b	591,68	39,10	1993,54	528,70	15,13
15750	13575	3	3b	1201,85	91,80	1975,28	363,80	13,09
15750	17400	3	3b	610,17	85,00	1980,54	484,50	7,18
15750	19575	3	3b	702,62	52,70	1939,32	438,60	13,33
15875	3500	3	3b	647,15	88,40	1811,58	402,90	7,32
15875	5975	3	3b	1775,04	149,60	1906,96	462,40	11,87
15875	7400	3	3b	887,52	59,50	1994,40	520,20	14,92
15875	13150	3	3b	924,50	34,00	1903,78	253,30	27,19
15875	13650	3	3b	1904,47	103,70	1990,88	496,40	18,37
15875	14675	3	3b	647,15	56,10	2024,02	538,90	11,54
15875	17450	3	3b	406,78	52,70	2036,78	542,30	7,72
15875	17525	3	3b	480,74	73,10	1977,00	479,40	6,58
15875	19625	3	3b	314,33	28,90	2010,58	508,30	10,88
15875	19700	3	3b	499,23	20,40	1921,90	416,50	24,47

(N-S)	X (E-W)	Area	Unit	Width (m)	Height (m)	Depth (mbsl)	Burial depth (m)	W/H ratio
15875	19925	3	3b	665,64	37,40	1954,20	448,80	17,80
15875	20000	3	3b	480,74	6,80	1984,66	477,70	70,70
16000	3650	3	3b	739,60	90,10	1826,60	414,80	8,21
16000	3825	3	3b	332,82	22,10	1852,24	442,00	15,06
16000	6075	3	3b	1590,14	93,50	1915,04	465,80	17,01
16000	7525	3	3b	480,74	44,20	1997,10	515,10	10,88
16000	13100	3	3b	979,97	42,50	1910,58	260,10	23,06
16000	13750	3	3b	1479,20	91,80	1995,84	499,80	16,11
16000	17575	3	3b	536,21	79,90	1974,88	472,60	6,71
16000	19850	3	3b	647,15	37,40	2008,32	499,80	17,30
16000	19950	3	3b	850,54	44,20	1960,72	452,20	19,24
16125	3750	3	3b	850,54	71,40	1823,20	411,40	11,91
16125	6125	3	3b	1812,02	122,40	1916,74	467,50	14,80
16125	7200	3	3b	517,72	42,50	1954,44	489,60	12,18
16125	7600	3	3b	499,23	39,10	2004,32	527,00	12,77
16125	7850	3	3b	351,31	30,60	1956,02	470,90	11,48
16125	13100	3	3b	979,97	51,00	1920,50	266,90	19,22
16125	13775	3	3b	1275,81	68,00	1998,96	499,80	18,76
16125	17675	3	3b	554,70	83,30	1986,78	484,50	6,66
16125	20075	3	3b	758,09	61,20	1962,00	448,80	12,39
16250	3900	3	3b	665,64	37,40	1839,92	425,00	17,80
16250	6525	3	3b	1090,91	76,50	1924,68	469,20	14,26
16250	7675	3	3b	425,27	39,10	2001,78	515,10	10,88
16250	7925	3	3b	425,27	22,10	1953,76	462,40	19,24
16250	8050	3	3b	406,78	57,80	1831,50	341,70	7,04
16250	13900	3	3b	1553,16	90,10	2002,94	491,30	17,24
16250	17700	3	3b	610,17	73,10	1988,06	481,10	8,35
16250	20025	3	3b	499,23	40,80	1975,18	457,30	12,24
16250	20150	3	3b	776,58	28,90	1928,28	418,20	26,87
16250	20300	3	3b	554,70	32,30	2003,94	484,50	17,17
16375	6300	3	3b	591,68	68,00	1902,44	445,40	8,70
16375	7650	3	3b	314,33	44,20	2001,64	513,40	7,11
16375	7975	3	3b	388,29	22,10	1967,22	474,30	17,57
16375	8300	3	3b	443,76	51,00	1841,56	350,20	8,70
16375	13925	3	3b	1386,75	73,10	2004,22	487,90	18,97
16375	17825	3	3b	721,11	90,10	1991,04	479,40	8,00
16375	20325	3	3b	979,97	35,70	1971,78	453,90	27,45
16500	5025	3	3b	665,64	23,80	1880,46	443,70	27,97
16500	5900	3	3b	573,19	40,80	1916,18	460,70	14,05
16500	5975	3	3b	813,56	32,30	1873,68	418,20	25,19
16500	6950	3	3b	554,70	47,60	1835,46	351,90	11,65
16500	7675	3	3b	850,54	57,80	1999,94	511,70	14,72
16500	8475	3	3b	610,17	51,00	1829,52	336,60	11,96
16500	9475	3	3b	665,64	32,30	1768,32	275,40	20,61
16500	12625	3	3b	351,31	34,00	1697,52	40,80	10,33
16500	13875	3	3b	406,78	35,70	1630,06	130,90	11,39
16500	14225	3	3b	1349,77	78,20	2003,92	503,20	17,26
16500	17875	3	3b	813,56	95,20	1999,96	493,00	8,55

(N-S)	X (E-W)	Area	Unit	Width (m)	Height (m)	Depth (mbsl)	Burial depth (m)	W/H ratio
16625	2650	3	3b	998,46	30,60	1508,70	96,90	32,63
16625	3125	3	3b	277,35	27,20	1867,12	452,20	10,20
16625	3275	3	3b	665,64	37,40	1819,38	402,90	17,80
16625	3925	3	3b	388,29	28,90	1817,54	399,50	13,44
16625	4825	3	3b	573,19	35,70	1875,64	442,00	16,06
16625	6100	3	3b	517,72	30,60	1918,60	452,20	16,92
16625	6900	3	3b	517,72	32,30	1930,10	440,30	16,03
16625	7250	3	3b	351,31	44,20	1828,24	340,00	7,95
16625	7325	3	3b	591,68	23,80	1962,54	474,30	24,86
16625	7775	3	3b	517,72	51,00	1999,66	508,30	10,15
16625	8125	3	3b	480,74	18,70	1965,24	469,20	25,71
16625	8250	3	3b	221,88	32,30	1770,16	278,80	6,87
16625	9800	3	3b	462,25	54,40	1704,58	202,30	8,50
16625	10025	3	3b	277,35	28,90	1610,38	100,30	9,60
16625	11550	3	3b	536,21	32,30	1603,14	107,10	16,60
16625	12450	3	3b	258,86	37,40	1696,96	34,00	6,92
16625	14200	3	3b	1553,16	78,20	2002,08	499,80	19,86
16625	14450	3	3b	610,17	34,00	1617,88	115,60	17,95
16625	18000	3	3b	665,64	85,00	2003,22	494,70	7,83
16625	20450	3	3b	1238,83	37,40	1976,74	457,30	33,12
16750	3075	3	3b	369,80	49,30	1877,60	465,80	7,50
16750	3225	3	3b	684,13	45,90	1824,76	411,40	14,90
16750	3825	3	3b	332,82	30,60	1817,54	399,50	10,88
16750	5100	3	3b	961,48	47,60	1883,02	436,90	20,20
16750	6000	3	3b	388,29	27,20	1871,42	409,70	14,28
16750	6900	3	3b	369,80	30,60	1924,86	433,50	12,08
16750	7100	3	3b	258,86	32,30	1842,98	348,50	8,01
16750	7425	3	3b	443,76	51,00	1982,66	491,30	8,70
16750	7425	3	3b	462,25	42,50	1793,68	299,20	10,88
16750	7800	3	3b	388,29	44,20	2005,76	506,60	8,78
16750	8050	3	3b	369,80	40,80	1768,04	272,00	9,06
16750	14275	3	3b	1368,26	78,20	2010,58	508,30	17,50
16750	15425	3	3b	351,31	27,20	1929,54	433,50	12,92
16750	18075	3	3b	739,60	90,10	2000,96	486,20	8,21
16750	22100	3	3b	684,13	34,00	1885,24	350,20	20,12
16875	2975	3	3b	480,74	25,50	1865,42	450,50	18,85
16875	4775	3	3b	536,21	30,60	1991,10	555,90	17,52
16875	5175	3	3b	1238,83	56,10	1885,72	431,80	22,08
16875	6650	3	3b	184,90	20,40	1845,38	358,70	9,06
16875	7100	3	3b	406,78	23,80	1934,78	440,30	17,09
16875	7850	3	3b	739,60	52,70	1993,86	494,70	14,03
16875	14325	3	3b	1072,42	69,70	2004,92	496,40	15,39
16875	15500	3	3b	351,31	22,10	1925,58	423,30	15,90
16875	16025	3	3b	1146,38	27,20	2028,86	521,90	42,15
16875	18225	3	3b	942,99	93,50	1999,26	484,50	10,09
16875	22325	3	3b	906,01	23,80	1900,40	363,80	38,07
17000	2925	3	3b	554,70	39,10	1868,82	453,90	14,19
17000	4075	3	3b	351,31	30,60	1971,12	540,60	11,48

(N-S)	X (E-W)	Area	Unit	Width (m)	Height (m)	Depth (mbsl)	Burial depth (m)	W/H ratio
17000	5100	3	3b	869,03	40,80	1872,54	423,30	21,30
17000	7050	3	3b	443,76	17,00	1929,40	431,80	26,10
17000	7825	3	3b	721,11	42,50	1963,26	464,10	16,97
17000	13300	3	3b	591,68	40,80	1953,26	266,90	14,50
17000	14425	3	3b	850,54	52,70	2010,30	504,90	16,14
17000	15600	3	3b	499,23	39,10	1924,02	423,30	12,77
17000	16050	3	3b	813,56	32,30	2025,74	521,90	25,19
17000	18275	3	3b	869,03	77,35	1993,31	478,55	11,24
17000	19000	3	3b	406,78	30,60	1901,66	379,10	13,29
17125	2950	3	3b	887,52	45,90	1882,28	465,80	19,34
17125	4825	3	3b	628,66	37,40	1998,90	555,90	16,81
17125	4900	3	3b	554,70	52,70	1876,22	430,10	10,53
17125	6175	3	3b	665,64	52,70	1860,68	374,00	12,63
17125	7875	3	3b	721,11	28,90	1966,66	467,50	24,95
17125	7925	3	3b	332,82	46,75	2019,93	517,65	7,12
17125	11150	3	3b	869,03	47,60	1895,14	375,70	18,26
17125	13750	3	3b	739,60	39,10	1946,76	244,80	18,92
17125	14475	3	3b	813,56	44,20	1992,18	474,30	18,41
17125	15150	3	3b	369,80	23,80	1952,78	450,50	15,54
17125	15600	3	3b	388,29	23,80	1932,52	431,80	16,31
17125	16175	3	3b	628,66	34,00	2028,58	518,50	18,49
17125	16925	3	3b	758,09	45,90	1927,58	409,70	16,52
17125	18375	3	3b	739,60	85,00	2005,50	484,50	8,70
17125	22375	3	3b	166,41	27,20	1953,10	416,50	6,12
17250	2825	3	3b	1127,89	78,20	1878,60	459,00	14,42
17250	4825	3	3b	647,15	30,60	1996,92	550,80	21,15
17250	5000	3	3b	462,25	30,60	1863,34	406,30	15,11
17250	8075	3	3b	813,56	27,20	1966,38	464,10	29,91
17250	11300	3	3b	924,50	32,30	1886,78	368,90	28,62
17250	13750	3	3b	721,11	34,00	1960,64	261,80	21,21
17250	14625	3	3b	1053,93	57,80	1989,06	474,30	18,23
17250	16125	3	3b	665,64	27,20	2025,04	513,40	24,47
17250	16900	3	3b	869,03	51,00	1940,76	418,20	17,04
17250	18425	3	3b	462,25	27,20	2053,10	532,10	16,99
17250	18500	3	3b	758,09	66,30	2002,10	481,10	11,43
17375	4875	3	3b	684,13	32,30	1848,18	392,70	21,18
17375	5250	3	3b	942,99	40,80	1881,92	404,60	23,11
17375	6200	3	3b	573,19	27,20	1878,40	380,80	21,07
17375	6825	3	3b	906,01	32,30	1852,90	355,30	28,05
17375	7775	3	3b	906,01	35,70	1966,38	464,10	25,38
17375	7875	3	3b	832,05	22,10	1959,58	457,30	37,65
17375	8025	3	3b	332,82	47,60	2039,34	535,50	6,99
17375	13750	3	3b	554,70	37,40	1951,72	248,20	14,83
17375	14300	3	3b	1072,42	37,40	1920,22	396,10	28,67
17375	14825	3	3b	942,99	44,20	1976,30	470,90	21,33
17375	16225	3	3b	628,66	51,00	2050,26	535,50	12,33
17375	16950	3	3b	850,54	51,00	1954,36	431,80	16,68
17375	18475	3	3b	480,74	11,05	2027,89	500,65	43,51

(N-S)	X (E-W)	Area	Unit	Width (m)	Height (m)	Depth (mbsl)	Burial depth (m)	W/H ratio
17375	18650	3	3b	813,56	68,00	2003,66	481,10	11,96
17500	2500	3	3b	1405,24	95,20	1869,10	457,30	14,76
17500	5000	3	3b	1016,95	32,30	1843,94	379,10	31,48
17500	6550	3	3b	832,05	30,60	1830,52	329,80	27,19
17500	8050	3	3b	406,78	28,90	2005,48	503,20	14,08
17500	13725	3	3b	684,13	40,80	1939,62	290,70	16,77
17500	14825	3	3b	739,60	25,50	1947,98	430,10	29,00
17500	15550	3	3b	221,88	25,50	1938,06	423,30	8,70
17500	17050	3	3b	869,03	61,20	1968,10	447,10	14,20
17500	18700	3	3b	758,09	68,00	2003,66	481,10	11,15
17500	20575	3	3b	1460,71	54,40	1952,68	411,40	26,85
17500	22175	3	3b	813,56	35,70	1935,82	396,10	22,79
17625	4925	3	3b	979,97	64,60	1862,64	397,80	15,17
17625	7150	3	3b	480,74	23,80	1828,68	326,40	20,20
17625	7875	3	3b	795,07	28,90	1954,34	450,50	27,51
17625	8125	3	3b	443,76	42,50	2016,82	508,30	10,44
17625	13675	3	3b	536,21	25,50	1929,32	241,40	21,03
17625	14725	3	3b	406,78	22,10	1949,82	433,50	18,41
17625	15525	3	3b	258,86	25,50	1941,46	426,70	10,15
17625	17150	3	3b	924,50	57,80	1964,70	443,70	15,99
17625	18725	3	3b	906,01	25,50	2027,04	499,80	35,53
17625	18800	3	3b	684,13	45,90	1984,68	459,00	14,90
17625	20750	3	3b	1516,18	42,50	1934,40	397,80	35,67
17625	20850	3	3b	758,09	30,60	2000,70	464,10	24,77
17750	4175	3	3b	758,09	32,30	1745,46	300,90	23,47
17750	8050	3	3b	813,56	28,90	1960,86	453,90	28,15
17750	8225	3	3b	443,76	44,20	2021,78	511,70	10,04
17750	11275	3	3b	184,90	28,90	1631,50	110,50	6,40
17750	13550	3	3b	610,17	35,70	1922,40	214,20	17,09
17750	15075	3	3b	721,11	20,40	1933,10	419,90	35,35
17750	17200	3	3b	869,03	51,00	1955,78	430,10	17,04
17750	18825	3	3b	795,07	34,00	2025,20	496,40	23,38
17750	18850	3	3b	554,70	44,20	1975,76	445,40	12,55
17750	21000	3	3b	813,56	35,70	2002,54	467,50	22,79
17875	8000	3	3b	591,68	26,00	536,00	455,60	22,76
17875	8325	3	3b	425,27	54,00	618,00	525,30	7,88
17875	11350	3	3b	277,35	32,00	128,00	108,80	8,67
17875	13625	3	3b	702,62	40,00	438,00	372,30	17,57
17875	15075	3	3b	665,64	36,00	484,00	411,40	18,49
17875	17350	3	3b	924,50	66,00	504,00	428,40	14,01
17875	18700	3	3b	203,39	30,00	544,00	462,40	6,78
17875	18750	3	3b	758,09	36,00	578,00	491,30	21,06
17875	18950	3	3b	739,60	64,00	526,00	447,10	11,56
17875	21300	3	3b	961,48	40,00	536,00	455,60	24,04
18000	7425	3	3b	351,31	34,00	314,00	266,90	10,33
18000	8175	3	3b	554,70	26,00	532,00	452,20	21,33
18000	8225	3	3b	554,70	60,00	610,00	518,50	9,25
18000	14175	3	3b	425,27	50,00	462,00	392,70	8,51

(N-S)	X (E-W)	Area	Unit	Width (m)	Height (m)	Depth (mbsl)	Burial depth (m)	W/H ratio
18000	17475	3	3b	702,62	52,00	498,00	423,30	13,51
18000	18800	3	3b	517,72	64,00	556,00	472,60	8,09
18000	19200	3	3b	240,37	44,00	510,00	433,50	5,46
18000	21625	3	3b	924,50	38,00	534,00	453,90	24,33
18125	8350	3	3b	499,23	72,00	612,00	520,20	6,93
18125	14400	3	3b	721,11	58,00	480,00	408,00	12,43
18125	17425	3	3b	684,13	60,00	474,00	402,90	11,40
18125	18975	3	3b	665,64	46,00	506,00	430,10	14,47
18125	19800	3	3b	295,84	30,00	452,00	384,20	9,86
18125	22000	3	3b	998,46	40,00	538,00	457,30	24,96
18250	8300	3	3b	721,11	64,00	616,00	523,60	11,27
18250	14550	3	3b	1035,44	78,00	488,00	414,80	13,27
18250	19025	3	3b	998,46	64,00	520,00	442,00	15,60
18375	8150	3	3b	702,62	60,00	606,00	515,10	11,71
18375	14725	3	3b	1146,38	68,00	488,00	414,80	16,86
18375	19025	3	3b	1109,40	48,00	518,00	440,30	23,11
18375	19450	3	3b	1442,22	48,00	462,00	392,70	30,05
18500	8425	3	3b	1238,83	72,00	618,00	525,30	17,21
18500	14875	3	3b	1164,87	60,00	472,00	401,20	19,41
18500	19100	3	3b	1627,12	86,00	514,00	436,90	18,92
18625	8575	3	3b	961,48	62,00	614,00	521,90	15,51
18625	19100	3	3b	1442,22	84,00	508,00	431,80	17,17
18625	22475	3	3b	1534,67	86,00	500,00	425,00	17,85
18750	8575	3	3b	979,97	76,00	636,00	540,60	12,89
18750	19100	3	3b	1127,89	46,00	500,00	425,00	24,52
18750	22425	3	3b	1386,75	84,00	490,00	416,50	16,51
18875	8600	3	3b	1090,91	79,90	2068,68	550,80	13,65
18875	19150	3	3b	1479,20	102,00	1996,46	450,50	14,50
18875	22200	3	3b	1109,40	85,00	1950,00	397,80	13,05
19000	8875	3	3b	1090,91	62,90	2056,66	518,50	17,34
19000	15875	3	3b	610,17	42,50	1908,48	367,20	14,36
19000	19125	3	3b	1257,32	54,40	1951,98	402,90	23,11
19125	8775	3	3b	1220,34	64,60	2057,80	513,40	18,89
19125	8850	3	3b	813,56	27,20	1991,36	445,40	29,91
19125	15975	3	3b	979,97	47,60	1920,38	379,10	20,59
19125	18975	3	3b	1460,71	54,40	1938,38	389,30	26,85
19250	8900	3	3b	1331,28	61,20	2055,54	504,90	21,75
19250	13775	3	3b	776,58	37,40	2116,52	374,00	20,76
19250	16050	3	3b	1201,85	57,80	1928,18	379,10	20,79
19250	19200	3	3b	1164,87	59,50	1954,96	401,20	19,58
19375	3000	3	3b	406,78	27,20	1819,56	367,20	14,96
19375	9050	3	3b	1090,91	62,90	2063,48	506,60	17,34
19375	16125	3	3b	924,50	42,50	1922,66	368,90	21,75
19375	19275	3	3b	721,11	49,30	1978,62	423,30	14,63
19500	8225	3	3b	221,88	32,30	1971,82	416,50	6,87
19500	9200	3	3b	832,05	45,90	2050,02	494,70	18,13
19500	19125	3	3b	1405,24	34,00	1925,92	370,60	41,33
19500	19150	3	3b	647,15	40,80	1973,66	419,90	15,86



(N-S)	X (E-W)	Area	Unit	Width (m)	Height (m)	Depth (mbsl)	Burial depth (m)	W/H ratio
19500	19475	3	3b	573,19	56,10	2017,72	462,40	10,22
19625	8350	3	3b	258,86	18,70	1965,02	409,70	13,84
19625	9250	3	3b	961,48	42,50	2039,82	484,50	22,62
19625	19125	3	3b	1571,65	44,20	1935,84	377,40	35,56
19625	19250	3	3b	850,54	51,00	1979,90	419,90	16,68
19750	8400	3	3b	277,35	27,20	1968,00	408,00	10,20
19750	9575	3	3b	795,07	47,60	2058,38	501,50	16,70
19750	11850	3	3b	1368,26	37,40	1879,04	312,80	36,58
19750	16575	3	3b	1275,81	47,60	1930,46	368,90	26,80
19750	19175	3	3b	1701,08	44,20	1940,80	380,80	38,49
19750	19325	3	3b	1016,95	35,70	1988,26	426,70	28,49
19750	19575	3	3b	573,19	22,10	2010,08	445,40	25,94
19875	8400	3	3b	351,31	25,50	1968,14	409,70	13,78
19875	9550	3	3b	776,58	40,80	2057,68	493,00	19,03
19875	11950	3	3b	1035,44	32,30	1919,70	351,90	32,06
19875	16625	3	3b	1275,81	66,30	1957,80	397,80	19,24
19875	19200	3	3b	1701,08	35,70	1936,84	370,60	47,65
19875	19550	3	3b	1201,85	71,40	1994,50	426,70	16,83
20000	6625	3	3b	332,82	20,40	1950,70	406,30	16,31
20000	8425	3	3b	425,27	27,20	1966,16	404,60	15,63
20000	9750	3	3b	739,60	56,10	2059,52	496,40	13,18
20000	12125	3	3b	906,01	51,00	1953,28	380,80	17,76
20000	16800	3	3b	1257,32	85,00	1992,94	426,70	14,79
20000	19450	3	3b	1294,30	85,00	1989,54	423,30	15,23
1	1275	1	3c	441,75	49,30	1092,26	154,7	8,96
1	4250	1	3c	279	30,60	1197,18	45,9	9,12
1	4975	1	3c	209,25	28,90	1155,68	129,2	7,24
1	6075	1	3c	186	40,80	1180,92	132,6	4,56
1	6100	1	3c	255,75	27,20	1135,3	90,1	9,40
1	6625	1	3c	302,25	28,90	1312,52	272	10,46
1	9475	1	3c	930	64,60	1469,96	384,2	14,40
1	14375	1	3c	627,75	37,40	1344,2	221	16,78
1	16450	1	3c	627,75	52,70	1240,08	112,2	11,91
1	16450	1	3c	302,25	71,40	1324,8	193,8	4,23
125	750	1	3c	302,25	30,60	1042,24	115,6	9,88
125	4275	1	3c	279	49,30	1213,06	49,3	5,66
125	6050	1	3c	279	47,60	1187,58	137,7	5,86
125	8125	1	3c	488,25	42,50	1118,48	37,4	11,49
125	8225	1	3c	558	45,90	1150,78	69,7	12,16
125	10250	1	3c	860,25	39,10	1280,28	183,6	22,00
125	10800	1	3c	395,25	45,90	1219,38	107,1	8,61
125	16400	1	3c	418,5	83,30	1320,56	180,2	5,02
125	16425	1	3c	744	45,90	1227,48	91,8	16,21
125	19100	1	3c	395,25	32,30	1196,56	95,2	12,24
250	825	1	3c	279	30,60	1050,18	117,3	9,12
250	4900	1	3c	279	40,80	1173,82	141,1	6,84
250	6050	1	3c	441,75	59,50	1189	136	7,42

(N-S)	X (E-W)	Area	Unit	Width (m)	Height (m)	Depth (mbsl)	Burial depth (m)	W/H ratio
250	8275	1	3c	465	62,90	1182,24	91,8	7,39
250	10850	1	3c	511,5	34,00	1235,26	110,5	15,04
250	16350	1	3c	418,5	79,90	1323,54	178,5	5,24
250	18800	1	3c	581,25	35,70	1210,44	112,2	16,28
375	950	1	3c	372	34,00	1061,38	120,7	10,94
375	1650	1	3c	441,75	56,10	1133,8	166,6	7,87
375	6025	1	3c	441,75	34,00	1120,58	62,9	12,99
375	6025	1	3c	302,25	52,70	1193,96	139,4	5,74
375	8350	1	3c	744	93,50	1193,86	100,3	7,96
375	16325	1	3c	441,75	78,20	1324,28	149,6	5,65
500	975	1	3c	209,25	34,00	1068,62	113,9	6,15
500	1750	1	3c	418,5	40,80	1129,28	149,6	10,26
500	4350	1	3c	302,25	39,10	1234,74	66,3	7,73
500	6000	1	3c	534,75	35,70	1113,36	51	14,98
500	6050	1	3c	279	42,50	1243,26	188,7	6,56
500	8450	1	3c	720,75	96,90	1191,74	93,5	7,44
500	11100	1	3c	488,25	49,30	1253,82	127,5	9,90
500	16275	1	3c	418,5	79,90	1326,42	137,7	5,24
500	16400	1	3c	395,25	68,00	1242,82	69,7	5,81
625	1075	1	3c	232,5	23,80	1081,8	122,4	9,77
625	1800	1	3c	302,25	32,30	1129	146,2	9,36
625	5975	1	3c	302,25	32,30	1232,5	171,7	9,36
625	11175	1	3c	372	35,70	1266,86	134,3	10,42
625	16250	1	3c	279	45,90	1324,72	136	6,08
625	16300	1	3c	372	37,40	1290,44	98,6	9,95
625	16400	1	3c	255,75	57,80	1246,94	62,9	4,42
750	1125	1	3c	162,75	22,10	1085,78	113,9	7,36
750	6175	1	3c	790,5	88,40	1513,3	436,9	8,94
750	8275	1	3c	418,5	34,00	1145,42	42,5	12,31
750	8400	1	3c	325,5	28,90	1175,46	66,3	11,26
750	8425	1	3c	395,25	35,70	1182,68	78,2	11,07
750	8500	1	3c	279	42,50	1225,18	120,7	6,56
750	8550	1	3c	302,25	32,30	1227,16	125,8	9,36
750	16300	1	3c	325,5	54,40	1329,68	139,4	5,98
875	1975	1	3c	604,5	28,90	1140,64	136	20,92
875	4475	1	3c	418,5	44,20	1393,56	214,2	9,47
875	4925	1	3c	255,75	45,90	1221,66	96,9	5,57
875	5650	1	3c	372	45,90	1214,38	141,1	8,10
875	6200	1	3c	1023	85,00	1515,58	426,7	12,04
875	8400	1	3c	1046,25	79,90	1478,64	357	13,09
875	11275	1	3c	348,75	23,80	1300,3	161,5	14,65
875	16325	1	3c	279	52,70	1336,2	142,8	5,29
1000	1700	1	3c	604,5	27,20	1239,66	239,7	22,22
1000	2025	1	3c	348,75	28,90	1140,08	129,2	12,07
1000	6275	1	3c	930	96,90	1529,04	438,6	9,60
1000	8050	1	3c	325,5	56,10	1180,72	54,4	5,80
1000	16325	1	3c	348,75	59,50	1324,44	132,6	5,86
1125	1975	1	3c	558	30,60	1138,24	125,8	18,24

(N-S)	X (E-W)	Area	Unit	Width (m)	Height (m)	Depth (mbsl)	Burial depth (m)	W/H ratio
1125	6200	1	3c	1209	102,00	1530,46	436,9	11,85
1125	7925	1	3c	488,25	57,80	1188,8	57,8	8,45
1125	11550	1	3c	418,5	28,90	1315,32	173,4	14,48
1125	16300	1	3c	511,5	52,70	1336,06	141,1	9,71
1250	1825	1	3c	651	22,10	1130,46	107,1	29,46
1250	5250	1	3c	558	85,00	1219	64,6	6,56
1250	5300	1	3c	581,25	76,50	1237,42	79,9	7,60
1250	5375	1	3c	372	49,30	1261,66	90,1	7,55
1250	7850	1	3c	581,25	66,30	1200,56	68	8,77
1250	7850	1	3c	395,25	25,50	1229,04	91,8	15,50
1250	8825	1	3c	302,25	35,70	1250	119	8,47
1250	11225	1	3c	255,75	45,90	1276,8	122,4	5,57
1250	11650	1	3c	395,25	35,70	1324,4	170	11,07
1250	16275	1	3c	534,75	66,30	1336,2	142,8	8,07
1250	17575	1	3c	604,5	63,20	1300,02	158,1	9,56
1375	1800	1	3c	279	30,60	1258,24	238	9,12
1375	2000	1	3c	581,25	34,00	1149,16	125,8	17,10
1375	5350	1	3c	325,5	52,70	1268,22	56,1	6,18
1375	6175	1	3c	1116	90,10	1513,04	414,8	12,39
1375	7725	1	3c	604,5	51,00	1188,38	52,7	11,85
1375	8825	1	3c	302,25	37,40	1256,8	125,8	8,08
1375	11075	1	3c	627,75	37,40	1477,26	321,3	16,78
1375	11200	1	3c	209,25	40,80	1274,82	117,3	5,13
1375	11800	1	3c	441,75	39,10	1327,8	173,4	11,30
1375	16275	1	3c	372	44,20	1337,9	144,5	8,42
1500	2075	1	3c	511,5	32,30	1153,42	120,7	15,84
1500	5425	1	3c	372	54,40	1268,5	59,5	6,84
1500	5450	1	3c	302,25	54,40	1266,38	52,7	5,56
1500	5950	1	3c	1069,5	62,90	1499,16	397,8	17,00
1500	7625	1	3c	395,25	34,00	1247,04	102	11,63
1500	8850	1	3c	418,5	52,70	1211,04	81,6	7,94
1500	11025	1	3c	953,25	32,30	1473,58	314,5	29,51
1625	1900	1	3c	720,75	32,30	1155,26	124,1	22,31
1625	5500	1	3c	279	54,40	1273,32	61,2	5,13
1625	6125	1	3c	1023	68,00	1483,72	380,8	15,04
1625	7550	1	3c	534,75	52,70	1212,06	56,1	10,15
1625	8800	1	3c	441,75	51,00	1186,82	52,7	8,66
1625	12000	1	3c	372	42,50	1341,7	171,7	8,75
1625	16675	1	3c	744	45,90	1339,2	122,4	16,21
1750	1875	1	3c	767,25	39,10	1154,98	120,7	19,62
1750	5600	1	3c	534,75	32,30	1285,52	57,8	16,56
1750	6225	1	3c	1023	59,50	1481,46	372,3	17,19
1750	7600	1	3c	465	68,00	1224,24	71,4	6,84
1750	12150	1	3c	418,5	49,30	1349,64	173,4	8,49
1750	16750	1	3c	720,75	37,40	1350,46	69,7	19,27
1875	2150	1	3c	837	54,40	1181,76	142,8	15,39
1875	5675	1	3c	372	51,00	1284,8	68	7,29
1875	6300	1	3c	883,5	42,50	1460,22	341,7	20,79

(N-S)	X (E-W)	Area	Unit	Width (m)	Height (m)	Depth (mbsl)	Burial depth (m)	W/H ratio
1875	7550	1	3c	488,25	98,60	1252,86	96,9	4,95
1875	12300	1	3c	418,5	45,90	1349,78	175,1	9,12
1875	13325	1	3c	418,5	28,90	1413,7	212,5	14,48
2000	2000	1	3c	627,75	45,90	1170,86	124,1	13,68
2000	7500	1	3c	534,75	93,50	1249,04	88,4	5,72
2000	12050	1	3c	511,5	57,80	1357,72	176,8	8,85
2125	2175	1	3c	930	37,40	1183,2	122,4	24,87
2125	5875	1	3c	395,25	40,80	1289,5	49,3	9,69
2125	6200	1	3c	581,25	28,90	1438,5	229,5	20,11
2125	7625	1	3c	534,75	100,30	1262,78	103,7	5,33
2125	11325	1	3c	860,25	35,70	1469,92	289	24,10
2125	12650	1	3c	581,25	35,70	1348,94	164,9	16,28
2250	1975	1	3c	1116	37,40	1282,36	227,8	29,84
2250	2100	1	3c	953,25	37,40	1183,34	124,1	25,49
2250	12750	1	3c	697,5	69,70	1368,08	170	10,01
2375	2225	1	3c	1139,25	69,70	1281,8	221	16,35
2375	5925	1	3c	767,25	39,10	1460,36	210,8	19,62
2375	8775	1	3c	930	71,40	1515,52	350,2	13,03
2375	9875	1	3c	441,75	32,30	1334,34	158,1	13,68
2375	12625	1	3c	372	42,50	1397,56	187	8,75
2500	1350	1	3c	1069,5	51,00	1177,8	132,6	20,97
2500	6325	1	3c	209,25	39,10	1298,58	45,9	5,35
2500	6575	1	3c	790,5	35,70	1424,5	192,1	22,14
2500	8200	1	3c	860,25	35,70	1339,3	161,5	24,10
2500	9850	1	3c	418,5	49,30	1345,68	163,2	8,49
2500	11600	1	3c	1325,25	78,20	1570,94	379,1	16,95
2500	12675	1	3c	372	34,00	1403,36	200,6	10,94
2625	1475	1	3c	1232,25	47,60	1186,88	129,2	25,89
2625	6250	1	3c	558	32,30	1464,62	205,7	17,28
2625	7425	1	3c	441,75	98,60	1284,34	100,3	4,48
2625	8000	1	3c	604,5	42,50	1485,08	302,6	14,22
2625	12825	1	3c	511,5	37,40	1414,84	207,4	13,68
2750	2400	1	3c	372	37,40	1196,4	112,2	9,95
2750	6100	1	3c	651	30,60	1473,38	236,3	21,27
2750	6600	1	3c	348,75	32,30	1328,12	139,4	10,80
2750	6800	1	3c	860,25	40,80	1442,66	185,3	21,08
2750	7975	1	3c	441,75	45,90	1483,1	297,5	9,62
2875	6875	1	3c	906,75	54,40	1484,2	197,2	16,67
2875	8275	1	3c	883,5	34,00	1338,2	129,2	25,99
3000	2575	1	3c	279	27,20	1212,98	124,1	10,26
3000	3650	1	3c	720,75	44,20	1275,34	161,5	16,31
3000	6875	1	3c	837	39,10	1511,12	221	21,41
3000	6950	1	3c	325,5	25,50	1330,22	32,3	12,76
3000	7325	1	3c	1511,25	52,70	1478,5	222,7	28,68
3000	8050	1	3c	279	32,30	1323,48	102	8,64
3000	13025	1	3c	860,25	45,90	1436,66	226,1	18,74
3000	13125	1	3c	534,75	40,80	1382,84	159,8	13,11
3125	1700	1	3c	883,5	37,40	1185,48	112,2	23,62

(N-S)	X (E-W)	Area	Unit	Width (m)	Height (m)	Depth (mbsl)	Burial depth (m)	W/H ratio
3125	6850	1	3c	441,75	47,60	1536,02	277,1	9,28
3125	7200	1	3c	162,75	42,50	1348,08	40,8	3,83
3125	7525	1	3c	1441,5	40,80	1466,9	195,5	35,33
3125	8925	1	3c	395,25	28,90	1456,6	278,8	13,68
3125	12875	1	3c	418,5	35,70	1495,74	280,5	11,72
3125	12900	1	3c	837	30,60	1431,56	221	27,35
3125	13200	1	3c	744	37,40	1376,46	158,1	19,89
3125	13500	1	3c	558	34,00	1339,48	125,8	16,41
3250	1700	1	3c	720,75	39,10	1215,66	137,7	18,43
3250	4900	1	3c	255,75	27,20	1245,06	96,9	9,40
3250	7525	1	3c	1325,25	74,80	1504,48	197,2	17,72
3250	8025	1	3c	372	39,10	1297,14	66,3	9,51
3250	8125	1	3c	604,5	51,00	1414,44	183,6	11,85
3250	12525	1	3c	1348,5	51,00	1429,86	219,3	26,44
3250	12925	1	3c	418,5	42,50	1553,54	338,3	9,85
3250	13450	1	3c	744	40,80	1347,56	129,2	18,24
3250	16125	1	3c	279	22,10	1389,08	27,2	12,62
3375	2800	1	3c	441,75	28,90	1210,88	98,6	15,29
3375	7675	1	3c	1092,75	81,60	1521,34	212,5	13,39
3375	12475	1	3c	1464,75	47,60	1437,94	222,7	30,77
3500	3000	1	3c	395,25	42,50	1227,6	112,2	9,30
3500	4175	1	3c	534,75	54,40	1484,04	346,8	9,83
3500	7550	1	3c	1069,5	66,30	1509,56	221	16,13
3500	7600	1	3c	255,75	47,60	1362,82	49,3	5,37
3500	8500	1	3c	372	39,10	1427,02	222,7	9,51
3500	12625	1	3c	1162,5	40,80	1444,32	224,4	28,49
3625	3150	1	3c	255,75	40,80	1242,34	120,7	6,27
3625	7625	1	3c	1278,75	64,60	1495,1	215,9	19,79
3625	7750	1	3c	232,5	52,70	1361,26	49,3	4,41
3625	9150	1	3c	534,75	34,00	1410,02	205,7	15,73
3625	12500	1	3c	604,5	34,00	1453,96	227,8	17,78
3625	12950	1	3c	581,25	57,80	1579,34	348,5	10,06
3625	16000	1	3c	232,5	49,30	1416,14	52,7	4,72
3750	2100	1	3c	1092,75	68,85	1228,01	126,65	15,87
3750	7300	1	3c	1441,5	59,50	1572,8	363,8	24,23
3750	9175	1	3c	581,25	40,80	1421,08	207,4	14,25
3875	650	1	3c	720,75	51,00	1216,64	149,6	14,13
3875	3500	1	3c	418,5	28,90	1248,16	115,6	14,48
3875	7375	1	3c	1348,5	56,10	1588,24	380,8	24,04
3875	7675	1	3c	1023	64,60	1528,1	256,7	15,84
3875	7950	1	3c	674,25	37,40	1380,68	57,8	18,03
3875	10400	1	3c	302,25	52,70	1364,56	146,2	5,74
3875	12600	1	3c	1767	61,20	1467,7	243,1	28,87
3875	15950	1	3c	209,25	34,00	1407,36	40,8	6,15
4000	2250	1	3c	790,5	54,40	1331,44	217,6	14,53
4000	4900	1	3c	651	28,90	1526,28	367,2	22,53
4000	7725	1	3c	1046,25	28,90	1497,52	207,4	36,20
4000	8050	1	3c	674,25	39,10	1378,7	52,7	17,24

(N-S)	X (E-W)	Area	Unit	Width (m)	Height (m)	Depth (mbsl)	Burial depth (m)	W/H ratio
4000	10700	1	3c	558	39,10	1384,82	164,9	14,27
4000	12675	1	3c	1697,25	66,30	1487,96	261,8	25,60
4000	16350	1	3c	418,5	40,80	1404,22	192,1	10,26
4125	550	1	3c	953,25	71,40	1256,32	176,8	13,35
4125	2475	1	3c	906,75	69,70	1343,2	227,8	13,01
4125	3800	1	3c	139,5	28,90	1262,06	113,9	4,83
4125	4700	1	3c	651	39,10	1509,14	348,5	16,65
4125	7250	1	3c	1674	88,40	1604,82	392,7	18,94
4125	10900	1	3c	627,75	44,20	1396,72	176,8	14,20
4125	12325	1	3c	1371,75	39,10	1443,48	214,2	35,08
4125	12750	1	3c	1488	69,70	1494,34	263,5	21,35
4125	16425	1	3c	581,25	61,20	1403,8	187	9,50
4250	1600	1	3c	906,75	32,30	1361,04	255	28,07
4250	1875	1	3c	1557,75	28,90	1204,5	96,9	53,90
4250	3950	1	3c	232,5	28,90	1274,96	119	8,04
4250	4300	1	3c	465	34,00	1388,58	229,5	13,68
4250	6350	1	3c	139,5	22,10	1299,94	100,3	6,31
4250	7575	1	3c	1395	66,30	1610,06	399,5	21,04
4250	8475	1	3c	999,75	20,40	1375,3	49,3	49,01
4250	9725	1	3c	441,75	37,40	1490,5	273,7	11,81
4250	10875	1	3c	418,5	32,30	1493,48	272	12,96
4250	10875	1	3c	302,25	25,50	1493,48	272	11,85
4250	10975	1	3c	604,5	37,40	1386,24	163,2	16,16
4250	12825	1	3c	1674	81,60	1502,28	265,2	20,51
4250	14175	1	3c	418,5	28,90	1370,84	108,8	14,48
4375	2525	1	3c	906,75	57,80	1330,18	202,3	15,69
4375	5150	1	3c	651	37,40	1497,26	317,9	17,41
4375	8100	1	3c	1232,25	54,40	1552,28	323	22,65
4375	8325	1	3c	837	44,20	1430,82	117,3	18,94
4375	8650	1	3c	1023	32,30	1386,92	57,8	31,67
4375	9775	1	3c	488,25	47,60	1496,04	265,2	10,26
4375	11175	1	3c	1185,75	35,70	1382,28	153	33,21
4375	12675	1	3c	2441,25	51,00	1420,4	180,2	47,87
4375	12850	1	3c	1767	79,90	1505,54	266,9	22,12
4375	14175	1	3c	348,75	40,80	1409,16	346,8	8,55
4375	16425	1	3c	627,75	61,20	1404,94	181,9	10,26
4500	2650	1	3c	744	44,20	1337,98	202,3	16,83
4500	4250	1	3c	488,25	47,60	1484,64	316,2	10,26
4500	5650	1	3c	279	35,70	1299,5	113,9	7,82
4500	6725	1	3c	534,75	39,10	1567,7	358,7	13,68
4500	7500	1	3c	1139,25	54,40	1618,42	406,3	20,94
4500	8175	1	3c	1302	40,80	1543,26	270,3	31,91
4500	12975	1	3c	1790,25	88,40	1514,06	256,7	20,25
4500	16350	1	3c	697,5	52,70	1411,32	183,6	13,24
4625	2875	1	3c	697,5	51,00	1331,04	193,8	13,68
4625	3000	1	3c	581,25	35,70	1385,3	246,5	16,28
4625	7050	1	3c	744	56,10	1579,04	363,8	13,26
4625	10625	1	3c	279	25,50	1281,44	27,2	10,94

(N-S)	X (E-W)	Area	Unit	Width (m)	Height (m)	Depth (mbsl)	Burial depth (m)	W/H ratio
4625	11400	1	3c	930	32,30	1383,14	144,5	28,79
4625	13075	1	3c	1999,5	105,40	1520,44	258,4	18,97
4625	14175	1	3c	302,25	71,40	1393,98	86,7	4,23
4625	15300	1	3c	1209	40,80	1471,28	78,2	29,63
4625	16250	1	3c	488,25	45,90	1417,42	181,9	10,64
4625	19325	1	3c	883,5	28,90	1461,6	244,8	30,57
4750	2175	1	3c	1371,75	42,50	1230,16	105,4	32,28
4750	7250	1	3c	860,25	52,70	1589,96	363,8	16,32
4750	8450	1	3c	837	52,70	1611,32	282,2	15,88
4750	8925	1	3c	465	32,30	1457,76	122,4	14,40
4750	10675	1	3c	255,75	28,90	1277,04	30,6	8,85
4750	13050	1	3c	1348,5	42,50	1589,48	282,2	31,73
4750	13075	1	3c	1860	102,00	1520,74	243,1	18,24
4750	14200	1	3c	255,75	66,30	1414,96	95,2	3,86
4750	15000	1	3c	651	27,20	1436,42	52,7	23,93
4750	16200	1	3c	651	57,80	1410,76	44,2	11,26
4875	2350	1	3c	348,75	37,40	1499,76	367,2	9,32
4875	2425	1	3c	511,5	35,70	1446,22	304,3	14,33
4875	4825	1	3c	418,5	37,40	1298,8	105,4	11,19
4875	5950	1	3c	953,25	44,20	1469,8	268,6	21,57
4875	8650	1	3c	279	25,50	1362,42	25,5	10,94
4875	9000	1	3c	976,5	59,50	1474,32	153	16,41
4875	13050	1	3c	1209	71,40	1519,64	210,8	16,93
4875	14100	1	3c	302,25	71,40	1415,26	79,9	4,23
4875	14950	1	3c	441,75	18,70	1429,78	28,9	23,62
4875	17825	1	3c	1116	32,30	1404,94	181,9	34,55
5000	2425	1	3c	1232,25	51,00	1247,74	110,5	24,16
5000	5025	1	3c	255,75	27,20	1298,66	103,7	9,40
5000	6000	1	3c	581,25	44,20	1328,14	120,7	13,15
5000	8550	1	3c	395,25	56,10	1380,54	56,1	7,05
5000	9000	1	3c	697,5	57,80	1484,64	183,6	12,07
5000	9450	1	3c	232,5	37,40	1390,06	39,1	6,22
5000	13175	1	3c	1139,25	64,60	1513,7	195,5	17,64
5000	14700	1	3c	279	17,00	1434,88	34	16,41
5000	15000	1	3c	186	22,10	1426,24	23,8	8,42
5000	17800	1	3c	1255,5	68,00	1446,16	227,8	18,46
5125	1775	1	3c	697,5	40,80	1521,86	389,3	17,10
5125	1875	1	3c	395,25	37,40	1549,48	421,6	10,57
5125	2600	1	3c	558	42,50	1578,26	430,1	13,13
5125	4325	1	3c	674,25	39,10	1572,2	394,4	17,24
5125	4425	1	3c	558	49,30	1657,92	469,2	11,32
5125	6075	1	3c	418,5	45,90	1338,2	129,2	9,12
5125	7725	1	3c	627,75	42,50	1584,76	319,6	14,77
5125	8400	1	3c	372	45,90	1375,02	45,9	8,10
5125	8725	1	3c	1046,25	49,30	1608,06	280,5	21,22
5125	9050	1	3c	790,5	56,10	1502,9	215,9	14,09
5125	9450	1	3c	279	45,90	1393,6	44,2	6,08
5125	13175	1	3c	1371,75	78,20	1545,3	219,3	17,54

(N-S)	X (E-W)	Area	Unit	Width (m)	Height (m)	Depth (mbsl)	Burial depth (m)	W/H ratio
5125	13350	1	3c	534,75	57,80	1647,56	343,4	9,25
5125	13400	1	3c	860,25	62,90	1472,32	166,6	13,68
5125	14500	1	3c	581,25	35,70	1442,96	37,4	16,28
5125	15225	1	3c	1116	49,30	1647,46	304,3	22,64
5125	18125	1	3c	1743,75	76,50	1452,56	210,8	22,79
5125	18650	1	3c	1209	34,00	1369,96	136	35,56
5250	3175	1	3c	302,25	25,50	1250,6	88,4	11,85
5250	5550	1	3c	348,75	37,40	1522,64	323	9,32
5250	7875	1	3c	581,25	45,90	1592,44	299,2	12,66
5250	8275	1	3c	395,25	45,90	1375,3	49,3	8,61
5250	13150	1	3c	558	56,10	1461,7	151,3	9,95
5250	14450	1	3c	418,5	45,90	1454,44	44,2	9,12
5250	15850	1	3c	441,75	28,90	1336,38	107,1	15,29
5250	18175	1	3c	1464,75	59,50	1438,12	187	24,62
5375	1925	1	3c	651	35,70	1541,84	404,6	18,24
5375	6175	1	3c	604,5	54,40	1346,28	132,6	11,11
5375	8150	1	3c	395,25	54,40	1375,3	49,3	7,27
5375	9350	1	3c	325,5	39,10	1491,2	149,6	8,32
5375	9475	1	3c	302,25	34,00	1387,08	40,8	8,89
5375	13075	1	3c	906,75	71,40	1599,7	273,7	12,70
5375	13525	1	3c	930	62,90	1505,94	158,1	14,79
5375	18250	1	3c	837	66,30	1505,26	263,5	12,62
5375	18400	1	3c	1813,5	93,50	1447,46	205,7	19,40
5500	1600	1	3c	1209	64,60	1513,5	382,5	18,72
5500	8075	1	3c	395,25	39,10	1363,54	39,1	10,11
5500	8100	1	3c	372	35,70	1360	34	10,42
5500	9375	1	3c	465	52,70	1509,2	159,8	8,82
5500	9500	1	3c	348,75	37,40	1391,62	39,1	9,32
5500	9525	1	3c	325,5	39,10	1394,88	40,8	8,32
5500	13125	1	3c	1023	54,40	1595,32	258,4	18,81
5500	13675	1	3c	1023	59,50	1518,14	154,7	17,19
5500	18525	1	3c	1488	79,90	1438,96	197,2	18,62
5625	1475	1	3c	1185,75	49,30	1492,4	353,6	24,05
5625	5025	1	3c	1185,75	69,70	1511,74	304,3	17,01
5625	6300	1	3c	674,25	73,10	1379,16	153	9,22
5625	8875	1	3c	930	51,00	1584,92	302,6	18,24
5625	9450	1	3c	627,75	47,60	1498,02	137,7	13,19
5625	9550	1	3c	348,75	40,80	1394,6	37,4	8,55
5625	13125	1	3c	697,5	57,80	1592,08	238	12,07
5625	13550	1	3c	790,5	39,10	1518	153	20,22
5625	13950	1	3c	465	32,30	1462,4	27,2	14,40
5625	18875	1	3c	1069,5	81,60	1449,6	193,8	13,11
5750	1525	1	3c	1185,75	56,10	1499,62	365,5	21,14
5750	5125	1	3c	906,75	78,20	1501,4	292,4	11,60
5750	8925	1	3c	930	54,40	1593,84	316,2	17,10
5750	9400	1	3c	465	39,10	1506,8	149,6	11,89
5750	9600	1	3c	325,5	42,50	1396,44	40,8	7,66
5750	13500	1	3c	1023	103,70	1683,82	253,3	9,86



(N-S)	X (E-W)	Area	Unit	Width (m)	Height (m)	Depth (mbsl)	Burial depth (m)	W/H ratio
5750	13750	1	3c	534,75	37,40	1471,04	37,4	14,30
5750	18925	1	3c	372	98,60	1459,24	197,2	3,77
5875	1350	1	3c	1092,75	47,60	1494,1	355,3	22,96
5875	6125	1	3c	697,5	57,80	1384,54	161,5	12,07
5875	9450	1	3c	395,25	49,30	1522,24	166,6	8,02
5875	9625	1	3c	372	42,50	1396,72	44,2	8,75
5875	13600	1	3c	558	49,30	1481,24	47,6	11,32
5875	18950	1	3c	1278,75	124,10	1475,66	226,1	10,30
6000	1225	1	3c	744	42,50	1485,46	345,1	17,51
6000	5950	1	3c	744	45,90	1375,48	146,2	16,21
6000	9550	1	3c	511,5	45,90	1521,96	163,2	11,14
6000	9750	1	3c	418,5	6,80	1364,14	8,5	61,54
6000	13450	1	3c	488,25	49,30	1483,08	51	9,90
6000	19025	1	3c	1232,25	113,90	1479,06	229,5	10,82
6125	1125	1	3c	581,25	44,20	1527,24	397,8	13,15
6125	1200	1	3c	953,25	40,80	1477,52	343,4	23,36
6125	5400	1	3c	441,75	35,70	1514,46	280,5	12,37
6125	5500	1	3c	348,75	22,10	1547,04	316,2	15,78
6125	5525	1	3c	767,25	39,10	1462,04	231,2	19,62
6125	6575	1	3c	395,25	23,80	1555,98	311,1	16,61
6125	9650	1	3c	441,75	32,30	1513,32	153	13,68
6125	9875	1	3c	488,25	51,00	1403,52	51	9,57
6125	9875	1	3c	465	42,50	1403,1	45,9	10,94
6125	12825	1	3c	348,75	42,50	1682,8	278,8	8,21
6125	13175	1	3c	720,75	74,80	1620,64	187	9,64
6125	13175	1	3c	558	40,80	1476,56	47,6	13,68
6125	13475	1	3c	604,5	45,90	1670,22	239,7	13,17
6125	19125	1	3c	1116	119,00	1489,54	243,1	9,38
6250	1100	1	3c	651	44,20	1528,94	399,5	14,73
6250	1125	1	3c	1116	49,30	1473,98	338,3	22,64
6250	5325	1	3c	511,5	47,60	1518	285,6	10,75
6250	5700	1	3c	1069,5	39,10	1387,24	156,4	27,35
6250	6075	1	3c	651	42,50	1549,6	309,4	15,32
6250	9675	1	3c	534,75	52,70	1514,46	147,9	10,15
6250	10050	1	3c	325,5	37,40	1397,86	39,1	8,70
6250	13025	1	3c	488,25	52,70	1484,08	44,2	9,26
6250	13300	1	3c	534,75	64,60	1657,9	222,7	8,28
6250	19125	1	3c	1185,75	110,50	1475,94	229,5	10,73
6375	4725	2	3c	627,75	49,30	1318,66	100,3	12,73
6375	5400	2	3c	581,25	47,60	1525,08	295,8	12,21
6375	5675	2	3c	1162,5	44,20	1386,54	147,9	26,30
6375	6125	2	3c	581,25	49,30	1559,24	312,8	11,79
6375	7350	2	3c	465	39,10	1406,44	105,4	11,89
6375	7550	2	3c	744	45,90	1619,08	319,6	16,21
6375	7800	2	3c	558	49,30	1508,44	207,4	11,32
6375	9125	2	3c	953,25	44,20	1633,1	338,3	21,57
6375	9200	2	3c	581,25	44,20	1636,64	343,4	13,15
6375	9700	2	3c	255,75	39,10	1620,14	256,7	6,54

(N-S)	X (E-W)	Area	Unit	Width (m)	Height (m)	Depth (mbsl)	Burial depth (m)	W/H ratio
6375	10100	2	3c	372	49,30	1412,74	49,3	7,55
6375	12775	2	3c	604,5	68,00	1501,5	66,3	8,89
6375	13225	2	3c	813,75	45,90	1598,34	219,3	17,73
6375	19200	2	3c	1023	112,20	1483,18	222,7	9,12
6500	4700	2	3c	604,5	39,10	1314,98	93,5	15,46
6500	5050	2	3c	627,75	42,50	1355,22	127,5	14,77
6500	5500	2	3c	930	56,10	1512,48	275,4	16,58
6500	5550	2	3c	953,25	51,00	1386,54	147,9	18,69
6500	5775	2	3c	441,75	30,60	1563,2	323	14,44
6500	9150	2	3c	744	42,50	1632,82	334,9	17,51
6500	9825	2	3c	441,75	45,90	1526,62	181,9	9,62
6500	9975	2	3c	744	45,90	1669,16	302,6	16,21
6500	10150	2	3c	348,75	54,40	1416,14	52,7	6,41
6500	12725	2	3c	511,5	71,40	1517,94	76,5	7,16
6500	13125	2	3c	558	40,00	1610,04	285,6	13,95
6500	13225	2	3c	813,75	40,80	1608,9	290,7	19,94
6500	14600	2	3c	279	40,80	1605,9	311,1	6,84
6500	19225	2	3c	1092,75	107,10	1475,96	210,8	10,20
6625	5350	2	3c	1069,5	51,00	1379,88	142,8	20,97
6625	9875	2	3c	441,75	42,50	1528,88	190,4	10,39
6625	10200	2	3c	372	52,70	1416,14	52,7	7,06
6625	12525	2	3c	372	45,90	1488,76	44,2	8,10
6625	13125	2	3c	604,5	56,10	1678,04	353,6	10,78
6625	19200	2	3c	418,5	61,20	1566,06	300,9	6,84
6625	19300	2	3c	1116	102,00	1474,68	214,2	10,94
6750	775	2	3c	488,25	49,30	1487,46	331,5	9,90
6750	5450	2	3c	441,75	34,00	1528,5	280,5	12,99
6750	9275	2	3c	581,25	45,90	1644,3	341,7	12,66
6750	9975	2	3c	790,5	25,50	1501,68	163,2	31,00
6750	10250	2	3c	488,25	54,40	1417,56	51	8,98
6750	12450	2	3c	255,75	54,40	1501,94	52,7	4,70
6750	14600	2	3c	465	35,70	1370,04	61,2	13,03
6750	19300	2	3c	883,5	85,00	1477,8	214,2	10,39
6875	775	2	3c	418,5	59,50	1492,86	321,3	7,03
6875	5275	2	3c	1046,25	44,20	1374,36	132,6	23,67
6875	10025	2	3c	813,75	28,90	1504,4	139,4	28,16
6875	10250	2	3c	441,75	47,60	1417	44,2	9,28
6875	12475	2	3c	372	56,10	1499,64	81,6	6,63
6875	13100	2	3c	953,25	54,40	1613,58	290,7	17,52
6875	19300	2	3c	930	76,50	1475,96	210,8	12,16
7000	5450	2	3c	651	45,90	1559,1	311,1	14,18
7000	10400	2	3c	581,25	47,60	1417,56	51	12,21
7000	12450	2	3c	348,75	40,80	1499,78	83,3	8,55
7000	13025	2	3c	860,25	56,10	1630,72	309,4	15,33
7000	14425	2	3c	418,5	28,90	1591,88	292,4	14,48
7000	14550	2	3c	441,75	34,00	1405,16	108,8	12,99
7000	14650	2	3c	255,75	25,50	1514,54	205,7	10,03
7000	14925	2	3c	395,25	23,80	1378,98	56,1	16,61

(N-S)	X (E-W)	Area	Unit	Width (m)	Height (m)	Depth (mbsl)	Burial depth (m)	W/H ratio
7000	19275	2	3c	418,5	71,40	1567,2	295,8	5,86
7000	19325	2	3c	883,5	110,50	1498,06	232,9	8,00
7125	1000	2	3c	558	42,50	1372,78	151,3	13,13
7125	5375	2	3c	1116	56,10	1385	129,2	19,89
7125	5425	2	3c	674,25	56,10	1563,78	311,1	12,02
7125	8025	2	3c	627,75	32,30	1602,1	283,9	19,43
7125	9650	2	3c	860,25	49,30	1652,52	346,8	17,45
7125	10250	2	3c	511,5	47,60	1548,6	183,6	10,75
7125	10325	2	3c	744	28,90	1494,2	129,2	25,74
7125	10625	2	3c	581,25	73,10	1449,3	76,5	7,95
7125	12450	2	3c	279	57,80	1523,56	125,8	4,83
7125	14600	2	3c	651	23,80	1406,3	103,7	27,35
7125	19300	2	3c	813,75	100,30	1488,86	215,9	8,11
7125	19325	2	3c	441,75	52,70	1548,08	272	8,38
7250	5375	2	3c	1395	45,90	1386,56	129,2	30,39
7250	9725	2	3c	1232,25	61,20	1664,14	355,3	20,13
7250	10375	2	3c	860,25	61,20	1549,86	198,9	14,06
7250	10725	2	3c	604,5	52,70	1437,98	52,7	11,47
7250	12975	2	3c	906,75	62,90	1620,38	297,5	14,42
7250	14700	2	3c	372	23,80	1420,18	120,7	15,63
7250	15075	2	3c	279	32,30	1399,38	76,5	8,64
7250	19300	2	3c	511,5	54,40	1550,92	268,6	9,40
7250	19375	2	3c	813,75	93,50	1485,46	212,5	8,70
7375	5475	2	3c	1023	47,60	1381,18	120,7	21,49
7375	9700	2	3c	1464,75	71,40	1673,78	358,7	20,51
7375	10400	2	3c	1046,25	56,10	1546,04	190,4	18,65
7375	10850	2	3c	1627,5	68,00	1454,42	62,9	23,93
7375	12475	2	3c	418,5	51,00	1497,2	108,8	8,21
7375	14525	2	3c	767,25	35,70	1430,38	130,9	21,49
7375	15200	2	3c	325,5	37,40	1368,64	44,2	8,70
7375	19400	2	3c	837	91,80	1490,7	219,3	9,12
7500	1100	2	3c	511,5	49,30	1414	197,2	10,38
7500	5025	2	3c	813,75	28,90	1457,82	198,9	28,16
7500	5600	2	3c	1092,75	51,00	1386,14	124,1	21,43
7500	7900	2	3c	488,25	44,20	1557,34	232,9	11,05
7500	9700	2	3c	1371,75	59,50	1671,38	348,5	23,05
7500	10500	2	3c	930	47,60	1537,68	183,6	19,54
7500	10950	2	3c	488,25	59,50	1452,44	57,8	8,21
7500	12550	2	3c	465	88,40	1541,84	139,4	5,26
7500	12950	2	3c	697,5	69,70	1695,04	370,6	10,01
7500	12975	2	3c	1023	69,70	1634,12	312,8	14,68
7500	13025	2	3c	1185,75	79,90	1560,88	238	14,84
7500	14750	2	3c	511,5	90,10	1477,98	178,5	5,68
7500	19350	2	3c	558	69,70	1572,46	283,9	8,01
7500	19400	2	3c	790,5	102,00	1495,24	217,6	7,75
7625	1250	2	3c	651	44,20	1330,26	127,5	14,73
7625	1275	2	3c	627,75	47,60	1416,68	210,8	13,19
7625	4975	2	3c	953,25	32,30	1456,26	198,9	29,51

(N-S)	X (E-W)	Area	Unit	Width (m)	Height (m)	Depth (mbsl)	Burial depth (m)	W/H ratio
7625	6125	2	3c	348,75	28,90	1538,8	197,2	12,07
7625	9875	2	3c	1511,25	64,60	1669,68	346,8	23,39
7625	10500	2	3c	558	37,40	1546,62	178,5	14,92
7625	11050	2	3c	581,25	66,30	1462,78	69,7	8,77
7625	12475	2	3c	395,25	66,30	1534,54	69,7	5,96
7625	13000	2	3c	1046,25	54,40	1567,12	238	19,23
7625	14750	2	3c	697,5	37,40	1423,58	124,1	18,65
7625	19400	2	3c	813,75	95,20	1494,68	210,8	8,55
7750	1300	2	3c	604,5	54,40	1335,36	132,6	11,11
7750	5225	2	3c	1046,25	35,70	1360,22	93,5	29,31
7750	5562,5	2	3c	488,25	32,30	1536,26	185,3	15,12
7750	9775	2	3c	1278,75	62,90	1676,06	348,5	20,33
7750	11075	2	3c	604,5	69,70	1468,02	76,5	8,67
7750	12475	2	3c	441,75	78,20	1535,24	78,2	5,65
7750	13025	2	3c	1441,5	78,20	1560,32	231,2	18,43
7750	14825	2	3c	790,5	57,80	1449,08	149,6	13,68
7750	19375	2	3c	744	91,80	1492,28	200,6	8,10
7875	1350	2	3c	720,75	47,60	1348,96	146,2	15,14
7875	6225	2	3c	511,5	18,70	1533,56	190,4	27,35
7875	12425	2	3c	395,25	81,60	1537,22	83,3	4,84
7875	14650	2	3c	906,75	64,60	1476	173,4	14,04
7875	19275	2	3c	418,5	10,20	1521,9	219,3	41,03
7875	19375	2	3c	767,25	115,60	1507,02	209,1	6,64
8000	950	2	3c	465	47,60	1473,06	270,3	9,77
8000	1350	2	3c	744	42,50	1351,22	154,7	17,51
8000	7325	2	3c	465	30,60	1460,16	132,6	15,20
8000	7800	2	3c	372	22,10	1536,8	210,8	16,83
8000	8050	2	3c	441,75	27,20	1579,02	249,9	16,24
8000	9625	2	3c	767,25	42,50	1686,42	341,7	18,05
8000	12900	2	3c	930	124,10	1703,4	377,4	7,49
8000	14825	2	3c	1023	44,20	1475,86	171,7	23,14
8000	19325	2	3c	813,75	130,90	1526,44	217,6	6,22
8125	7500	2	3c	604,5	32,30	1461,86	134,3	18,72
8125	9750	2	3c	883,5	37,40	1693,76	374	23,62
8125	12300	2	3c	534,75	73,10	1533,12	71,4	7,32
8125	12900	2	3c	953,25	103,70	1700,72	363,8	9,19
8125	14900	2	3c	1116	45,90	1489,46	185,3	24,31
8125	19250	2	3c	488,25	71,40	1587,22	273,7	6,84
8125	19275	2	3c	720,75	88,40	1499,24	190,4	8,15
8250	1000	2	3c	465	64,60	1496,86	294,1	7,20
8250	7475	2	3c	697,5	28,90	1456,76	129,2	24,13
8250	11900	2	3c	418,5	44,20	1758,08	302,6	9,47
8250	12900	2	3c	999,75	93,50	1691,94	351,9	10,69
8250	14675	2	3c	1139,25	56,10	1496,12	190,4	20,31
8250	19225	2	3c	441,75	76,50	1604,92	299,2	5,77
8250	19250	2	3c	744	98,60	1501,92	204	7,55
8375	12275	2	3c	534,75	71,40	1540,78	69,7	7,49
8375	12850	2	3c	1092,75	107,10	1692,08	353,6	10,20

(N-S)	X (E-W)	Area	Unit	Width (m)	Height (m)	Depth (mbsl)	Burial depth (m)	W/H ratio
8375	14875	2	3c	1209	66,30	1507,46	195,5	18,24
8375	19225	2	3c	372	68,00	1589,2	278,8	5,47
8375	19250	2	3c	813,75	91,80	1495,68	204	8,86
8500	7475	2	3c	488,25	52,70	1475,9	134,3	9,26
8500	8225	2	3c	418,5	37,40	1629,04	289	11,19
8500	10150	2	3c	1185,75	35,70	1672,02	280,5	33,21
8500	10325	2	3c	1092,75	73,10	1754,9	358,7	14,95
8500	12275	2	3c	511,5	68,00	1538,94	66,3	7,52
8500	12850	2	3c	1185,75	117,30	1698,46	355,3	10,11
8500	15050	2	3c	1395	96,90	1530,84	214,2	14,40
8500	19225	2	3c	767,25	76,50	1486,9	192,1	10,03
8625	10350	2	3c	1278,75	69,70	1732,94	338,3	18,35
8625	12150	2	3c	604,5	66,30	1538,38	59,5	9,12
8625	19275	2	3c	790,5	78,20	1471,6	176,8	10,11
8750	1800	2	3c	1371,75	32,30	1341,34	110,5	42,47
8750	7625	2	3c	860,25	40,80	1472,5	130,9	21,08
8750	10375	2	3c	1418,25	69,70	1707,02	307,7	20,35
8750	12250	2	3c	581,25	54,40	1539,38	52,7	10,68
8750	15075	2	3c	1185,75	88,40	1521,22	192,1	13,41
8750	19175	2	3c	976,5	83,30	1481,66	185,3	11,72
8875	1825	2	3c	488,25	47,60	1356,78	127,5	10,26
8875	7700	2	3c	674,25	47,60	1491,06	147,9	14,16
8875	12875	2	3c	1395	96,90	1693,1	328,1	14,40
8875	15150	2	3c	1278,75	113,90	1553,24	221	11,23
8875	18925	2	3c	976,5	113,90	1517,08	217,6	8,57
8875	18950	2	3c	558	62,90	1569,22	263,5	8,87
9000	1875	2	3c	534,75	35,70	1348,56	122,4	14,98
9000	7675	2	3c	534,75	42,50	1482	132,6	12,58
9000	12275	2	3c	534,75	64,60	1545,32	68	8,28
9000	12900	2	3c	930	62,90	1695,22	334,9	14,79
9000	15175	2	3c	1139,25	88,40	1518,96	183,6	12,89
9000	18850	2	3c	976,5	88,40	1489,04	180,2	11,05
9125	12425	2	3c	604,5	54,40	1539,66	56,1	11,11
9125	12825	2	3c	1046,25	79,90	1698,76	340	13,09
9125	15225	2	3c	1488	85,00	1515,7	181,9	17,51
9125	18700	2	3c	1046,25	79,90	1503,64	187	13,09
9125	18700	2	3c	697,5	49,30	1562,58	239,7	14,15
9250	11475	2	3c	581,25	37,40	1540,4	159,8	15,54
9250	12400	2	3c	488,25	52,70	1541,5	59,5	9,26
9250	12850	2	3c	1116	56,10	1697,92	329,8	19,89
9250	15225	2	3c	1348,5	62,90	1516,56	173,4	21,44
9250	18525	2	3c	837	68,00	1572,22	243,1	12,31
9250	18925	2	3c	1092,75	52,70	1477,58	154,7	20,74
9375	1350	2	3c	674,25	20,40	1349,14	110,5	33,05
9375	11425	2	3c	558	45,90	1543,94	164,9	12,16
9375	12425	2	3c	395,25	56,10	1542,92	57,8	7,05
9375	12825	2	3c	1185,75	102,00	1714,5	341,7	11,63
9375	15250	2	3c	1418,25	78,20	1514,58	168,3	18,14

(N-S)	X (E-W)	Area	Unit	Width (m)	Height (m)	Depth (mbsl)	Burial depth (m)	W/H ratio
9375	18600	2	3c	953,25	83,30	1492,46	164,9	11,44
9500	1400	2	3c	860,25	28,90	1367,7	127,5	29,77
9500	7675	2	3c	767,25	47,60	1483,56	132,6	16,12
9500	12375	2	3c	395,25	52,70	1534,42	49,3	7,50
9500	12800	2	3c	1232,25	113,90	1717,06	334,9	10,82
9500	15325	2	3c	1464,75	81,60	1521,1	171,7	17,95
9500	18750	2	3c	1023	78,20	1496,28	173,4	13,08
9625	1375	2	3c	581,25	39,10	1364,3	124,1	14,87
9625	6250	2	3c	534,75	28,90	1593,34	253,3	18,50
9625	12225	2	3c	534,75	68,00	1544,04	71,4	7,86
9625	12725	2	3c	1441,5	100,30	1696,66	314,5	14,37
9625	15350	2	3c	1139,25	88,40	1524,78	178,5	12,89
9625	15825	2	3c	744	79,90	1837,3	487,9	9,31
9625	15975	2	3c	883,5	64,60	1738,7	389,3	13,68
9625	18475	2	3c	953,25	51,00	1468,24	136	18,69
9750	625	2	3c	348,75	20,40	1352,84	98,6	17,10
9750	2050	2	3c	395,25	39,10	1376,64	122,4	10,11
9750	12150	2	3c	465	59,50	1544,06	52,7	7,82
9750	15425	2	3c	953,25	73,10	1513,6	156,4	13,04
9750	18550	2	3c	651	61,20	1483,12	146,2	10,64
9875	12050	2	3c	511,5	62,90	1554,96	71,4	8,13
9875	12100	2	3c	441,75	51,00	1547,46	56,1	8,66
9875	12200	2	3c	488,25	59,50	1652,72	159,8	8,21
9875	12700	2	3c	1046,25	93,50	1725	336,6	11,19
9875	15600	2	3c	813,75	69,70	1513,6	156,4	11,68
9875	15725	2	3c	534,75	32,30	1705,28	343,4	16,56
9875	15950	2	3c	813,75	119,00	1861,54	498,1	6,84
9875	16025	2	3c	976,5	78,20	1745,94	382,5	12,49
9875	17575	2	3c	372	32,30	1505,68	136	11,52
9875	18000	2	3c	627,75	47,60	1720,14	372,3	13,19
9875	18200	2	3c	674,25	51,00	1669,58	307,7	13,22
9875	18250	2	3c	837	56,10	1781,2	431,8	14,92
9875	18650	2	3c	744	73,10	1498,28	159,8	10,18
10000	575	2	3c	232,5	40,80	1437,28	176,8	5,70
10000	675	2	3c	581,25	49,30	1389,96	132,6	11,79
10000	12100	2	3c	488,25	54,40	1553,12	68	8,98
10000	12650	2	3c	1348,5	95,20	1712,82	321,3	14,16
10000	15600	2	3c	697,5	44,20	1500,86	134,3	15,78
10000	17425	2	3c	837	59,50	1522,54	151,3	14,07
10000	18700	2	3c	348,75	52,70	1464,86	113,9	6,62
10125	525	2	3c	325,5	39,10	1435,72	176,8	8,32
10125	2350	2	3c	441,75	52,70	1524,14	246,5	8,38
10125	7025	2	3c	1139,25	28,90	1466,14	110,5	39,42
10125	7450	2	3c	651	44,20	1598,88	244,8	14,73
10125	12075	2	3c	558	52,70	1549,02	56,1	10,59
10125	12600	2	3c	1418,25	85,00	1708,86	311,1	16,69
10125	12625	2	3c	1348,5	93,50	1703,06	164,9	14,42
10125	17525	2	3c	813,75	56,10	1534,02	158,1	14,51

(N-S)	X (E-W)	Area	Unit	Width (m)	Height (m)	Depth (mbsl)	Burial depth (m)	W/H ratio
10250	600	2	3c	906,75	45,90	1384,72	125,8	19,75
10250	2275	2	3c	441,75	68,00	1552,62	270,3	6,50
10250	3425	2	3c	441,75	27,20	1608,42	341,7	16,24
10250	12575	2	3c	999,75	45,90	1699,52	292,4	21,78
10250	17500	2	3c	906,75	74,80	1547,34	168,3	12,12
10375	525	2	3c	790,5	37,40	1379,48	119	21,14
10375	1850	2	3c	534,75	35,70	1408,68	132,6	14,98
10375	2625	2	3c	325,5	27,20	1401,34	100,3	11,97
10375	10425	2	3c	1836,75	59,50	1731,92	363,8	30,87
10375	11950	2	3c	488,25	66,30	1562,62	69,7	7,36
10375	12575	2	3c	1116	61,20	1719,64	309,4	18,24
10375	17525	2	3c	930	81,60	1560,52	176,8	11,40
10500	1800	2	3c	511,5	56,10	1429,22	154,7	9,12
10500	2225	2	3c	465	73,10	1554,74	277,1	6,36
10500	2725	2	3c	418,5	37,40	1417,06	120,7	11,19
10500	12000	2	3c	441,75	69,70	1565,6	68	6,34
10500	17475	2	3c	1069,5	79,90	1561,22	185,3	13,39
10625	2200	2	3c	488,25	39,10	1542,42	260,1	12,49
10625	17475	2	3c	1302	76,50	1573,98	188,7	17,02
10750	2225	2	3c	488,25	42,50	1549,64	272	11,49
10750	2775	2	3c	418,5	42,50	1418,76	122,4	9,85
10750	11850	2	3c	441,75	56,10	1558,38	56,1	7,87
10750	12675	2	3c	976,5	45,90	1704,92	282,2	21,27
10750	17275	2	3c	1302	64,60	1571,86	181,9	20,15
10875	1175	2	3c	697,5	34,00	1420,22	83,3	20,51
10875	2125	2	3c	906,75	44,20	1531,8	244,8	20,51
10875	2825	2	3c	418,5	25,50	1412,96	108,8	16,41
10875	11350	2	3c	627,75	47,60	1754,24	312,8	13,19
10875	11950	2	3c	418,5	52,70	1570	64,6	7,94
10875	12725	2	3c	1162,5	47,60	1707,76	278,8	24,42
10875	17200	2	3c	1325,25	86,70	1597,8	193,8	15,29
11000	1150	2	3c	813,75	57,80	1466,7	117,3	14,08
11000	2250	2	3c	1371,75	44,20	1531,1	236,3	31,04
11000	11775	2	3c	348,75	45,90	1552,58	42,5	7,60
11000	12725	2	3c	906,75	49,30	1706,34	280,5	18,39
11000	13275	2	3c	534,75	47,60	1603,78	171,7	11,23
11125	11675	2	3c	325,5	45,90	1552,72	44,2	7,09
11125	12750	2	3c	860,25	37,40	1712,74	263,5	23,00
11125	17175	2	3c	1488	69,70	1575,7	171,7	21,35
11250	7100	2	3c	627,75	35,70	1585,46	195,5	17,58
11250	11800	2	3c	372	52,70	1562,78	52,7	7,06
11250	12750	2	3c	999,75	69,70	1718,84	261,8	14,34
11250	17175	2	3c	1069,5	57,80	1555,86	158,1	18,50
11375	1350	2	3c	534,75	54,4	1467,3	86,7	9,83
11375	7075	2	3c	581,25	40,8	1585,6	197,2	14,25
11375	11800	2	3c	418,5	62,9	1574,68	64,6	6,65
11500	1500	2	3c	558	147,9	1530,48	153	3,77
11500	2325	2	3c	1046,25	37,4	1615,98	300,9	27,97

(N-S)	X (E-W)	Area	Unit	Width (m)	Height (m)	Depth (mbsl)	Burial depth (m)	W/H ratio
11500	2550	2	3c	581,25	54,4	1586,8	268,6	10,68
11500	11825	2	3c	325,5	47,6	1568,3	62,9	6,84
11500	17250	2	3c	1418,25	68	1562,38	161,5	20,86
11625	2225	2	3c	1162,5	47,6	1565,98	243,1	24,42
11625	2350	2	3c	1418,25	56,1	1643,9	317,9	25,28
11625	6700	2	3c	465	40,8	1504,58	103,7	11,40
11625	11575	2	3c	581,25	110,5	1500,72	125	5,26
11625	11725	2	3c	511,5	68	1575,1	69,7	7,52
11625	13625	2	3c	883,5	40,8	1605,5	154,7	21,65
11625	17375	2	3c	953,25	64,6	1566,06	168,3	14,76
11750	1600	2	3c	534,75	42,5	1456,96	74,8	12,58
11750	2275	2	3c	1371,75	49,3	1573,94	226,1	27,82
11750	2425	2	3c	1302	40,8	1623,66	280,5	31,91
11750	6725	2	3c	441,75	34	1493,54	83,3	12,99
11750	8925	2	3c	744	30,6	1535,34	117,3	24,31
11750	11750	2	3c	488,25	68	1572,98	62,9	7,18
11750	13550	2	3c	860,25	42,5	1612,02	158,1	20,24
11750	15375	2	3c	511,5	28,9	1554,6	142,8	17,70
11750	16575	2	3c	372	23,8	1532,66	103,7	15,63
11750	17475	2	3c	813,75	42,5	1563,1	151,3	19,15
11875	1750	2	3c	511,5	51	1468,02	76,5	10,03
11875	1975	2	3c	767,25	39,1	1629,06	270,3	19,62
11875	2300	2	3c	1092,75	57,8	1592,92	248,2	18,91
11875	7000	2	3c	790,5	40,8	1509,54	107,1	19,38
11875	7400	2	3c	697,5	32,3	1573,86	168,3	21,59
11875	8650	2	3c	1023	39,1	1722,2	302,6	26,16
11875	11800	2	3c	534,75	83,3	1580,76	81,6	6,42
11875	16575	2	3c	395,25	27,2	1547,54	113,9	14,53
12000	1775	2	3c	558	61,2	1493,52	102	9,12
12000	2275	2	3c	767,25	54,4	1641,96	275,4	14,10
12000	2600	2	3c	1139,25	56,1	1599,58	253,3	20,31
12000	3425	2	3c	534,75	45,9	1464,62	73,1	11,65
12000	3500	2	3c	860,25	42,5	1465,84	125,8	20,24
12000	4875	2	3c	2232	27,2	1563,84	255	82,06
12000	7200	2	3c	837	40,8	1505,86	100,3	20,51
12000	9000	2	3c	999,75	40,8	1555,6	136	24,50
12000	13675	2	3c	837	47,6	1599,84	142,8	17,58
12000	15250	2	3c	697,5	25,5	1547,52	132,6	27,35
12000	15450	2	3c	534,75	49,3	1627,42	212,5	10,85
12000	16625	2	3c	418,5	35,7	1559,44	125,8	11,72
12000	17550	2	3c	720,75	54,4	1539,72	132,6	13,25
12125	2600	2	3c	1092,75	57,8	1609,5	260,1	18,91
12125	13925	2	3c	1046,25	44,2	1598	139,4	23,67
12125	16800	2	3c	1604,25	37,4	1557,32	119	42,89
12125	18700	2	3c	348,75	56,1	1464,78	56,1	6,22
12250	1825	2	3c	604,5	51	1467,88	74,8	11,85
12250	2275	2	3c	744	73,1	1658,82	290,7	10,18
12250	2525	2	3c	1371,75	57,8	1599,6	234,6	23,73



(N-S)	X (E-W)	Area	Unit	Width (m)	Height (m)	Depth (mbsl)	Burial depth (m)	W/H ratio
12250	3475	2	3c	604,5	32,3	1475,62	130,9	18,72
12250	12200	2	3c	697,5	64,6	1592,1	86,7	10,80
12250	14275	2	3c	976,5	47,6	1601,26	141,1	20,51
12250	16925	2	3c	1348,5	51	1574,46	137,7	26,44
12250	18675	2	3c	534,75	54,4	1486,18	69,7	9,83
12375	1900	2	3c	558	52,7	1469,44	74,8	10,59
12375	2450	2	3c	1162,5	115,6	1713,34	365,5	10,06
12375	2650	2	3c	1395	35,7	1579,04	231,2	39,08
12375	3500	2	3c	418,5	37,4	1481	139,4	11,19
12375	12475	2	3c	813,75	47,6	1590,44	47,6	17,10
12375	14525	2	3c	1092,75	47,6	1595,74	130,9	22,96
12375	16900	2	3c	906,75	30,6	1594,72	156,4	29,63
12500	1900	2	3c	465	54,4	1478,08	85	8,55
12500	2650	2	3c	1162,5	107,1	1711,08	357	10,85
12500	2750	2	3c	1185,75	35,7	1577,34	229,5	33,21
12500	3600	2	3c	348,75	25,5	1447,28	108,8	13,68
12500	8675	2	3c	558	32,3	1722,36	285,6	17,28
12500	9600	2	3c	395,25	37,4	1788,64	370,6	10,57
12500	12625	2	3c	837	34	1586,62	39,1	24,62
12500	14600	2	3c	1046,25	45,9	1585,82	124,1	22,79
12500	17125	2	3c	1046,25	57,8	1622,48	190,4	18,10
12625	1900	3	3c	395,25	40,80	1457,4	61,2	9,69
12625	2575	3	3c	1209	105,40	1708,96	350,2	11,47
12625	2775	3	3c	1464,75	51,00	1586,28	224,4	28,72
12625	15075	3	3c	1023	61,20	1610,9	144,5	16,72
12625	17125	3	3c	1023	66,30	1625,18	185,3	15,43
12625	18625	3	3c	395,25	62,90	1527,84	102	6,28
12750	1975	3	3c	372	47,60	1462,36	64,6	7,82
12750	2575	3	3c	1162,5	83,30	1698,76	340	13,96
12750	2800	3	3c	1302	45,90	1589,66	246,5	28,37
12750	14950	3	3c	953,25	71,40	1615,86	147,9	13,35
12750	15400	3	3c	953,25	56,10	1650,3	168,3	16,99
12750	17100	3	3c	1162,5	68,00	1630,56	193,8	17,10
12750	18500	3	3c	348,75	59,50	1532,8	105,4	5,86
12875	2175	3	3c	604,5	51,00	1489,56	91,8	11,85
12875	2725	3	3c	1139,25	103,70	1714,92	346,8	10,99
12875	2875	3	3c	1418,25	37,40	1577,8	197,2	37,92
12875	15175	3	3c	744	66,30	1606,94	134,3	11,22
12875	15525	3	3c	976,5	78,20	1678,22	185,3	12,49
12875	17100	3	3c	1092,75	88,40	1655,22	209,1	12,36
12875	18475	3	3c	418,5	76,50	1544,84	119	5,47
13000	2100	3	3c	674,25	68,00	1486,16	88,4	9,92
13000	2825	3	3c	1511,25	49,30	1586,18	185,3	30,65
13000	2850	3	3c	1278,75	113,90	1727,14	324,7	11,23
13000	13325	3	3c	418,5	47,60	1596,12	40,8	8,79
13000	15375	3	3c	813,75	59,50	1588,1	113,9	13,68
13000	15575	3	3c	1302	88,40	1699,04	210,8	14,73
13000	17075	3	3c	1162,5	119,00	1689,5	246,5	9,77

(N-S)	X (E-W)	Area	Unit	Width (m)	Height (m)	Depth (mbsl)	Burial depth (m)	W/H ratio
13000	18450	3	3c	651	85,00	1565,24	139,4	7,66
13125	2150	3	3c	627,75	44,20	1490,84	88,4	14,20
13125	2675	3	3c	1209	100,30	1707,46	294,1	12,05
13125	2900	3	3c	1395	39,10	1575,28	166,6	35,68
13125	8675	3	3c	767,25	28,90	1568,38	120,7	26,55
13125	15625	3	3c	1348,5	71,40	1688,42	195,5	18,89
13125	17150	3	3c	1092,75	110,50	1682,42	236,3	9,89
13125	18450	3	3c	488,25	93,50	1573,6	146,2	5,22
13250	2775	3	3c	1278,75	122,40	1571,46	158,1	10,45
13250	2775	3	3c	1139,25	85,00	1706,04	295,8	13,40
13250	8650	3	3c	697,5	23,80	1561,44	112,2	29,31
13250	13500	3	3c	302,25	44,20	1609,7	73,1	6,84
13250	15150	3	3c	720,75	54,40	1603,4	129,2	13,25
13250	15675	3	3c	1069,5	74,80	1695,92	210,8	14,30
13250	17075	3	3c	883,5	81,60	1683,84	234,6	10,83
13250	17425	3	3c	767,25	34,00	1783,72	329,8	22,57
13250	18350	3	3c	558	85,00	1563,12	132,6	6,56
13375	2375	3	3c	1092,75	44,20	1509,12	102	24,72
13375	2850	3	3c	1302	57,80	1584,06	178,5	22,53
13375	2900	3	3c	1185,75	79,90	1705,04	302,6	14,84
13375	8525	3	3c	767,25	42,50	1611,88	156,4	18,05
13375	11050	3	3c	767,25	64,60	1838,42	368,9	11,88
13375	12375	3	3c	1139,25	45,90	1831,58	266,9	24,82
13375	15750	3	3c	1116	68,00	1702,72	217,6	16,41
13375	17200	3	3c	674,25	62,90	1685,82	239,7	10,72
13375	17425	3	3c	767,25	49,30	1796,32	350,2	15,56
13375	18525	3	3c	372	54,40	1533,38	93,5	6,84
13500	2450	3	3c	1023	54,40	1525,7	113,9	18,81
13500	2825	3	3c	1627,5	56,10	1577,26	171,7	29,01
13500	2875	3	3c	1255,5	108,80	1724,02	324,7	11,54
13500	8475	3	3c	860,25	42,50	1618,68	163,2	20,24
13500	17100	3	3c	581,25	42,50	1734,56	282,2	13,68
13500	17450	3	3c	744	52,70	1804,54	355,3	14,12
13625	2750	3	3c	697,5	30,60	1501,04	98,6	22,79
13625	2800	3	3c	1511,25	44,20	1582,78	181,9	34,19
13625	2800	3	3c	1302	139,40	1767,52	360,4	9,34
13625	8325	3	3c	813,75	57,80	1635,4	176,8	14,08
13625	12125	3	3c	418,5	56,10	1681,6	74,8	7,46
13625	16100	3	3c	1581	57,80	1693,9	243,1	27,35
13625	16950	3	3c	1046,25	20,40	1587,08	139,4	51,29
13625	17475	3	3c	744	42,50	1814,6	363,8	17,51
13625	18575	3	3c	255,75	40,80	1536,52	74,8	6,27
13750	2150	3	3c	651	35,70	1511,68	95,2	18,24
13750	2900	3	3c	1325,25	93,50	1721,48	312,8	14,17
13750	2925	3	3c	1348,5	37,40	1575,42	168,3	36,06
13750	8300	3	3c	837	59,50	1641,92	180,2	14,07
13750	11975	3	3c	325,5	59,50	1676,94	56,1	5,47
13750	16250	3	3c	1325,25	40,80	1712,46	260,1	32,48

(N-S)	X (E-W)	Area	Unit	Width (m)	Height (m)	Depth (mbsl)	Burial depth (m)	W/H ratio
13750	16975	3	3c	860,25	28,90	1577,6	119	29,77
13750	17500	3	3c	813,75	52,70	1811,78	348,5	15,44
13750	18250	3	3c	302,25	27,20	1529,56	85	11,11
13750	18575	3	3c	372	62,90	1547,28	91,8	5,91
13875	2150	3	3c	627,75	40,80	1505,16	91,8	15,39
13875	2900	3	3c	1627,5	45,90	1585,78	161,5	35,46
13875	2900	3	3c	1395	105,40	1711,3	283,9	13,24
13875	8275	3	3c	999,75	69,70	1655,66	195,5	14,34
13875	8650	3	3c	697,5	39,10	1573,92	112,2	17,84
13875	16450	3	3c	1139,25	42,50	1718,98	263,5	26,81
13875	17150	3	3c	860,25	27,20	1583,12	129,2	31,63
13875	17500	3	3c	976,5	61,20	1823,82	362,1	15,96
13875	18600	3	3c	395,25	61,20	1560,6	102	6,46
14000	2525	3	3c	1162,5	52,70	1521,46	100,3	22,06
14000	2825	3	3c	1302	130,90	1736,38	304,3	9,95
14000	2900	3	3c	1743,75	66,30	1582,1	154,7	26,30
14000	8300	3	3c	860,25	40,80	1648,58	185,3	21,08
14000	16900	3	3c	790,5	57,80	1753,7	287,3	13,68
14000	16900	3	3c	651	25,50	1604,24	139,4	25,53
14000	17600	3	3c	930	62,90	1818,02	348,5	14,79
14000	18600	3	3c	395,25	74,80	1588,1	113,9	5,28
14125	2650	3	3c	1581	88,40	1578,7	151,3	17,88
14125	2800	3	3c	1371,75	129,20	1736,1	300,9	10,62
14125	8275	3	3c	883,5	49,30	1651,84	187	17,92
14125	16900	3	3c	953,25	37,40	1602,54	137,7	25,49
14125	17000	3	3c	744	54,40	1752	285,6	13,68
14125	17675	3	3c	999,75	56,10	1813,2	346,8	17,82
14125	18575	3	3c	395,25	66,30	1578,9	96,9	5,96
14250	2775	3	3c	1441,5	141,10	1737,66	300,9	10,22
14250	2875	3	3c	1720,5	90,10	1590,32	159,8	19,10
14250	8350	3	3c	930	62,90	1665,16	197,2	14,79
14250	16000	3	3c	1255,5	23,80	1643,76	183,6	52,75
14250	16900	3	3c	813,75	23,80	1600,7	134,3	34,19
14250	17050	3	3c	999,75	62,90	1736,14	263,5	15,89
14250	17650	3	3c	906,75	49,30	1815,76	340	18,39
14250	18650	3	3c	418,5	35,70	1572,38	93,5	11,72
14375	2825	3	3c	1767	81,60	1588,9	161,5	21,65
14375	2825	3	3c	1209	120,70	1736,94	311,1	10,02
14375	8300	3	3c	883,5	47,60	1661,76	193,8	18,56
14375	13950	3	3c	1116	23,80	1638,38	175,1	46,89
14375	16925	3	3c	1116	35,70	1661,34	188,7	31,26
14375	16950	3	3c	1906,5	44,20	1594,9	120,7	43,13
14375	17100	3	3c	790,5	51,00	1737,7	263,5	15,50
14375	18625	3	3c	720,75	32,30	1567,84	95,2	22,31
14500	2825	3	3c	1092,75	105,40	1728,58	304,3	10,37
14500	2875	3	3c	1255,5	54,40	1597,68	173,4	23,08
14500	3300	3	3c	930	30,60	1535,08	95,2	30,39
14500	8300	3	3c	697,5	39,10	1661,34	188,7	17,84

(N-S)	X (E-W)	Area	Unit	Width (m)	Height (m)	Depth (mbsl)	Burial depth (m)	W/H ratio
14500	13450	3	3c	1302	40,80	1638,52	176,8	31,91
14500	17125	3	3c	744	59,50	1718,72	241,4	12,50
14500	18550	3	3c	372	30,60	1572,1	90,1	12,16
14625	2875	3	3c	1162,5	86,70	1711,86	290,7	13,41
14625	3525	3	3c	627,75	32,30	1535,22	96,9	19,43
14625	8250	3	3c	813,75	42,50	1659,22	181,9	19,15
14625	16925	3	3c	534,75	25,50	1617,86	134,3	20,97
14625	17150	3	3c	790,5	39,10	1708,24	227,8	20,22
14625	18625	3	3c	465	35,70	1580,6	98,6	13,03
14750	1900	3	3c	395,25	32,30	1496,94	86,7	12,24
14750	2825	3	3c	1185,75	79,90	1708,32	285,6	14,84
14875	1925	3	3c	465	25,50	1494,52	95,2	18,24
14875	2825	3	3c	1255,5	93,50	1735,38	311,1	13,43
14875	3500	3	3c	465	37,40	1606,34	164,9	12,43
14875	3500	3	3c	418,5	34,00	1607,9	164,9	12,31
14875	4000	3	3c	953,25	47,60	1543,9	69,7	20,03
14875	4025	3	3c	930	47,60	1548,14	83,3	19,54
14875	7725	3	3c	674,25	42,50	1591,94	103,7	15,86
14875	8325	3	3c	883,5	39,10	1665,88	187	22,60
14875	11500	3	3c	999,75	39,10	1668,02	42,5	25,57
14875	15675	3	3c	976,5	61,20	1858,12	380,8	15,96
14875	17825	3	3c	999,75	51,00	1828,66	345,1	19,60
15000	2725	3	3c	2441,25	86,70	1733,96	312,8	28,16
15000	2725	3	3c	1418,25	25,50	1634,08	217,6	55,62
15000	3500	3	3c	744	54,40	1618,24	176,8	13,68
15000	4250	3	3c	1627,5	42,50	1554,94	90,1	38,29
15000	11000	3	3c	418,5	30,60	1671,86	32,3	13,68
15000	11500	3	3c	2301,75	54,40	1854,18	219,3	42,31
15000	15625	3	3c	1371,75	76,50	1858,26	382,5	17,93
15000	17200	3	3c	627,75	54,40	1806,28	319,6	11,54
15000	17800	3	3c	976,5	57,80	1837,74	341,7	16,89
15000	18700	3	3c	511,5	51,00	1623,12	122,4	10,03
15125	2025	3	3c	720,75	34,00	1520,74	110,5	21,20
15125	2675	3	3c	1395	100,30	1753,94	328,1	13,91
15125	7825	3	3c	744	85,00	1603,84	115,6	8,75
15125	12625	3	3c	767,25	44,20	1611,46	151,3	17,36
15125	16300	3	3c	1209	27,20	1680,2	190,4	44,45
15125	17300	3	3c	534,75	18,70	1625,66	134,3	28,60
15125	18650	3	3c	581,25	54,40	1622	108,8	10,68
15250	2075	3	3c	813,75	57,80	1539,58	130,9	14,08
15250	2650	3	3c	1488	105,40	1757,76	336,6	14,12
15250	4075	3	3c	674,25	23,80	1554,64	105,4	28,33
15250	7825	3	3c	790,5	27,20	1598,88	112,2	29,06
15250	12800	3	3c	999,75	59,50	1621,38	158,1	16,80
15250	16475	3	3c	1255,5	40,80	1698,9	209,1	30,77
15250	18800	3	3c	720,75	39,10	1618,6	105,4	18,43
15375	1925	3	3c	906,75	42,50	1531,22	124,1	21,34
15375	2150	3	3c	674,25	34,00	1609,56	204	19,83

(N-S)	X (E-W)	Area	Unit	Width (m)	Height (m)	Depth (mbsl)	Burial depth (m)	W/H ratio
15375	2900	3	3c	1348,5	90,10	1748,26	334,9	14,97
15375	7900	3	3c	674,25	25,50	1600,44	112,2	26,44
15375	10950	3	3c	255,75	39,10	1681,5	35,7	6,54
15375	13050	3	3c	604,5	47,60	1621,94	164,9	12,70
15375	16450	3	3c	1325,25	45,90	1702,44	214,2	28,87
15375	18650	3	3c	441,75	44,20	1629,08	119	9,99
15500	1925	3	3c	930	37,40	1524	112,2	24,87
15500	2875	3	3c	1534,5	90,10	1747,56	326,4	17,03
15500	11150	3	3c	651	51,00	1689,84	61,2	12,76
15500	18825	3	3c	790,5	56,10	1624,98	107,1	14,09
15625	2075	3	3c	790,5	42,50	1619,2	207,4	18,60
15625	2925	3	3c	1604,25	74,80	1744,3	324,7	21,45
15625	6925	3	3c	255,75	27,20	1584,14	103,7	9,40
15625	8675	3	3c	999,75	28,90	1605,12	112,2	34,59
15625	11375	3	3c	488,25	37,40	1690,72	34	13,05
15750	1900	3	3c	976,5	42,50	1527,82	120,7	22,98
15750	2075	3	3c	790,5	35,70	1620,62	205,7	22,14
15750	2925	3	3c	1790,25	69,70	1741,46	328,1	25,69
15750	5200	3	3c	1092,75	32,30	1738,82	277,1	33,83
15750	8975	3	3c	930	30,60	1615,74	127,5	30,39
15750	12050	3	3c	1418,25	93,50	1987,9	498,1	15,17
15750	15925	3	3c	744	90,10	1978,84	482,8	8,26
15875	1725	3	3c	1023	34,00	1519,18	110,5	30,09
15875	1975	3	3c	1139,25	40,80	1621,04	210,8	27,92
15875	2375	3	3c	883,5	39,10	1653,2	241,4	22,60
15875	3000	3	3c	2185,5	64,60	1740,48	316,2	33,83
15875	4200	3	3c	511,5	32,30	1589,48	149,6	15,84
15875	5675	3	3c	2069,25	44,20	1740,52	278,8	46,82
15875	7450	3	3c	860,25	35,70	1602,42	117,3	24,10
15875	8325	3	3c	1278,75	61,20	1657,4	159,8	20,89
15875	11625	3	3c	395,25	44,20	1696,24	44,2	8,94
16000	1875	3	3c	1046,25	40,80	1527,54	117,3	25,64
16000	2075	3	3c	1185,75	44,20	1627,7	215,9	26,83
16000	2350	3	3c	1023	30,60	1655,18	246,5	33,43
16000	2700	3	3c	1511,25	62,90	1737,64	319,6	24,03
16000	8425	3	3c	2115,75	71,40	1659,38	164,9	29,63
16000	11575	3	3c	441,75	45,90	1696,38	45,9	9,62
16000	13050	3	3c	976,5	27,20	1603,42	110,5	35,90
16125	1675	3	3c	1278,75	42,50	1527,12	112,2	30,09
16125	2175	3	3c	1116	34,00	1658,16	244,8	32,82
16125	2975	3	3c	1069,5	74,80	1754,92	340	14,30
16125	7300	3	3c	883,5	40,80	1597,18	110,5	21,65
16125	8125	3	3c	1581	68,00	1683,32	190,4	23,25
16125	11525	3	3c	325,5	30,60	1687,04	27,2	10,64
16125	13125	3	3c	953,25	35,70	1603,14	107,1	26,70
16250	2925	3	3c	2022,75	57,80	1751,1	331,5	35,00
16250	5825	3	3c	558	28,90	1781,06	297,5	19,31
16250	8075	3	3c	1209	69,70	1718,74	222,7	17,35

(N-S)	X (E-W)	Area	Unit	Width (m)	Height (m)	Depth (mbsl)	Burial depth (m)	W/H ratio
16250	11375	3	3c	302,25	40,80	1697,52	40,8	7,41
16250	17625	3	3c	2115,75	22,10	1669,88	159,8	95,74
16375	1625	3	3c	1488	39,10	1525,28	108,8	38,06
16375	2975	3	3c	3022,5	61,20	1757,9	338,3	49,39
16375	8100	3	3c	1116	47,60	1698,34	202,3	23,45
16375	8475	3	3c	534,75	40,80	1626,24	122,4	13,11
16375	9475	3	3c	976,5	44,20	1807,14	311,1	22,09
16375	11300	3	3c	395,25	40,80	1700,5	39,1	9,69
16750	1500	3	3c	1883,25	56,10	1639,46	226,1	33,57
16750	6600	3	3c	604,5	42,50	1759,68	265,2	14,22
16750	8300	3	3c	488,25	62,90	1702,74	198,9	7,76
16750	8500	3	3c	395,25	32,30	1641,26	134,3	12,24
16750	10900	3	3c	348,75	45,90	1710,42	45,9	7,60
16750	17850	3	3c	2487,75	25,50	1691,28	173,4	97,56
16875	6425	3	3c	790,5	69,70	1768,18	273,7	11,34
16875	8350	3	3c	627,75	56,10	1709,26	202,3	11,19
16875	8600	3	3c	348,75	30,60	1642,54	130,9	11,40
16875	12900	3	3c	651	20,40	1620,44	108,8	31,91
16875	17925	3	3c	2557,5	23,80	1685,62	161,5	107,46
17000	5975	3	3c	372	47,60	1815,78	321,3	7,82
17000	6325	3	3c	813,75	66,30	1773	275,4	12,27
17000	8525	3	3c	558	81,60	1742,98	232,9	6,84
17000	8750	3	3c	604,5	39,10	1649,06	134,3	15,46
17000	12775	3	3c	651	27,20	1618,6	105,4	23,93
17000	18025	3	3c	2441,25	23,80	1688,88	163,2	102,57
17125	1350	3	3c	1092,75	61,20	1641,02	226,1	17,86
17125	6050	3	3c	302,25	23,80	1796,52	295,8	12,70
17125	6150	3	3c	674,25	59,50	1771,3	273,7	11,33
17125	8750	3	3c	1162,5	52,70	1707,28	197,2	22,06
17125	8950	3	3c	651	45,90	1662,94	151,3	14,18
17125	18050	3	3c	2487,75	18,70	1685,76	163,2	133,03
17250	4725	3	3c	418,5	18,70	1705,28	210,8	22,38
17250	6075	3	3c	604,5	52,70	1764,36	265,2	11,47
17250	8700	3	3c	1162,5	35,70	1712,52	204	32,56
17250	8825	3	3c	511,5	51,00	1754,46	239,7	10,03
17250	9150	3	3c	511,5	35,70	1658,84	139,4	14,33
17250	18225	3	3c	2232	18,70	1688,88	163,2	119,36
17375	725	3	3c	651	37,40	1804,92	397,8	17,41
17375	1275	3	3c	883,5	59,50	1642,72	227,8	14,85
17375	1325	3	3c	1604,25	74,80	1877,18	460,7	21,45
17375	4450	3	3c	418,5	15,30	1703,02	202,3	27,35
17375	6000	3	3c	511,5	35,70	1752,6	255	14,33
17375	9175	3	3c	627,75	34,00	1648,64	129,2	18,46
17375	18300	3	3c	2069,25	27,20	1693,98	168,3	76,08
17500	1275	3	3c	790,5	57,80	1647,68	231,2	13,68
17500	4275	3	3c	279	25,50	1698,9	209,1	10,94
17500	9475	3	3c	604,5	61,20	1672,44	153	9,88
17500	12125	3	3c	511,5	39,10	1737,88	95,2	13,08

(N-S)	X (E-W)	Area	Unit	Width (m)	Height (m)	Depth (mbsl)	Burial depth (m)	W/H ratio
17500	12700	3	3c	395,25	37,40	1658,42	134,3	10,57
17500	18350	3	3c	2441,25	34,00	1698,8	170	71,80
17625	900	3	3c	1488	83,30	1853,24	435,2	17,86
17625	1800	3	3c	1511,25	49,30	1652,22	229,5	30,65
17625	5850	3	3c	1743,75	25,50	1616,18	113,9	68,38
17625	8525	3	3c	418,5	25,50	1633,2	112,2	16,41
17625	9575	3	3c	511,5	52,70	1673,86	151,3	9,71
17625	12025	3	3c	534,75	45,90	1738,08	40,8	11,65
17625	12675	3	3c	581,25	35,70	1661,54	134,3	16,28
17625	18325	3	3c	2441,25	35,70	1700,08	166,6	68,38
17750	1225	3	3c	581,25	42,50	1615,24	197,2	13,68
17750	9575	3	3c	395,25	49,30	1679,38	161,5	8,02
17750	11875	3	3c	325,5	25,50	1737,1	28,9	12,76
17875	2700	3	3c	744	32	352	299,2	23,25
17875	6925	3	3c	604,5	52	300	255	11,63
17875	9600	3	3c	418,5	52	182	154,7	8,05
17875	11825	3	3c	279	28	34	28,9	9,96
18000	1425	3	3c	348,75	48	244	207,4	7,27
18000	6000	3	3c	744	66	270	229,5	11,27
18000	9500	3	3c	511,5	46	194	164,9	11,12
18000	9500	3	3c	418,5	40	216	183,6	10,46
18000	9775	3	3c	348,75	54	174	147,9	6,46
18000	9825	3	3c	209,25	30	350	297,5	6,98
18000	9900	3	3c	302,25	38	128	108,8	7,95
18000	11725	3	3c	255,75	38	38	32,3	6,73
18125	1325	3	3c	348,75	60	242	205,7	5,81
18125	4950	3	3c	1255,5	54	310	263,5	23,25
18125	5800	3	3c	953,25	46	250	212,5	20,72
18125	9900	3	3c	372	60	166	141,1	6,20
18250	3250	3	3c	1325,25	52	352	299,2	25,49
18250	5475	3	3c	1534,5	58	248	210,8	26,46
18250	8800	3	3c	1697,25	48	260	221	35,36
18250	9850	3	3c	790,5	40	168	142,8	19,76
18250	11675	3	3c	232,5	38	40	34	6,12
18375	4350	3	3c	976,5	64	316	268,6	15,26
18375	4875	3	3c	1116	60	258	219,3	18,60
18375	8300	3	3c	441,75	48	248	210,8	9,20
18375	8800	3	3c	1185,75	54	254	215,9	21,96
18375	11725	3	3c	279	56	42	35,7	4,98
18500	3100	3	3c	581,25	36	322	273,7	16,15
18500	3975	3	3c	860,25	50	314	266,9	17,21
18500	4575	3	3c	1697,25	50	242	205,7	33,95
18500	5600	3	3c	906,75	32	162	137,7	28,34
18500	5700	3	3c	1743,75	40	120	102	43,59
18500	8225	3	3c	558	64	256	217,6	8,72
18500	9900	3	3c	395,25	42	218	185,3	9,41
18500	11775	3	3c	372	48	50	42,5	7,75
18625	2850	3	3c	488,25	20	320	272	24,41

(N-S)	X (E-W)	Area	Unit	Width (m)	Height (m)	Depth (mbsl)	Burial depth (m)	W/H ratio
18625	3450	3	3c	1209	48	320	272	25,19
18625	4300	3	3c	1209	46	226	192,1	26,28
18625	5250	3	3c	1604,25	52	144	122,4	30,85
18625	8200	3	3c	488,25	62	250	212,5	7,88
18625	10025	3	3c	372	42	214	181,9	8,86
18625	11775	3	3c	348,75	42	40	34	8,30
18750	5000	3	3c	1441,5	34	128	108,8	42,40
18750	8150	3	3c	534,75	68	240	204	7,86
18750	8175	3	3c	744	36	124	105,4	20,67
18750	10075	3	3c	418,5	40	222	188,7	10,46
18750	11925	3	3c	534,75	60	54	45,9	8,91
18875	1850	3	3c	488,25	49,3	1665,42	219,3	9,90
18875	2725	3	3c	813,75	44,2	1757,66	297,5	18,41
18875	8000	3	3c	558	71,4	1745	200,6	7,82
18875	8925	3	3c	1441,5	37,4	1744,86	198,9	38,54
18875	10125	3	3c	418,5	39,1	1720,06	181,9	10,70
19000	2425	3	3c	767,25	37,4	1749,58	294,1	20,51
19000	7900	3	3c	558	47,6	1712,7	168,3	11,72
19000	10350	3	3c	953,25	59,5	1724,88	183,6	16,02
19125	2025	3	3c	488,25	35,7	1656,5	205,7	13,68
19125	2350	3	3c	558	44,2	1758,5	307,7	12,62
19125	4425	3	3c	720,75	28,9	1659,24	163,2	24,94
19125	4950	3	3c	627,75	27,2	1589,7	76,5	23,08
19125	7900	3	3c	511,5	32,3	1703,92	156,4	15,84
19125	8000	3	3c	348,75	40,8	1758,32	210,8	8,55
19125	8125	3	3c	953,25	42,5	1662,98	113,9	22,43
19125	9025	3	3c	581,25	32,3	1824,2	272	18,00
19125	10275	3	3c	1139,25	42,5	1722,48	173,4	26,81
19125	12225	3	3c	348,75	35,7	1771,98	35,7	9,77
19250	2275	3	3c	418,5	45,9	1761,48	306	9,12
19250	2575	3	3c	976,5	35,7	1662,46	202,3	27,35
19250	8075	3	3c	860,25	45,9	1662,98	113,9	18,74
19250	10300	3	3c	1209	42,5	1723,9	171,7	28,45
19250	12200	3	3c	441,75	51	1778,64	40,8	8,66
19375	2175	3	3c	558	34	1717	258,4	16,41
19375	2225	3	3c	372	40,8	1762,9	304,3	9,12
19375	4375	3	3c	1720,5	35,7	1655,56	156,4	48,19
19375	7975	3	3c	720,75	87	1740,76	187	8,28
19375	8025	3	3c	837	39,1	1660,86	107,1	21,41
19375	10575	3	3c	1069,5	47,6	1730,56	176,8	22,47
19375	12100	3	3c	418,5	69,7	1805,98	69,7	6,00
19500	2200	3	3c	813,75	45,9	1658,64	193,8	17,73
19500	2225	3	3c	720,75	66,3	1759,36	299,2	10,87
19500	7925	3	3c	1534,5	52,7	1677,72	122,4	29,12
19500	10550	3	3c	1046,25	35,7	1721,78	164,9	29,31
19500	12050	3	3c	395,25	49,3	1784,6	37,4	8,02
19625	2150	3	3c	558	59,5	1767,44	302,6	9,38
19625	2250	3	3c	744	44,2	1650	183,6	16,83



(N-S)	X (E-W)	Area	Unit	Width (m)	Height (m)	Depth (mbsl)	Burial depth (m)	W/H ratio
19625	5700	3	3c	558	25,5	1647,54	96,9	21,88
19625	11950	3	3c	348,75	49,3	1796,5	49,3	7,07
19750	2125	3	3c	720,75	62,9	1776,36	316,2	11,46
19750	2175	3	3c	767,25	39,1	1653,12	183,6	19,62
19750	5875	3	3c	1627,5	27,2	1647,82	100,3	59,83
19750	8300	3	3c	558	18,7	1662,14	103,7	29,84
19750	11950	3	3c	302,25	44,2	1791,12	40,8	6,84
19875	1375	3	3c	767,25	25,5	1670,1	219,3	30,09
19875	2000	3	3c	720,75	51	1772,26	304,3	14,13
19875	5325	3	3c	744	20,4	1638,04	95,2	36,47
19875	5425	3	3c	604,5	34	1721,06	175,1	17,78
19875	11950	3	3c	302,25	40,8	1788	40,8	7,41
20000	1100	3	3c	767,25	28,9	1638,36	193,8	26,55
20000	1925	3	3c	790,5	54,4	1767,86	307,7	14,53
20000	5000	3	3c	837	27,2	1703,34	168,3	30,77
20000	5825	3	3c	1185,75	32,3	1657,6	105,4	36,71
20000	6325	3	3c	1836,75	40,8	1757,62	202,3	45,02
20000	8025	3	3c	767,25	18,7	1761,88	197,2	41,03
20000	8175	3	3c	488,25	20,4	1668,1	100,3	23,93
20000	11925	3	3c	279	52,7	1799,48	47,6	5,29
1	1532	1	MC (C4)	550	183,60	1274,52	0	3,00
10	1532	1	MC (C4)	575	183,60	1280,76	0	3,13
10	462	1	MC (C4)	825	154,70	1165,32	0	5,33
20	1532	1	MC (C4)	575	181,90	1282,32	0	3,16
20	460	1	MC (C4)	750	151,30	1166,88	0	4,96
30	1528	1	MC (C4)	650	180,20	1282,32	0	3,61
30	466	1	MC (C4)	850	139,40	1165,32	0	6,10
40	1528	1	MC (C4)	550	170,00	1283,88	0	3,24
40	472	1	MC (C4)	900	139,40	1170	0	6,46
50	1524	1	MC (C4)	575	176,80	1288,56	0	3,25
50	478	1	MC (C4)	775	136,00	1176,24	0	5,70
60	1526	1	MC (C4)	625	175,10	1290,12	0	3,57
60	486	1	MC (C4)	850	144,50	1187,16	0	5,88
70	1528	1	MC (C4)	650	171,70	1287	0	3,79
70	490	1	MC (C4)	875	141,10	1193,4	0	6,20
80	1526	1	MC (C4)	675	171,70	1290,12	0	3,93
80	500	1	MC (C4)	1025	129,20	1194,96	0	7,93
90	1522	1	MC (C4)	650	163,20	1288,56	0	3,98
90	510	1	MC (C4)	950	127,50	1196,52	0	7,45
100	524	1	MC (C4)	1100	124,10	1202,76	0	8,86
110	1526	1	MC (C4)	800	166,60	1291,68	0	4,80
110	540	1	MC (C4)	1025	139,40	1213,68	0	7,35
120	1526	1	MC (C4)	800	163,20	1291,68	0	4,90
120	552	1	MC (C4)	1000	124,10	1210,56	0	8,06
130	1524	1	MC (C4)	650	171,70	1293,24	0	3,79
130	558	1	MC (C4)	825	134,30	1221,48	0	6,14
140	1476	1	MC (C4)	850	171,70	1296,36	0	4,95

(N-S)	X (E-W)	Area	Unit	Width (m)	Height (m)	Depth (mbsl)	Burial depth (m)	W/H ratio
140	568	1	MC (C4)	900	132,60	1226,16	0	6,79
150	1456	1	MC (C4)	925	198,90	1329,12	0	4,65
150	574	1	MC (C4)	875	149,60	1244,88	0	5,85
160	1452	1	MC (C4)	725	180,20	1324,44	0	4,02
160	582	1	MC (C4)	875	137,70	1241,76	0	6,35
180	1436	1	MC (C4)	900	193,80	1338,48	0	4,64
180	600	1	MC (C4)	950	124,10	1244,88	0	7,66
190	1424	1	MC (C4)	950	188,70	1346,28	0	5,03
190	610	1	MC (C4)	1100	122,40	1251,12	0	8,99
200	1424	1	MC (C4)	800	190,40	1347,84	0	4,20
200	622	1	MC (C4)	1100	112,20	1252,68	0	9,80
210	1420	1	MC (C4)	900	183,60	1349,4	0	4,90
210	632	1	MC (C4)	1050	125,80	1274,52	0	8,35
220	1416	1	MC (C4)	800	195,50	1352,52	0	4,09
220	644	1	MC (C4)	1075	146,20	1282,32	0	7,35
230	1414	1	MC (C4)	850	181,90	1360,32	0	4,67
230	660	1	MC (C4)	1050	139,40	1291,68	0	7,53
240	1414	1	MC (C4)	700	168,30	1355,64	0	4,16
240	678	1	MC (C4)	1200	132,60	1294,8	0	9,05
250	1412	1	MC (C4)	825	161,50	1363,44	0	5,11
250	692	1	MC (C4)	1250	137,70	1299,48	0	9,08
260	1408	1	MC (C4)	850	175,10	1360,32	0	4,85
260	706	1	MC (C4)	1375	139,40	1305,72	0	9,86
270	1408	1	MC (C4)	775	164,90	1361,88	0	4,70
270	718	1	MC (C4)	1350	141,10	1311,96	0	9,57
280	1402	1	MC (C4)	850	159,80	1365	0	5,32
280	730	1	MC (C4)	1325	129,20	1315,08	0	10,26
290	1402	1	MC (C4)	775	163,20	1368,12	0	4,75
290	738	1	MC (C4)	1125	113,90	1311,96	0	9,88
300	1400	1	MC (C4)	675	158,10	1366,56	0	4,27
300	750	1	MC (C4)	1025	129,20	1319,76	0	7,93
310	1398	1	MC (C4)	825	170,00	1374,36	0	4,85
310	758	1	MC (C4)	1050	117,30	1319,76	0	8,95
320	1394	1	MC (C4)	750	176,80	1382,16	0	4,24
320	766	1	MC (C4)	1125	119,00	1324,44	0	9,45
330	1392	1	MC (C4)	875	185,30	1382,16	0	4,72
330	774	1	MC (C4)	1100	15,30	1221,48	0	71,90
340	788	1	MC (C4)	1150	148,50	1535,04	0	7,74
340	1382	1	MC (C4)	950	171,70	1385,28	0	5,53
350	1370	1	MC (C4)	975	185,30	1389,96	0	5,26
350	806	1	MC (C4)	1675	117,30	1333,8	0	14,28
360	1362	1	MC (C4)	1050	180,20	1396,2	0	5,83
360	814	1	MC (C4)	1525	127,50	1343,16	0	11,96
370	1348	1	MC (C4)	1150	178,50	1399,32	0	6,44
370	832	1	MC (C4)	1750	125,80	1343,16	0	13,91
380	1332	1	MC (C4)	1075	185,30	1394,64	0	5,80
380	838	1	MC (C4)	1350	112,20	1343,16	0	12,03
390	1322	1	MC (C4)	1225	166,60	1397,76	0	7,35

(N-S)	X (E-W)	Area	Unit	Width (m)	Height (m)	Depth (mbsl)	Burial depth (m)	W/H ratio
390	840	1	MC (C4)	1500	96,90	1329,12	0	15,48
400	1308	1	MC (C4)	1100	153,00	1399,32	0	7,19
400	874	1	MC (C4)	700	117,30	1349,4	0	5,97
400	806	1	MC (C4)	1050	90,10	1329,12	0	11,65
410	1310	1	MC (C4)	1100	156,40	1402,44	0	7,03
410	872	1	MC (C4)	725	127,50	1350,96	0	5,69
410	804	1	MC (C4)	975	85,00	1333,8	0	11,47
420	1282	1	MC (C4)	925	175,10	1411,8	0	5,28
420	876	1	MC (C4)	675	100,30	1350,96	0	6,73
430	1264	1	MC (C4)	975	139,40	1419,6	0	6,99
430	880	1	MC (C4)	750	86,70	1354,08	0	8,65
430	776	1	MC (C4)	1025	71,40	1326	0	14,36
440	1250	1	MC (C4)	1525	204,00	1428,96	0	7,48
440	882	1	MC (C4)	750	96,90	1357,2	0	7,74
440	766	1	MC (C4)	2250	68,00	1326	0	33,09
450	1234	1	MC (C4)	1575	161,50	1428,96	0	9,75
450	884	1	MC (C4)	925	98,60	1355,64	0	9,38
460	1222	1	MC (C4)	2000	175,10	1432,08	0	11,42
460	890	1	MC (C4)	1250	103,70	1355,64	0	12,05
470	1208	1	MC (C4)	1925	185,30	1435,2	0	10,39
470	1194	1	MC (C4)	1150	98,60	1354,08	0	11,66
480	1190	1	MC (C4)	1950	176,80	1433,64	0	11,03
480	902	1	MC (C4)	1200	93,50	1354,08	0	12,83
490	1174	1	MC (C4)	1850	163,20	1435,2	0	11,34
490	910	1	MC (C4)	1100	105,40	1358,76	0	10,44
500	1160	1	MC (C4)	1575	149,60	1433,64	0	10,53
500	918	1	MC (C4)	1100	102,00	1357,2	0	10,78
510	1150	2	MC (C4)	1300	142,80	1435,2	0	9,10
510	928	2	MC (C4)	1050	96,90	1360,32	0	10,84
520	1134	2	MC (C4)	1325	149,60	1436,76	0	8,86
520	932	2	MC (C4)	1000	105,40	1361,88	0	9,49
530	1122	2	MC (C4)	1075	180,20	1452,36	0	5,97
530	938	2	MC (C4)	1050	73,10	1365	0	14,36
540	1118	2	MC (C4)	1000	173,40	1450,8	0	5,77
540	940	2	MC (C4)	1150	79,90	1365	0	14,39
550	1110	2	MC (C4)	975	154,70	1450,8	0	6,30
550	948	2	MC (C4)	1250	78,20	1368,12	0	15,98
560	1108	2	MC (C4)	950	153,00	1458,6	0	6,21
560	952	2	MC (C4)	1100	73,10	1371,24	0	15,05
570	1104	2	MC (C4)	1000	159,80	1467,96	0	6,26
570	958	2	MC (C4)	1200	64,60	1369,68	0	18,58
580	1104	2	MC (C4)	925	161,50	1469,52	0	5,73
580	968	2	MC (C4)	1000	110,50	1404	0	9,05
590	1102	2	MC (C4)	1050	159,80	1471,08	0	6,57
590	976	2	MC (C4)	1000	81,60	1391,52	0	12,25
600	1102	2	MC (C4)	950	164,90	1469,52	0	5,76
600	986	2	MC (C4)	975	88,40	1393,08	0	11,03
620	1104	2	MC (C4)	1000	149,60	1461,72	0	6,68

(N-S)	X (E-W)	Area	Unit	Width (m)	Height (m)	Depth (mbsl)	Burial depth (m)	W/H ratio
620	994	2	MC (C4)	1025	91,80	1393,08	0	11,17
630	1100	2	MC (C4)	1150	134,30	1463,28	0	8,56
640	1102	2	MC (C4)	1150	141,10	1464,84	0	8,15
650	1098	2	MC (C4)	1075	144,50	1461,72	0	7,44
660	1102	2	MC (C4)	1000	144,50	1467,96	0	6,92
670	1104	2	MC (C4)	975	134,30	1471,08	0	7,26
680	1108	2	MC (C4)	1150	127,50	1466,4	0	9,02
690	1102	2	MC (C4)	1375	144,50	1478,88	0	9,52
700	1102	2	MC (C4)	1225	134,30	1480,44	0	9,12
710	1112	2	MC (C4)	1150	137,70	1482	0	8,35
730	1114	2	MC (C4)	1000	134,30	1483,56	0	7,45
740	1112	2	MC (C4)	750	124,10	1482	0	6,04
750	1114	2	MC (C4)	900	129,20	1485,12	0	6,97
760	1108	2	MC (C4)	700	129,20	1485,12	0	5,42
770	1104	2	MC (C4)	1250	120,70	1489,8	0	10,36
780	1100	2	MC (C4)	950	113,90	1489,8	0	8,34
800	1086	2	MC (C4)	1125	115,60	1485,12	0	9,73
810	1082	2	MC (C4)	1050	141,10	1497,6	0	7,44
820	1084	2	MC (C4)	425	69,70	1567,16	0	6,10
830	1078	2	MC (C4)	1425	142,80	1494,48	0	9,98
840	1072	2	MC (C4)	950	132,60	1494,48	0	7,16
850	1072	2	MC (C4)	1600	142,80	1503,84	0	11,20
860	1066	2	MC (C4)	750	134,30	1505,4	0	5,58
870	1062	2	MC (C4)	650	132,60	1502,28	0	4,90
880	1060	2	MC (C4)	700	141,10	1511,64	0	4,96
890	1054	2	MC (C4)	725	132,60	1506,96	0	5,47
900	1054	2	MC (C4)	700	134,30	1513,2	0	5,21
910	1050	2	MC (C4)	650	130,9	1514,76	0	4,97
920	1046	2	MC (C4)	800	132,6	1516,32	0	6,03
940	1042	2	MC (C4)	625	127,5	1527,24	0	4,90
950	1048	2	MC (C4)	775	124,1	1525,68	0	6,24
960	1054	2	MC (C4)	600	144,5	1538,16	0	4,15
970	1060	2	MC (C4)	650	149,6	1539,72	0	4,34
980	1066	2	MC (C4)	1000	149,6	1555,32	0	6,68
1000	1122	2	MC (C4)	1650	130,9	1550,64	0	12,61
1010	1156	3	MC (C4)	1150	137,70	1552,2	0	8,35
1020	1172	3	MC (C4)	1175	130,90	1550,64	0	8,98
1030	1178	3	MC (C4)	1075	139,40	1555,32	0	7,71
1040	1194	3	MC (C4)	750	136,00	1553,76	0	5,51
1050	1202	3	MC (C4)	1100	127,50	1553,76	0	8,63
1060	1098	3	MC (C4)	575	120,70	1572,48	0	4,76
1060	1208	3	MC (C4)	700	115,60	1552,2	0	6,06
1070	1100	3	MC (C4)	875	154,70	1611,48	0	5,66
1070	1214	3	MC (C4)	600	115,60	1552,2	0	5,19
1080	1034	3	MC (C4)	1450	181,90	1667,64	0	7,97
1090	1088	3	MC (C4)	750	219,30	1622,4	0	3,42
1090	1124	3	MC (C4)	350	139,40	1605,24	0	2,51
1090	1214	3	MC (C4)	550	115,60	1560	0	4,76

(N-S)	X (E-W)	Area	Unit	Width (m)	Height (m)	Depth (mbsl)	Burial depth (m)	W/H ratio
1100	1078	3	MC (C4)	800	164,90	1622,4	0	4,85
1100	1214	3	MC (C4)	650	124,10	1567,8	0	5,24
1100	1124	3	MC (C4)	450	78,20	1605,24	0	5,75
1110	1066	3	MC (C4)	750	171,70	1628,64	0	4,37
1110	1126	3	MC (C4)	650	147,90	1606,8	0	4,39
1110	1208	3	MC (C4)	675	125,80	1563,12	0	5,37
1120	1066	3	MC (C4)	825	175,10	1636,44	0	4,71
1120	1162	3	MC (C4)	875	100,30	1558,44	0	8,72
1130	1068	3	MC (C4)	850	181,90	1641,12	0	4,67
1130	1158	3	MC (C4)	900	85,00	1558,44	0	10,59
1150	1074	3	MC (C4)	825	170,00	1638	0	4,85
1150	1154	3	MC (C4)	650	74,80	1539,72	0	8,69
1160	1072	3	MC (C4)	700	171,70	1639,56	0	4,08
1170	1378	3	MC (C4)	1300	164,90	1631,76	0	7,88
1180	1034	3	MC (C4)	1700	153,00	1619,28	0	11,11
1190	1036	3	MC (C4)	1875	187,00	1633,32	0	10,03
1200	1020	3	MC (C4)	1850	175,10	1630,2	0	10,57
1230	984	3	MC (C4)	1650	192,10	1650,48	0	8,59
1240	998	3	MC (C4)	1375	170,00	1647,36	0	8,09
1250	1022	3	MC (C4)	1475	171,70	1656,72	0	8,59
1260	1038	3	MC (C4)	1800	187,00	1658,28	0	9,63
1270	1054	3	MC (C4)	1550	176,80	1652,04	0	8,77
1280	1052	3	MC (C4)	1500	170,00	1656,72	0	8,82
1290	1040	3	MC (C4)	1450	175,10	1659,84	0	8,28
1300	1028	3	MC (C4)	1475	171,70	1656,72	0	8,59
1310	1018	3	MC (C4)	1475	171,70	1658,28	0	8,59
1320	1010	3	MC (C4)	1325	164,90	1656,72	0	8,04
1340	994	3	MC (C4)	1125	180,20	1664,52	0	6,24
1340	1060	3	MC (C4)	1000	93,50	1584,96	0	10,70
1350	986	3	MC (C4)	900	205,70	1686,36	0	4,38
1350	1062	3	MC (C4)	1150	119,00	1622,4	0	9,66
1360	986	3	MC (C4)	900	197,20	1686,36	0	4,56
1360	1074	3	MC (C4)	1250	187,00	1689,48	0	6,68
1370	1064	3	MC (C4)	1325	207,40	1706,64	0	6,39
1370	990	3	MC (C4)	875	185,30	1681,68	0	4,72
1380	1094	3	MC (C4)	975	212,50	1712,88	0	4,59
1380	1016	3	MC (C4)	1325	200,60	1698,84	0	6,61
1390	1098	3	MC (C4)	1000	204,00	1714,44	0	4,90
1390	1010	3	MC (C4)	900	185,30	1689,48	0	4,86
1400	1098	3	MC (C4)	1525	187,00	1705,08	0	8,16
1410	1094	3	MC (C4)	1350	183,60	1705,08	0	7,35
1420	1078	3	MC (C4)	1075	193,80	1709,76	0	5,55
1430	1066	3	MC (C4)	950	228	1710	0	4,17
1440	1060	3	MC (C4)	1050	224	1715	0	4,69
1450	1054	3	MC (C4)	900	250	1713	0	3,60
1460	1050	3	MC (C4)	1175	232	1715	0	5,06
1470	1048	3	MC (C4)	1350	234	1732	0	5,77
1480	1052	3	MC (C4)	1400	220	1730	0	6,36

(N-S)	X (E-W)	Area	Unit	Width (m)	Height (m)	Depth (mbsl)	Burial depth (m)	W/H ratio
1490	1056	3	MC (C4)	1300	208	1735	0	6,25
1500	1064	3	MC (C4)	1425	222	1740	0	6,42
1510	1080	3	MC (C4)	1275	207,4	1747,2	0	6,15
1520	1092	3	MC (C4)	1275	198,9	1745,64	0	6,41
1530	1096	3	MC (C4)	1225	188,7	1737,84	0	6,49
1540	1104	3	MC (C4)	1200	183,6	1742,52	0	6,54
1550	1102	3	MC (C4)	1125	185,3	1745,64	0	6,07
1560	1096	3	MC (C4)	1250	183,6	1747,2	0	6,81
1570	1084	3	MC (C4)	1275	188,7	1753,44	0	6,76
1580	1078	3	MC (C4)	1250	180,2	1751,88	0	6,94
1590	1074	3	MC (C4)	1200	170	1745,64	0	7,06
1600	1068	3	MC (C4)	1125	171,7	1751,88	0	6,55
1610	1066	3	MC (C4)	1125	166,6	1751,88	0	6,75
1620	1064	3	MC (C4)	1125	164,9	1748,76	0	6,82
1630	1064	3	MC (C4)	1150	159,8	1750,32	0	7,20
1640	1066	3	MC (C4)	1150	159,8	1753,44	0	7,20
1650	1072	3	MC (C4)	1125	159,8	1755	0	7,04
1660	1072	3	MC (C4)	1025	151,3	1753,44	0	6,77
1670	1072	3	MC (C4)	975	147,9	1748,76	0	6,59
1680	1072	3	MC (C4)	1200	139,4	1744,08	0	8,61
1690	1070	3	MC (C4)	1350	158,1	1755	0	8,54
1700	1068	3	MC (C4)	1175	151,3	1758,12	0	7,77
1710	1068	3	MC (C4)	1200	151,3	1755	0	7,93
1720	1066	3	MC (C4)	1150	153	1753,44	0	7,52
1730	1062	3	MC (C4)	1300	149,6	1759,68	0	8,69
1740	1056	3	MC (C4)	1350	6,8	1617,72	0	198,53
1750	1052	3	MC (C4)	1425	147,9	1762,8	0	9,63
1760	1044	3	MC (C4)	1425	149,6	1769,04	0	9,53
1770	1028	3	MC (C4)	1475	147,9	1775,28	0	9,97
1790	1004	3	MC (C4)	1350	161,5	1781,52	0	8,36
1800	1002	3	MC (C4)	1300	163,2	1786,2	0	7,97
1810	1000	3	MC (C4)	1250	153	1784,64	0	8,17
1820	998	3	MC (C4)	1225	153	1783,08	0	8,01
1830	1004	3	MC (C4)	1300	153	1783,08	0	8,50
1840	1004	3	MC (C4)	1350	151,3	1784,64	0	8,92
1850	1014	3	MC (C4)	1275	141,1	1779,96	0	9,04
1860	1010	3	MC (C4)	700	91,8	1781,52	0	7,63
1870	1012	3	MC (C4)	775	91,8	1779,96	0	8,44
1880	1014	3	MC (C4)	625	73,1	1775,28	0	8,55
1890	1010	3	MC (C4)	1225	117,3	1779,96	0	10,44
1900	1014	3	MC (C4)	1375	127,5	1787,76	0	10,78
1910	1016	3	MC (C4)	1337,5	134,3	1786,2	0	9,96
1920	1014	3	MC (C4)	1150	107,1	1789,32	0	10,74
1930	1014	3	MC (C4)	1075	108,8	1792,44	0	9,88
1930	900	3	MC (C4)	550	39,1	1705,08	0	14,07
1940	1018	3	MC (C4)	1250	125,8	1789,32	0	9,94
1950	1016	3	MC (C4)	2175	137,7	1794	0	15,80
1960	1018	3	MC (C4)	2000	134,3	1787,76	0	14,89

(N-S)	X (E-W)	Area	Unit	Width (m)	Height (m)	Depth (mbsl)	Burial depth (m)	W/H ratio
1970	1022	3	MC (C4)	1925	136	1795,56	0	14,15
1980	1024	3	MC (C4)	2100	136	1797,12	0	15,44
1990	1024	3	MC (C4)	2050	139,4	1801,8	0	14,71
2000	1024	3	MC (C4)	1950	137,7	1800	0	14,16

**Table A.7.** Table with calculated Poisson probability, Poisson expected CP frequency and observed CP frequencies in the total area of the slope analysed in Chapter 6.

CP nr per cell	Poisson prob.	Observed Freq.	Expected Freq.
0	0.00	0	0.00
1	0.00	1	0.00
2	0.00	3	0.00
3	0.00	7	0.00
4	0.00	3	0.00
5	0.00	3	0.00
6	0.00	3	0.00
7	0.00	6	0.00
8	0.00	6	0.01
9	0.00	1	0.01
10	0.00	4	0.04
11	0.00	3	0.09
12	0.00	5	0.18
13	0.00	2	0.36
14	0.00	6	0.66
15	0.01	4	1.13
16	0.01	5	1.80
17	0.02	2	2.71
18	0.03	3	3.85
19	0.04	3	5.18
20	0.05	3	6.63
21	0.06	1	8.07
22	0.07	5	9.38
23	0.07	0	10.43
24	0.08	5	11.12
25	0.08	3	11.38
26	0.08	2	11.19
27	0.07	0	10.60
28	0.07	3	9.68
29	0.06	4	8.54
30	0.05	1	7.28
31	0.04	1	6.01
32	0.03	1	4.80
33	0.03	4	3.72
34	0.02	0	2.80
35	0.01	2	2.05
36	0.01	2	1.45
37	0.01	2	1.00
38	0.00	2	0.68
39	0.00	0	0.44
40	0.00	2	0.28
41	0.00	1	0.18
42	0.00	3	0.11
43	0.00	1	0.06
44	0.00	3	0.04
45	0.00	1	0.02
46	0.00	1	0.01
47	0.00	1	0.01
48	0.00	2	0.00



CP nr per cell	Poisson prob.	Observed Freq.	Expected Freq.
49	0.00	0	0.00
50	0.00	1	0.00
51	0.00	2	0.00
52	0.00	0	0.00
53	0.00	1	0.00
54	0.00	1	0.00
55	0.00	1	0.00
56	0.00	0	0.00
57	0.00	0	0.00
58	0.00	1	0.00
59	0.00	1	0.00
60	0.00	0	0.00
61	0.00	0	0.00
62	0.00	1	0.00
63	0.00	1	0.00
64	0.00	0	0.00
65	0.00	1	0.00
66	0.00	0	0.00
67	0.00	0	0.00
68	0.00	0	0.00
69	0.00	1	0.00
70	0.00	0	0.00
71	0.00	1	0.00
72	0.00	0	0.00
73	0.00	0	0.00
74	0.00	1	0.00
75	0.00	0	0.00
76	0.00	1	0.00
77	0.00	0	0.00
78	0.00	0	0.00
79	0.00	0	0.00
80	0.00	0	0.00
81	0.00	0	0.00
82	0.00	0	0.00
83	0.00	0	0.00
84	0.00	1	0.00
85	0.00	0	0.00
86	0.00	0	0.00
87	0.00	1	0.00
88	0.00	0	0.00
89	0.00	0	0.00
90	0.00	1	0.00
<b>TOTAL</b>	<b>1</b>	<b>144</b>	<b>144</b>

**Table A.8.** Table with calculated Poisson probability, Poisson expected CP frequency and observed CP frequencies in Area A1.

CP nr per cell	Poisson prob.	Observed Freq.	Expected Freq.
0	0.00	0	0.00
1	0.00	0	0.00
2	0.00	1	0.00
3	0.00	0	0.00
4	0.00	0	0.00
5	0.00	0	0.00
6	0.00	0	0.00
7	0.00	0	0.00
8	0.00	0	0.00
9	0.00	0	0.00
10	0.00	0	0.00
11	0.00	1	0.00
12	0.00	1	0.00
13	0.00	0	0.00
14	0.00	0	0.00
15	0.00	1	0.00
16	0.00	2	0.00
17	0.00	0	0.00
18	0.00	1	0.00
19	0.00	1	0.00
20	0.00	1	0.00
21	0.00	0	0.01
22	0.00	0	0.01
23	0.00	0	0.02
24	0.00	2	0.04
25	0.00	1	0.06
26	0.00	0	0.10
27	0.00	0	0.16
28	0.01	1	0.24
29	0.01	2	0.34
30	0.01	0	0.48
31	0.01	0	0.65
32	0.02	1	0.86
33	0.02	1	1.09
34	0.03	0	1.35
35	0.04	2	1.62
36	0.04	0	1.89
37	0.05	1	2.15
38	0.05	1	2.38
39	0.06	0	2.56
40	0.06	0	2.69
41	0.06	0	2.76
42	0.06	3	2.76
43	0.06	0	2.70
44	0.06	3	2.58
45	0.05	1	2.41
46	0.05	1	2.21
47	0.04	0	1.97
48	0.04	1	1.73

CP nr per cell	Poisson prob.	Observed Freq.	Expected Freq.
49	0.03	0	1.48
50	0.03	1	1.25
51	0.02	2	1.03
52	0.02	0	0.83
53	0.01	1	0.66
54	0.01	0	0.51
55	0.01	1	0.39
56	0.01	0	0.29
57	0.00	0	0.22
58	0.00	1	0.16
59	0.00	0	0.11
60	0.00	0	0.08
61	0.00	0	0.05
62	0.00	0	0.04
63	0.00	1	0.02
64	0.00	0	0.02
65	0.00	1	0.01
66	0.00	0	0.01
67	0.00	0	0.00
68	0.00	0	0.00
69	0.00	1	0.00
70	0.00	0	0.00
71	0.00	1	0.00
72	0.00	0	0.00
73	0.00	0	0.00
74	0.00	1	0.00
75	0.00	0	0.00
76	0.00	1	0.00
77	0.00	0	0.00
78	0.00	0	0.00
79	0.00	0	0.00
80	0.00	0	0.00
81	0.00	0	0.00
82	0.00	0	0.00
83	0.00	0	0.00
84	0.00	1	0.00
85	0.00	0	0.00
86	0.00	0	0.00
87	0.00	1	0.00
88	0.00	0	0.00
89	0.00	0	0.00
90	0.00	1	0.00
<b>TOTAL</b>	1	45	45

**Table A.9.** Table with calculated Poisson probability, Poisson expected CP frequency and observed CP frequencies in Area A2.

CP nr per cell	Poisson prob.	Observed Freq.	Expected Freq.
0	0.00	0	0.00
1	0.00	0	0.00
2	0.00	0	0.00
3	0.00	1	0.00
4	0.00	0	0.00
5	0.00	1	0.00
6	0.00	1	0.00
7	0.00	2	0.00
8	0.00	1	0.00
9	0.00	0	0.00
10	0.00	0	0.01
11	0.00	2	0.02
12	0.00	1	0.04
13	0.00	1	0.08
14	0.00	3	0.14
15	0.01	0	0.25
16	0.01	1	0.42
17	0.01	0	0.65
18	0.02	1	0.95
19	0.03	2	1.31
20	0.04	1	1.73
21	0.05	1	2.17
22	0.06	2	2.60
23	0.07	0	2.98
24	0.07	1	3.28
25	0.08	1	3.45
26	0.08	0	3.50
27	0.08	0	3.42
28	0.07	2	3.22
29	0.06	2	2.92
30	0.06	1	2.57
31	0.05	1	2.18
32	0.04	0	1.80
33	0.03	3	1.44
34	0.02	0	1.11
35	0.02	0	0.84
36	0.01	2	0.61
37	0.01	1	0.44
38	0.01	1	0.30
39	0.00	0	0.20
40	0.00	2	0.14
41	0.00	1	0.09
42	0.00	0	0.05
43	0.00	1	0.03
44	0.00	0	0.02
45	0.00	0	0.01
46	0.00	0	0.01
47	0.00	1	0.00
48	0.00	1	0.00

CP nr per cell	Poisson prob.	Observed Freq.	Expected Freq.
49	0.00	0	0.00
50	0.00	0	0.00
51	0.00	0	0.00
52	0.00	0	0.00
53	0.00	0	0.00
54	0.00	1	0.00
55	0.00	0	0.00
56	0.00	0	0.00
57	0.00	0	0.00
58	0.00	0	0.00
59	0.00	1	0.00
60	0.00	0	0.00
61	0.00	0	0.00
62	0.00	1	0.00
63	0.00	0	0.00
64	0.00	0	0.00
65	0.00	0	0.00
66	0.00	0	0.00
67	0.00	0	0.00
68	0.00	0	0.00
69	0.00	0	0.00
70	0.00	0	0.00
71	0.00	0	0.00
72	0.00	0	0.00
73	0.00	0	0.00
74	0.00	0	0.00
75	0.00	0	0.00
76	0.00	0	0.00
77	0.00	0	0.00
78	0.00	0	0.00
79	0.00	0	0.00
80	0.00	0	0.00
81	0.00	0	0.00
82	0.00	0	0.00
83	0.00	0	0.00
84	0.00	0	0.00
85	0.00	0	0.00
86	0.00	0	0.00
87	0.00	0	0.00
88	0.00	0	0.00
89	0.00	0	0.00
90	0.00	0	0.00
<b>TOTAL</b>	1	45	45

**Table A.10.** Table with calculated Poisson probability, Poisson expected CP frequency and observed CP frequencies in Area A3.

CP nr per cell	Poisson prob.	Observed Freq.	Expected Freq.
0	0.00	0	0.00
1	0.00	1	0.01
2	0.00	2	0.05
3	0.00	6	0.17
4	0.01	3	0.48
5	0.02	2	1.08
6	0.04	2	2.02
7	0.06	4	3.23
8	0.08	5	4.53
9	0.10	1	5.64
10	0.12	4	6.32
11	0.12	0	6.43
12	0.11	3	6.01
13	0.10	1	5.18
14	0.08	3	4.14
15	0.06	3	3.09
16	0.04	2	2.17
17	0.03	2	1.43
18	0.02	1	0.89
19	0.01	0	0.52
20	0.01	1	0.29
21	0.00	0	0.16
22	0.00	3	0.08
23	0.00	0	0.04
24	0.00	2	0.02
25	0.00	1	0.01
26	0.00	2	0.00
27	0.00	0	0.00
28	0.00	0	0.00
29	0.00	0	0.00
30	0.00	0	0.00
31	0.00	0	0.00
32	0.00	0	0.00
33	0.00	0	0.00
34	0.00	0	0.00
35	0.00	0	0.00
36	0.00	0	0.00
37	0.00	0	0.00
38	0.00	0	0.00
39	0.00	0	0.00
40	0.00	0	0.00
41	0.00	0	0.00
42	0.00	0	0.00
43	0.00	0	0.00
44	0.00	0	0.00
45	0.00	0	0.00
46	0.00	0	0.00
47	0.00	0	0.00
48	0.00	0	0.00

CP nr per cell	Poisson prob.	Observed Freq.	Expected Freq.
49	0.00	0	0.00
50	0.00	0	0.00
51	0.00	0	0.00
52	0.00	0	0.00
53	0.00	0	0.00
54	0.00	0	0.00
55	0.00	0	0.00
56	0.00	0	0.00
57	0.00	0	0.00
58	0.00	0	0.00
59	0.00	0	0.00
60	0.00	0	0.00
61	0.00	0	0.00
62	0.00	0	0.00
63	0.00	0	0.00
64	0.00	0	0.00
65	0.00	0	0.00
66	0.00	0	0.00
67	0.00	0	0.00
68	0.00	0	0.00
69	0.00	0	0.00
70	0.00	0	0.00
71	0.00	0	0.00
72	0.00	0	0.00
73	0.00	0	0.00
74	0.00	0	0.00
75	0.00	0	0.00
76	0.00	0	0.00
77	0.00	0	0.00
78	0.00	0	0.00
79	0.00	0	0.00
80	0.00	0	0.00
81	0.00	0	0.00
82	0.00	0	0.00
83	0.00	0	0.00
84	0.00	0	0.00
85	0.00	0	0.00
86	0.00	0	0.00
87	0.00	0	0.00
88	0.00	0	0.00
89	0.00	0	0.00
90	0.00	0	0.00
TOTAL	1	54	54

**Table A.11.** Table with calculated Negative Binomial probability and expected CP frequency, and observed CP frequencies in the total area.

CP nr per cell	Negative Binomial Prob.	Expected Freq.	Observed Freq.
0	0.01	1.12	0
1	0.01	1.86	1
2	0.02	2.42	3
3	0.02	2.84	7
4	0.02	3.18	3
5	0.02	3.43	3
6	0.03	3.62	3
7	0.03	3.76	6
8	0.03	3.86	6
9	0.03	3.92	1
10	0.03	3.95	4
11	0.03	3.95	3
12	0.03	3.93	5
13	0.03	3.90	2
14	0.03	3.84	6
15	0.03	3.78	4
16	0.03	3.71	5
17	0.03	3.62	2
18	0.02	3.54	3
19	0.02	3.44	3
20	0.02	3.34	3
21	0.02	3.24	1
22	0.02	3.14	5
23	0.02	3.03	0
24	0.02	2.93	5
25	0.02	2.82	3
26	0.02	2.72	2
27	0.02	2.61	0
28	0.02	2.51	3
29	0.02	2.41	4
30	0.02	2.31	1
31	0.02	2.22	1
32	0.01	2.12	1
33	0.01	2.03	4
34	0.01	1.94	0
35	0.01	1.86	2
36	0.01	1.77	2
37	0.01	1.69	2
38	0.01	1.62	2
39	0.01	1.54	0
40	0.01	1.47	2
41	0.01	1.40	1
42	0.01	1.33	3
43	0.01	1.27	1
44	0.01	1.21	3
45	0.01	1.15	1
46	0.01	1.09	1
47	0.01	1.04	1
48	0.01	0.99	2



CP nr per cell	Negative Binomial Prob.	Expected Freq.	Observed Freq.
49	0.01	0.94	0
50	0.01	0.89	1
51	0.01	0.85	2
52	0.01	0.80	0
53	0.01	0.76	1
54	0.01	0.72	1
55	0.00	0.68	1
56	0.00	0.65	0
57	0.00	0.62	0
58	0.00	0.58	1
59	0.00	0.55	1
60	0.00	0.52	0
61	0.00	0.50	0
62	0.00	0.47	1
63	0.00	0.44	1
64	0.00	0.42	0
65	0.00	0.40	1
66	0.00	0.38	0
67	0.00	0.36	0
68	0.00	0.34	0
69	0.00	0.32	1
70	0.00	0.30	0
71	0.00	0.28	1
72	0.00	0.27	0
73	0.00	0.25	0
74	0.00	0.24	1
75	0.00	0.23	0
76	0.00	0.21	1
77	0.00	0.20	0
78	0.00	0.19	0
79	0.00	0.18	0
80	0.00	0.17	0
81	0.00	0.16	0
82	0.00	0.15	0
83	0.00	0.14	0
84	0.00	0.14	1
85	0.00	0.13	0
86	0.00	0.12	0
87	0.00	0.11	1
88	0.00	0.11	0
89	0.00	0.10	0
90	0.00	0.10	1
<b>TOTAL</b>	0.99	142.45	144

**Table A.12.** Table with calculated Negative Binomial probability and expected CP frequency, and observed CP frequencies in Area A1.

CP nr per cell	Negative Binomial Prob.	Expected Freq.	Observed Freq.
0	0.00	0.00	0
1	0.00	0.01	0
2	0.00	0.02	1
3	0.00	0.03	0
4	0.00	0.05	0
5	0.00	0.08	0
6	0.00	0.11	0
7	0.00	0.15	0
8	0.00	0.19	0
9	0.01	0.23	0
10	0.01	0.28	0
11	0.01	0.33	1
12	0.01	0.37	1
13	0.01	0.42	0
14	0.01	0.47	0
15	0.01	0.52	1
16	0.01	0.57	2
17	0.01	0.61	0
18	0.01	0.65	1
19	0.02	0.69	1
20	0.02	0.73	1
21	0.02	0.76	0
22	0.02	0.79	0
23	0.02	0.82	0
24	0.02	0.85	2
25	0.02	0.87	1
26	0.02	0.89	0
27	0.02	0.90	0
28	0.02	0.91	1
29	0.02	0.92	2
30	0.02	0.93	0
31	0.02	0.93	0
32	0.02	0.93	1
33	0.02	0.92	1
34	0.02	0.92	0
35	0.02	0.91	2
36	0.02	0.90	0
37	0.02	0.89	1
38	0.02	0.88	1
39	0.02	0.86	0
40	0.02	0.85	0
41	0.02	0.83	0
42	0.02	0.81	3
43	0.02	0.80	0
44	0.02	0.78	3
45	0.02	0.76	1
46	0.02	0.73	1
47	0.02	0.71	0
48	0.02	0.69	1

CP nr per cell	Negative Binomial Prob.	Expected Freq.	Observed Freq.
49	0.01	0.67	0
50	0.01	0.65	1
51	0.01	0.63	2
52	0.01	0.61	0
53	0.01	0.58	1
54	0.01	0.56	0
55	0.01	0.54	1
56	0.01	0.52	0
57	0.01	0.50	0
58	0.01	0.48	1
59	0.01	0.46	0
60	0.01	0.44	0
61	0.01	0.42	0
62	0.01	0.40	0
63	0.01	0.38	1
64	0.01	0.37	0
65	0.01	0.35	1
66	0.01	0.33	0
67	0.01	0.32	0
68	0.01	0.30	0
69	0.01	0.29	1
70	0.01	0.27	0
71	0.01	0.26	1
72	0.01	0.25	0
73	0.01	0.24	0
74	0.00	0.22	1
75	0.00	0.21	0
76	0.00	0.20	1
77	0.00	0.19	0
78	0.00	0.18	0
79	0.00	0.17	0
80	0.00	0.16	0
81	0.00	0.15	0
82	0.00	0.14	0
83	0.00	0.14	0
84	0.00	0.13	1
85	0.00	0.12	0
86	0.00	0.11	0
87	0.00	0.11	1
88	0.00	0.10	0
89	0.00	0.10	0
90	0.00	0.09	1
<b>TOTAL</b>	0.97	43.64	45

**Table A.13.** Table with calculated Negative Binomial probability and expected CP frequency, and observed CP frequencies in area A2.

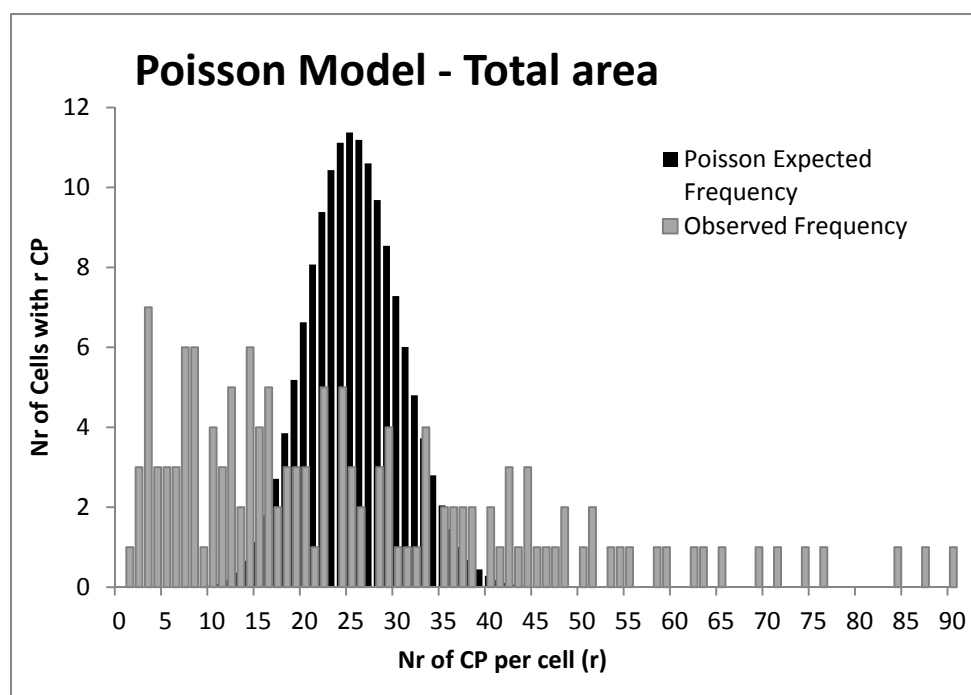
CP nr per cell	Negative Binomial Prob.	Expected Freq.	Observed Freq.
0	0.00	0.02	0
1	0.00	0.07	0
2	0.00	0.14	0
3	0.01	0.23	1
4	0.01	0.34	0
5	0.01	0.45	1
6	0.01	0.57	1
7	0.02	0.69	2
8	0.02	0.80	1
9	0.02	0.90	0
10	0.02	1.00	0
11	0.02	1.09	2
12	0.03	1.16	1
13	0.03	1.23	1
14	0.03	1.28	3
15	0.03	1.32	0
16	0.03	1.35	1
17	0.03	1.37	0
18	0.03	1.38	1
19	0.03	1.38	2
20	0.03	1.37	1
21	0.03	1.35	1
22	0.03	1.33	2
23	0.03	1.30	0
24	0.03	1.27	1
25	0.03	1.24	1
26	0.03	1.20	0
27	0.03	1.15	0
28	0.02	1.11	2
29	0.02	1.06	2
30	0.02	1.02	1
31	0.02	0.97	1
32	0.02	0.92	0
33	0.02	0.88	3
34	0.02	0.83	0
35	0.02	0.78	0
36	0.02	0.74	2
37	0.02	0.70	1
38	0.01	0.66	1
39	0.01	0.61	0
40	0.01	0.58	2
41	0.01	0.54	1
42	0.01	0.50	0
43	0.01	0.47	1
44	0.01	0.44	0
45	0.01	0.41	0
46	0.01	0.38	0
47	0.01	0.35	1
48	0.01	0.33	1

CP nr per cell	Negative Binomial Prob.	Expected Freq.	Observed Freq.
49	0.01	0.30	0
50	0.01	0.28	0
51	0.01	0.26	0
52	0.01	0.24	0
53	0.00	0.22	0
54	0.00	0.20	1
55	0.00	0.19	0
56	0.00	0.17	0
57	0.00	0.16	0
58	0.00	0.15	0
59	0.00	0.13	1
60	0.00	0.12	0
61	0.00	0.11	0
62	0.00	0.10	1
63	0.00	0.10	0
64	0.00	0.09	0
65	0.00	0.08	0
66	0.00	0.07	0
67	0.00	0.07	0
68	0.00	0.06	0
69	0.00	0.06	0
70	0.00	0.05	0
71	0.00	0.05	0
72	0.00	0.04	0
73	0.00	0.04	0
74	0.00	0.04	0
75	0.00	0.03	0
76	0.00	0.03	0
77	0.00	0.03	0
78	0.00	0.02	0
79	0.00	0.02	0
80	0.00	0.02	0
81	0.00	0.02	0
82	0.00	0.02	0
83	0.00	0.01	0
84	0.00	0.01	0
85	0.00	0.01	0
86	0.00	0.01	0
87	0.00	0.01	0
88	0.00	0.01	0
89	0.00	0.01	0
90	0.00	0.01	0
TOTAL	1.00	44.93	45

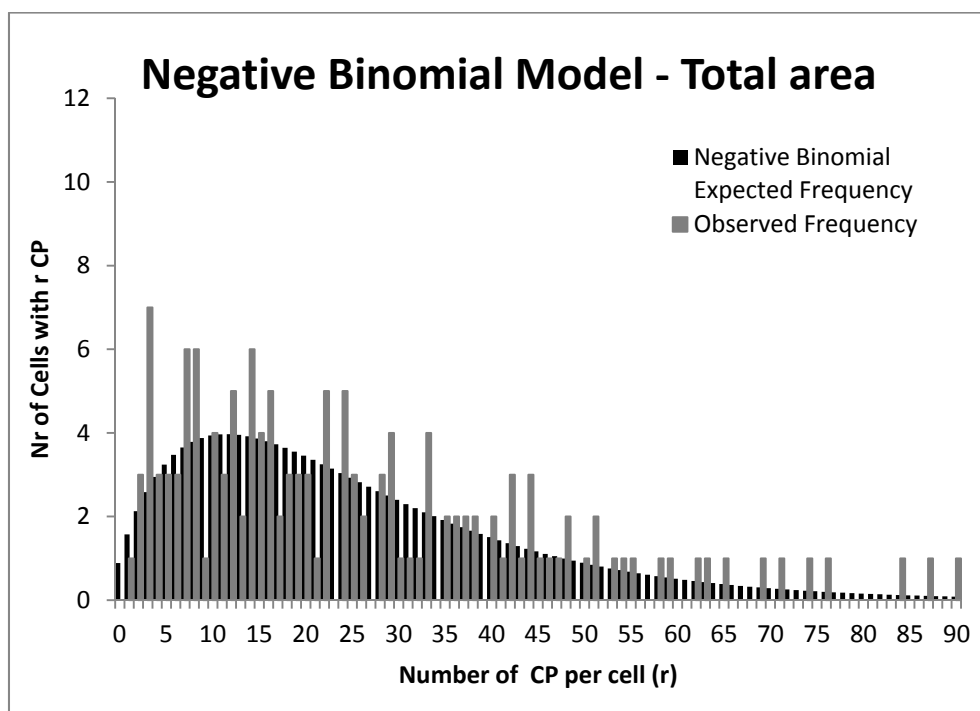
**Table A.14.** Table with calculated Negative Binomial probability and expected CP frequency, and observed CP frequencies in area A3.

CP nr per cell	Negative Binomial Prob.	Expected Freq.	Observed Freq.
0	0.01	0.46	0
1	0.02	1.12	1
2	0.03	1.81	2
3	0.04	2.43	6
4	0.05	2.91	3
5	0.06	3.25	2
6	0.06	3.44	2
7	0.07	3.51	4
8	0.06	3.48	5
9	0.06	3.36	1
10	0.06	3.19	4
11	0.06	2.98	0
12	0.05	2.74	3
13	0.05	2.49	1
14	0.04	2.24	3
15	0.04	2.00	3
16	0.03	1.77	2
17	0.03	1.56	2
18	0.03	1.36	1
19	0.02	1.18	0
20	0.02	1.02	1
21	0.02	0.88	0
22	0.01	0.75	3
23	0.01	0.64	0
24	0.01	0.55	2
25	0.01	0.46	1
26	0.01	0.39	2
27	0.01	0.33	0
28	0.01	0.28	0
29	0.00	0.23	0
30	0.00	0.20	0
31	0.00	0.16	0
32	0.00	0.14	0
33	0.00	0.11	0
34	0.00	0.09	0
35	0.00	0.08	0
36	0.00	0.06	0
37	0.00	0.05	0
38	0.00	0.04	0
39	0.00	0.04	0
40	0.00	0.03	0
41	0.00	0.02	0
42	0.00	0.02	0
43	0.00	0.02	0
44	0.00	0.01	0
45	0.00	0.01	0
46	0.00	0.01	0
47	0.00	0.01	0
48	0.00	0.01	0

CP nr per cell	Negative Binomial Prob.	Expected Freq.	Observed Freq.
49	0.00	0.00	0
50	0.00	0.00	0
51	0.00	0.00	0
52	0.00	0.00	0
53	0.00	0.00	0
54	0.00	0.00	0
55	0.00	0.00	0
56	0.00	0.00	0
57	0.00	0.00	0
58	0.00	0.00	0
59	0.00	0.00	0
60	0.00	0.00	0
61	0.00	0.00	0
62	0.00	0.00	0
63	0.00	0.00	0
64	0.00	0.00	0
65	0.00	0.00	0
66	0.00	0.00	0
67	0.00	0.00	0
68	0.00	0.00	0
69	0.00	0.00	0
70	0.00	0.00	0
71	0.00	0.00	0
72	0.00	0.00	0
73	0.00	0.00	0
74	0.00	0.00	0
75	0.00	0.00	0
76	0.00	0.00	0
77	0.00	0.00	0
78	0.00	0.00	0
79	0.00	0.00	0
80	0.00	0.00	0
81	0.00	0.00	0
82	0.00	0.00	0
83	0.00	0.00	0
84	0.00	0.00	0
85	0.00	0.00	0
86	0.00	0.00	0
87	0.00	0.00	0
88	0.00	0.00	0
89	0.00	0.00	0
90	0.00	0.00	0
<b>TOTAL</b>	1.00	54.00	54

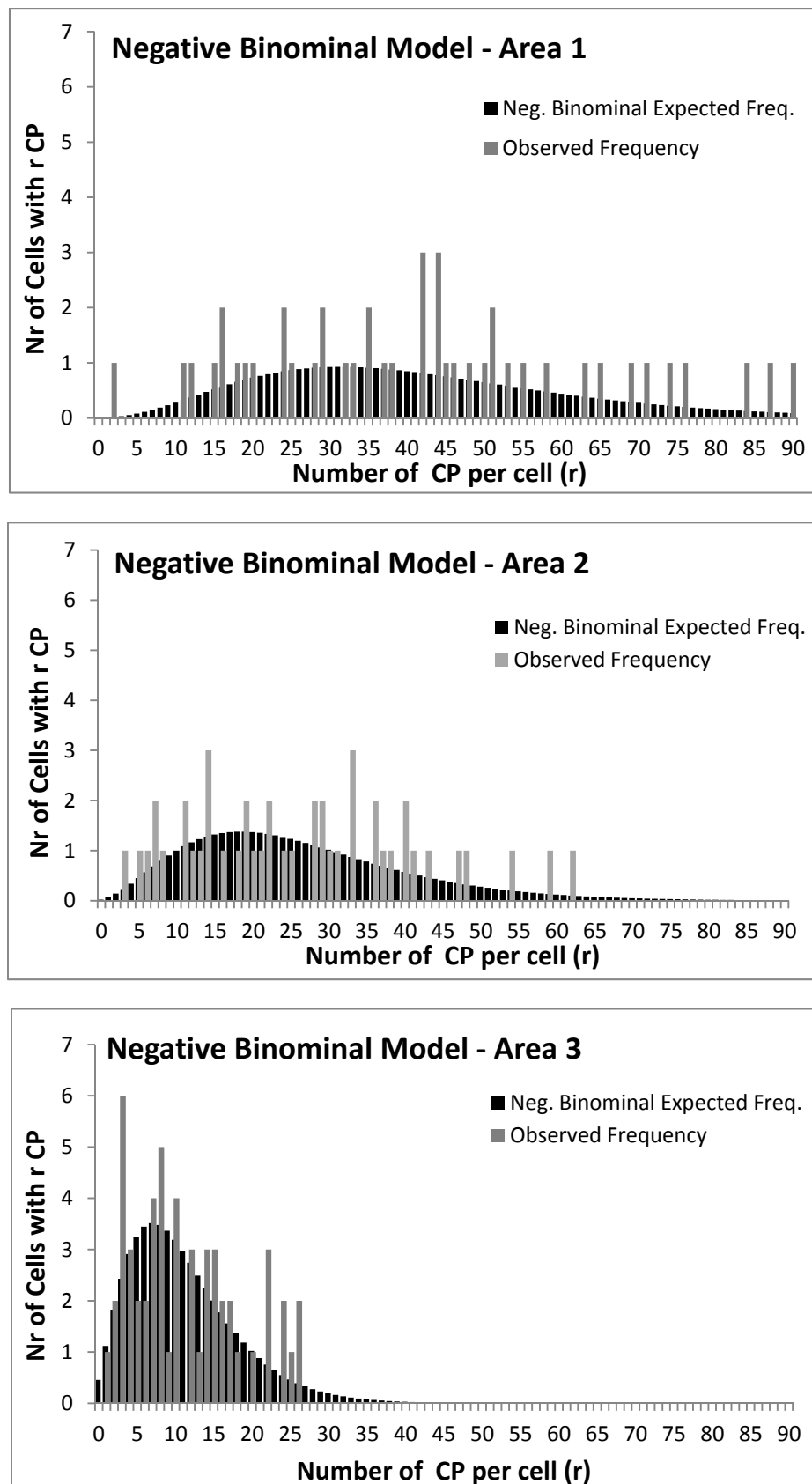


**Figure A.6.** Plot contrasting the Poisson expected frequency and observed frequencies in the total area



**Figure A.7.** Plot contrasting the Negative Binomial expected frequency and observed frequencies in the total area.





**Figure A.8.** Plots representing the Negative Binomial expected frequencies and the observed frequencies in the three studied areas.

## A5. Supplementary data for Chapter 7

**Table A.15.** Average dimensions of MTDs in Units 2 and 3.

Unit	MTD	Avg W (m)	Avg H (m)
<b>2</b>	MTD-A1	24000	110
	MTD-2	30000	90
	MTD-3	21000	60
	MTD-Top-1	12000	75
	MTD-Top-2	15000	70
<b>3</b>	1	9480	48.45
	2	6555	22.1
	3	6430	40.8
	4	7200	33.15

**Table A.16.** Average dimensions of turbidites in Unit 2.

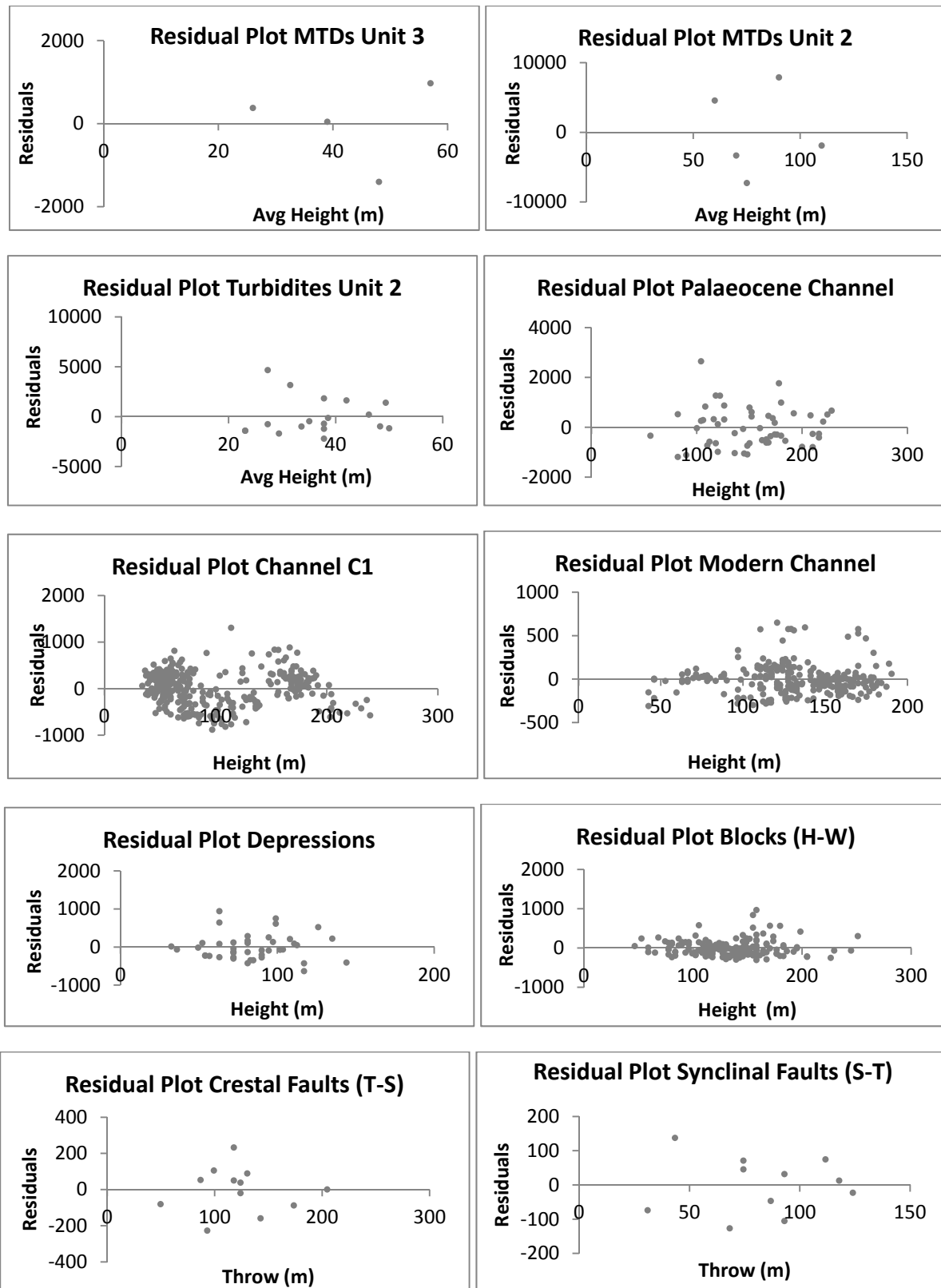
Horizon	Avg W (m)	Avg H (m)	Lenght (m)	Area (sq. Km)
<b>1</b>	1620	37.8	10380	22.24
<b>2</b>	5231	49.35	29970	257
<b>3</b>	2145	29.4	6640	15
<b>4</b>	4040	46.2	7688	13.8
<b>5</b>	3704	38.577	16620	62.78
<b>6</b>	2660	49.98	13690	42
<b>7a</b>	3079	27.3	22000	95
<b>7b</b>	3375	35.07	13880	45
<b>8a</b>	2427	23.1	9340	26
<b>8b</b>	2427	23.1	8064	23
<b>9a</b>	8500	27.3	10000	71
<b>10</b>	2607	37.8	11180	27.25
<b>12</b>	3120	37.8	20300	65
<b>14</b>	7000	31.5	18700	154
<b>17</b>	2856	48.3	4645	8.3
<b>18</b>	2847	33.6	9150	19
<b>20a</b>	5463	42	8500	37
<b>20b</b>	5661	37.8	12980	71
<b>min</b>	1620	23.1	4645	8.3
<b>max</b>	8500	49.98	29970	257

**Table A.17.** Length, Throw and Spacing data of the Crestal and Synclinal fault families.

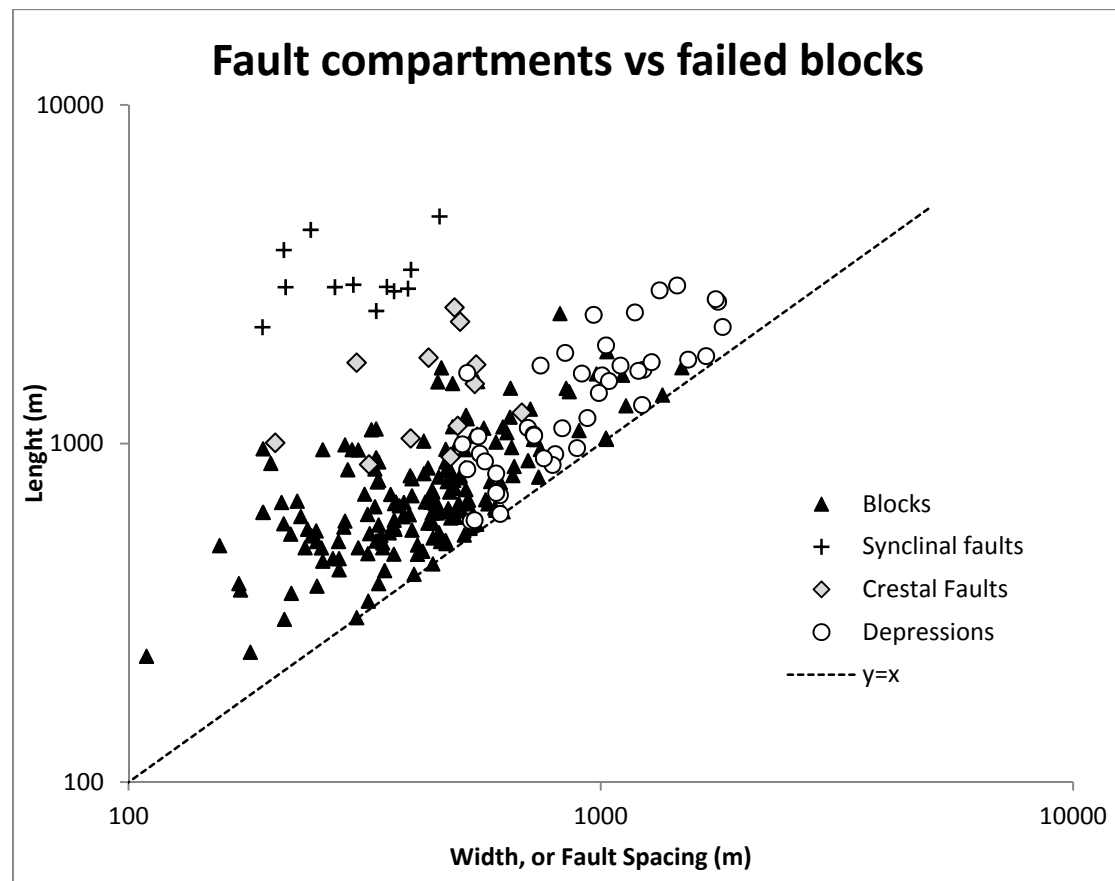
Type	Length (m)	Throw (m)	Spacing (m)
Crestal	1036.0	173.6	395.5
	1501.1	99.2	540.6
	913.3	86.8	480.4
	1005.4	93.0	204.3
	867.7	49.6	322.8
	2523.0	124.0	489.7
	1793.9	124.0	431.6
	1733.5	142.6	303.9
	1127.9	117.8	497.4
	1711.7	130.2	544.3
	1233.8	117.8	679.9
	2290.5	204.6	503.2
Synclinal	3728.3	80.6	213.1
	4277.3	31.0	243.0
	2897.1	86.8	273.3
	2895.8	93.0	214.9
	2205.9	68.2	192.1
	2902.4	93.0	352.2
	2816.8	74.4	364.8
	2866.2	74.4	390.4
	2463.2	117.8	334.4
	2945.0	124.0	299.1
	4684.6	43.4	455.2
	3260.2	111.6	396.1
<b>Avg. Crestal</b>	1478.2	121.9	449.5
<b>Avg. Syncl.</b>	3161.9	83.2	310.7
<b>Max Crestal</b>	2523.0	204.6	679.9
<b>Max Syncl.</b>	4684.6	124.0	455.2
<b>Min. Crestal</b>	867.7	49.6	204.3
<b>Min. Syncl.</b>	2205.9	31.0	192.1

**Table A.18.** Table with dimensional data of the morphometric depressions in sub-unit 3b.

ID	Width (m)	Height (m)	Length (m)	Area (sq Km)	W/L ratio
2	521	54	1617	0.9	0.32
5	1331	108	2835	3.1	0.47
9	1810	99	2210	2.1	0.82
10	1180	97	2440	2.7	0.48
11	1005	102	1590	1.1	0.63
11	1040	81	1530	1.2	0.68
11	1530	135	1770	2.4	0.86
13	521	54	840	0.5	0.62
14	800	81	931	0.5	0.86
14	600	72	816	0.3	0.74
15	1100	81	1700	1.7	0.65
16b	1770	126	2624	3.5	0.67
16b	790	90	865	0.5	0.91
16c	700	50	1113	0.5	0.63
16d	612	32	620	0.3	0.99
16d	554	36	934	0.3	0.59
17a	1222	81	1300	1.0	0.94
17c	1230	111	1652	1.7	0.74
17c	890	63	970	0.6	0.92
18b	965	144	2400	2.0	0.40
18c	1450	63	2930	4.2	0.49
19	1670	99	1813	2.1	0.92
19	611	85	704	0.3	0.87
19	509	81	995	0.4	0.51
21	1280	95	1740	1.5	0.74
21	745	72	1700	1.3	0.44
23	990	72	1411	1.0	0.70
24	720	72	1063	0.7	0.68
30	568	72	886	0.5	0.64
30	530	57	590	0.2	0.90
31a	911	90	1610	1.2	0.57
35	550	117	1050	0.3	0.52
36	1200	113	1640	1.4	0.73
37	936	95	1190	1.0	0.79
39	828	72	1110	0.7	0.75
39	722	90	1056	0.6	0.68
49	600	83	715	0.4	0.84
53	757	117	905	0.61	0.84
54	540	63	594	0.3	0.91
<b>Avg.</b>	930.5	84.7	1396.4	1.2	0.7



**Figure A.9.** Linear regression residual plots of the width-height, or fault spacing-throw, relations obtained for the different data series analysed in this thesis.



**Figure A.10.** Log-Log plot comparing the width and length of MTD Blocks and morphological depressions, and spacing and length of crestal faults and synclinal faults. The size of blocks overlaps the sizes of crestal faults, thus confirming their genetic relation.